Strategies for Reserve Growth in Tirrawarra Field

Final Report to
Santos Ltd., Adelaide, South Australia

by

Noel Tyler, H. Scott Hamlin, Shirley P. Dutton,
Bob A. Hardage, and Joseph S. Yeh
Bureau of Economic Geology

Robert Seggie and Peter Lansom
Santos Ltd.

and
George Asquith
Texas Tech University

Bureau of Economic Geology
W. L. Fisher, Director
The University of Texas at Austin
Austin, Texas 78713-7508

October 1993

QAe7726

CONTENTS

I. EXECUTIVE SUMMARY 1

II. INTRODUCTION 3

Background 3

Objectives 5

Data 6

Methodology 8

III. GEOLOGICAL SETTING 11

Structural Geology 11

Regional Setting 11

Field Area 11

Palynology 18

Stratigraphic Setting 19

IV. GEOPHYSICAL INTERPRETATION 23

Introduction 23

Interpretational Procedure 25

Correlation and Interpretation of Seismic Sections 26

Structural Mapping 79

Time-Structure Maps 79

Velocity Maps 79

Depth Maps 83

Structural Style 83

Discussion 90

Comparison of Santos and BEG Interpretations 90

Use of Revised Structure Map in OOIP Calculations 92

Recommendations 92

VSP Calibration Control 92

3-D Seismic Imaging....93
V. DEPOSITIONAL SYSTEMS....94
Methodology....94
Core Description....94
Characterization of Facies and Flow Units....95
Tirrawarra Facies....97
Facies 1....97
Core Description....97
Interpretation....107
Facies 2....107
Core Description....107
Interpretation....110
Facies 3....110
Core Description....110
Interpretation....118
Facies 4....120
Core Description....120
Interpretation....127
Differentiation of Flow Units....127
Well Log Patterns....129
Flow Unit 1U....129
Flow Units 2L and 2U....129
Flow Units 3L and 3U....130
Flow Unit 4....130
Petrophysical Properties from Core....131
Architecture of Facies and Flow Units....141
Facies 1 (Flow Unit 1U)....149

Facies 2 (Flow Unit 2L) 155
Facies 3 (Flow Units 3L and 3U) 159
Facies 2 (Flow Unit 2U) 168
Facies 4 (Flow Unit 4) 168
Summary of Facies-Related Reservoir Properties 177
VI. PETROGRAPHIC COMPOSITION OF TIRRAWARRA SANDSTONES 179
Methodology 179
Texture 181
Framework Mineralogy 181
Matrix 183
Cements 185
Quartz 188
Authigenic Clays 188
Siderite 191
Reservoir Bitumen 204
Porosity 205
Diagenetic Bands 206
Diagenetic Controls on Reservoir Quality 209
Flow Unit 1U 212
Flow Unit 2L 212
Flow Unit 3L 214
Flow Unit 3U 219
Flow Unit 4 219
Spatial Variation in Petrographic Parameters 220
Conclusions 223
VII. PETROPHYSICS 225
Introduction 225

Review and Analysis....225
General....225
Problems with the Log Data....226
Review of Santos Methods....229
Volume of Shale (Vsh) Determination....229
Porosity Determination....229
Effective Water Saturation Determination....232
Petrophysical Verification of Flow Units....235
Determination of Cutoff Values for Net Pay Calculation....249
Volume of Shale Cutoff....263
Porosity Cutoff....271
Water Saturation Cutoff....279
Other Issues....280
Saturation Exponent (n)....280
Rw Determination....289
Background....289
Rw Determination from Water Analysis....295
Rw Estimation from Log Analysis....295
Foot-by-Foot Log Analysis....297
Determination of Input Parameters for Log Analysis....297
Log Analysis Results and Adjustments....298
Implications....298
VIII. VOLUMETRICS....299
Original Oil in Place (OOIP) Mapping Procedure....299
Oil/Water Contact Interpretation....306
OOIP Calculation and Distribution....315
OOIP Distribution—Net Pay and Hydrocarbon Pore Volume....315

Flow Unit 1U 322
Flow Unit 2L 333
Flow Unit 3L 333
Flow Unit 3U 333
Flow Unit 2U 334
Flow Unit 4 334
Calculated OOIP and Distribution Summary 335
IX. PRODUCTION ANALYSIS 338
Engineering Review 338
SCAL Data 338
Capillary Pressure 340
Relative Permeability 340
RFT/PLT Results 344
Production Data 345
Pattern Performance 348
Tirrawarra No. 15 Pattern 349
Tirrawarra No. 18 Pattern 352
Tirrawarra No. 29 Pattern 354
Tirrawarra No. 38 Pattern 354
Tirrawarra Nos. 50, 60, and 61 Patterns 354
Permeability Analysis 355
Permeability Calculation 355
Permeability Distribution 358
Production Allocation by kh 361
Remaining Oil in Place 362
West Area 363
East Area 363

North Area 364
Validation and Sensitivity of kh-Apportioned Method 364
X. OPPORTUNITIES FOR INCREMENTAL DEVELOPMENT 366
New Pattern Development 366
Optimization of Existing EOR Activities 368
General 368
Low Pressure Flood 368
CO_2 Injection 370
Pattern Soak 370
Flank Location Huff-and-Puff 370
Infill Well Locations 371
Strategic Infill and Recompletion Opportunities 372
Horizontal Well 372
Recompletion Strategies 372
XI. CONCLUSIONS 373
XII. RECOMMENDATIONS 378
ACKNOWLEDGMENTS 379
REFERENCES 380
APPENDICES
A. Well Data Tables
B. Core Descriptions
C. Petrographic Data
D. Flow Units on Well Logs
E. Production History Plots

Figures

II-1. Map of Tirrawarra field in the Cooper Basin, South Australia 4
II-2. Map of Tirrawarra field showing distribution of Tirrawarra Sandstone core 7

III-1. Location map of Cooper Basin and Tirrawarra oil field in east-central Australia.....12

III-2. Generalized structure map of the southern Cooper Basin, South Australia.....13

III-3. Schematic cross section A–A', southern Cooper Basin.....14

III-4. Late Carboniferous–Triassic stratigraphy of the Cooper Basin.....15

III-5. Isopach map of the interval between the red and orange correlation horizons, Tirrawarra field.....17

IV-1. Seismic grid and well control - Tirrawarra field.....in pocket and 24

IV-2. Interpretation of seismic line 80 T-1.....27

IV-3. Interpretation of seismic line 80 T-3.....29

IV-4. Interpretation of seismic line 80 T-5.....31

IV-5. Interpretation of seismic line 80 T-7.....33

IV-6. Interpretation of seismic line 80 T-9.....35

IV-7. Interpretation of seismic line 80 T-11.....37

IV-8. Interpretation of seismic line 80 T-13.....39

IV-9. Interpretation of seismic line 80 T-15.....41

IV-10. Interpretation of seismic line 80 T-17.....43

IV-11. Interpretation of seismic line 80 T-19.....45

IV-12. Interpretation of seismic line 80 T-21.....47

IV-13. Interpretation of seismic line 80 T-23.....49

IV-14. Interpretation of seismic line 80 T-2.....51

IV-15. Interpretation of seismic line 80 T-4.....53

IV-16. Interpretation of seismic line 80 T-6.....55

IV-17. Interpretation of seismic line 80 T-8.....57

IV-18. Interpretation of seismic line 80 T-10.....59

IV-19. Interpretation of seismic line 80 T-12.....61

IV-20. Interpretation of seismic line 80 T-14.....63

IV-21. Interpretation of seismic line 80 T-16.....65

IV-22. Interpretation of seismic line 80 T-18.....67

IV-23. Interpretation of seismic line 80 T-20 69

IV-24. Interpretation of northeast portion of seismic line 90-CJQ 72

IV-24. (cont.) Interpretation of the southwest portion of seismic line 90-CJQ 73

IV-25. Interpretation of seismic line 90-CJR. Ignore fault 15 as projected onto this line 75

IV-26. Interpretation of seismic line 90-CJS 77

IV-27. Tirrawarra Project - Orange Horizon - 2-way time map ..... in pocket and 80

IV-28. Tirrawarra Project - Reservoir Horizon - 2-way time map ..... in pocket and 81

IV-29. Tirrawarra Project - Merrimelia Horizon - 2-way time map ..... in pocket and 82

IV-30. Tirrawarra Project - Orange Horizon - Velocity map ..... in pocket and 84

IV-31. Tirrawarra Project - Reservoir Horizon - Velocity map ..... in pocket and 85

IV-32. Tirrawarra Project - Merrimelia Horizon - Velocity map ..... in pocket and 86

IV-33. Tirrawarra Project - Orange Horizon - Depth map ..... in pocket and 87

IV-34. Tirrawarra Project - Reservoir Horizon - Depth map ..... in pocket and 88

IV-35. Tirrawarra Project - Merrimelia Horizon - Depth map ..... in pocket and 89

IV-36. Depth to top Tirrawarra map ..... in pocket

V-1. Core description, log responses, and petrophysical properties from facies 1 and 2, Tirrawarra well 8 100

V-2. Photographs of core from facies 1 and 2 ..... 102 and 105

V-3. Depositional model for facies 1 and 2 108

V-4. Core description, log responses, and petrophysical properties from facies 1, 2, 3, and 4, Tirrawarra well 20 109

V-5. Core description, log responses, and petrophysical properties from facies 2 and 3, Tirrawarra well 2 111

V-6. Photographs of core from facies 3 ..... 113 and 115

V-7. Depositional model for facies 2 and 3 119

V-8. Core description, log responses, and petrophysical properties from facies 4, Tirrawarra well 16 121

V-9. Photographs of core from facies 4 ..... 123 and 125

V-10. Depositional model for facies 4 128

V-11. Graph of porosity versus permeability, flow unit 1U 132
V-12. Graph of porosity versus permeability, flow unit 2U 133
V-13. Graph of porosity versus permeability, flow unit 2L 134
V-14. Graph of porosity versus permeability, flow unit 3U 135
V-15. Graph of porosity versus permeability, flow unit 3L 136
V-16. Graph of porosity versus permeability, flow unit 4 137
V-17. Graph of porosity versus permeability, flow unit 4, showing only core data from wells in the central and western parts of Tirrawarra field 139
V-18. Graph of average porosity versus geometric mean permeability for each Tirrawarra flow unit 140
V-19. Mercury-injection capillary-pressure curve for a core sample from flow unit 1U 142
V-20. Mercury-injection capillary-pressure curve for a core sample from flow unit 2U 143
V-21. Mercury-injection capillary-pressure curves for core samples from flow unit 2L 144
V-22. Mercury-injection capillary-pressure curves for core samples from flow unit 3U 145
V-23. Mercury-injection capillary-pressure curves for core samples from flow unit 3L 146
V-24. Mercury-injection capillary-pressure curves for core samples from flow unit 4 147
V-25. Average capillary-pressure curves for each flow unit 148
V-26. Schematic south–north cross section, Tirrawarra field 150
V-27. Schematic west–east cross section, Tirrawarra field 151
V-28. Isopach map of Tirrawarra flow unit 1U 152
V-29. Net porous sandstone map of Tirrawarra flow unit 1U 153
V-30. Permeability-thickness (kh) map of Tirrawarra flow unit 1U 154
V-31. Isopach map of Tirrawarra flow unit 2L 156
V-32. Net porous sandstone map of Tirrawarra flow unit 2L 157
V-33. Permeability-thickness (kh) map of Tirrawarra flow unit 2L 158

V-34. Isopach map of Tirrawarra facies 3, which includes both flow units 3L and 3U.....160

V-35. Isopach map of Tirrawarra flow unit 3L.....162

V-36. Net porous sandstone map of Tirrawarra flow unit 3L.....163

V-37. Net porous sandstone map of Tirrawarra flow unit 3U.....164

V-38. Permeability-thickness (kh) map of Tirrawarra flow unit 3L.....166

V-39. Permeability-thickness (kh) map of Tirrawarra flow unit 3U.....167

V-40. Isopach map of Tirrawarra flow unit 2U.....169

V-41. Net porous sandstone map of Tirrawarra flow unit 2U.....170

V-42. Permeabilility-thickness (kh) map of Tirrawarra flow unit 2U.....171

V-43. Isopach map of Tirrawarra flow unit 4.....172

V-44. Net porous sandstone map of Tirrawarra flow unit 4.....174

V-45. Permeability-thickness (kh) map of Tirrawarra flow unit 4.....175

VI-1. Compositional classification of Tirrawarra sandstones by flow unit.....184

VI-2. Relative proportions of quartz, siderite, and kaolinite cements by flow unit.....186

VI-3. Generalized paragenetic sequence for Tirrawarra sandstones, Tirrawarra field, Cooper Basin.....187

VI-4. Quartz cement volume decreases with increasing proportion of detrital rock fragments.....189

VI-5. Volume of quartz cement and primary porosity have a positive correlation, indicating that quartz cement volume is not the primary reason for occlusion of intergranular porosity.....190

VI-6. Relative proportions of primary, secondary, and micropores by flow unit.....207

VI-7. Permeability increases with increasing grain size in the total population of Tirrawarra sandstones.....211

VI-8. Permeability decreases with increasing volume of ductile grains, defined as metamorphic and sedimentary rock fragments (including chert), biotite, and muscovite.....213

VI-9. Permeability in flow unit 2L sandstones increases with increasing grain size.....215

VI-10. Permeability in flow unit 3L sandstones decreases with increasing volume of ductile grains.....217

VI-11. Permeability in flow unit 3L sandstones increases with increasing grain size.....218

VI-12. Permeability in flow unit 4 increases with increasing grain size....222

VII-1. Environmental corrected log for the Tirrawarra well 21....227

VII-2. Cross plot of core porosity versus volume of shale (Vsh) for the Tirrawarra well 12....230

VII-3. Cross plot of core permeability versus volume of shale for the Tirrawarra well 12....231

VII-4a. Cross plot of core-derived porosity versus effective sonic porosity for the Tirrawarra wells 12 and 16....233

VII-4b. Sonic log porosity versus core porosity cross plot for the total edited core porosity data base....234

VII-5. Cross plot of Sw (Simandoux) versus Sw (Automatic Compensation) for the Tirrawarra well 21....237

VII-6. Dew plot of the Tirrawarra well 21 with reservoir flow unit 4 shown in red....239

VII-7. Dew plot of the Tirrawarra well 21 with reservoir flow unit 3U shown in red....241

VII-8. Dew plot of the Tirrawarra well 21 with reservoir flow unit 3L shown in red....243

VII-9. Dew plot of the Tirrawarra well 21 with reservoir flow unit 2 shown in red....245

VII-10. Dew plot of the Tirrawarra well 21 with reservoir flow unit 1 shown in red....247

VII-11. Bulk volume water plot of the Tirrawarra well 21 with reservoir flow unit 4 shown in red....251

VII-12. Bulk volume water plot of the Tirrawarra well 21 with reservoir flow unit 3U shown in red....253

VII-13. Bulk volume water plot of the Tirrawarra well 21 with reservoir flow unit 3L shown in red....255

VII-14. Bulk volume water plot of the Tirrawarra well 21 with reservoir flow unit 2L shown in red....257

VII-15. Bulk volume water plot of the Tirrawarra well 21 with reservoir flow unit 1U shown in red....259

VII-16. Dew plot of the downdip Rakoona well 1....261

VII-17. Cross plot of core permeability against log analysis calculated Volume of Shale (vsh) for all edited core data....264

VII-18. Cross plot of core permeability against log analysis calculated Volume of Shale (vsh) for all edited core data from flow unit 4....265

VII-19. Cross plot of core permeability against log analysis calculated Volume of Shale (vsh) for all edited core data from flow unit 2U....266

VII-20. Cross plot of core permeability against log analysis calculated Volume of Shale (vsh) for all edited core data from flow unit 3U....267

VII-21. Cross plot of core permeability against log analysis calculated Volume of Shale (vsh) for all edited core data from flow unit 3L....268

VII-22. Cross plot of core permeability against log analysis calculated Volume of Shale (vsh) for all edited core data from flow unit 2L....269

VII-23. Cross plot of core permeability against log analysis calculated Volume of Shale (vsh) for all edited core data from flow unit 1U....270

VII-24. Cross plot of core permeability against core porosity for all edited core data....272

VII-25. Cross plot of core permeability against core porosity for edited core data for flow unit 4....273

VII-26. Cross plot of core permeability against core porosity for edited core data for flow unit 2U....274

VII-27. Cross plot of core permeability against core porosity for edited core data for flow unit 3U....275

VII-28. Cross plot of core permeability against core porosity for edited core data for flow unit 3L....276

VII-29. Cross plot of core permeability against core porosity for edited core data for flow unit 2L....277

VII-30. Cross plot of core permeability against core porosity for edited core data for flow unit 1U....278

VII-31. Net pay summary for the downdip Tirrawarra well 3....281

VII-32. Net pay summary for the downdip Tirrawarra well 3....283

VII-33. Net pay summary for the Tirrawarra well 21 near the top of the structure....285

VII-34. Net pay summary for the downdip Rakoona well 1....287

VII-35. Net pay summary for the Tirrawarra well 64....291

VII-36. Net pay summary for the Tirrawarra well 67....293

VII-37. Location map of accepted water resistivities....296

VIII-1. Net pay map of flow unit 1U....300

VIII-2. Net pay map of flow unit 2L....301

VIII-3. Net pay map of flow unit 3L....302

VIII-4. Net pay map of flow unit 3U....303

VIII-5. Net pay map of flow unit 2U....304
VIII-6. Net pay map of flow unit 4....305
VIII-7. Map of effective oil/water contact surface....307
VIII-8. Map of hydrocarbon pore volume, flow unit 1U....316
VIII-9. Map of hydrocarbon pore volume, flow unit 2L....317
VIII-10. Map of hydrocarbon pore volume, flow unit 3L....318
VIII-11. Map of hydrocarbon pore volume, flow unit 3U....319
VIII-12. Map of hydrocarbon pore volume, flow unit 2U....320
VIII-13. Map of hydrocarbon pore volume, flow unit 4....321
VIII-14. Map of pay connectivity between flow units 2L and 1U....323
VIII-15. Map of pay connectivity between flow units 3L and 2L....324
VIII-16. Map of pay connectivity between flow units 3U and 3L....325
VIII-17. Map of pay connectivity between flow units 4 and 3U....326
VIII-18. Contour map of the number of separate pay zones in flow unit 2L....327
VIII-19. Contour map of the number of separate pay zones in flow unit 3L....328
VIII-20. Contour map of the number of separate pay zones in flow unit 3U....329
VIII-21. Contour map of the number of separate pay zones in flow unit 2U....330
VIII-22. Contour map of the number of separate pay zones in flow unit 4....331
VIII-23. Map showing regions used in OOIP calculations....336
IX-1. Map showing distribution of available engineering data....339
IX-2. Graph showing capillary pressure versus water saturation at reservoir conditions for averaged Tirrawarra flow unit data....341
IX-3. Graph showing height above the free water level versus water saturation for Tirrawarra flow units....342
IX-4. Graph showing average oil/water relative permeabilities, Tirrawarra reservoir....343
IX-5. Contour map of initial oil production rates from Tirrawarra oil wells....346
IX-6. Graph of cumulative oil production since injection start-up versus cumulative solvent injected, both on a displaceable pore volume (DPV) basis, for the Tirrawarra EOR patterns....350
IX-7. Graph of cumulative solvent produced versus cumulative solvent injected for the Tirrawarra EOR patterns....351

IX-8. Map of Tirrawarra field showing cumulative oil production to breakthrough 353

IX-9. Map of Tirrawarra field showing existing EOR patterns and scaling factors.....357

X-1. Map of Tirrawarra field showing potential future EOR patterns in the north part of the field.....367

X-2. Map of Tirrawarra field showing potential infill drilling and recompletion locations 369

Tables

IV-1. Tirrawarra check-shot wells.....25

V-1. Characteristics of facies 1.....98

V-2. Characteristics of facies 2.....98

V-3. Characteristics of facies 3.....99

V-4. Characteristics of facies 4.....99

V-5. Petrophysical properties from core.....138

VI-1. Comparison of petrographic features by flow unit 182

VI-2. Porosity and permeability parameters in Tirrawarra Sandstone.....210

VI-3. Comparison of flow unit 2 petrographic features 216

VI-4. Comparison of flow unit 3L petrographic features 219

VI-5. Comparison of flow unit 3U petrographic features.....221

VI-6. Comparison of flow unit 4 petrographic features 221

VII-1. Cutoff values for Tirrawarra flow units.....249

VIII-1. OOIP distribution 332

VIII-2. Original oil in place by flow unit and region.....335

IX-1. Tirrawarra RFT pressure results 345

IX-2. Pattern performance summary 348

IX-3. Comparison between well log and production test-derived flow capacity.....356

IX-4. Aggregate Tirrawarra volumetrics 362

IX-5. Remaining oil in place calculated by the production allocation method for west, east, and north areas.....363

IX-6. Comparison of kh-method with volumes remaining assuming flow unit 3L produces 90 percent (CP_{90}) of Tirrawarra production.....364

Plates

III-1. East-west cross section T7 showing well log curves and correlation horizons in the Tirrawarra Sandstone and the Patchawarra Formation.....in pocket

III-2. East-west cross section T15 showing well log curves and correlation horizons in the Tirrawarra Sandstone and the Patchawarra Formation.....in pocket

III-3. East-west cross section T21 showing well log curves and correlation horizons in the Tirrawarra Sandstone and the Patchawarra Formation.....in pocket

III-4. North-south cross section T12 showing well log curves and correlation horizons in the Tirrawarra Sandstone and the Patchawarra Formation.....in pocket

V-1. Stratigraphic cross section T7 showing Tirrawarra reservoir flow unit boundaries and well log curves.....in pocket

V-2. Stratigraphic cross section T11 showing Tirrawarra reservoir flow unit boundaries and well log curves.....in pocket

V-3. Stratigraphic cross section T15 showing Tirrawarra reservoir flow unit boundaries and well log curves.....in pocket

V-4. Stratigraphic cross section T17 showing Tirrawarra reservoir flow unit boundaries and well log curves.....in pocket

V-5. Stratigraphic cross section T19 showing Tirrawarra reservoir flow unit boundaries and well log curves.....in pocket

V-6. Stratigraphic cross section T21 showing Tirrawarra reservoir flow unit boundaries and well log curves.....in pocket

V-7. Stratigraphic cross section OB1 showing Tirrawarra reservoir flow unit boundaries and well log curves.....in pocket

V-8. Stratigraphic cross section T10 showing Tirrawarra reservoir flow unit boundaries and well log curves.....in pocket

V-9. Stratigraphic cross section T12 showing Tirrawarra reservoir flow unit boundaries and well log curves.....in pocket

V-10. Stratigraphic cross section T14 showing Tirrawarra reservoir flow unit boundaries and well log curves.....in pocket

V-11. Stratigraphic cross section T16 showing Tirrawarra reservoir flow unit boundaries and well log curves.....in pocket

V-12. Stratigraphic cross section X1 showing Tirrawarra reservoir flow unit boundaries and well log curves.....in pocket

V-13. Stratigraphic cross section X2 showing Tirrawarra reservoir flow unit boundaries and well log curves ..... in pocket

VI-1a. Illite fibers inside a secondary pore. Sample is from flow unit 3L in Tirrawarra well 17 at 9,724 ft 193

VI-1b. Kaolinite and illite in an altered and partly dissolved rock fragment 193

VI-1c. Typical sandstone from flow unit 1U 193

VI-1d. Typical sandstone from flow unit 2L, showing ductile grain deformation, kaolinite in secondary pores, and siderite replacement of framework grains 193

VI-2a. Typical sandstone from flow unit 3L, showing primary and secondary pores and quartz overgrowths 196

VI-2b. Typical sandstone from flow unit 3U, showing fewer primary pores than flow unit 3L 196

VI-2c. Typical high-permeability sandstone from flow unit 4, showing primary pores 196

VI-2d. Low-permeability sandstone from flow unit 4, with less primary porosity than the sample from two feet away, shown in Plate VI-2c 196

VI-3a. Illite fibers and flakes that line primary pores and extend into and across secondary pores 199

VI-3b. Large cluster of kaolinite crystals in a secondary pore (lower right) 199

VI-3c. Typical flow unit 1U sandstone 199

VI-3d. Typical flow unit 2L sandstone 199

VI-4a. Typical flow unit 3L sandstone 202

VI-4b. Typical flow unit 3U sandstone 202

VI-4c. Typical high-permeability flow unit 4 sandstone; note primary pores (P) and quartz overgrowths (Q) 202

VI-4d. Typical low-permeability flow unit 4 sandstone 202

VIII-1. Stratamodel cross section T12 showing LOGCALC calculated water saturations 310

VIII-2. Stratamodel cross section T17 showing LOGCALC calculated water saturations 313

I. EXECUTIVE SUMMARY

Predictions of reservoir performance at Tirrawarra field based on the existing reservoir simulation model have proved unsatisfactory. Further, drilling results of recent infill wells have been poor. The need for an improved and quantified descriptive model of Tirrawarra led to a characterization project jointly undertaken by the Bureau of Economic Geology and Santos Ltd. The objectives of the project were to characterize the stratigraphic and structural complexity of the field and within this framework to quantify the residency of the original and remaining oil resource base. All well log, core, geophysical, petrophysical, and production and other engineering data were incorporated into an integrated reservoir model to be used as the basis for continued development of this field.

The overall results of the study were the development of a detailed facies based flow-unit model within which petrophysical parameters and pay distribution have been mapped in detail. The excellent match between the production and other engineering data and this new reservoir model attests to the reliability of the model for use in reservoir engineering studies and the identification of opportunities for incremental development of the large resource remaining in the field.

The main results of the study are:

- The environments of deposition have been shown to control the detailed fabric of the rock, which in turn controls its reservoir properties and productivity. The reservoir is interpreted to have been deposited as a braid delta, which has been reworked by lacustrine shoreface transgressing and regressing across the area in response to rapid and frequent changes in lake level. The final result is that the two main flow units are relatively uniform in character, with much of the production-reducing shale being removed.
- The identification of four principal facies from which six flow units have been characterized in detail. This has been the basis for the detailed three-dimensional mapping of the original oil in place (OOIP).
- The increase in OOIP of 36.051 MMSTBO from 127.17 MMSTBO to 163.221 MMSTBO. This increase in OOIP is primarily due to the use of more appropriate pay cutoffs.
- A new field Rw of 0.65 ohm-m at 75°F to replace the current field Rw of 0.58 ohm-m at 75°F.
- Only 50 MMSTBO of the OOIP is currently accessed by miscible flood, and a further 50 MMSTBO is potentially accessible by expanding the current miscible flood through

deployment of new EOR patterns in the north of the field and by expanding and optimizing existing patterns.

- Potential reserve appreciation of 17.5 MMSTBO may be achievable through continued development of existing and new EOR patterns. This assumes a 35 percent recovery of the additional 50 MMSTBO of OOIP accessed by EOR.
- The majority of the remaining 60 MMSTBO of OOIP is located in flank areas with poor production characteristics due to proximity to the wedge edge and relative permeability effects. These areas will be risky to access but may prove to be worthwhile if new development approaches are undertaken.
- Relative permeability effects largely explain why crestal wells outperform structurally lower wells.
- Fluvial flow unit 4, not previously identified as a significant contributor to OOIP, is sparsely developed but holds 24 MMSTBO of OOIP.

In addition to deployment of new EOR patterns and optimization and expansion of existing patterns several other avenues for reserve appreciation have been identified. These include the drilling of strategic infill wells and recompletion of existing wells targeting flow unit 4, which has been vertically bypassed by the EOR process. Infill drilling and recompletion could be undertaken in conjunction with other approaches to development (including EOR soak and huff-and-puff) so that structurally narrow areas, tight areas and areas with adjacent or underlying moveable water can be accessed. The potential appreciation in reserves resulting from these approaches amounts to a volume of oil equivalent to the current cumulative production from Tirrawarra field.

II. INTRODUCTION

Background

Tirrawarra field was discovered in 1969, and to date 73 wells have been drilled (fig. II-1). The Tirrawarra Sandstone, a fluvial-lacustrine sandstone reservoir of earliest Permian age, lies at a depth of approximately 10,000 ft, and current volumetric mapping shows an original oil in place (OOIP) of 127 MMbbl. The cumulative production to December 1992 is 17.2 MMbbl. The average net pay thickness is 60 ft over an area of 12,000 acres, with an average porosity of approximately 10 percent and an initial oil saturation of roughly 70 percent. The reservoir contains a volatile oil with a solution GOR of 2714 scf/rcf (C5+/C4–). At the initial pressure of 4,280 psia and temperature of 285°F the oil formation volume factor was 2.9 rb/stb (C5+) and the oil viscosity was 0.09 cp.

Early reviews and production trends indicated that recovery would be low without some method of improved or enhanced recovery. Laboratory and screening studies using reservoir oil and various injection fluids resulted in the conclusion that satellite separator gas from several local Patchawarra Formation gas (PCSG) reservoirs, gas from the de-ethanizer tower at the nearby Moomba gas plant, and CO_2 were all first contact miscible at or above 3,200 psia.

A pilot seven-spot pattern in the area of best reservoir productivity was started up in 1984, using PCSG as an injection fluid. After the production decline in this area was largely arrested, four more patterns (approximate seven spots) were added over the next couple of years. Three more have been added during 1992–93. Injection of the Moomba de-ethanizer gas was phased in during 1987.

Due to the low permeability range in the Tirrawarra Sandstone (0.1–10 md), all but three production and injection wells have undergone hydraulic fracture stimulation to ensure injection and offtake is on a commercial scale. The induced fracture orientation is unknown. Fracture half lengths are between 200 and 500 ft with well spacing of 1,800 to 2,400 ft.

Radioactive tracers were placed in the first five injectors in 1985 and 1986, and active sampling occurred until mid 1991. Results were disappointing, most likely due to injection of insufficient amounts of two of the tracers and questionable analytical practices by the laboratory, however, there was a clear indication of uniform sweep.

For the last several years, simulation work has consisted of three-dimensional regional studies using TCA's MULTIFLOOD miscible flood simulator. Current reservoir descriptions have been unable to match or predict injection gas breakthrough or new well productivity. This is

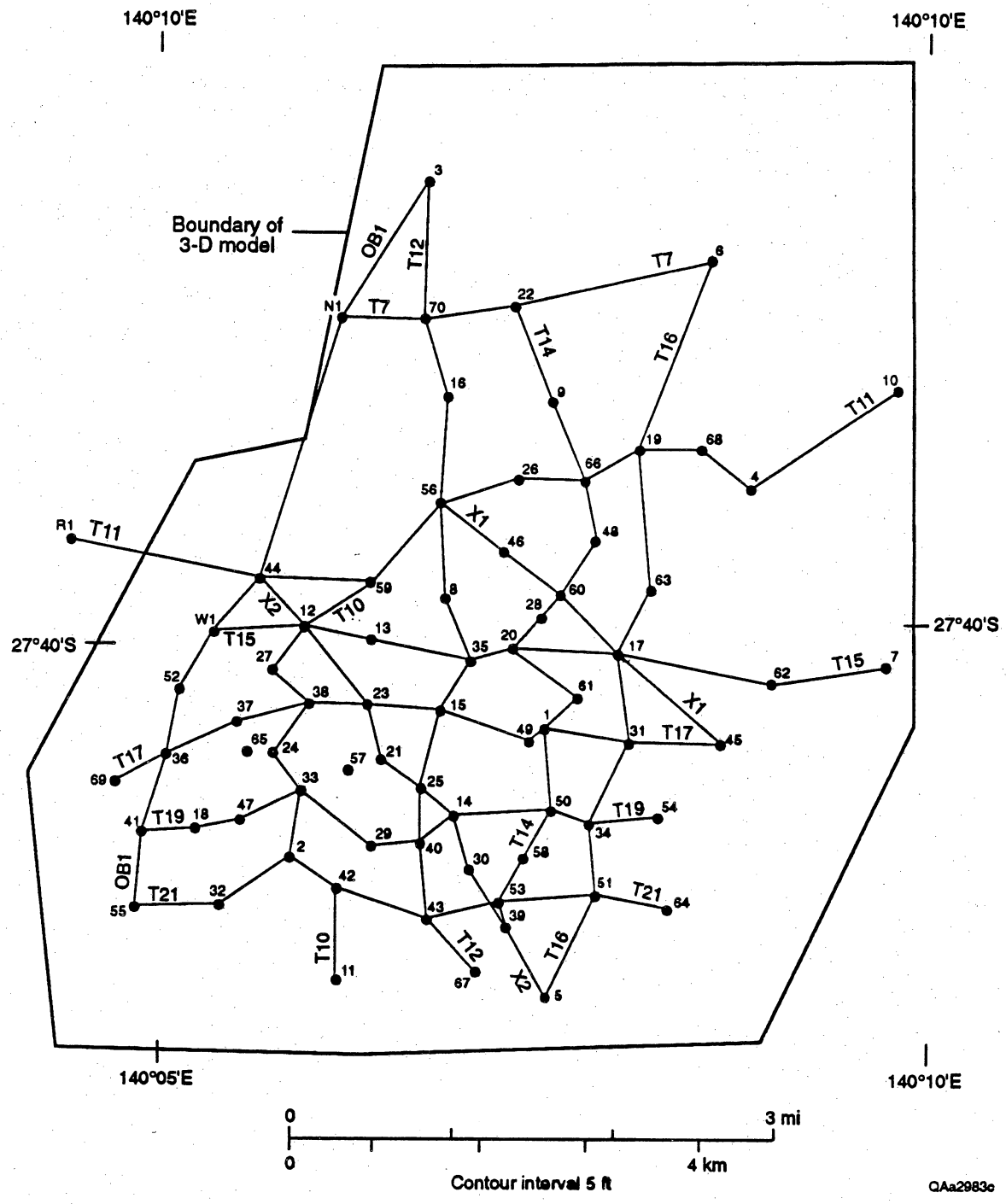

Figure II-1. Map of Tirrawarra field in the Cooper Basin, South Australia, showing well locations and numbers, lines of cross sections referred to in parts III and V, and boundary of the three-dimensional model.

partly due to simplifications made because of limits on computer processing capacity which necessitated the use of a simple reservoir description.

Estimated current reservoir pressures in the flood patterns are between 3,500 and 4,200 psia. Recent analysis of individual patterns has indicated a very high recovery to date in areas effectively swept (up to 50 percent). Other patterns, while less mature, appear not to be performing as well. Outside the flood patterns, recovery to date is quite low (less than 3 percent), and expansion of the flood or other recovery strategies may be required to improve recovery.

Gas breakthrough occurred in most patterns between 1 and 3 years after injection start-up. However, some wells in the older patterns still have not shown breakthrough. The current simulation model had limited success in predicting breakthrough.

Recent drilling results have been disappointing, with both poor reservoir quality and water being encountered. Most of these recent wells have been drilled on the flanks or in the northern, less developed part of the field. Water production was a minor problem until recently.

The large undeveloped resource remaining in this field, together with problems encountered with simulation predictions and recent drilling results, have resulted in the need for the development of an integrated geological and engineering description of the reservoir and its recovery mechanism. A preliminary geological study undertaken by Santos included a full data compilation and a review of core from key wells and indicated the potential for an increase in OOIP in the north of the field. Further, the key issues pertaining to the field were identified. These issues became the project objectives and are listed below. The Bureau of Economic Geology, The University of Texas at Austin (BEG), was thereupon chosen to undertake, jointly with SANTOS, an integrated geological, geophysical, and production engineering analysis of Tirrawarra field. This report describes the approach and results of the study and proposes several advanced recovery strategies for realizing reserve appreciation in this heterogeneous reservoir.

Objectives

The overall project goal was to characterize Tirrawarra oil field in detail for use in future reservoir engineering studies. The key issues identified by Santos' preliminary geological study became the foundation for the project objectives, which are listed below:

- Determine the structural and stratigraphic framework of the field
- Identify mappable facies units and from these identify mappable flow units

- Identify stratigraphic datums (time lines) and discontinuities to enable structural and stratigraphic analysis
- Establish a diagenetic framework and relate permeability and porosity to the diagenetic fabric, especially pore type
- Assess current methods of log analysis and evaluate alternative methods
- Identify structural and stratigraphic discontinuities that might affect production
- Relate all production characteristics and anomalies to rock properties/characteristics and to larger scale geological features
- Produce a detailed three-dimensional petrophysical model of the field incorporating flow unit geometry and characteristics, all engineering data, and the structural framework
- Determine the distribution of original oil in place (OOIP)
- Identify the remaining oil in place (ROIP) and its distribution
- Identify areas for new EOR patterns, recompletions, infill drilling, and new exploitation techniques.

These objectives have been met, resulting in the development of a detailed facies model for the field, within which the petrophysical parameters and pay distribution have been mapped. The strong relation between production data and well-test data and the reservoir model attests to the reliability of the model for use in reservoir simulation and the identification of opportunities for incremental development of the remaining oil in place.

Data

The available data included (1) well logs and completion information from all 73 wells in and near Tirrawarra field; (2) 3,000 ft of whole core from 29 of those wells (fig. II-2); (3) gamma scans and photographs of all core; (4) porosity, permeability, and capillary pressure data from core; (5) a two-dimensional seismic grid covering the field at 1 to 1.5 km spacing; (6) pressure, production, and other well-test data; and (7) reports from previous studies. This broad-based data set permitted thorough analyses to be conducted of the several geological and engineering aspects of this study as well as a complete synthesis of results in order to accomplish our ultimate objectives: to increase both our understanding of the Tirrawarra oil reservoir and ultimate recovery from that reservoir.

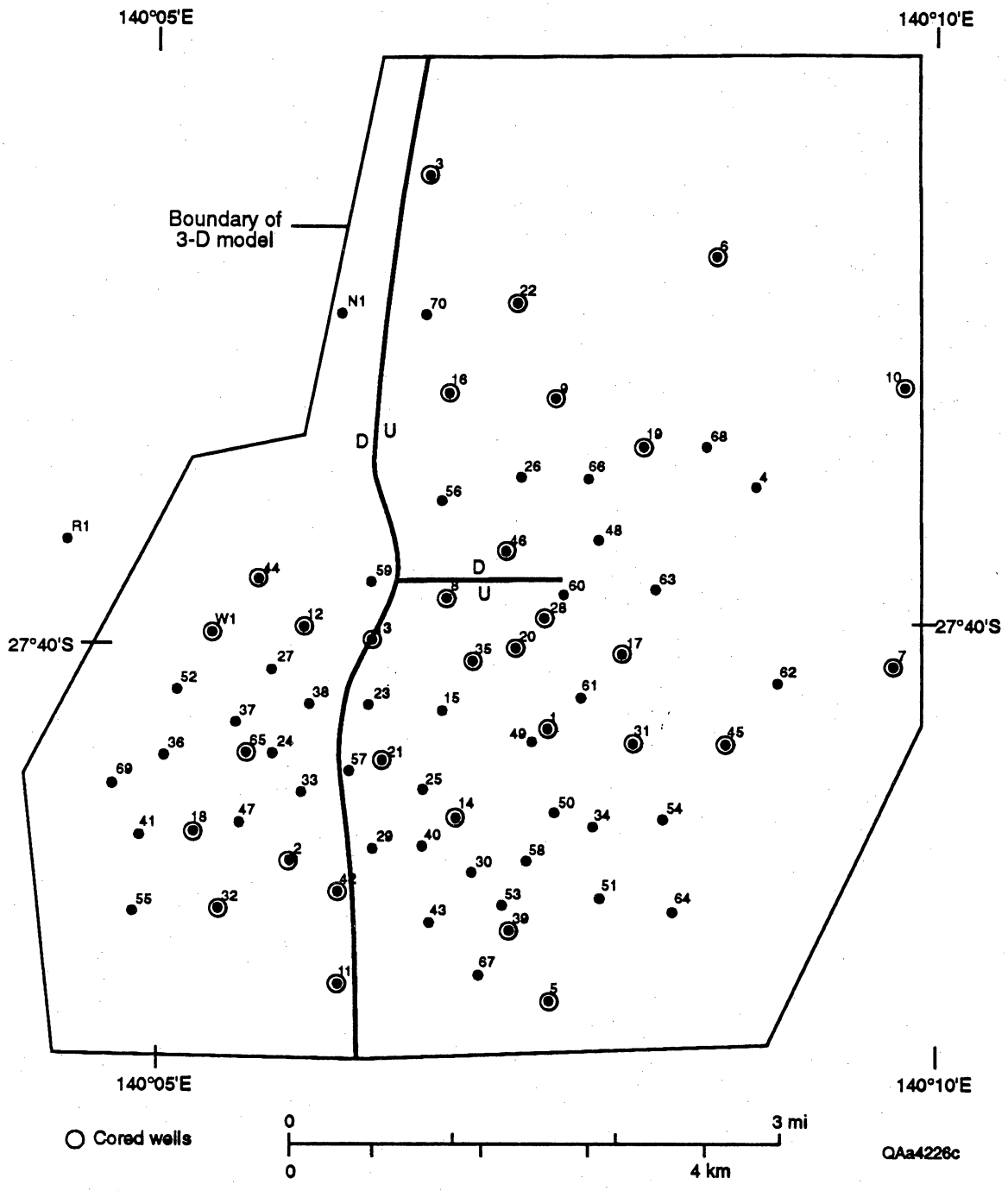

Figure II-2. Map of Tirrawarra field showing distribution of Tirrawarra Sandstone core. Wells having core from the Tirrawarra reservoir interval are circled.

Methodology

A broad range of methods and expertise was brought to bear during this geological and engineering analysis of the Tirrawarra reservoir. All available data were reviewed and analyzed. Detailed descriptions of methods are included in each of the major sections of this report. A brief summary of the methodology is given below.

Task 1: Data Compilation

All available data, including logs, cores, core analyses, production data, pressure data, and drill stem and other well test data, were assembled and compiled as part of Santos' preliminary project. Engineering data were compiled and summarized as plots against time and were also summarized on the geological strip logs that displayed all available geological and petrophysical data. This effective compilation enabled all data to be considered during every aspect of the project. As a result, full synergy between all of the different specialists and their studies was attained. The match between the result of these studies and the fact that the final geological model can be used to explain production trends, including anomalous behavior, attests to the success of the data compilation.

Task 2: Depositional Systems Analysis

Depositional systems and their component facies form the primary building blocks of reservoirs and exert fundamental control on reservoir quality, behavior, and recovery efficiency. Facies provide the context for mapping reservoir flow units, which more precisely describe variations in the rock properties that control fluid flow. Tirrawarra facies were identified on the basis of core observations combined with well log characteristics and petrophysical properties. Within each facies, one or more flow units was delineated according to fluid-transmission abilities. The dimensions, orientations, and internal heterogeneities of each flow unit were documented using core descriptions, well-to-well correlations, contour maps, stratigraphic cross sections, and a three-dimensional computer modeling program. The detailed reservoir architecture thus established provided the framework for mapping pay distribution, calculating original oil in place, evaluating reservoir performance, and developing strategies for increasing ultimate recovery.

Task 3: Geological Setting

Palynological age dating was used to determine the broad structural and stratigraphic framework of the reservoir. Correlatable horizons thus identified, together with regional correlation horizons and seismic, were used to analyse the structural history of the field area.

Task 4: Geophysical Interpretation

The structural configuration of Tirrawarra field was mapped using a grid of two-dimensional seismic lines. Migrated seismic data were interpreted and surfaces and faults were mapped with the help of a DEC5000 workstation and geophysics software. Faults were interpreted and the style of faulting characterized. Velocity control for depth-conversion maps was obtained from all 73 wells in and near the field, and depth-structure maps were constructed. Finally, important details and implications of the interpretation of the structural configuration of Tirrawarra field are discussed. As the full seismic data base was not used in the interpretation the pre-existing SANTOS map was used for mapping OOIP distribution.

Task 5: Petrography

Petrographic analysis was conducted in the context of the stratigraphic framework. For each Tirrawarra facies, the petrographic characteristics were determined from thin-section analysis and related to petrophysical properties measured in core. Scanning electron microscopy (SEM) with an energy dispersive X-ray spectrometer (EDX) supplemented thin-section petrography. Thin-section point counts were used to quantify grain size, sorting, detrital mineralogy, authigenic cements, and primary and secondary porosity. Diagenetic controls on reservoir quality were determined to be closely related to depositional facies.

Task 6: Petrophysics

The petrophysics task of the project is composed of three main subtasks:

- Review and analysis of all aspects of the petrophysics of the field
- Review and analysis of the water resistivity data for the field
- Calculation of foot-by-foot porosity, water saturation, and pay for each well This includes foot-by-foot editing of the final results to honor core and engineering data.

The purposes of the petrophysical review and analysis have been to:

(i) review the Santos methods that have been used to determine porosity and water saturation,

(ii) compare the reservoir flow units with core porosities, permeabilities and rock types to determine if reservoir cutoffs (i.e., Vcl, porosity, and Sw) need to be adjusted for each reservoir flow unit,

(iii) petrophysically verify reservoir flow unit definition

(iv) suggest improvements to Santos' petrophysical analysis.

During the petrophysical review, 46 wells were examined through the Tirrawarra Sandstone. The wells were selected so that different logging suites, different flow units and water versus oil productive zones could be examined and compared. The review was performed using "SSA," a PC based shaly sand analysis program developed by George Asquith and The Logic Group, Inc. This program is designed to quickly analyze and compare results from different log analysis techniques and equations. It thereby enables qualitative and quantitative assessment of the different techniques. The results of this review were incorporated into the foot-by-foot log analysis that was run in-house by Santos.

Task 7: Original Oil in Place Calculation and Residency

This task addressed the original oil volumetrics and the areal and flow unit-based variation in the distribution of oil-in-place. The existing structure map was used as the basis for oil-in-place calculations, which together with flow-unit isopachs and a revised oil/water contact interpretation, were incorporated into Stratamodel. Edited LOGCALC output formed the foundation for net pay and hydrocarbon pore volume mapping and ultimately OOIP calculations, which were both compiled and calculated in Stratamodel.

Task 8: Engineering Review

This review of the relevant available engineering data has been undertaken to confirm the geologically derived reservoir description and to provide a basis for further engineering studies and projects. Engineering data provide valuable information on the reservoir quality, layering, preferred flow paths, stratigraphic heterogeneity, and structural partitioning by sealing faults within reservoir units, which can then be used to refine the geological model.

Task 9: Remaining Oil in Place

Critical to the determination of remaining resources is the calculation of the relative contribution of each flow unit to cumulative well production. Santos provided detailed analysis of historical and areal production trends. Spatial production trends were related to the sedimentary architecture of the well reservoir on the basis of kh apportioning of well production. These data were used to estimate remaining oil volumes for each reservoir interval.

III. GEOLOGICAL SETTING

Structural Geology

Regional Setting

Tirrawarra oil field is located in the Patchawarra Trough in the South Australian sector of the Permo-Triassic Cooper Basin (fig. III-1). The Patchawarra Trough is separated from the rest of the Cooper Basin by a northeast-trending elongate horst block, the Gidgealpa-Merrimelia-Innamincka Ridge. Two other troughs occur to the southeast: the Nappamerri and the Tenappera (fig. III-2). These are separated by the Nappacoongee-Murteree Ridge. Both ridges are asymmetric features and were emergent during deposition of the Lower Permian strata. The troughs are relatively unstructured, being broad and flat, but are transected by minor faults and ridges that often intersect (figs. III-2 and III-3).

A major tectonic event preceded Permian deposition, resulting in folding and faulting of the thick underlying Cambro-Ordovician strata. This is evidenced some 50 km to the west of the study area in the folding and faulting of the pre-Permian Kalladiena beds. The complex structural framework exhibited throughout the basin was established prior to the deposition of any Cooper Basin strata and has been frequently reactivated in response to the stress regime prevailing at any one time.

Minor structural events occured during Permian deposition, except for the Daralingie Unconformity, which divides Lower and Upper Permian strata (fig. III-4). This was accompanied by significant uplift and erosion, especially along sympathetic basement features. These features were again reactivated at the close of Triassic deposition. Deposition was slow during the Jurassic, indicating slow subsidence, but the Cretaceous saw rapid subsidence with a substantial marine sequence being deposited. Paludal and finally thick braid plain deposition followed. No major structural reactivation is indicated during the rapid subsidence of the Cretaceous. The Tertiary section is insignificant, with substantial uplift and peneplanation separating it from the Cretaceous. The Tertiary saw reactivation of most structural features in the basin, and widespread listric faulting of the Cretaceous section occurred.

Field Area

Tirrawarra field straddles one of the basin transecting faults, a north-south, down-to-the-west, high-angle, normal fault. Cross sections T7, T15, T21 (plates III-1 through

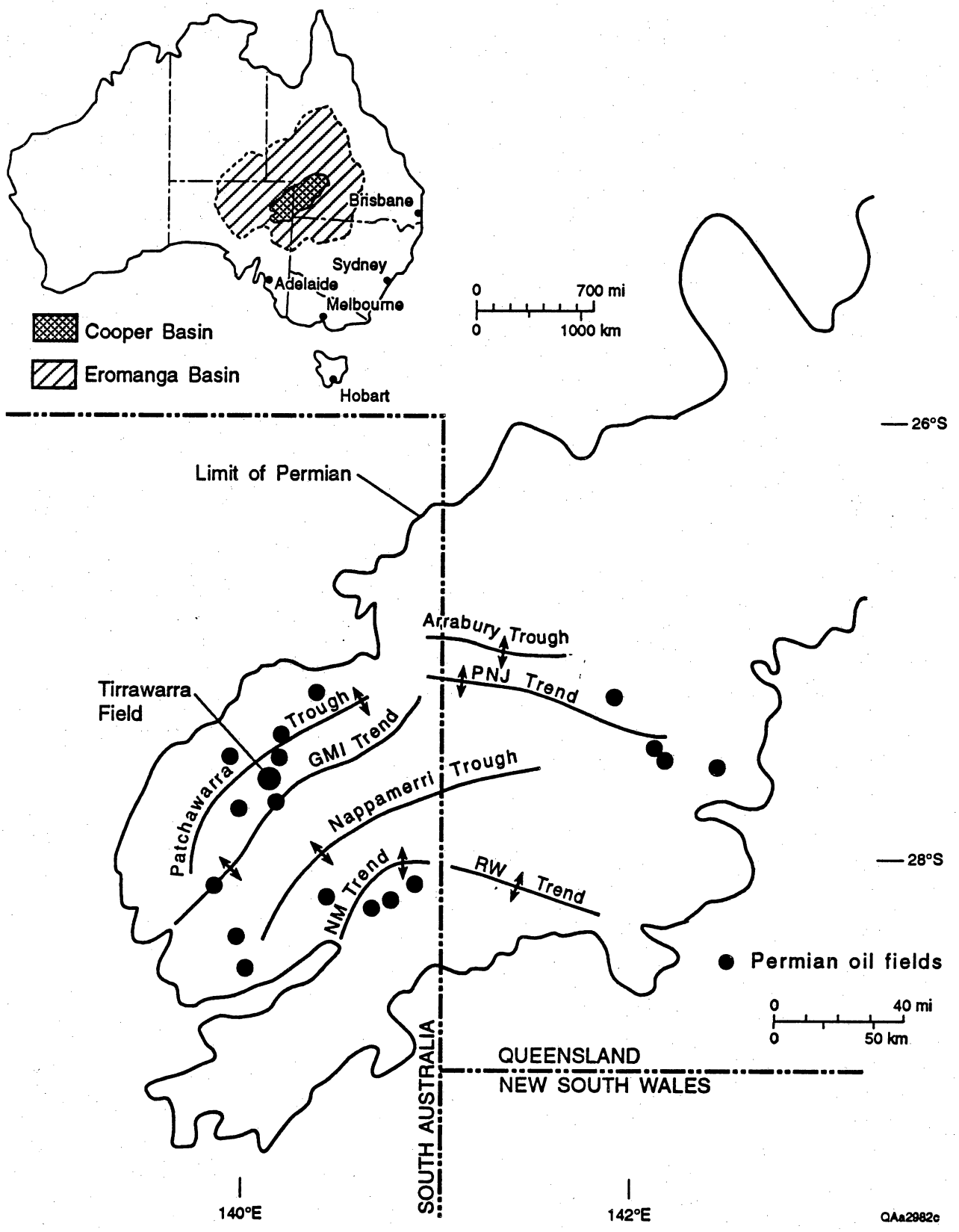

Figure III-1. Location map of Cooper Basin and Tirrawarra oil field in east-central Australia.

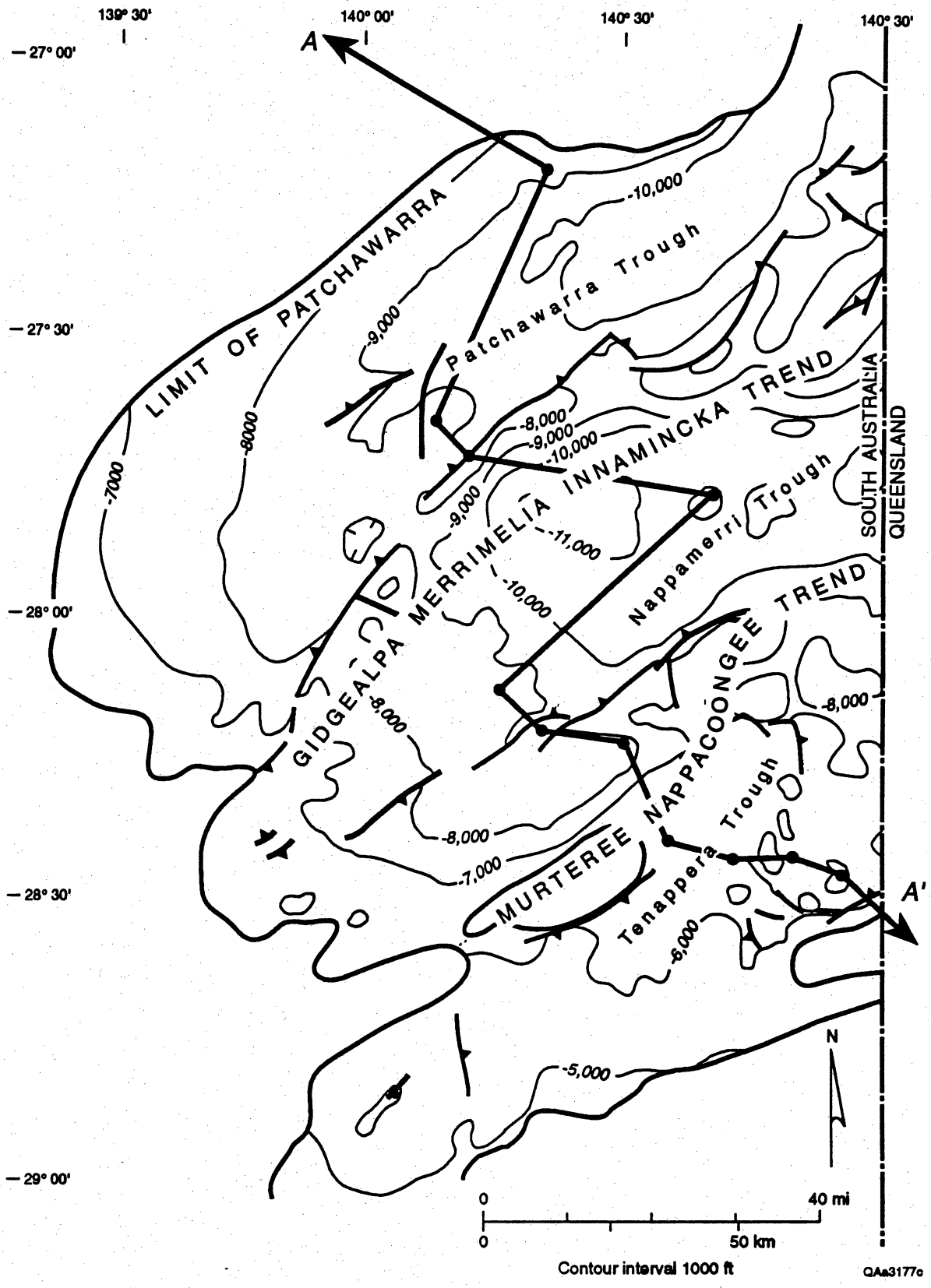

Figure III-2. Generalized structure map of the southern Cooper Basin, South Australia.

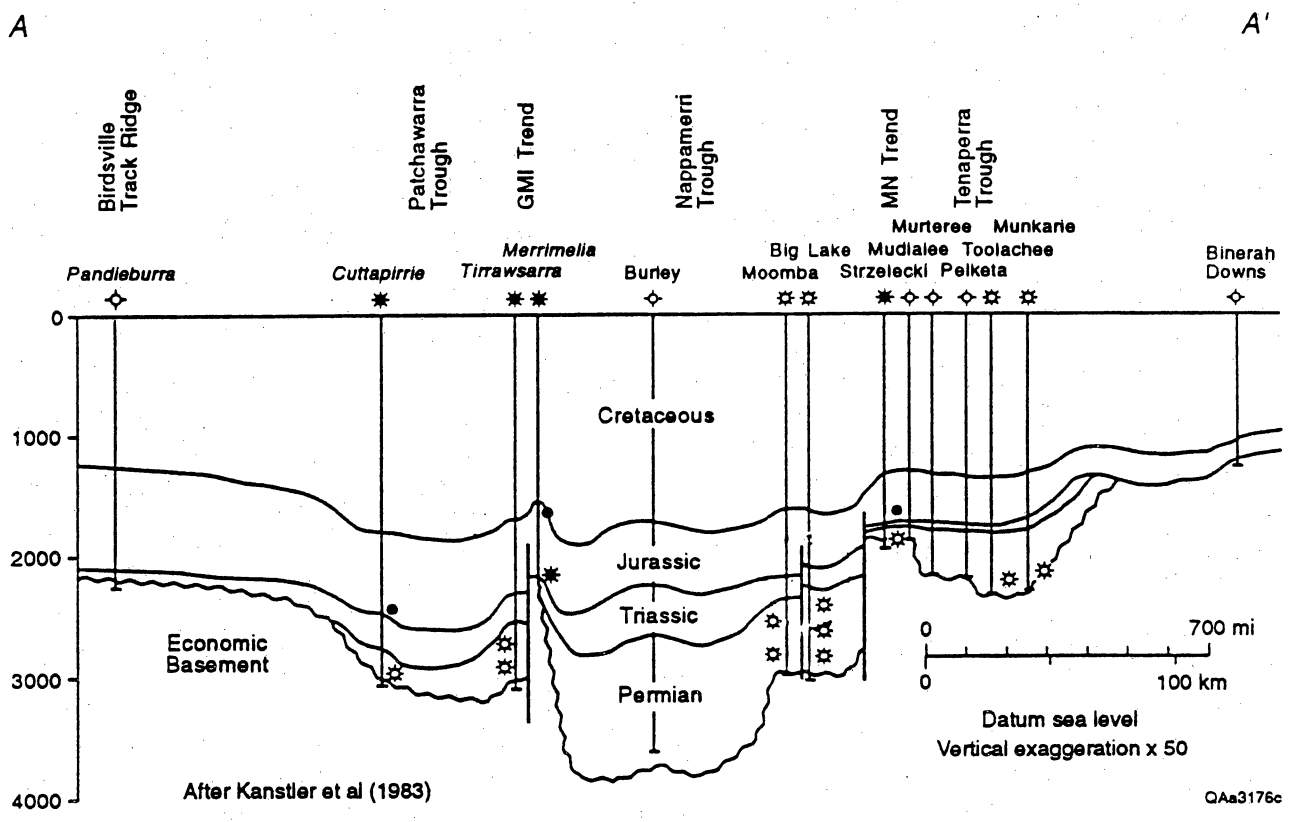

Figure III-3. Schematic cross section A–A,' southern Cooper Basin. Line of section shown in figure III-2. Modified from Kanstler and others (1983).

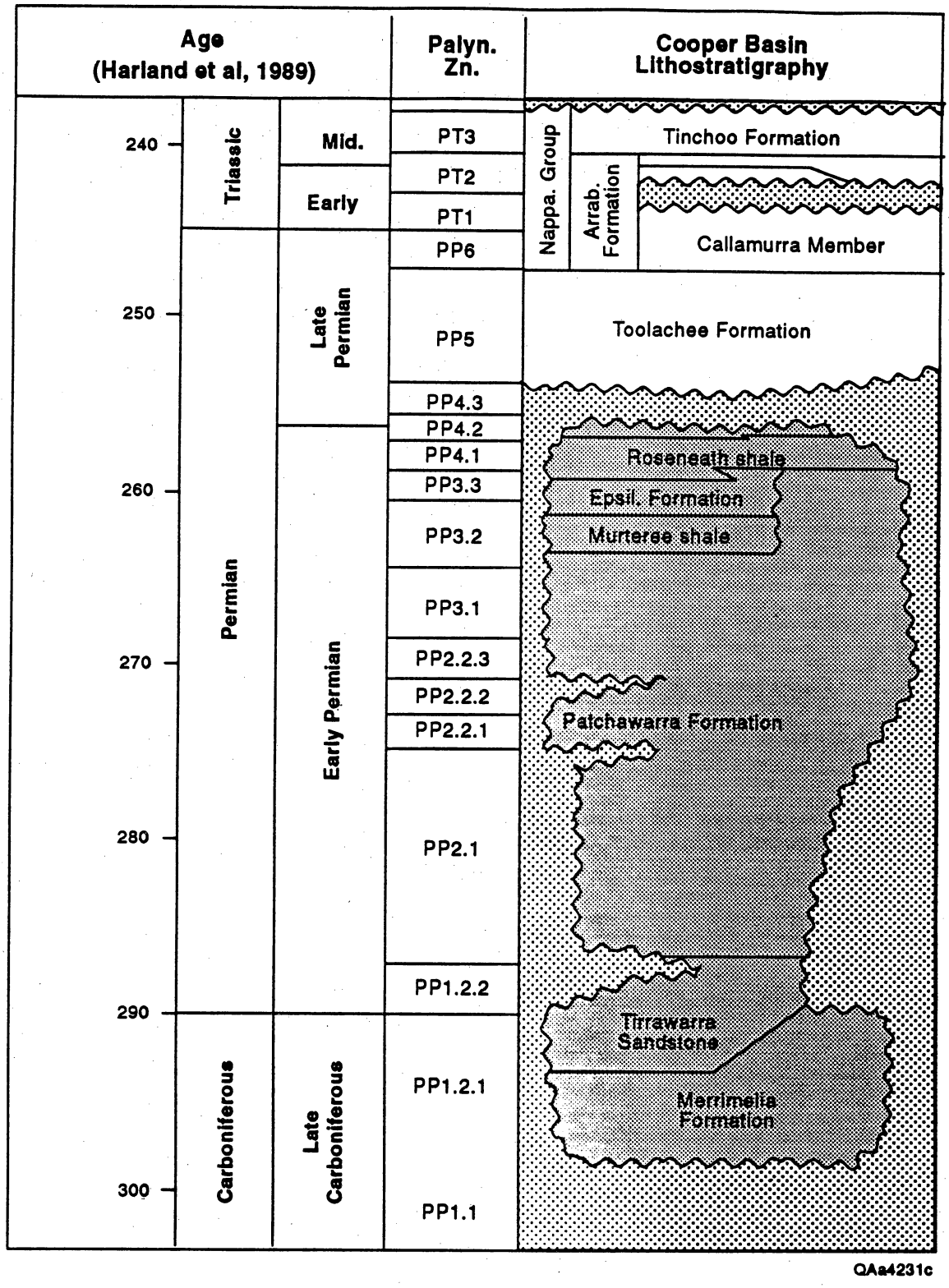

Figure III-4. Carboniferous through Triassic stratigraphy of the Cooper Basin.

III-3) are datumed and are oriented east–west, showing this fault to be syndepositional; thickening to the west occurs between each of the correlation horizons. Further, cross section T-12 (plate III-4), oriented north–south, shows substantial regional thinning of the strata in a northerly direction. Both of these phenomena are evidenced on the isopach map of the interval bounded by the Orange and Red correlation horizons, which include the Tirrawarra Sandstone reservoir unit (fig. III-5). From this it has been interpreted that the same tectonic stress regime was active in this area from before Tirrawarra Sandstone deposition until after Patchawarra Formation deposition.

The time markers are based on widespread stratigraphic correlation and sequence stratigraphy.

The Brown Marker corresponds with the base of the Murteree Shale a widespread lacustrine shale unit, representing a flooding surface.

The Green Marker is the top of a widespread coal horizon which occurs close to the PP3.1/ PP2.2.3 palynological boundary and underlies a radioactive shale with coal stringers.

The Yellow Marker corresponds with the top of a very thick coal bed which is interpreted as a flooding unit.

The Green Marker is the base of another coal which is widespread and is easily correlated due to the presence of another diagnostic coal 50 ft below.

The Blue Marker is a thin coal whose correlation is based on adjacent log character, other coal spikes and radioactivity profile.

The Orange marker is also a thin coal spike which occurs over much of the field area. Surrounding log character is used for picking this horizon in the north east where this characteristic spike is absent.

The red horizon underlies the reservoir and corresponds with a low gamma spike underlain and overlain by high gamma shales. This unit and horizon is consistent over the whole field and represents a tempestite within a flooding surface.

The structural and stratigraphic observations are confirmed by the seismic data (see Section IV) with the brown, green, yellow orange and red marker horizons corresponding with the V, V2, Vc, orange and X seismic horizons. Only the Orange, X and W (corresponding with the near top of the reservoir) seismic horizons are interpreted on the seismic sections. (see Section IV)

Seismic data afford a much more comprehensive view of the fields' structure than the very detailed but imperfect view provided by well correlations alone. The seismic data show small normal faults transecting the structure with major faulting associated with the main north–south fault. A significant feature of the structure is the horst block on which Tirrawarra 13 and 23 wells are sited. In map view, this structural high has a narrow triangular shape caused by short

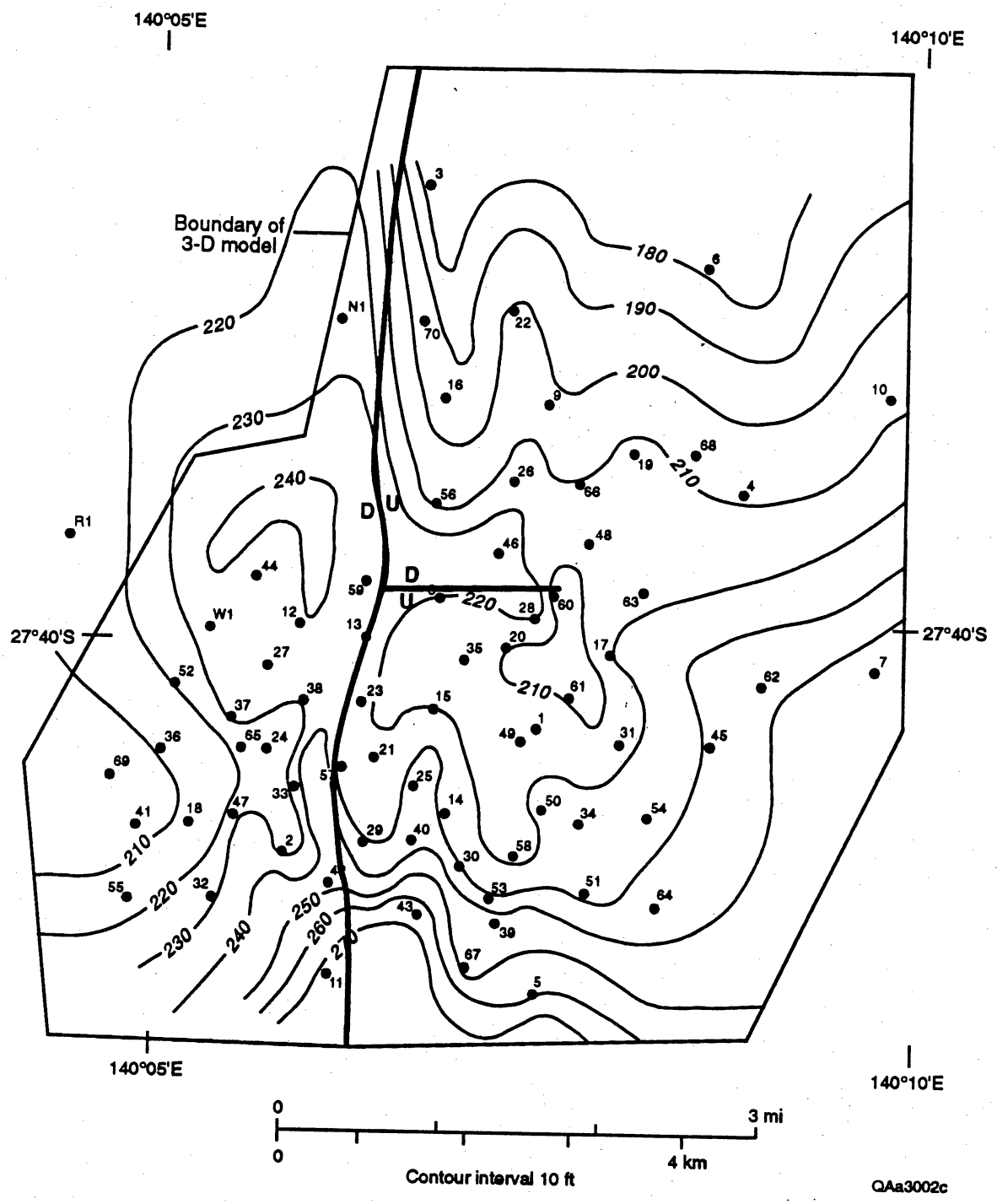

Figure III-5. Isopach map of the interval between the red and orange correlation horizons, Tirrawarra field.

but high-throw east–west and northeast–southwest faults intersecting the main north–south fault and is consistent with some minor left-lateral shear occurring along the main north–south fault. Minor pop-up wedges and drop-down wedges can occur with this interpretation and may be regarded as "flower structures." The overall trend of the anticlinal structure is oriented northeast–southwest, which is also consistent with this model.

An alternative model is that all the structuring is simple normal faulting. The presence of widespread listric faulting in the whole Cretaceous section, combined with substantial anticlinal arching at that level and the presence of arching with minimal faulting in the Jurassic section, implies substantial compressive stress acting on the basal section. Wedges would therefore be expected to "pop-up" at maximum stress locations.

The presence of different oil/water contacts across the main north–south fault attests to it being a sealing fault. The northeast–southwest fault bounding the crestal horst block cannot be a seal because Tirrawarra 13 sees pressure support from the Tirrawarra 15 well. The fact that nearly all observed fractures in the core have stylolites or mineralisation attests to the predominance of closed (sealing) fractures over open fractures. This may be used to infer that faults also tend to seal rather than leak. It is recommended that an analysis of the fractures, faulting and stress regime be attempted so that structural boundaries to fluid flow may be better identified and quantified.

Palynology

Almost 60 palynological samples from 16 wells have been reviewed for dating. Of these, 45 had enough preservation, yield and diversity to give an age date.

The goals of this sampling and dating were:

1. To determine the thickness of the newly identified G confluens (PP1.2.2 zone). This zone is absent in nearby fields, specifically and tightly sampled Fly Lake/Brolga Field, indicating the presence of a significant depositional/erosional hiatus between the overlying PP2.1 and underlying PP1.2.1 zones.
2. To identify the boundary between the PP1.2.2 and PP2.1 zones as early dating indicates that it represents an unconformity and divides the reservoir, presumably resulting in different reservoir characteristics above and below this boundary.
3. To provide a basis for choosing geological time lines for the purpose of datuming and hence correlation.

As a result of the integration of this data, the PP1/PP2 boundary has been restricted to narrow depth ranges in many of the sampled wells. This has provided added control for correlation of facies. Further, the underlying PP1.2.1 zone has been encountered within 50 ft

of the base of the reservoir, limiting the thickness of the PP1.2.2 zone to its maximum encountered thickness of approximately 100 feet. Still, this indicates a significant thickness of strata to be absent, due to erosion, from the nearby fields which lack the PP1.2.2 zone. An unconformity is therefore interpreted at, or near, the PP1.2.2/PP2.1 boundary. This unconformity surface is sub-parallel to both the orange and red horizons and is therefore a useful "internal" datum surface for the reservoir for in-field interpretation.

The unconformity has been placed at the Facies 4/Upper Facies 2 boundary, however, the age dating has not been as definitive as had been envisaged. Upper Facies 2 always gives a PP1.2.2 age but lower Facies 4 can yield either a PP2.1 or PP1.2.2 age. There are two possible explanations:

i) The time boundary is slightly above the unconformity;

ii) reworking of PP1.2.2 age strata has resulted in contamination of basal Facies 4.

The former explanation is preferred as the PP1.2.2 assemblage is very sparse and is species limited compared with PP2.1 so any reworked PP1.2.2 would be overwhelmed by a PP2.1 assemblage.

The basal boundary of PP1.2.2 is located beneath the reservoir section and is above the silty section located 50ft below the reservoir. In between is a high gamma, finely laminated shale which persists over the entire field area. This shale is interpreted to be a flooding surface and as such represents very slow deposition. The basal boundary of PP1.2.2 is interpreted to be in this shale. The red horizon coincides with a silty unit within this shale.

Stratigraphic Setting

In the southern Cooper Basin (fig. III-1), the Tirrawarra Sandstone is part of a intracratonic succession of nonmarine clastic rocks deposited during the Late Carboniferous–Triassic (fig. III-4). Because regional Cooper Basin stratigraphy is well described (Kapel, 1966, 1972; Martin, 1967; Gatehouse, 1972; Battersby, 1976; Thornton, 1979), only a brief outline is presented here. The Cooper Basin succession unconformably overlies Cambro-Ordovician and Proterozoic basement (Heath, 1989). The Eromanga Basin, a petroliferous succession of Mesozoic clastics, unconformably overlies the Cooper Basin. The Merrimelia Formation, which fills the lowermost part of the Cooper Basin, comprises glaciogenic fluvial sandstones and conglomerates, diamictites, and lacustrine mudstones. The Tirrawarra Sandstone was deposited by a bed-load-dominated fluvial system in a braidplain/braid-delta setting. Although channel-base erosion is widespread, the Merrimelia Formation and the overlying Tirrawarra Sandstone are regionally conformable and intergradational (Williams and Wild, 1984). The upper part of the Tirrawarra Sandstone interfingers regionally with the overlying Patchwarra

Formation, a thick succession of fluvial, floodplain, and lacustrine sandstones, mudstones, and coals. The Permo-Triassic formations that fill the upper part of the Cooper Basin are composed of fluvial-lacustrine lithofacies similar, although less coally, to those in the Patchawarra Formation (Thornton, 1979).

The main oil reservoir in Tirrawarra field comprises the Tirrawarra Sandstone plus the uppermost part of the Merrimelia Formation. This Tirrawarra reservoir is 90 to 180 ft thick and is composed of four main facies. Facies 1, which is the Merrimelia part of the reservoir, comprises 0 to 17 ft of very fine grained sandstone and siltstone. Facies 2 is coarser grained but more heterogeneous than facies 1. Facies 2, which is 0 to 40 ft thick, includes clean sandstone and abundant mudstone but is dominated by muddy sandstone. Facies 1 and 2 form the lower part of the reservoir but are not continuous across the field, owing to depositional pinchout and erosional truncation. Facies 3 is continuous across the field and forms the main body of the reservoir. Facies 3 is 40 to 100 ft thick and is composed primarily of porous sandstone, although it also includes numerous thin mudstone laminations and interbeds. Facies 3 encompasses several bodies of facies 2-type rock, one of which reaches 30 ft in thickness along the southwest margin of the field. Facies 4, which forms the uppermost part of the Tirrawarra reservoir, is 10 to 60 ft thick and includes sandstone, mudstone, conglomerate, and coal. These facies are the basic components of the Tirrawarra reservoir and control reservoir quality.

A sequence stratigraphic framework (as defined by Van Wagoner and others, 1988) for the Tirrawarra reservoir can be constructed using the results of this study in the context of the regional stratigraphic setting. Although the direct influence of sea-level changes (eustatic or relative) could not be determined in this entirely nonmarine succession, vertical and lateral facies interrelationships could be used to determine parasequence stacking patterns and to identify depositional systems tracts. Fine-grained lake-center facies near the top of the Merrimelia Formation record maximum flooding at Tirrawarra field. The uppermost Merrimelia Formation and the lower part of the Tirrawarra Sandstone are composed of delta-front and distributary-channel facies (facies 1 and 2) in a progradational parasequence set. The main body of the Tirrawarra Sandstone consists of braided-stream facies (facies 3), which aggraded the former lake basin, but which may also represent a basinward shift in facies relative to underlying strata. A basinward shift in facies implies the presence of a sequence boundary, but our study suggests that the deltaic facies interfinger with the overlying fluvial facies and that together they form a highstand systems tract. In the upper part of the Tirrawarra Sandstone, an erosional unconformity (sequence boundary) truncates the highstand systems tract and is overlain by proximal braidplain facies (facies 4) representing incised-valley-fill deposits of a lowstand systems tract. The incised-valley-fill conglomeratic sandstone is relatively thin and grades upward into lenticular channel-fill sandstones enclosed in floodplain mudstones and

coals. The top of the Tirrawarra Sandstone is usually picked at the uppermost thick channel-fill sandstone; the overlying Patchawarra Formation is dominated by floodplain and lacustrine facies. Thus, the Tirrawarra/Patchawarra transition encompasses a retrogradational parasequence set in a transgressive systems tract.

The sequence stratigraphy of the Tirrawarra reservoir provides a framework for identification and correlation of facies and for delineation of reservoir architecture. Within each depositional systems tract, the lateral and vertical distribution of facies is systematic and predictable. Generalities concerning sandstone continuities and trend directions may also be derived from the sequence stratigraphic framework, although depositional models are needed to guide detailed characterization of facies geometries and internal properties. Sequence stratigraphy also provides a framework for high-resolution chronostratigraphic correlations throughout the basin (Van Wagoner and others, 1990). Palynological analysis indicates that the sequence boundary within the Tirrawarra Sandstone approximately coincides with the boundary between Cooper Basin biostratigraphic zones PP1 and PP2 (fig. III-4). Palynological sampling undertaken as a part of our study provides data for regional stratigraphic, structural, and environmental evaluations.

There is evidence that tectonic activity accompanied deposition of the Tirrawarra reservoir, although the effects of this activity on stratigraphy and reservoir quality are subtle. A close interrelationship between regional structure and stratigraphy in the Cooper Basin is well documented (Thornton, 1979; Heath, 1989). An interval that includes the Tirrawarra Sandstone as well as parts of the underlying Merrimelia Formation and the overlying Patchawarra Formation thickens southward across Tirrawarra field but also thickens abruptly westward across the main north–south fault (fig. III-5). Much of this thickening occurs within the lower Patchawarra Formation; thickness patterns within the Tirrawarra reservoir are similar but more irregular. Individually, the Tirrawarra facies display distinctive thickness trends that can be related to depositional and erosional processes but that show no obvious relationship to the present structural configuration of the field. Channel-sandstone trends, for example, are not diverted toward the downthrown side of faults or away from the crest of the field. The cumulative effects on the entire reservoir of individual facies thickness variations are (1) an irregular southward thickening (from approximately 100 to 150 ft), (2) several closed thin areas (less than 120 ft) over the crest, and (3) local thickening on the downthrown side of faults. Reservoir quality is enhanced in some wells on the crest of the field, possibly because they include relatively fewer fine grained low-permeability layers. Fine-grained interchannel deposits are more likely to be removed by lateral channel migration in areas where subsidence is low than they are in areas where subsidence is high. Thus, variable rates of subsidence,

controlled by syndepositional tectonics, can result in variations in both the amounts and the types of sediment preserved.

IV. GEOPHYSICAL INTERPRETATION

Introduction

A grid of two-dimensional seismic lines covering Tirrawarra field was provided to the Bureau in digital SEGY format so that the structural character and faulting relationships within, and adjacent to, Tirrawarra production could be determined. Most of the seismic grid was recorded in 1980 as a series of north–south and east–west lines spaced 1 to 1.5 km apart. Within this grid, even-numbered lines 80-T2 through 80-T20 are oriented north–south and odd-numbered lines 80-T1 through 80-T23 are oriented east–west. All of these 1980 lines were provided as migrated images. In addition to the 1980 coverage, three 1990 vintage lines (90-CJQ, 90-CJR, 90-CJS), one 1984 line (84-TSP) and one 1985 line (85-YXC) were provided in a migrated format. Other 1984 and 1986 lines (84-TSQ, 84-TSR, 86-MW02) were provided only as stacked, not migrated, images.

The seismic interpretation described in this section is based on the 1980 and 1990 migrated data. The 1984 and 1986 unmigrated data were excluded because unmigrated images do not correctly image the spatial attributes of faults. The single 1985 migrated line (85-YXC) was not used because only a small portion of the line was inside the 1980 grid coverage. The single 1984 migrated line (84-TSP) was also excluded because its reflection character differed from the 1980 data because of different vibrator sweep parameters, different receiver arrays and group intervals, and slightly different processing parameters being used in the 1984 seismic program. Only those seismic lines used in the interpretation are displayed in figure IV-1 and in subsequent seismic-based maps (large format versions of these maps are included in the enclosure pocket). The migrated data were interpreted using a DEC5000 workstation and Sierra Geophysics 2DI software. Structural surfaces and attendant faulting were mapped with Radian's CPS-1 software.

Velocity check shot information was provided for the 19 wells listed in table IV-1. The three wells marked with an asterisk were not used in the interpretational process. The time-versus-depth information in the remaining 16 wells formed the basis by which formation tops, determined from log control, were converted into functions of seismic two-way travel time at each check shot well.

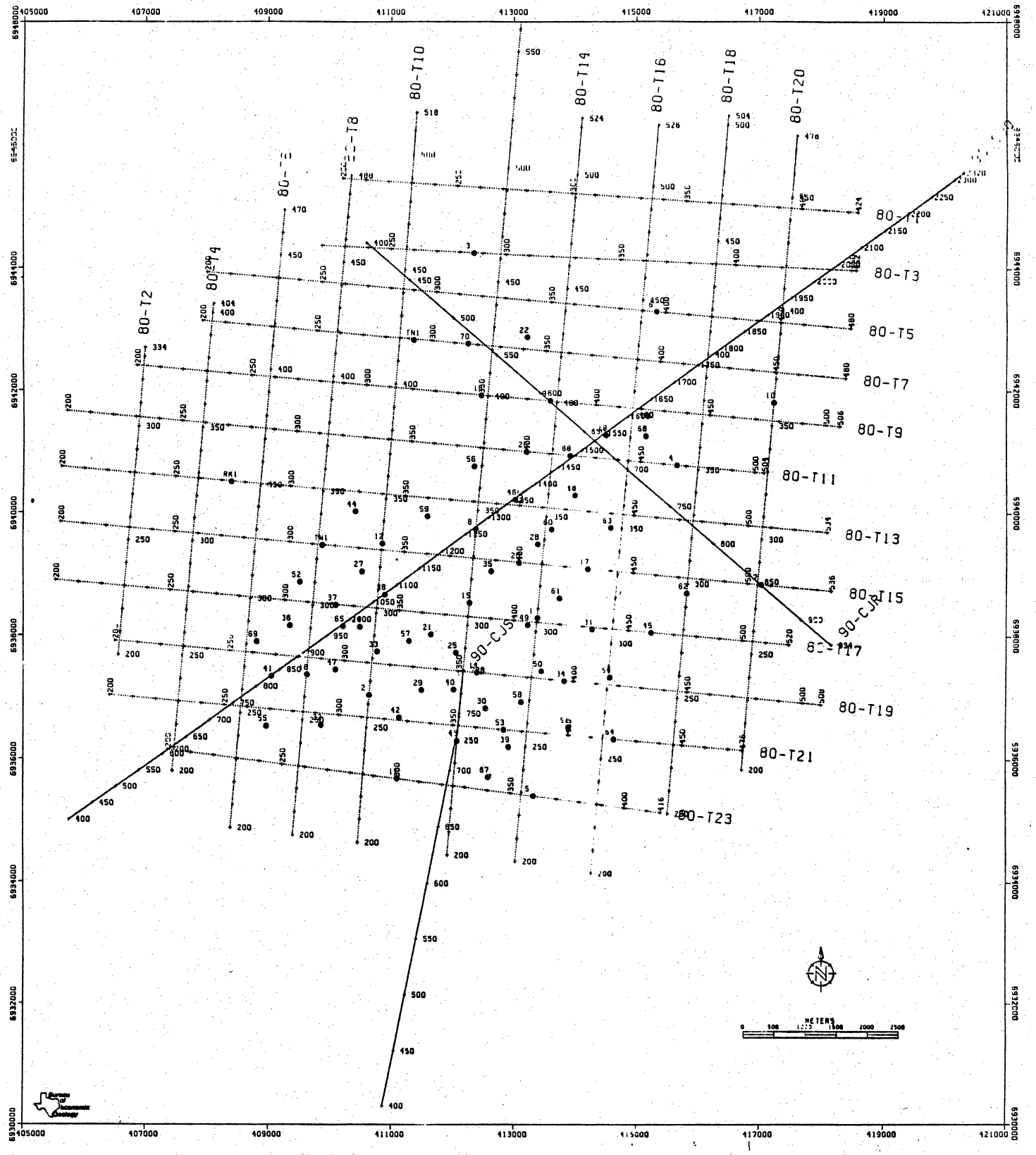

SEISMIC GRID AND WELL CONTROL – TIRRAWARRA FIELD
ENCLOSURE IV - 1

Table IV-1. Tirrawarra check-shot wells.

Brolga No. 2*	Tirrawarra 17	Tirrawarra 27
Rakoona No. 1	Tirrawarra 18	Tirrawarra 29
Tirrawarra 13*	Tirrawarra 19	Tirrawarra 31
Tirrawarra 14	Tirrawarra 20	Tirrawarra 32
Tirrawarra 15	Tirrawarra 21	Tirrawarra 46*
Tirrawarra 16	Tirrawarra 26	North No. 1
		West No. 1

* Not used to define interpreted seismic surfaces.

Interpretational Procedure

The seismic interpretation was based on the assumption that vertical seismic profiles and check shot data provide the definitive relationship between stratigraphic depth and seismic travel time. Consequently, the check shot information from the wells listed in table IV-I was used together with log-determined depths of key stratigraphic units to determine the vertical two-way travel time to three critical horizons; these being:

- Orange—a reasonably good seismic reflection event approximately 80 to 100 ft above the Tirrawarra reservoir
- Reservoir—a seismic horizon defining the approximate top of the productive Tirrawarra interval
- Merrimelia—a seismic horizon defining the approximate top of the Merrimelia interval.

At each check shot well, the check shot-based times for each of these three horizon depths were transferred to the nearest migrated seismic line to identify the specific reflection peak or trough associated with that horizon. Rarely, a check shot pick had to be excluded because the associated reflection phase did not agree with the reflection phase defined by the other check shots. This occasional disagreement among a sizable number of check shot measurements is not uncommon when projecting well control onto sparse, migrated, 2-D seismic lines that image significant faulting and structural relief such as occur in Tirrawarra field. Using this check shot-based method, the optimum reflection peaks or troughs associated with the Orange, Reservoir, and Merrimelia horizons were identified on several seismic lines near the velocity control wells, and these interpretations were then extended to all of the 1980 and 1990 seismic lines in the grid.

The check-shot approach for depth-time conversion was utilized in preference to synthetic seismograms because of the undesirable signal-to-noise characteristics of the 80-T grid of lines at the Orange, Reservoir and Merimelia horizons, and because of the likelihood that

strong intrabed multiples contaminate the data. This contamination results from large reflection coefficients at the boundaries of the deep coal-bearing units present at Tirrawarra field. Consideration of these factors led to the conclusion that in the Tirrawarra reservoir the synthetic seismogram correlation technique would not be as robust a method for establishing an accurate subsurface-to-surface calibration as is the use of high-quality check shot information. Thus, based on past experience in interpreting reservoir systems from seismic data having characteristics similar to the Tirrawarra data, the synthetic seismogram interpretational approach was not used to define the Orange, Reservoir and Merimelia horizons.

Correlation and Interpretation of Seismic Sections

The Orange, Reservoir, and Merrimelia horizons, as interpreted for the 1980 and 1990 migrated seismic lines, are displayed as figures IV-2 through IV-26. The check shot-based interpretation philosophy described in the preceding section was used to establish the horizon picks shown on each of these 2-D seismic images. Each interpreted horizon is labeled and also color coded to ensure that the seismic phases used to define the surfaces are obvious across the entire Tirrawarra structure.

By definition, migrated 2-D seismic lines do not tie when they image significant structural relief. (In contrast, migrated 3-D seismic lines do tie, regardless of structural complexity, which is one reason why 3-D seismic imaging is so important for precise interpretation.) Since the Tirrawarra seismic data base is composed of migrated 2-D lines, mis-ties sometimes exist at the Orange, Reservoir and Merimelia horizons when these 2-D lines cross each other in areas of high dip or near faulted zones. Examples of mis-ties can be seen at the intersections of line 80-T9 with lines 80-T12 and 80-T18.

When mis-ties such as these were observed, all neighboring line ties were examined to determine if the mis-tie was areally consistent or is isolated to a single tie point. In the case of line 80-T9, reasonably good line ties exist at the intersections with lines 80-T10 and 80-T14, for example, and these locations are close to the mis-ties at lines 80-T12 and 80-T18. When all other neighboring line ties around each mis-tie were examined, consistent picks for the Orange, Reservoir and Merimelia horizons were determined and then extrapolated through each mis-tie point.

The seismic displays also show the interpreted faults that appear as areal fault patterns in the structural maps discussed later in this chapter. These faults are individually labeled in each figure to aid in tracing any particular fault interpretation across the field. All faults identified in the interpretation and shown in the structural maps are positioned and oriented based on close examination of adjacent lines.

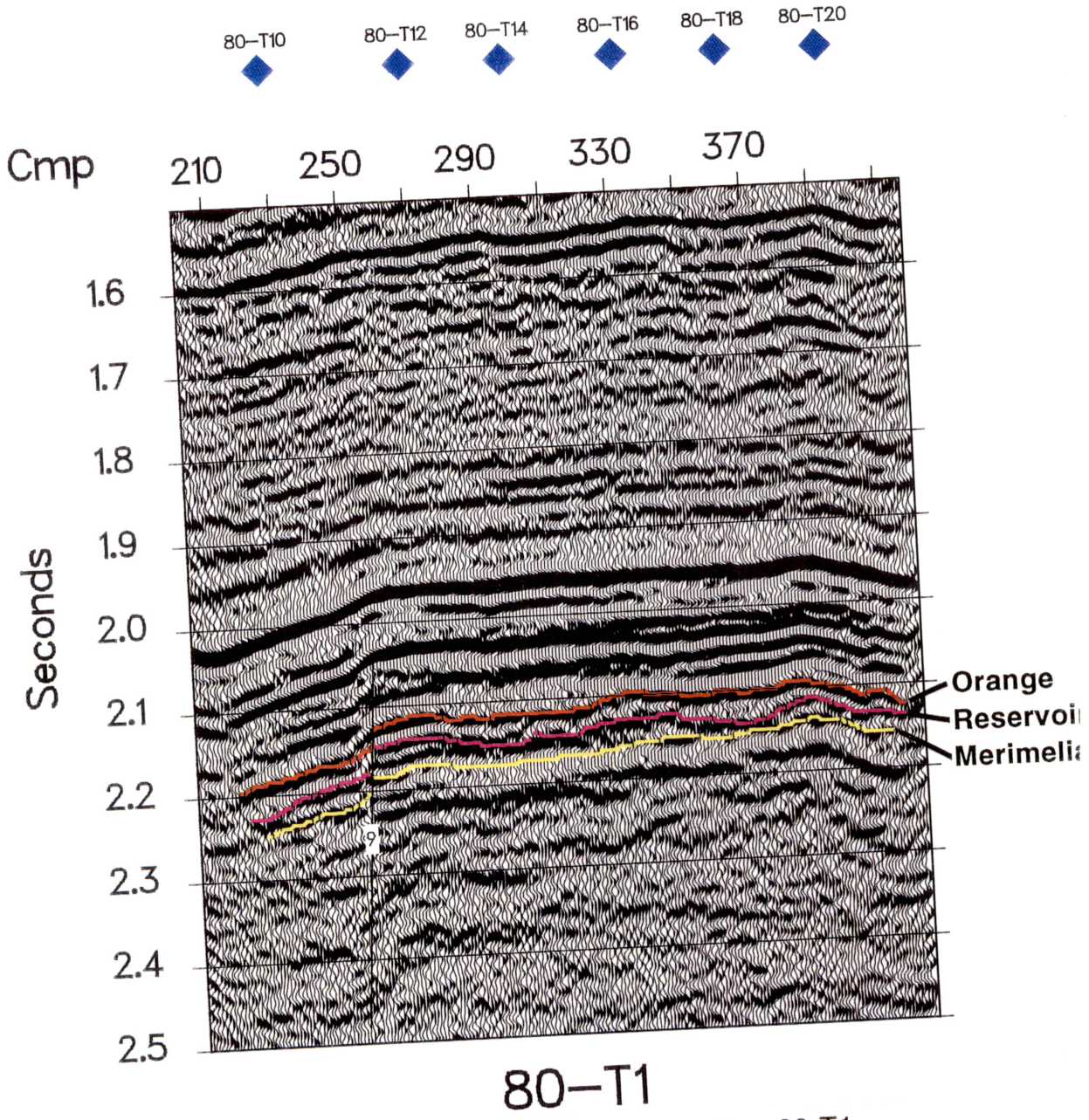

Figure IV - 2. Interpretation of seismic line 80-T1.

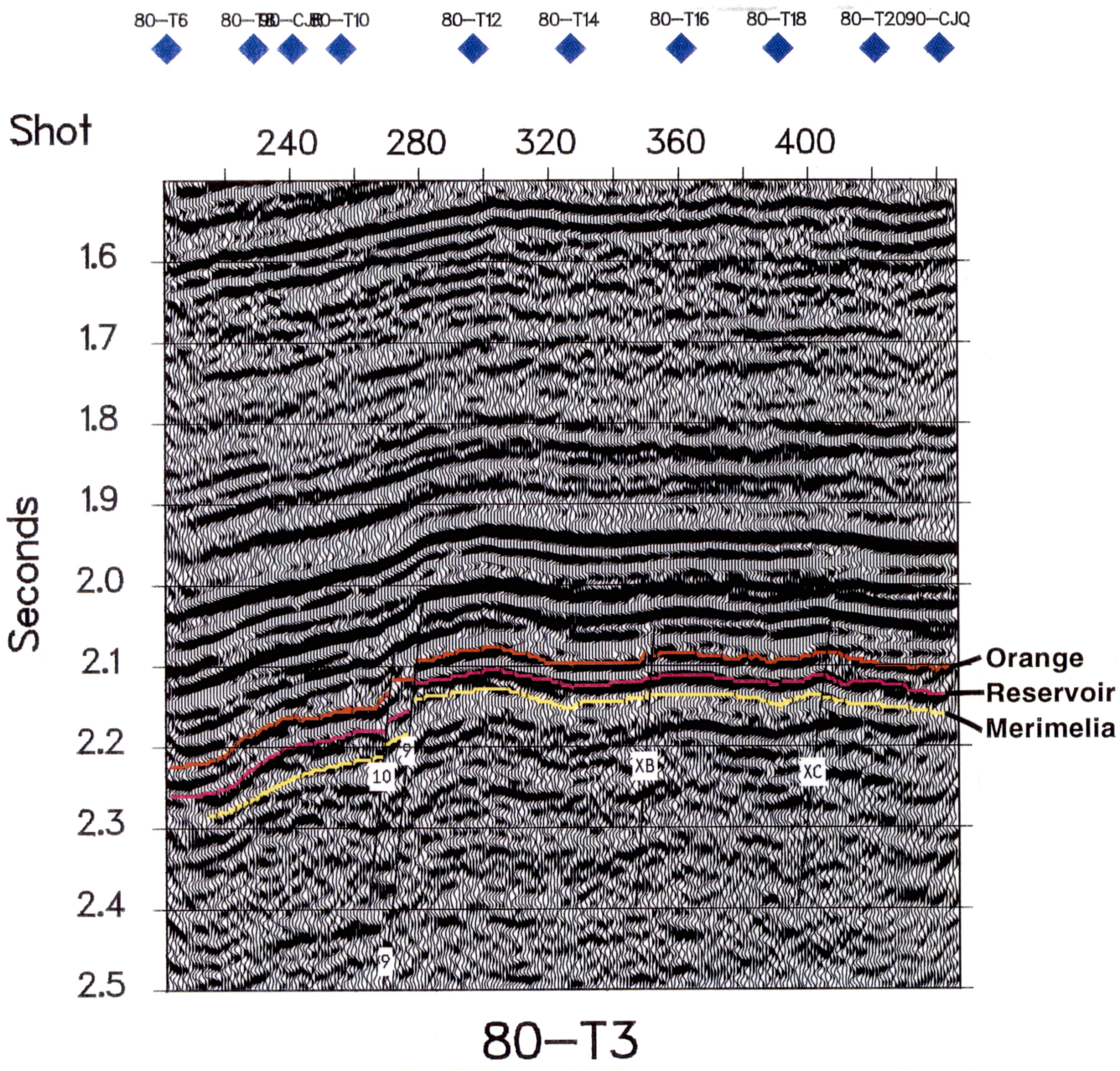

Figure IV - 3. Interpretation of seismic line 80-T3.

QAa3122

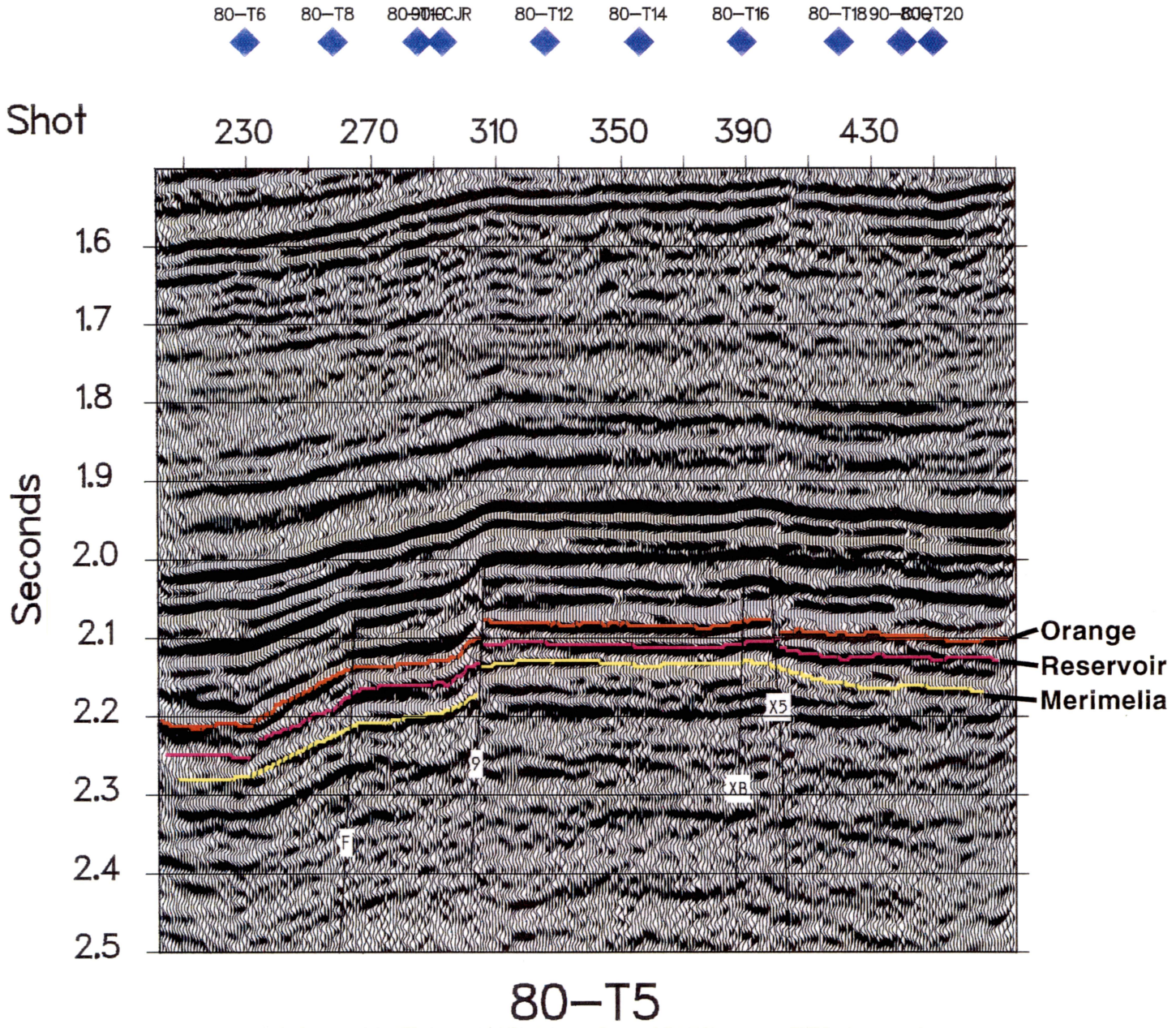

Figure IV - 4. Interpretation of seismic line 80-T5.

QAa3123

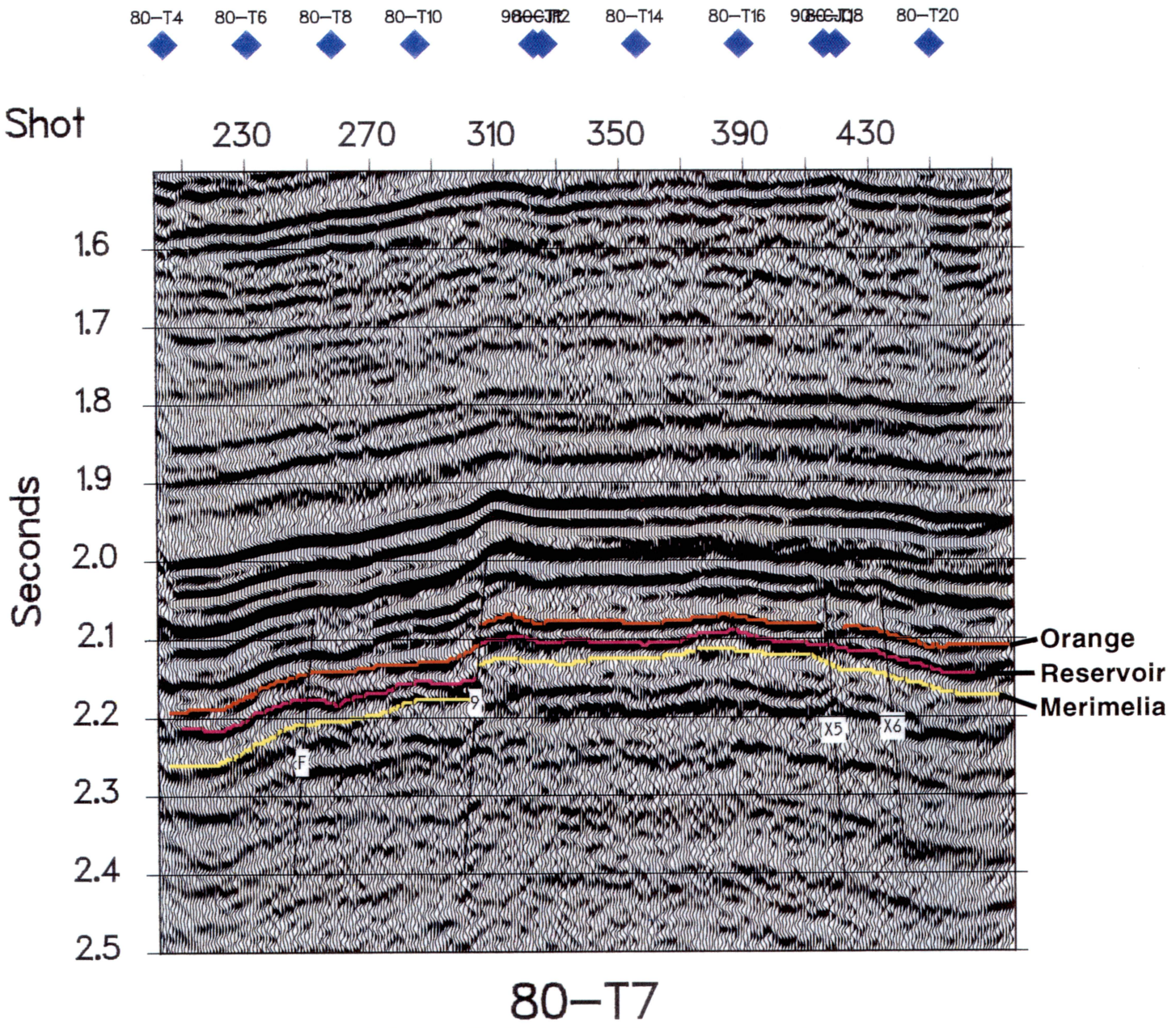

Figure IV - 5. Interpretation of seismic line 80-T7.

QAa3124

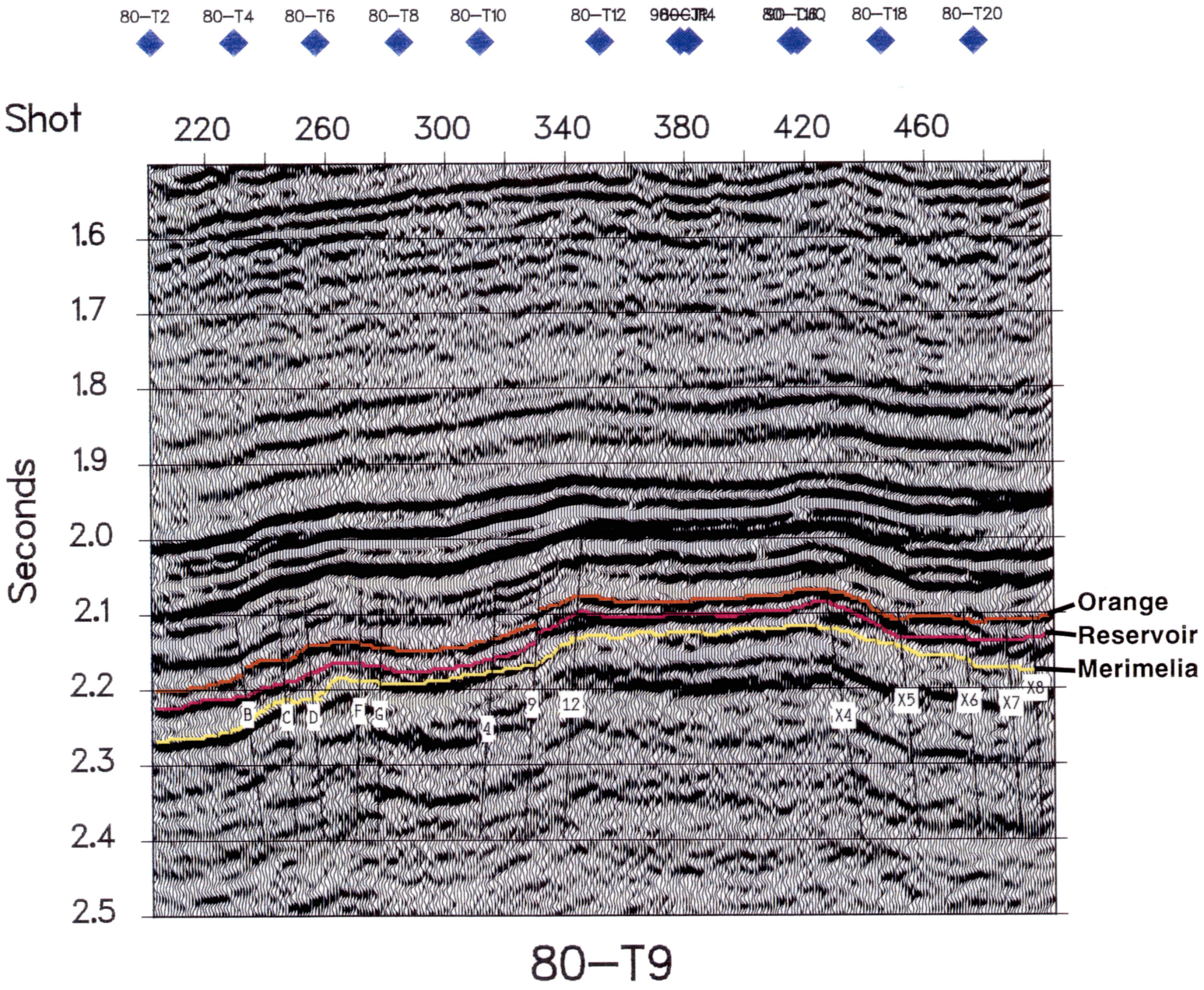

Figure IV - 6. Interpretation of seismic line 80-T9.

QAa3125

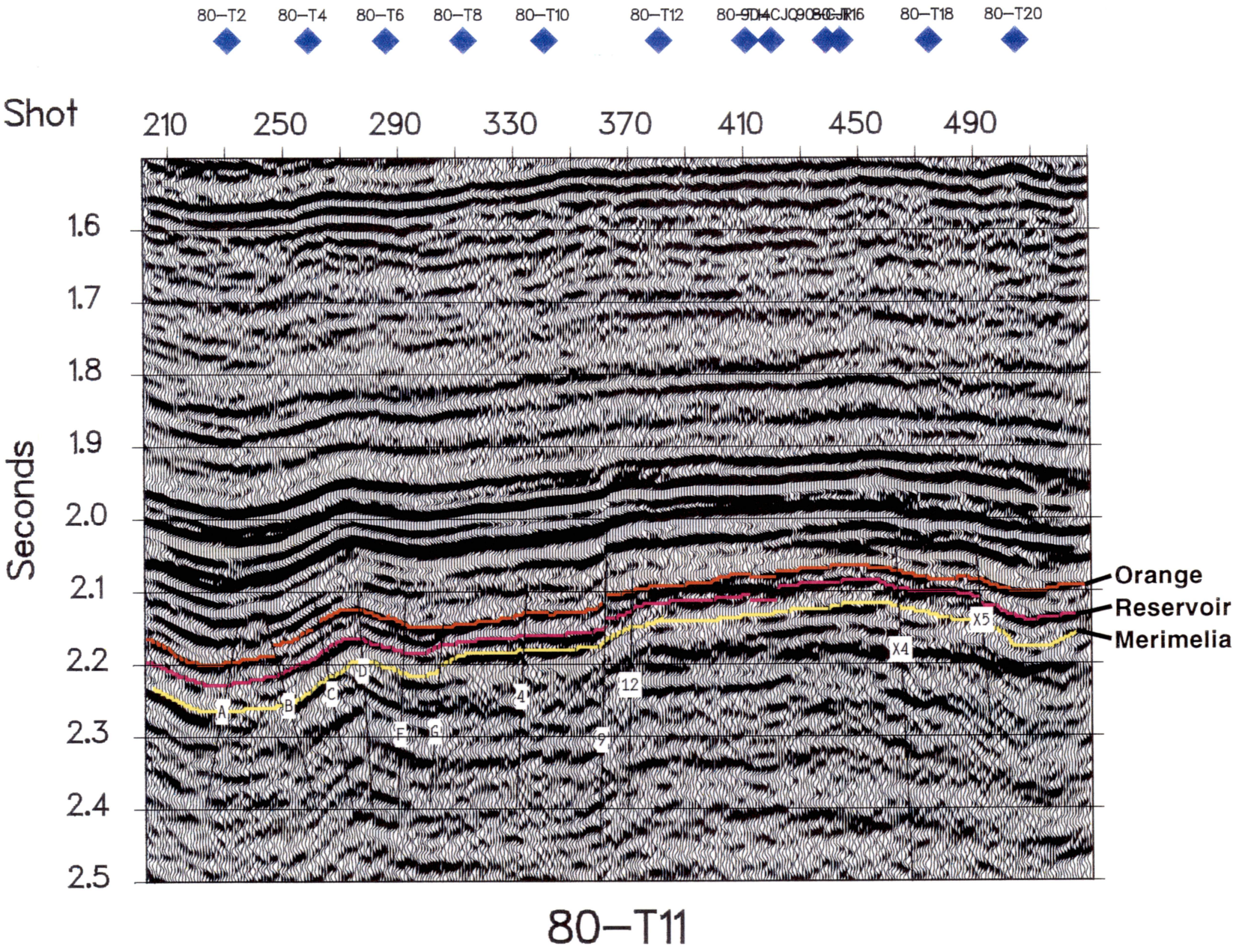

Figure IV - 7. Interpretation of seismic line 80-T11.

QAa3126

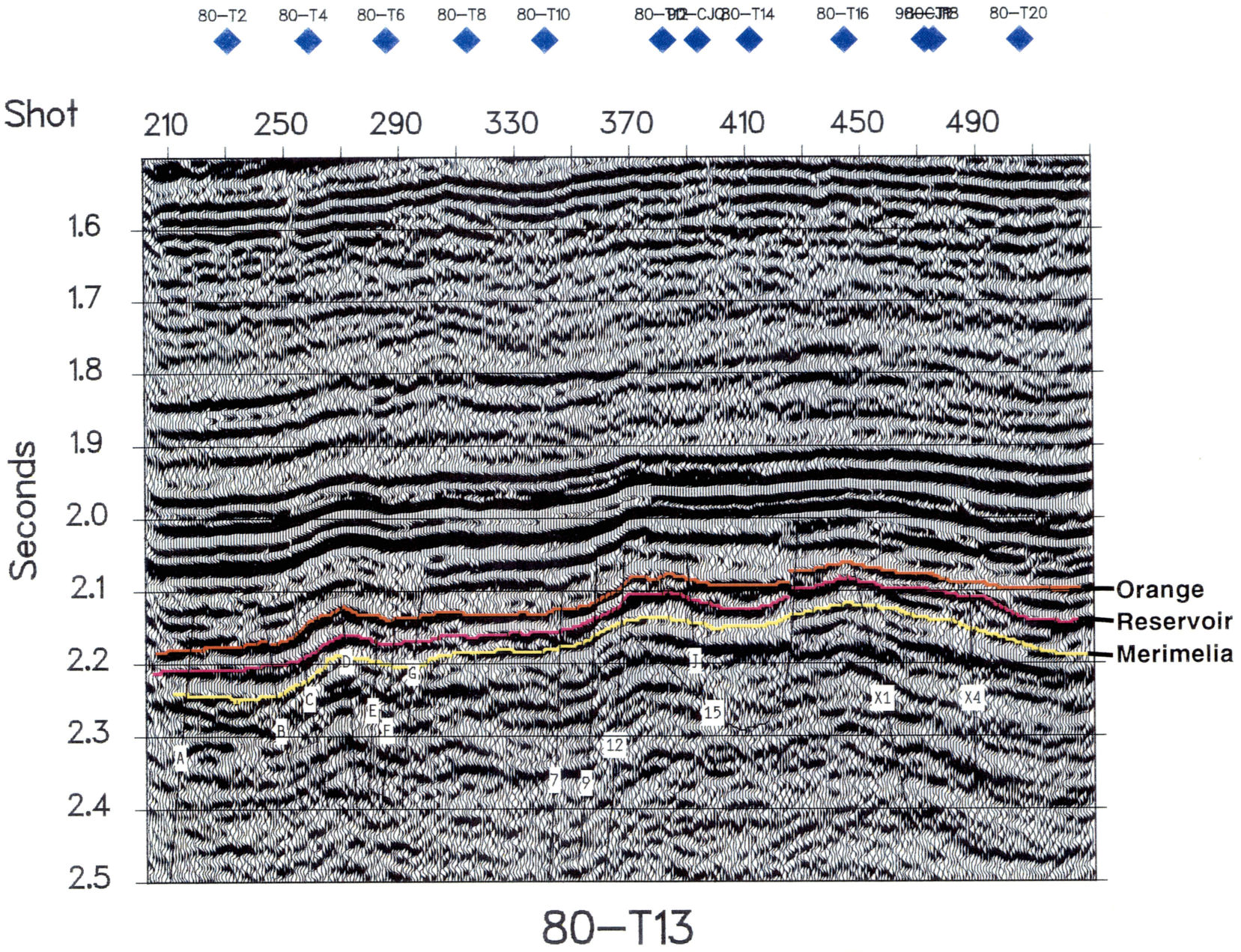

Figure IV - 8. Interpretation of seismic line 80-T13.
Fault 15 is incorrectly plotted.

QAa3127

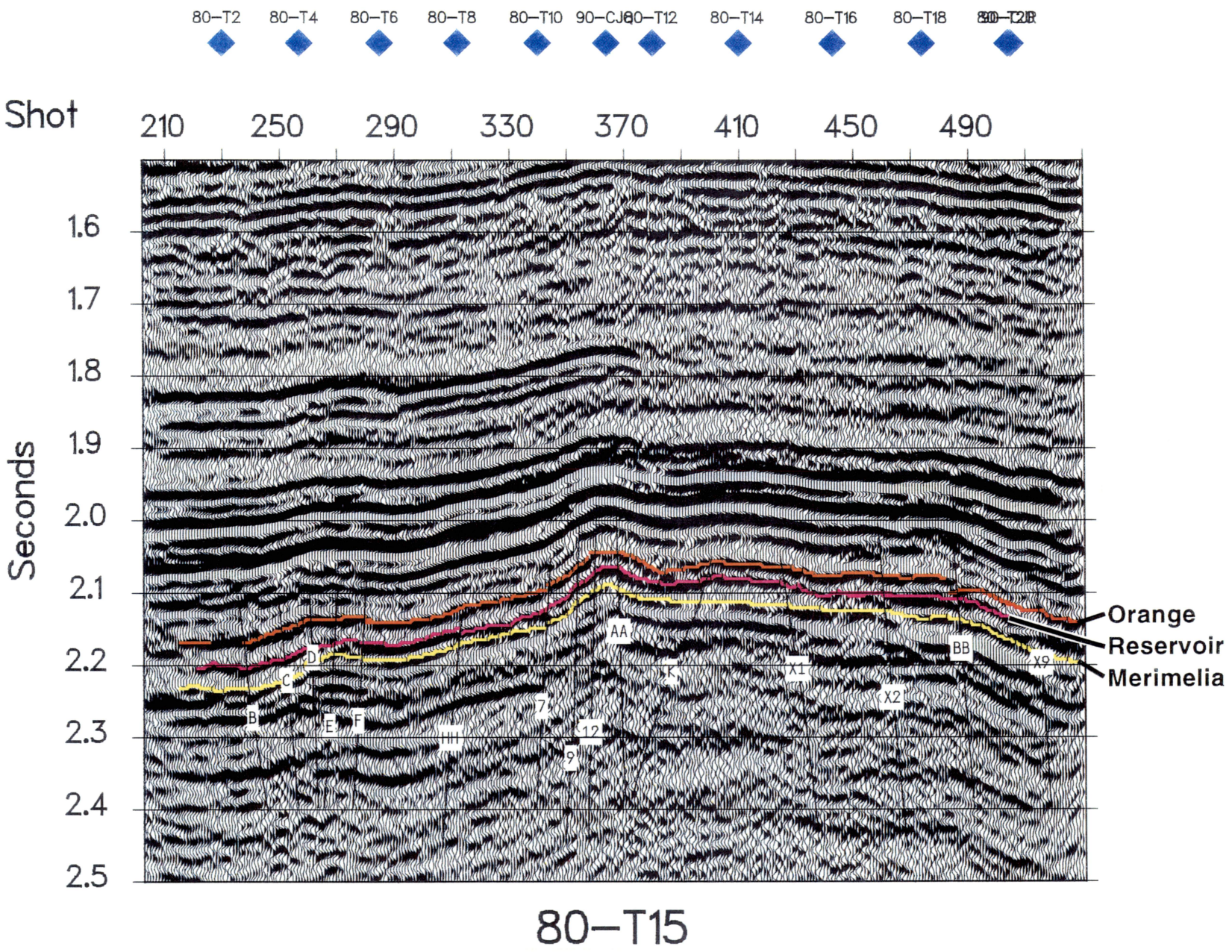

Figure IV - 9. Interpretation of seismic line 80-T15.

QAa3128

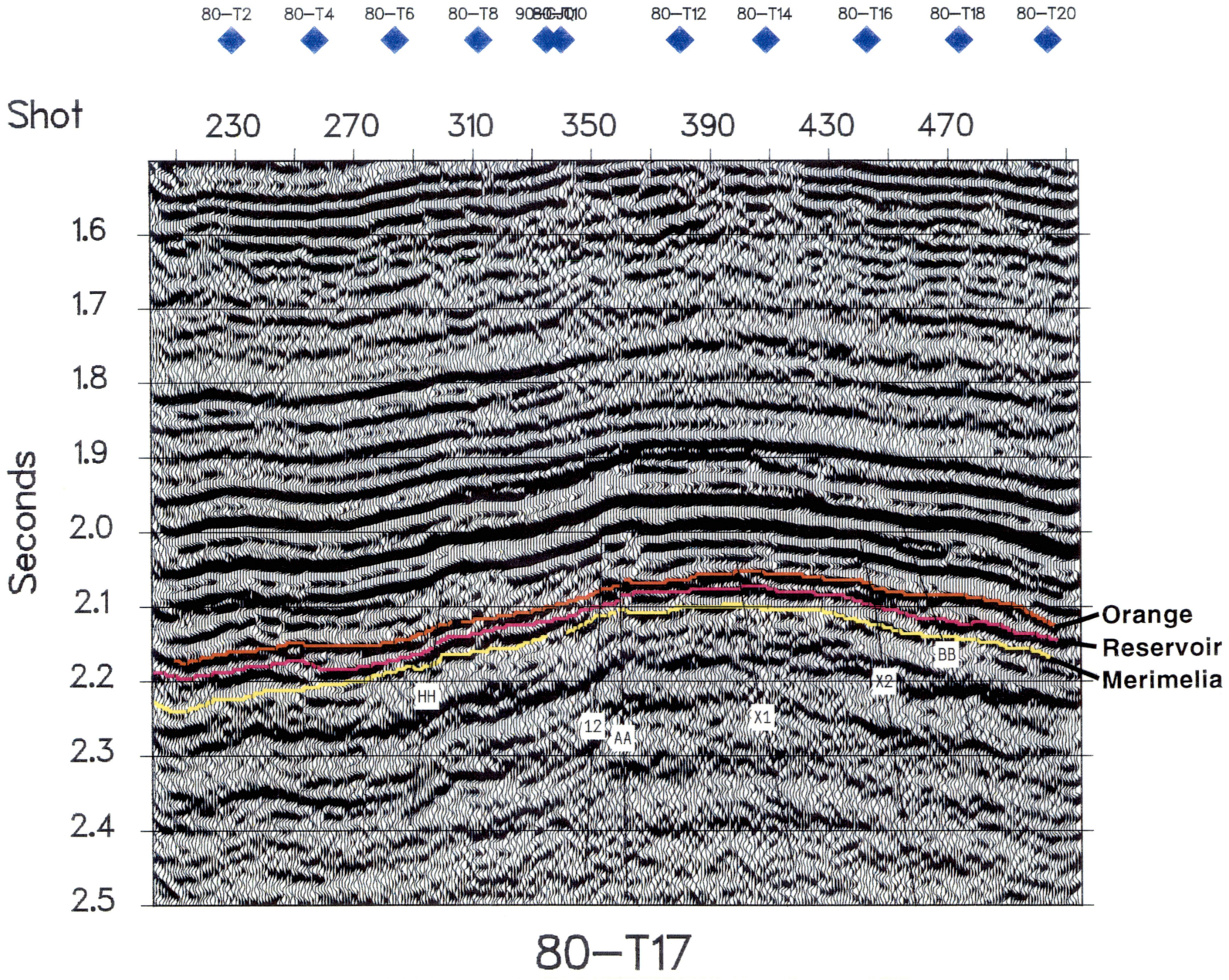

Figure IV - 10. Interpretation of seismic line 80-T17.

QAa3129

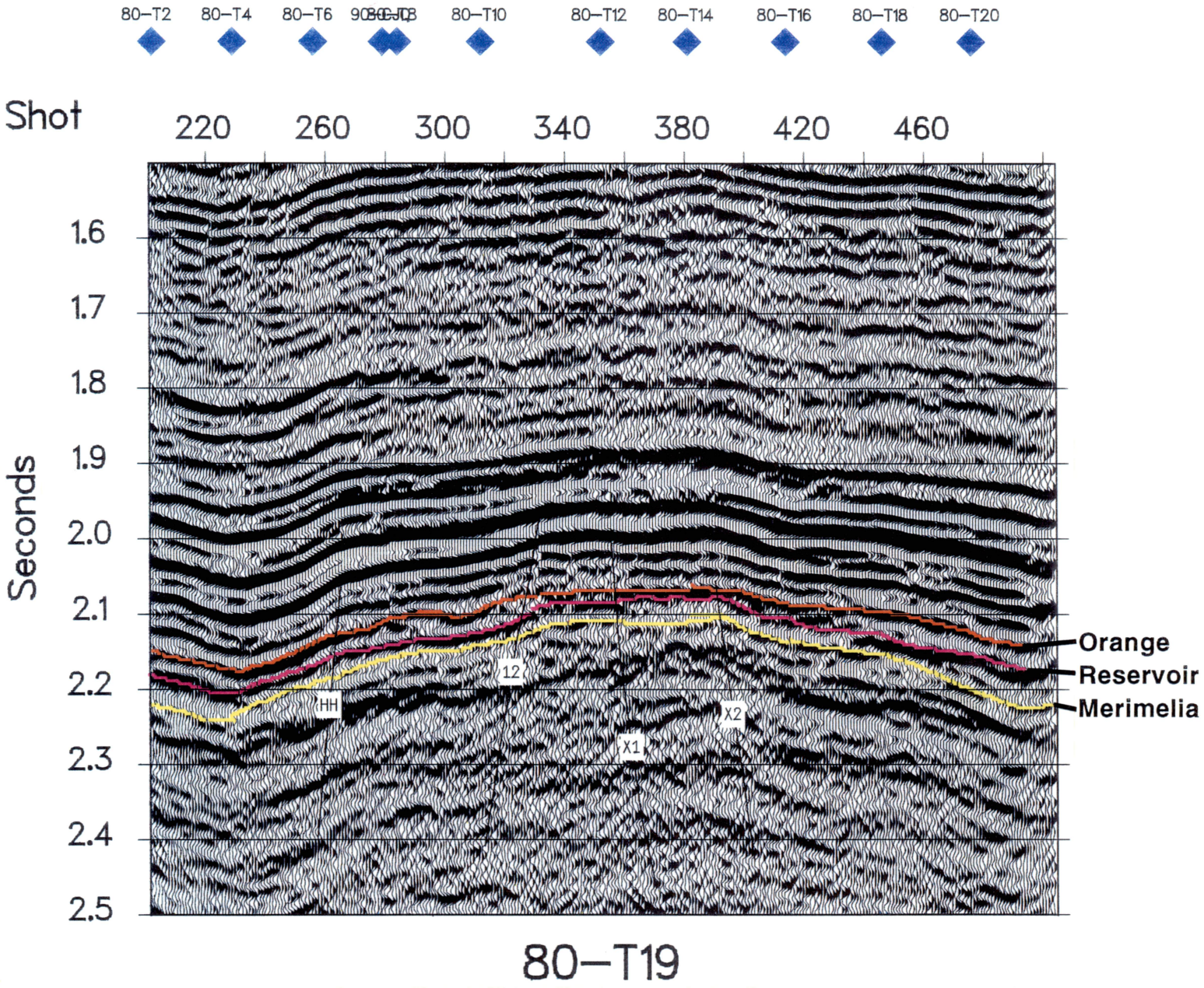

Figure IV - 11. Interpretation of seismic line 80-T19.

QAa3130

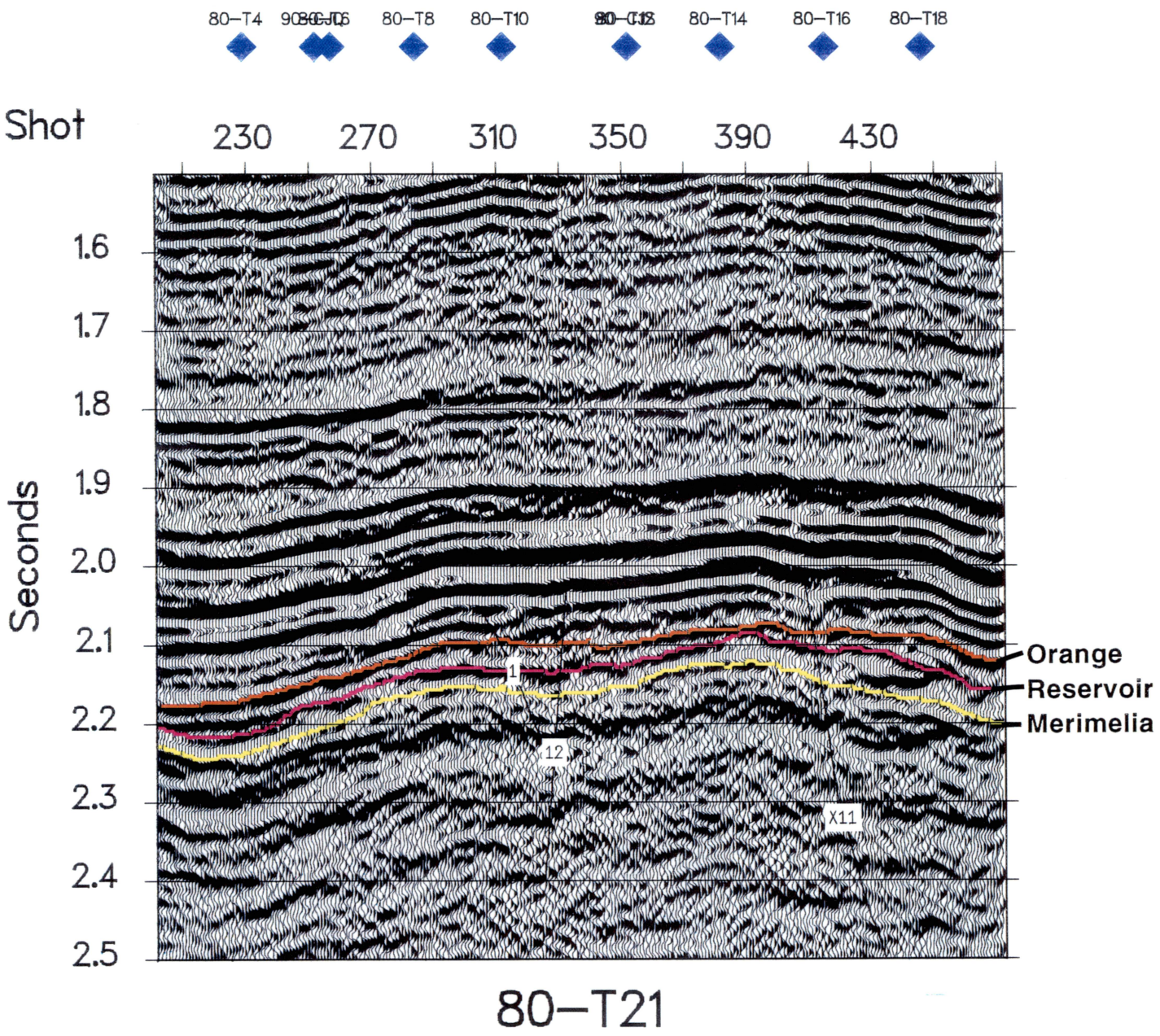

Figure IV - 12. Interpretation of seismic line 80-T21.

QAa3131

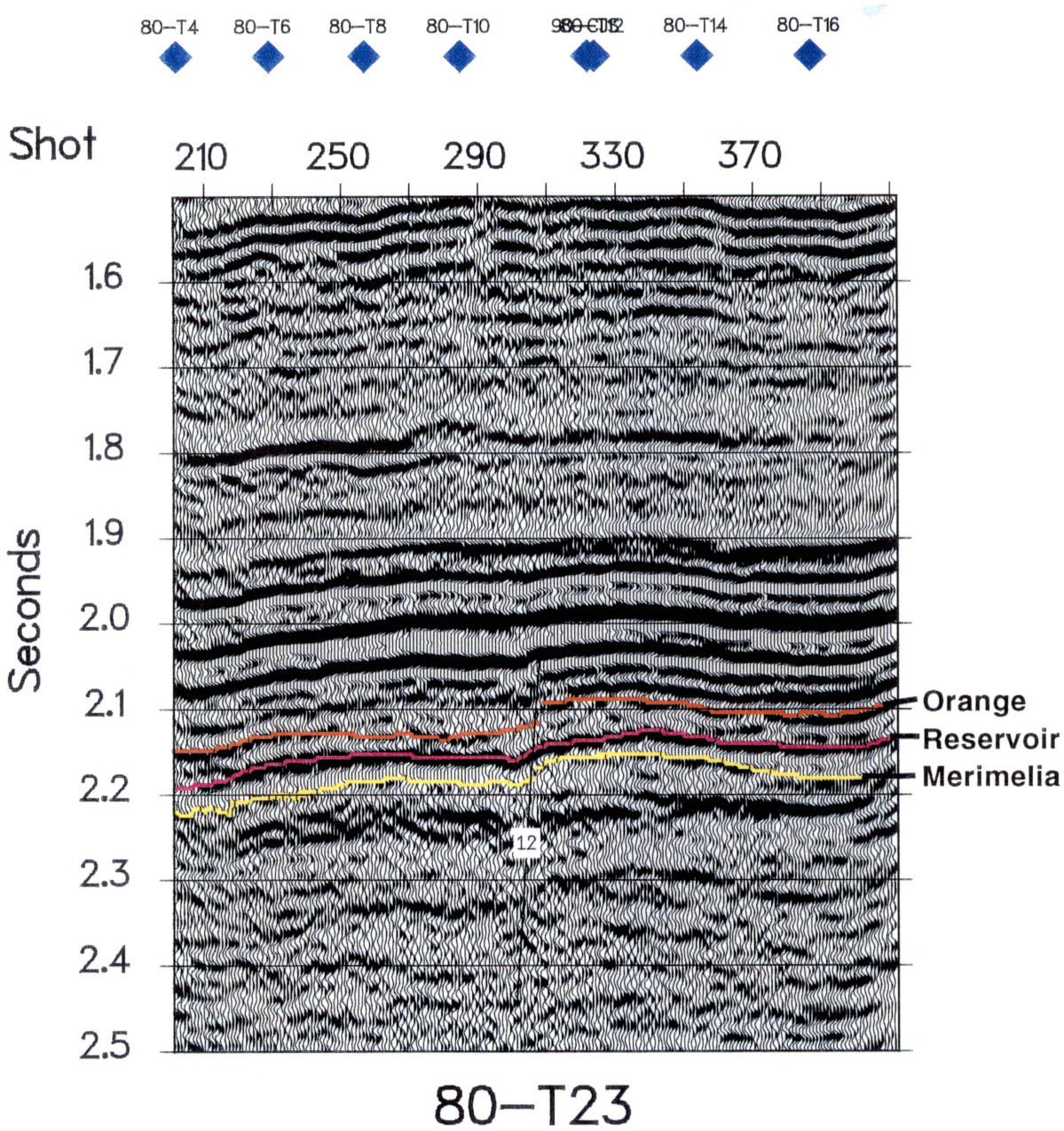

Figure IV - 13. Interpretation of seismic line 80-T23.

QAa3132

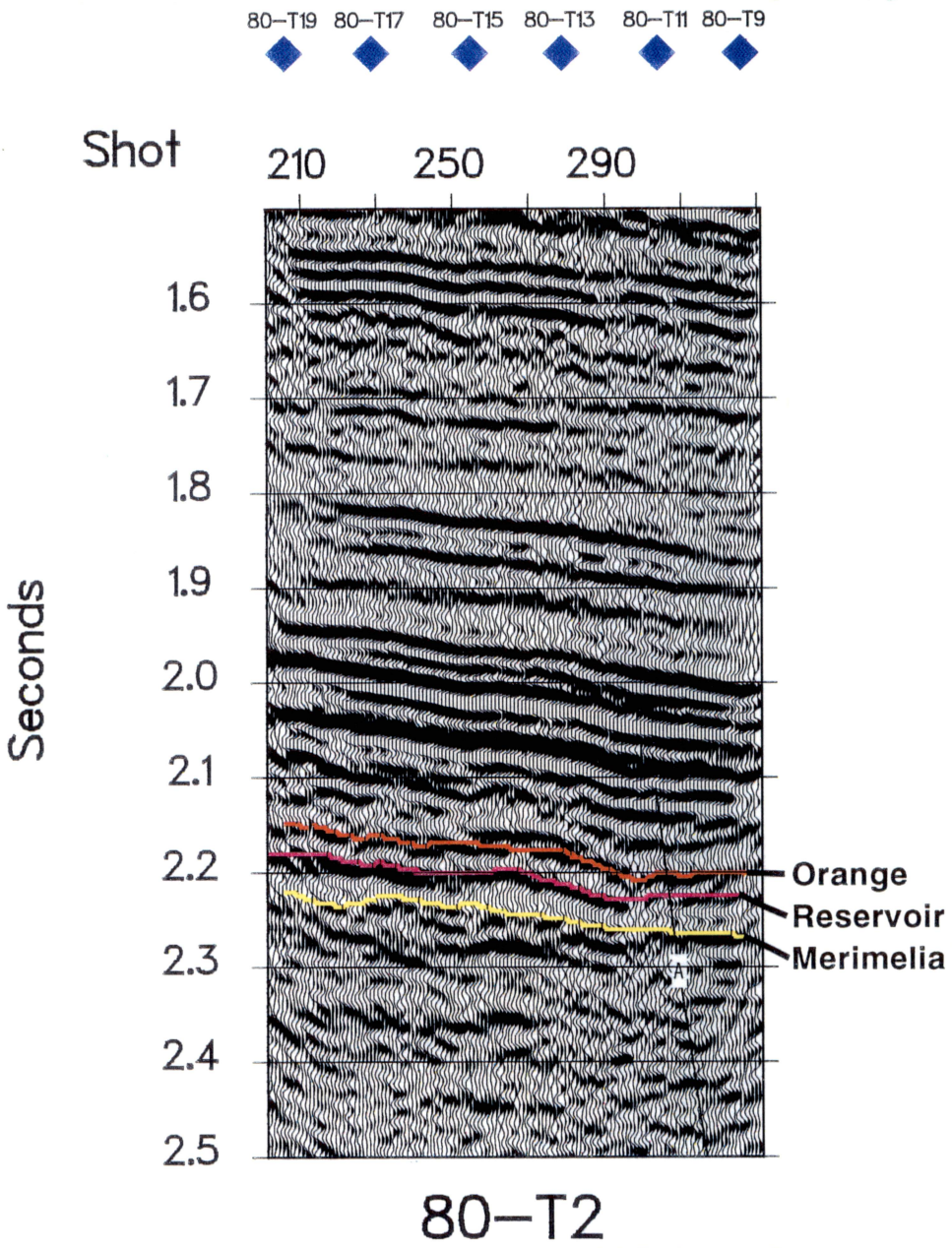

Figure IV - 14. Interpretation of seismic line 80-T2.

QAa3133

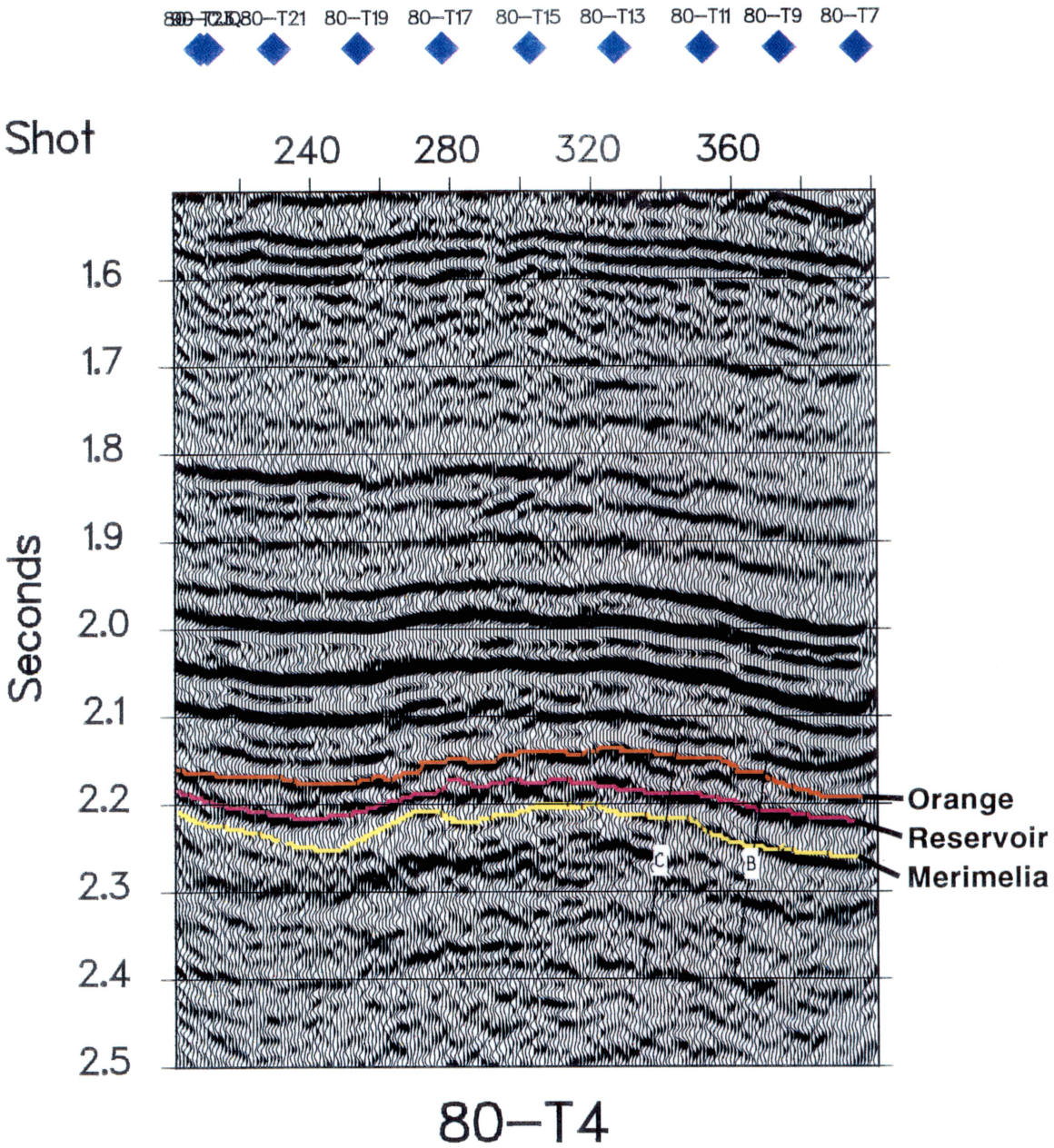

Figure IV - 15. Interpretation of seismic line 80-T4.

QAa3134

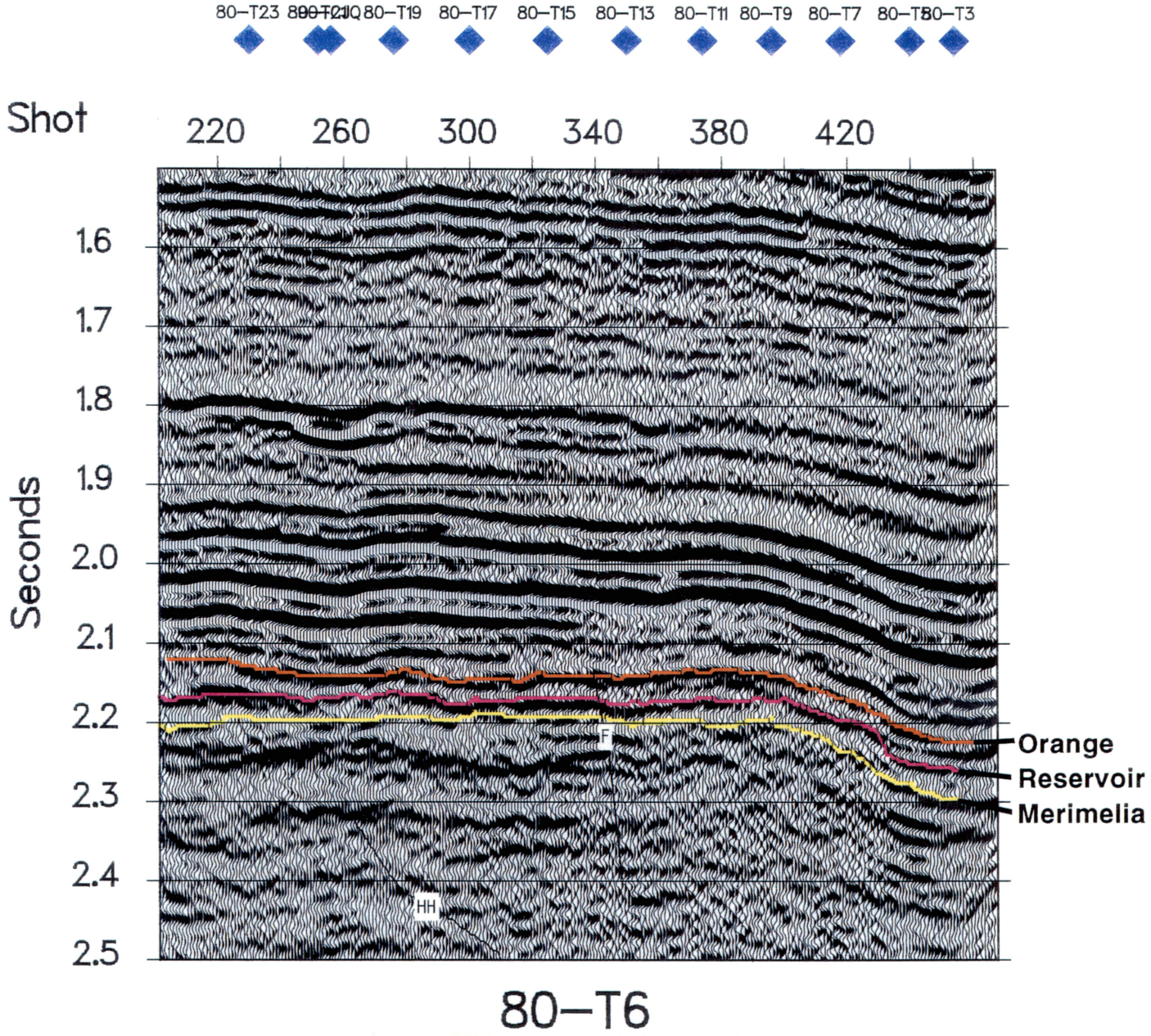

Figure IV - 16. Interpretation of seismic line 80-T6.
Ignore fault HH which software projected onto this line.

QAa3135

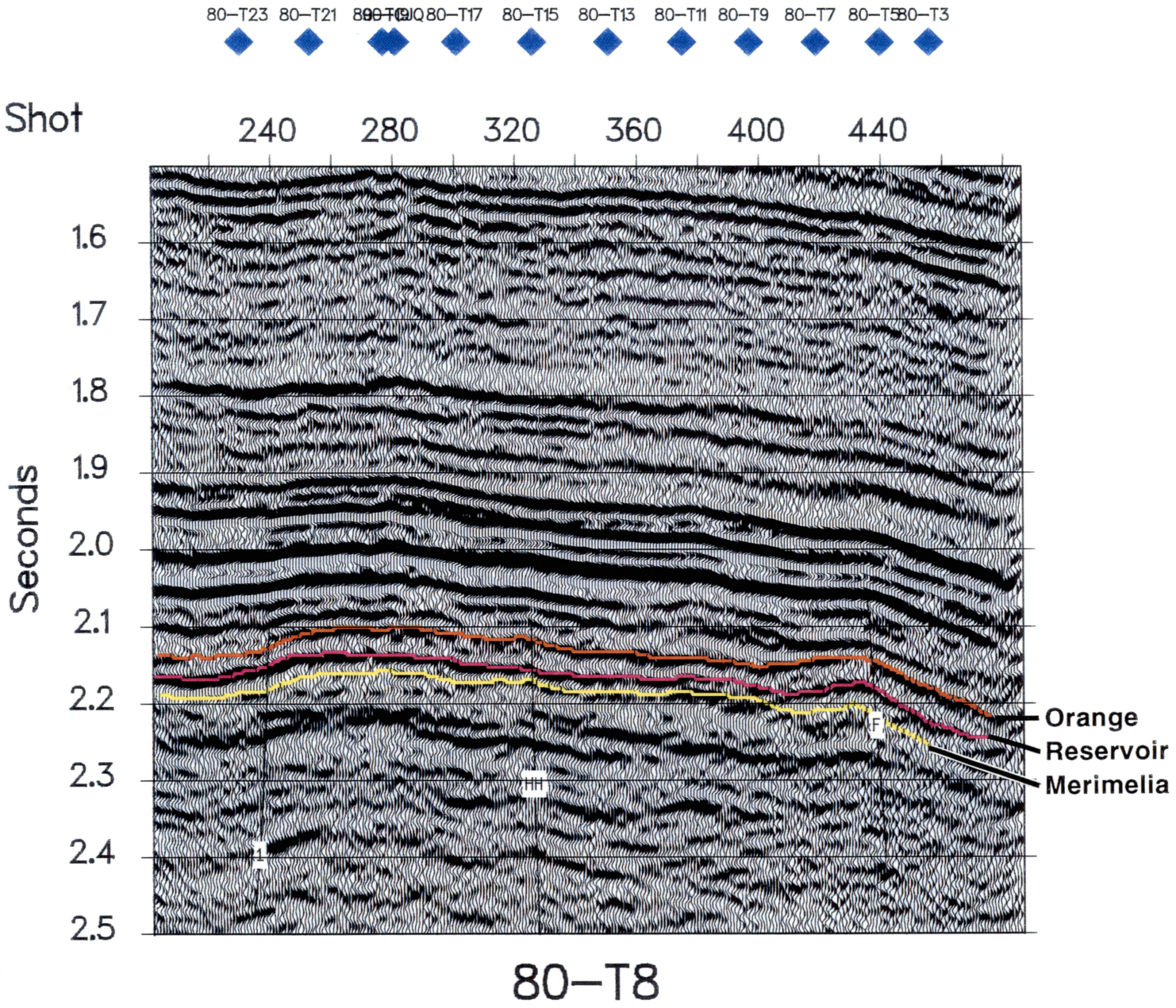

Figure IV - 17. Interpretation of seismic line 80-T8.

QAa3136

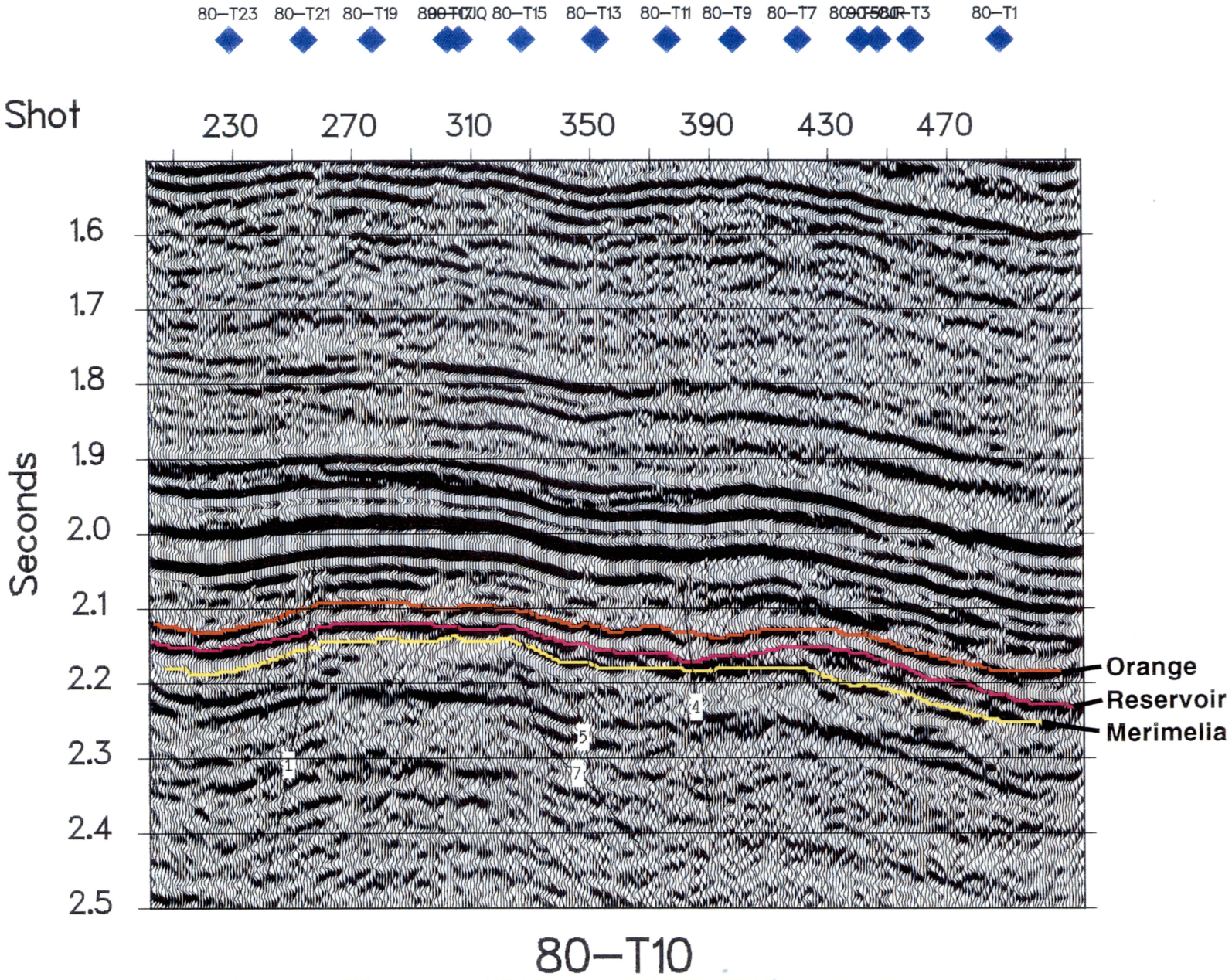

Figure IV - 18. Interpretation of seismic line 80-T10.
Ignore fault 5 which software projected onto this line.

QAa3137

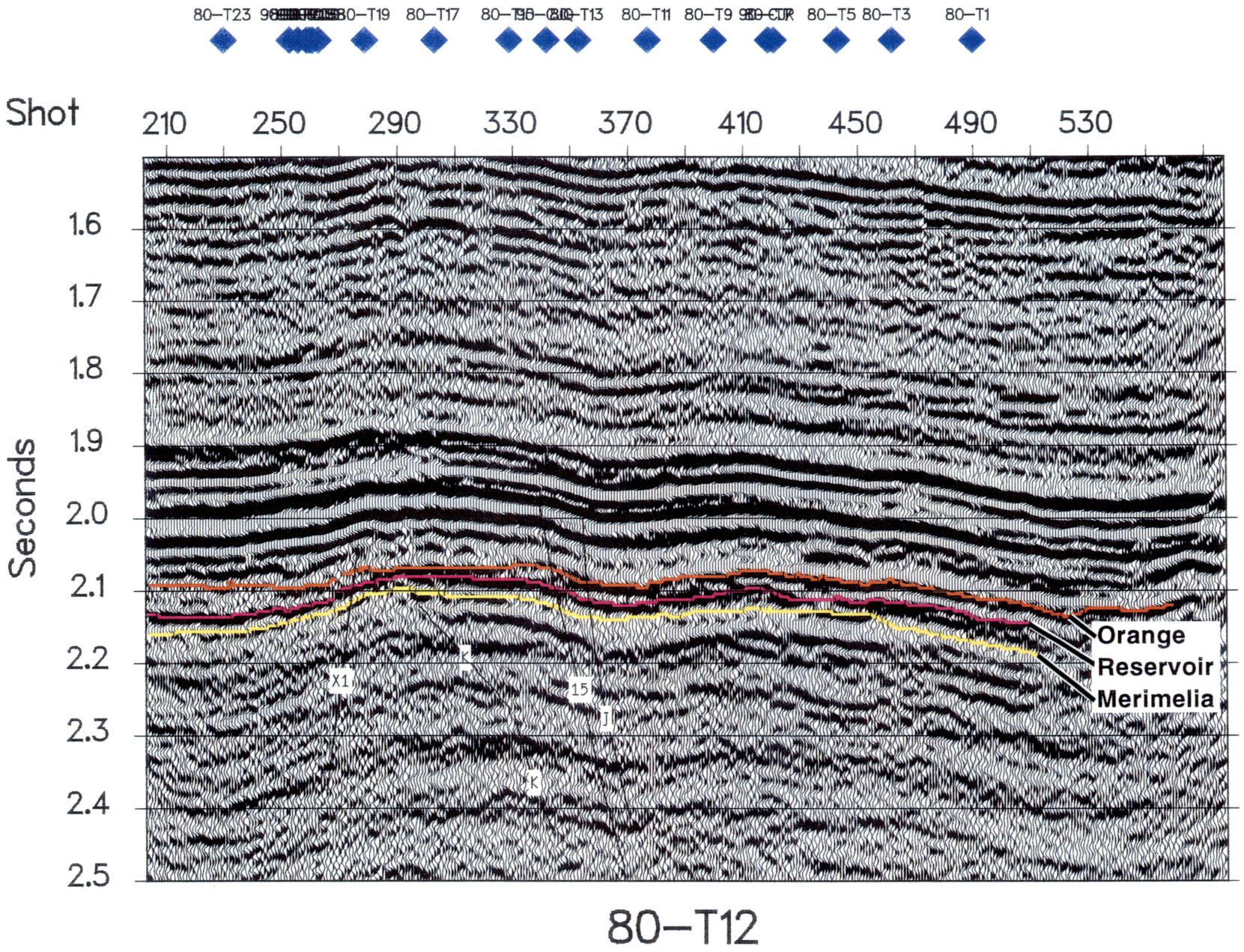

Figure IV - 19. Interpretation of seismic line 80-T12.
Ignore fault K as projected onto this line.

QAa3138

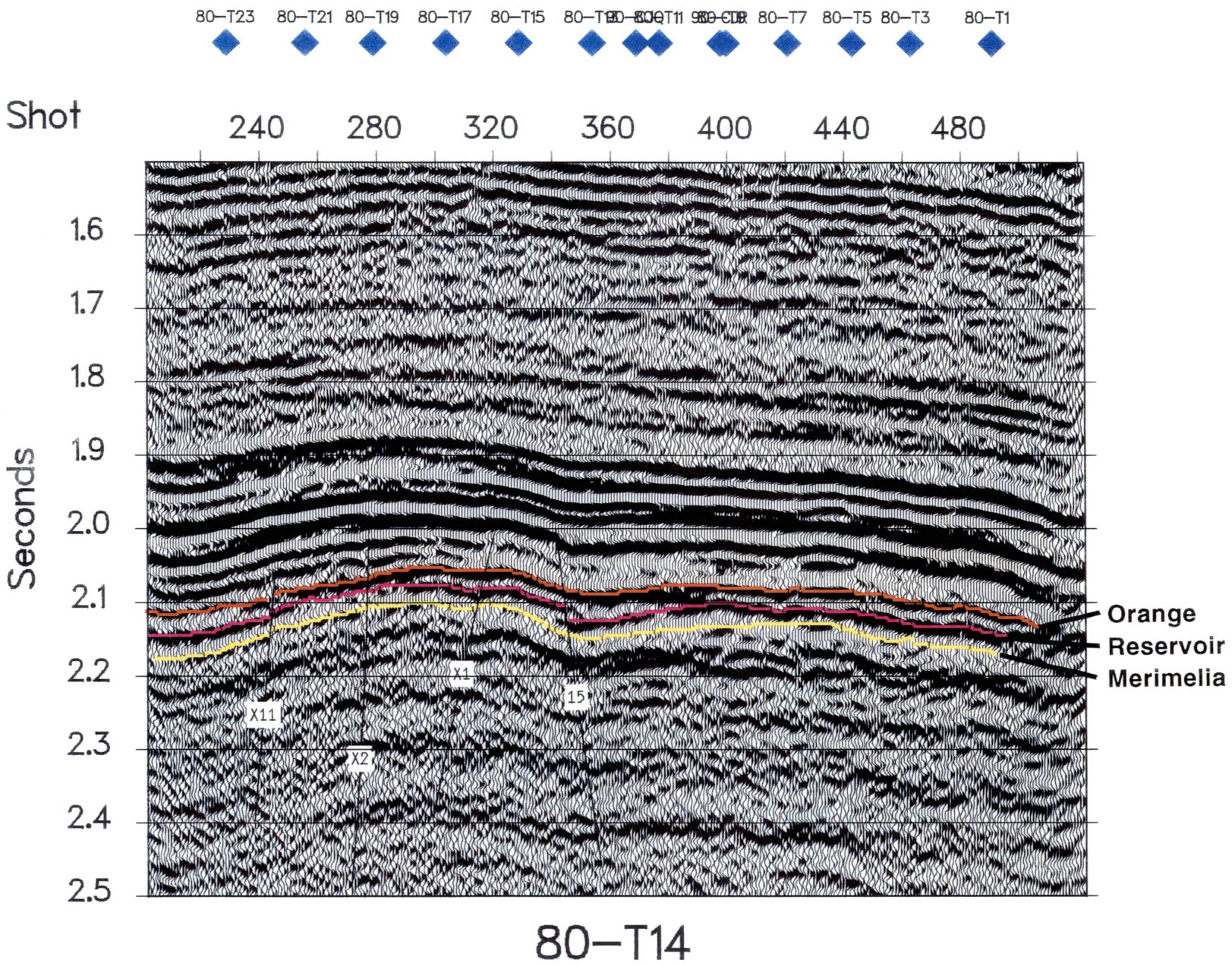

Figure IV - 20. Interpretation of seismic line 80-T14.

QAa3139

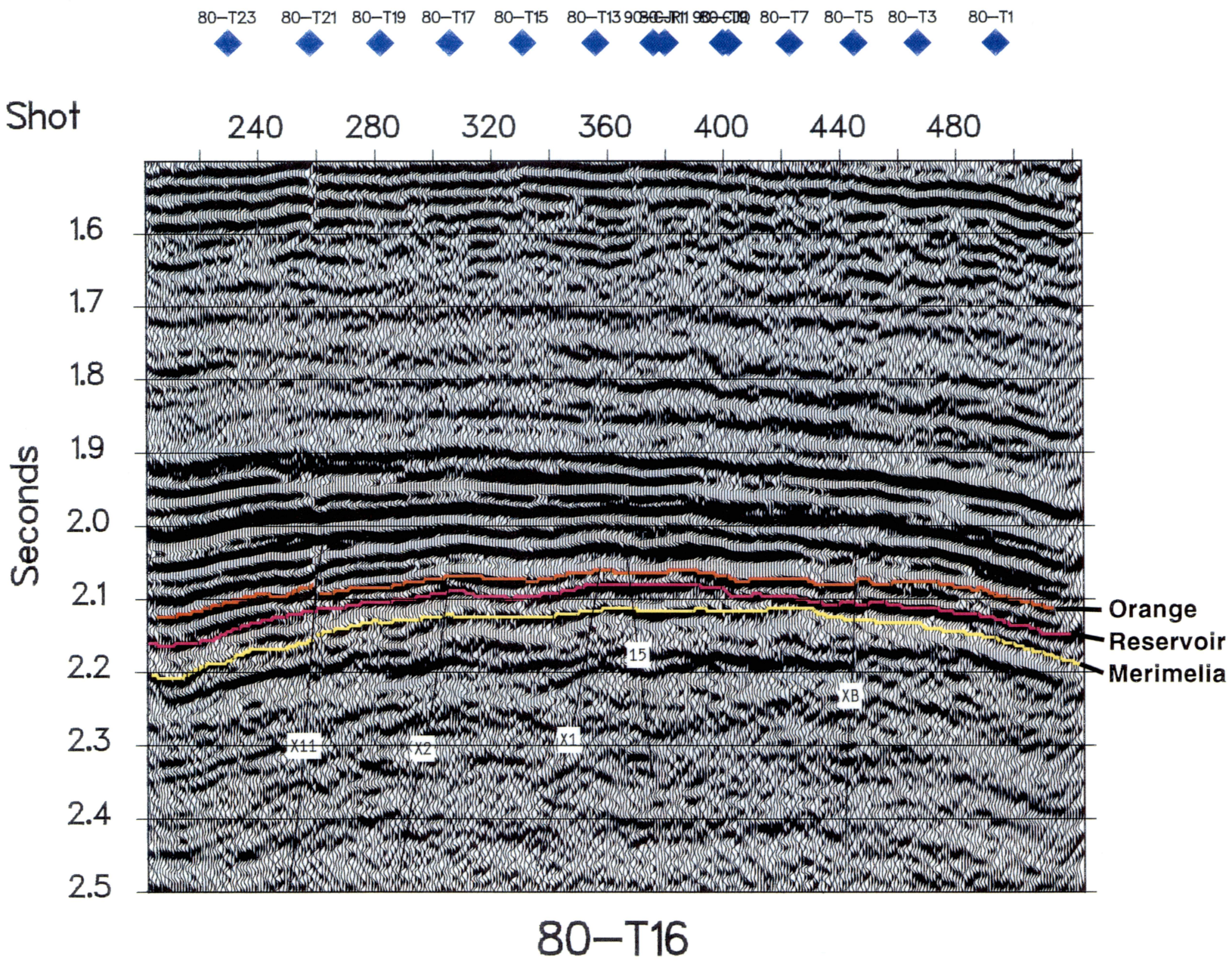

Figure IV - 21. Interpretation of seismic line 80-T16.

QAa3140

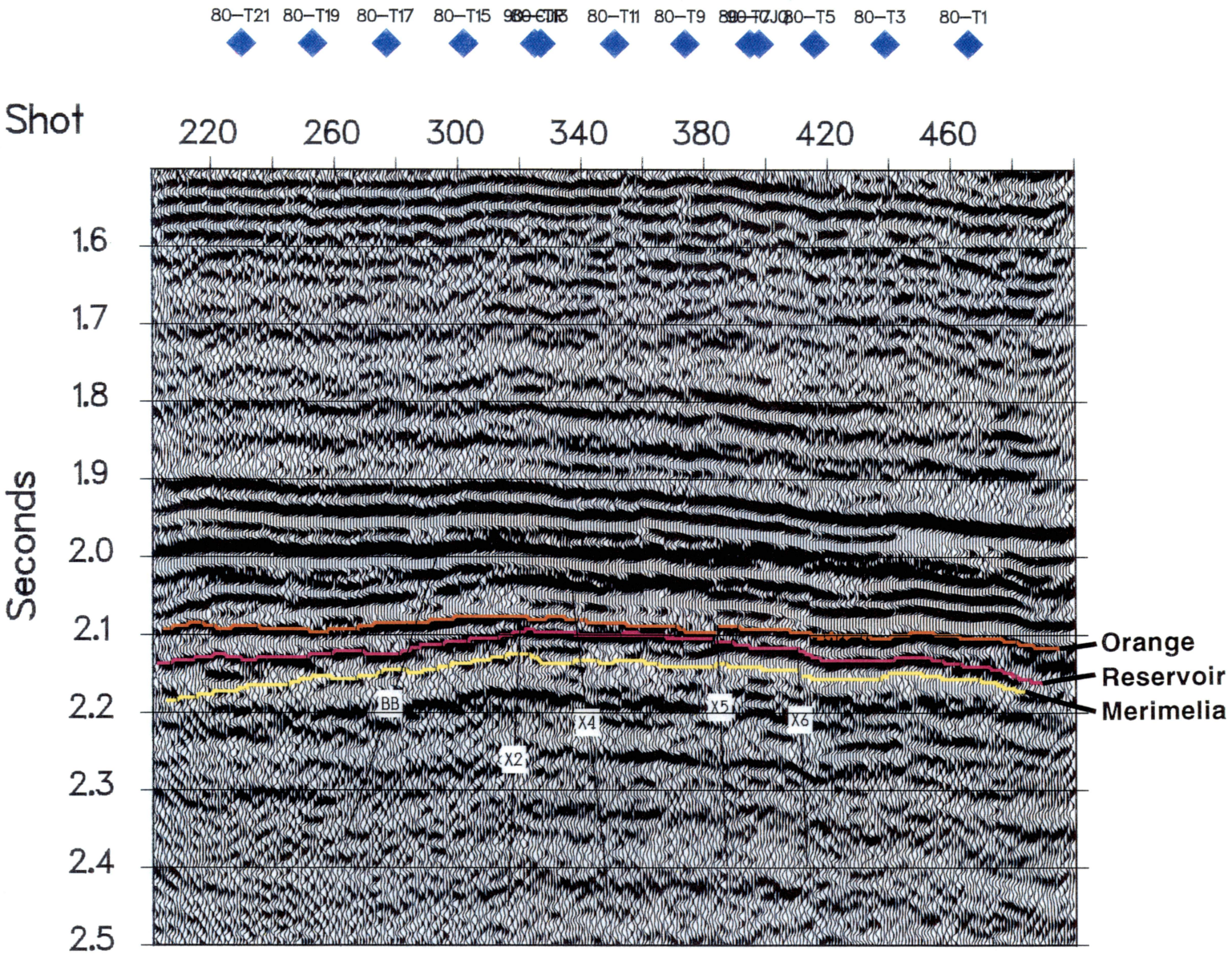

Figure IV - 22. Interpretation of seismic line 80-T18.

QAa3141

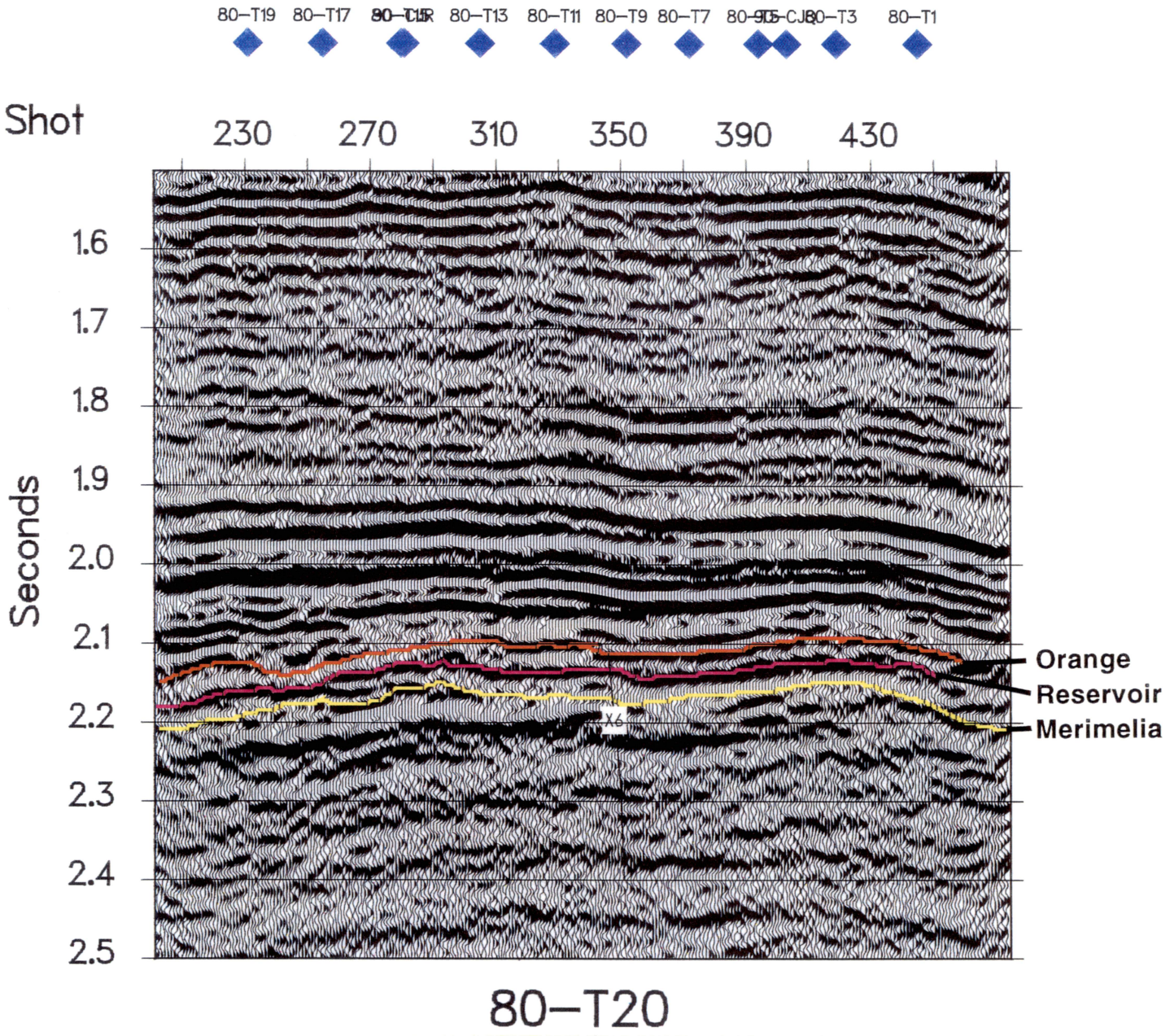

Figure IV - 23. Interpretation of seismic line 80-T20.

QAa3142

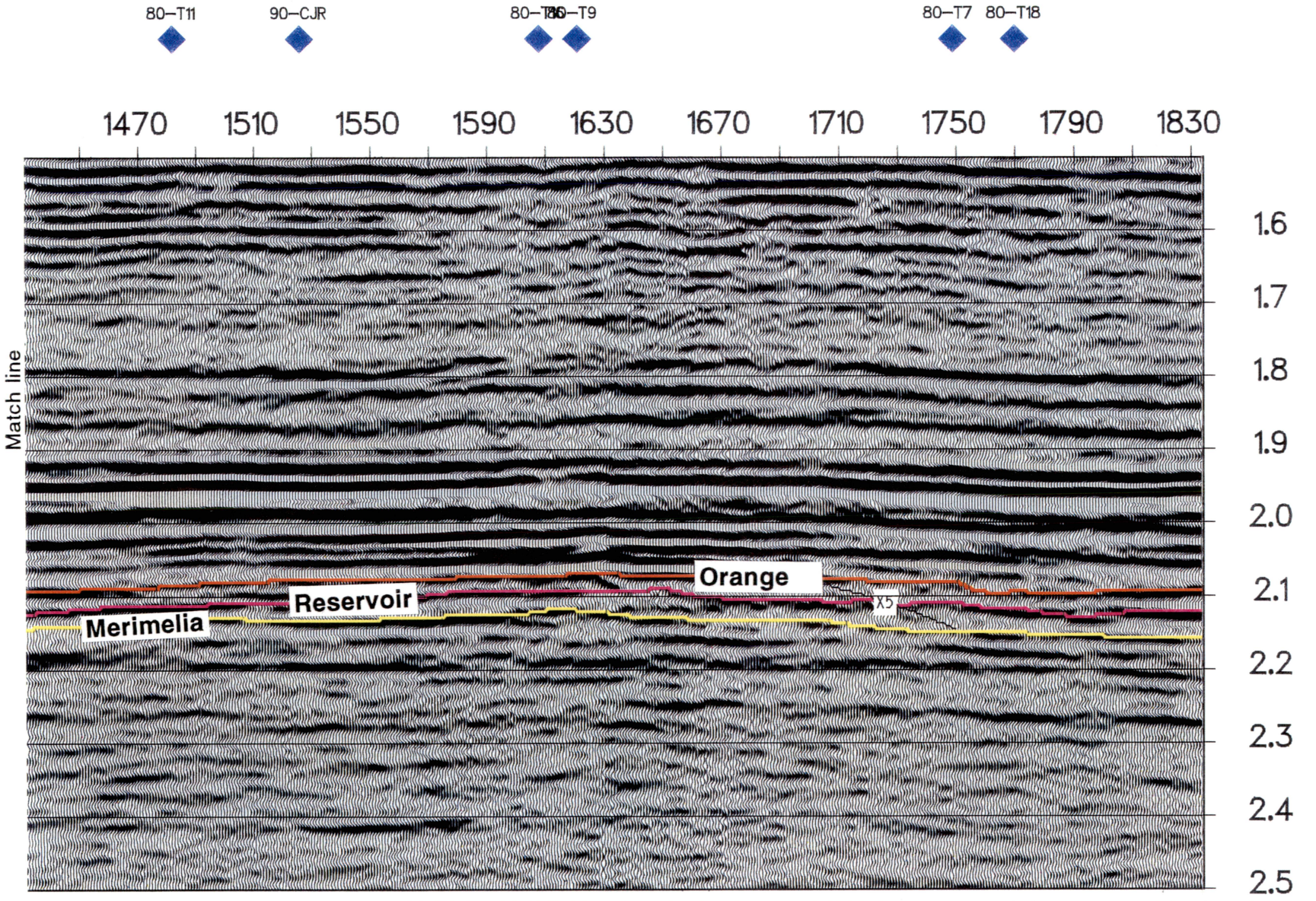

Figure IV - 24. Interpretation of northeast portion of seismic line 90-CJQ.

QAa3143(b)

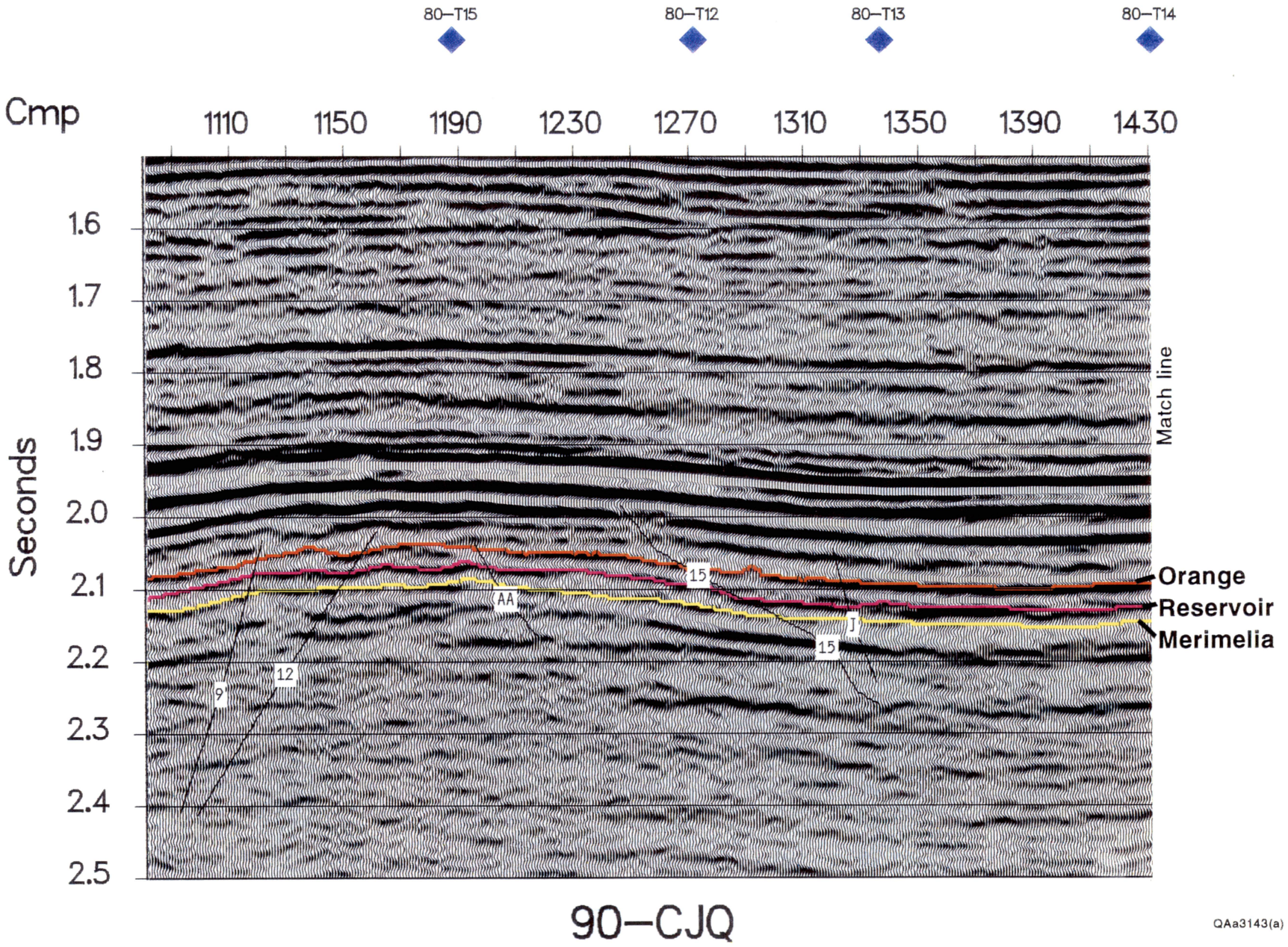

Figure IV - 24, continued - Interpretation of the southwest portion of seismic line 90-CJQ. Note match line to previous page.

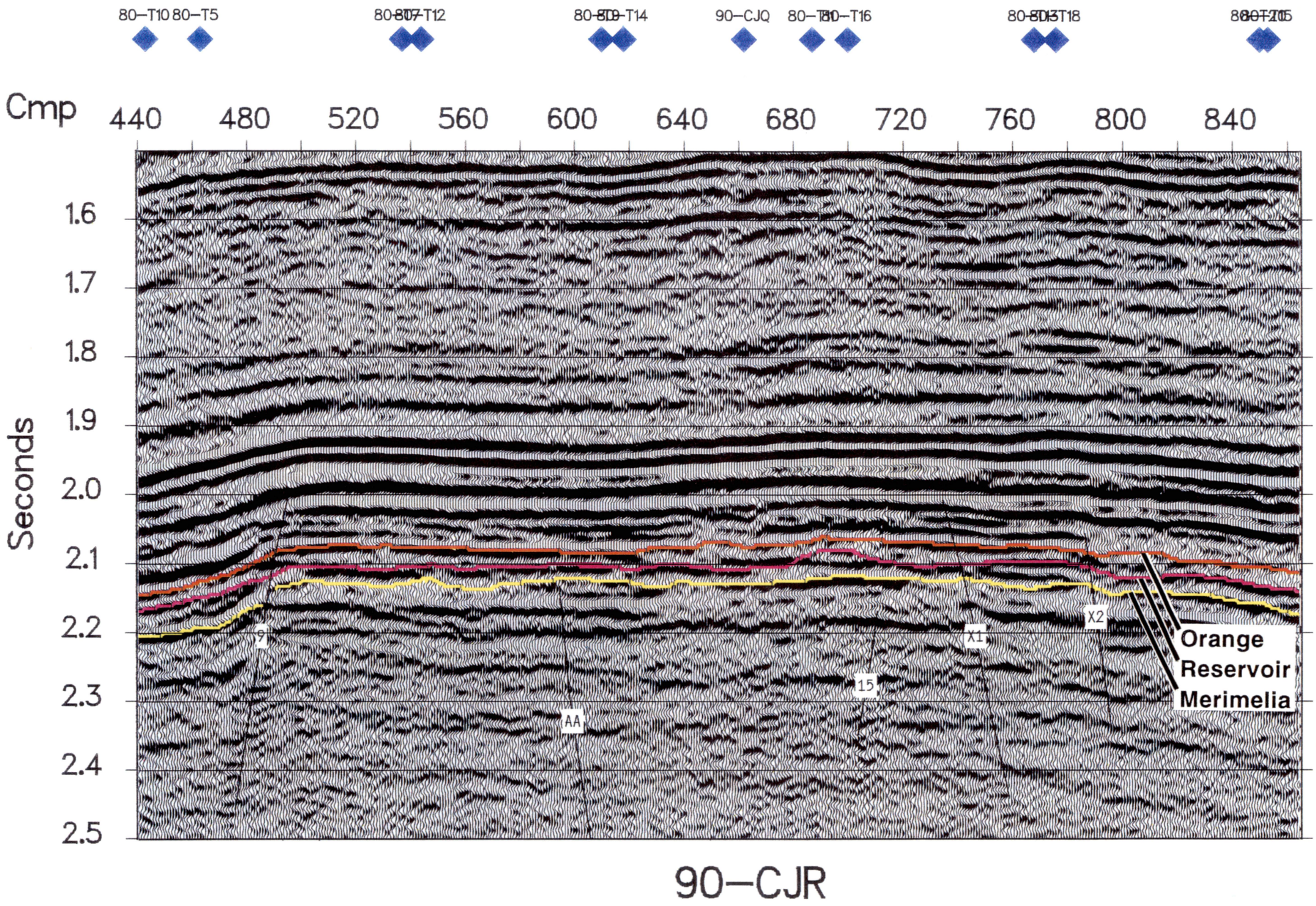

Figure IV - 25. Interpretation of seismic line 90-CJR.
Ignore fault 15 as projected onto this line.

QAa3144c

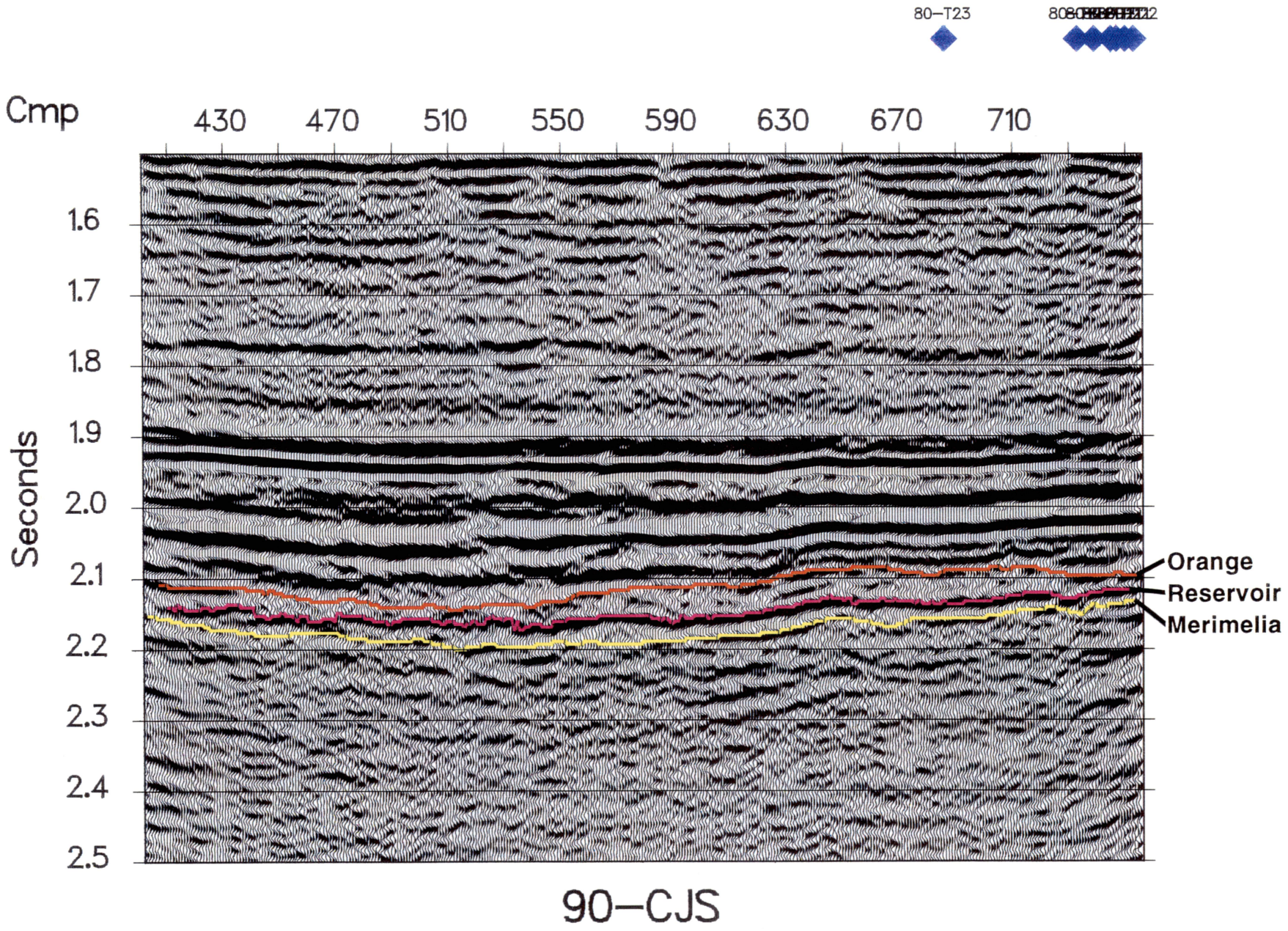

Figure IV - 26. Interpretation of seismic line 90-CJS.

QAa3145

Structural Mapping

Time-Structure Maps

Time structure maps of the Orange, Reservoir, and Merrimelia horizons are displayed as figures IV-27, 28, and 29, respectively. These maps were computer generated and then edited. Editing was required only to modify contours inside two narrow fault blocks, and occasionally to modify a portion of a computer-generated contour. Only a modest amount of editing was necessary for each map.

Velocity Maps

All of the wells in the field (73) were used to construct the velocity control that converted the time-structure maps into depth maps. The methodology consisted of the following steps:

1. The subsea depths to the Orange, Reservoir, and Merrimelia horizons were picked from log control in each of the 73 wells.
2. At the X-Y coordinates of each well, the seismic two-way time to each seismically interpreted horizon was extracted from the digital time structure files generated by the CPS-1 mapping software.
3. Using these log-determined depths and the seismically measured times, the vertical velocity to each horizon was calculated at each of the 73 well locations.
4. These 73 velocity control points were then contoured using the CPS-1 mapping software.
5. Because the 73 wells were located in the centre of the seismic grid, the machine-generated velocity contours were poorly constrained at the edges of the seismic grid where there were no control wells to guide the contouring. Consequently, considerable hand editing was done to each first-pass velocity map to produce more realistic velocity contours at the outer edges of the seismic grid.
6. Using the edited map as a guide, additional velocity control points were added at the edges of the seismic grid to supplement the velocity control established at the 73 well coordinates. The locations of these edge control points appear on the velocity control maps as unnumbered well symbols.
7. A new velocity map of each horizon was then machine generated using the velocity values calculated at the 73 control wells together with the velocity values defined at the pseudo-well locations around the edge of the seismic grid.

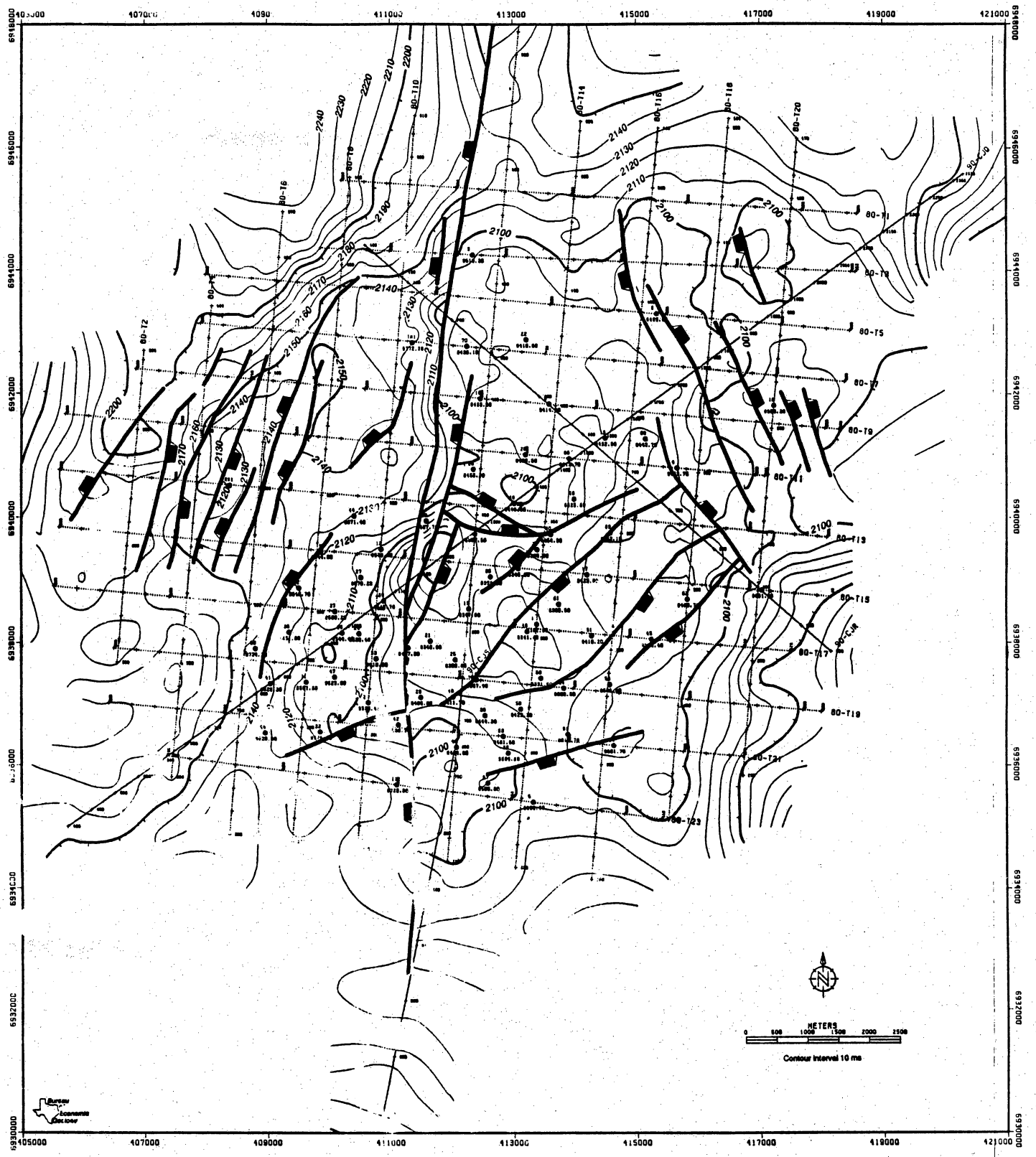

Tirrawarra Project – Orange Horizon – 2-w y time map

ENCLOSURE IV - 27

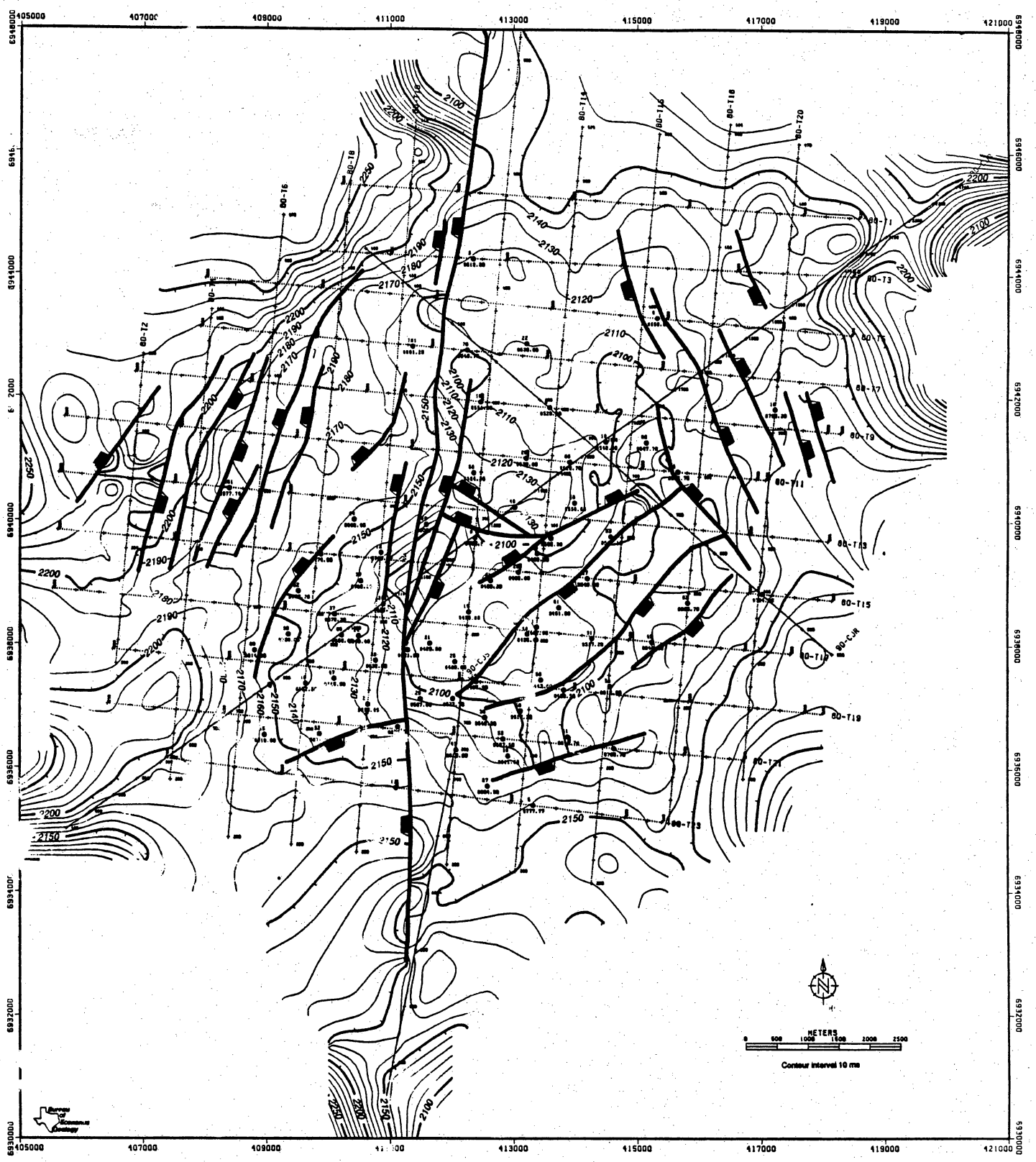

Tirrawarra Project – Reservoir Horizon – 2-way time map

ENCLOSURE IV - 28

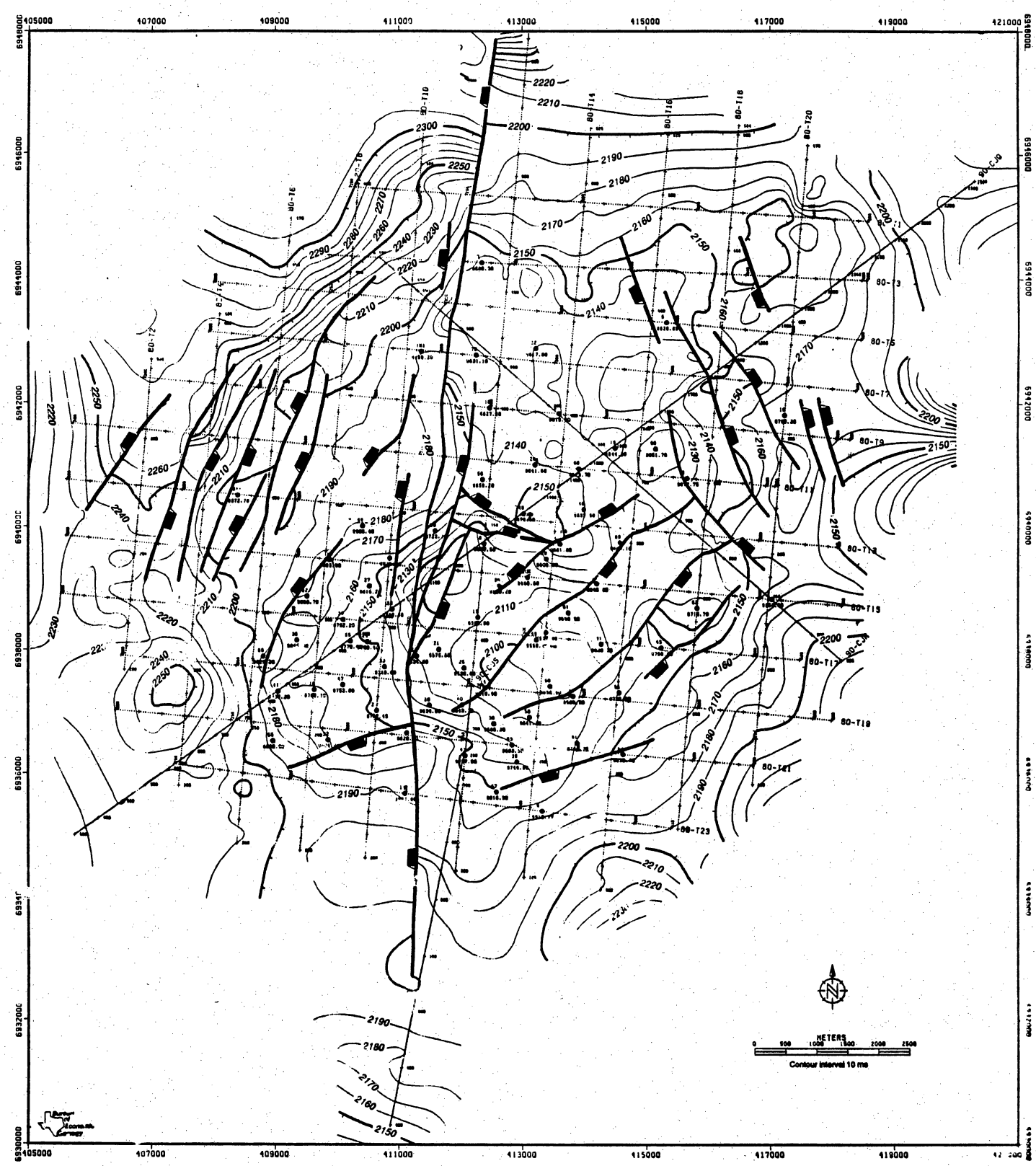

Tirrawarra Project – Merimelia Horizon – 2-way time map

ENCLOSURE IV - 29

The final depth-conversion velocity maps of the Orange, Reservoir, and Merrimelia horizons are displayed in figures IV-30, 31, and 32. These maps show that the velocities are reduced across the central portion of the Tirrawarra anticlinal structure. This low-velocity trend is oriented in an approximate northeast–southwest direction, causing the highest depth-conversion velocity values to occur on the northwest and southeast flanks of the structure. The northeast–southwest orientation of this low velocity trend across the structure is the same orientation that Heath (1989) shows for the regional troughs and ridges in the basin.

Depth Maps

Depth maps were produced by multiplying the time structure map for each horizon by the velocity map for that same horizon and dividing this product by 2 to convert the two-way seismic travel time values to one-way times. These seismically calculated depth values were then compared with the log-measured depths to that same horizon at the 73 field well locations to create a final depth map file composed of both log-measured depths and seismically calculated depths. These log/seismic depth values were then contoured using CPS-1 software. The resulting depth maps are shown in figures IV-33, 34, and 35.

Structural Style

All faults in Tirrawarra field are interpreted to be normal faults. Due to their steep throws, the faults on each time-structure map (and on the depth maps that follow) move laterally only short distances as the structure rises from the deeper Merrimelia level (figs. IV-29 and 35) to the shallower Orange horizon (figs. IV-27 and 33). These structure maps show Tirrawarra field to be a faulted anticline. A major normal fault downthrown to the west cuts the entire north–south dimension of the field at all three seismically mapped levels and divides the field into western and eastern portions. The remaining normal faults in the field are shorter, with many extending across only one or two seismic lines. The normal faults in the western portion of the field are oriented north–south as is the major bisecting fault. One exception to this behavior is the southernmost fault in the western block, which cuts across lines 80-T8, 80-T10, and 80-T21. This fault is oriented almost east–west.

In contrast, the normal faults in the eastern portion of the field are oriented either northeast–southwest or northwest–southeast, implying that different tectonic forces were active in the eastern and western parts of the anticlinal feature. The fault patterns in both the

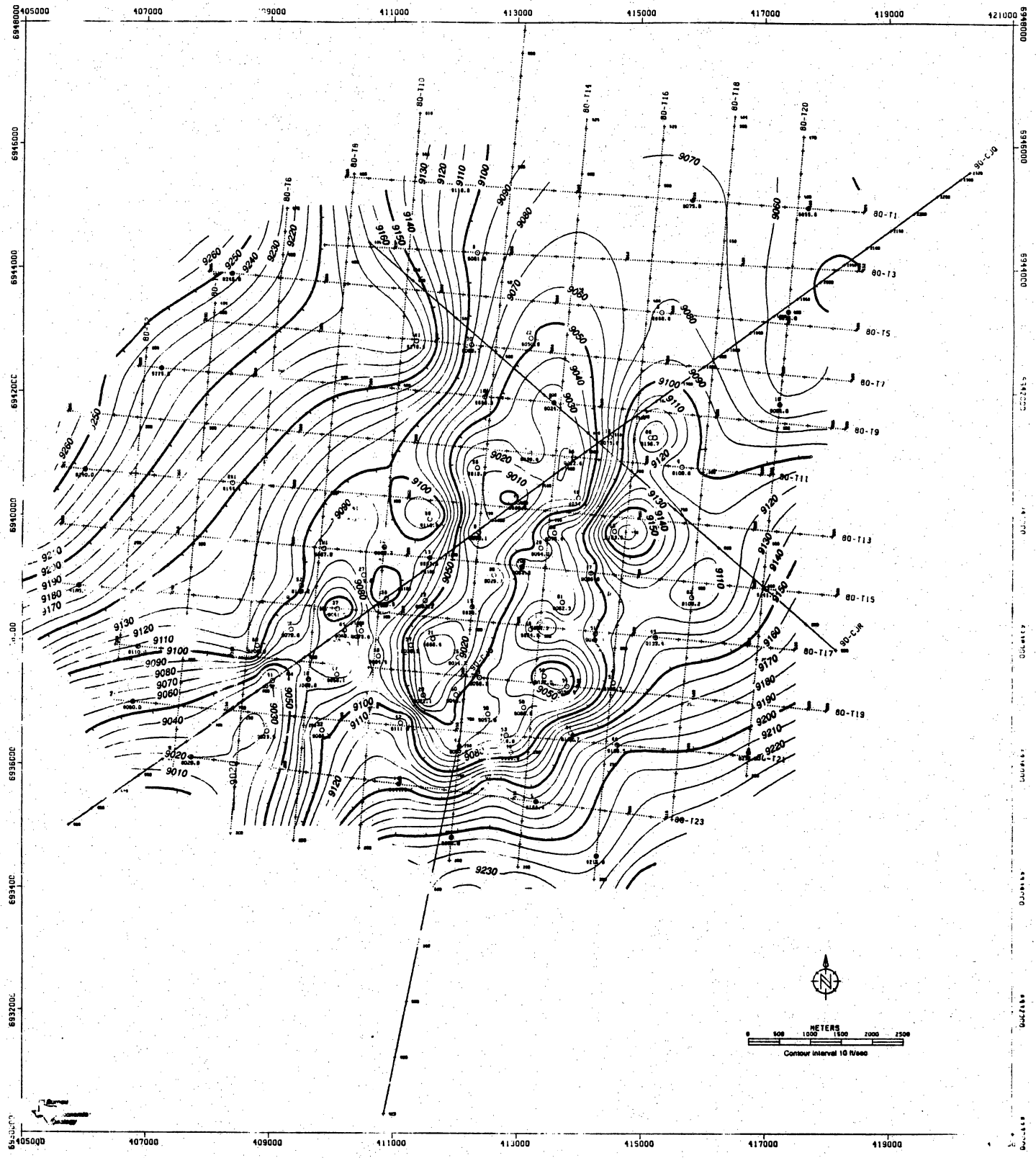

Tirrawarra Project – Orange Horizon – Velocity map
ENCLOSURE IV - 30

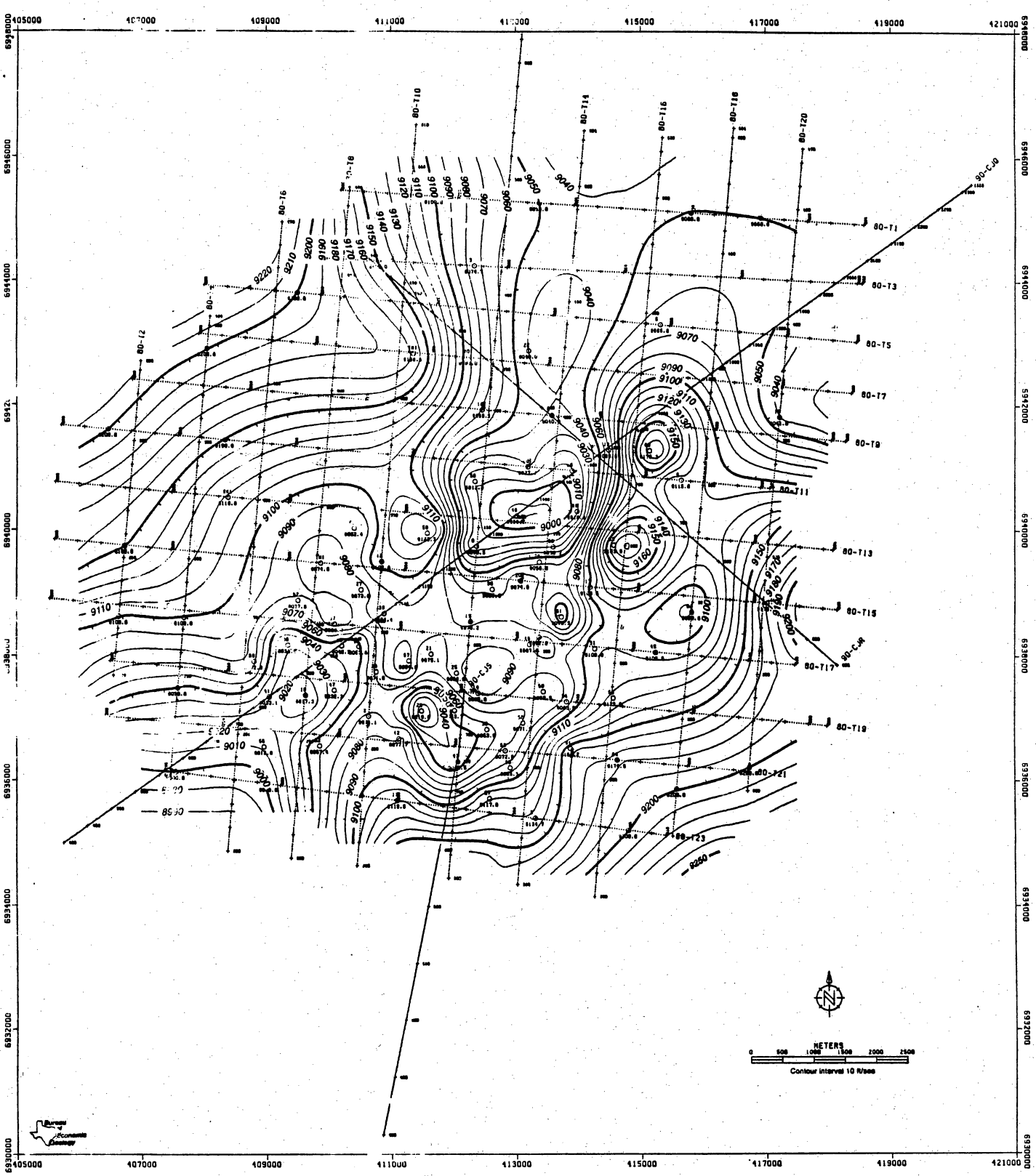

Tirrawarra Project – Reservoir Horizon – Velocity map
ENCLOSURE IV - 31

OAs3181

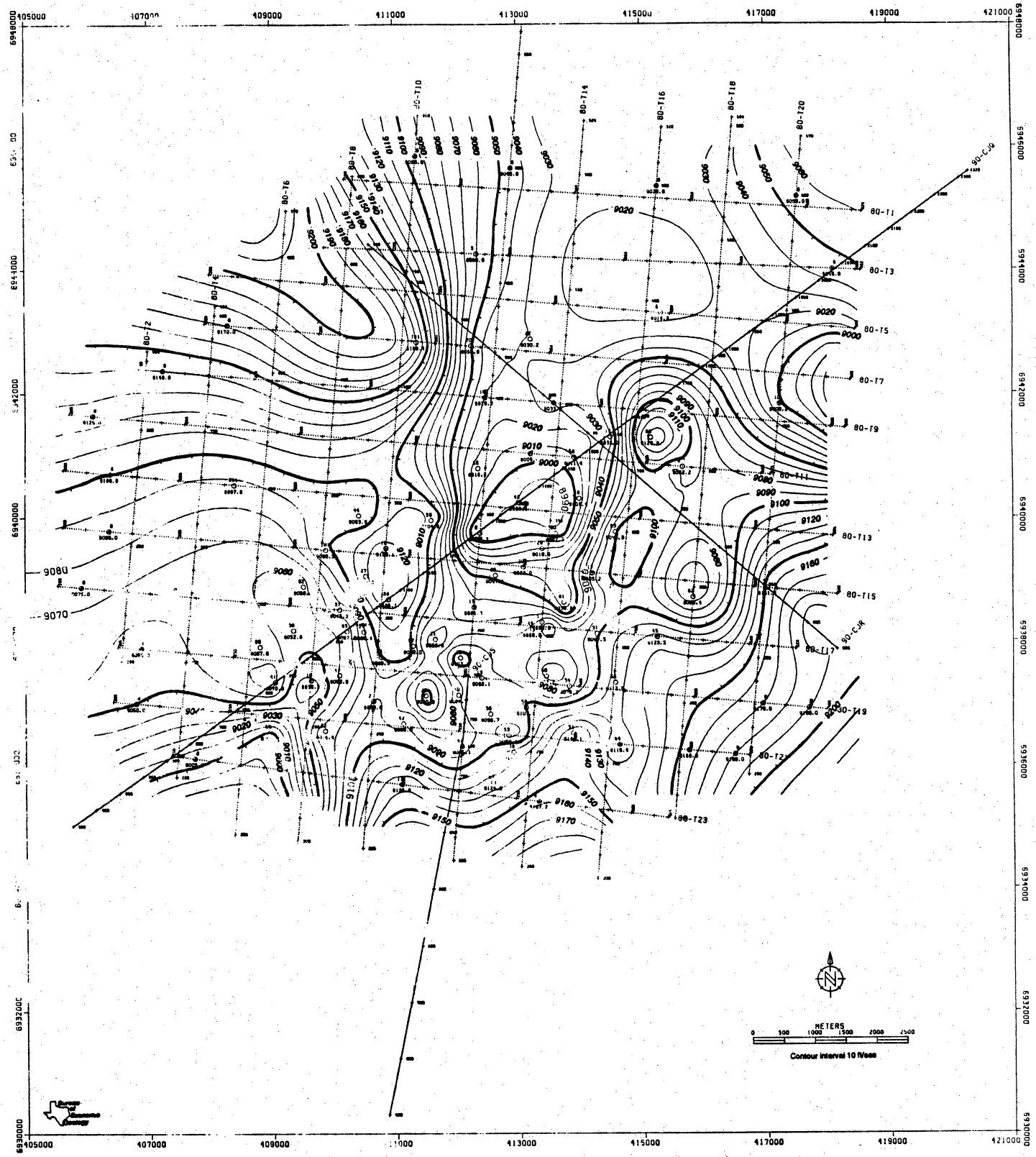

Tirrawarra Project - Merimelia Horizon - Velocity map

ENCLOSURE IV - 32

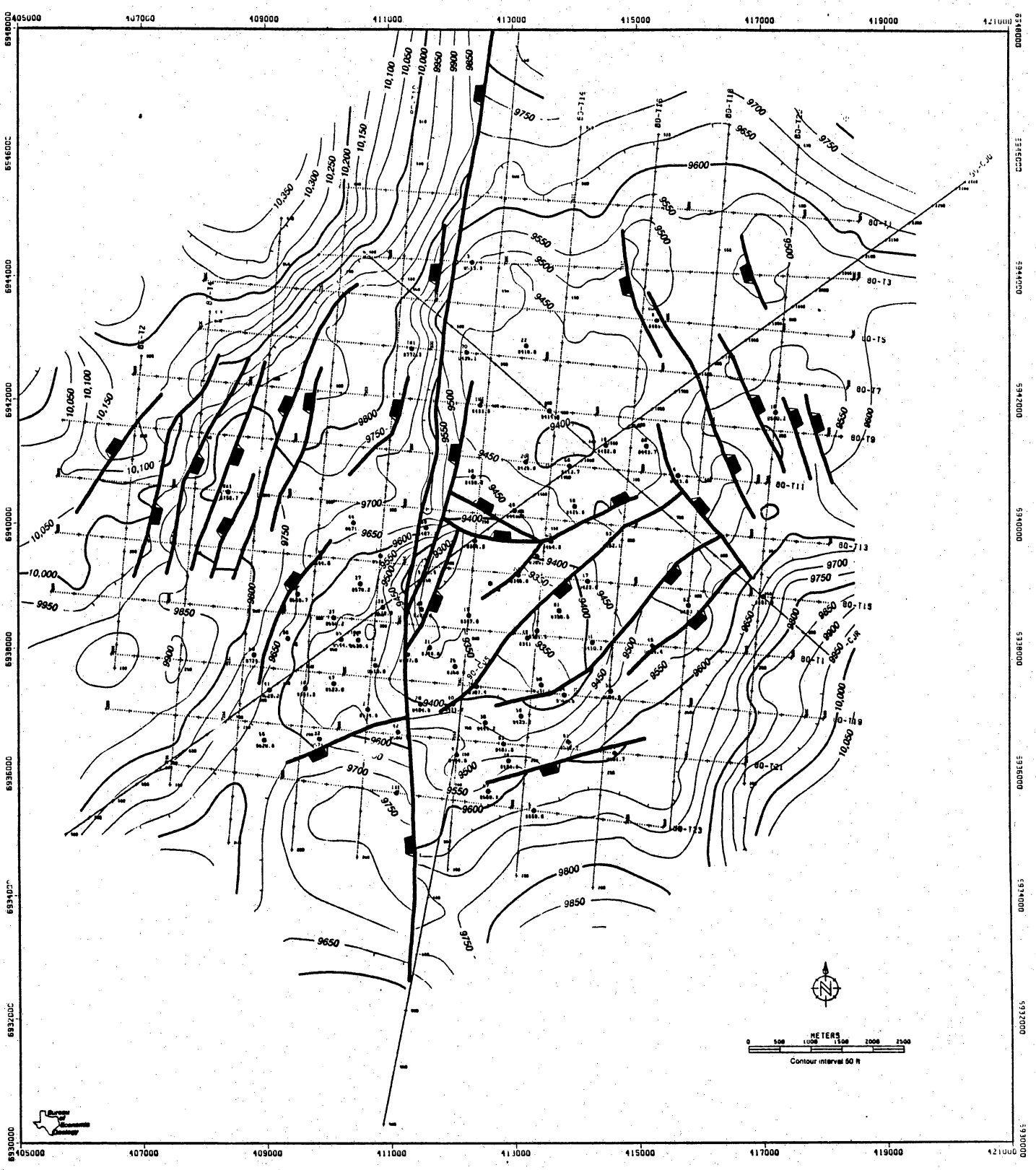

Tirrawarra Project – Orange Horizon – Depth map
ENCLOSURE IV 33

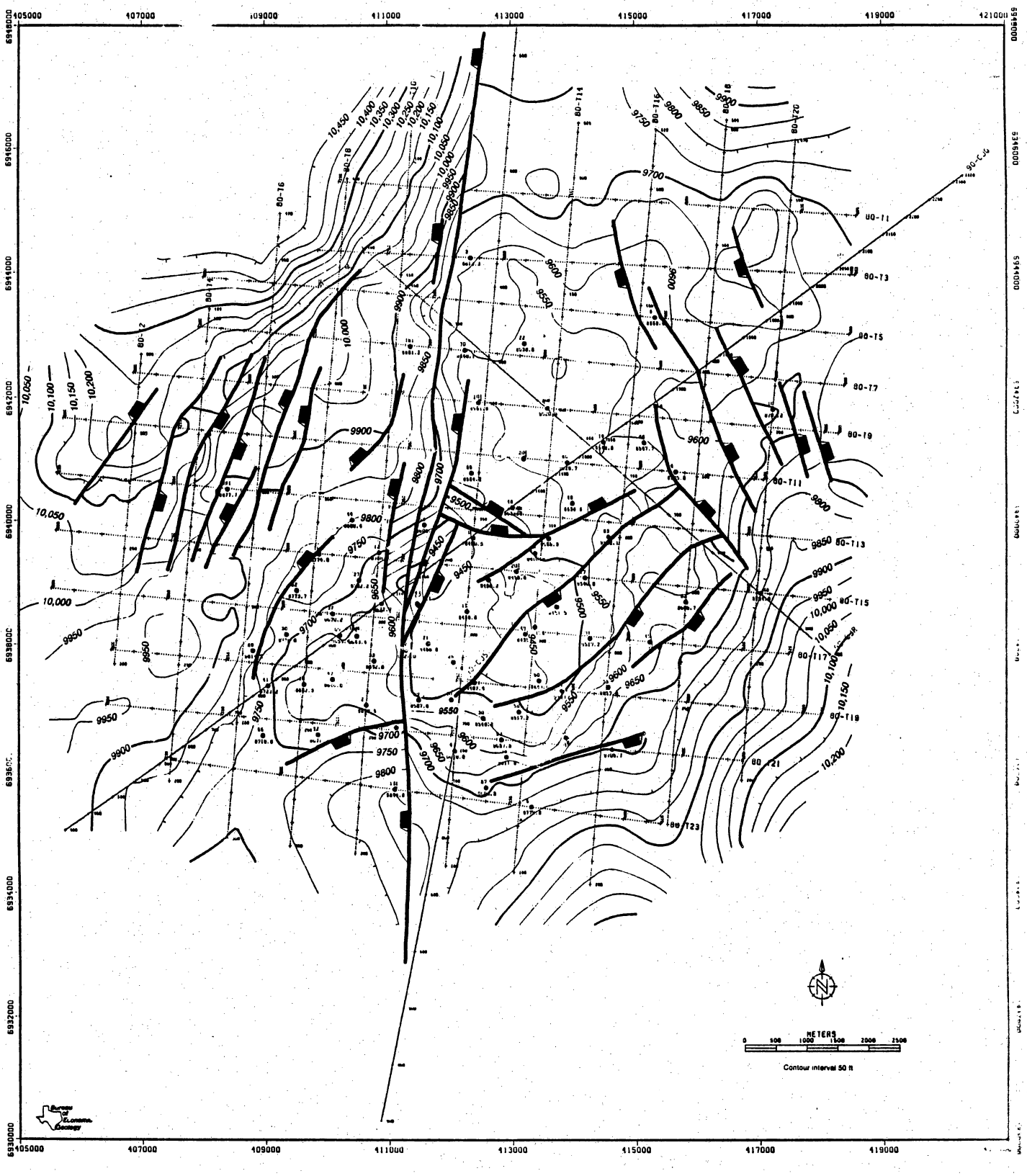

Tirrawarra Project – Reservoir Horizon – Depth map
ENCLOSURE IV - 34

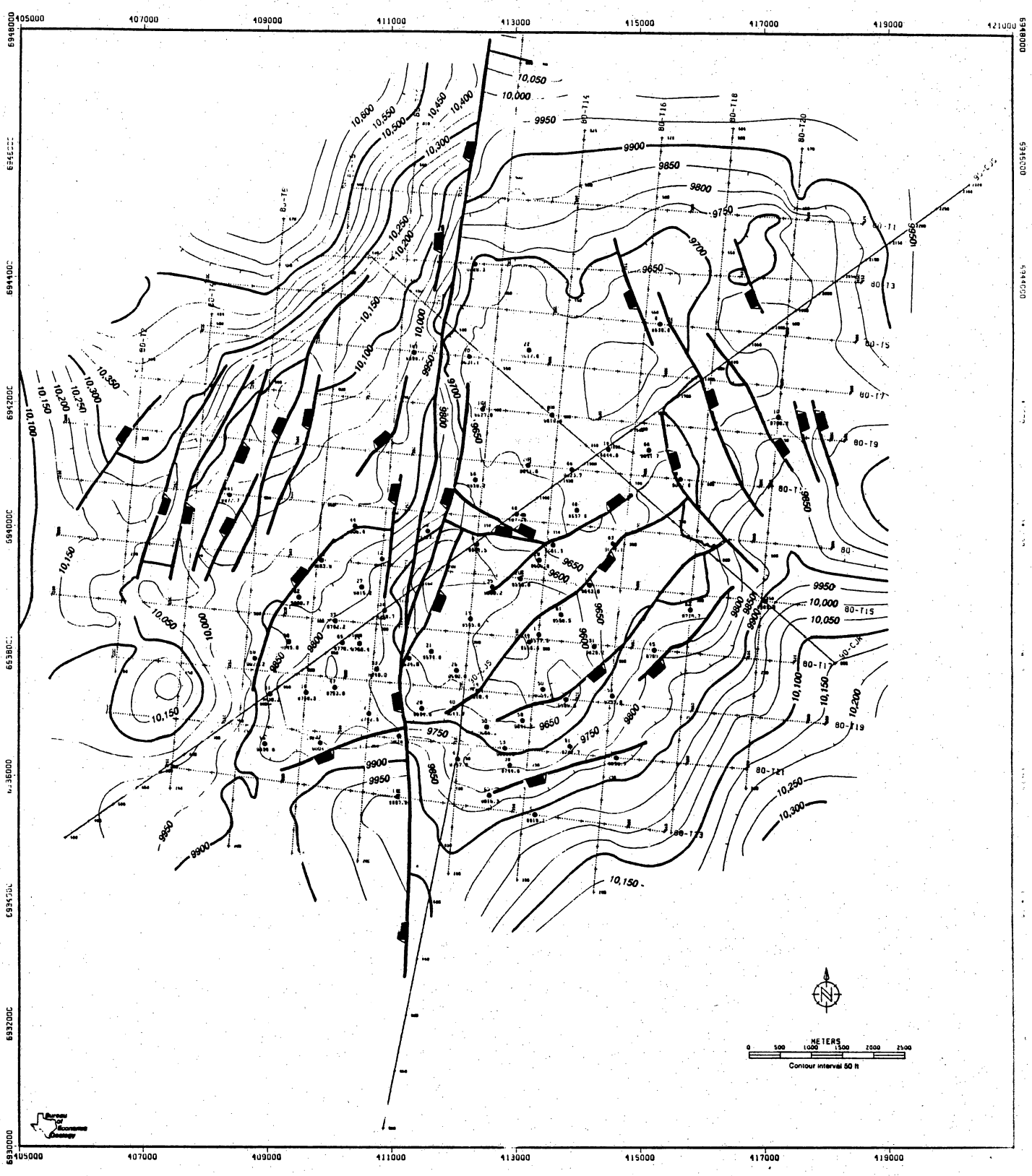

Tirrawarra Project – Merimelia Horizon – Depth map
ENCLOSURE IV - 35

east and west parts of the field are consistent with the regional fault orientations published by Heath (1989).

Discussion

Comparison of Santos and BEG Interpretations

The Santos technique used to construct depth maps in the report, *Tirrawarra Field Geophysical Mapping Status Report (Post no. 70),* is basically a three-step process consisting of (1) identification of the stratigraphic depth to the deepest, continuous seismic reflection event pervasive over the entire field, (2) use of well-based average velocities to convert the time picks for that reflection to depth values, and (3) construction of deeper depth structures by adding log-based depth isopachs to this reference depth structure. This approach to depth mapping should produce reliable depth structures when there is abundant well control to construct the incremental isopach maps.

The depth mapping technique used in this study also made extensive use of well control but differed from the Santos approach. The Bureau technique was to (1) determine the two-way travel time to the reservoir at as many velocity survey wells as possible, (2) identify the seismic reflection event corresponding to the reservoir at each of these check shot times, (3) extrapolate these reservoir picks across the entire seismic grid to construct a reservoir time structure map, (4) construct an average velocity map of the reservoir using log depths and interpolated travel times from the time structure maps at the field wells, and (5) combine this areal velocity map with the time structure map to create a reservoir depth map.

Both the Santos and the Bureau depth mapping techniques will produce reliable maps if care is taken at all steps of each process. As a consequence, the major difference between the Bureau depth maps and the Santos maps is not the depth values that are contoured but the fault patterns superimposed on these depth values. Since the seismic data allow a variety of reservoir fault interpretations to be made, reservoir pressure information and injector well-to-producer well connectivity test data provided by Santos was used to confirm the location of faults determined on seismic. Alternately, if well performance implied a fault existed, the seismic data were then examined to find evidence of the fault throw and orientation.

Several features exhibited by the BEG depth maps support known log correlations and well performances. For example,

- Tirrawarra 46 has received no pressure support from the Tirrawarra 60 injector whereas Tirrawarra 48 has received pressure support. The east-west fault in the center

of the field is therefore interpreted to be sealing and to be located to the north of Tirrawarra 60 but does not extend east of this well.

- Wells 13 and 23 are positioned on a narrow horst oriented NNE–SSW, and the fault on the west side of this horst block can explain why the reservoir at well 59, only 1 km to the north, is approximately 250 lower than it is in well 13.
- The fault on the east side of the horst where Tirrawarra 13 is located provides a possible explanation as to why there is reduced communication between Tirrawarra 13 and the injector well 15 about 1 km to the southeast (compared with other wells in this EOR pattern).
- The major north–south fault across the central part of the field separates production well 42 from the injection well 29, which can explain why production performance demonstrates these two wells are not in communication.

There are some differences between the reservoir depth structure map produced in this study and the "Depth to Top Tirrawarra" map dated 12/17/91 and issued as a part of the Santos report, *Tirrawarra Field Geophysical Mapping Status Report (Post no. 70)*, which will be referred to as the Santos map (enclosure IV-36, this report). The major differences between the BEG reservoir map and the Santos map are:

- The BEG map identifies more faults in the western part of the field near the Rakoona no. 1 well.
- In the northeast portion of the field, faults on the BEG map are oriented roughly northwest–southeast, but the faults on the Santos map are north–south. This interpretational difference occurs near the intersections of east–west seismic lines 80T-3, 5, 7, and 9 and north–south lines 80T-16, 18, and 20.
- In the southeast portion of the field, faults on the BEG map are oriented southwest–northeast, whereas the Santos-mapped faults are essentially north–south. The BEG interpretation also places a NE–SW-trending, low-throw fault near wells 17, 49, and 14, and this fault is absent in the Santos map. This fault is labeled X1 in the displays of seismic lines 80T-13, 15, 17, and 19 (figs. VI-8 through VI-11).
- The BEG map shows an additional fault immediately west of well 23 in the horst block in the center of the field (near the intersection of line 80T-15 with lines 80T-10 and 12).
- In the southwest portion of the field, the Santos map shows more faults than does the BEG map. Perhaps more importantly, the Santos faults are oriented northwest–southeast, but the faults most identified and mapped in this study trend southwest–northeast.

Certainly, elements of the BEG and Santos maps are in agreement. The differences in the two interpretations simply emphasize the difficulty that seismic interpreters have in constructing an image of a complicated, faulted structure using only 2-D seismic profiles across the structure.

Use of Revised Structure Map in OOIP Calculations

The revised structure map was not used in OOIP calculations. Because of problems with seismic interpretational software and difficulties in resolving and interpreting the poor quality Tirrawarra data, field structure was finalized late in the project. However, because preliminary versions of the revised structure map indicated broad similarity with the existing structure map the existing structure map (enclosure IV-36) was used to calculate OOIP.

Recommendations

VSP Calibration Control

Vertical seismic profiles (VSPs) are invaluable for calibrating subsurface stratigraphy to seismic travel time. In thin bed studies or in complex stratigraphic interpretations, VSP control has proven to be definitive for identifying the proper reflection phase to associate with a stratigraphic unit and superior to the velocity check shot approach. Consequently, VSP control should be considered in future seismic efforts in Tirrawarra field.

VSPs can be undertaken in either cemented or uncemented cased holes. Excellent VSP control has been recorded inside 2-7/8 inch tubing using slim-hole receivers. Good-quality VSP control could be acquired in several existing Tirrawarra wells by avoiding well intervals where there are *multiple* strings of casing which have an open annulus between the receiver and the formation. When there is only one string of casing, experience shows that usable VSP data can almost always be recorded in open annulus (i.e., uncemented) intervals. However, when there is more than one casing string, any open annulus seems to create resonating, unusable data.

Since mobilization/demobilization is a large component of the cost of a VSP, it is suggested that Santos could arrange for multiple VSPs to be run in existing wells during a single mobilization of a VSP crew to Tirrawarra field.

3-D Seismic Imaging

3-D seismic imaging is proving an invaluable source of information for reservoir characterization. The emphasis on 3-D seismic acquisition is now so strong in the U.S. that no 2-D seismic crews can be contracted; all seismic service companies offer strictly 3-D seismic recording. This dramatic switch from 2-D to 3-D imaging is in large part due to the advantages that 3-D seismic data offer in understanding producing reservoirs (i.e. in exploitation applications), and has been less influenced by exploration applications. As a result, the demand for 3-D seismic recording across onshore producing properties is now so great that the typical lead time between the signing of a contract with a service company and the arrival of the 3-D crew at the prospect is 6 to 10 months.

In high resolution seismic applications amazingly subtle reservoir stratigraphy can be revealed when a 3-D seismic program is properly designed and executed. Specifically, Bureau projects have imaged meandering channels as thin as 10 ft and as narrow as 200 ft at depths of 7,000 ft in Gulf Coast rocks. Based on the results of 3-D seismic evaluations of complex reservoirs done both within and outside of the Bureau, we encourage Santos to consider a 3-D seismic program at Tirrawarra field.

V. DEPOSITIONAL SYSTEMS

Genetic stratigraphy controls reservoir distribution and quality at several levels. At the largest scale, the depositional systems framework of the Cooper Basin controls regional sandstone distribution. Depositional systems are three-dimensional assemblages of sedimentary facies, which are deposited in genetically related environments (Fisher and McGowen, 1967). The fluvial-lacustrine depositional systems framework of the Cooper Basin provides a perspective for predicting geometry, spatial arrangement, and composition of component facies. The scale and focus of our study of the Tirrawarra reservoir was the facies level. Facies create discrete compartments in reservoirs, determine paths of fluid movement, influence saturations, and affect ultimate drainage efficiency (Tyler and Gholston, 1988).

Methodology

Core Description

Careful study and detailed description of cores from 29 Tirrawarra field wells provided the basis for identification and characterization of depositional facies. Macroscopic sedimentary characteristics of the cores were logged using standard sedimentologic techniques. A hand lens and binocular microscope were used to resolve small details and to estimate the range in sediment grain sizes present. The vertical scale of the core descriptions is 1 inch = 10 ft (appendix B). Color photographs were made of each box of Tirrawarra core. These photographs became especially valuable when used in conjunction with the core descriptions during subsequent facies evaluation and petrographic analysis in the United States.

Rock type is the first major feature noted on the descriptive log. In the Tirrawarra cores, three major rock types are present: sandstone, mudstone (silt + clay), and coal. Clean siltstone (without clay) was also noted in facies 1 in a few cores. The relative abundance of each rock type was estimated on a foot-by-foot basis and represented in the Rock Type column by the width of the corresponding symbol. For example, a shaly (muddy) sandstone might be represented as 60 percent sandstone and 40 percent mudstone. This permits core-to-log comparisons of approximate clay volumes. In the Rock Type column, single horizontal lines, whose lengths are roughly proportional to continuity and clay volume, represent mudstone layers less than 0.5 ft thick. Stylolites and contacts between different rock types are recorded in the column to the left of the Rock Type column.

Sedimentary structures, such as bedding and lamination styles, reflect flow dynamics in the depositional environment and commonly cause permeability anisotropy in the reservoir. Sedimentary structures are represented schematically and symbolically in the Structure column. Burrowing, organic fragments, mud clasts, and root traces are common sedimentary accessories in Tirrawarra cores; these features are noted in the narrow column to the left of the Structure column. The presence or absence of these accessories, along with bedding and lamination, provides important clues for environmental interpretation.

Grain size and sorting are controlled by both the sediment source area and the depositional environment. Sorting, a measure of grain-size range in sandstones, was judged qualitatively and noted in the Texture column. In the Grain Size column, the observed range of grain sizes is shaded. For example, a well-sorted sandstone that contained only fine and medium grains is represented by a narrow shaded column, whereas a muddy coarse sandstone is represented by a broad shaded column. The Grain Size column heading is calibrated with increasing grain size to the left. Grain size is an important control on Tirrawarra reservoir quality.

On the core description form, the columns to the right of the Grain Size column were used for miscellaneous notations and comments. Siderite cementation is noted in the narrow column to the right of the Grain Size column. Because it is easily obtainable from the core photos, Color was not always recorded. Stratification has already been described in the Structure column, and so this group of narrow columns was used for porosity, permeability, core-to-log depth correction, and sample locations for thin sections, palynology, and special core analyses. In the Comments column, boundaries between facies are shown, facies are briefly described, and any important features not adequately recorded elsewhere are noted. For example, natural fractures are noted in the Comments column, although fractures are also commonly shown graphically in the narrow column to the left of the Texture column.

Characterization of Facies and Flow Units

Tirrawarra depositional facies were identified on the basis of core observations combined with well log characteristics and petrophysical properties. Well logs, production and test data, and porosity and permeability data were continuously monitored during the core description process. Recurring bodies of rock having similar lithologies, sedimentary structures and textures, log expressions, and petrophysical properties were interpreted to have been deposited in similar environments and thus were identified as the major Tirrawarra facies as well as the fundamental reservoir divisions. Previous studies on the regional stratigraphic and paleogeographic framework provided the larger scale context for preliminary characterization

of Tirrawarra depositional environments. Assigning a specific environment to each Tirrawarra facies allowed predictions to be made about three-dimensional geometries and interwell heterogeneities on the basis of well-established depositional facies models.

Because well logs respond to rock properties such as lithology, porosity, and permeability, distinctive log patterns were used to identify Tirrawarra facies in uncored wells. Accurate core gamma scans, which were made during the core-description phase of the project, allowed us to correctly match core properties to well log responses to within 0.5 ft. Typical log responses through cored intervals of each facies were documented. Correlations between cored and uncored wells were made systematically along a grid of closely spaced cross sections (plates V-1 through V-13). Correlation of continuous horizons above and below the Tirrawarra reservoir provided the stratigraphic context for facies correlation within the reservoir. Alignment of these continuous horizons along well log cross sections correctly juxtaposed the reservoir intervals on adjacent logs. The well-to-well continuity of each facies was then delineated by similarity both to the established typical log responses and to the actual log responses in the nearest cored wells. Facies boundaries were picked where log responses changed significantly between wells. These techniques were reiterated until consistency was achieved throughout all the wells in the field.

Petrophysical data measured in core samples at ambient conditions provide the basis for quantifying facies-related variability in reservoir properties in order to identify flow units. A flow unit is a discrete reservoir zone having a characteristic range of geologic and petrophysical properties (Hearn and others, 1984). Facies are bodies of rock having lithologies, textures, and structures that can be attributed to deposition in a specific type of environment. Reservoir properties are strongly influenced by depositional facies. Within each facies, one or more flow units can be delineated according to fluid-transmission abilities. A facies may vary in stratigraphic position and internal properties, but a flow unit is a specific zone that has quantifiable, although not necessarily homogeneous, properties. Petrophysical data were statistically analyzed to obtain averages, variabilities, porosity/permeability relationships, and pay cutoff values for each flow unit.

Contour maps were constructed to document lateral variations in thickness and reservoir quality in each flow unit. Maps of gross unit thickness (isopach), net porous sandstone, and permeability-thickness (kh) display the basic facies-related dimensions and internal properties of each flow unit. Sandstone geometries and trend orientations provided data for environmental interpretation and paleogeographic reconstruction. Flow unit maps also provided the basic input for (1) modeling three-dimensional reservoir architecture on Stratamodel, (2) mapping pay distribution, and (3) calculating and allocating original oil in place. Well log responses, correlations, and lateral continuities are displayed on a grid of detailed

stratigraphic cross sections. Geological characterizations of Tirrawarra facies and their component flow units are primarily based on the contour maps, stratigraphic cross sections, and core descriptions.

Tirrawarra Facies

On the basis of studies of core, well log responses, and petrophysical properties, Tirrawarra depositional facies were characterized and depositional environments were interpreted. Depositional facies are bodies of sedimentary rock in which distinctive lithologies and sedimentary structures and textures can be attributed to the physical processes of deposition in a specific environment. Facies display a variable (but systematic) distribution within the larger depositional system, and reservoir properties commonly vary within facies. Because of these variations, flow units were identified to document and quantify facies-dependent reservoir behavior in Tirrawarra field. A flow unit is a reservoir zone that has similar petrophysical properties and well log responses and is continuous laterally and vertically (Hearn and others, 1984). Basic descriptions and depositional interpretations of each Tirrawarra facies are given below and summarized in tables V-1 through V-4.

Facies 1

Core Description

Facies 1 is composed of mudstone, siltstone, and very fine grained sandstone (fig. V-1, table V-1). These rocks are generally light to dark gray in color; organic (carbonaceous) debris appears to be a minor component. Bands and patches of siderite cement are common in the silt and sand fraction. The lower part of facies 1 is dominated by thin (mm) varve-like laminations of alternating mudstone and siltstone. The siltstone laminations are slightly lenticular (small ripples). Horizontally laminated mudstone beds up to several feet thick are also common. Soft-sediment deformation is abundant throughout the lower part of facies 1. Finely laminated beds are commonly folded, contorted, and microfaulted. Bioturbation occurs as isolated burrows, churned zones, and bedding plane feeding trails. The lower part of facies 1 includes a distinctive siltstone/sandstone bed, 2 to 5 ft thick, displaying wave and current ripples and hummocky to wavy lamination (fig. V-2). This bed is continuous across Tirrawarra field and forms the "red" correlation horizon, which is essentially the lower limit of our study interval.

Table V-1. Characteristics of facies 1.

Composition	sandstone, siltstone, minor mudstone
Texture	very fine grained, poorly to moderately sorted
Sedimentary Structures	climbing ripples, ripple trough crossbeds, hummocky bedding, wave ripples, wavy/lenticular lamination
Sedimentary Accessories	soft-sediment deformation, burrows, rare mud clasts
Vertical Trend	lower contact gradational, upward coarsening
Tectonic Structures	rare small faults and natural fractures
Well Log Patterns	gamma ray upward decreasing, resistivities baseline to slightly upward increasing
Interpretation	delta front prograding into lacustrine basin
Unit Thickness	lobes, 10-17 ft thick, 2-3 km long, 0.5-2 km wide
Porous Sandstone	isolated pods,
Reservoir Quality	marginal but homogeneous internally
Boundary Conditions	upper boundary rarely permeable

Table V-2. Characteristics of facies 2.

Composition	sandstone, mudstone, minor conglomerate
Texture	wide range of grain sizes, very poorly to moderately sorted
Sedimentary Structures	sandstone: small to medium trough crossbeds, wavy/lenticular lamination, gently inclined and horizontal lamination; mudstone: poorly laminated, mottled, horizontal lamination
Sedimentary Accessories	mud clasts, organic debris, soft-sediment deformation, root traces and burrows in mudstone
Vertical Trend	lower contact generally sharp to erosional but locally gradational, multiple fining upward sequences, internal scour and erosional surfaces
Tectonic Structures	stylolites and fractures common locally in clean sandstone
Well Log Patterns	gamma ray high and variable, borehole irregular
Interpretation	deltaic distributary channel and channel mouth bar
Unit Thickness	unit 2L: sinuous belts (northwest), 10-30 ft thick, 1-3 km wide, broad lobe (southeast), 20 ft thick unit 2U: lobate wedge in southwest, 0-35 ft thick
Porous Sandstone	unit 2L: coincides with thickness trends, southeast unit 2U: isolated wells in southwest,
Reservoir Quality	internally heterogeneous, interlayered discontinuous k trends, kh coincides with porous sandstone
Boundary Conditions	unit 2L: boundaries rarely permeable unit 2U: boundaries generally impermeable

Table V-3. Characteristics of facies 3.

Composition	sandstone, minor mudstone
Texture	fine to coarse sand, minor gravel, moderate to well sorted
Sedimentary Structures	gently inclined and horizontal plane beds, trough and tabular crossbeds, massive
Sedimentary Accessories	thin muddy sandstone and mudstone interbeds, soft-sediment deformation, minor mud clasts and organic fragments
Vertical Trend	lower contact generally sharp but locally erosional ro gradational, homogeneous to slightly upward fining
Tectonic Structures	stylolites abundant throughout, fractures and small faults abundant locally
Well Log Patterns	gamma ray low and smooth, resistivities decrease upward, sonic log porosities high, borehole enlargement in unit 3U
Interpretation	braid delta plain composed of broad shallow channels, some lacustrine shorezone reworking
Unit Thickness	tabular, 40-100 ft thick (3L + 3U), multidirectional thickness trends, "sheet with holes"
Porous Sandstone	similar to thickness patterns, unit 3L is 30-60 ft thick except in northeast, unit 3U is 30-60 ft thick in broad belts and pods
Reservoir Quality	generally good but variable k distribution, kh dominated by high k thin zones, low k zones thin and discontinuous
Boundary Conditions	unit 3L: lower boundary (with 2L) commonly impermeable, upper boundary (with 3U) mostly permeable unit 3U: upper boundary with 2U impermeable, and with 4 impermeable except in north and in center of field

Table V-4. Characteristics of facies 4.

Composition	sandstone, mudstone, conglomerate, coal
Texture	wide range of grain sizes, very poorly to moderately sorted
Sedimentary Structures	sandstone: trough and tabular crossbeds, ripple crossbeds, horizontal and wavy lamination; conglomerate: lags, single pebble layers, granule beds up to several ft thick; mudstone: wispy/irregular lamination, mottled, poorly laminated
Sedimentary Accessories	mud clasts, organic fragments, soft-sediment deformation, root traces and burrows in mudstone, coal laminations and beds up to several ft thick
Vertical Trend	lower contact erosional, abundant internal erosional surfaces, multiple upward fining sequences, mudstone and coal become more abundant upward
Tectonic Structures	stylolites locally abundant in clean sandstone, minor fractures
Well Log Patterns	gamma ray variable with large-scale upward increase, resistivities highest in reservoir
Interpretation	braidplain evolving into meandering stream system, lacustrine basin now subaerial and heavily vegetated
Unit Thickness	southeast trending belts, 30-60 ft thick, 1-3 km wide, interbelt areas, 10-30 ft thick, 1-2 km wide, general northeast thickening
Porous Sandstone	coincides with unit thickness trends, 10-40 ft thick in belts,
Reservoir Quality	partly to completely isolated k compartments, kh best developed in stacked channel belts
Boundary Conditions	upper boundary marked by lenticular sandstones enclosed in mudstone and coal, lower boundary impermeable except in north and in central part of field

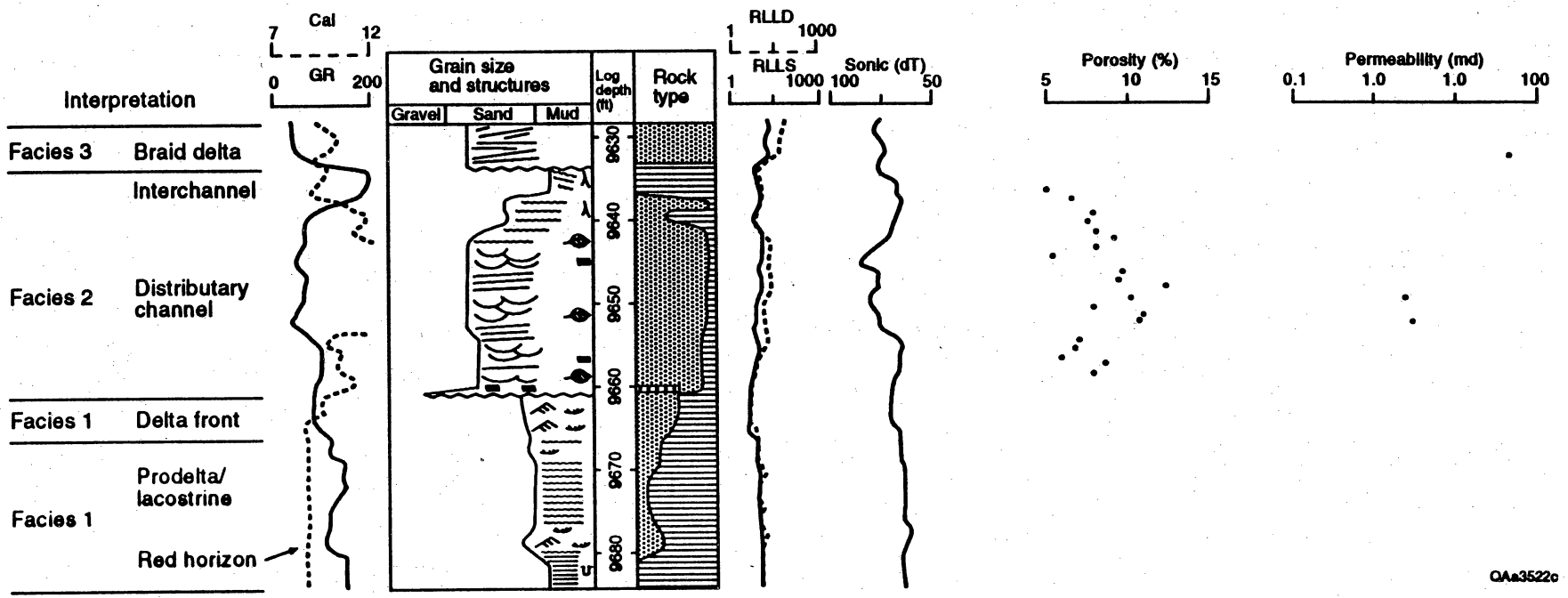

Figure V-1. Core description, log responses, and petrophysical properties from facies 1 and 2, Tirrawarra well 8. For explanation of symbols see appendix B.

T2 9883'

Figure V-2. Photographs of core from facies 1 and 2: (a) siltstone and very fine sandstone from facies 1 displaying wave and current ripples and wavy to hummocky lamination (core diameter is 10 cm), and (b) ripple drift cross-lamination in white, very fine sandstone (facies 1) erosionally truncated and overlain by conglomeratic sandstone having large mud clasts and coal fragments (facies 2).

INCH
DEAN
MADE IN
ENGLAND
FIBREGLASS
TAPE
CM
TIRRAWARRA No 21. CORE 4.
9709'3"---9710'1"
TOP.
BOTTOM.

The mudstone-dominated lower part of facies 1 grades upward into the more sandstone rich upper part of facies 1 (fig. V-1). Climbing ripple (ripple drift) cross lamination in very fine grained sandstone and siltstone characterize this interval (fig. V-2). Mudstone generally occurs as isolated laminations and lenses (flasers) and is volumetrically minor. Soft-sediment deformation, bioturbation, and rare mud clasts are also present. Stylolites and visible organic material are absent. An upward-coarsening/cleaning trend is well developed in the upper part of facies 1. Relatively clean siltstone/sandstone, 1 to 15 ft thick, caps the sequence except where it has been erosionally truncated by overlying facies.

Interpretation

Facies 1 exhibits features consistent with deposition in a glaciolacustrine basin. The thinly interlaminated mudstone and siltstone layers are probably seasonal rhythmites—glacial varves—that were transported into the center of the lake by turbidity currents (Ashley, 1975). These deposits formed a prodelta platform over which coarser, more proximal delta front facies prograded (fig. V-3). Deposition of the laterally extensive "red horizon" bed records either a major storm or a catastrophic flood caused by glacial melting. In the upper part of facies 1, the climbing ripple lamination and the upward-coarsening trend support deposition in a prograding delta front environment (Gustavson and others, 1975).

Facies 2

Core Description

Facies 2 comprises a heterogeneous suite of sandstone, mudstone, and minor conglomerate (figs. V-1 and V-4, table V-2). Mud clasts and organic debris (coal fragments) are ubiquitous, finely disseminated in mudstones, and up to gravel sized in coarser grained rocks (fig. V-2). The different facies 2 rock types are complexly interbedded and intermixed. Muddy sandstone is volumetrically dominant, composing the entire facies in some wells. In muddy sandstone detrital silt and clay occur as pore-filling matrix, interlaminations, and clasts. Mudstone-dominated rocks are generally poorly laminated; mottled textures and root traces are common. Mudstone layers locally reach 10 to 20 ft in thickness. Sandstones typically contain variable amounts of mud, but clean sandstone occurs locally, generally in beds less than 4 ft thick but rarely reaching 10 ft. Clean sandstone in facies 2 is visually similar to facies 3 sandstone. Stylolites and natural fractures in facies 2 are generally restricted to clean sandstone layers. Conglomerate occurs as thin pebble layers and in thicker beds of conglomeratic sandstone.

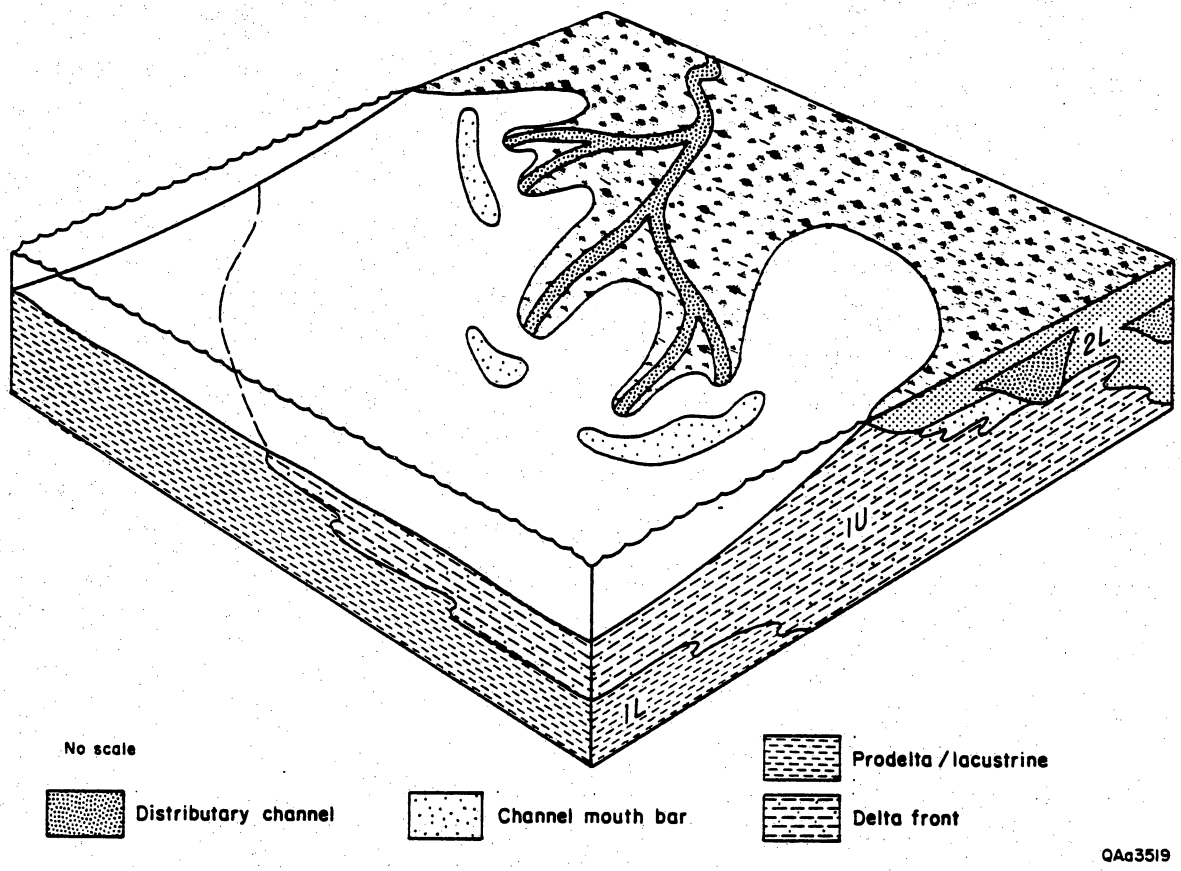

Figure V-3. Depositional model for facies 1 and 2 showing a fluvially dominated delta prograding across fine-grained lacustrine deposits. Both channel mouth-bar and delta-front deposits are truncated locally by downcutting distributary channels.

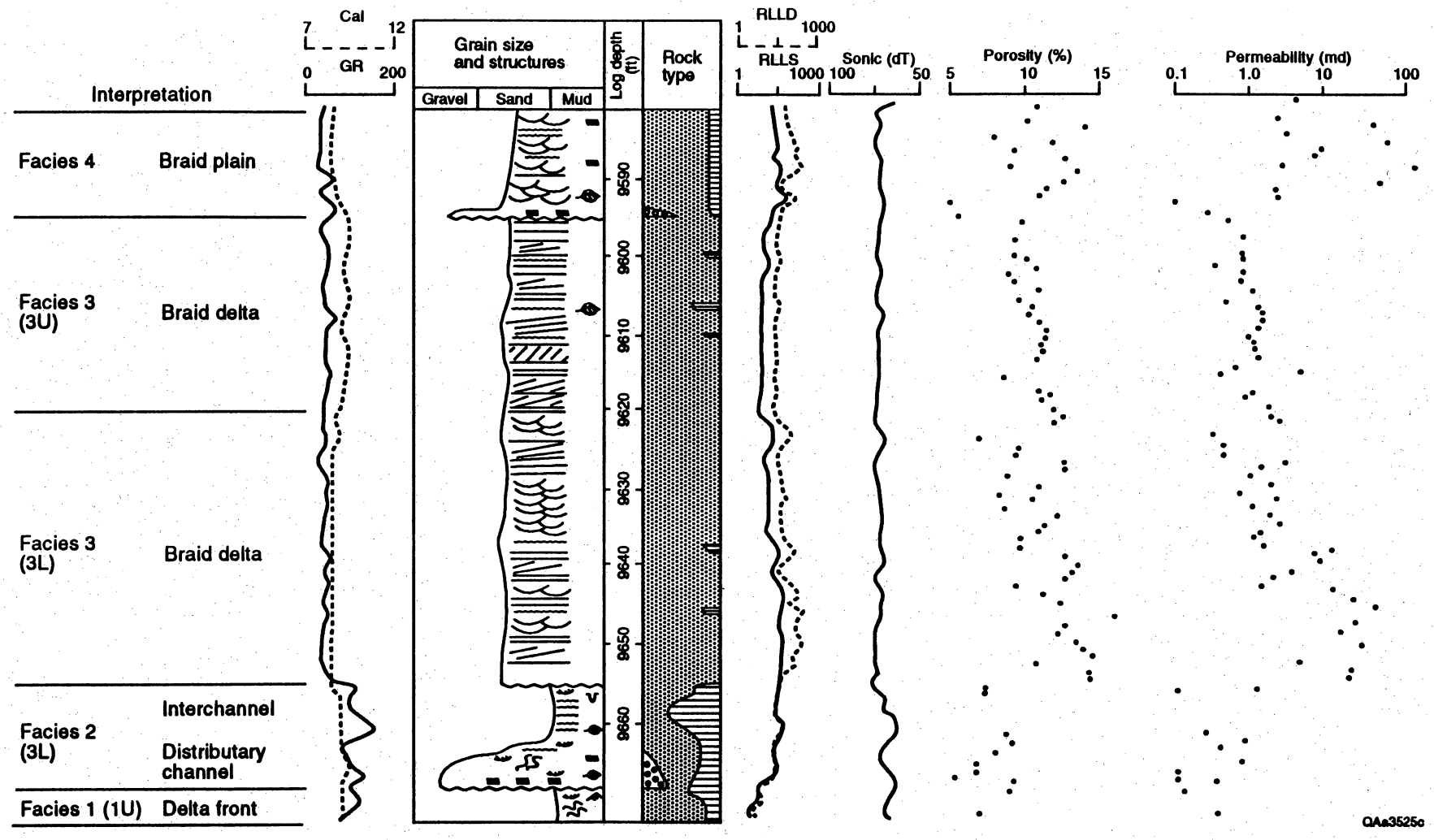

Figure V-4. Core description, log responses, and petrophysical properties from facies 1, 2, 3, and 4, Tirrawarra well 20. For explanation of symbols see appendix B.

A diverse range of sedimentary structures and accessories characterize facies 2 sandstones. Small (ripple) trough crossbeds, and wavy/lenticular lamination are most abundant in finer grained, muddier sandstone. Coarser, cleaner sandstones generally contain somewhat larger trough crossbed sets (up to 1 ft thick), massive bedding, and (more rarely) gently inclined to horizontal lamination. All sandstone bedding types are commonly disrupted by syndepositional slumping and folding (soft-sediment deformation). Internal erosion surfaces overlain by mud clast and pebble lags occur throughout facies 2. Upward-fining sequences commonly overlie these erosion surfaces. Where facies 2 overlies facies 1, its lower contact may be erosional, sharp, or (less commonly) gradational (fig. V-2).

Interpretation

The deposition of facies 2 probably records progradation of deltaic distributary channels across the delta front (fig. V-3). The cleaner, coarser grained sandstones in facies 2 were deposited in distributary channels and proximal channel mouth bars, although many of the channel-fill sequences were choked with mud clasts and plant debris. The finer grained, muddier sandstones were deposited in channel-flank environments, such as natural levees and crevasse splays, and in the more distal and marginal parts of the channel mouth bars. The poorly laminated, carbonaceous mudstones were deposited in abandoned distributary channels, whereas bioturbated mudstones were probably deposited in interdistributary marshes and bays. Because subsidence rates were probably relatively low in this intracratonic basin, facies 2 distributary channels commonly incised into underlying channel mouth bar and delta-front sediments.

Facies 3

Core Description

Facies 3 is composed primarily of clean sandstone that is moderately to well sorted and fine- to coarse-grained (figs. V-4 and V-5, table V-3). Gravel and mud clasts are common but volumetrically minor, displaying an isolated or scattered distribution. Oil staining is prominent locally in facies 3 sandstone (fig. V-6). Clean sandstones (lacking muddy laminations) are generally 3 to 10 ft thick, although 20-ft clean layers are common, and clean zones up to 40 ft thick are present in a few Tirrawarra cores. Silt and clay are typically restricted to thin laminations of sandy mudstone and muddy sandstone, where organic debris and siderite cement

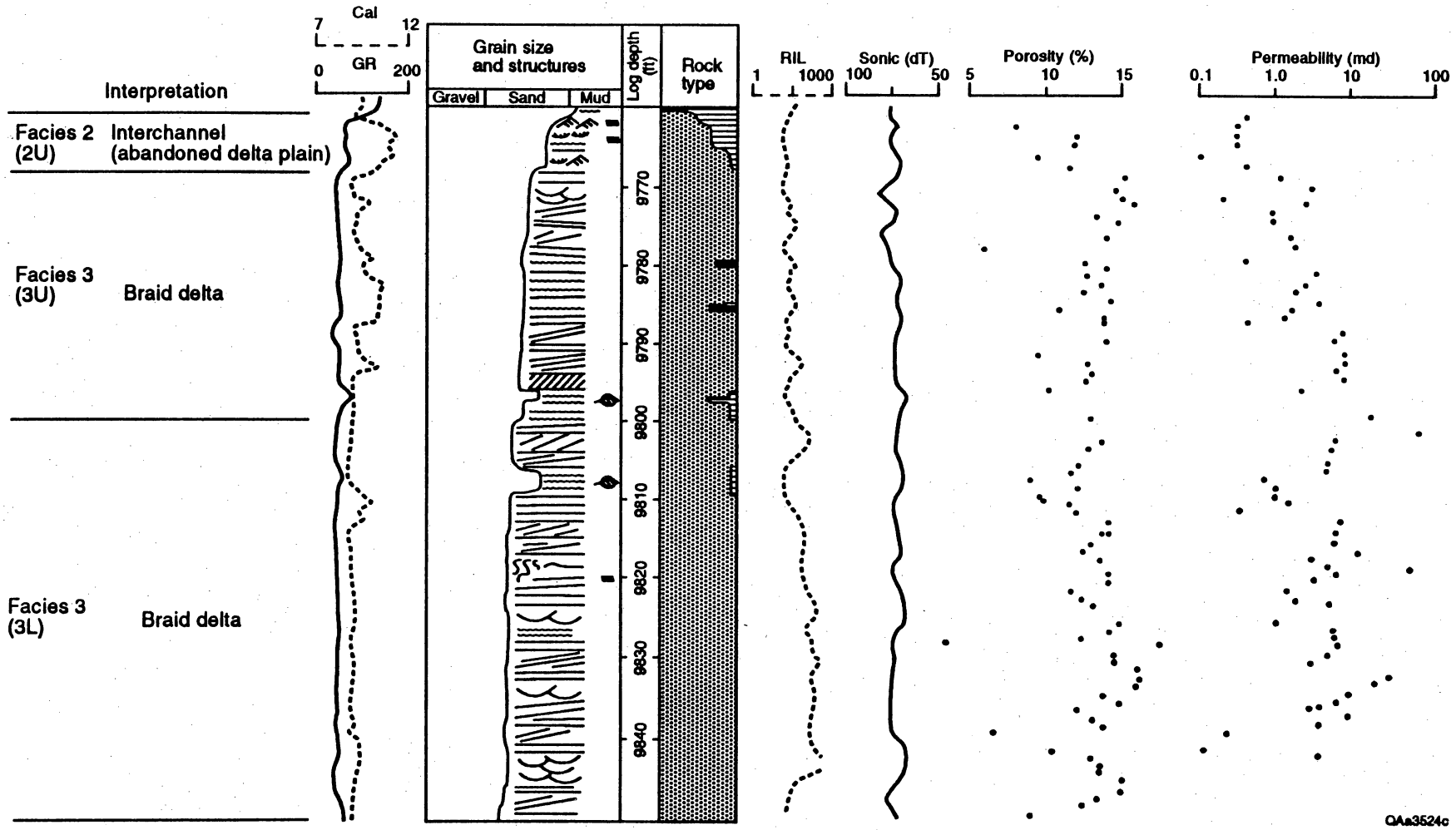

Figure V-5. Core description, log responses, and petrophysical properties from facies 2 and 3, Tirrawarra well 2. For explanation of symbols see appendix B.

Figure V-6. Photographs of core from facies 3: (a) well-sorted medium-grained sandstone displaying horizontal lamination and light brown oil stains, and (b) medium- to fine-grained sandstone displaying abundant small stylolites parallel to lamination and a thin organic-rich muddy sandstone bed at the top.

TIRRAWARRA No 21. CORE 2.
9665'4"---9666'1"
TOP.
BOTTOM.

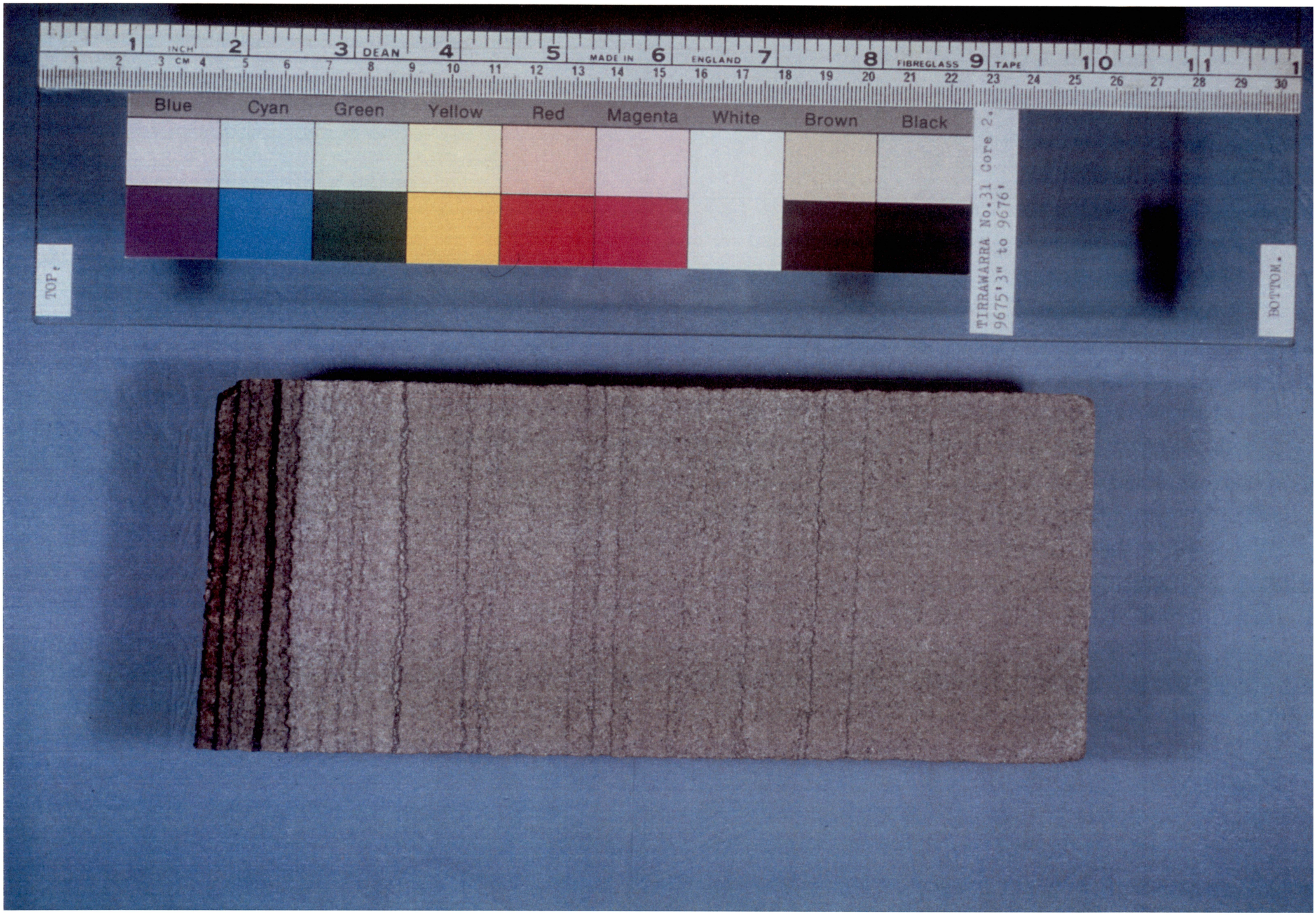
Blue
Cyan
Green
Yellow
Red
Magenta
White
Brown
Black
TOP.
TIRRAWARRA No.31 Core 2.
9675'3" to 9676'
BOTTOM.

are common accessory components. These muddy layers are generally less than 5 cm thick, but thicker layers (up to 3 ft), composed of fine grained sandstone with muddy lenses and laminations, occur locally (fig. V-5). Less commonly present in facies 3 are zones, composed of poorly sorted carbonaceous sandstone, that appear transitional with facies 2.

Horizontal to gently inclined planar bedding is the dominant sedimentary structure in facies 3 sandstone (fig. V-6). Low-angle discordances are common within the planar bedded sequences. Shallow trough crossbeds, having gently inclined, curving cross-laminae, are the second most abundant structure in facies 3 sandstone. Trough and tabular crossbeds, having more steeply inclined cross-laminae, are also common locally. Facies 3 crossbeds range in thickness from a few inches to about 2 ft. In clean sandstone, lamination is sufficiently indistinct locally to give the rock a massive appearance. In the finer grained sandstones and muddy sandstones, ripple trough cross-lamination and wavy/lenticular lamination are well displayed. Soft-sediment deformation is present locally in all facies 3 rock types. Bioturbation is rare in the clean sandstones but is common in the muddy sandstones. Internal scour surfaces occur locally, but lags of pebbles or mud clasts are rare. The basal contact of facies 3 is generally sharp to erosional. Large-scale vertical trends either are not apparent or are slightly upward fining.

Stylolites are ubiquitous in facies 3. The stylolites, which are pressure-solution fronts, typically appear in core as irregularly serrated dark lines. Rare truncated pebbles document the rock dissolution that generated the stylolite. The dark material may be insoluble residue or muddy/carbonaceous laminae that have become incorporated in the stylolite. This material probably results in low permeability across the stylolite. Most stylolites in facies 3 have amplitudes of about 1 mm, but a few have amplitudes reaching 1 cm. Tiny stylolites commonly occur closely spaced within a few centimeters of rock (fig. V-6), larger ones are typically more widely spaced. Stylolites are generally concentrated in groups, several meters of rock having relatively few stylolites alternating with densely stylolitized rock. In Tirrawarra cores, there does not appear to be any relationship between stylolitization and depth or location within the field. Unlike in the other facies, stylolites in facies 3 are not preferentially concentrated in clean sandstone; most of the thin muddy layers also contain stylolites. Most stylolites in facies 3 are horizontal and parallel to lamination (fig. V-6), but there are numerous exceptions. Steeply dipping and complexly crosscutting stylolites occur locally. Prominent dipping stylolites parallel inclined lamination in crossbeds, but these same crossbeds can also contain horizontal stylolites that cut across lamination.

Natural fractures and small faults are common in core from facies 3. These fractures are generally vertical to subvertical and closed; importantly, no open fractures were observed. The vertical extent of these fractures, where their terminations lie within the core, is typically only

a few inches to about 1 ft. Multiple, closely spaced fracture strands are common. Many facies 3 fractures are filled with an unknown black material; fractures filled with white clay or quartz are less common. Some vertical stylolites appear to be associated with fractures. Complex crosscutting relationships indicate multiple generations of both fractures and stylolites. Differences in oil staining and cementation occur locally across fractures, indicating some control on permeability and fluid migration. Minor fractures were observed in most cores, but prominent facies 3 fractures occur in cores from Tirrawarra wells 3, 5, 18, 31, and West 1, and they are especially abundant in cores from wells 11, 13, 21, and 42.

Interpretation

The depositional style of facies 3 represents a distinct change from that of underlying facies. Based on sedimentary features in facies 3, together with its stratigraphic context, this facies formed when a large braid delta (as defined by McPherson and others, 1987) prograded into the lake basin (fig. V-7). Most of facies 3 was deposited in broad, shallow, laterally coalescing fluvial channels. The abundance of gently inclined to horizontal planar bedding suggests that poorly channelized sheet floods were an important depositional mechanism (McGowen, 1970; Miall, 1981). Sheet flooding implies highly variable fluvial discharge, which is consistent with a glacial outwash plain (sandur) setting (Church and Gilbert, 1975). During periods of low fluvial discharge, the lower delta plain may have been partly reworked by lacustrine shorezone processes (principally storm waves). Transgressive shorezone deposits are typically thin, and lack of bioturbation suggests that the thick clean sandstones are primarily fluvial in origin. The thin muddy sandstones, which are commonly bioturbated, may have originated in several different environments: channel flank (overbank), abandoned channel, and transgressive lake margin.

Deposition of facies 3 largely postdates that of the lower development of facies 2, which appears to be erosionally truncated in places by facies 3. Nevertheless, local gradational contacts between facies 2 and facies 3 and the presence of transitional lithologies in both facies suggest at least some concurrent deposition.

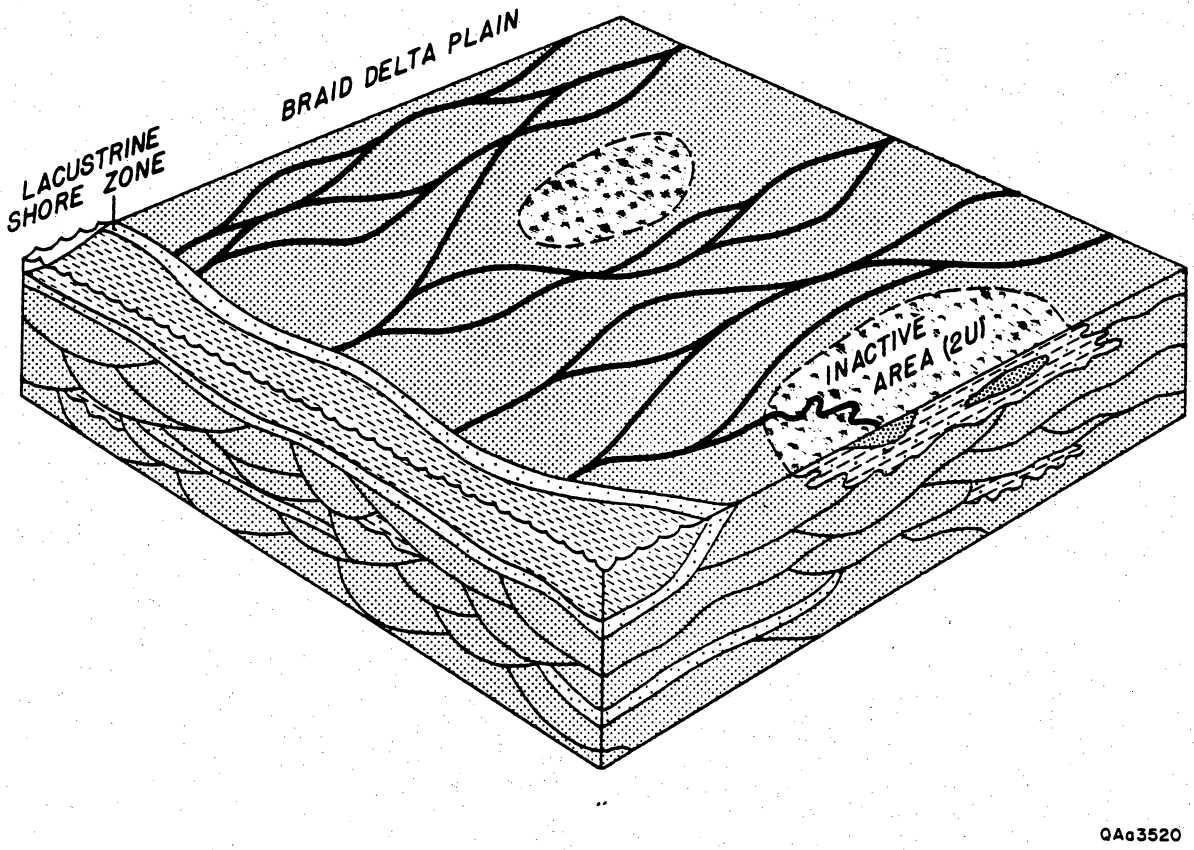

Figure V-7. Depositional model for facies 2 and 3 showing a braid delta composed of laterally coalescing fluvial channels and a narrow lacustrine shore zone. Facies 3 was deposited primarily by active bed-load-dominated channels and associated sheet floods, whereas the upper part of facies 2 accumulated in vegetated areas away from active channel migration.

Facies 4

Core Description

Facies 4 comprises sandstone, conglomerate, mudstone, and coal (figs. V-4 and V-8, table V-4). Muddy sandstone and sandy mudstone are probably the most important volumetrically, although clean sandstone is better developed in facies 4 than it is in facies 2. As in facies 2, organic fragments and mud clasts are abundant throughout. Thin pebble conglomerates, which are rare in facies 2, are common in facies 4 (fig. V-9). These conglomerates are typically less than 1 ft thick, although the individual pebbles reach several inches in diameter locally. These pebbles are locally sutured together along stylolitic boundaries. Finer grained conglomerates, composed of small pebbles, granules, and very coarse sand, occur in beds up to 3 ft thick in several cores (fig. V-9). Clean sandstones range in thickness from a few inches to about 10 ft generally but reach 20 ft in thickness more rarely. In several cores, relatively clean sandstones displayed visually enhanced porosity, owing to apparent dissolution of coarse sand grains. Thin mudstone beds and laminations are common in facies 4 sandstone and conglomerate. Thicker organic-rich mudstones reach 20 to 30 ft in thickness in a few cores and typically have thin sandstone and coal interbeds. Coal is present in beds ranging from a few inches to 3 ft in thickness (fig. V-8). Stylolites similar to those in facies 3 occur in most facies 4 clean sandstone, but natural fractures are relatively rare in facies 4 cores.

A variety of sedimentary structures and associated features were observed in facies 4 cores. Cleaner, coarser sandstones display (common) trough and tabular crossbeds and (less common) gently inclined to horizontal plane beds. Crossbeds are generally less than 1 ft thick. Finer grained sandstones and interlaminated mudstone and sandstone typically have ripple cross lamination and wavy/lenticular lamination. Mudstones are either poorly laminated or contain irregular horizontal laminations. Finely disseminated organic debris, mottled textures, root traces, and burrows are common in facies 4 mudstones. Gravel-size mud clasts and coal fragments are common in the sandstones and conglomerates (fig. V-9). Soft-sediment deformation is present in all lithologies but is most abundant in sandstones. The lower contact of facies 4 is commonly erosional, and internal erosion surfaces are common. Pebble and mud clast lags and thin (less than about 10 ft) upward-fining sequences overlie most erosional surfaces. The larger-scale upward trend in facies 4 (although irregularly developed) is thinner and fewer sandstones and thicker and more numerous mudstones and coals. Conglomerate also decreases in abundance upward in facies 4.

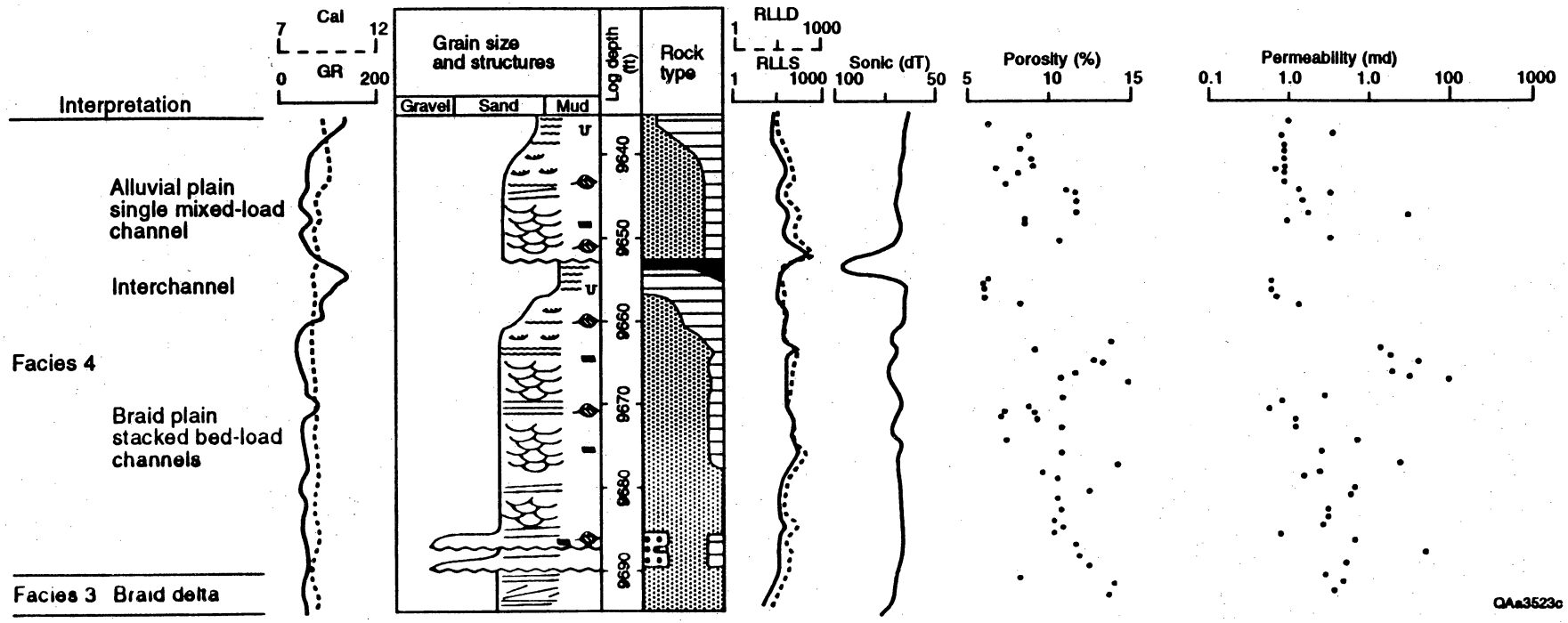

Figure V-8. Core description, log responses, and petrophysical properties from facies 4, Tirrawarra well 16. For explanation of symbols see appendix B.

Figure V-9. Photographs of core from facies 4: (a) conglomeratic sandstone with abundant flat mud clasts and organic fragments and a pebble layer near the base, and (b) crossbedded granule conglomerate at the base of facies 4 overlying fine-grained sandstone at the top of facies 3. The erosional unconformity at the base of facies 4 is marked in (b) by a thin dark bed of flattened mud clasts and coal fragments.

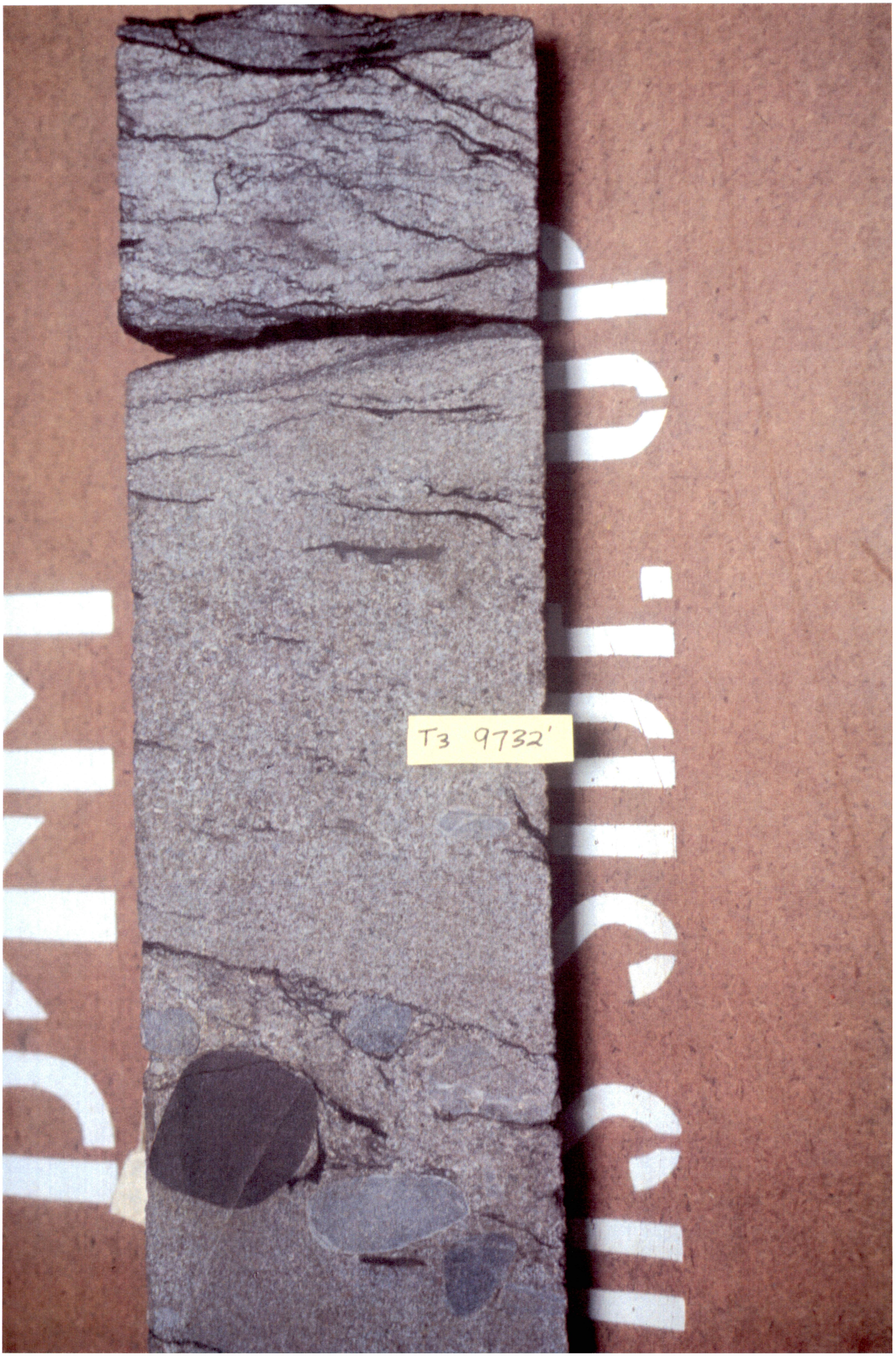
T3 9732'

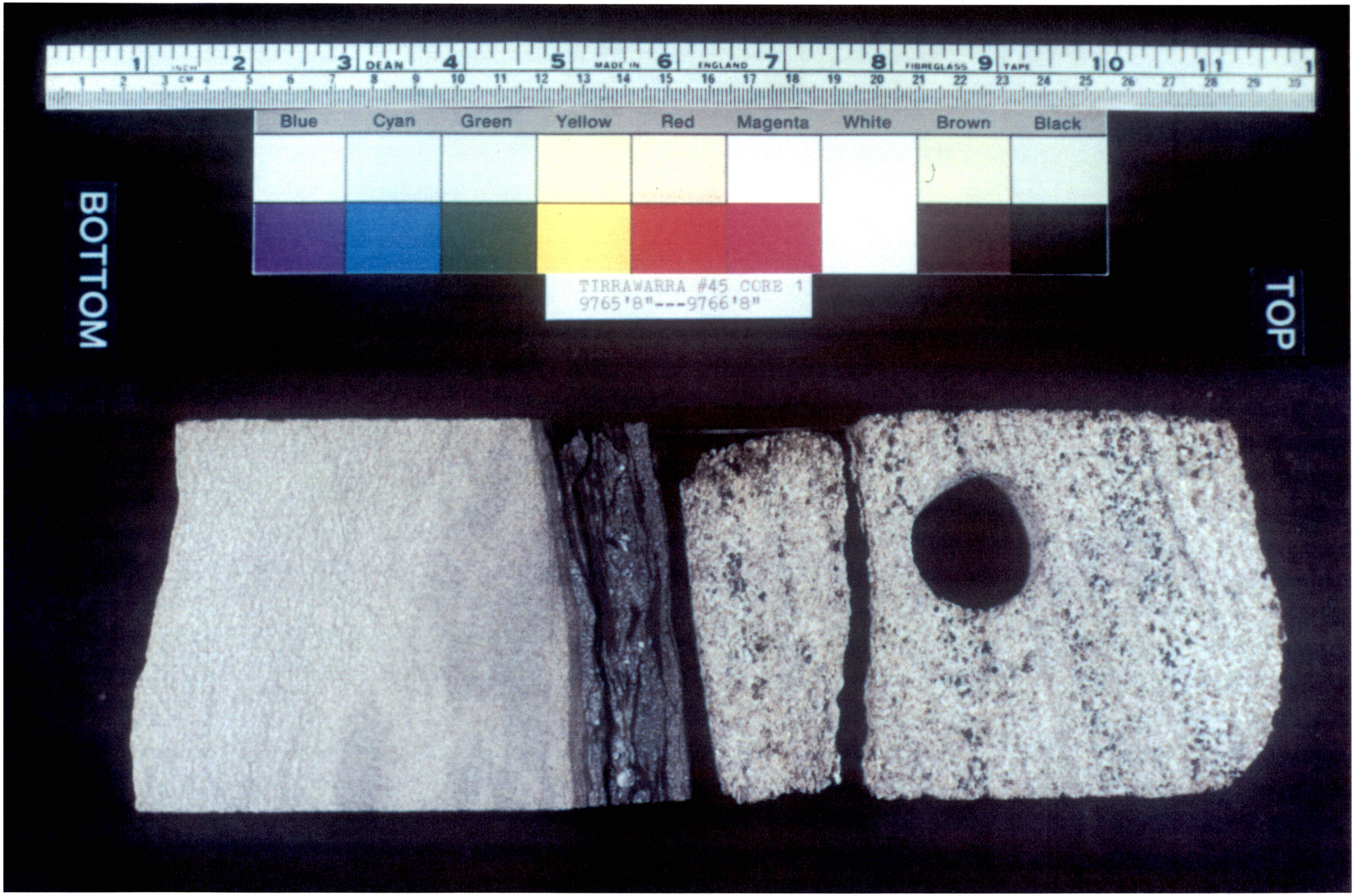
Blue
Cyan
Green
Yellow
Red
Magenta
White
Brown
Black
TIRRAWARRA #45 CORE 1
9765'8"---9766'8"
BOTTOM
TOP

Interpretation

The depositional environment of facies 4 is probably a bed-load dominated fluvial system that evolved through time into a more mixed-load fluvial system (fig. V-10). The lower part of facies 4 overlies an erosional surface and contains the largest maximum clast size and most abundant conglomerate in the Tirrawarra reservoir. Sedimentary structures in this part of the facies are consistent with a braidplain setting (McPherson and others, 1987), representing a landward shift in facies from the more distal braid delta setting of facies 3. A trend of increasing grain size toward the source area is well documented in modern and ancient braidplains, braided outwash fans, and other fluvial systems (Boothroyd and Ashley, 1975; Galloway and Hobday, 1983). The abundance of organic debris (plant fragments) and mud clasts, however, suggests that facies 4 was deposited in better developed channels with vegetation-stabilized banks than those of facies 3. Facies 4 mudstones and coals record the increasing persistence of interchannel vegetated floodplain areas. Through time lateral channel migration became more restricted until the braided channel system evolved into a meandering channel system. This evolution was accompanied by a decrease in the relative abundance of the sand and gravel bed load and an increase in the silt and clay suspended load being transported by facies 4 streams. Widespread coals in the upper part of and overlying facies 4 indicate that peat bogs were encroaching upon this part of the lake basin (fig. V-10).

Differentiation of Flow Units

Depositional facies provide the stratigraphic basis for identifying and characterizing reservoir flow units. The Tirrawarra reservoir flow units were differentiated on the basis of stratigraphic context, well log responses, and petrophysical properties. Because of variability in reservoir quality and stratigraphic position, Tirrawarra facies 1, 2, and 3 were divided into flow units 1U, 2L, 2U, 3L, and 3U, whereas facies 4 (undivided) coincides with flow unit 4. Recurring log responses were used to correlate the flow units into uncored wells. Petrophysical log analysis confirmed that many reservoir properties measured during well logging are facies dependent (see Section VII). Petrophysical data from core allowed statistical analysis of porosity and permeability in order to develop pay cutoff values for each flow unit.

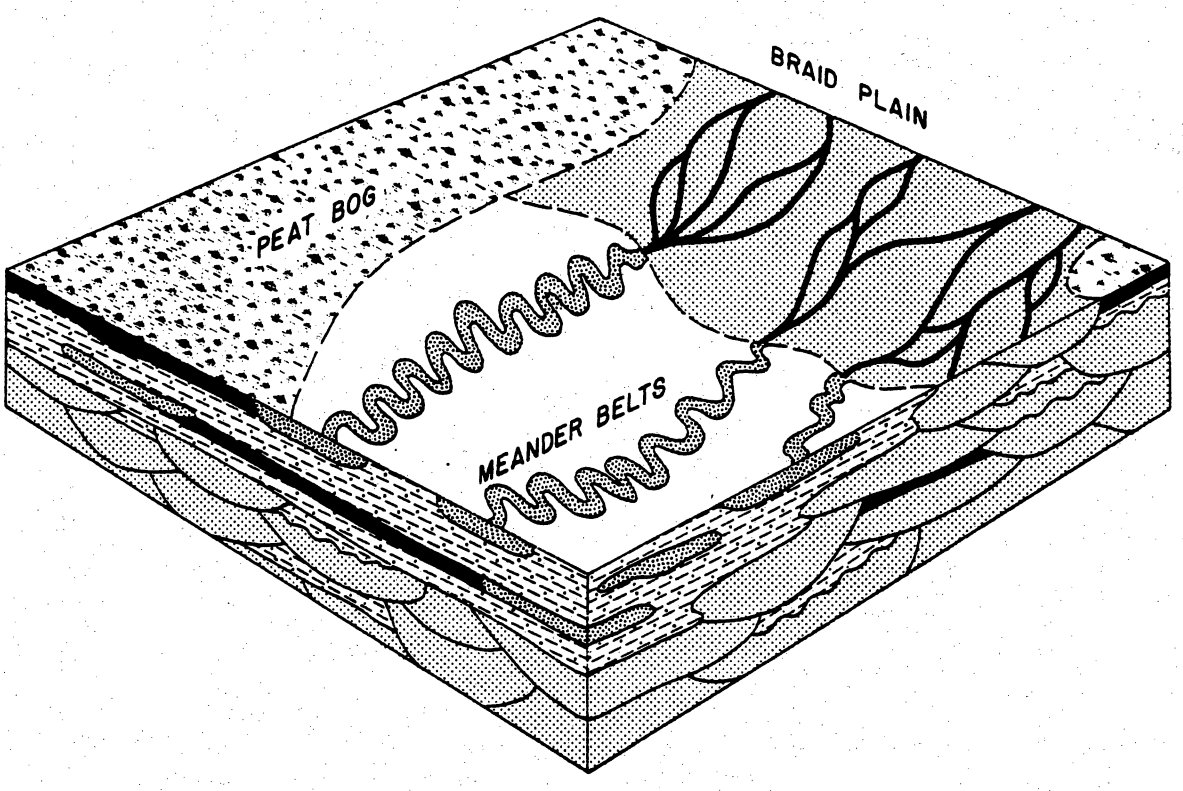

Figure V-10. Depositional model for facies 4 showing a braided fluvial system grading basinward (and through time) into a meandering fluvial system. Heavily vegetated peat-forming areas flanked active channels.

Well Log Patterns

Tirrawarra depositional facies and their component reservoir flow units can be recognized in part by distinctive well log patterns. Because log responses in each unit are generally not unique, log identification of facies must proceed within the context of stratigraphic correlation and core calibration. Comparisons of log responses among the different units are also important for identification and for boundary location. Typical gamma-ray, caliper, resistivity, and sonic porosity log responses for each flow unit are qualitatively described below.

Flow Unit 1U

Below flow unit 1U, the gamma-ray and resistivity curves are essentially shale baselines, except for small thin zones having slightly lower gamma ray, such as the "red horizon" siltstone/sandstone (fig. V-1). From the lower part of facies 1 upward into flow unit 1U, the gamma ray decreases and the resistivity slightly increases. Flow unit 1U generally displays a smooth to slightly erratic gamma-ray profile, which is commonly lower than that in overlying flow unit 2L but rarely is as low as that in flow unit 3L. The caliper log indicates that the hole is smooth to slightly irregular in flow unit 1U. The sonic log porosity profile for flow unit 1U is similar to but locally higher than that for flow unit 2L.

Flow Units 2L and 2U

Log responses in the two flow units derived from facies 2 are qualitatively similar; their distinction in uncored wells is based mainly on stratigraphic position. Gamma-ray curves in flow units 2L and 2U average significantly higher and are more variable than those in flow units 3L, 3U, and 4 (fig. V-4). Organic-rich mudstones cause high gamma-ray deflections, and abundant mud clasts and organic debris result in "shale baseline" gamma-ray curves in many sandstones. The gamma-ray response in the lower part of unit 2L is commonly higher than that in unit 1U. The resistivity logs show less variability than does the gamma-ray log. Resistivities are, on average, similar in units 2L and 3L, but are generally slightly higher in unit 2U than in unit 3U. Caliper logs reveal that bore holes are typically irregular and enlarged in flow units 2L and 2U (figs. V-1 and V-5). Overall sonic log porosity trends are similar in units 2L, 2U, and 4, but high log porosity zones are thinner and less common in the facies 2 flow units than they are in flow unit 4.

Flow Units 3L and 3U

On well logs facies 3 can be divided into flow units based on distinctive log responses, although the differences are commonly gradational and rarely universal. Gamma-ray curves in facies 3 are consistently low (20 to 40 API units) and display minor fluctuation. Thin muddy sandstones generally cause deflections of 60 to 100 API units. Gamma-ray deflections above 100 API are rare. A slightly upward-increasing gamma-ray trend is typical, and flow unit 3U has, on average, a slightly higher response than does flow unit 3L (figs. V-4 and V-5). Borehole enlargement is more common in unit 3U than it is in unit 3L. Thus, the caliper log helps to define the boundary between them in many wells. A significant number of wells, however, show no borehole enlargement through the entire reservoir or show no vertical trends in borehole enlargement. Resistivities commonly decrease upward in facies 3; the maximum range being approximately 200 to 30 ohm-m. Resistivities in flow unit 3U average lower than do those in flow unit 3L (figs. V-4 and V-5). Some wells, however, display no vertical resistivity trends in these units. The sonic log porosity trend in facies 3 is the highest in the Tirrawarra reservoir, displaying minor fluctuation. In the majority of the wells, sonic porosities are slightly higher in flow unit 3L than they are in flow unit 3U, but the reverse is also common. Because of these numerous exceptions to the "typical" well log responses in flow units 3L and 3U, the entire log suite must be considered carefully in order to determine the boundary between them.

Flow Unit 4

On most Tirrawarra well logs, flow unit 4 is readily distinguishable from underlying units. Resistivities in unit 4 are commonly 3 to 10 times higher than are those in units 3U or 2U, ranging from approximately 60 to 600 ohm-m (figs. V-4 and V-8). Coal beds, which are only present in flow unit 4, cause off-scale resistivity and sonic log responses. In wells where the resistivity difference is more subtle, the base of unit 4 is generally picked where an upwardly decreasing resistivity trend in unit 3U is reversed. Gamma-ray curves in flow unit 4 are, on average, higher and more variable than they are in flow unit 3U but are similar to those in flow unit 2U. As in units 2L and 2U, sandstones having abundant mud clasts and organic debris can appear as mudstones on gamma-ray logs. The large-scale gamma-ray trend in flow unit 4 is upwardly increasing. Boreholes are commonly irregular but smaller in unit 4 than they are in unit 3U. Sonic log porosity is, on average, lower in unit 4 than it is in unit 3U or 3L, although local clean sandstone and conglomerate beds in unit 4 commonly have much higher sonic porosities.

Petrophysical Properties from Core

Petrophysical data measured in core samples at ambient conditions provide the basis for quantifying facies-related variability in reservoir properties in order to identify and characterize reservoir flow units. Porosity and permeability data derived from Tirrawarra cores at ambient conditions are summarized in table V-5 and displayed on a series of graphs (figs. V-11 through V-16). Although the core data reveal a large amount of variability and overlap in porosity and permeability distribution, distinct average values and porosity/permeability relationships support the facies-based flow unit delineations. The data scatter and the variable correlations between porosity and permeability reflect (1) the heterogeneity within flow units, owing to subfacies-level depositional and diagenetic variations, and (2) the gradational and interrelated nature of facies within the larger Tirrawarra depositional system. However, core data also contain biases resulting from coring and sampling practices and so may not be completely representative of the field as a whole.

Based on core properties, flow unit 3L is the least heterogeneous and most consistently porous and permeable part of the Tirrawarra reservoir (table V-5, fig. V-15). This reflects deposition in an environment where reworking and winnowing of the sediment by lateral channel migration and by shorezone processes allowed little silt or clay to accumulate. Because flow unit 3U was deposited in an environment similar to that of unit 3L, the comparatively low average permeability and wide data scatter that characterize unit 3U (table V-5, fig. V-14) appear somewhat anomalous. Core and well log analyses, however, suggest that muddy sandstone beds are more abundant in unit 3U than they are in 3L. The depositional environment was apparently becoming less efficient in removing fine-grained sediment.

Flow unit 4 is characterized by a relatively low average core porosity but generally favorable core permeabilities (table V-5, fig. V-16). The relationship between porosity and permeability in flow unit 4 is the most positive in the Tirrawarra reservoir; that is, unit 4 has the greatest permeability increase for a given porosity increase (fig. V-16). The highest core permeabilities (up to 370 md) in the reservoir lie in the porous sandstones and conglomerates of flow unit 4 (fig. V-8). High-quality reservoir rock in flow unit 4 formed in a proximal setting on the braidplain, where high flow energies resulted in coarse-grained channel-fill deposits. Unfortunately, silt, clay, and organic material in nearby channel-flank environments were commonly ripped up and incorporated into the channel fill, reducing the reservoir quality of large parts of flow unit 4.

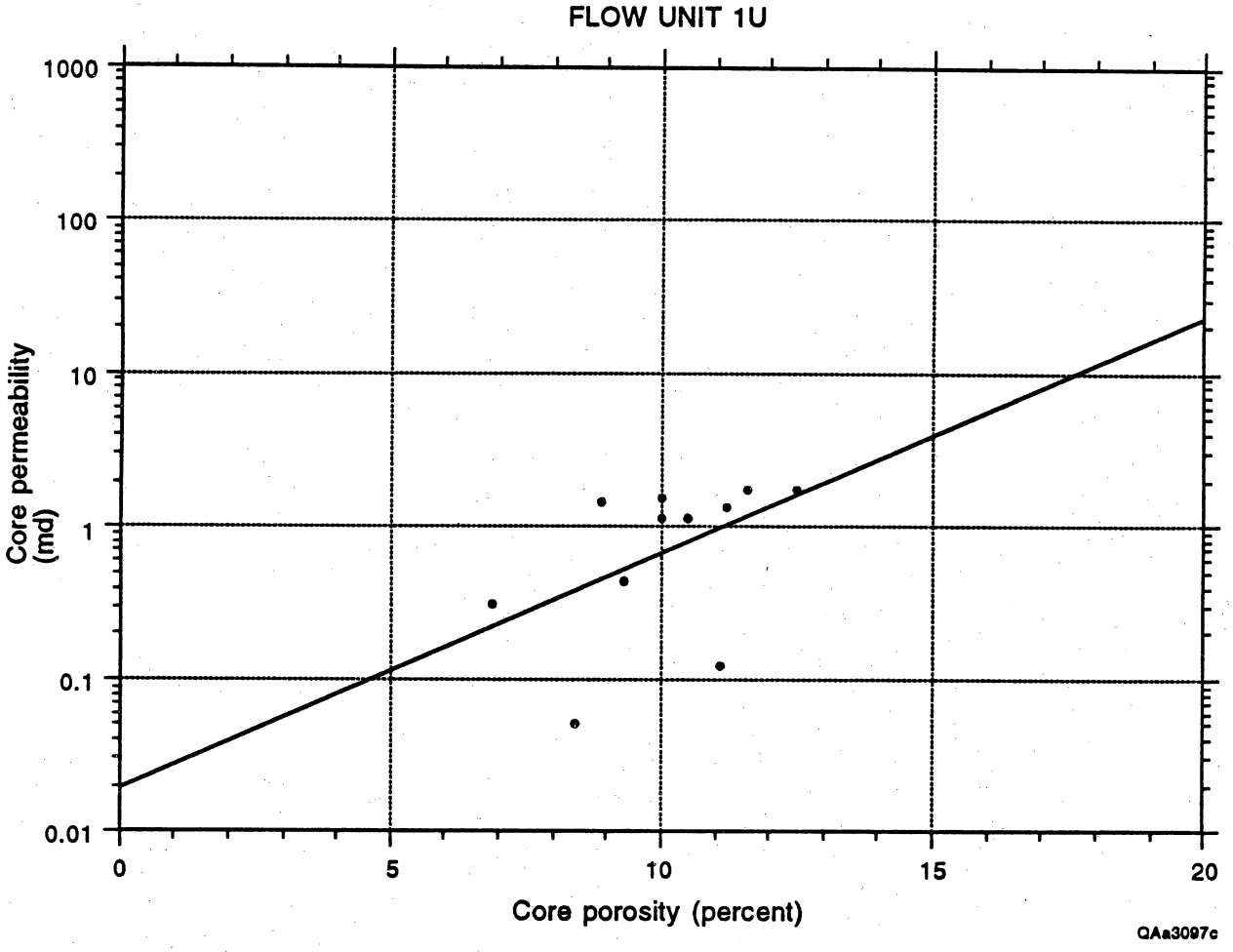

Figure V-11. Graph of porosity versus permeability, flow unit 1U. Data are from plugs taken from whole core at ambient conditions. Linear regression best fit line (conventional least squares) is shown. See table V-5.

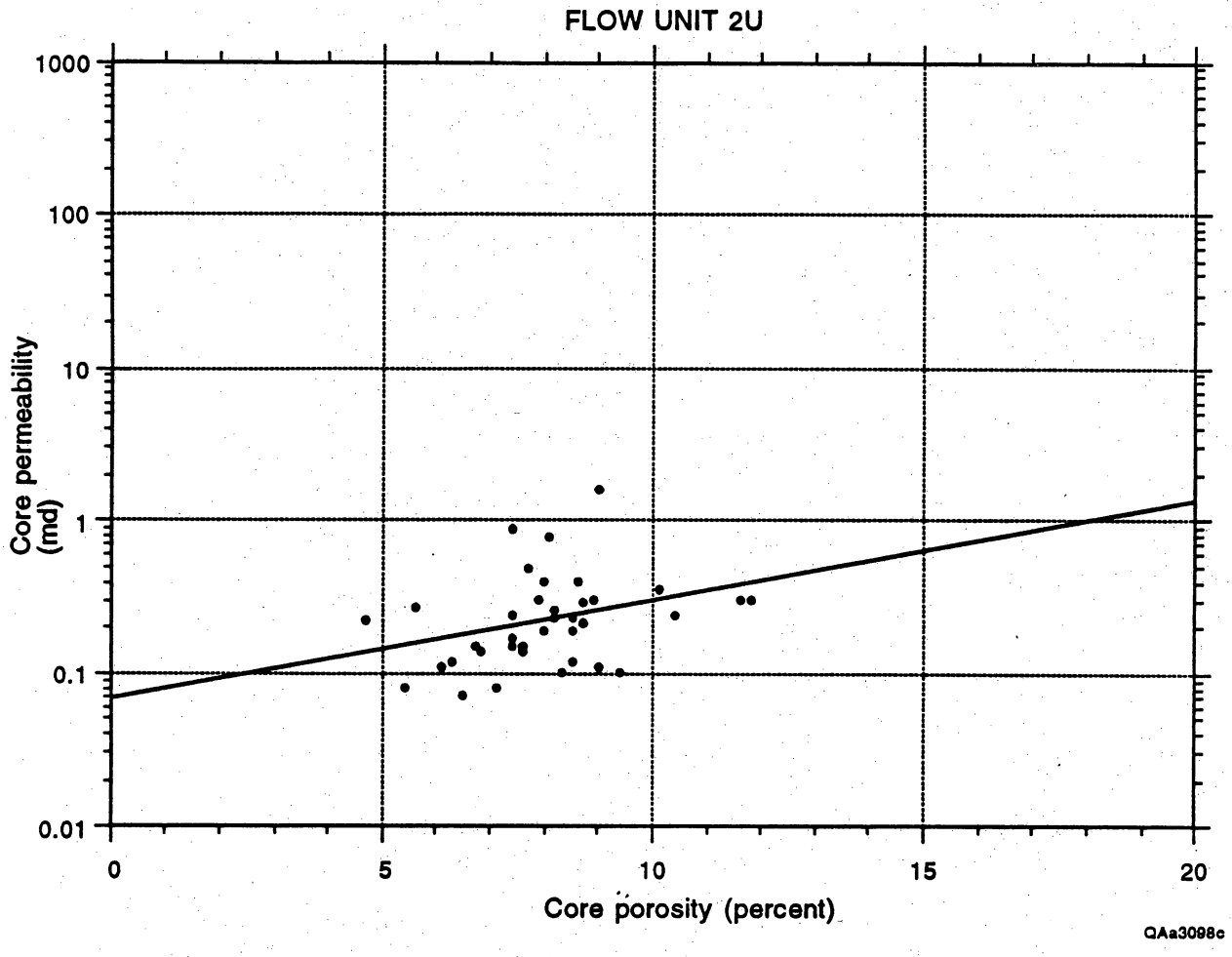

Figure V-12. Graph of porosity versus permeability, flow unit 2U. Data are from plugs taken from whole core at ambient conditions. Linear regression best fit line (conventional least squares) is shown. See table V-5.

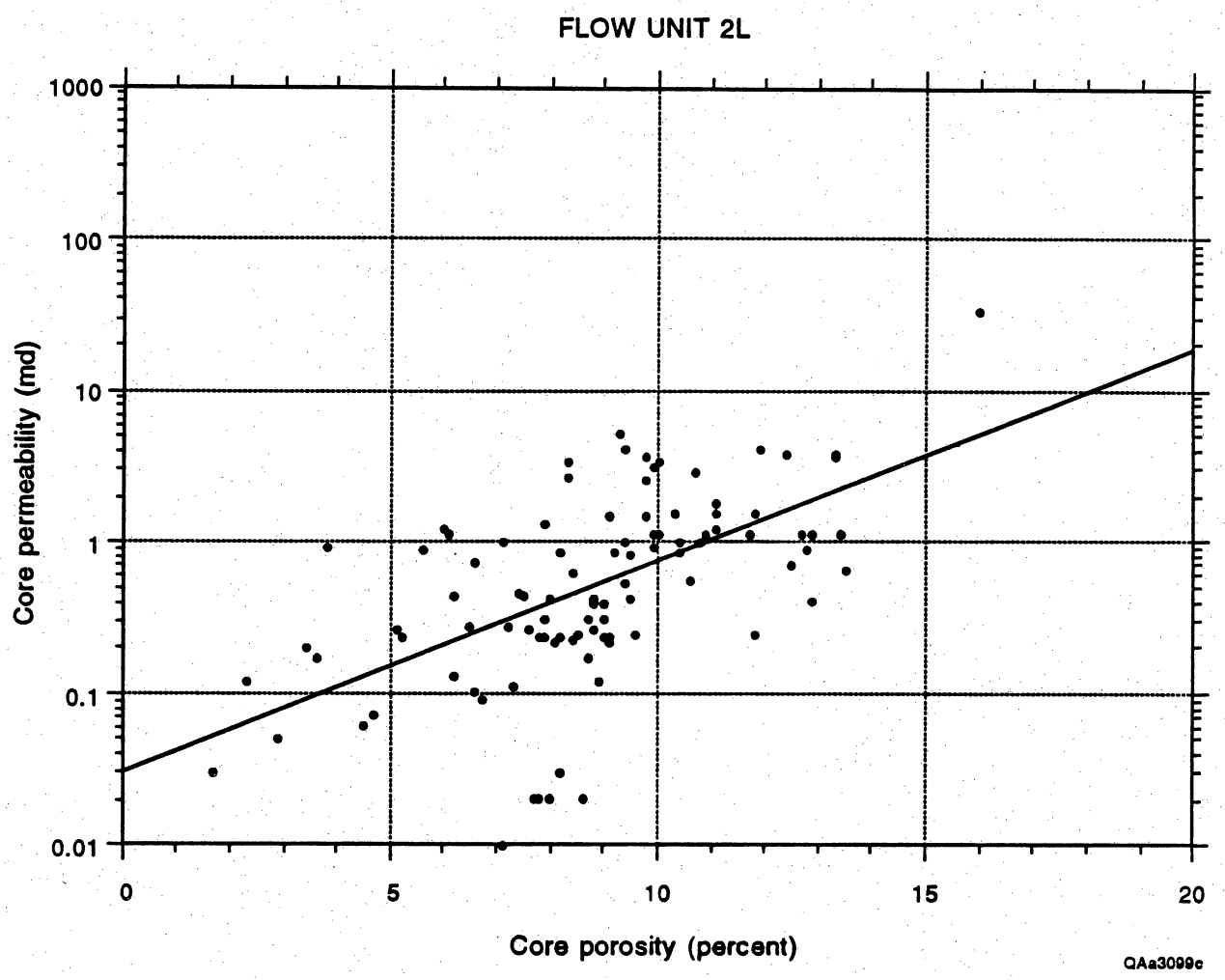

Figure V-13. Graph of porosity versus permeability, flow unit 2L. Data are from plugs taken from whole core at ambient conditions. Linear regression best fit line (conventional least squares) is shown. See table V-5.

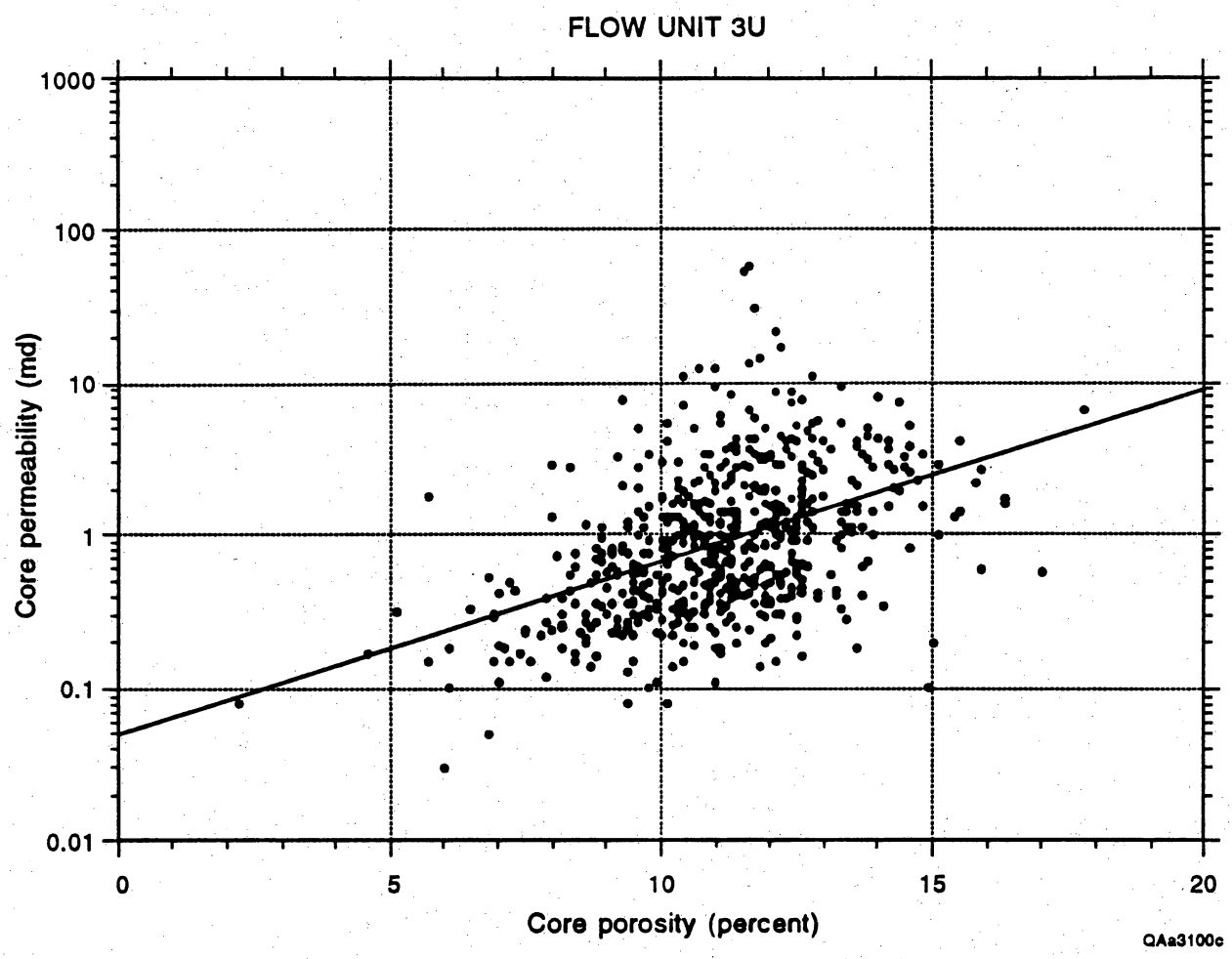

Figure V-14. Graph of porosity versus permeability, flow unit 3U. Data are from plugs taken from whole core at ambient conditions. Linear regression best fit line (conventional least squares) is shown. See table V-5.

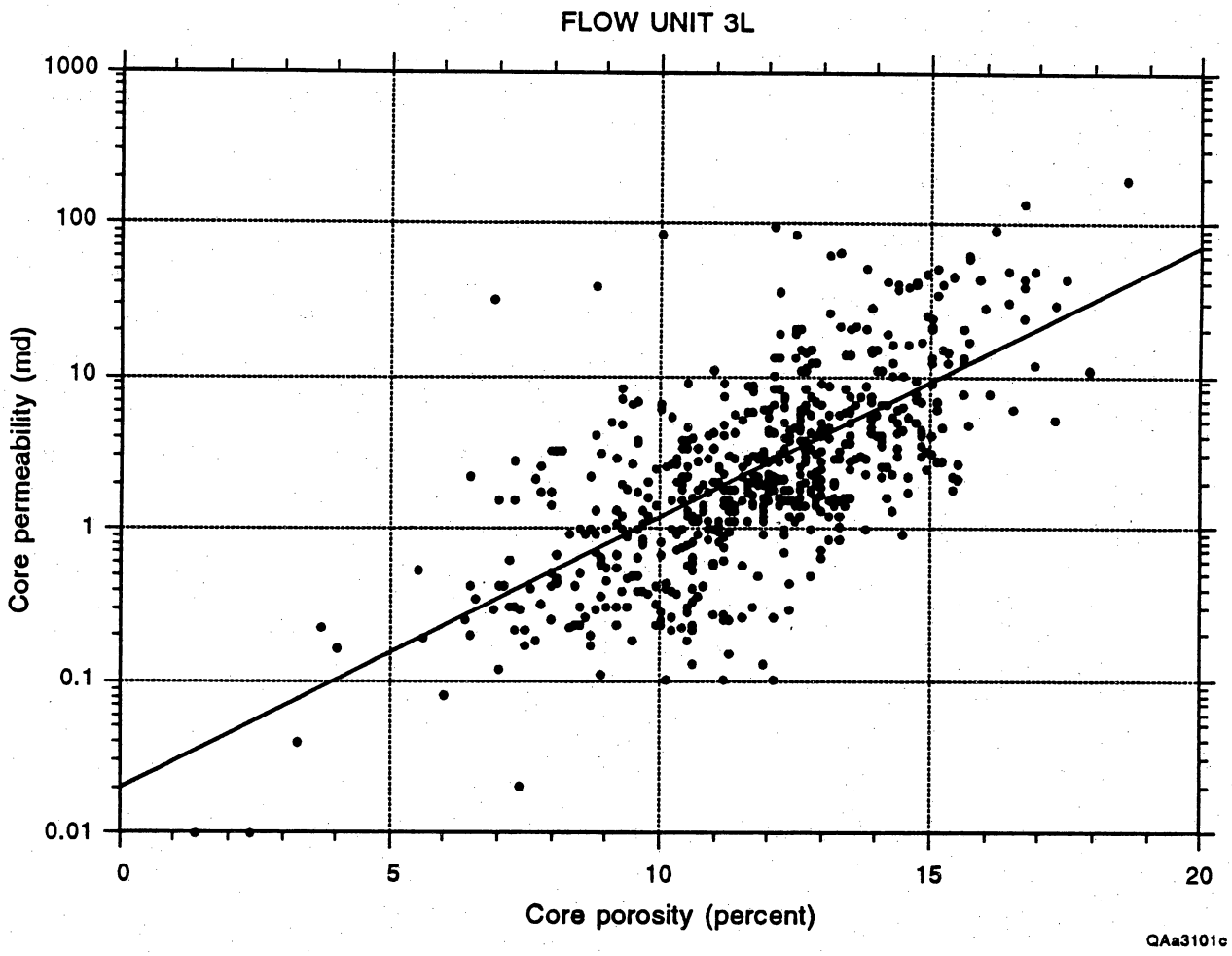

Figure V-15. Graph of porosity versus permeability, flow unit 3L. Data are from plugs taken from whole core at ambient conditions. Linear regression best fit line (conventional least squares) is shown. See table V-5.

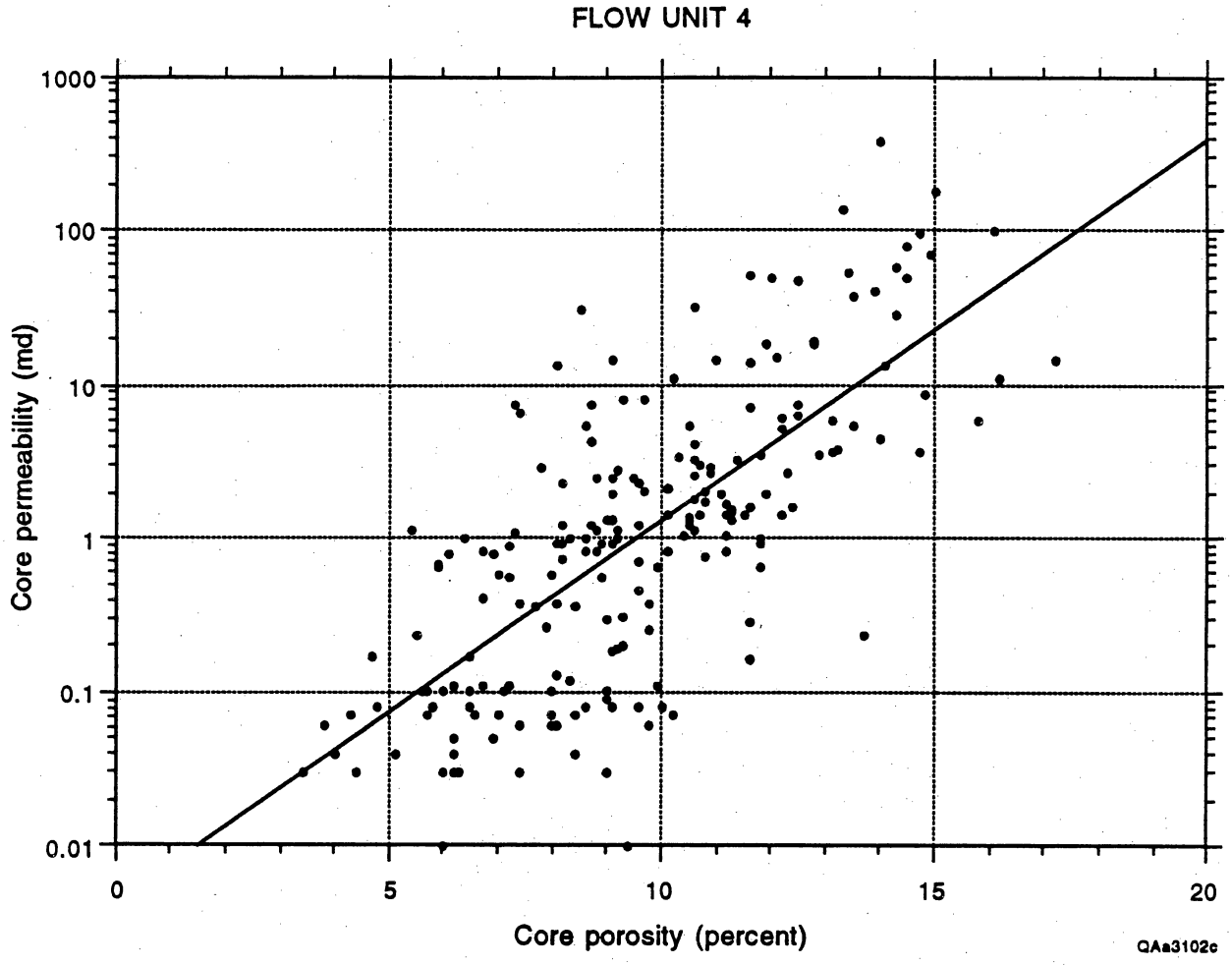

Figure V-16. Graph of porosity versus permeability, flow unit 4. Data are from plugs taken from whole core at ambient conditions. Linear regression best fit line (conventional least squares) is shown. See table V-5.

Table V-5. Petrophysical Properties from Core.[1]

Flow Unit	Mean ø[2]	Mean k[3]	k/ø Relationship[4]	r[5]	n[6]
4	9.3	1.02	$\log_{10}k = -2.37 + 0.25ø$	0.72	203
3U	10.9	0.88	$\log_{10}k = -1.30 + 0.11ø$	0.46	598
3L	11.6	2.19	$\log_{10}k = -1.68 + 0.17ø$	0.68	621
2U	8.1	0.22	$\log_{10}k = -1.20 + 0.07ø$	0.33	37
2L	8.5	0.51	$\log_{10}k = -1.51 + 0.14ø$	0.58	99
1U	10.2	0.65	$\log_{10}k = -1.75 + 0.16ø$	0.48	11

[1]See figures V-11 through V-18
[2]Arithmetic average
[3]Geometric mean
[4]Conventional least squares linear regression equation
[5]Correlation coefficient
[6]Number of data points

Unlike the other flow units, unit 4 displays marked areal variation in reservoir quality within Tirrawarra field. Core porosities and permeabilities from wells in the central part of the field are consistently higher than are those from wells in the western part of the field (fig. V-17). Wells in the northern part of the field (not shown on fig. V-17) have core properties that span the ranges of both the central and western parts. Facies maps (discussed in the next section) reveal that variations in thickness and interconnectedness of channel-fill sandstones and conglomerates in flow unit 4 can be related to these reservoir quality differences.

Flow units 1U, 2L, and 2U are not well represented in the core data, and thus statistics and relationships derived from these data are less meaningful. Nevertheless, the core data support facies characterization and well log analysis in confirming that these flow units contain the poorest quality rock in the Tirrawarra reservoir (table V-5, figs. V-11 through V-13). The distal deltaic depositional setting of flow unit 1U resulted in its fine grain size and generally low porosity and permeability. The few data available from flow unit 1, however, suggest that this thin and marginal zone contains intervals of pay quality rock. Flow units 2L and 2U, on the other hand, contain abundant nonreservoir rock, primarily mudstone, sandy mudstone, and muddy sandstone. The core porosities and permeabilities correctly show that clean sandstone is poorly developed in unit 2U but is somewhat more common in unit 2L.

A cross plot of average core permeability against average core porosity in each flow unit (fig. V-18) reveals interrelationships among the facies in the larger Tirrawarra depositional system. The flow units having abundant mud clasts and organic debris incorporated in reservoir quality sandstone (units 2U, 2L, and 4) are, on average, less porous than are those having only minor amounts of these components (units 1U, 3U, and 3L). In the Tirrawarra braid plain and lacustrine delta system, mud clasts and organic debris are most abundant in fluvial and distributary channels flanked by heavily vegetated banks and interchannel areas, features

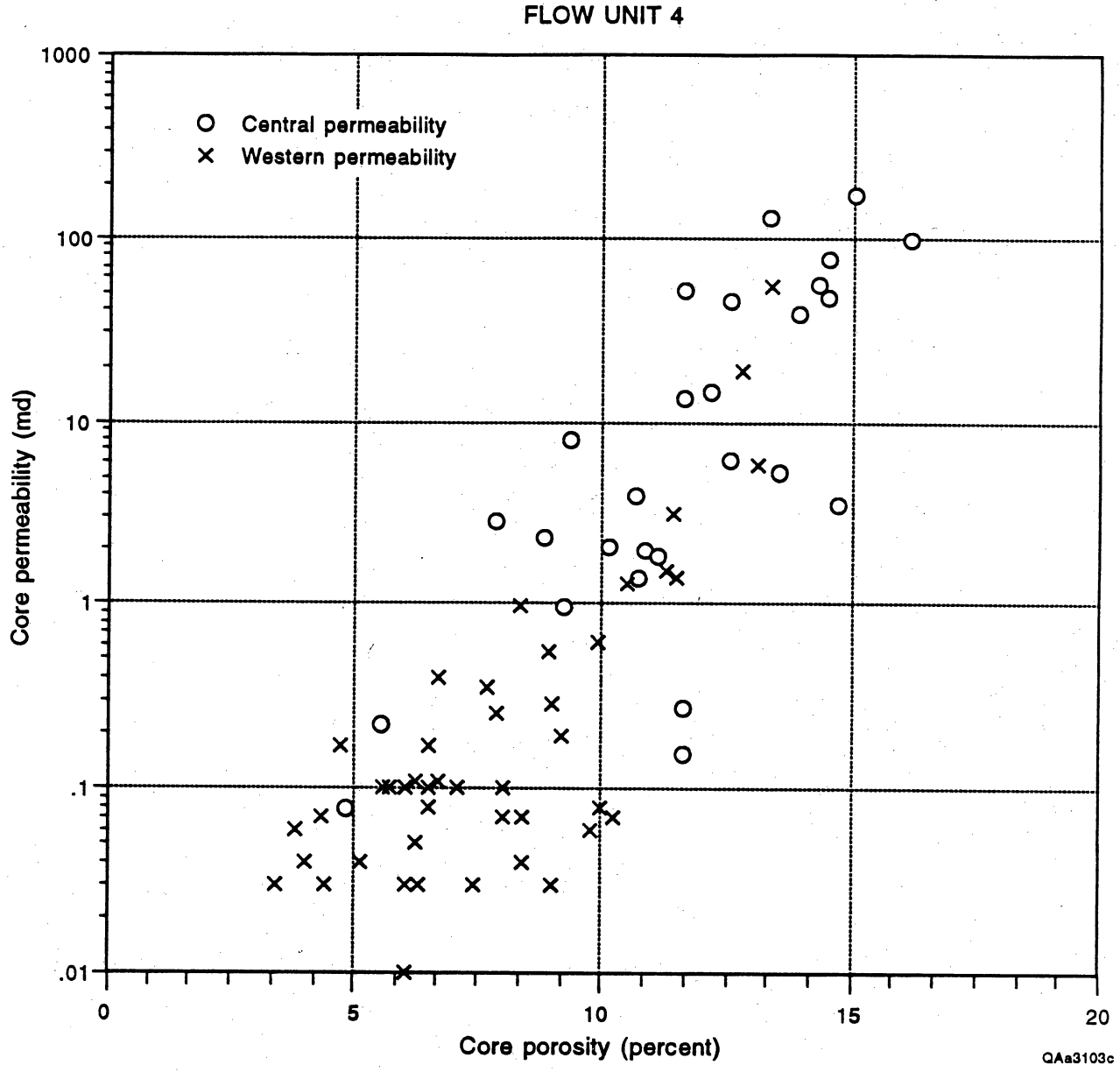

Figure V-17. Graph of porosity versus permeability, flow unit 4, showing only core data from wells in the central and western parts of Tirrawarra field.

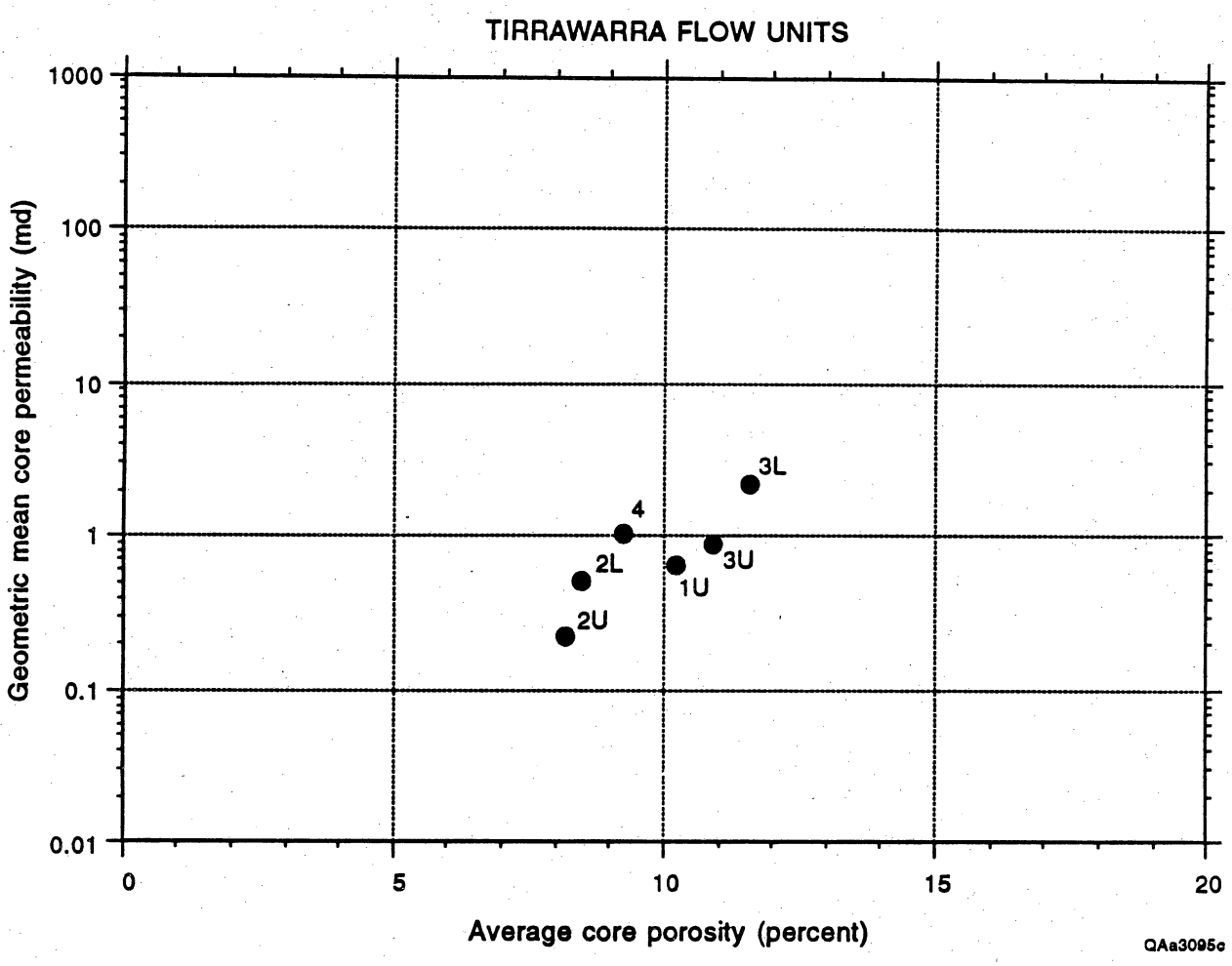

Figure V-18. Graph of average porosity versus geometric mean permeability for each Tirrawarra flow unit. Data are from plugs taken from whole core at ambient conditions.

common to both facies 2 and 4. The sand-rich poorly channelized fluvial system of facies 3 lacked heavily vegetated interchannel areas, because sediment on the braid delta-plain surface was continuously mobilized and reworked. Poorly consolidated mud clasts and organic debris did not easily survive transport to the delta front (flow unit 1U) or reworking in the lacustrine shorezone environment. Thus, flow units 1U, 3L, and 3U are related by depositional processes working toward development of clean sandstone. Within each of these two groups, reservoir quality variations (fig. V-18) can be attributed in part to grain size trends. Flow unit 4 contains larger clast sizes as well as greater volumes of coarse grained rock than does flow unit 2L, whereas unit 2U is, on average, the finest grained of the three. Flow unit 3L is slightly coarser grained than is 3U, and both of these are significantly coarser grained than is flow unit 1U. Although the postdepositional processes of diagenetic modification and tectonic deformation also influence reservoir quality, depositional environment exerts a fundamental and systematic control on porosity and permeability in the Tirrawarra reservoir.

Capillary pressure data can provide information about pore-size distribution in reservoir rocks (Hearn and others, 1984; Vavra and others, 1992). Although the capillary pressure data available from Tirrawarra cores could not be used for quantitative evaluation, qualitative comparisons can be made. Mercury injection capillary pressure curves from Tirrawarra flow units (figs. V-19 through V-25) support porosity and permeability data in the ranking of reservoir quality. Core samples from flow units 3L and 4 have well-connected pore networks with large pore throat, although unit 4 also includes samples resistant to mercury injection (figs. V-24 and V-25). Capillary pressure curves from flow unit 3U suggest a somewhat less well connected pore network with smaller pore throats (fig. V-25). Small pore throat sizes and intergranular clay matrix typically result in a convoluted, poorly interconnected pore network. Capillary pressure curves from flow units 1U, 2L, and 2U show low saturations at high pressures (fig. V-25), indicating small pore sizes and resistance to flow.

Architecture of Facies and Flow Units

Depositional architecture comprises the three-dimensional distribution of facies and bedding surfaces in a genetic stratigraphic interval. The Tirrawarra reservoir is a genetic stratigraphic interval that was deposited in a fluvial-deltaic system in a proglacial-lacustrine setting and that possesses sand-body geometries and orientations inherited from the depositional environment. Gross unit thickness (isopach) maps and net porous sandstone maps display tabular, lenticular, and lobate geometries resulting from deposition in braid plain, distributary channel, and channel mouth bar environments, respectively. A general northwest-to-southeast elongation common to many of the Tirrawarra facies delineates the

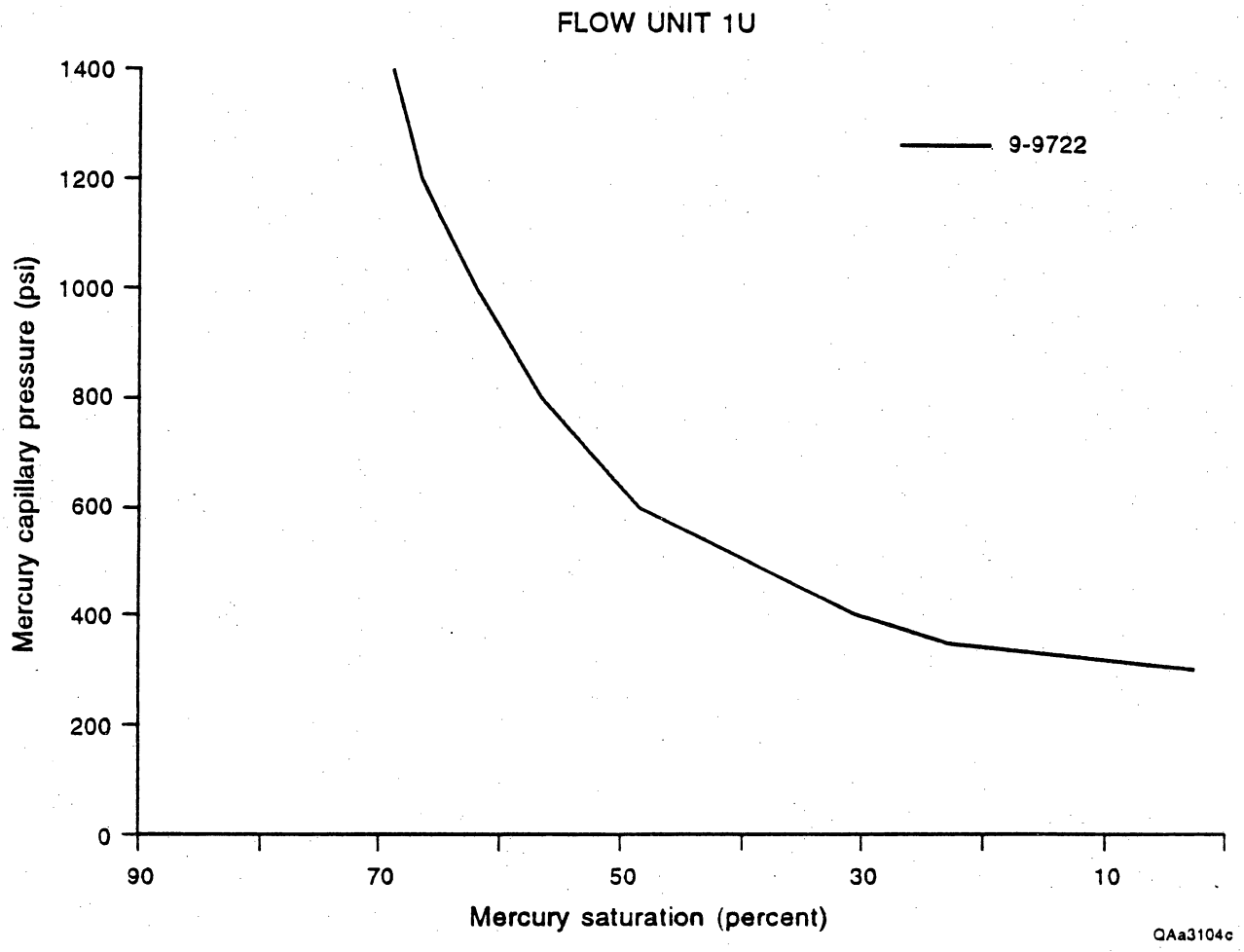

Figure V-19. Mercury-injection capillary-pressure curve for a core sample from flow unit 1U. Tirrawarra well number and sample depth (ft) are also shown.

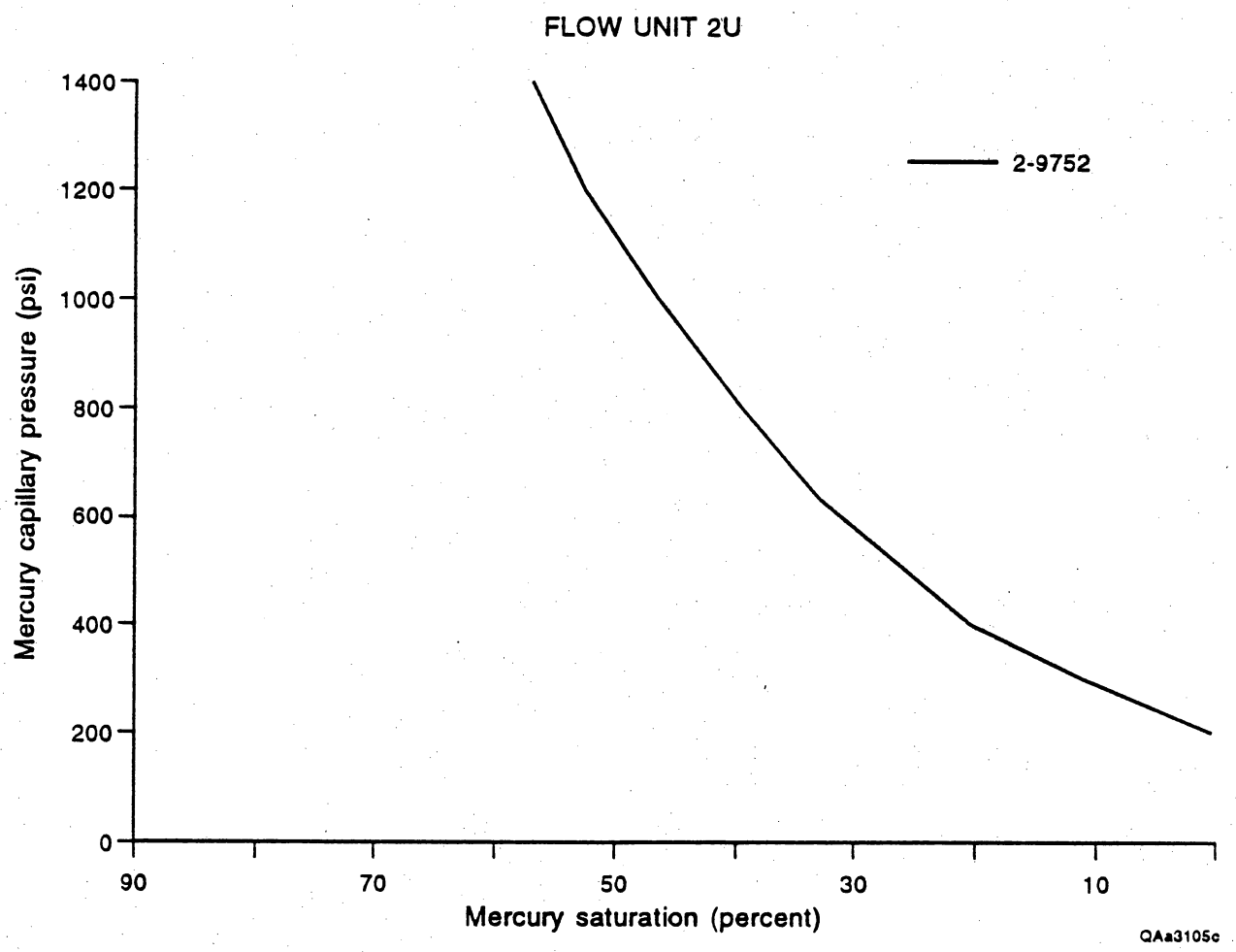

Figure V-20. Mercury-injection capillary-pressure curve for a core sample from flow unit 2U. Tirrawarra well number and sample depth (ft) are also shown.

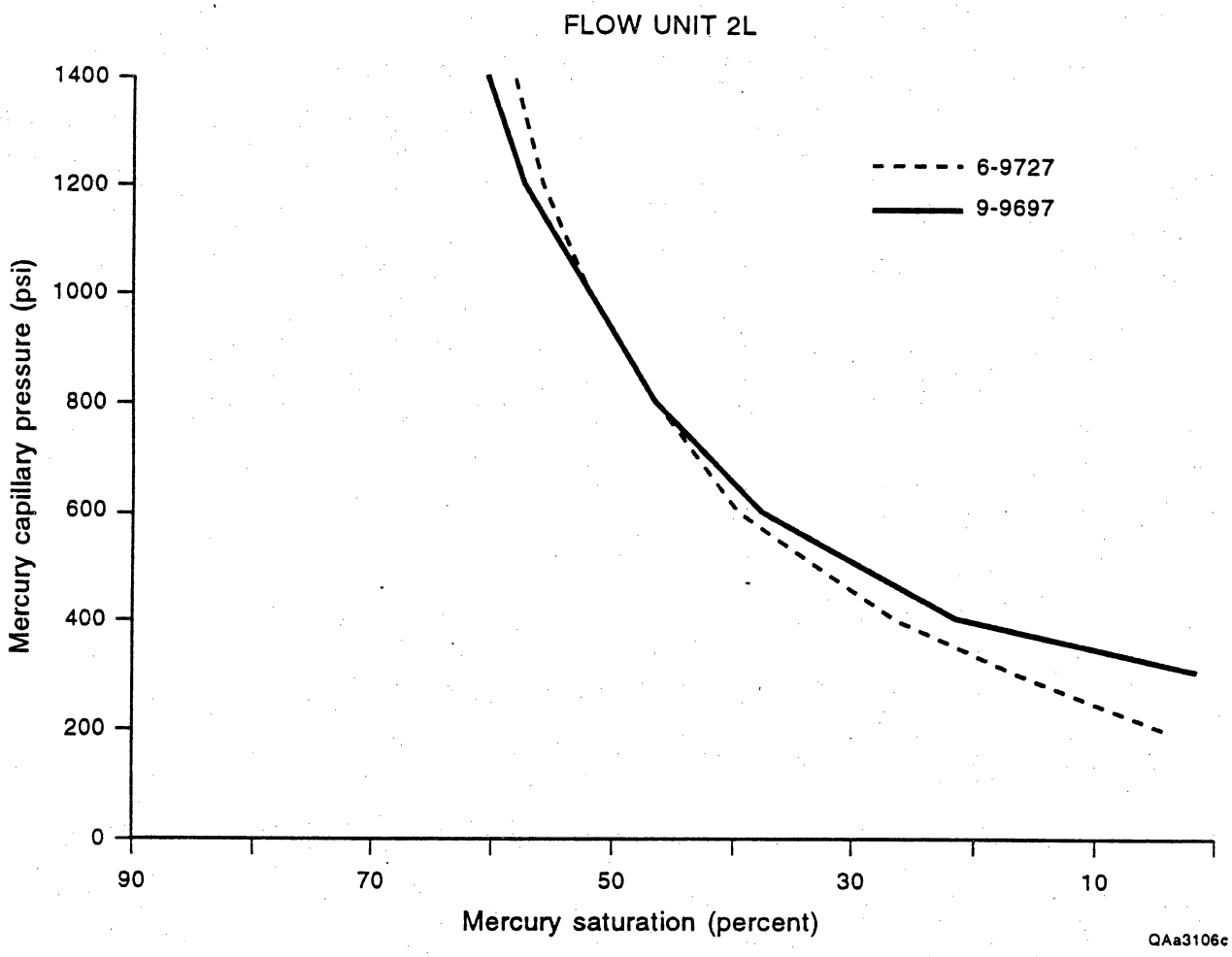

Figure V-21. Mercury-injection capillary-pressure curves for core samples from flow unit 2L. Tirrawarra well numbers and sample depths (ft) are also shown.

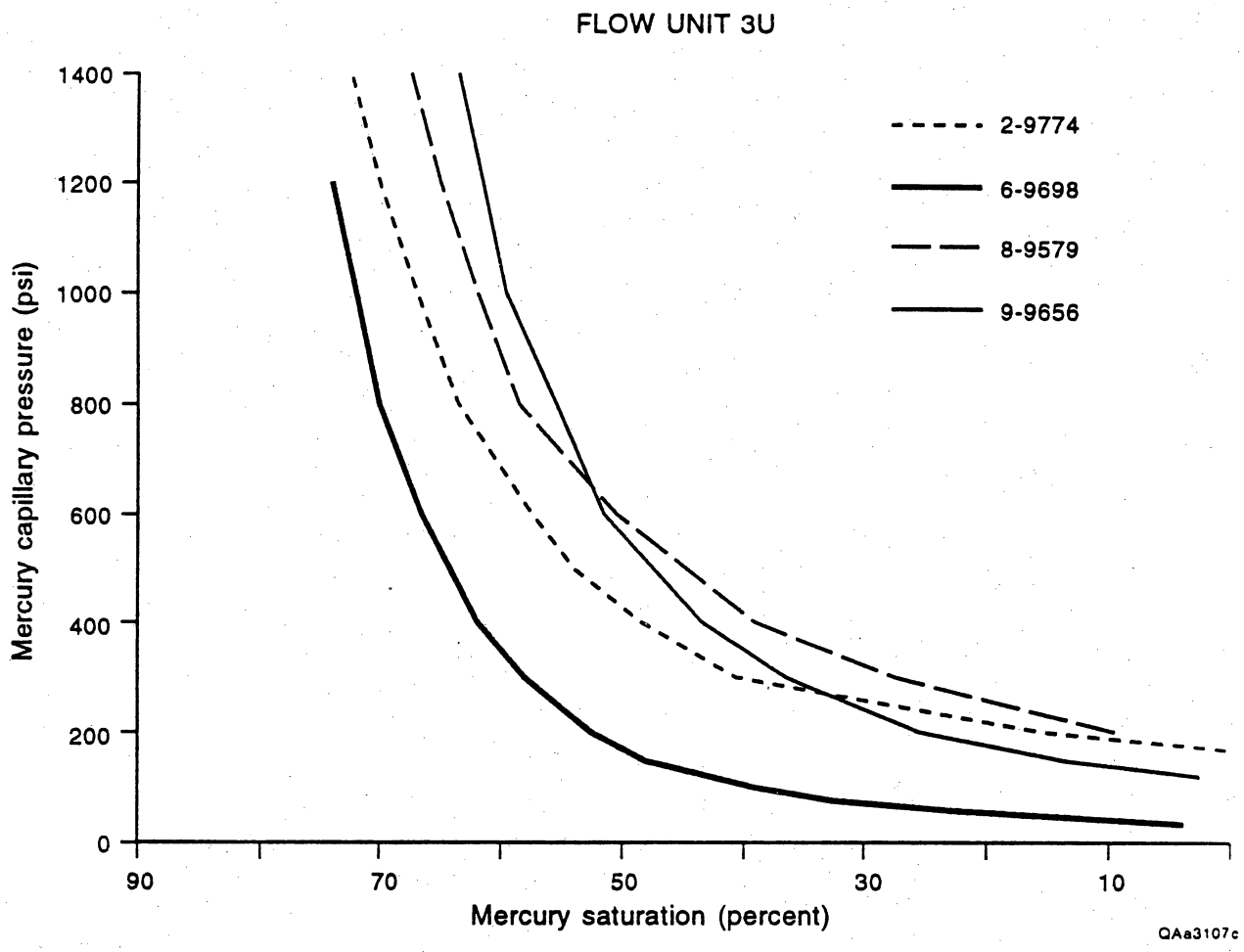

Figure V-22. Mercury-injection capillary-pressure curves for core samples from flow unit 3U. Tirrawarra well numbers and sample depths (ft) are also shown.

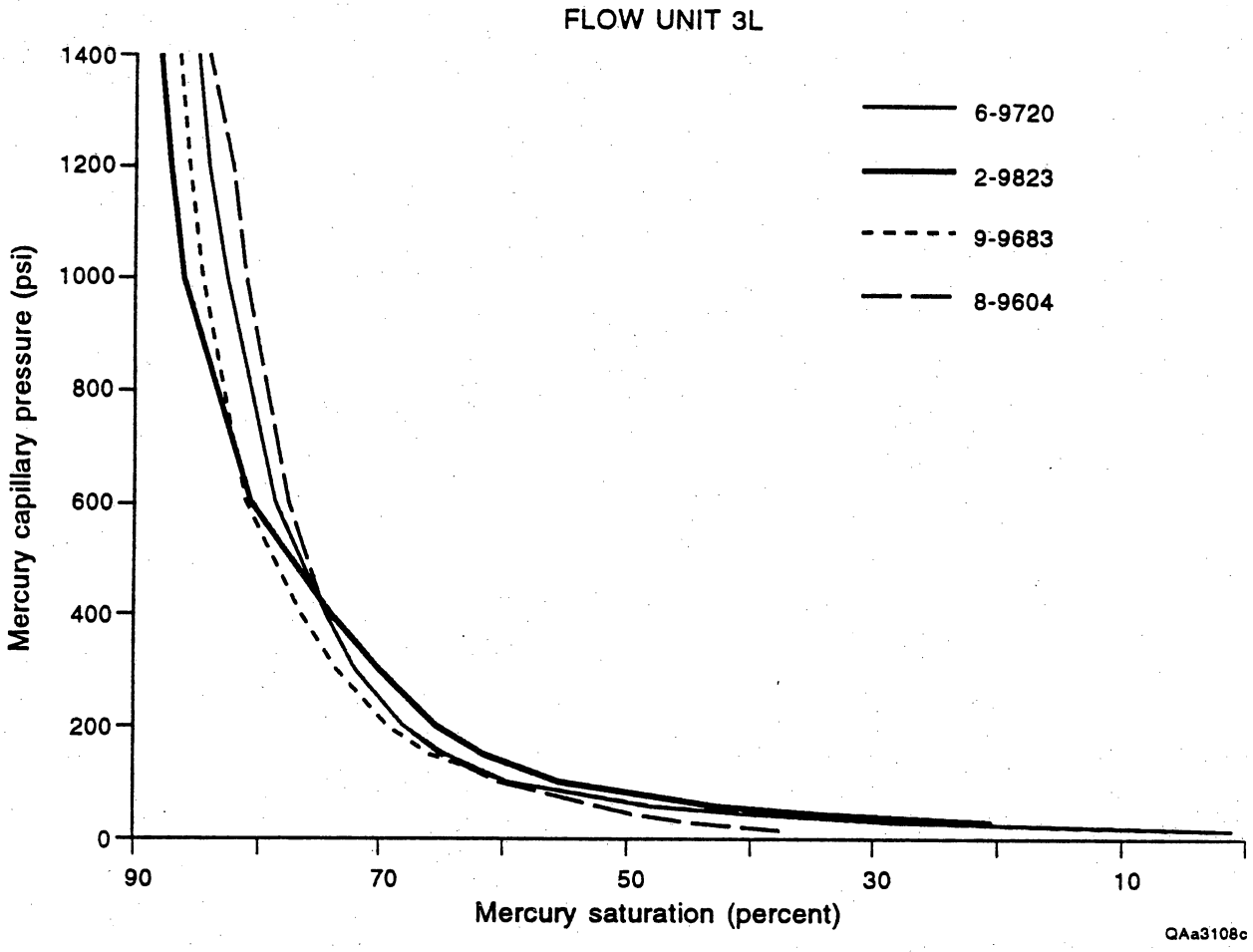

Figure V-23. Mercury-injection capillary-pressure curves for core samples from flow unit 3L. Tirrawarra well numbers and sample depths (ft) are also shown.

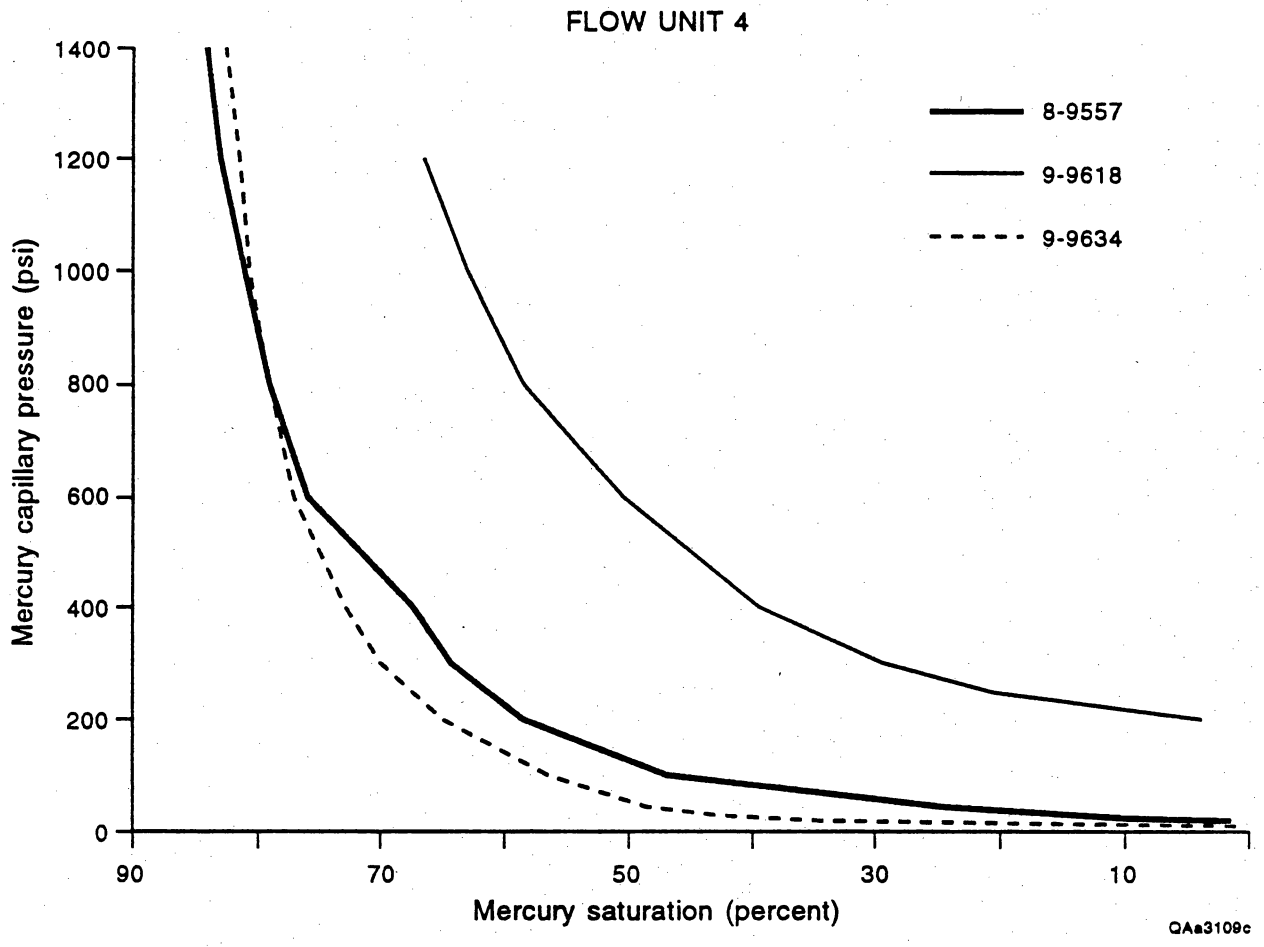

Figure V-24. Mercury-injection capillary-pressure curves for core samples from flow unit 4. Tirrawarra well numbers and sample depths (ft) are also shown.

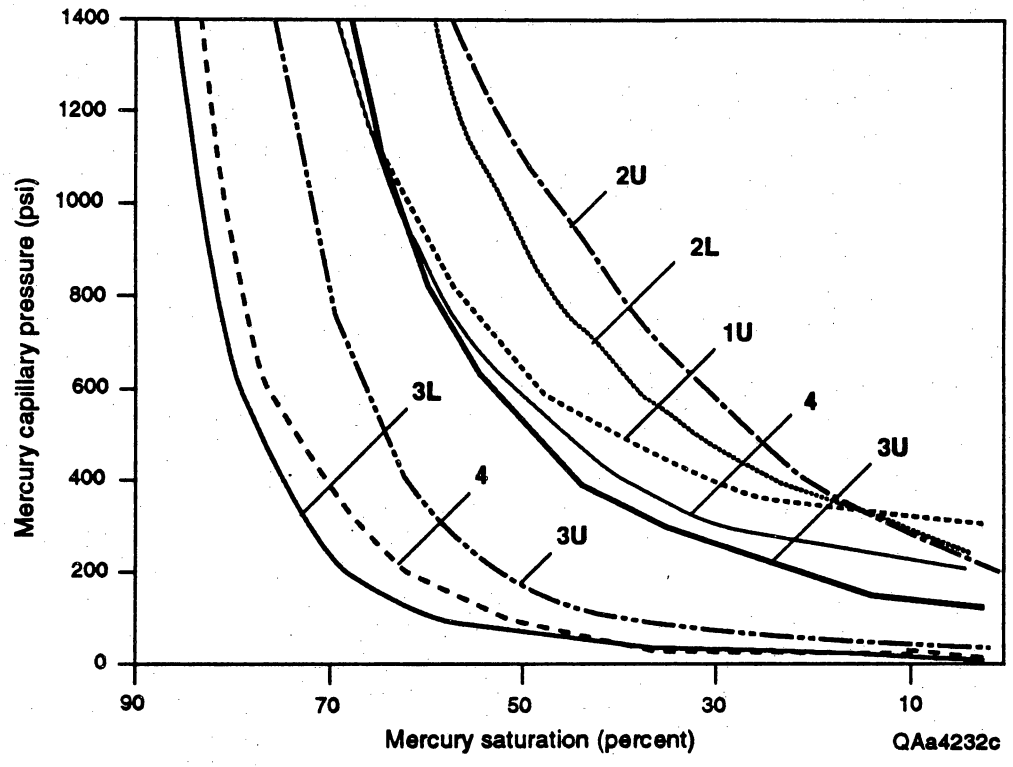

Figure V-25. Average capillary-pressure curves for each flow unit. Based on data shown in figures V-19 through V-24.

direction of progradation (depositional dip). The long dimensions of lenticular sandstones and permeability compartments commonly parallel this direction. Cross sections (plates V-1 through V-13) reveal the vertical distribution and lateral continuity of flow units and of low-permeability layers within and between flow units. Bedding characteristics within flow units control permeability anisotropy and influence flow paths. The depositional architecture of each Tirrawarra facies and its component flow units is described below and summarized in tables V-1 though V-4. Schematic cross sections display the vertical and lateral distribution of the flow units (figs. V-26 and V-27).

Facies 1 (Flow Unit 1U)

The lower, mudstone-dominated part of facies 1 is continuous across Tirrawarra field but is of undetermined thickness. Individual thin beds within the lower part of facies 1, such as the "red" horizon, are also continuous across the field, indicating that the lacustrine basin in which these rocks were deposited was much larger than the present size of Tirrawarra field.

The upper part of facies 1 (flow unit 1U) is also continuous except where erosionally truncated. Flow unit 1U thickness variations, however, are largely depositional. As is the case with the other flow units except unit 4, general thickness trends are inherited from the depositional environment but are modified by later erosional truncation. The isopach map of flow unit 1U displays a southeast-oriented, elongate to lobate geometry (fig. V-28). Because erosional truncation by overlying facies 2 and 3 increases toward the northwest, narrow trends in the west and north are erosional remnants. Flow unit 1U geometries in the west and north were probably similar originally to those extant in the south and southeast: lobate with a slight southeastward elongation (fig. V-28). Flow unit 1U lobes are 10 to 17 ft thick, 2 to 3 km long, and 0.5 to 2 km wide. These lobes form a coalesced delta-front platform; fine grained sand and silt entered the lake through multiple distributary channels and were spread across the nearshore environment by waves and currents.

Flow unit 1U is thin and relatively homogeneous internally, grading upward from siltstone to very fine grained sandstone. This grain size trend was produced by gradual shoaling as the delta front prograded across the lake basin. Clean, porous sandstone, however, occurs in isolated pods (fig. V-29). Net porous sandstone in flow unit 1U is 0 to 5 ft thick in small areas that each encompass only 1 or 2 wells, and permeability is similarly limited (fig. V-30). A somewhat larger lobe of porous sandstone is centered around wells 70, 16, and 26 in the north (fig. V-29). Poor development of porous and permeable sandstone in flow unit 1U can be attributed to low wave and current energies in the lacustrine nearshore environment and to trapping of coarser grained sediment updip in the delta-plain environment. Additionally, clean

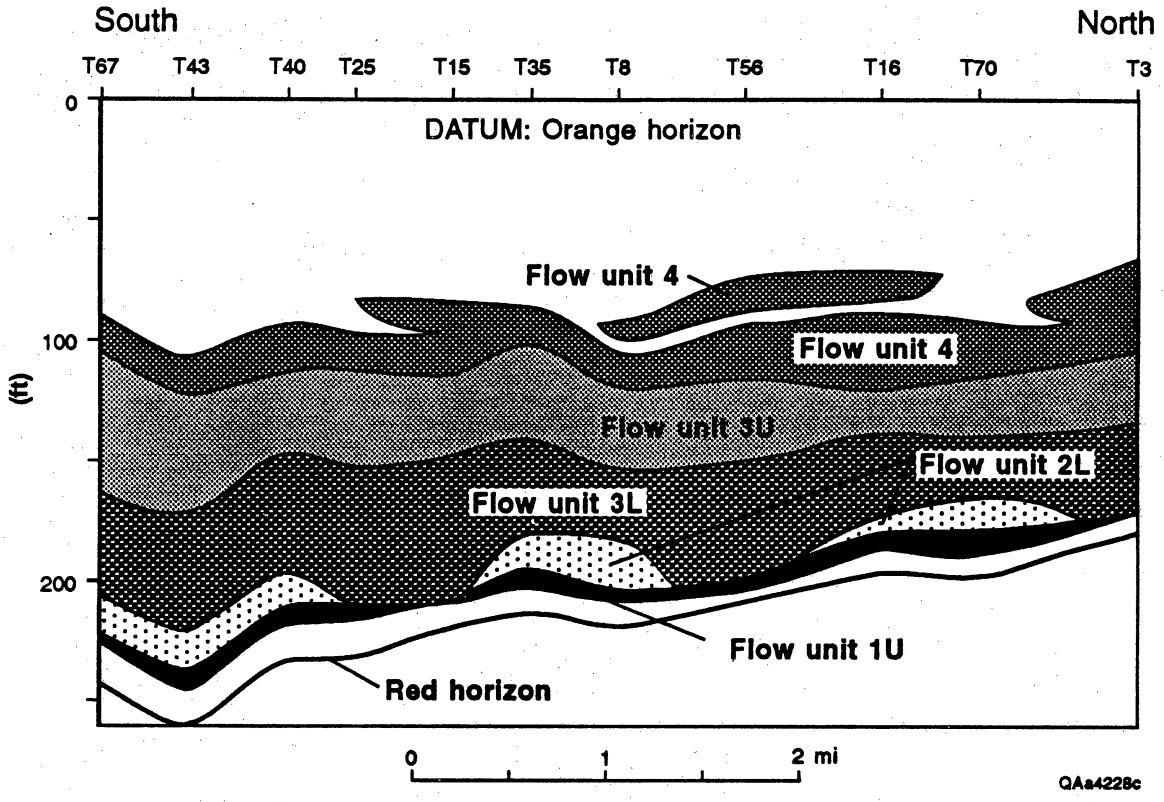

Figure V-26. Schematic south–north cross section (T12, fig. II-1), showing Tirrawarra flow units, Tirrawarra field.

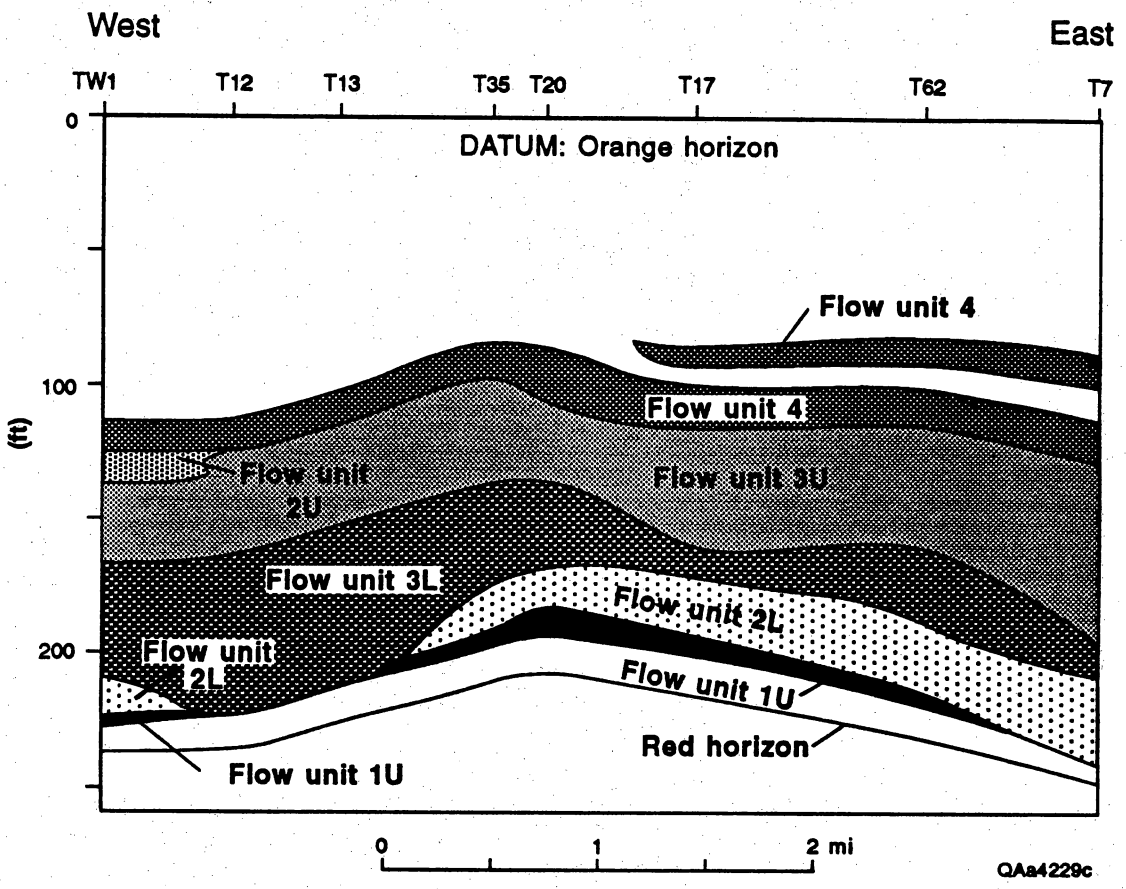

Figure V-27. Schematic west–east cross section (T15, fig. II-1), showing Tirrawarra flow units, Tirrawarra field.

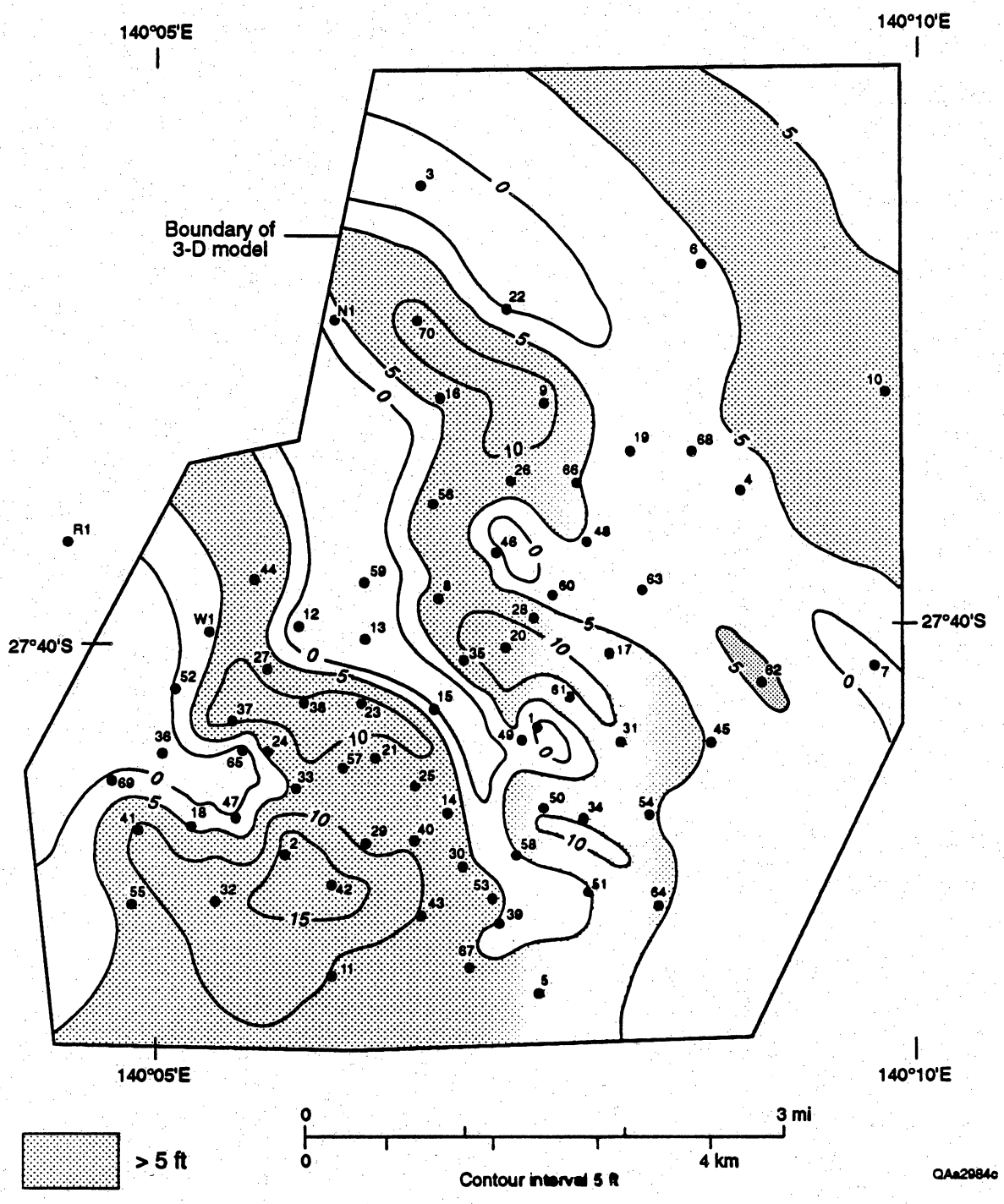

Figure V-28. Isopach map of Tirrawarra flow unit 1U.

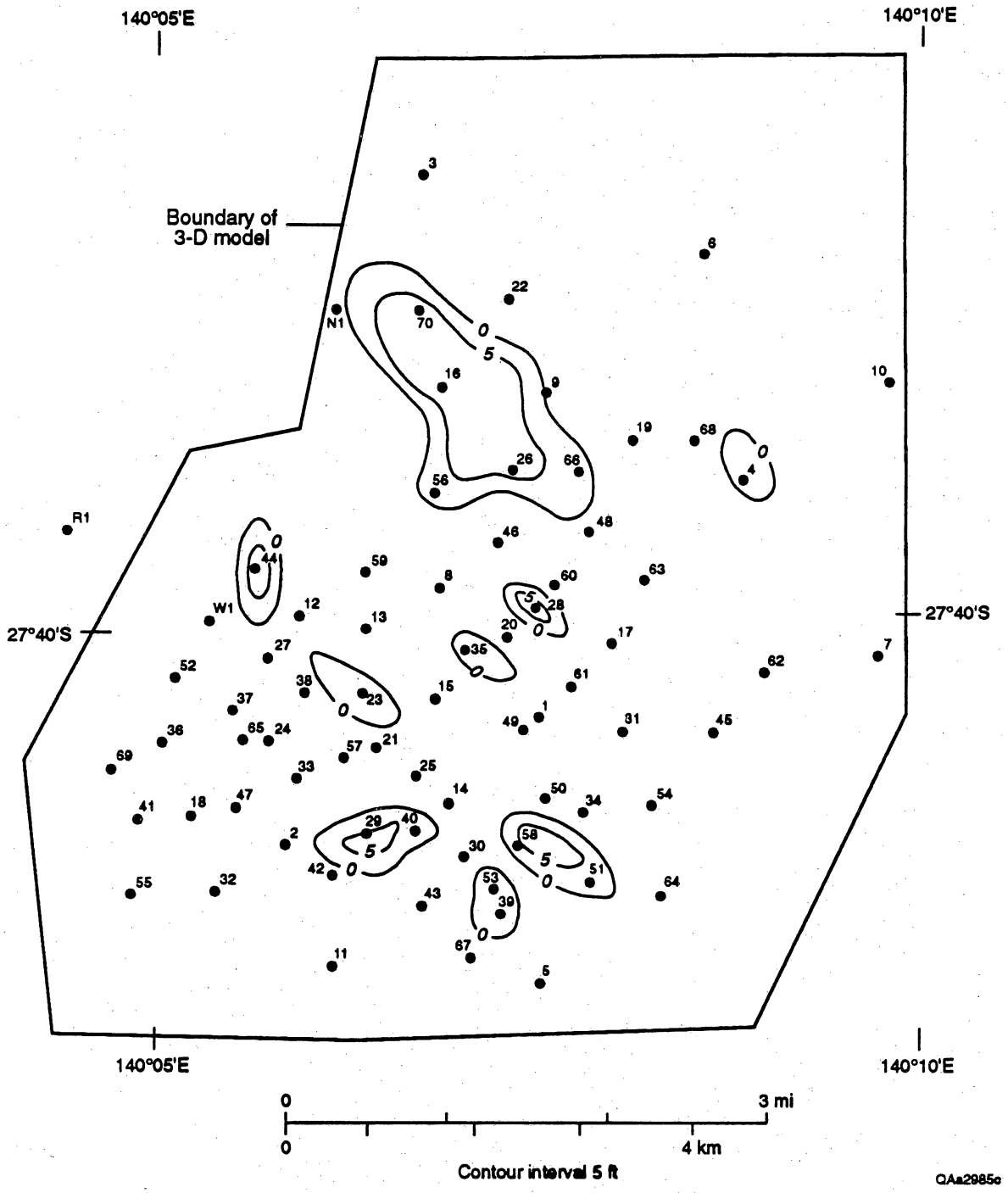

Figure V-29. Net porous sandstone map of Tirrawarra flow unit 1U.

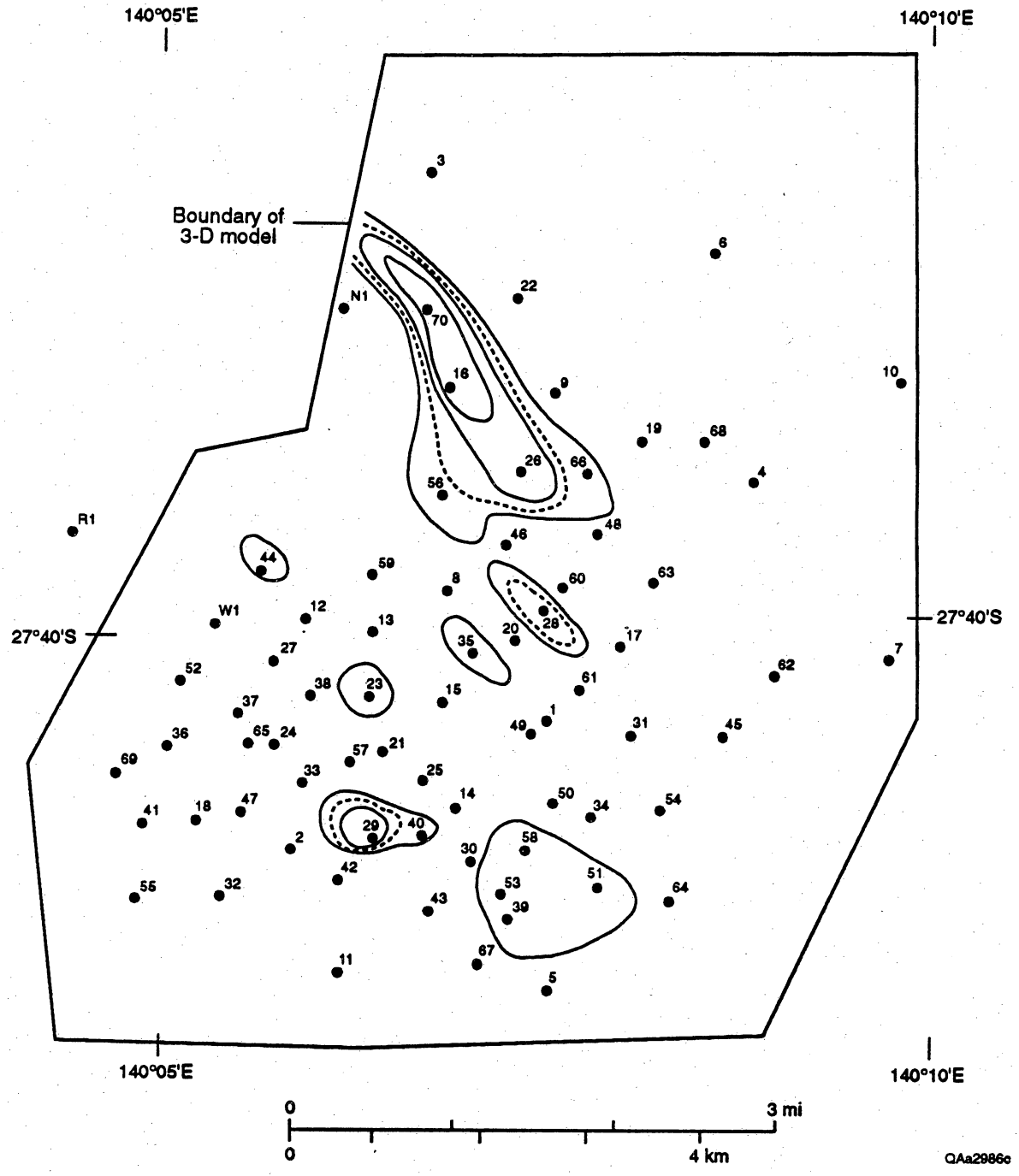

Figure V-30. Permeability-thickness (kh) map of Tirrawarra flow unit 1U.

sandstone in the uppermost part of flow unit 1U may have originally been more widespread but was removed by subsequent erosion.

Facies 2 (Flow Unit 2L)

Flow unit 2L, which includes both sandstone and mudstone, displays thickness trends having a pronounced southeastward elongation (fig. V-31). Sinuous belts, 10 to 30 ft thick and 1 to 3 km wide, extend across the field and merge in the southeast to form broad lobes. Flow unit 2L is greater than 20 ft thick across most of the southeast part of the field (fig. V-31). These geometries support a distributary channel and channel mouth bar interpretation for flow unit 2L. Distributary channels entered the area from the northwest, while channel mouth bars coalesced in the southeast. Net porous sandstone trends (fig. V-32) coincide closely with gross unit thickness trends (fig. V-31), suggesting that the deposition of both sand and mud occurred mainly in and near the channels. Thick mudstones in flow unit 2L were probably deposited in abandoned channels and channel-flank natural levees, whereas thin mudstones formed in interdistributary bay and marsh environments. Thin muddy sandstones in the interchannel areas formed as crevasse splays. Clean sand accumulated mainly in the lower parts of active channels and the upper parts of the channel mouth bars. The preserved thicknesses and widths of porous sandstone in flow unit 2L document the relatively small size of this delta system. Net porous sandstone in the channel belts is generally less than 10 ft thick and less than 2 km wide (fig. V-32). The coalesced channel mouth bars in the southeast, where sand was reworked and spread out in the lacustrine shorezone, contain 10 to 17 ft of porous sandstone across an area of about 12 km^2 (fig. V-32). Permeability-thickness patterns (fig. V-33) closely coincide with net porous sandstone trends, indicating that permeability in flow unit 2L is distributed throughout the porous sandstone and that highly permeable thin beds are probably not common in unit 2L.

Well log cross sections display the internal stratigraphy and the boundary conditions of flow unit 2L as well as of the other Tirrawarra flow units (plates V-1 through V-13). The bulk of flow unit 2L is composed of irregularly interbedded sandy mudstone, muddy sandstone, and clean sandstone. Individual bed sets are not typically traceable between wells, although a general upward increase in mud content commonly recurs. Some mudstones in the upper part of unit 2L, however, are 5 to 15 ft thick and extend 1 to 3 km, being generally more elongate in a north to northwest direction. These mudstones, which are probably abandoned channel fill deposits, occur at the contact between flow units 2L and 3L in most wells in the south and west but are also common in the rest of the field (plates V-1 through V-13). Thus, the boundary between units 2L and 3L is typically impermeable. The boundary between units 2L and 1U is

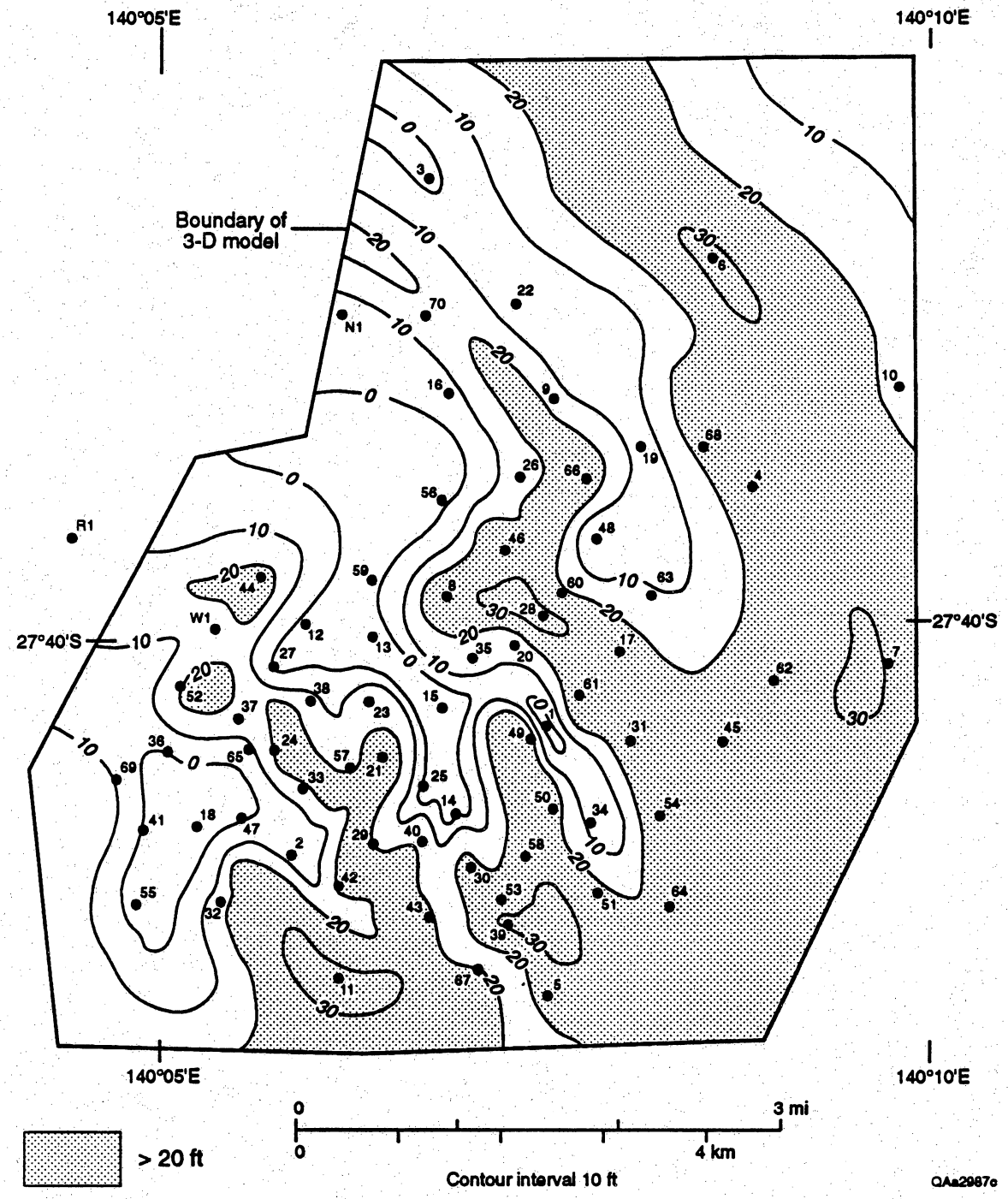

Figure V-31. Isopach map of Tirrawarra flow unit 2L.

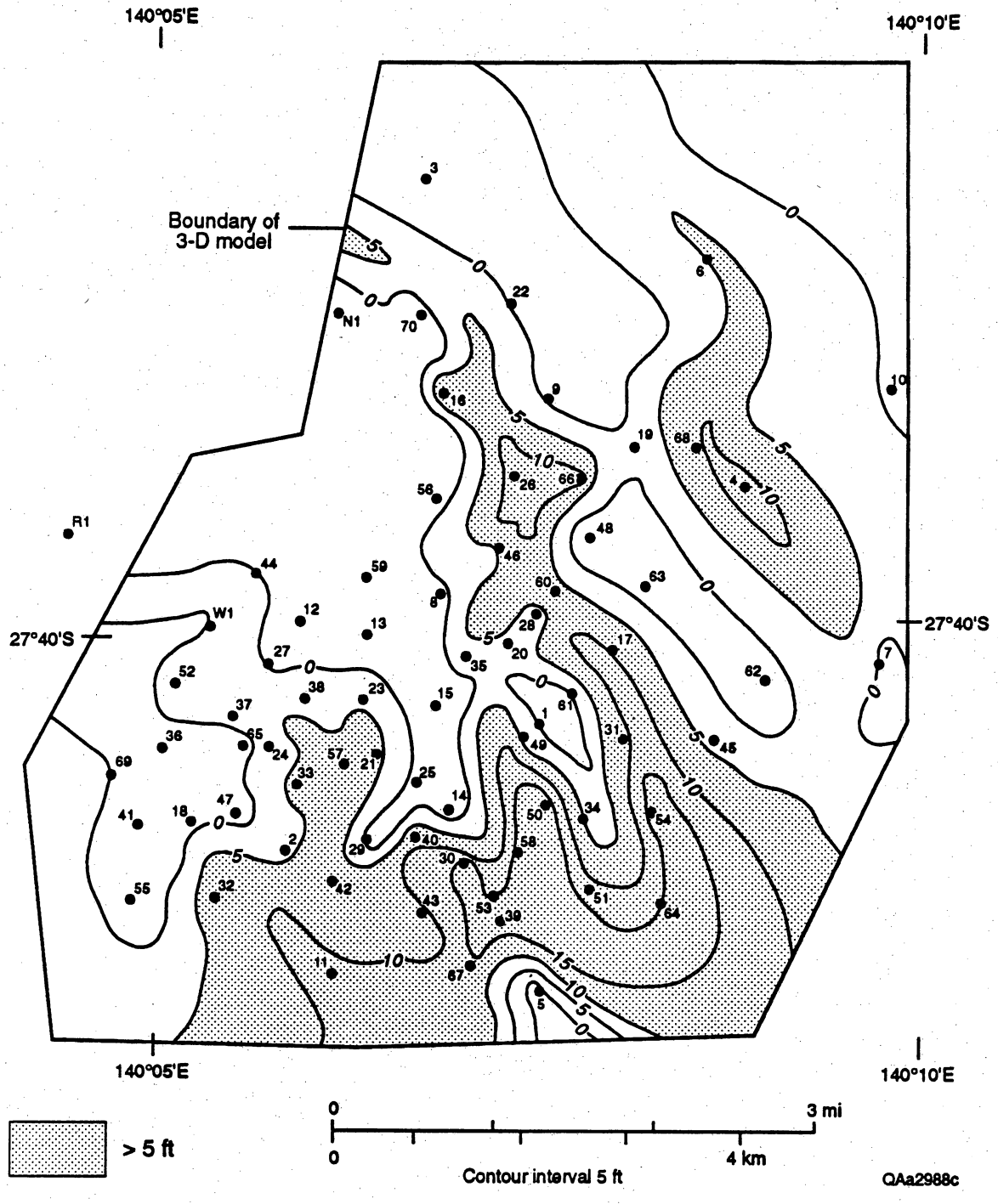

Figure V-32. Net porous sandstone map of Tirrawarra flow unit 2L.

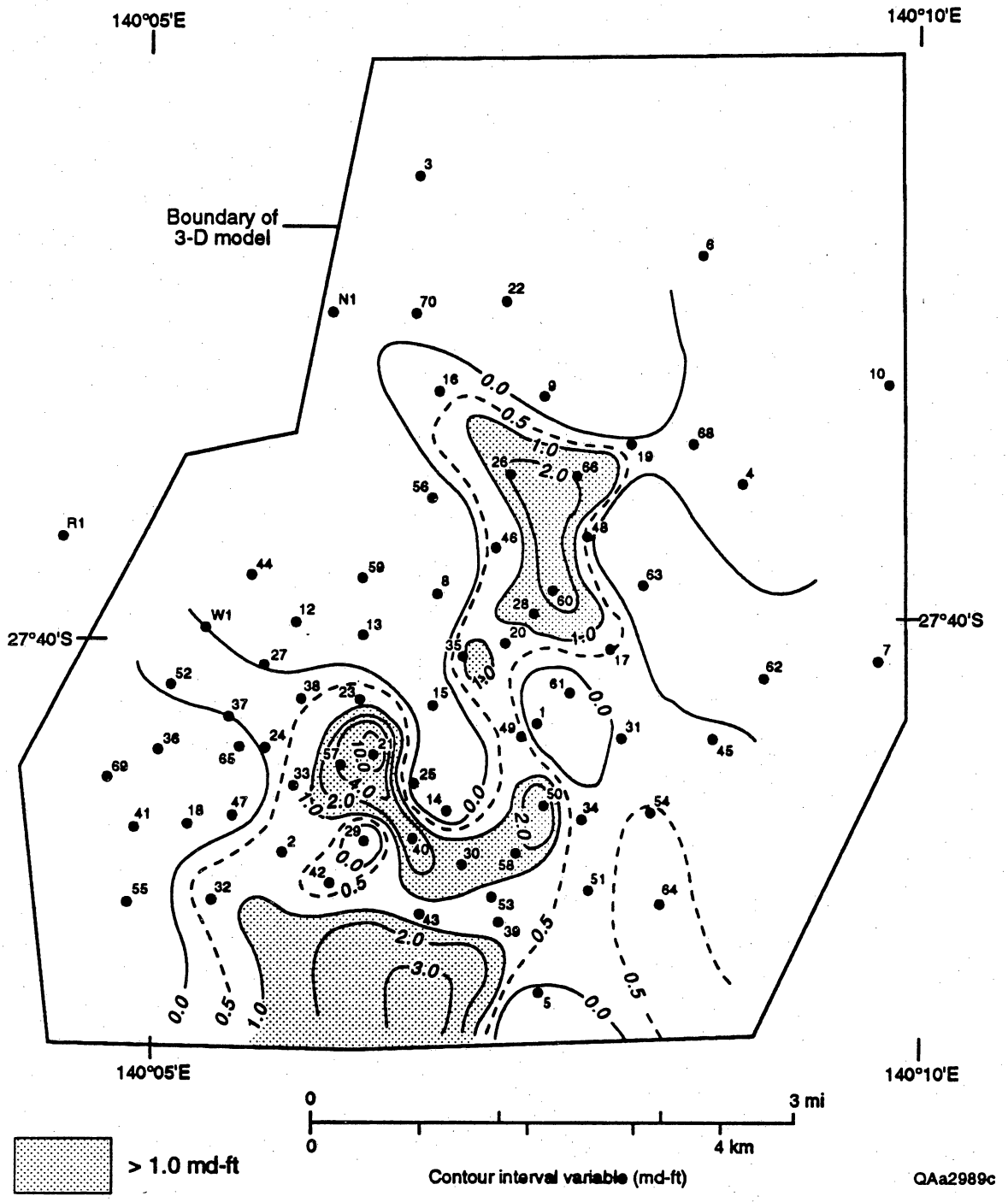

Figure V-33. Permeability-thickness (kh) map of Tirrawarra flow unit 2L.

more likely to be permeable, because clean sandstone is best developed at the top of unit 1U and at the base of unit 2L. Unfortunately, abundant mud clasts and organic debris decrease permeability in the lower part of flow unit 2L in many wells.

Flow unit 2L geometries appear to be primarily depositional, but erosional truncation of unit 2L is likely in places where flow unit 3L rests directly on the lower part of facies 1 (figs. V-26 and V-27). In these areas truncation of flow unit 1U is documented, and a comparison of isopach maps reveals that the areas where units 1U and 2L are missing commonly coincide (figs. V-28 and V-31). On the other hand, local gradational contacts between units 2L and 3L, transitional lithologies, and bodies of facies 2-type rock within unit 3L suggest that deposition of the upper part of unit 2L and the lower part of unit 3L was at least partly contemporaneous. As the fluvial system on the delta plain was evolving into a more sand-rich, bed-load dominated one, the narrow channels of flow unit 2L were replaced with the broad channels of unit 3L. Early unit 3L channels were probably preferentially located in the topographically low, interchannel areas of unit 2L.

Facies 3 (Flow Units 3L and 3U)

Facies 3 is continuous across Tirrawarra field, ranging in thickness from approximately 40 to 100 ft (figs. V-26, V-27, and V-34). Thickness variations in facies 3 are in part erosional, although the general northwest trend is probably depositional. The larger scale, gradational thinning of facies 3 toward the north and northeast is attributable to erosional truncation by the overlying facies 4, and facies 3 is relatively thicker where it truncates underlying facies 2 and 1. The broad multidirectional trends displayed on the facies 3 isopach map (especially in the south half of the field, fig. V-34) are typical geometries for bed-load fluvial channel systems, although Tirrawarra field probably encompasses only a small part of the facies 3 depositional system. Bed-load channels are characterized by high width/depth ratios, poorly developed banks, and rapid lateral migration (Galloway and Hobday, 1983). Bed-load fluvial systems form laterally continuous sheet or tabular sand bodies that are composed internally of interlensing sandstones and isolated remnant mudstones (Campbell, 1976).

Because of lateral coalescence, the dimensions of individual channels in facies 3 could not be determined directly from well and core data. Studies of outcrops of similar fluvial systems reveal that individual channel sandstones are typically less than 20 ft thick and several hundred to several thousand feet wide (Campbell, 1976; Davies and others, 1991). Because most clean sandstones in facies 3 are 3 to 20 ft thick between mud-rich interbeds, they could represent single channel deposits. Width/depth ratios greater than 40 are typical for bed-load fluvial channels (Schumm, 1977), and using this relationship, facies 3 channel sandstones would

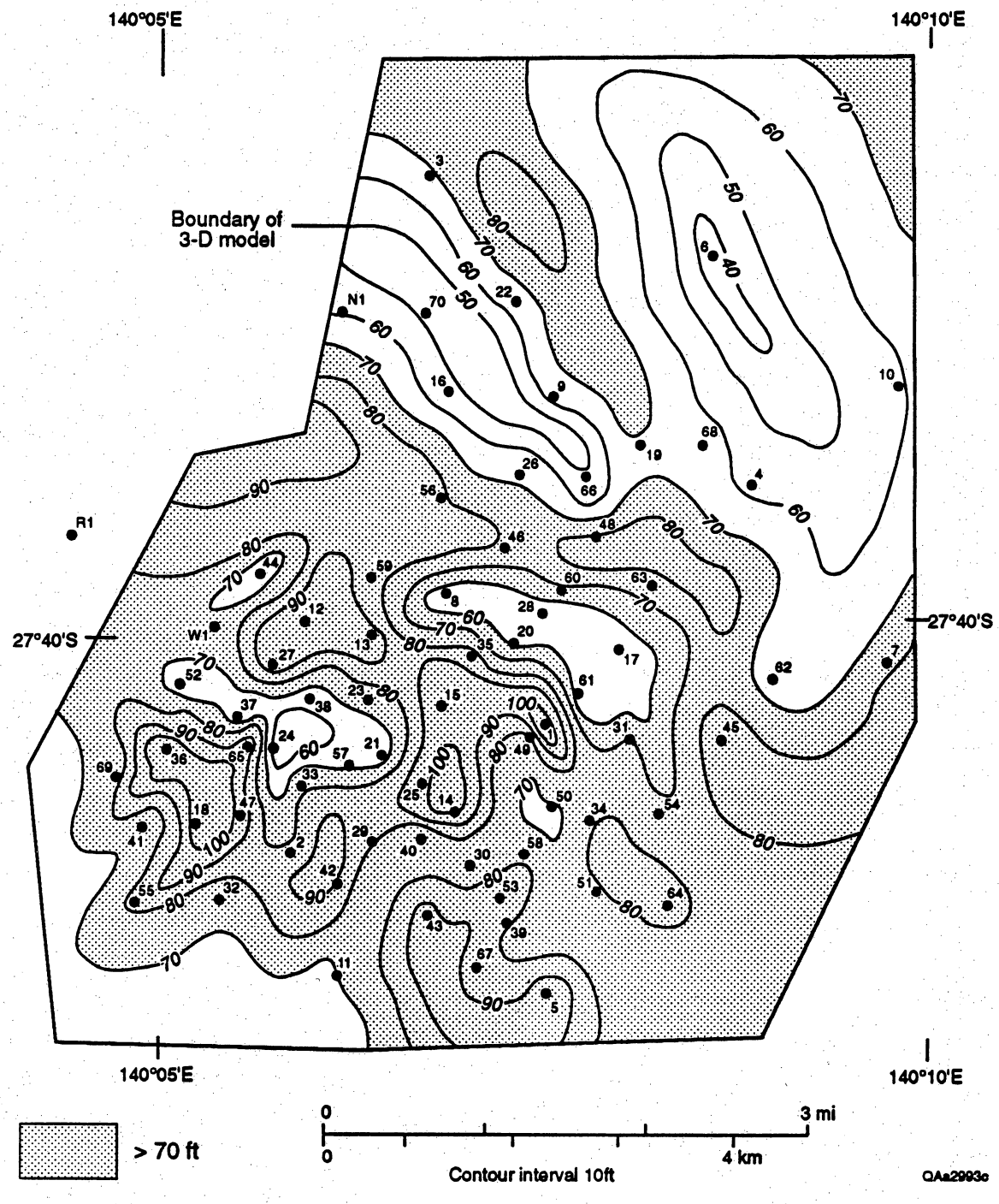

Figure V-34. Isopach map of Tirrawarra facies 3, which includes both flow units 3L and 3U.

be at least 120 to 800 ft wide (similar results are obtained using statistics presented by Fielding and Crane [1987]). Complexes of laterally coalesced and vertically stacked channels may reach 100 ft in thickness and more than 10 km in width. Sandstones within these complexes are not greatly compartmentalized by discontinuous erosional remnants of abandoned channel fill and floodplain mudstone. Thus, the facies 3 flow units probably lack significant flow barriers that can be related to their depositional framework.

Thickness patterns in flow units 3L and 3U are similar to those in facies 3. The boundary between flow units 3L and 3U represents a rather subtle and gradational change in rock properties but not a significant change in depositional facies. Therefore, thickness trends in facies 3, which are closely related to depositional environment, served to guide mapping of its component flow units. An isopach map of unit 3L suffices to document both units; unit 3U thicknesses can be obtained by subtracting (in Stratamodel) the unit 3L isopach map from the facies 3 isopach map. Flow unit 3L is thickest (greater than 50 ft) in the west and west-central parts of the field, whereas it is mostly less than 30 ft thick in the east and north (fig. V-35). By comparison, flow unit 3U is thickest in the southeast and east-central parts of the field, where facies 3 is thick (fig. V-34), but where flow unit 3L is thin (fig. V-35). Unit 3U is also thick in isolated wells, where unit 3L is atypically thin (wells 6, 17, and 68).

Net porous sandstone patterns in flow units 3L and 3U are similar to interval thickness patterns, because these units are composed primarily of porous sandstone in most wells. Exceptions to this similarity exist where mud-rich interbeds or transitional facies are atypically abundant. Transitional facies are bodies of facies 2-type rock that occur within facies 3 but that are not sufficiently extensive to be treated as separate flow units. Net porous sandstone in flow unit 3L is 30 to 60 ft thick in much of the central and west parts of the field but is less than 30 ft thick in most of the north and northeast (fig. V-36). Net porous sandstone in flow unit 3U is thickest in the east-central, southeast, and west and is thinnest in the north and locally around the margins of the field (fig. V-37). Unit 3U porous sandstone forms pods and belts that are 40 to 60 ft thick, 1 to 2 km wide, and 2 to 4 km long. Unit 3L porous sandstone is more sheetlike in distribution, although "thins" having less than 30 ft of net sandstone occur around wells 17 and 38 (fig. V-36). These thins coincide with net sandstone thicks on the unit 3U map (fig. V-37).

Flow units 3L and 3U are not entirely homogeneous. As discussed previously, thin interbeds of muddy sandstone and sandy mudstone occur, on average, about every 10 ft. Core data document low permeabilities in these interbeds, which are mostly less than 2 ft thick but locally reach 10 ft in thickness. Almost none of these low-permeability layers, however, are traceable between wells, and therefore their lateral continuities are probably less than 0.5 km. This is typical of abandoned channel fill and interchannel mudstones in a bed-load fluvial

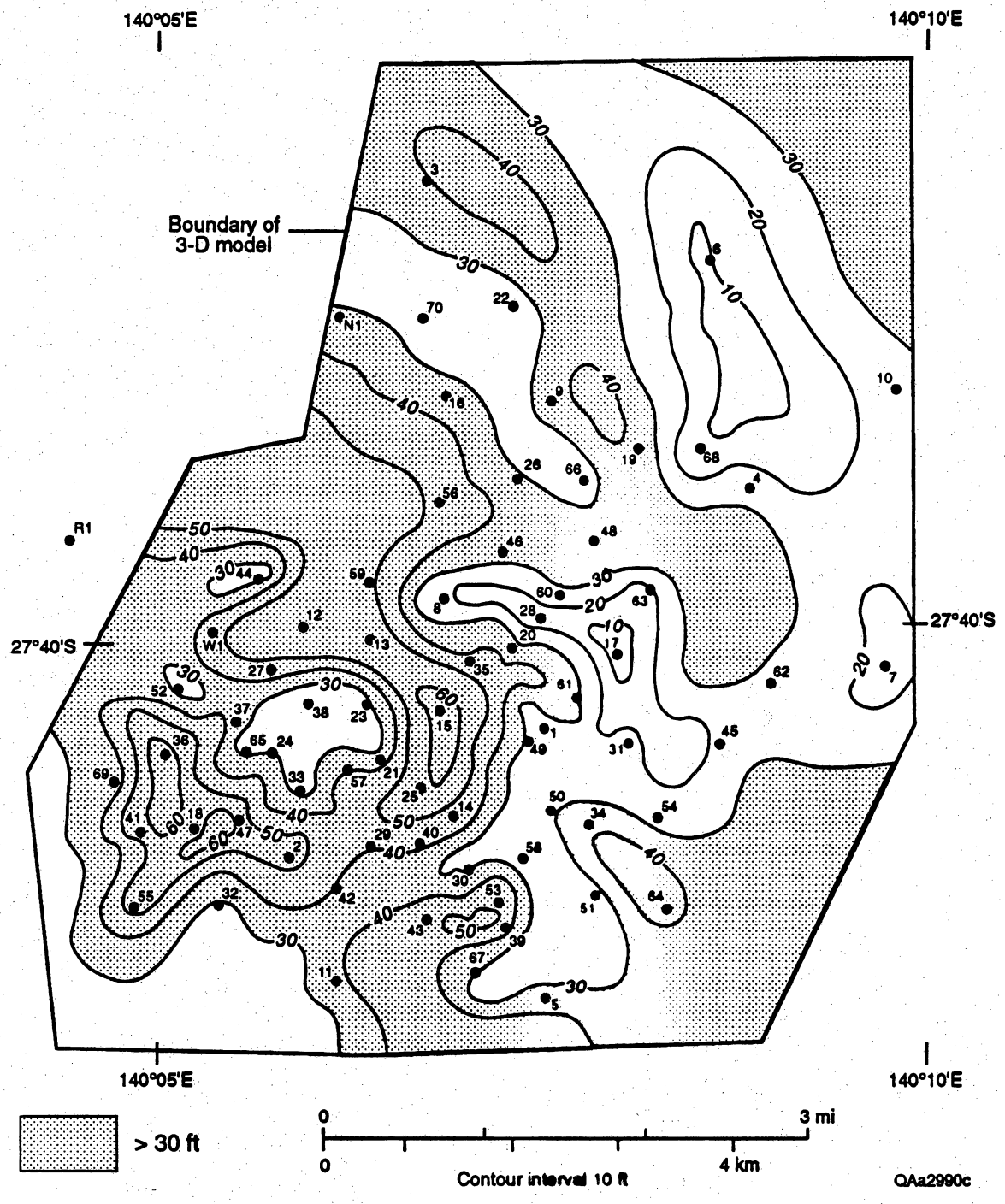

Figure V-35. Isopach map of Tirrawarra flow unit 3L.

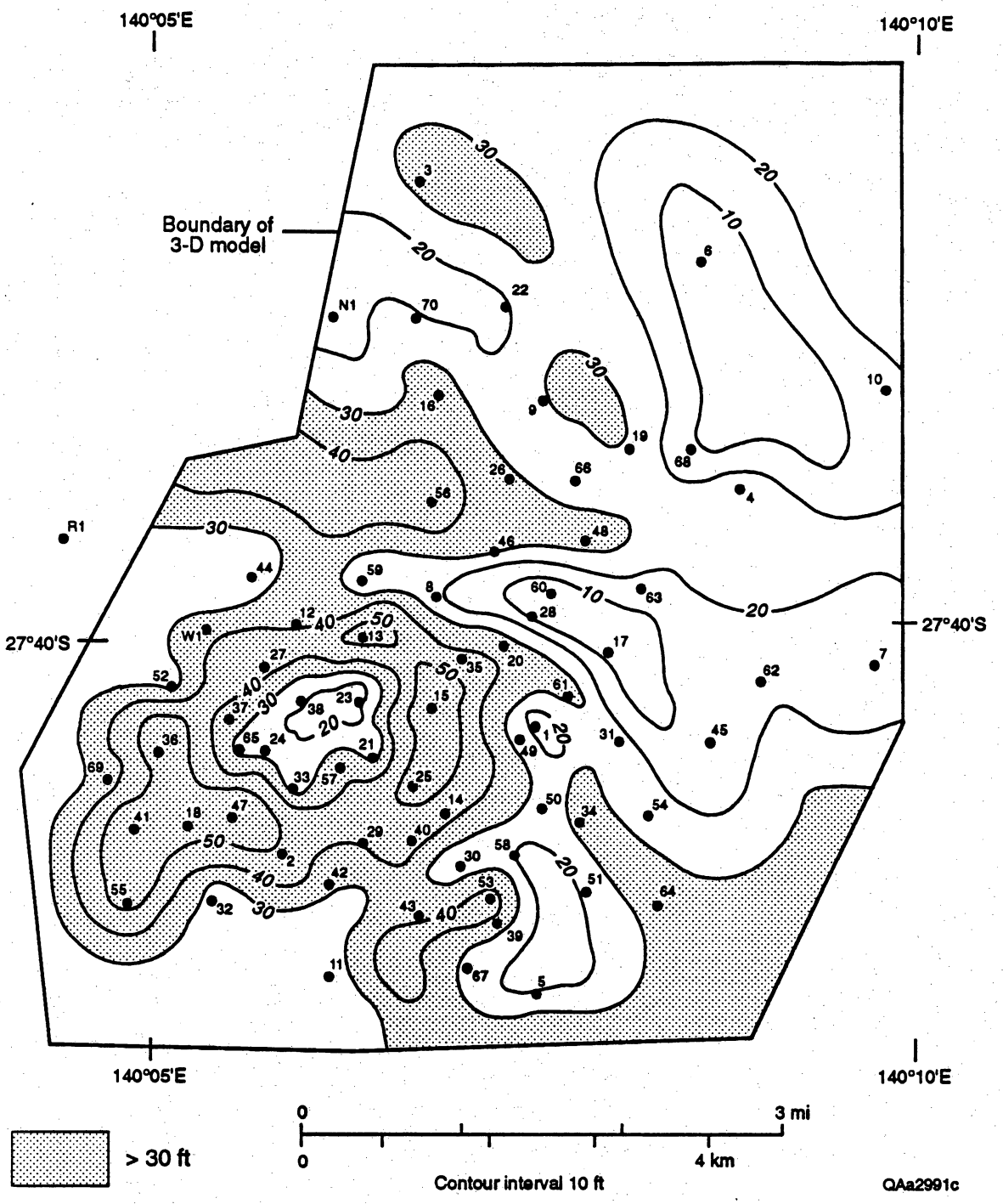

Figure V-36. Net porous sandstone map of Tirrawarra flow unit 3L.

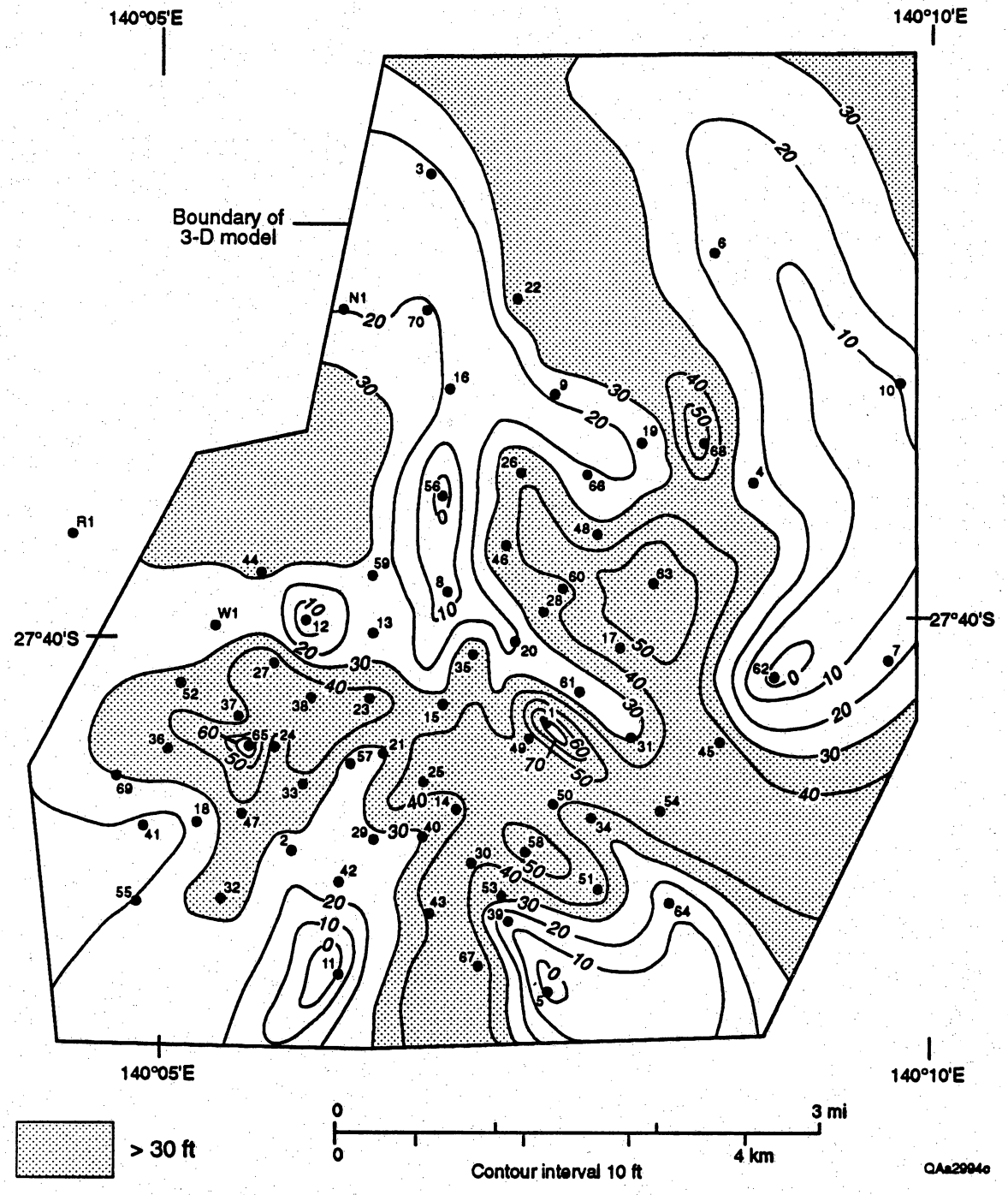

Figure V-37. Net porous sandstone map of Tirrawarra flow unit 3U.

system (Hamlin, 1988); efficient lateral channel migration removes most fine-grained deposits from the floodplain, leaving only isolated erosional remnants. Some of the mud-rich interbeds may record lacustrine flooding events, but because of the depositional topography that typifies bed-load fluvial systems (Miall, 1981), episodes of flooding may have incompletely inundated the delta plain. In any case, mud-rich interbeds in units 3L and 3U could only rarely be correlated between adjacent wells.

Permeability is probably anisotropic in flow units 3L and 3U, although directional permeability measurements are unavailable. Vertical permeability is inhibited by abundant horizontal lamination, low-permeability interbeds, and stylolites. In reservoirs having similar sedimentary features, the most common vertical/horizontal permeability ratios are less than 0.25 (Hearn and others, 1984). Medium to large-scale crossbedding, which is common locally in facies 3, imparts significant anisotropy to permeability, although oriented core is needed for directional determination (Weber, 1982).

Despite the apparent relative homogeneity of facies 3, internal permeability distribution is variable. Permeability-thickness trends in flow units 3L and 3U (figs. V-38 and V-39) display only an approximate coincidence with net porous sandstone trends (figs. V-36 and V-37). In some wells, porous sandstone development is poorly related to permeability, suggesting that thin zones having very high permeability may be controlling fluid flow locally. In flow unit 3L, core data indicate that layers having permeabilities greater than 50 md are generally less than 3 ft thick and are relatively rare. In well 8, for example, which includes several of these high-permeability thin beds, flow unit 3L has a high permeability-thickness (fig. V-38) even though porous sandstone is relatively thin (fig. V-36). In other wells having below-average thicknesses of porous sandstone in flow unit 3L (well 21, for example), permeabilities are consistently above average, and the resulting permeability-thickness is high.

Permeability variations within facies 3 are probably related to local differences within the depositional environment. High-permeability zones in cored intervals of facies 3 are relatively coarse grained and well sorted and include few mud-rich interbeds. Thin channel-base lag deposits or channel sands winnowed by shorezone processes are examples of subenvironments in facies 3 where high permeabilities could be produced. Unfortunately, as with low-permeability layers in facies 3, high-permeability deposits are also subject to subsequent removal (partial or complete) by migrating fluvial channels. Bed-load fluvial systems, although sand-dominated and grossly homogeneous, are composed internally of nested channel deposits that are truncating each other laterally and vertically. The bed-load channel system as a whole has excellent continuity, but its component channel and interchannel deposits are extremely discontinuous. Because these systems are, on average, permeable, and their fluid transmission

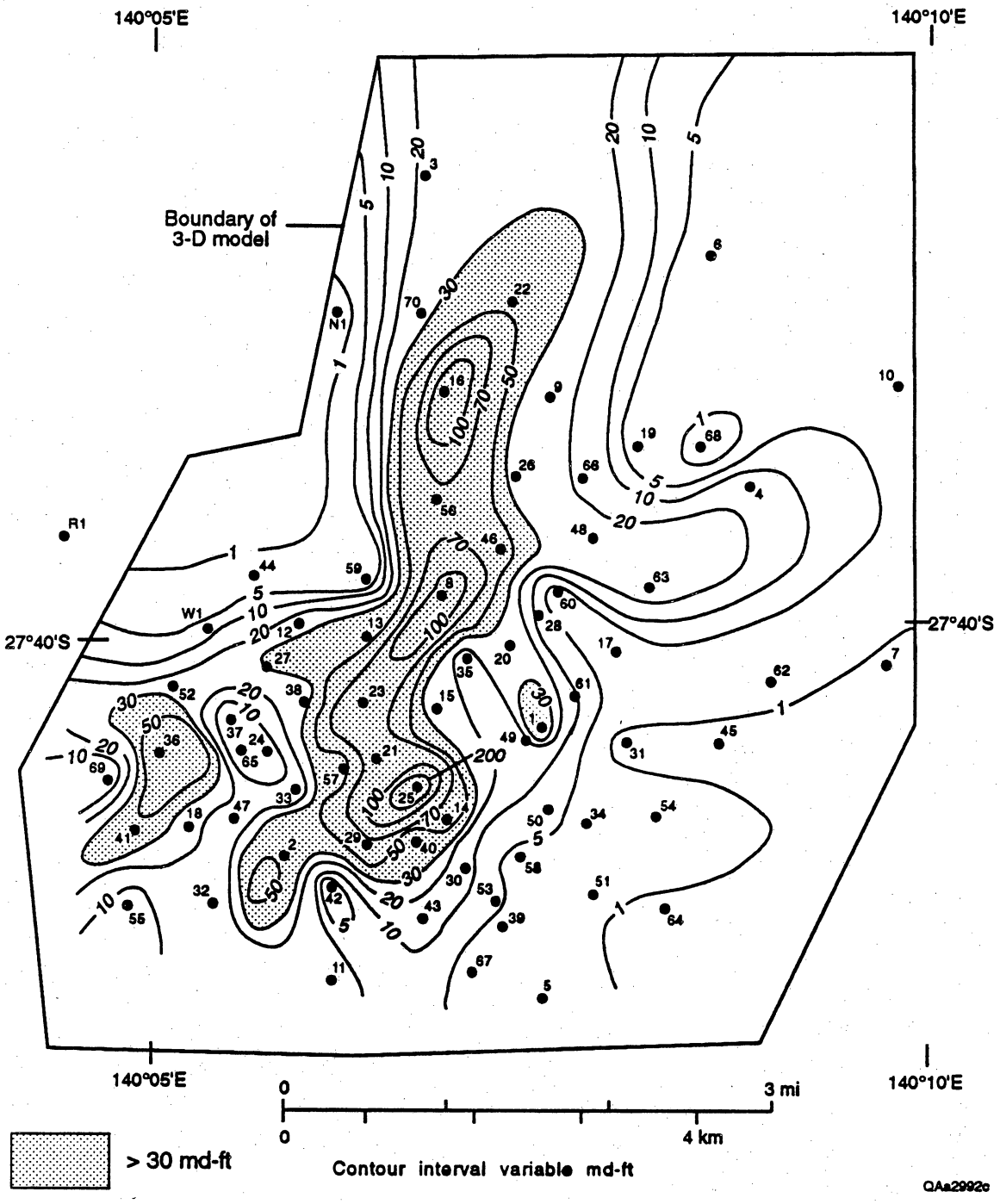

Figure V-38. Permeability-thickness (kh) map of Tirrawarra flow unit 3L.

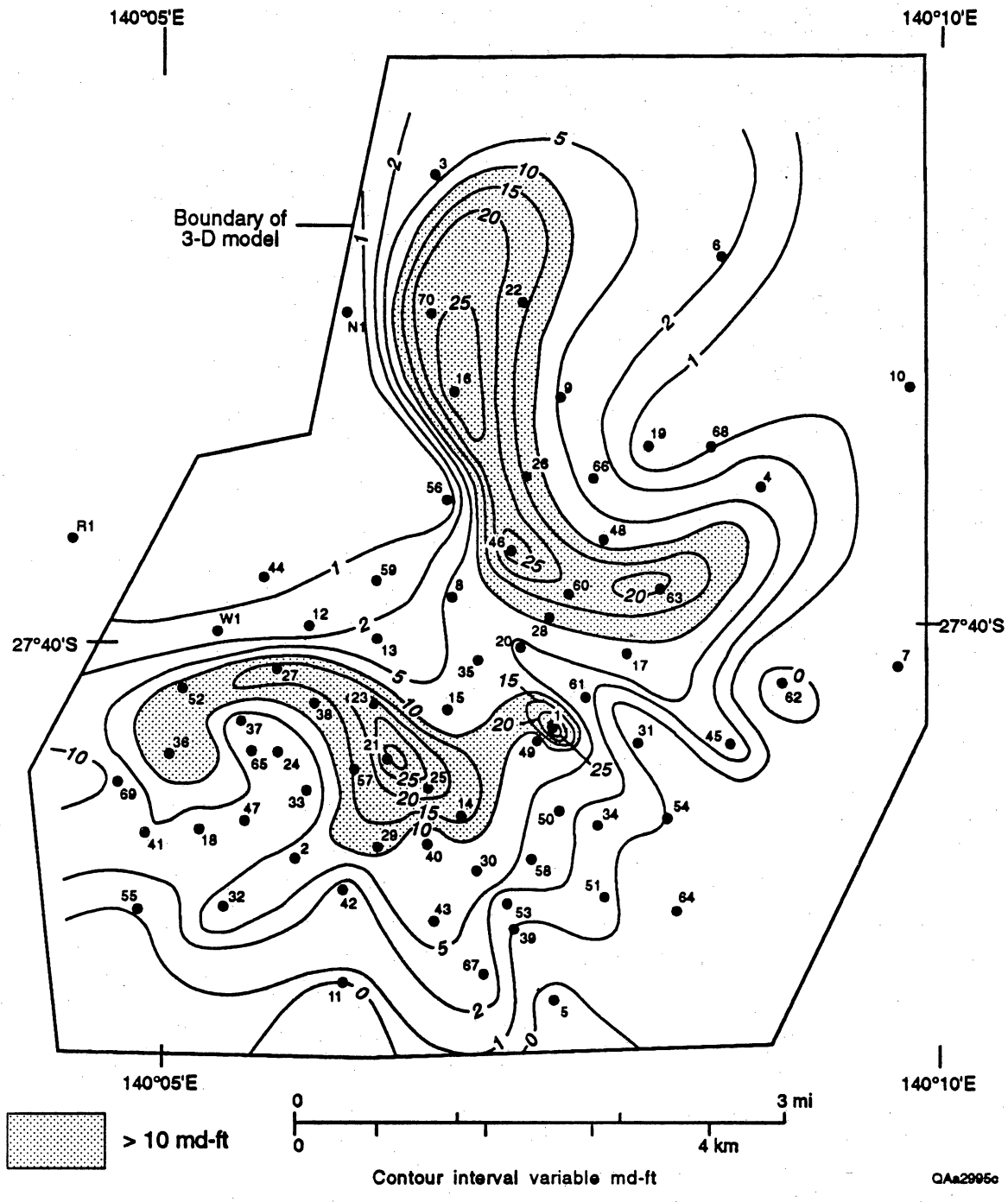

Figure V-39. Permeability-thickness (kh) map of Tirrawarra flow unit 3U.

capacities are typically high, they are usually modeled as single flow units (Davies and others, 1991).

Permeability conditions vary across the boundaries of flow units 3L and 3U. The boundary between flow units 3L and 3U is not a significant stratigraphic break, although it is marked locally by thin mud-rich layers. As discussed above, the boundary between unit 2L and 3L is commonly impermeable. Mudstone beds are common near the base of both flow units 2U and 4 (cross section plates), limiting permeability between these units and unit 3U, especially in the south and west. Across the northern part of the field and locally in the central part, sandstone in unit 3U is in erosional contact with sandstone and conglomerate at the base of unit 4, and studies of core indicate that this contact is usually permeable.

Facies 2 (Flow Unit 2U)

Flow unit 2U is a development of facies 2 lying between flow units 3U and 4 in the west and southwest parts of Tirrawarra field. Flow unit 2U grades laterally into unit 3U and is erosionally overlain by unit 4 (plates V-1 through V-13). Thus, part of the sand-dominated bed-load fluvial system represented by facies 3 was abandoned and replaced primarily by the fine-grained interchannel and lake-margin facies that characterize unit 2U. Mixed-load channel sandstones, having abundant mud clasts and organic debris, are common to both flow units 2L and 2U, but unit 2U apparently includes fewer channel sandstones than does unit 2L. The unit 2U isopach map displays a simple southwest-thickening wedge having a lobate margin where it interfingers with unit 3U (fig. V-40). Porous and permeable sandstone is poorly developed in flow unit 2U and is restricted to a few wells in the southwest part of the field (figs. V-41 and V-42). Studies of well logs and core indicate that unit 2U is composed mainly of muddy sandstone in which mudstone interbeds are abundant but clean sandstone is rare. Porous sandstone in flow unit 2U is isolated from flow unit 4 by thick mudstone or muddy sandstone everywhere except possibly around wells 24 and 55.

Facies 4 (Flow Unit 4)

Flow unit 4, although continuous across the field (figs. V-26 and V-27), varies widely in thickness and reservoir quality. Flow unit 4 is thickest in belts that trend southeast generally but are more south- to southwest-trending in the northeast part of the field (fig. V-43). These belts, which are 30 to 60 ft thick, are 1 to 2 km wide in the southwest, south, and central parts of the field but are 2 to 3 km wide in the north and east. The areas in between the belts, where

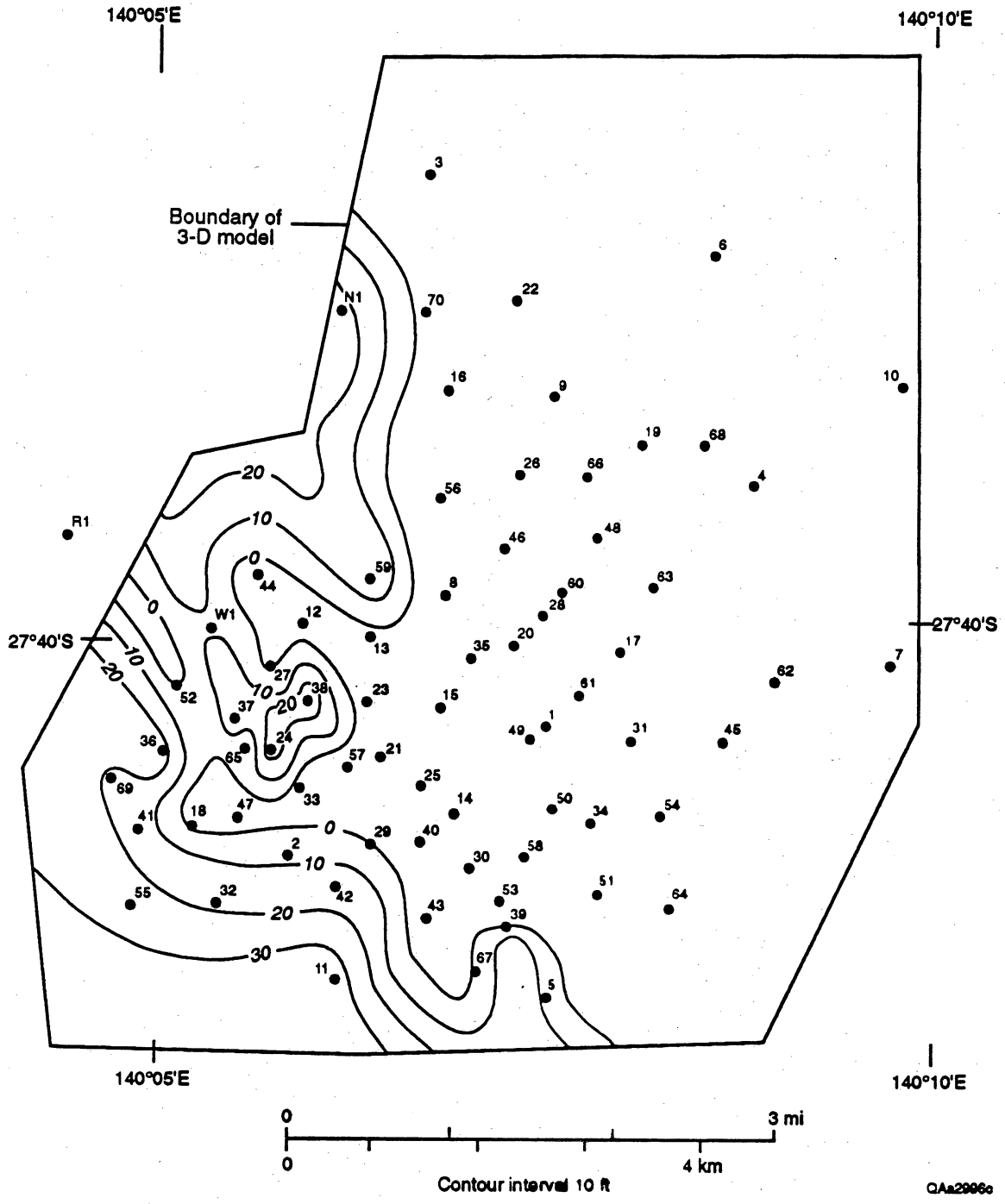

Figure V-40. Isopach map of Tirrawarra flow unit 2U.

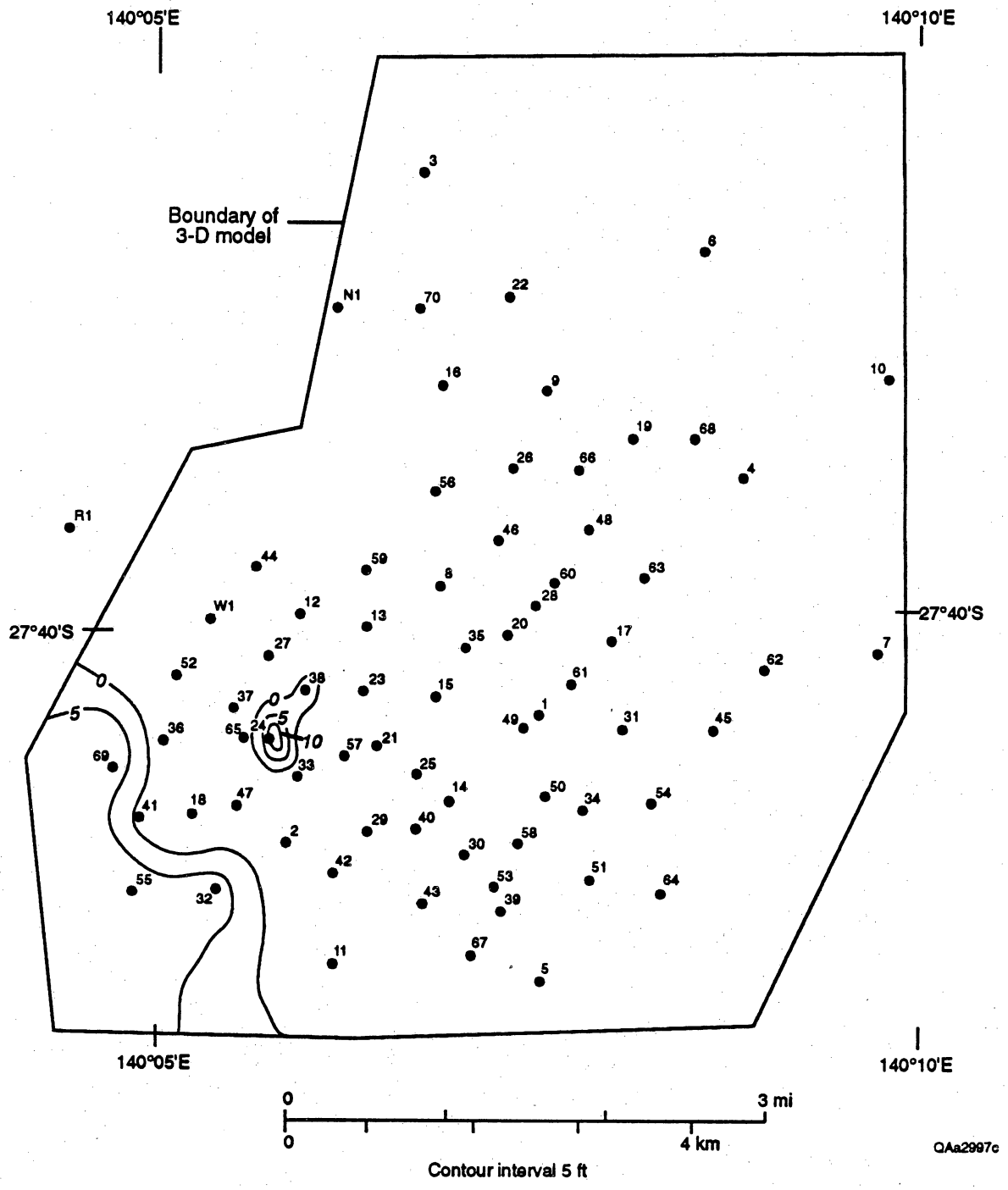

Figure V-41. Net porous sandstone map of Tirrawarra flow unit 2U.

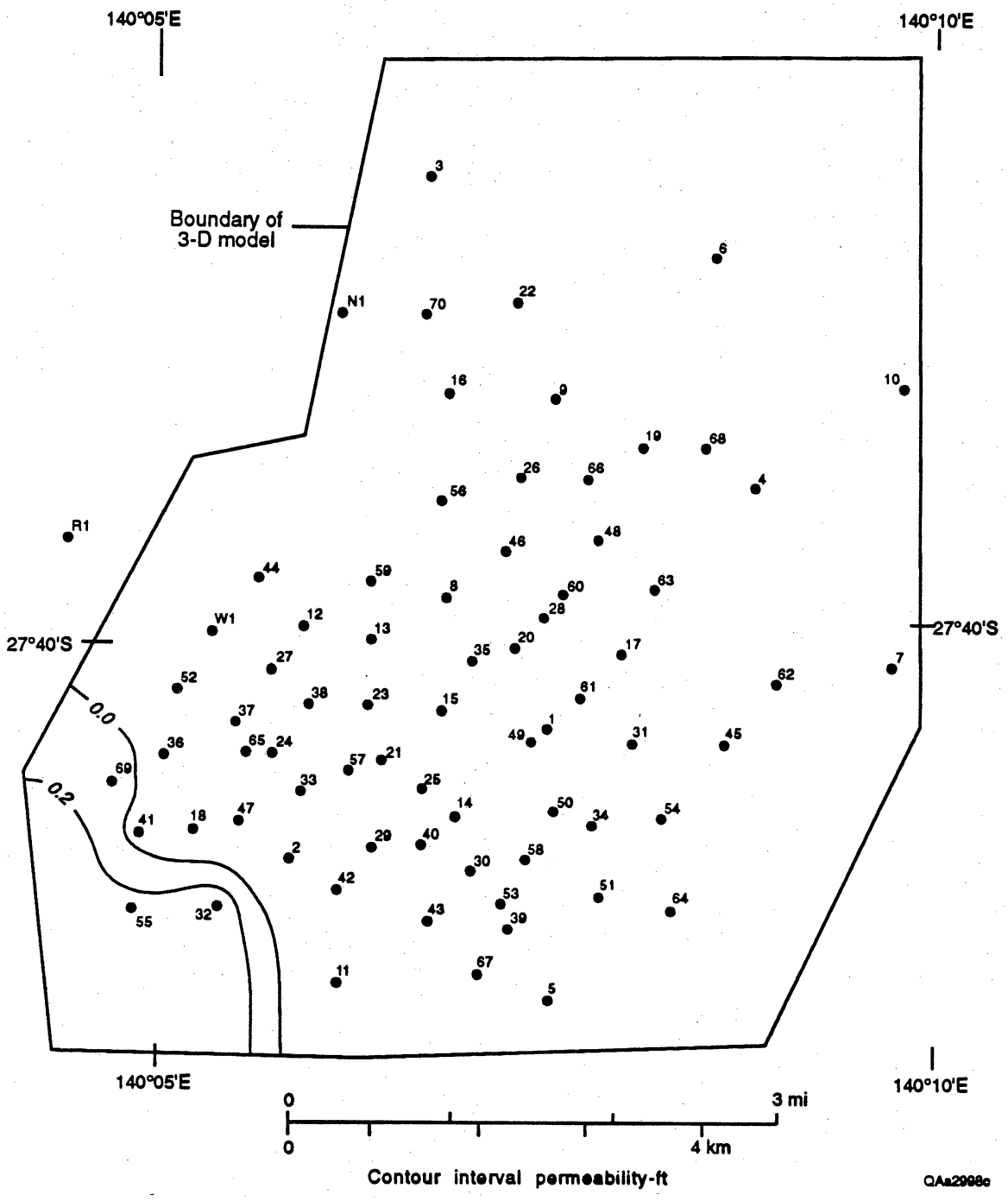

Figure V-42. Permeabililty-thickness (kh) map of Tirrawarra flow unit 2U.

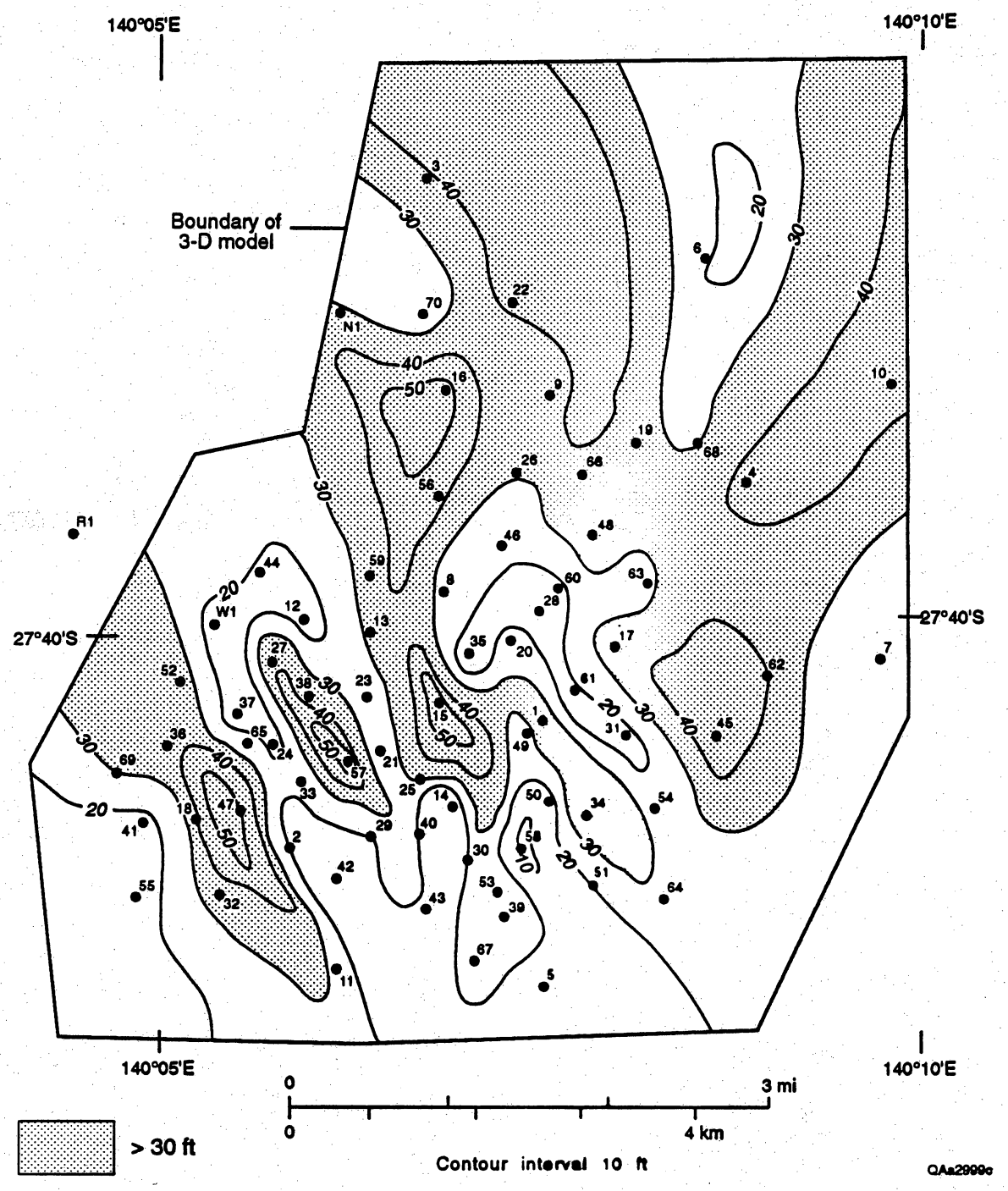

Figure V-43. Isopach map of Tirrawarra flow unit 4.

unit 4 is 10 to 30 ft thick, are larger in the south half of the field than they are in the north half (fig. V-43). Belts of relatively thicker unit 4 delineate areas where fluvial channel sandstones are vertically stacked. The areas in between these belts generally contain channel sandstone only in the lower part of unit 4. In a few areas, such as around wells 12 and 58, unit 4 includes only interchannel deposits. Since the top of flow unit 4 is defined as the top of the uppermost sandstone, vertical stacking strongly influences isopach patterns. Porous sandstone in flow unit 4 is best developed within the belts of stacked channel sandstones. Areas where unit 4 is 30 to 60 ft thick (fig. V-43) coincide with areas where net porous sandstone is 10 to 40 ft thick (fig. V-44). In the interbelt areas where only one channel sandstone is typically present, net porous sandstone is generally less than 10 ft thick. Permeability thickness is also best developed within the channel belts (fig. V-45).

The laterally continuous channel sandstone complex in the lower part of flow unit 4 was deposited in a bed-load fluvial system, having low-sinuosity braided channels. This sandstone is 5 to 25 ft thick and is generally coarser grained than is facies 3 sandstone. Conglomerate interbeds up to 3 ft thick are common in sandstone in the lower part of unit 4, especially in the southeast part of the field. These features suggest that sandstone in the lower part of flow unit 4 was deposited in a more proximal, braidplain setting, compared with the more distal, braid delta-plain setting of facies 3. These two facies, however, cannot be considered as parts of the same depositional systems tract. Facies 3 belonged to an earlier depositional system, which was more sand-dominated than the succeeding facies 4 system. Partial erosion of the older facies 3 delta plain accompanied deposition of facies 4. Channel banks were somewhat better stabilized in facies 4 than they were in facies 3, so that larger remnants of fine grained interchannel deposits were preserved, and mud clasts and organic debris became incorporated in the channel fills.

Bed-load fluvial channels in the lower part of flow unit 4 probably have similar dimensions to their counterparts in units 3L and 3U but are likely to be more compartmentalized. Individual channel sandstones in the lower part of unit 4 are generally less than 20 ft thick and, based on statistically derived width/depth ratios (Schumm, 1977; Davies and others, 1991), range from 200 to 800 ft wide. Cross sections reveal that the lower unit 4 sandstone is continuous across most of Tirrawarra field (plates V-1 through V-13), and it must, therefore, represent a laterally coalesced channel complex. Remnants of fine-grained interchannel deposits are probably preserved locally along the contacts between individual channels within this complex. Permeability compartments thus created would be elongate parallel to trends displayed on the unit 4 maps (figs. V-43 through V-45) and would most likely be in partial communication with each other, owing to incomplete preservation of fine grained barriers.

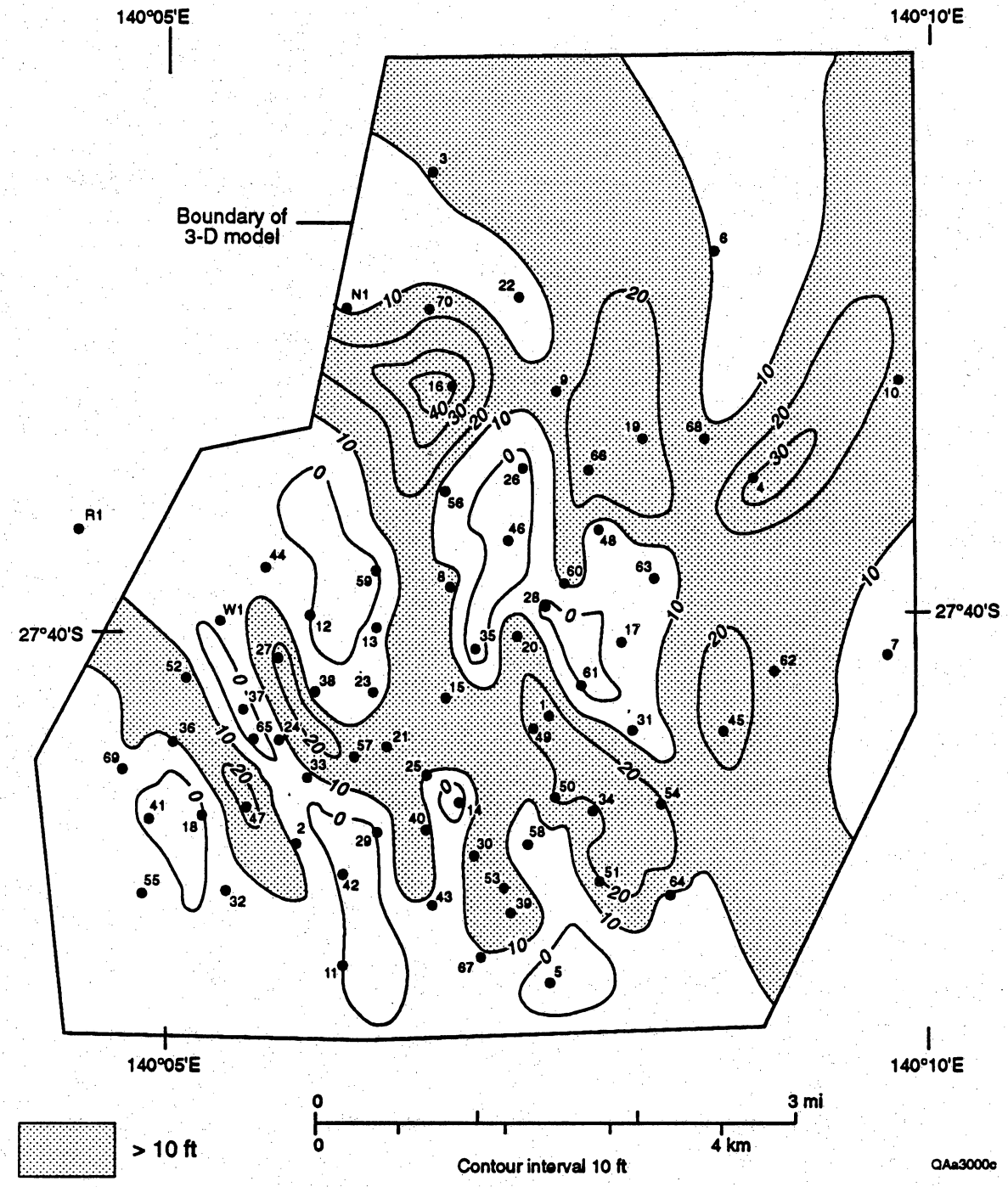

Figure V-44. Net porous sandstone map of Tirrawarra flow unit 4.

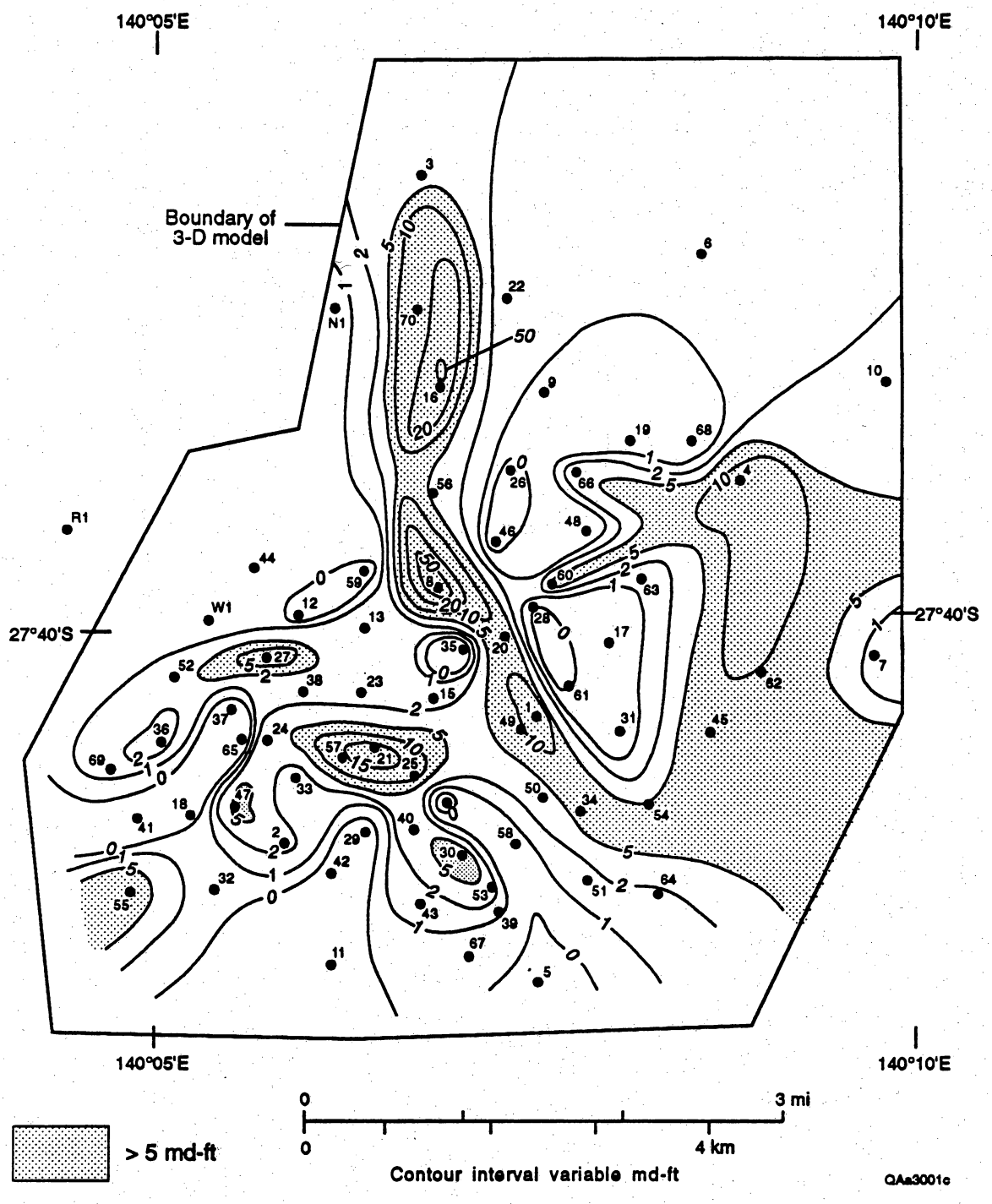

Figure V-45. Permeability-thickness (kh) map of Tirrawarra flow unit 4.

Conglomeratic beds in flow unit 4 represent lag deposits or bar forms that are discontinuous within individual channels. Within sandstone-dominated channels having the dimensions discussed above, conglomeratic beds would not exceed a few feet in thickness, a few hundred feet in width, or a few thousand feet in length. Studies of well log and core data confirm these general dimensions for conglomeratic beds in flow unit 4 and also reveal that locally they have low permeabilities owing to abundant matrix-filling mud clasts and carbonaceous debris. Nevertheless, thin conglomeratic beds in flow unit 4 are potential high-permeability flow conduits.

Lenticular sandstone, mudstone, and coal interbedded in the upper part of flow unit 4 record deposition in a mixed-load fluvial system in which sand, silt, and clay are subequally preserved. Individual channels in this system probably resemble the classic meandering stream model: sinuous channel-fill deposits composed of laterally accreting point-bar sandstones and abandoned channel fill mudstones and enclosed in floodplain mudstones and coals. Meandering channels migrate laterally in a systematic way within the confines of a meanderbelt. Lenticular sandstones in the upper part of flow unit 4, which probably are individual meanderbelt deposits, are 10 to 20 ft thick and 0.5 to 2 km wide, although they appear wider on cross sections (plates V-1 through V-13) because of oblique section orientations. These meanderbelt deposits are confined to the areas where the unit 4 isopach is greater than 30 ft (fig. V-43), coinciding with the stacked channel belts described above. Individual sandstones within the meanderbelts are compartmentalized by mud drapes along point-bar accretion surfaces and abandoned channel fill mudstones.

Channel sandstones in both the upper and lower parts of flow unit 4 are internally heterogeneous. Mudstone clasts, laminations, and thin beds are more abundant in facies 4 than they are in facies 3. Most of the unit 4 sandstones that were studied in core, however, include zones of relatively clean sandstone and conglomerate, 3 to 15 ft thick. Core data show that, similar to units 3L and 3U, high-permeability zones in unit 4 are typically thin and interlayered with thicker zones having low permeability. Zones having permeability greater than 10 md (common) are generally less than 5 ft thick, and those having permeability greater than 100 md (rare) are 1 ft or less thick.

Channel sandstones in the upper part of flow unit 4 are enclosed in interchannel mudstones and coals. These fine-grained layers are generally less than 20 ft thick, extend up to one-third of the distance across the field, and are typically truncated against the margins of channel sandstones (plates V-1 through V-13). These fine-grained layers isolate upper four meanderbelt sandstones from the lower four tabular bed-load channel sandstone across most of the field except locally in the north and northeast. Sandstone in the lower part of unit 4 is

isolated from underlying flow units by mudstone and sandy mudstone across the west and southwest and locally in the central and east parts of the field.

Summary of Facies-Related Reservoir Properties

The Tirrawarra reservoir is a sandstone-dominated interval, 100 to 150 ft thick, composed of four depositional facies. The Tirrawarra facies record progradation of several fluvial-deltaic systems across an intracratonic lacustrine basin. The reservoir is bounded below by fine-grained lake-center sediments and above by flood-basin mudstones and coals. The core of the reservoir formed when a major bed-load fluvial system prograded into and aggraded the lake basin (fig. V-7). The resulting deposit (facies 3) extends throughout the field, is 40 to 100 ft thick, and is 60 to 90 percent porous sandstone. Although facies 3 as a whole is a sheet sandstone, it is composed internally of laterally discontinuous layers, which are erosional remnants of channel-fill and interchannel deposits. Most of these layers are thick, permeable sandstone beds (3 to 20 ft, 0.5 to 3 md), but numerous thin layers (less than 3 ft) occur in facies 3 that are either impermeable or very permeable (greater than 10 md). Models of bed-load fluvial systems suggest that individual layers in facies 3 generally do not extend more than 0.5 km and are, therefore, not readily mappable at current well spacing in Tirrawarra field. The inherent discontinuity of layering (both permeable and impermeable layers) indicates that the overall permeability structure of facies 3 is well interconnected. Facies 3 was divided into two reservoir flow units on the basis of variations in well log responses and petrophysical properties. The available core data indicate that flow unit 3L has, on average, higher porosities and permeabilities than does flow unit 3U (table V-5, figs. V-14 and V-15).

Facies 3 prograded over a small delta system comprising a fine-grained delta-front sandstone/siltstone (facies 1) and a heterogeneous distributary channel and channel mouth bar complex (lower development of facies 2) (fig. V-3). The upper part of facies 1 is flow unit 1U, which is relatively homogeneous but has only marginal reservoir quality. Overlying flow unit 1U is flow unit 2L, which comprises sinuous belts of channel sandstone merging southeastward into lobate channel mouth bar sandstone. Isolated permeable zones in flow units 1U and 2L are locally in communication with the more widespread permeability structure of flow unit 3L. Net porous sandstone in units 1U and 2L combined, however, rarely exceeds 10 ft. Although dominated by laterally coalesced fluvial channel sandstones, facies 3 also contains isolated bodies of facies 2-type muddy sandstone, which represent preserved remnants of interchannel and lake-margin environments on the braid delta plain (fig. V-7). These muddy sandstone bodies limit reservoir quality locally, especially in flow unit 3U, where one such body (unit 2U)

is sufficiently extensive to be mappable as a distinct reservoir flow unit. Porous sandstone in flow unit 2U is restricted to a few wells in the southwest part of the field.

The fluvial-deltaic system that deposited facies 1, 2, and 3 was subsequently truncated and buried by a more proximal fluvial system (facies 4, fig. V-10). Facies 4 includes sandstone and conglomerate that is coarser grained than any found in the underlying facies, but it also includes abundant muddy sandstone, mudstone, and coal. The sequence bounding unconformity that underlies facies 4 marks the end of the progradational style of deposition in the Tirrawarra reservoir. Above this unconformity, sandstone content decreases upward, recording gradual replacement of fluvial channels with swamps, bogs, and lakes. Multilateral bed-load channel sandstones in the lower part of facies 4 are overlain by more isolated mixed-load channel sandstones in the upper part. Porous sandstone development reflects channel sandstone distribution. Net porous sandstone is thin (less than 15 ft) but widespread in the lower part of facies 4 but is thick (15 to 40 ft) where lenticular channel sandstones in the upper part are vertically stacked above the more continuous lower part. Because this change in channel sandstone geometry is gradational, facies 4 is defined as a single flow unit. More widespread preservation of low-permeability interchannel and abandoned-channel deposits resulted in more compartmentalization of flow unit 4 relative to flow units 3L and 3U.

VI. PETROGRAPHIC COMPOSITION OF TIRRAWARRA SANDSTONES

Original porosity and permeability of Tirrawarra sandstones were determined by their depositional environment, but diagenesis has significantly altered reservoir characteristics after deposition by compaction and cementation. However, depositional facies remains the major control of porosity and permeability in Tirrawarra sandstones. The main effect of diagenesis has been to lower porosity and permeability, but it has not changed the relative reservoir quality of different facies. Previous studies by Martin (1981, 1984) and Bever and others (1987) did an excellent job of describing and illustrating the general diagenetic features of Tirrawarra sandstones and interpreting the paragenetic sequence. Our petrographic study builds on the previous ones but focuses on differences in mineralogy, texture, and diagenesis among the flow units. The goal is to determine the influence of detrital composition, texture (grain size and sorting), and cementation on porosity and permeability in each flow unit.

Methodology

A key to our approach is to conduct petrographic analyses in the context of the stratigraphic framework. The composition of Tirrawarra sandstones was determined from thin sections made from representative samples of the different flow units. It was then possible to quantify the petrographic characteristics of each flow unit—grain size, sorting, detrital mineralogy, authigenic cements, and porosity. Matrix-free (clean) sandstones were sampled preferentially because most reservoirs are in clean sandstones. The chips used to make the thin sections were taken immediately adjacent to the core-analysis plugs so that petrographic parameters could be compared to porosity and permeability. The plugs themselves were not available for this study, but in general it is preferable to make thin sections from end trims off the core-analysis plugs. Composition of Tirrawarra sandstones was determined by standard thin-section petrography and scanning electron microscopy (SEM) with an energy dispersive X-ray spectrometer (EDX).

Point counts were done on 81 thin sections chosen as representative of the range of Tirrawarra sandstones. A total of 200 counts were made on each thin section. This number of counts allows reasonable statistical accuracy compared with counting 300 points, but because each sample takes less time, more samples can be completed. Counting error varies with the percentage of the constituent. For a sample in which 200 points are counted, a constituent that composes 50 percent of the sample has an error of ±3.6 percent, whereas a constituent

that is 10 percent has an error of ±2.1 percent and one that is 2 percent of the sample has an error of ±0.9 percent (Folk, 1974). In comparison, if 300 points were counted, a constituent that composes 50 percent of the sample has an error of ±3.0 percent, one that is 10 percent has an error of ±1.7 percent, and a constituent that is 2 percent of the sample has an error of ±0.7 percent.

Framework grain size and sorting were estimated by comparing the thin sections to standard diagrams. Grain size estimated from viewing thin sections averages only 85 percent of grain size measured by sieving (R. L. Folk, personal communication, 1975), so raw values of grain size should be divided by 0.85 to give actual grain size. All values of grain size reported in text and tables in this report are the raw values determined from thin section and should be divided by 0.85 if the sieve-equivalent size is desired.

Point counts recognize four major categories of rock volume: detrital framework grains, matrix, authigenic cements and replacive minerals, and pores. Framework grains are subdivided by composition. The essential framework grains are those used to classify the sandstone: quartz, feldspar, and rock fragments, including chert. Other framework grains, such as biotite or zircon, are counted but are excluded from the calculation of sandstone type.

Detrital clay matrix is defined as grains too small to be identified in thin section. Detrital clay was distinguished from authigenic clay by using many of the criteria summarized by Wilson and Pittman (1977), including the following: (1) detrital clay commonly fills primary pores and occurs at grain-to-grain contacts; (2) it may form distinct laminae; (3) it has been compacted and does not contain porosity visible in thin section between clay particles, and (4) crystal size is generally smaller than that of authigenic clays. Where sand-size detrital clay clasts were recognized, they were counted separately from clay matrix. However, where clay clasts were deformed by compaction and were no longer recognizable as distinct grains, they were counted as matrix.

Authigenic cements were categorized by composition and location, that is, whether they filled intergranular pores or occurred within secondary pores that formed by dissolution of a framework grain. It is necessary to make this distinction in order to calculate "minus-cement porosity," which is the sum of primary porosity plus the volume of cements that occur in primary pores. Minus-cement porosity provides an indication of the relative amount of porosity lost by compaction, and the total volume of cements in primary pores provides an estimate of the amount of porosity lost by cementation.

Porosity is identified during point counting as primary, intergranular porosity or secondary porosity that formed by dissolution of a framework grain or cement. It is difficult to recognize intergranular pores that were filled with carbonate cement that has subsequently dissolved. Unless the cement enlarged the intergranular pore space by dissolving adjacent framework

grains or overgrowths, cement-dissolution porosity generally cannot be recognized except in places where part of the cement remains.

The point count data from each of the thin sections in this study are tabulated in appendix B. Each sample is identified by well number and core depth. The values listed in the table are in percent of total rock volume, including porosity. The data for each sample continue on two pages; detrital minerals and detrital clay matrix are on one page and authigenic minerals and porosity are on the second page. Flow units and mean grain size are also listed on the second page.

Texture

Most Tirrawarra sandstone samples viewed in this study are medium grained (2.0 to 1.0 phi [0.25 to 0.5 mm]) or fine grained (3.0 to 2.0 phi [0.125 to 0.25 mm]). They are moderately well sorted (0.5 to 0.71 phi) to moderately sorted (0.71 to 1.0 phi), according to the definition of Folk (1974). Significant differences exist among the flow units in grain size and sorting (table VI-1). Flow unit 1U samples are the finest grained, averaging only 0.074 mm, and flow unit 2L samples are coarsest, averaging 0.222 mm. Sandstones from flow unit 3L have the best sorting. The average sorting value for flow unit 3L is 0.5 phi, which is the borderline between good and moderately good sorting. Flow unit 3U is moderately well sorted, and flow units 1U, 2L, and 4 are moderately sorted (table VI-1).

Framework Mineralogy

Tirrawarra sandstones are mostly sublitharenites, and the average composition is $Q_{84}F_{0}R_{16}$. Detrital quartz composes an average of 65 percent of the total rock volume and forms between 59 and 93 percent of the essential constituents. Feldspar is extremely rare; only a few highly altered grains were observed. Average feldspar abundance is 0.1 percent, and feldspar volume ranges from 0 to 1.4 percent of the essential framework grains. The almost complete loss of feldspar is interpreted to be a diagenetic change that resulted in dissolution of feldspar to generate secondary pores. Many of the secondary pores are now filled with kaolinite, which is likely to be a product of the feldspar dissolution. If all the kaolinite in these sandstones used to be feldspar, the original composition of the sandstones would have been $Q_{79}F_{6}R_{15}$.

Rock fragments range from 2 to 40 percent of the essential framework grains. Metamorphic rock fragments composed predominantly of muscovite and quartz are the most

Table VI-1. Comparison of petrographic features by flow unit.[1]

	Flow unit 1U	Flow unit 2L	Flow unit 2U	Flow unit 3L	Flow unit 3U	Flow unit 4
Detrital composition	$Q_{85}F_0R_{15}$	$Q_{79}F_0R_{21}$	$Q_{74}F_1R_{25}$	$Q_{87}F_0R_{13}$	$Q_{83}F_0R_{17}$	$Q_{85}F_0R_{15}$
Ductile grains (%)	11.6	14.7	18.0	8.7	11.7	11.1
Quartz cement (%)	7.7	5.2	8.0	9.7	8.8	9.9
Kaolinite (%)	3.7	8.2	4.5	6.3	5.3	3.9
Illite (%)	4.7	1.9	6.0	2.6	2.8	2.9
Siderite (%)	1.3	4.7	1.0	0.4	0.4	0.4
Total cement (%)	17.3	20.0	19.5	19.1	17.4	17.2
Total primary-pore-filling cement (%)	12.0	11.8	7.7	11.6	10.8	12.1
Primary porosity (%)	0.5	0.7	1.5	2.1	1.1	1.6
Secondary porosity (%)	1.1	2.4	3.0	3.8	3.5	2.7
Minus-cement porosity (%)	12.3	8.4	13.5	13.7	11.9	13.7
Grain size (mm)	0.074	0.222	0.149	0.212	0.214	0.208
Sorting (phi st. dev.)	0.9	0.8	0.6	0.5	0.7	0.8
Porosimeter porosity (%)	11.9	9.2	9.3	12.5	11.4	11.3
Permeability (md) (geometric mean)	0.5	0.5	#	5.2	2.0	3.4
No. of samples	3	13	1	27	19	17

[1]Arithmetic average except as indicated.
*High average value due to one sample with 41% siderite
#Below detection limit

common lithic grains. These include foliated grains, such as slate and phyllite, and nonfoliated grains such as hornfels, which appears to be the result of contact metamorphism of sandstones. Sedimentary rock fragments include detrital grains of sandstone, siltstone, shale (some of which may be contemporaneous mud rip-up clasts), and chert. Igneous rock fragments, including grains interpreted to be devitrified volcanic rock fragments and plutonic rock fragments, are rare. Most rock fragments in the Tirrawarra sandstones are ductile and deform during compaction. Ductile grain deformation, a form of mechanical compaction, is an important cause of porosity loss in the sandstones.

Other framework grains in Tirrawarra sandstones include biotite and muscovite, which are present in volumes of less than 2 percent in most samples. As will be discussed in the section on clay minerals, biotite was probably more common in these sandstones at the time of deposition, but much of it has altered to illite and kaolinite. Rare grains of glauconite occur in flow unit 2L samples, and abundant ostracod shells occur in one sample of flow unit 2L (T21 9,702 ft). Tourmaline, zircon, and leucoxene (altered ilmenite) occur in a few samples in volumes less than 1 percent. Woody organic matter is present in volumes ranging from 0 to 2 percent and is most common in flow unit 2L samples.

Framework-grain composition of Tirrawarra sandstones varies among flow unit. The most quartz-rich samples occur in flow unit 3L (fig. VI-1). Flow units 1U, 4, and 3U have intermediate framework-grain compositions, and flow units 2L and 2U contain the greatest volume of rock fragments (fig. VI-1). The reason for this variation in proportion of rock fragments is that flow unit 3L sandstones were deposited in a high-energy braid-delta-platform environment and experienced wave abrasion that removed some of the mechanically unstable rock fragments. Sands deposited in flow units 2L and 4 were not winnowed and thus contain more rock fragments. Sandstones with higher proportions of rock fragments are in general more susceptible to loss of porosity by mechanical compaction compared with quartz-rich sandstones.

Matrix

Detrital clay matrix composes only 0 to 4 percent of the volume of Tirrawarra sandstones in the samples chosen for this study. However, these samples were particularly chosen to emphasize clean sandstones and thus may not accurately represent the average volume of detrital clay in all Tirrawarra sandstones. In many cases it is difficult to distinguish detrital and authigenic clays, so some of the volume of clay reported as authigenic may actually be detrital (table VI-1). No X-ray diffraction analyses of matrix were done for this study, but previous X-ray work by Martin (1981) indicates that illite and kaolinite (variety dickite) are the most abundant clays in Tirrawarra sandstones. Minor chlorite and mixed-layer illite-smectite with <20 percent

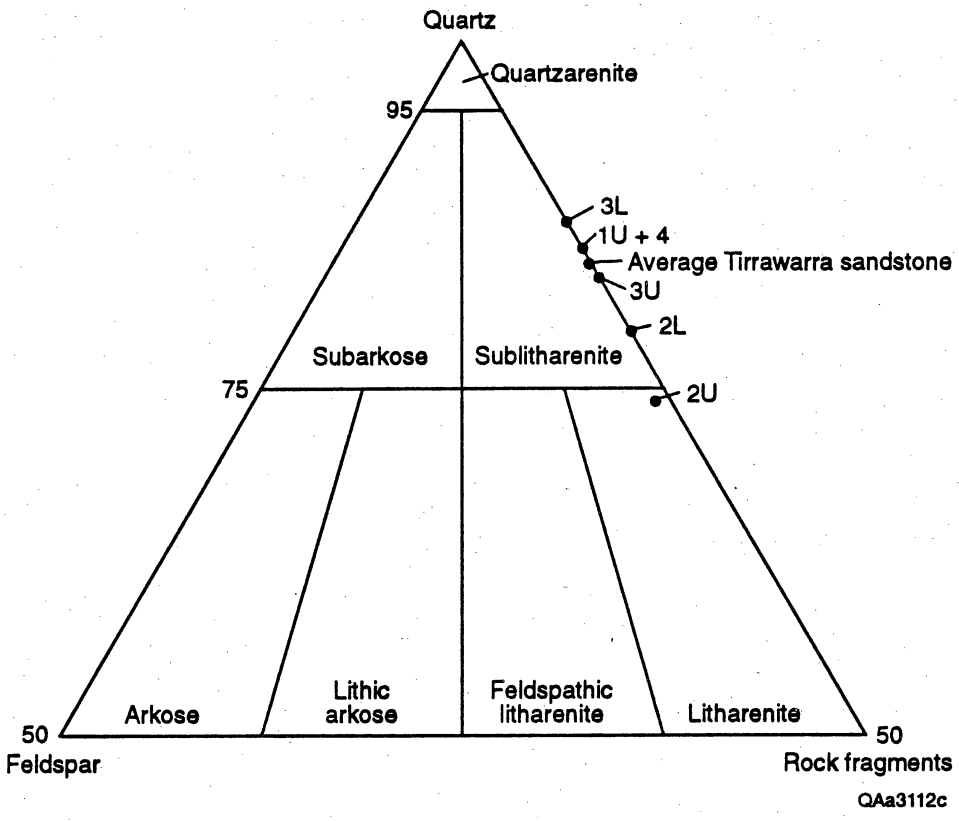

Figure VI-1. Compositional classification of Tirrawarra sandstones by flow unit. Note that this diagram shows only the upper half of Folk's (1974) sandstone classification triangle, from 50 to 100 percent quartz.

smectite layers were identified in a few samples (Martin, 1981). Martin did not specify whether his X-ray samples contained detrital clay, but his data suggest that the Tirrawarra matrix is predominantly illite and kaolinite. Clay-size quartz probably also is a component of matrix.

Cements

Cements and replacive minerals constitute between 0 and 44 percent of the sandstone volume in Tirrawarra samples. Cement is most abundant in clean sandstones that contain little detrital clay matrix. Because clean sandstones were preferentially sampled for this study, the average volume of 18 percent cement may not accurately represent the average volume of cement in all Tirrawarra sandstones. It should, however, be representative of the volume of cement in reservoir sandstones. The highest average volume of cement is in flow unit 2L (table VI-1), the result of a large amount of siderite cement (41 percent) in one sample. Without this sample the average total cement volume in flow unit 2L is 18 percent, and all the flow units are approximately equal in cement volume.

Quartz, kaolinite, illite, and siderite are the only volumetrically important cements in Tirrawarra sandstones. The relative proportion of quartz, siderite, and kaolinite varies in the different flow units, with flow unit 2L having the greatest proportion of kaolinite and siderite and flow unit 4 the most quartz (fig. VI-2). Flow units 3U and 3L are essentially identical in their cementation history. The only other authigenic mineral observed in these sandstones was pyrite, which is rare and occurs in trace amounts. Reservoir bitumen ("dead oil"), a solid hydrocarbon residue that occurs in some sandstones, is also considered a cement in this study, although it is not a mineral. On the basis of petrographic evidence, the relative order of occurrence of the major events in the diagenetic history of Tirrawarra sandstones was found to be (1) mechanical compaction by grain rearrangement and deformation of ductile grains, (2) formation of illite rims, (3) precipitation of quartz overgrowths, (4) generation of secondary porosity by dissolution of feldspars and rock fragments, (5) precipitation of kaolinite and illite in secondary pores, (6) precipitation of siderite, (7) chemical compaction by intergranular pressure solution and stylolitization and additional precipitation of a second generation of quartz cement, and (8) migration of hydrocarbons into the reservoirs. Many of these events overlapped in time (fig. VI-3).

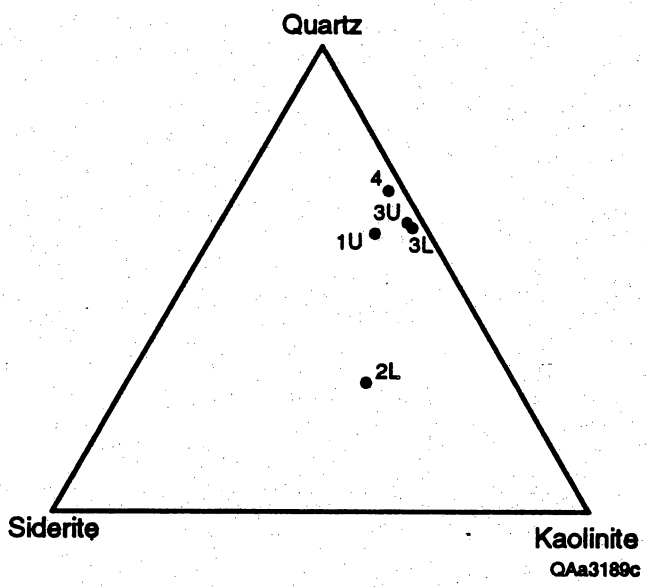

Figure VI-2. Relative proportions of quartz, siderite, and kaolinite cements by flow unit.

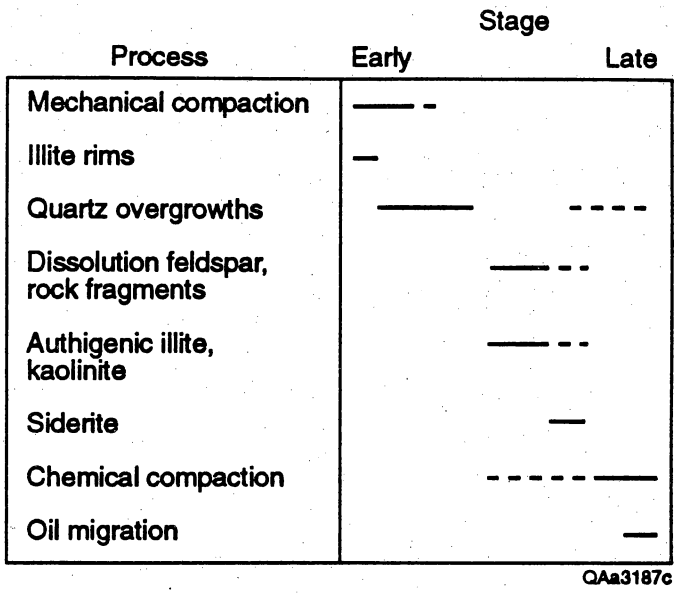

Figure VI-3. Generalized paragenetic sequence for Tirrawarra sandstones, Tirrawarra field, Cooper Basin.

Quartz

Quartz overgrowths are well developed in most Tirrawarra sandstones, having an average volume of 9 percent and ranging from 0 to 16 percent. No correlation exists between volume of quartz cement and grain size, but quartz cement volume decreases significantly with poorer sorting. There is a significant inverse trend between volume of quartz cement and volume of rock fragments (fig. VI-4), which indicates that quartz cement developed preferentially in quartz-rich sandstones that provided abundant sites for quartz nucleation. The correlation between better sorting and higher quartz cement volume probably is a result of well sorted sandstones being quartz rich. A significant inverse correlation also exists between quartz cement and kaolinite. The cause of this trend is probably the fact that kaolinite is most abundant in samples with abundant rock fragments, and dissolution of those grains provided the source of material for the kaolinite. Those samples lacked nucleation sites for quartz cement, so less quartz cement occurs in them.

Average volume of quartz cement varies from a low of 5 percent in the 2L flow unit, with its abundant rock fragments, to a high of 10 percent in quartz-rich flow units 3L and 4. The highest volumes of quartz cement occur in sandstones with the greatest volume of remaining primary porosity (fig. VI-5). This relationship indicates that volume of quartz cement is not an important control on porosity or permeability in Tirrawarra sandstones. Instead, quartz-rich sandstones, which developed the most quartz cement, have also retained the most porosity and are the best reservoirs, despite the quartz cement that has precipitated in them.

Quartz is interpreted to have precipitated relatively early in the burial history of Tirrawarra sandstones because it was the first cement to precipitate in primary pores after clay rims. However, some petrographic evidence suggests multiple or prolonged periods of quartz cementation. For example, some quartz cement clearly precipitated before framework grain dissolution because quartz overgrowths do not extend beyond where the feldspar grains used to be. A second generation of quartz precipitation is indicated by quartz cement that projects into some secondary pores. We have also observed kaolinite cement partly engulfed by quartz overgrowths, although in general quartz cement appears to have precipitated before kaolinite.

Authigenic Clays

Authigenic illite and kaolinite are pervasive in the Tirrawarra sandstones, occurring not only in primary and secondary pores but also in many metamorphic rock fragments and biotite grains that have partly to completely altered to clay. Some illite occurs as rims of tangentially

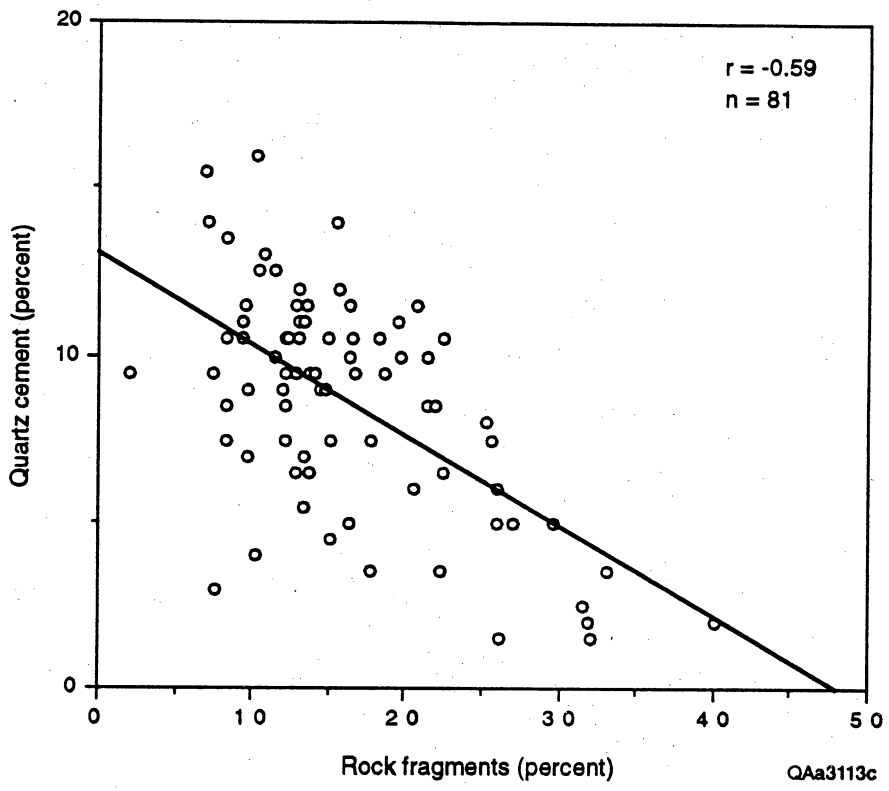

Figure VI-4. Quartz cement volume decreases with increasing proportion of detrital rock fragments. (The percent rock fragments plotted represents the proportion of rock fragments in the essential framework grains.) Relationship is significant at the 99-percent confidence level.

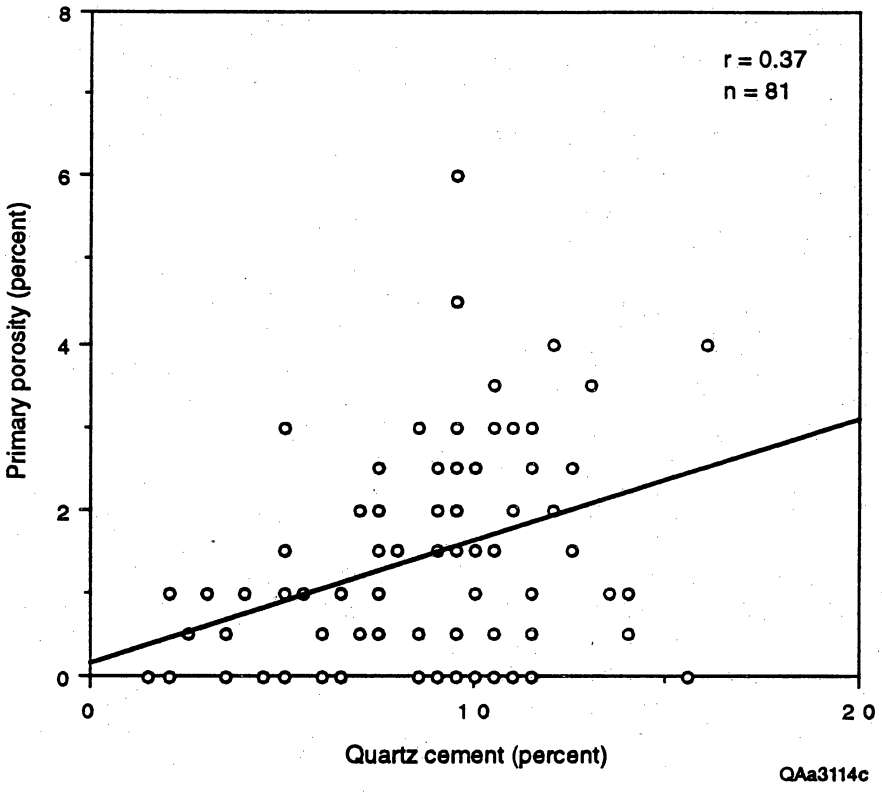

Figure VI-5. Volume of quartz cement and primary porosity have a positive correlation, indicating that quartz cement volume is not the primary reason for occlusion of intergranular porosity. Relationship is significant at the 99-percent confidence level.

oriented flakes that developed around detrital grains early in the diagenetic history. The tangentially oriented illite may have entered the sandstone by mechanical infiltration and may have been recrystallized during burial diagenesis. Other illite having a flaky to fibrous morphology is clearly authigenic and extends into and across primary and secondary pores (plates VI-1a, 3a).

Most kaolinite occurs in secondary pores and is a reaction product of dissolution of framework grains (plates VI-1b, 3b). Much of the kaolinite cement appears loosely packed (plate VI-3b) and thus may be susceptible to being dislodged during production, creating a mobile fines problem. The kaolinite was identified by X-ray diffraction analysis as the variety dickite (Martin, 1981), which is in the kaolin group but has a different stacking order than does kaolinite. Dickite is polymorphous with kaolinite, and it is referred to as kaolinite in this report.

Much of the kaolinite is probably derived from dissolution of feldspars, but loss of feldspar has been so complete that this is only an assumption. No partly dissolved feldspars with kaolinite in the intragranular pores were seen in any of the samples. Some partly dissolved metamorphic rock fragments and biotite grains contain kaolinite, and it is possible that all the kaolinite has this origin.

Dissolution and alteration of framework grains to illite and kaolinite are interpreted to be relatively late events in the diagenetic history of these sandstones that occurred after mechanical compaction had ended and quartz cementation had provided a rigid framework to the sandstones. The large secondary pores filled with delicate clay fibers would otherwise have been compacted and crushed out of their present shape. No correlation exists between volume of either illite or kaolinite or their total volume and permeability.

Siderite

The average volume of siderite in Tirrawarra sandstones is 1 percent, and it is most abundant in flow units 1U and 2L (table VI-1). It is interpreted to be the last major cement to precipitate because it appears to replace both quartz overgrowths and kaolinite cement in secondary pores. Most sandstones contain only a few percent siderite by volume, but one sample in this study was extensively cemented and replaced with 41 percent siderite. This sample, from flow unit 2L in the T21 well at 9,702 ft, contains abundant fossil shells, probably fresh-water ostracods. Siderite cement has replaced shells and silicate grains and filled all the primary and secondary pores. Two other intervals were reported by Martin (1981) as having extensive siderite cement, one in the T6 well at 9,730 ft and the other in the T8 well at 9,633 ft, which are both in the 2L flow unit. These extensively siderite-cemented layers have very low porosity and permeability and may compartmentalize the reservoir. The source of the

Plate VI-1a.

Illite fibers inside a secondary pore. Sample is from flow unit 3L in Tirrawarra well 17 at 9,724 ft. Long dimension of photo is 0.65 mm; plane-polarized light.

Figure VI-1b.

Kaolinite and illite in an altered and partly dissolved rock fragment. Siderite (upper right corner) has partly replaced framework grains. Sample is from flow unit 2L in Tirrawarra well 8 at 9,640 ft. Long dimension of photo is 0.65 mm; cross-polarized light.

Plate VI-1c.

Typical sandstone from flow unit 1U. Alternating fine sandstone and very fine sandstone to siltstone laminations are inclined along a ripple. Sample is from Tirrawarra well 10 at a depth of 9,911 ft. Long dimension of photo is 2.6 mm; plane-polarized light.

Plate VI-1d.

Typical sandstone from flow unit 2L, showing ductile grain deformation, kaolinite in secondary pores, and siderite replacement of framework grains. Sample is from Tirrawarra well 20 at a depth of 9,649 ft. Long dimension of photo is 2.6 mm; plane-polarized light.

(a)
I
(b)
I
K
S
(c)
(d)
S
K
D
K

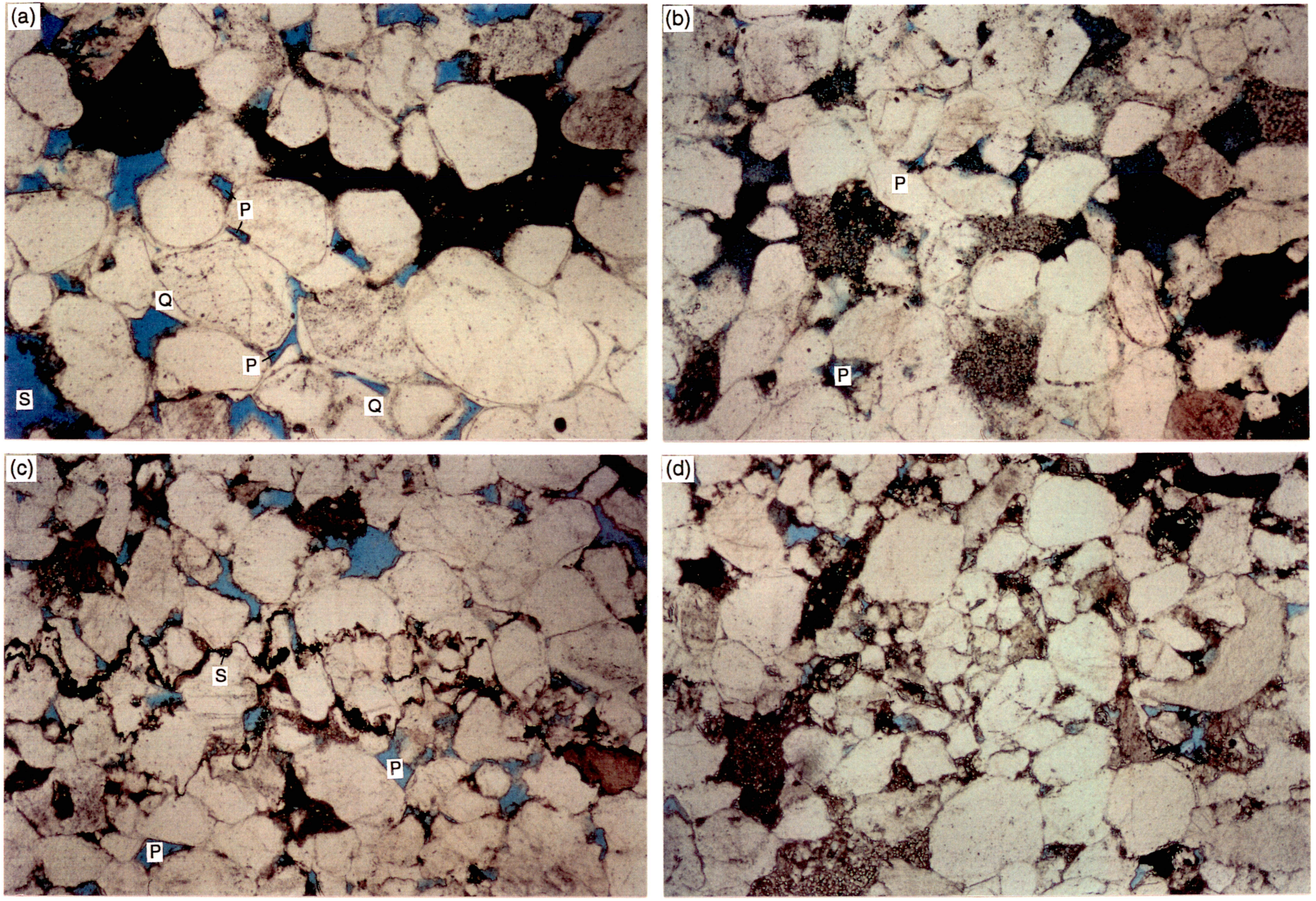
(a)
P
Q
P
S
Q
(b)
P
P
(c)
S
P
P
(d)

Plate VI-2a.

Typical sandstone from flow unit 3L, showing primary and secondary pores and quartz overgrowths. Sample is from Tirrawarra well 8 at a depth of 9,604 ft. Long dimension of photo is 2.6 mm; plane-polarized light.

Plate VI-2b.

Typical sandstone from flow unit 3U, showing fewer primary pores than flow unit 3L. Sample is from Tirrawarra well 19 at a depth of 9,697 ft. Long dimension of photo is 2.6 mm; plane-polarized light.

Plate VI-2c.

Typical high-permeability sandstone from flow unit 4, showing primary pores. Note stylolite in upper right corner of photo. Sample is from Tirrawarra well 8 at a depth of 9,562 ft. Long dimension of photo is 2.6 mm; plane-polarized light.

Plate VI-2d.

Low-permeability sandstone from flow unit 4, with less primary porosity than the sample from two feet away, shown in Plate VI-2c. This particular sample has poor sorting, although that is not generally the cause of low permeability in flow unit 4 sandstones. Sample is from Tirrawarra well 8 at a depth of 9,560 ft. Long dimension of photo is 2.6 mm.

Plate VI-3a.

Illite fibers and flakes that line primary pores and extend into and across secondary pores. Sample is from flow unit 3L in Tirrawarra well 13 at 9,528 ft. SEM photo by J. M. Mendenhall. Scale bar is 10 μm.

Figure VI-3b.

Large cluster of kaolinite crystals in a secondary pore (lower right). Much of the kaolinite cement appears loosely packed and thus may be dislodged during production, creating a mobile fines problem. Sample is from flow unit 4 in the Tirrawarra well 8 from a depth of 9,560 ft. SEM photo by J. M. Mendenhall. Scale bar is 100 μm.

Plate VI-3c.

Typical flow unit 1U sandstone. Note fine grain size and abundant kaolinite (K) cement. Sample is from Tirrawarra well 14 from a depth of 9,709 ft. SEM photo by J. M. Mendenhall. Scale bar is 100 μm.

Plate VI-3d.

Typical flow unit 2L sandstone. Abundant ductile grains and kaolinite (K) filling secondary pores are characteristic of this facies. Sample is from Tirrawarra well 20 from a depth of 9,649 ft. SEM photo by J. M. Mendenhall. Scale bar is 100 μm. Illite fibers inside a secondary pore. Sample is from facies 3L in the T17 well at 9,724 ft. Long dimension of photo is 0.65 mm; plane-polarized light.

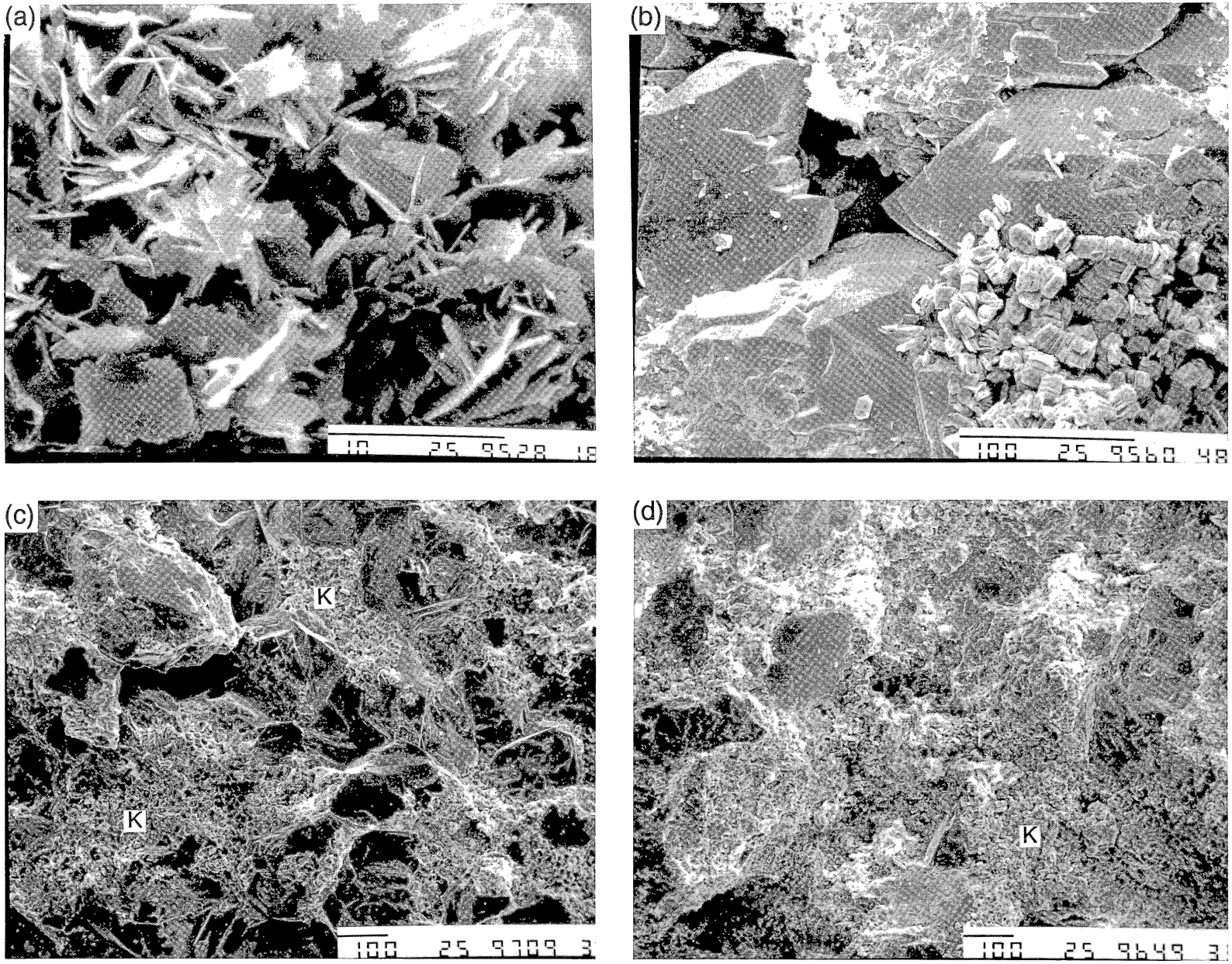
(a)
(b)
(c)
K
K
(d)
K

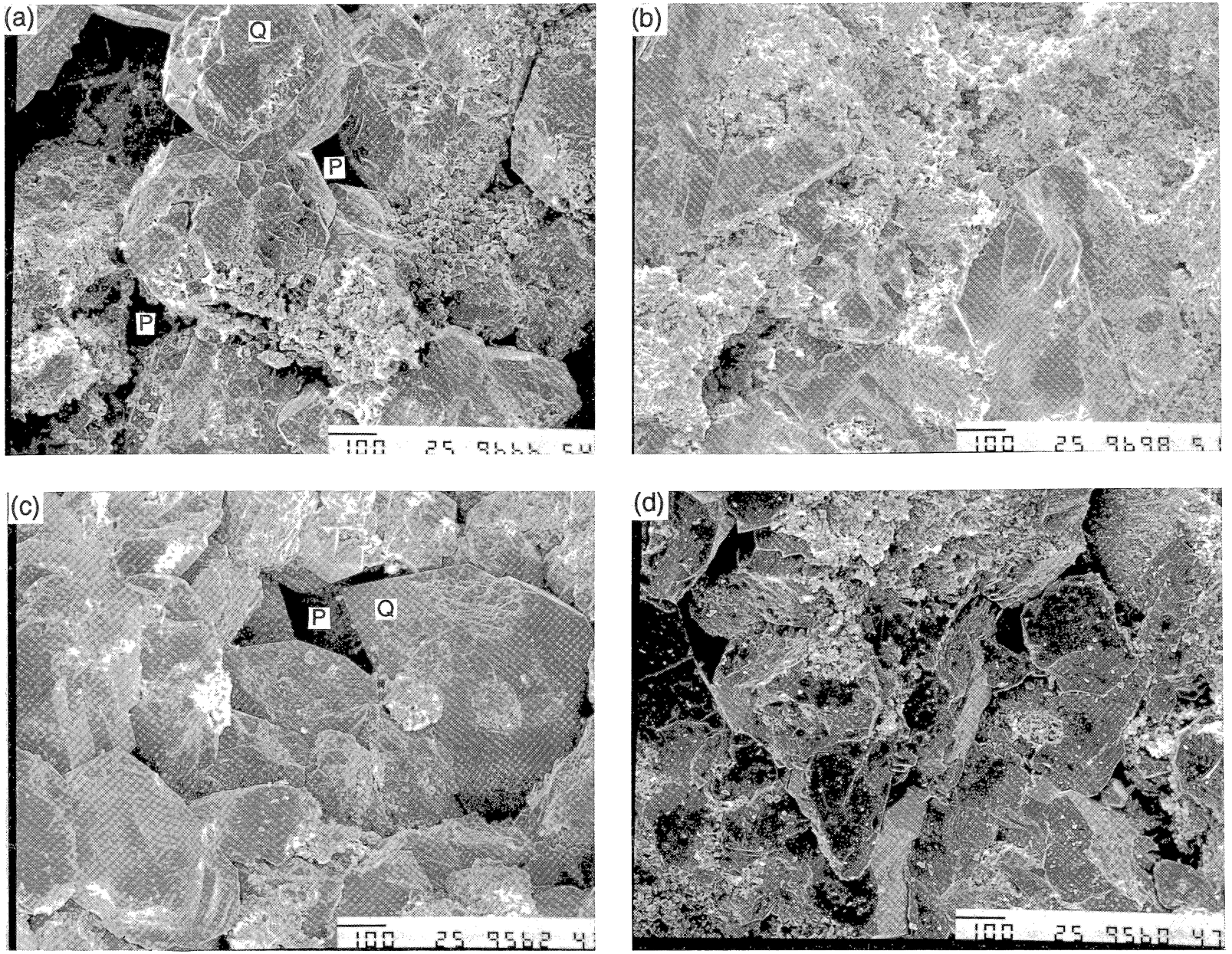
(a)
Q
P
P
(b)
(c)
P
Q
(d)

Plate VI-4a.

Typical flow unit 3L sandstone. Abundant primary porosity (P) and well-developed quartz overgrowths (Q) are characteristic of this flow unit. Sample is from well 21 from a depth of 9,666 ft. SEM photo by J. M. Mendenhall. Scale bar is 100 μm.

Plate VI-4b.

Typical flow unit 3U sandstone. Primary porosity is somewhat lower than in flow unit 3L because of an increased volume of ductile grains. Sample is from well 6 from a depth of 9,698 ft. SEM photo by J. M. Mendenhall. Scale bar is 100 μm.

Plate VI-4c.

Typical high-permeability flow unit 4 sandstone; note primary pores (P) and quartz overgrowths (Q). This sample has 6 percent primary porosity and permeability of 99 md. Sample is from well 8 from a depth of 9,562 ft. SEM photo by J. M. Mendenhall. Scale bar is 100 μm.

Plate VI-4d.

Typical low-permeability flow unit 4 sandstone. This sample has 2.5 percent primary porosity and permeability below the detection limit. Sample is from well 8 from a depth of 9,560 ft, only two feet away from the sample shown in Plate VI-4c. SEM photo by J. M. Mendenhall. Scale bar is 100 μm.

carbonate in siderite probably was calcite fossils, and zones with particularly extensive siderite may represent layers in which shell material was concentrated. Siderite is most abundant in flow units 1U and 2L because these flow units, the delta front and channel-mouth bar, respectively, were the ones in which ostracods lived. Precipitation of siderite and replacement of calcite by siderite indicates that the late pore fluids responsible for this phase of diagenesis were strongly reducing and had a very high ratio of Fe^{+2} to Ca^{+2}.

Dissolution of some siderite cement may have generated additional secondary porosity late in the diagenetic history of the Tirrawarra sandstones. Enlarged intergranular pores containing remnants of siderite cement and deeply embayed quartz grains and overgrowths were observed in several samples, including well T16 at a depth of 9,651 ft, and these features suggest carbonate dissolution. Siderite dissolution was also noted by Martin (1981, 1984) and Bever and others (1987). The extent of cement-dissolution porosity in Tirrawarra sandstones is unclear, but textural evidence in thin section and SEM suggests it was not extensive. Therefore, it seems likely that siderite dissolution has been relatively restricted, and most secondary pores were not previously cemented by siderite. Instead, secondary pores probably formed directly by dissolution of feldspars and other framework grains, without going through an intermediate stage of being replaced by siderite cement.

Reservoir Bitumen

Immovable, black hydrocarbon accumulations line pores in a flow unit 4 sample from the T45 well. In other thin sections, kaolinite books have a brownish tinge, which may be caused by oil staining. This black or brown material is interpreted to be reservoir bitumen, which was defined by Rogers and others (1974, p. 1806) as "solid asphaltic or graphitic coatings and particles within reservoir porosity." Reservoir bitumen fills both primary and secondary pores in the T45 sample and coats quartz overgrowths. Emplacement of reservoir bitumen appears to have been a late diagenetic event that occurred after quartz and kaolinite precipitation and also after migration of hydrocarbons into the Tirrawarra reservoirs. We interpret the reservoir bitumen to be a product of deasphalting of crude oil present in the reservoir sandstones; the deasphalting was probably caused by solution of gas into the oil. The gas that caused the deasphalting may have been generated by the pooled oil as it matured. The oil presently in the reservoir is very light (40° API gravity and lighter), but it probably was heavier when it first was generated and migrated into the reservoir. As the pooled oil was buried and heated after emplacement, it is likely that it underwent thermal alteration and generated gas that caused deasphalting. Because extensive reservoir bitumen was observed in only one sample, it is not interpreted to have much effect on permeability in Tirrawarra field.

Reservoir bitumen is a common feature in both sandstone and carbonate reservoirs (Lomando, 1992). It can form by (1) thermal alteration of oil to dry gas and solid bitumen, (2) deasphalting of oil after solution of large amounts of gas, causing precipitation of asphaltenes, or (3) biodegradation or water washing (Rogers and others, 1974). Reservoir bitumen in the Travis Peak Formation in East Texas is believed to have formed by deasphalting, the same process that is interpreted to have formed the reservoir bitumen in Tirrawarra sandstones (Dutton, 1987; Dutton and others, 1987). In the Travis Peak, the soluble fraction of reservoir bitumen is similar to normal producible oil but enriched in saturates and depleted in aromatics and polars. The insoluble fraction of the reservoir bitumen probably contains more polar and aromatic molecules. Geochemical parameters measured in both Travis Peak oil and reservoir bitumen provide evidence that the reservoir bitumen was derived from oil similar to oil now in the Travis Peak (API gravity ranges from 45° to 58°). The oil, however, is more mature (contains more normal alkanes) than the reservoir bitumen from the same well. Either the reservoir bitumen precipitated out of the oil when it was not as mature as it is today, or pristane and phytane were preferentially precipitated into the bitumen when gas entered the pooled oil, leaving more of the normal alkanes in the oil.

Porosity

Porosity in Tirrawarra sandstones observed in thin section ranges from 0 to 12 percent; porosimeter-measured porosity for the equivalent samples ranges from 3.3 to 18.6 percent. Average porosimeter porosity in the 81 Tirrawarra sandstones that were included in this petrographic study is 11.2 percent, compared with an average of 4.5 percent thin-section porosity. In general, thin-section porosity is lower than porosimeter porosity because accurately identifying the volume of microporosity in thin section is difficult. When the microscope cross hair lands on authigenic illite or kaolinite, it is counted as the clay mineral, but abundant microporosity actually exists between the clay flakes (plate VI-1a). The two measures of porosity in Tirrawarra sandstones are related by the following equation: thin-section porosity = $-1.3 + 0.5 \times$ (porosimeter porosity) ($r = 0.57$).

Thin-section porosity was divided into (1) primary, intergranular pores and (2) secondary pores that result from dissolution of framework grains or cements. On the basis of thin-section identification, average primary porosity has been found to be 1.4 percent, and average secondary porosity, 3.1 percent. Most secondary pores formed by the dissolution of framework grains, particularly rock fragments, biotite, and, presumably, feldspar. Most secondary pores contain remnants of the original detrital grains and the reaction products illite and kaolinite.

Both primary and secondary porosity identified in thin section correlate significantly with porosimeter porosity (r = 0.54 and 0.44, respectively).

Microporosity, defined as pores having pore-aperture radii <0.5 μm (Pittman, 1979), is abundant in Tirrawarra sandstones. Microporosity cannot be accurately quantified by routine thin-section point counts, but an estimate of the volume of microporosity can be obtained by taking the difference between porosimeter-measured porosity and thin-section porosity. This method is predicated on the fact that pores that cannot be distinguished in thin section are micropores. The average volume of microporosity in Tirrawarra sandstones estimated by this method is 6.7 percent. The different facies of the Tirrawarra sandstone can be distinguished by their relative proportions of primary, secondary, and microporosity (fig. VI-6). Microporosity is most abundant in flow unit 1U; flow units 3L and 4 have the highest proportion of primary porosity.

Much of the depositional porosity in Tirrawarra sandstones was lost by mechanical and chemical compaction. Intergranular pressure solution and stylolitization are examples of chemical compaction. Many rock fragments and quartz grains have undergone intergranular pressure solution; stylolites, oriented both parallel and at a high angle to bedding, are common in Tirrawarra sandstones. Intergranular pressure solution appears to have developed preferentially where grains were separated by an illite rim, suggesting the presence of the illite enhanced pressure solution (e.g., Houseknecht, 1988). Stylolites commonly developed along thin clay drapes, probably for the same reason. Whereas chemical compaction reduces porosity by causing closer packing of framework grains, mechanical compaction is bulk volume reduction resulting from processes other than framework-grain dissolution, such as reorientation of competent grains and deformation of ductile grains (Houseknecht, 1987). Many of the sedimentary and metamorphic rock fragments in Tirrawarra sandstones are ductile and have been deformed during compaction, causing a reduction of primary porosity. Minus-cement porosity, which is a measure of the amount of porosity remaining after compaction, averages only 12 percent in Tirrawarra sandstones. At the time of deposition, moderately well sorted Tirrawarra sandstones probably had a porosity of about 40 percent (Pryor, 1973; Atkins and McBride, 1992). Thus, about 28 percent porosity (70 percent of the original porosity) was lost by compaction. Much of the remaining intergranular porosity was occluded by precipitation of an average of 11 percent primary-pore-filling cement.

Diagenetic Bands

Some Tirrawarra cores have white bands that are visible in hand sample and are most commonly oriented vertically or inclined at a high angle to bedding. These bands, termed

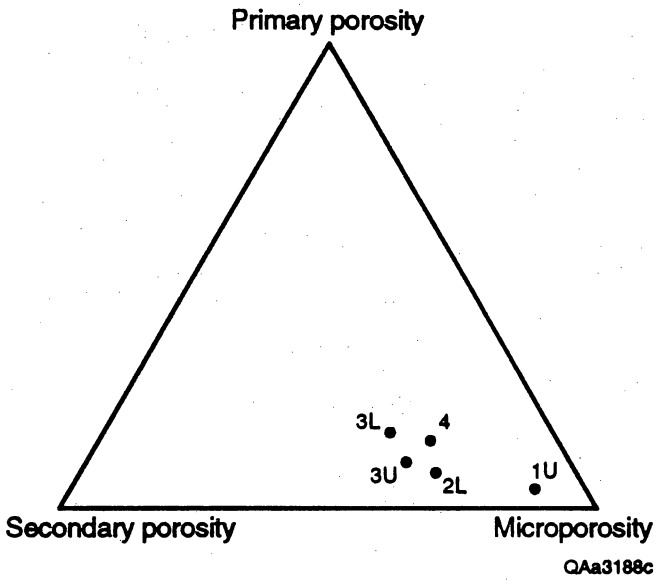

Figure VI-6. Relative proportions of primary, secondary, and micropores by flow unit.

"diagenetic bands," were previously observed and described by Bever and others (1987). The bands extend vertically for several feet in the core, are regular in width (approximately 4 mm) and orientation, but may bifurcate, deviate, or stop suddenly within the core (Bever and others, 1987). No fractures were observed in the bands, nor offset of features on opposite sides of the bands.

Three of these white bands, all from flow unit 3L, were sampled in thin section for this study. The band from well 13 at 9,518 ft is about 3 mm wide and inclined at an angle of 40° from the horizontal; no stylolites are associated with this band. The sandstone within the band is extensively cemented by quartz and therefore is less porous than the surrounding sandstone. Furthermore, the sandstone in the band lacks the abundant, dark clay that is very common in the rest of the sample. The cause of the dark appearance of the clays is not clear, but it may be a result of oil staining. A second band from well 13 is from a depth of 9,528 ft. This band is 2 to 3 mm wide and is inclined 80° from horizontal, nearly perpendicular to bedding. This band is defined by stylolites on each side. The difference between the sandstone inside the band and that outside is not as obvious as in the previous sample. The main difference is less dark (oil-stained?) kaolinite and fewer rock fragments inside the band compared to the rest of the sandstone. The sandstone inside the band also appears to be more quartz cemented, but the difference is less clear than in the sample at 9,518 ft. The third sample of a band is from well 42 at a depth of 9,895.5 ft. This band is vertical and 2 to 3 mm wide. Only one side is bounded by a stylolite. Similar to the other two bands, the sandstone inside the band seems to be somewhat more cemented by quartz and to contain fewer rock fragments than the surrounding sandstones. The three bands viewed in this study do not appear to be more porous than the surrounding sandstone, and the sample from well 13 9,518 ft probably is less porous. This observation is the opposite to of Bever and others (1987), who indicated that the bands were more porous than the rest of the sandstone.

The origin of the diagenetic bands is enigmatic. The appearance of the bands in the cores is reminiscent of natural fractures, but no evidence of fractures could be found along the bands. The greater volume of quartz cement inside the bands may be caused by release of silica from the bounding stylolites, however the band not associated with stylolites had the greatest increase in quartz cementation. As first noted by Bever and others (1987), the sandstone within the bands contains fewer rock fragments but no corresponding increase in secondary porosity. This fact may suggest that the feature developed early in the diagenetic history of the sandstones, and compaction rearranged the remaining detrital grains, destroying the secondary pores. The bands evidently formed prior to hydrocarbon migration because oil was able to migrate into the more porous sandstone around the band at well 13 9,518 ft but did not enter the already well-cemented sandstone along the band.

Additional study of the diagenetic bands is warranted because of their potential as fluid-flow pathways where they are more porous than the surrounding sandstones or as flow barriers where they are less porous. We are unaware of any similar features described in the literature.

Diagenetic Controls on Reservoir Quality

By comparing point-count data of thin sections with core analyses, we were able to evaluate the influence of parameters such as grain size, sorting, compaction, volume of authigenic cements, and pore type (primary vs. secondary) on porosity and permeability (table VI-2). Eight samples reported as having 0 permeability were omitted from permeability calculations, which has the effect of increasing average permeabilities somewhat. When the entire Tirrawarra sandstone data base is taken as a whole, combining samples from all flow units, two parameters emerge as having the major control on porosity and permeability: grain size and volume of ductile grains. Although the range of grain sizes is not large, there is a clear trend of increasing permeability with increasing grain size (fig. VI-7), and the relationship is statistically significant at the 99 percent confidence level. However, there is sufficient scatter in the relationship that grain size alone is a poor predictor of permeability. For example, permeability ranges from >100 to 0.1 md in sandstones with a grain size of 2.25 phi (0.21 mm).

Table VI-2. Porosity and permeability versus petrographic parameters in Tirrawarra sandstone.*

Porosimeter porosity vs. petrographic parameters

Parameter	Correlation Coefficient
Total thin-section porosity (%)	+0.57**
Primary porosity (%)	+0.54**
Secondary porosity (%)	+0.44**
Ductile grains (%)	-0.38**
Grain size (phi)	-0.31**†
Illite cement (%)	+0.20
Siderite cement (%)	-0.16
Total cement (%)	-0.08
Quartz cement (%)	+0.03
Kaolinite cement (%)	-0.03

Permeability vs. petrographic parameters

Parameter	Correlation Coefficient
Porosimeter porosity (%)	+0.75**
Primary porosity (%)	+0.56**
Total thin-section porosity (%)	+0.56**
Secondary porosity (%)	+0.42**
Grain size (phi)	-0.37**†
Ductile grains (%)	-0.36**
Total cement (%)	-0.17
Illite cement (%)	+0.13
Siderite cement (%)	-0.11
Kaolinite cement (%)	-0.07
Quartz cement (%)	-0.06

*Linear regression correlation coefficients are shown for porosimeter porosity versus various textural and mineralogic parameters; n = 78. Linear regression correlation coefficients are shown for log permeability versus various parameters; n = 70.

**Significant at the 99-percent confidence level.

†Grain size in phi accounts for negative r value.

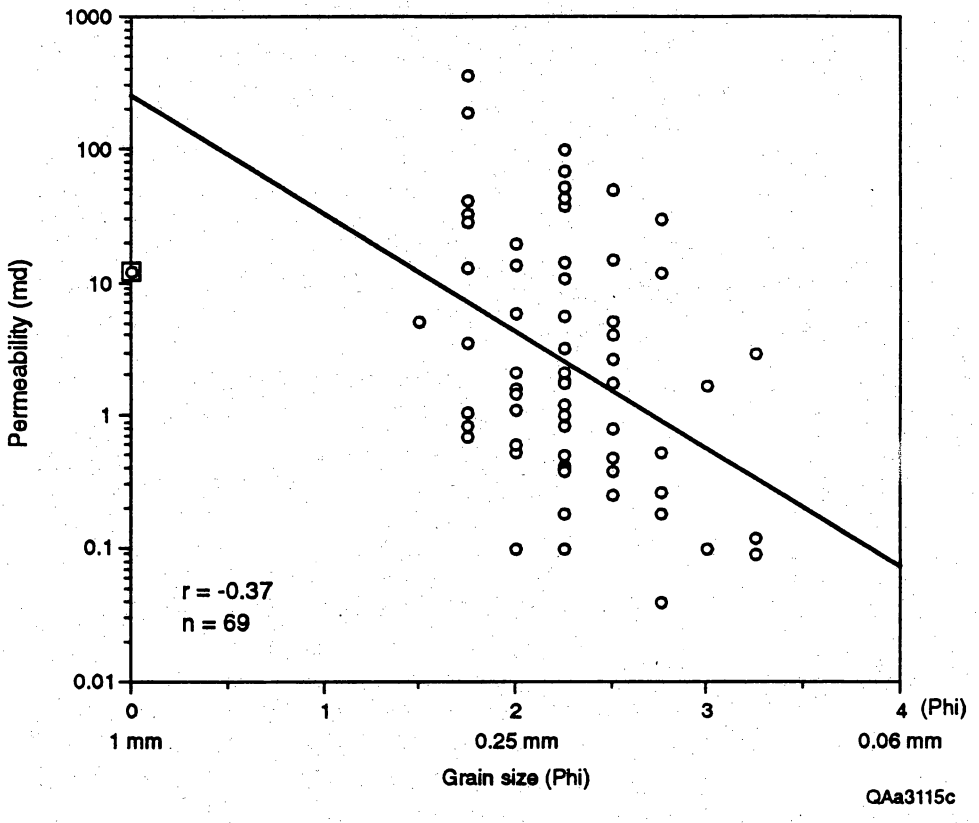

Figure VI-7. Permeability increases with increasing grain size in the total population of Tirrawarra sandstones. The linear regression equation relating grain size and log permeability is: log permeability (md) = 2.4 – 0.9 × grain size (phi units). The regression line was calculated by omitting one data outlier (shown inside box). The reason for the inverse trend line is that grain size is plotted in phi units, in which larger numbers indicate smaller grain sizes.

The other major control on porosity and permeability in the total Tirrawarra sandstone data base is the volume of ductile grains, defined as metamorphic and sedimentary rock fragments, biotite, and muscovite. All of these grains are easily deformed during burial, resulting in loss of porosity by mechanical compaction. Thus, as the volume of ductile grains increases, permeability decreases (fig. VI-8). This relationship also is significant at the 99 percent confidence level.

The linear regression correlation coefficients for other petrographic parameters versus porosity and permeability are listed in table VI-2. Porosity has the best correlation with permeability, but it is controlled, in turn, by grain size and volume of ductile grains. Primary and secondary porosity are both significantly correlated with permeability, but primary porosity has a higher value of r^2, the coefficient of determination (0.31 vs. 0.18), and thus accounts for more of the permeability variation. Although less abundant in Tirrawarra sandstones (table VI-1), primary porosity is more important in determining permeability than is secondary porosity. Petrographic observations show that primary pores are better connected than are secondary pores, resulting in a greater contribution to permeability.

Both grain size and volume of ductile grains are functions of the energy of the depositional environment. We conclude, therefore, that original depositional environment is the main control on porosity and permeability in Tirrawarra sandstones. Porosity and permeability have been reduced from what they were at the time of deposition by diagenesis—compaction and cementation—but those sandstones deposited in the highest energy settings retain the best reservoir quality. These relationships can be seen even more clearly when the total petrographic data base is subdivided on the basis of facies.

Flow Unit 1U

Flow unit 1U, deposited in a delta-front environment, is the finest grained flow unit and has among the lowest average permeabilities (table VI-1). Overall sorting is poor because the sandstones are commonly composed of alternating laminations of fine sandstone and very fine sandstone or siltstone (plate VI-1c). Illite and kaolinite cement are abundant (plate VI-3c).

Flow Unit 2L

Sandstones in flow unit 2L were deposited in a channel-mouth-bar/distributary-channel complex. These sandstones contain the most abundant ductile grains of any of the Tirrawarra flow units and have lost most of their intergranular porosity by mechanical compaction

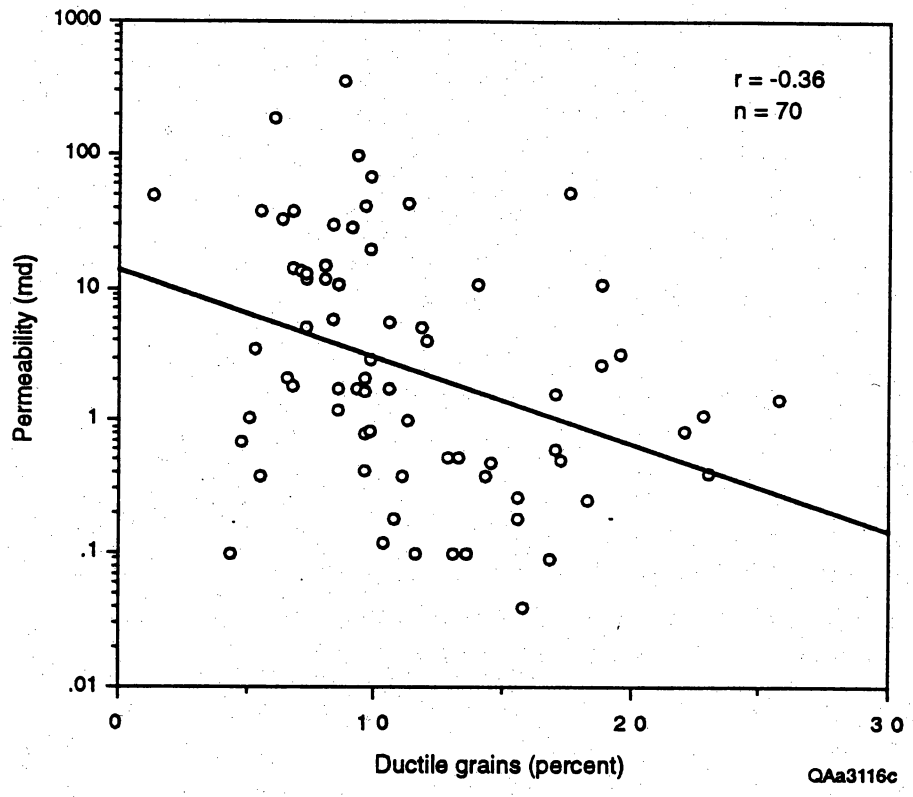

Figure VI-8. Permeability decreases with increasing volume of ductile grains, defined as metamorphic and sedimentary rock fragments (including chert), biotite, and muscovite. The linear regression equation relating grain size and log permeability is: log permeability = 1.1 – 6.5 × volume of ductile grains (percent).

(tables VI-1 and VI-3). Minus-cement porosity averages 8 percent in these sandstones, and geometric mean permeability is only 0.5 md (table VI-1). However, permeability of 2L sandstones is strongly controlled by grain size (fig. VI-9). Flow unit 2L sandstones with permeability >0.5 md have an average grain size of 0.257 mm, whereas 2L sandstones with permeability <0.5 md have an average grain size of 0.195 mm (table VI-3). The coarsest flow unit 2L sandstones occur in wells 17 and 20, near the crest of the Tirrawarra structure, but there is no obvious geographic trend to grain size distribution based on the 13 flow unit 2L samples used in this study.

Flow unit 2L sandstones are characterized by abundant kaolinite cement in secondary pores (plate VI-3d) and siderite rhombs that replace framework grains and fill pores (plate VI-1d). Only one sample from flow unit 2U was examined (table VI-3). It is finer grained than the 2L sandstones but also has abundant ductile grains.

Flow Unit 3L

Flow unit 3L was deposited in a braid-delta-platform environment in which the sandstones were locally winnowed by wave action. As a result, flow unit 3L sandstones are the most quartz rich of the Tirrawarra sandstones and have retained the highest primary porosity and permeability (table VI-1). Flow unit 3L sandstones have well developed quartz overgrowths because there are large primary pores into which the quartz could grow (plates VI-2a and VI-4a). Quartz cementation is not so extensive that it occludes all the primary porosity, and no correlation exists between volume of quartz cement and permeability. As in the other Tirrawarra flow units, volume of quartz cement is not a control on permeability in the 3L sandstones.

The main controls on porosity and permeability in flow unit 3L are volume of ductile grains (fig. VI-10) and grain size (fig. VI-11). Average grain size in the more permeable sandstones is 0.217 mm, compared with an average of 0.193 mm for the less permeable 3L sandstones (table VI-4). The average volume of ductile grains in 3L sandstones with permeability >0.5 md is 8 percent, but 3L sandstones having permeability <0.5 md contain an average of 14 percent ductile grains (table VI-4). No geographic trend was observed in the distribution of ductile grains in the 27 flow unit 3L samples in this study. Wells Tirrawarra 2, 6, 8, 13, 17, and 42 and Tirrawarra West 1 all contain an average of 5 percent or fewer metamorphic rock fragments in flow unit 3L sandstones.

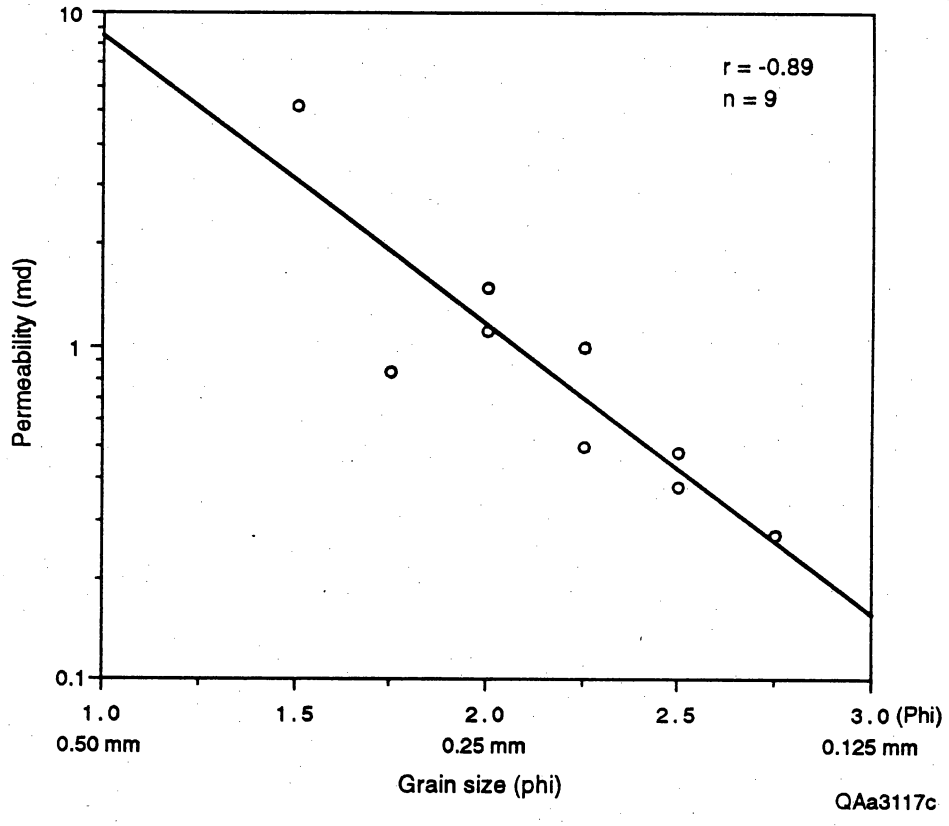

Figure VI-9. Permeability in flow unit 2L sandstones increases with increasing grain size. The reason for the inverse trend line is that grain size is plotted in phi units in which larger numbers indicate smaller grain sizes. The linear regression equation relating grain size and log permeability is: log permeability (md) = 1.8 – 0.9 × grain size (phi units). Relationship is significant at the 99-percent confidence level.

Table VI-3. Comparison of flow unit 2 petrographic features.[1]

	Flow unit 2U	Flow unit 2L (k ≥0.5 md)	Flow unit 2L (k <0.5 md)
Detrital composition	$Q_{74}F_1R_{25}$	$Q_{74.3}F_{0.3}R_{24.4}$	$Q_{82}F_0R_{18}$
Ductile grains (%)	18	18	12
Quartz cement (%)	8	4	6
Kaolinite (%)	5	10	7
Illite (%)	6	2	2
Siderite (%)	1	2.3	7*
Total cement (%)	20	19	21*
Primary porosity (%)	1.5	0.5	0.9
Secondary porosity (%)	3.0	3.0	1.9
Minus-cement porosity (%)	14	7	10
Grain size (mm)	0.149	0.257	0.195
Sorting (phi st. dev.)	0.6	0.8	0.8
Porosimeter porosity (%)	9.3	10.3	8.3
Permeability (md) (geometric mean)	#	1.2	0.4
No. of samples	1	6	7

[1]Arithmetic average except as indicated.
*High average value due to one sample with 41% siderite
#Below detection limit

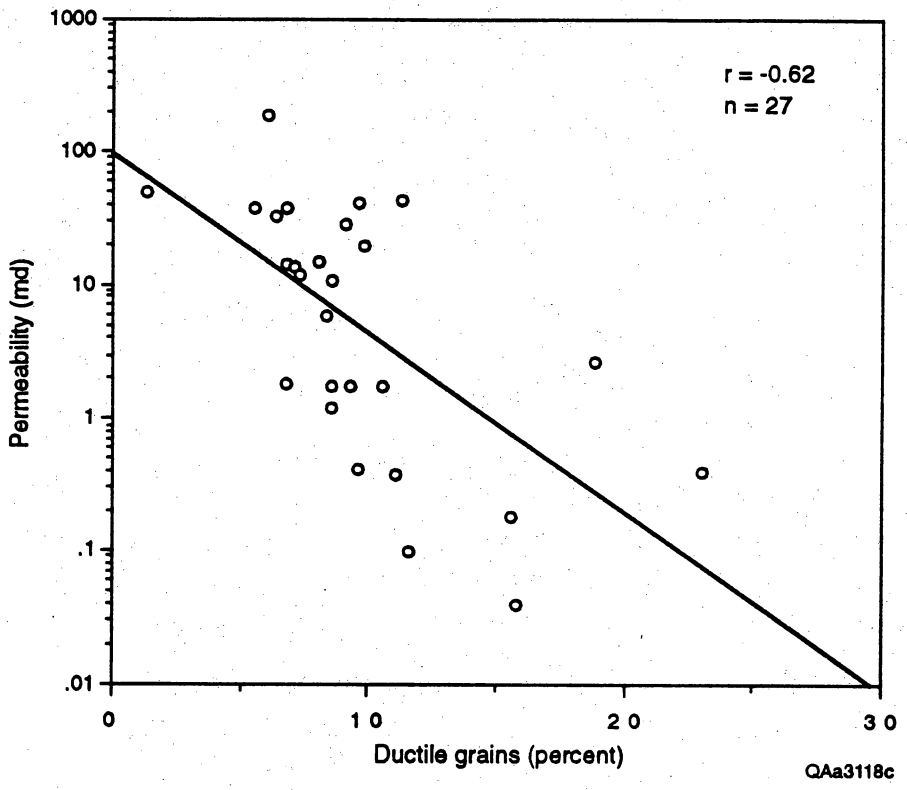

Figure VI-10. Permeability in flow unit 3L sandstones decreases with increasing volume of ductile grains. The linear regression equation relating grain size and log permeability is: log permeability = 2.0 – 0.1 × volume of ductile grains (percent). Relationship is significant at the 99-percent confidence level.

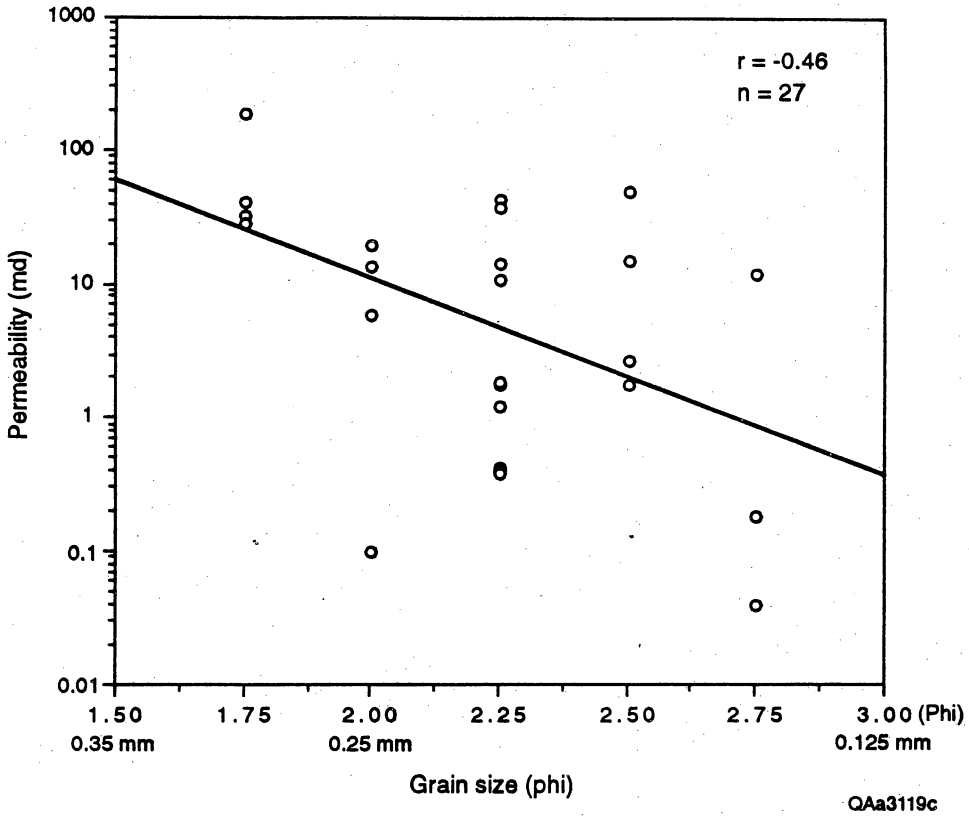

Figure VI-11. Permeability in flow unit 3L sandstones increases with increasing grain size. The reason for the inverse trend line is that grain size is plotted in phi units in which larger numbers indicate smaller grain sizes. The linear regression equation relating grain size and log permeability is: log permeability (md) = 4.0 – 1.5 × grain size (phi units). Relationship is significant at the 98-percent confidence level.

Table VI-4. Comparison of flow unit 3L petrographic features.[1]

	Flow unit 3L (k ≥0.5 md)	Flow unit 3L (k <0.5 md)
Detrital composition	$Q_{88}F_0R_{12}$	$Q_{80}F_0R_{20}$
Ductile grains (%)	8	14
Quartz cement (%)	10	9
Kaolinite (%)	6	9
Illite (%)	3	2
Siderite (%)	0.4	0.7
Total cement (%)	19	20
Primary porosity (%)	2.4	0.9
Secondary porosity (%)	4.1	2.5
Minus-cement porosity (%)	14	13
Grain size (mm)	0.217	0.193
Sorting (phi st. dev.)	0.5	0.6
Porosimeter porosity (%)	13.6	8.0
Permeability (md) (geometric mean)	11.9	0.2
No. of samples	22	6

[1]Arithmetic average except as indicated.

Flow Unit 3U

Sandstones in flow unit 3U are similar to those of flow unit 3L but on average they have more ductile grains and poorer sorting (plates VI-2b and VI-4b), which results in lower primary and secondary porosity and permeability (table VI-1). No petrographic parameters correlated significantly with permeability in these 19 flow unit 3U sandstones. Only two of the 3U sandstones sampled for this study have permeability <0.5 md, so it is difficult to compare the better 3U samples to the poorer ones (table VI-5). It appears, however, that the low permeability 3U sandstones are finer grained than are the more permeable 3U samples (table VI-5) and have lower primary and secondary porosity.

Flow Unit 4

Sandstones of flow unit 4 were deposited in a braid-plain environment, and they are quite variable in terms of their porosity and permeability. Permeability varies from 0.1 to 370 md and porosity from 5.7 to 16.1 percent. A comparison of facies 4 sandstones with permeability

>0.5 md to those with permeability less than the 0.5 md pay cutoff indicates that the more permeable samples are coarser grained and have fewer ductile grains (table VI-6). These slight changes in grain size and composition result in large differences in porosity and permeability. The more permeable flow unit 4 sandstones have an average of 12.8 porosimeter porosity (2 percent primary and 3.5 percent secondary porosity) and 17 md permeability, whereas the less permeable sandstones have an average of only 8.9 porosimeter porosity (0.9 percent primary and 1.5 percent secondary porosity) and 0.1 md permeability (table VI-6). The difference in volume of primary porosity between the good and poor flow unit 4 sandstones is obvious in the SEM and thin-section photomicrographs (plates VI-2c, d and plates VI-4c, d). The only petrographic parameter than correlates significantly with permeability in flow unit 4 samples is grain size (fig. VI-12). The wells with the coarsest flow unit 4 samples are 9, 16, and 31, but there is no obvious geographic trend to grain-size distribution across the field.

Spatial Variation in Petrographic Parameters

No clear-cut, systematic variations in framework-grain composition, grain size, or cementation were observed between wells on the crest of the structure and those on the flanks, although minor spatial variations were noted in some facies. For example, the two finest grained samples in flow unit 4 occur on the northern flank of the structure, in wells 3 and 22, but one of the coarsest flow unit 4 samples also occurs on the northern flank, in well 16. Similarly, the volume of ductile metamorphic rock fragments in flow unit 3L is lowest in two wells on the crest of the structure, but a low volume of metamorphic rock fragments also occurs in well W1, on the western flank of the structure. Volume of quartz cement in flow unit 3L is actually highest in some of the wells on the crest of the structure, not on the flanks. Dissolution of siderite cement was observed in a flow unit 4 sample from well 16, and qualitative observations suggest that siderite dissolution may have been more common in flow unit 4 sandstones from the northern flank of the structure than from other parts of the field. Other than these somewhat contradictory observations, however, there is no evidence that the Tirrawarra structure influenced original detrital mineral composition or grain size of the sandstones or subsequent cementation.

Table VI-5. Comparison of flow unit 3U petrographic features.[1]

	Flow unit 3U (k ≥0.5 md)	Flow unit 3U (k <0.5 md)
Detrital composition	$Q_{84}F_0R_{16}$	$Q_{80}F_0R_{20}$
Ductile grains (%)	11	17
Quartz cement (%)	9	9
Kaolinite (%)	5	5
Illite (%)	3	1
Siderite (%)	0.4	1
Total cement (%)	18	16
Primary porosity (%)	1.2	0.8
Secondary porosity (%)	3.8	0.9
Minus-cement porosity (%)	12	13
Grain size (mm)	0.219	0.177
Sorting (phi st. dev.)	0.7	0.7
Porosimeter porosity (%)	11.5	11.2
Permeability (md) (geometric mean)	2.2	0.4
No. of samples	17	2

Table VI-6. Comparison of flow unit 4 petrographic features.[1]

	Flow unit 4 (k ≥0.5 md)	Flow unit 4 (k <0.5 md)
Detrital composition	$Q_{86}F_0R_{14}$	$Q_{82}F_0R_{18}$
Ductile grains (%)	10	13
Quartz cement (%)	9	11
Kaolinite (%)	5	2
Illite (%)	2	4
Siderite (%)	0.5	0.3
Total cement (%)	17	17
Primary porosity (%)	2.0	0.9
Secondary porosity (%)	3.5	1.5
Minus-cement porosity (%)	13	15
Grain size (mm)	0.237	0.167
Sorting (phi st. dev.)	0.9	0.7
Porosimeter porosity (%)	12.8	8.9
Permeability (md) (geometric mean)	17.0	0.1
No. of samples	10	7

[1]Arithmetic average except as indicated.

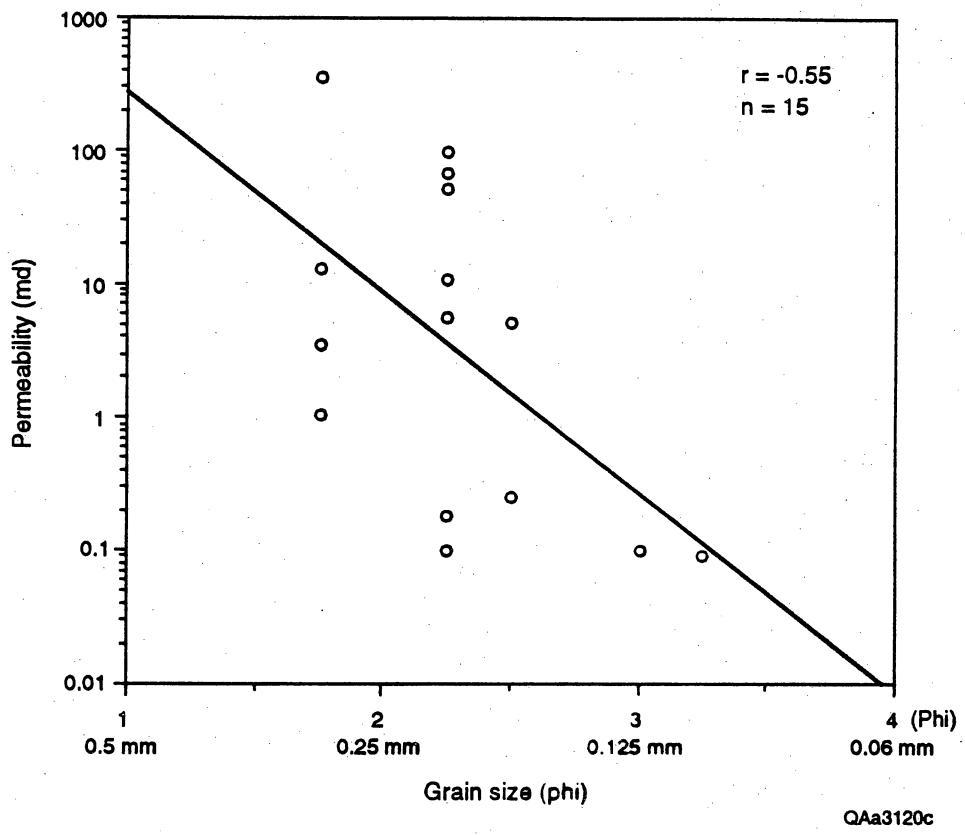

Figure VI-12. Permeability in flow unit 4 increases with increasing grain size. The reason for the inverse trend line is that grain size is plotted in phi units in which larger numbers indicate smaller grain sizes. The linear regression equation relating grain size and log permeability is: log permeability (md) = 3.9 - 1.5 × grain size (phi units). This equation is very close to that of facies 3L, shown in figure VI-11. Relationship is significant at the 95-percent confidence level.

Conclusions

Tirrawarra sandstones are medium- to fine-grained sublitharenites. Quartz and metamorphic and sedimentary rock fragments are the most abundant detrital grains; feldspar is almost completely absent. Rock fragments have been extensively altered to illite and kaolinite during diagenesis. Secondary pores developed by dissolution of rock fragments and biotite, but complete dissolution of detrital feldspar is believed to be responsible for the generation of many of the secondary pores. Dissolved feldspars probably are the source of the kaolinite cement common in secondary pores. Quartz overgrowths and siderite are the other major cements in these sandstones. Volume of cement is not a significant control on porosity or permeability in Tirrawarra sandstones.

Mechanical compaction of ductile grains and chemical compaction by intergranular pressure solution and stylolitization are major causes of porosity loss in Tirrawarra sandstones. The average sandstone lost about 28 percent porosity (70 percent of the original porosity) by compaction. An additional 11 percent porosity was lost on average by precipitation of primary-pore-filling cements. The main controls on permeability in these sandstones are grain size and volume of ductile grains, which are both functions of the original depositional environment of the sandstones. The effect of diagenesis has been to lower porosity and permeability but with depositional texture and composition determining the magnitude of loss. The highest porosity and permeability occur in those sandstones of flow units 3L and 4 that have coarser grain size, relatively quartz-rich detrital mineral composition, and high values of primary porosity.

Depositional flow units of the Tirrawarra sandstone have distinct petrographic characteristics. Flow unit 1U is a moderately sorted, very fine grained sandstone to siltstone. It contains moderate amounts of siderite and more illite cement than the other facies. Microporosity is the dominant pore type in flow unit 1U, and the volume of primary and secondary porosity are both low. Flow unit 2L is the coarsest grained, and it has moderate sorting. Detrital rock fragments and siderite and kaolinite cements are more abundant in flow unit 2L sandstones than in the other Tirrawarra flow units. The main control on permeability in flow unit 2L sandstones is grain size. Flow units 3L and 3U are very similar in terms of their grain size and types and volumes of cements, but 3L samples have fewer rock fragments and are better sorted. Primary porosity is more abundant in flow unit 3L, and thus it has higher average permeability than flow unit 3U. Grain size and volume of ductile grains are the main controls on permeability in flow unit 3L sandstones. Grain size, sorting, and detrital mineral composition are quite variable in flow unit 4 sandstones, and the highest permeability occurs in the coarsest samples. Flow unit 4 sandstones with permeability $\geq$0.5 md have an average grain size of

0.24 mm, whereas flow unit 4 sandstones with <0.5 md permeability have an average grain size of 0.17 mm.

VII. PETROPHYSICS

Introduction

The petrophysics task of the project is composed of three main tasks:

- The review and analysis of all aspects of the petrophysics of the field.
- The review and analysis of the water resistivity data for the field.
- The calculation of foot-by-foot porosity, water saturation and pay for each well. This includes foot-by-foot editing of the final results to honour core and engineering data.

Review and Analysis

General

The purposes of the petrophysical review and analysis have been to:

i) review the Santos methods that have been used to determine porosity and water saturation,

ii) compare the reservoir flow units with core porosities, permeabilities and rock types to determine if reservoir cut-offs (i.e., Vsh, porosity, and Sw) need to be adjusted for each reservoir flow unit,

iii) determine if reservoir flow units could be verified by petrophysics, and

iv) make any suggestions that could improve the petrophysical analysis.

During the petrophysical review, 46 wells were examined through the Tirrawarra Sandstone. The wells were selected so that different logging suites, different flow units and water versus oil productive zones could be examined and compared. The review was performed using "SSA," a PC based shaly sand analysis program developed by George Asquith and The Log Group Inc. This program is designed to quickly analyze and compare results from different log analysis techniques and equations. It thereby enables qualitative and quantitative assessment of the different techniques. The results of this review were incorporated into the foot by foot log analysis which was run by SANTOS in-house.

As the Rw determination had not been finalised at the time of the Petrophysics Review and Analysis, the previous Rw of 0.58 ohm-m @ 75°F was used (revised Rw = 0.65 ohm-m @

75°F). This only had minimal impact on the analysis of the water saturations (up to 2 percent) and had no impact on the cut-offs or other parameters derived during this task.

Problems with the Log Data

Three potential log problems were noted early in the study. The first was that on some wells, such as the Tirrawarra 12, the resistivity of the mud filtrate (Rmf) was much lower than the resistivity of the formation water (Rw). On Tirrawarra 12 the Rmf was 0.11 at 75°F and the Rw was 0.58 at 75°F. Since a dual laterolog–MSFL was run on the Tirrawarra 12 a more compatible Rmf-Rw combination would have been to have Rmf approximately equal to Rw (Asquith, 1982). For example, in the Tirrawarra 16 the Rmf was 0.49 at 75°F, which is much closer to Rw and therefore a better mud for a dual laterolog–MSFL log. It is important to have Rmf approximately equal to Rw when running laterologs because any separation between deep and shallow resistivity traces is due to filtrate displacing hydrocarbons and the hydrocarbon resistivity profiles and the degree of hydrocarbon moveability are therefore easier to observe on the logs. However, it is important to remember that the drilling muds used in these wells do not negate the calculated values of water saturation (Sw).

The second problem was the excessive porosity calculated from the density log at some depths (fig. VII-1). These excessive streaks of density porosity were suspected of being the result of mud-filled or hydrocarbon-filled fractures near the well causing the density log to record a very low density. However, no open fractures have been identified in core corresponding to these zones. To overcome the problem with the density log the sonic log was used in all porosity calculations.

The third problem was the high degree of hole washout in some wells. This problem proved not to be too serious because porosity and water saturation values from wells with and without wash-out were similar and the sonic tool largely compensates for borehole size. Two exceptions were the Tirrawarra 6 and 9 wells, where sonic porosities were sometimes 20 percent or greater. Therefore, caution must be used in using the data from the badly caved portions of these wells.

Rakoona 1 also shows this effect, however, the density anomalies correspond closely with low Vsh values and high sonic porosity values. In the case of this well, a gas effect is suspected and should be investigated.

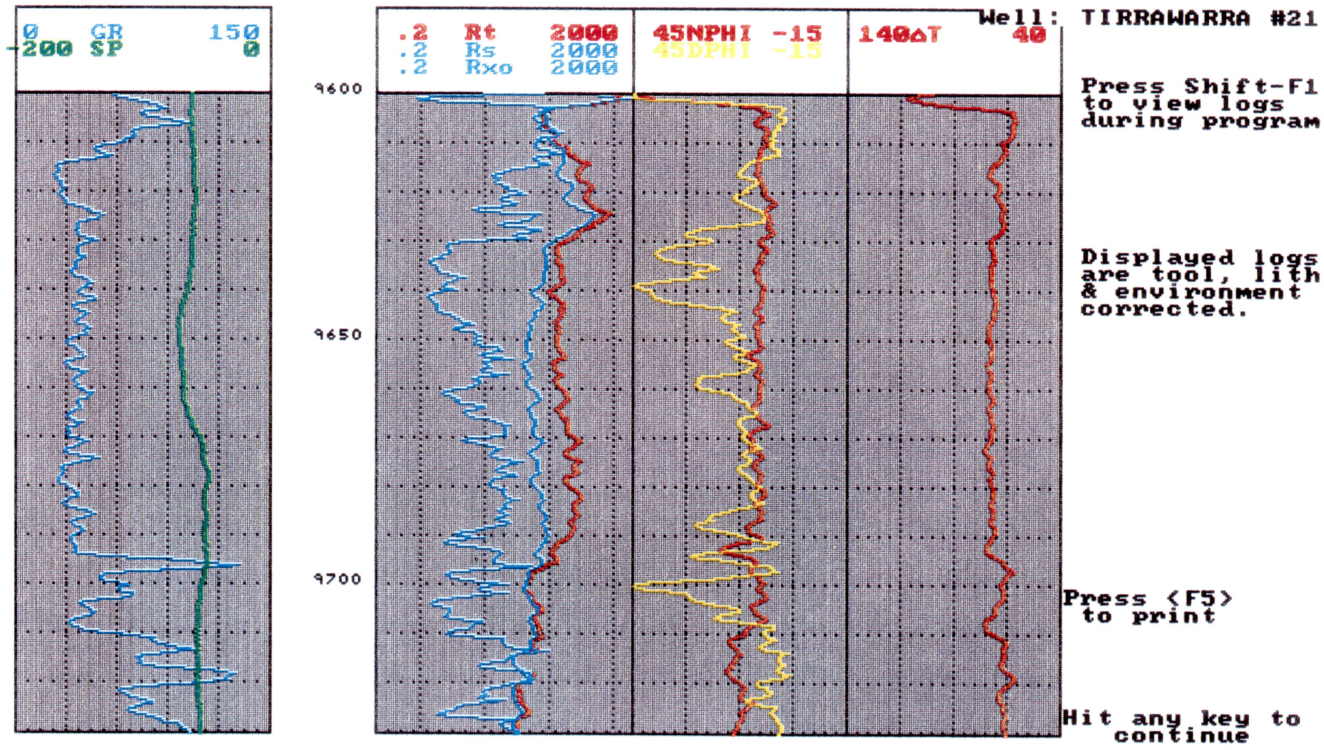

Figure VII-1. Environmental corrected log for the Tirrawarra well 21. The neutron and density porosities are both corrected to a sand matrix. Note the local streaks of very high porosity on the density log (yellow curve) that may be due to fractures.

Review of Santos Methods

Volume of Shale (Vsh) Determination

The previous work on the Tirrawarra Sandstone used the linear relation between the gamma ray log and the volume of shale (eq. 1).

$$Vsh = (GR-GRmin)/(GRmax-GRmin)$$

where

Vsh = volume of shale

GR = gamma-ray reading from shaly sand

GRmin = gamma-ray reading from clean sand (average = 25 API)*

GRmax = gamma-ray reading from shale (average = 130 API)*

*For this analysis, these values were selected for each well.

This linear relationship between the gamma-ray log and the Vsh often results in a slight overestimation of Vsh in some reservoirs. However, because the gamma ray log is not very sensitive to the presence of kaolinite or dickite due to their low radioactivity, the linear relationship should be adequate. The preferred Vsh method for reservoirs with kaolinite or dickite would be to use the neutron-density logs (Asquith, 1990) but that was impossible because of the excessive porosity recorded by the density log (fig. VII-1).

Figures VII-2 and VII-3 are cross plots of core porosity and core permeability versus Vsh for the Tirrawarra 12 well. Note that there is an increase in both porosity and permeability with a decrease in Vsh. An examination of the cross plots reveals that there is more scatter on the Vsh versus porosity cross plot (fig. VII-2). However, the high Vsh (40 percent or greater) values with high porosity (fig. VII-2) are probably the result of shale clasts and/or laminated shale in the reservoir in addition to the dispersed clay. Normally a volume of dispersed clay of 40 percent or more destroys effective porosity (solid line; fig. VII-2). Therefore, figure VII-2 illustrates that there are different Vsh cutoffs depending on the type of clay distribution.

Porosity Determination

For this review a different sonic porosity equation was used to allow a comparison with the Overton porosity equation used by SANTOS.

As with the previous work done on the Tirrawarra Sandstone the sonic log was also chosen to determine porosity. However, the sonic porosity was adjusted to core porosity by the matrix travel time (Dtma), not the travel time of the fluid in the borehole (Dtf) as is used in the

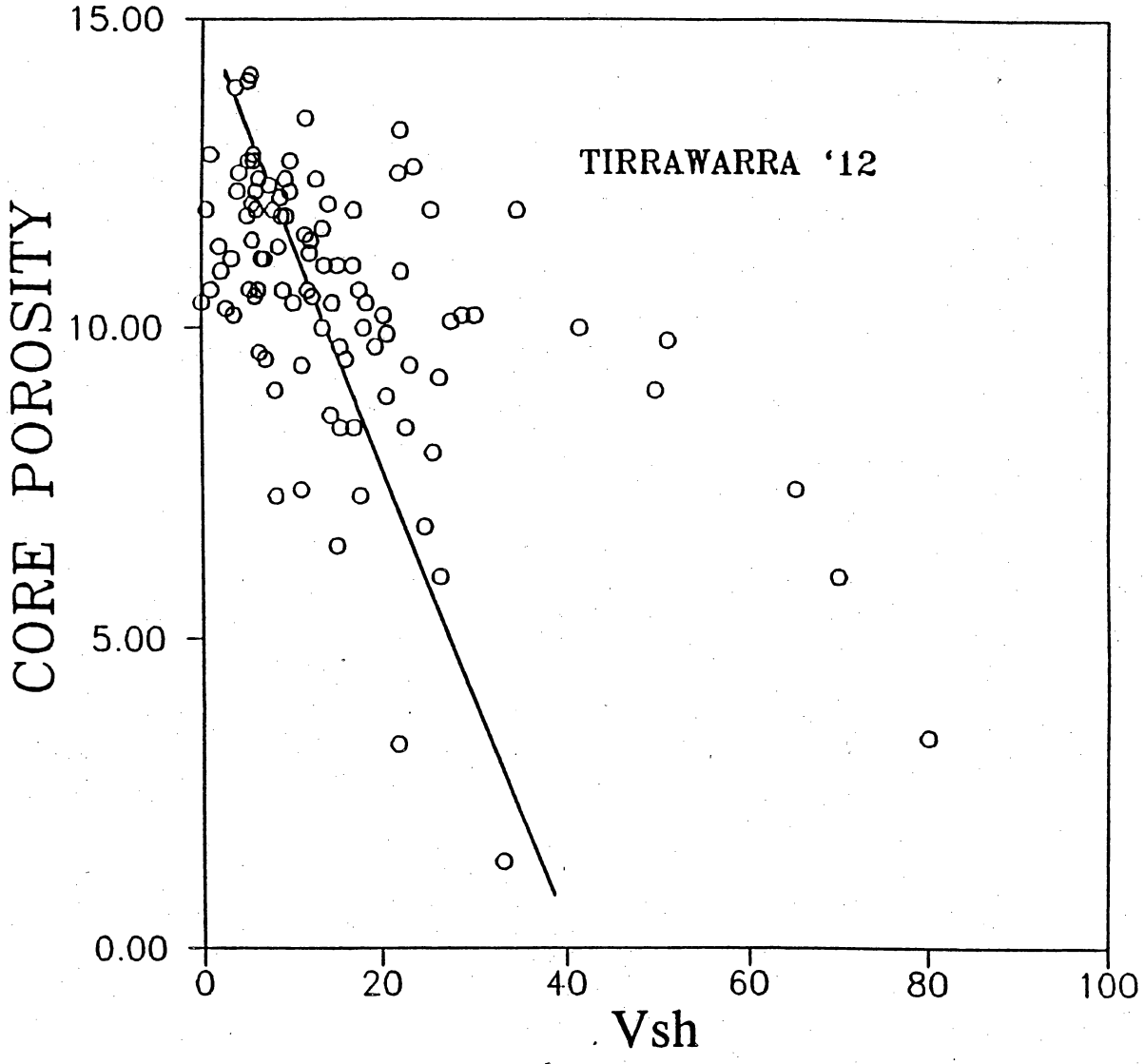

Figure VII-2. Cross plot of core porosity versus volume of shale (Vsh) for the Tirrawarra well 12. The data that have high values of Vsh (40 percent or greater) and high porosity probably have shale clasts and/or shale laminations in addition to dispersed clay. The data along the solid line represent a normal porosity versus Vsh trend for a reservoir with dispersed clay.

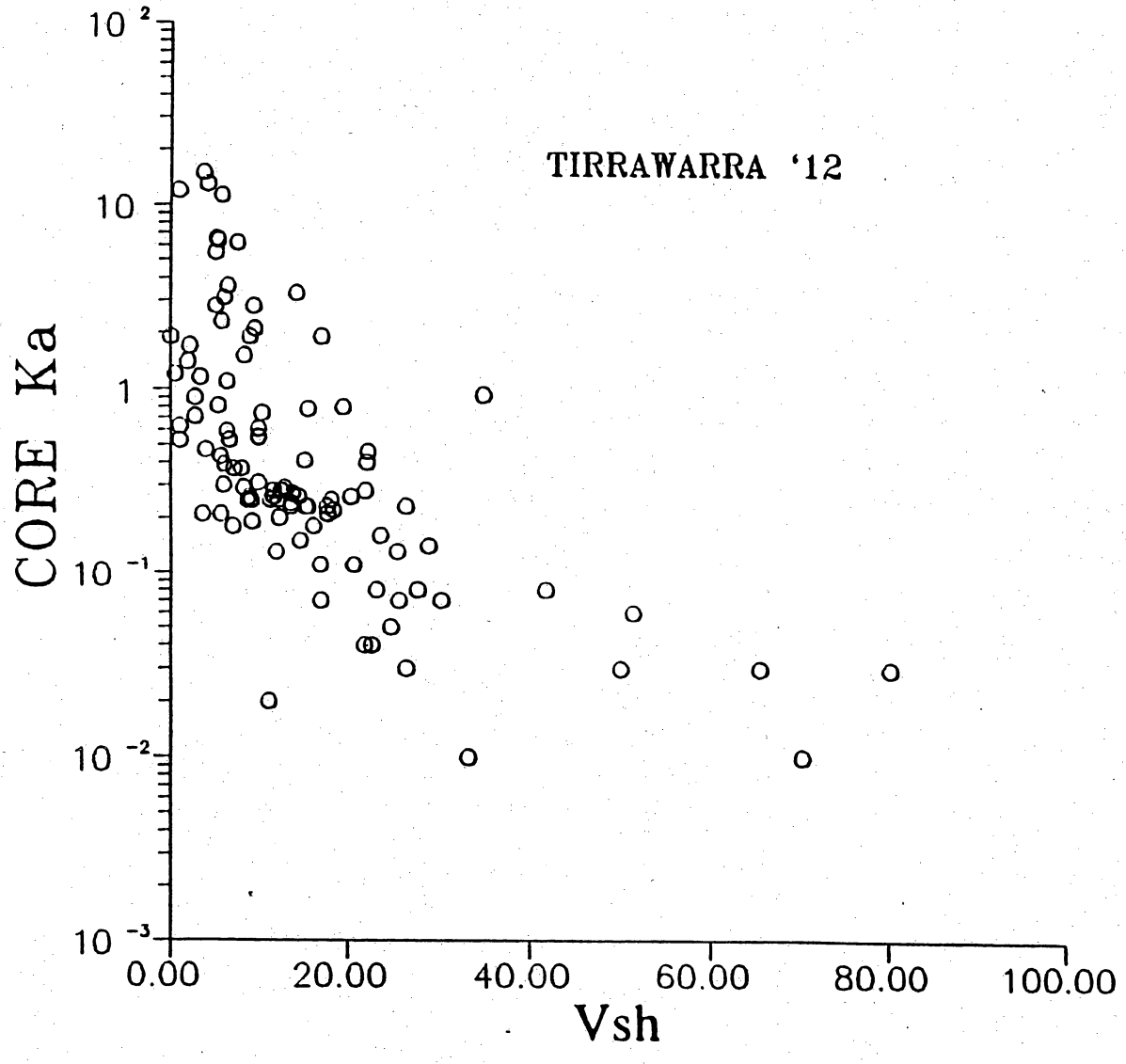

Figure VII-3. Cross plot of core permeability versus volume of shale for the Tirrawarra well 12. Note the good relationship between Vsh and permeability, which illustrates the effect an increase in Vsh has on permeability.

Overton porosity equation (Overton and Hamilton, 1986). It is important to note that both methods are valid because both are based on core porosity. For the foot-by-foot porosity determination the Overton porosity equation was used and calculated by Santos. The formula used in this review of sonic porosity (eq. 2) is:

$$PHIsonic = [(Dtsa-Dtma)/(Dtf-Dtma)] - Vsh \times [(Dtsh-Dtma)/(Dtf-Dtma)]$$

where

PHIsonic = effective sonic (Vsh corrected) porosity

Dtsa = interval transit time of sandstone

Dtma = interval transit time of matrix (55 usec/ft)

Dtsh = interval transit time of shale (66 usec/ft)*

Vsh = volume of shale

*For this analysis Dtsh was picked for each well. Note that Dtsh is not required for the Overton equation.

Figure VII-4a is a cross plot of sonic porosity calculated using the above equation versus core porosity for data from the Tirrawarra 12 and 16 wells. The good correlation between log porosity and core porosity indicates that the sonic log porosity is a good approximation of core porosity. The dotted line in figure VII-4a is not a best fit line but is only a line along which sonic porosity is equal to core porosity. Figure VII-4b is the same cross plot but for the whole edited core-porosity data base for Tirrawarra field, using the Overton porosity equation. Despite a larger scatter of data the relationship still holds. The scatter is explained by the fact that core samples are a very specific point in a well, whereas the sonic log averages many cubic feet of rock, including any shale laminae, high-porosity stringers, or other porosity-affecting heterogeneities. The presence of the clay mineral dickite is largely unnoticed by the gamma-ray tool, so core porosities will correspond to higher log-calculated porosities, resulting in scatter. Scatter may also be due to the Overton equation using uncorrected gamma-ray values. The gamma-ray tool is sensitive to variation in both bore hole diameter and logging speed.

Effective Water Saturation Determination

Based on the log suites used for the wells and the problems with the density log (fig. VII-1) the best shaly sand method for determining effective water saturation in the Tirrawarra sandstone is the Simandoux equation. The Dual Water, Fertl, and Dispersed Clay methods all require density logs, and density logs in the Tirrawarra sandstone were unusable. The Indonesian (Poupon) method is an equation developed for a particular shaly sand area. In contrast, the Simandoux equation has been applied successfully to the analysis of shaly sands in many different basins. The Automatic Compensation method (Dewan, 1984) is also appropriate.

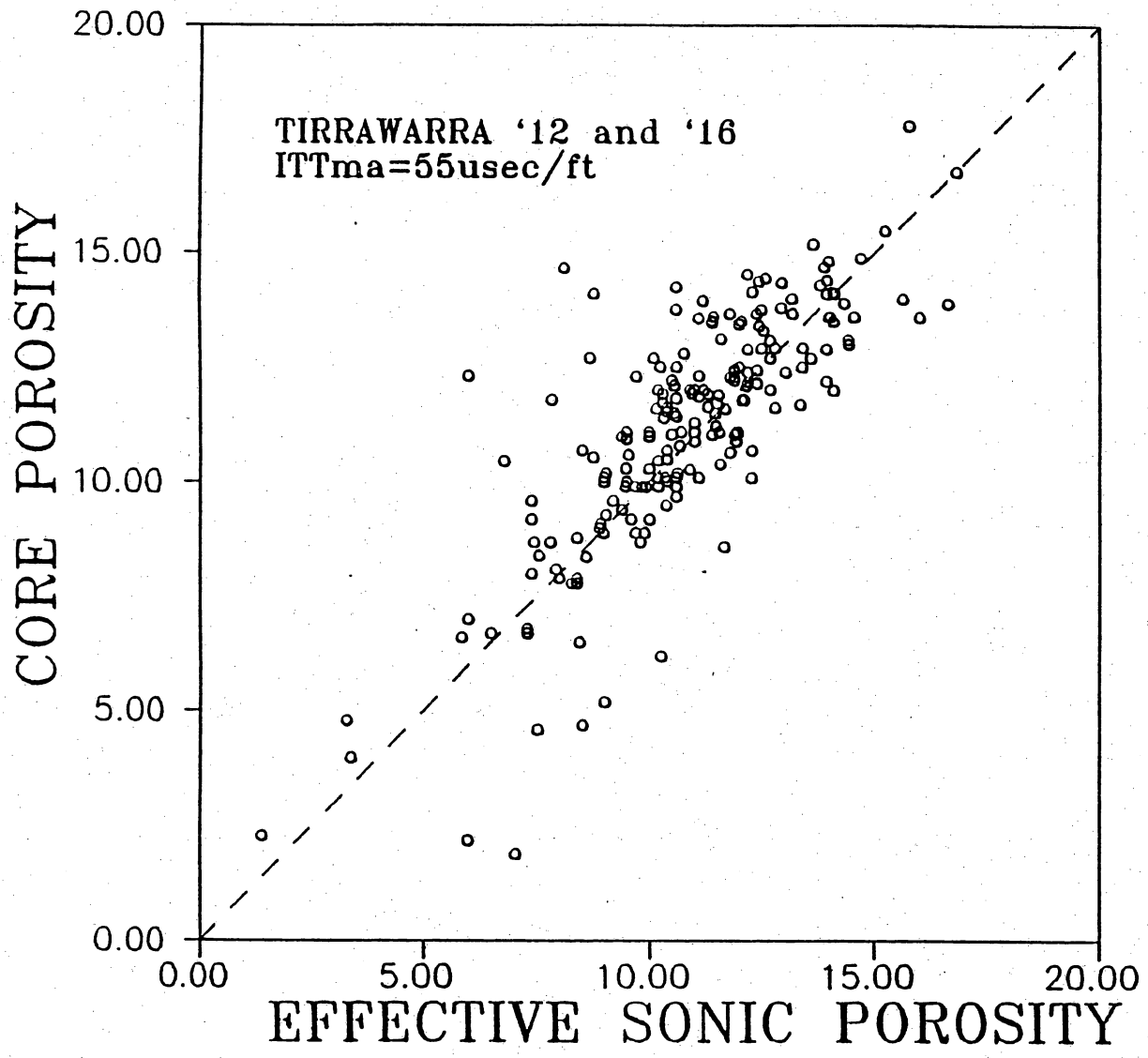

Figure VII-4a. Cross plot of core-derived porosity versus effective sonic porosity for the Tirrawarra wells 12 and 16. The dotted line is not a best-fit line but only a line along which core porosity is equal to sonic porosity.

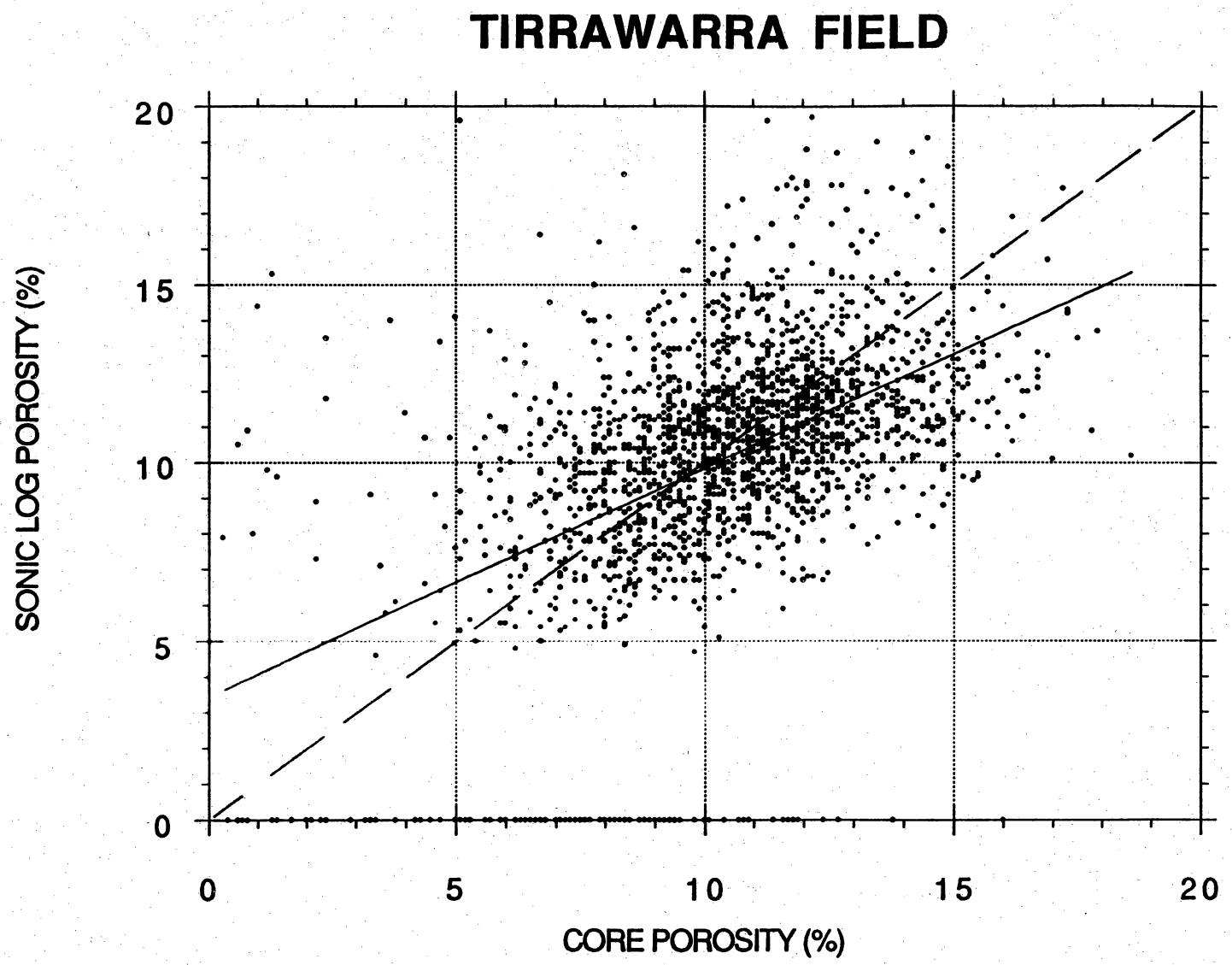

Figure VII-4b. Sonic log porosity versus core porosity cross plot for the total edited core porosity data base. Core porosity equals sonic porosity along the dashed line. The solid line is a linear regression (conventional least squares) best fit line.

To effectively use the Simandoux equation, a value for the resistivity of the shale or clay (Rsh) in the reservoir is needed (Asquith, 1990). An examination of the shale units below the Tirrawarra sandstone revealed minimum shale resistivities of 23–50 (ave. 34) ohm-m. The shales above the Tirrawarra Sandstone were not used because their organic content is high and the presence of organic matter in shales raises resistivity.

To determine if the Rsh value used is compatible with the resistivity of the shale or clay in the reservoir, a cross plot of effective water saturations calculated by an equation that requires Rsh and an equation that does not require Rsh is used (Asquith, 1990). In this case a cross plot (fig. VII-5) of Sw, calculated by the Simandoux equation, which requires a value of Rsh (Y-axis), versus Sw calculated by the Automatic Compensation equation (Dewan, 1984), which does not require a value of Rsh (X-axis) is made for Tirrawarra 21. This plot illustrates that values for corresponding depths, from each method, are the same (fig. VII-5) so the value for Rsh for Tirrawarra 21 (35 ohm-m) is compatible with the adjacent shale and is correct. This was also true for the other analysed wells. Therefore the Simandoux Equation appears to be appropriate for this reservoir.

A further check on the value of Rsh is to calculate a value of Rsh assuming the clay minerals are predominantly dickite or kaolinite. Using the method of calculating Rsh outlined by Dewan (1984) and assuming the clay is dickite, the value for Rsh is 16–50 ohm-m, which is close to the 23–50 ohm-m determined from logs. In conclusion, the effective water saturations for the Tirrawarra Sandstone were calculated by the Simandoux Equation using effective sonic porosity and a Rsh value of 23–50 ohm-m (determined for each well):

$$1/Rt = [(Vsh/Rsh)*Sw] + [Phie^2/(a*Rw)]*Sw^2$$

where

Rt = true formation resistivity

Vsh = volume of shale

Rsh = shale resistivity

Sw = water saturation

Phie = effective sonic (GR corrected porosity)

Rw = water resistivity

Petrophysical Verification of Flow Units

Log-derived parameters, such as resistivity, water saturation, and density, are strongly influenced by formation lithology. Reservoir flow units determined from geological attributes were verified to have different petrophysical characteristics: using Dew plots, (cross plot of the ratios of Rt/Rw versus Rxo/Rmf; figs. VII-6 through VII-10) identified flow units plot in discrete

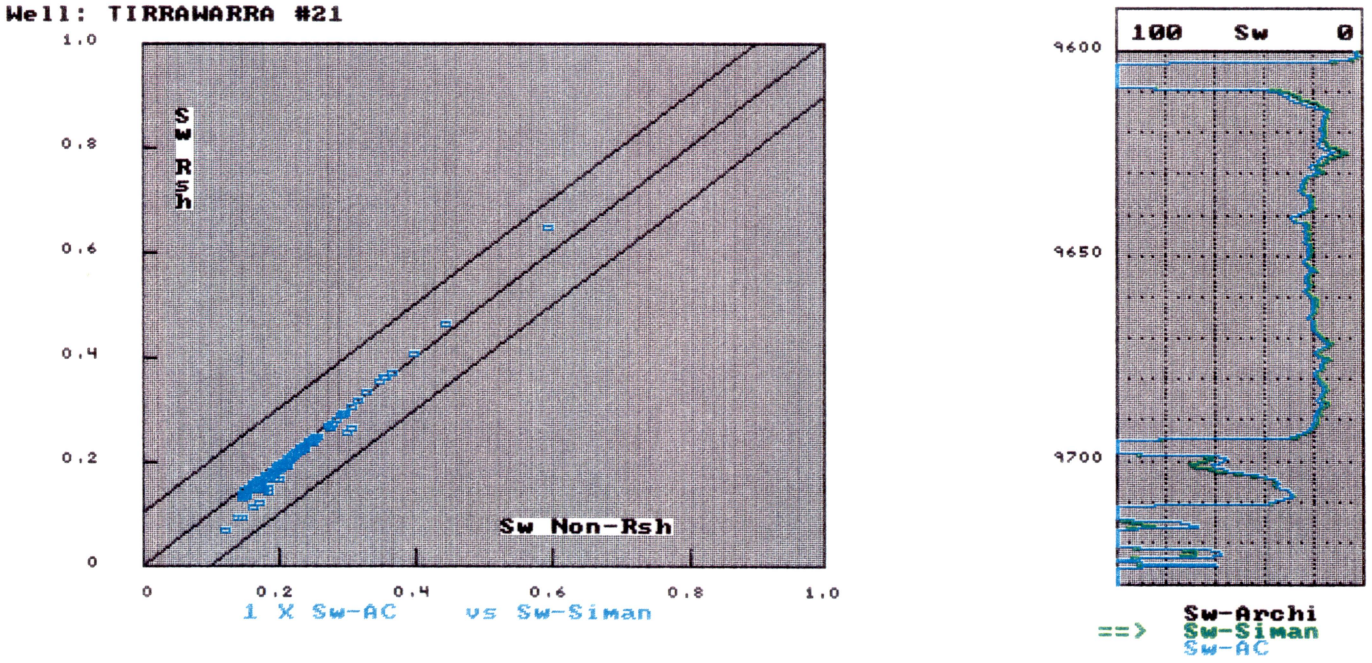

Figure VII-5. Cross plot of Sw (Simandoux) versus Sw (Automatic Compensation) for the Tirrawarra well 21. Note that the two Sw methods give the same Sw values, which indicates that the Rsh value (Rsh = 20 ohm-m) used in Simandoux equation is correct.

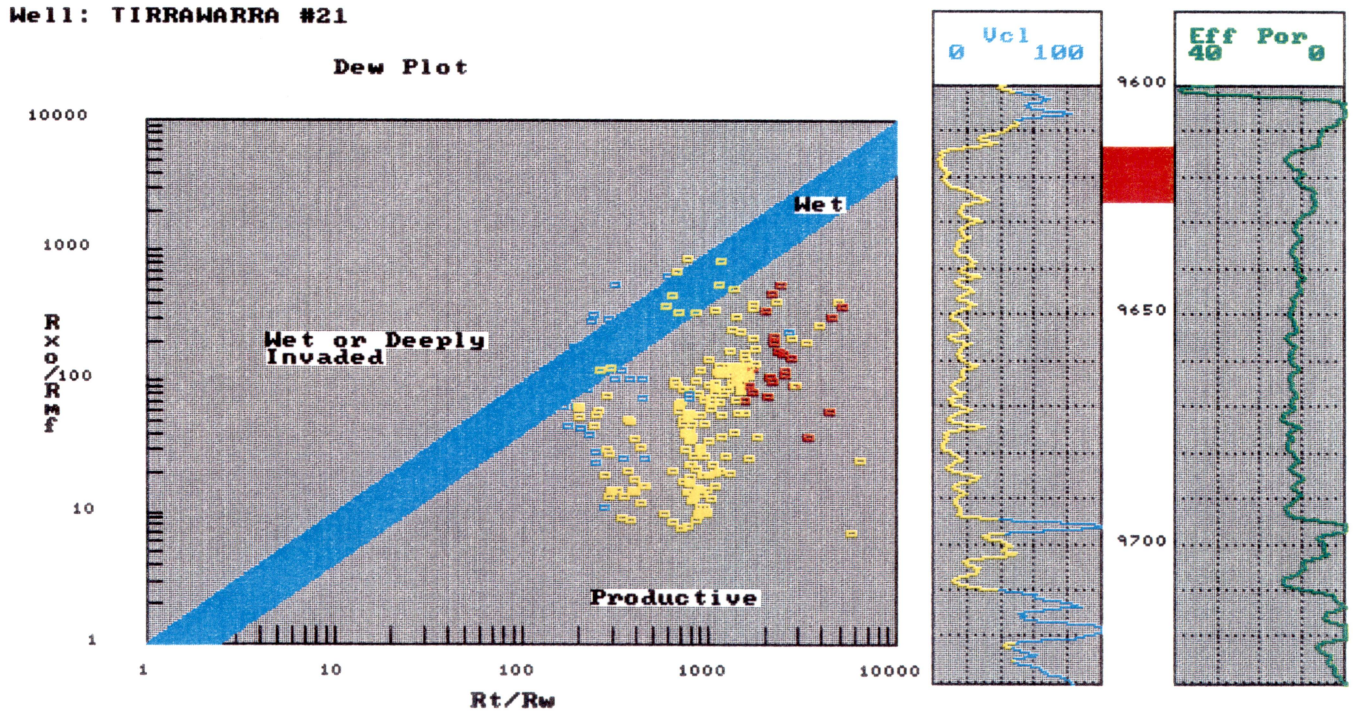

Figure VII-6. Dew plot of the Tirrawarra well 21 with reservoir flow unit 4 shown in red. Note that each of the different reservoir facies cluster in a different region of the plot (figures VII-6 to VII-10).

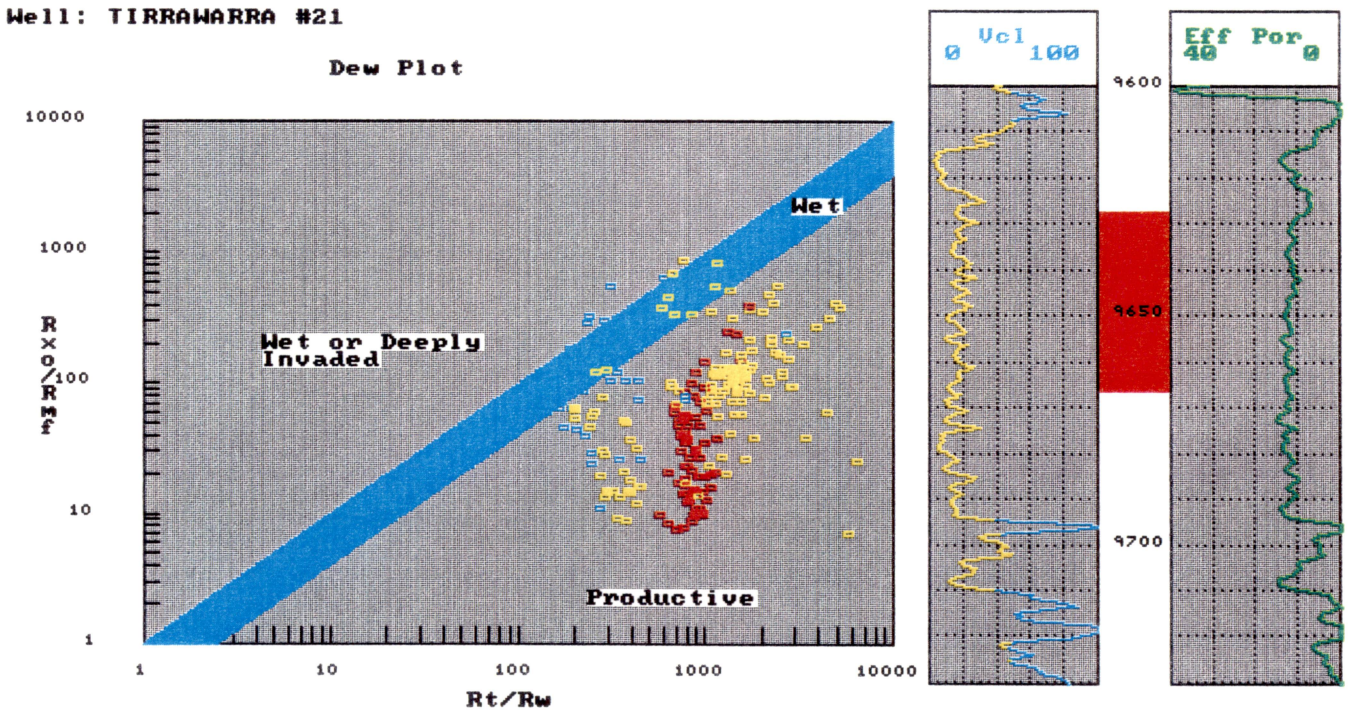

Figure VII-7. Dew plot of the Tirrawarra well 21 with reservoir flow unit 3U shown in red.

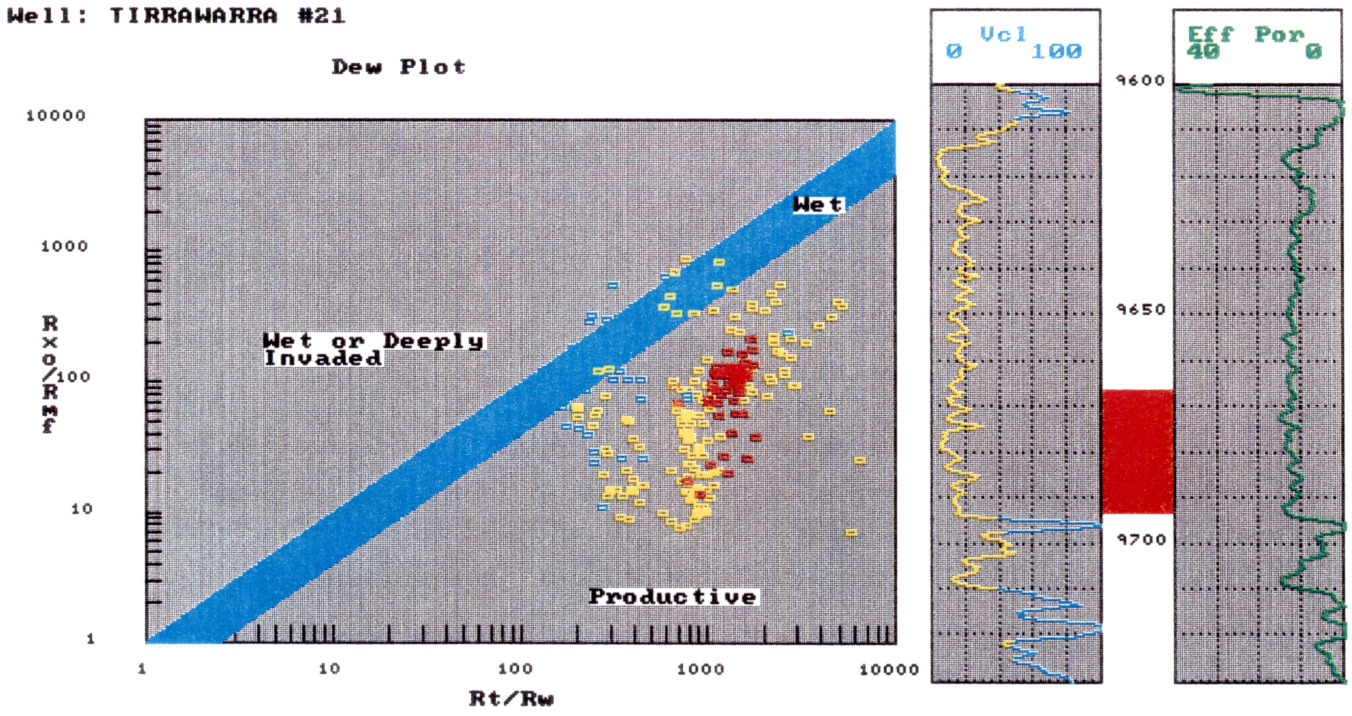

Figure VII-8. Dew plot of the Tirrawarra well 21 with reservoir flow unit 3L shown in red.

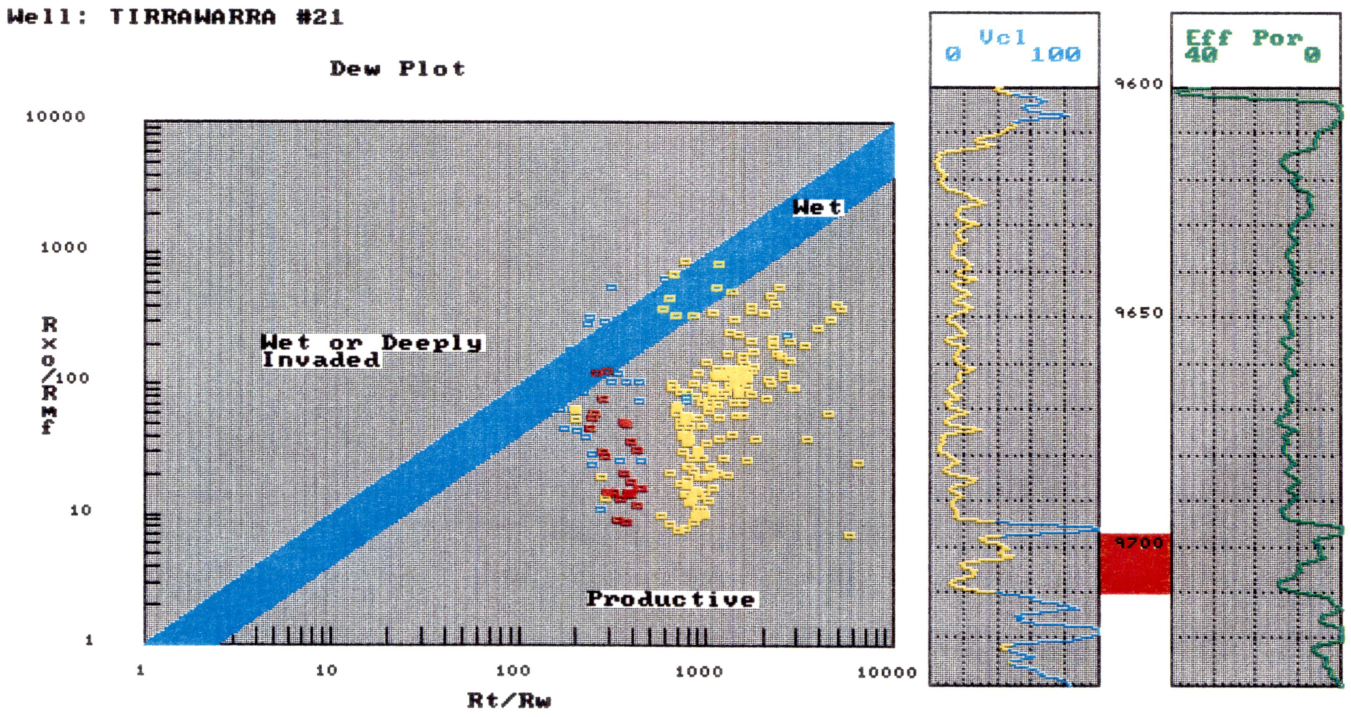

Figure VII-9. Dew plot of the Tirrawarra well 21 with reservoir flow unit 2 shown in red.

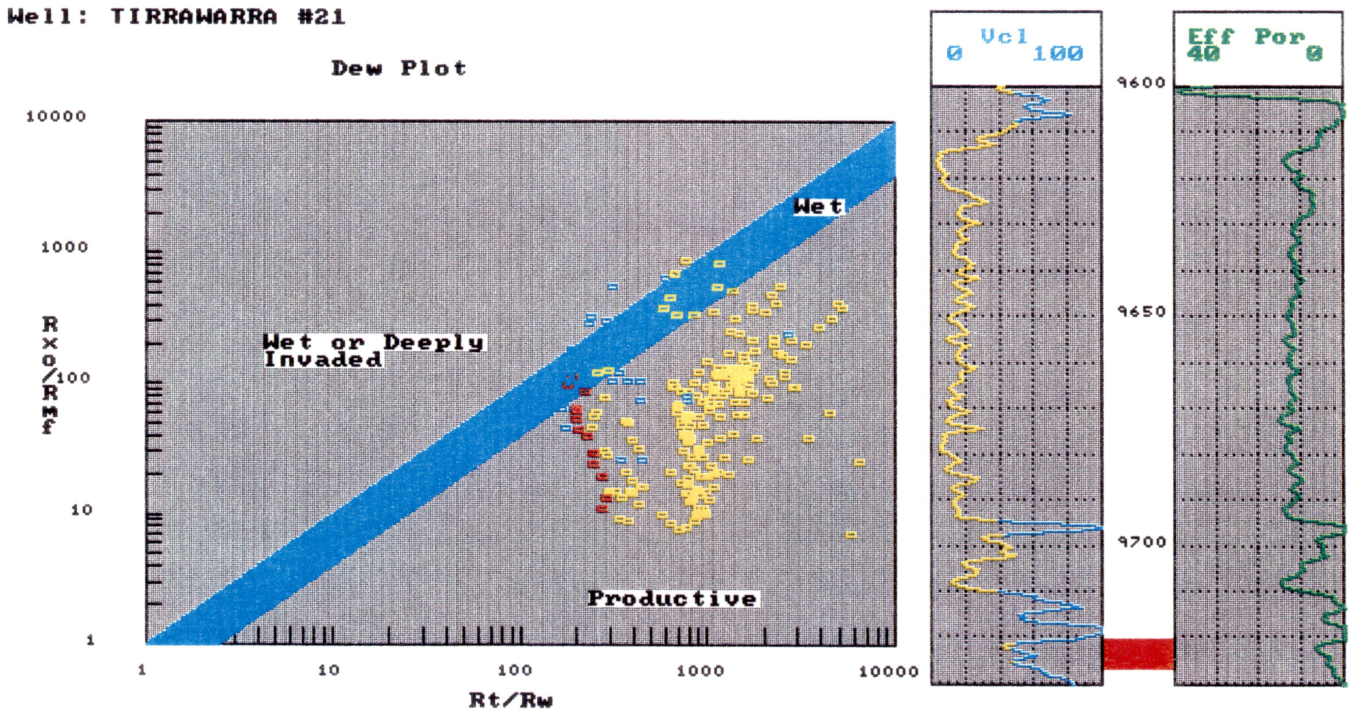

Figure VII-10. Dew plot of the Tirrawarra well 21 with reservoir flow unit 1 shown in red.

fields. In figures VII-6 to VII-10 (Tirrawarra 21 well) the depth intervals of each reservoir flow unit was isolated on the Dew plots as indicated by the red areas. The flow unit differentiation on the Dew plots is the result of slight changes in porosity or pore type due to changes in grain size and/or volume of clay in the different reservoir flow units. The best quality reservoir cluster further to the right on the cross plot. Bulk volume water (BVW) plots from the Tirrawarra 21 well also illustrate differentiation of the reservoir flow units (figs. VII-11 to VII-15). Note that the individual reservoir flow units also have distinct patterns on the BVW plots (figs. VII-11 to VII-15) with the best reservoir unit forming a curve closest to the origin of the plot. As BVW plots require a density log to be effective, this cross-plot was run on fewer wells. These two plots therefore indicate that the identified geological flow units have distinct petrophysical differences that can be identified and mapped. Therefore, net pay and hydrocarbon pore-feet were determined for each of these reservoir flow units separately. Further, both methods confirm flow unit 4 as having the best reservoir characteristics, followed in decreasing order of reservoir quality by 3L, 3U, and 2L, with 1U having the poorest characteristics.

The location of data clustering on the Dew plots identifies the potential for production. In figures VII-6 to VII-10, the reservoir flow units cluster below the blue line on the Dew plot indicates productive moved hydrocarbons in the Tirrawarra 21 well. In contrast, the data from the lower 45 ft of the downdip Rakoona no. 1 well cluster in the blue area of the Dew plot (fig. VII-16), which indicates a lack of moved hydrocarbons because the zone is wet.

Determination of Cutoff Values for Net Pay Calculation

The parameters requiring cutoff definition for the purpose of pay determination are Vsh, porosity, and Sw. The cutoff values established for the foot-by-foot pay determinations are presented in table VII-1 by flow unit:

Table VII-1. Cutoff Values for Tirrawarra Flow Units.

Flow unit	Vsh (%)	Porosity (%)	Sw (%)
4	40	8	50
2U	40	8	50
3U	30	8	50
3L	30	8	50
2L	40	8	50
1U	40	8	60

These cutoff values are based on a 0.5 md permeability cutoff for core derived values and on production and test results. (Overton, 1986; Pecanek and Gulayets, 1986). Previous log analysis interpretations used the following cutoffs for the whole reservoir section:

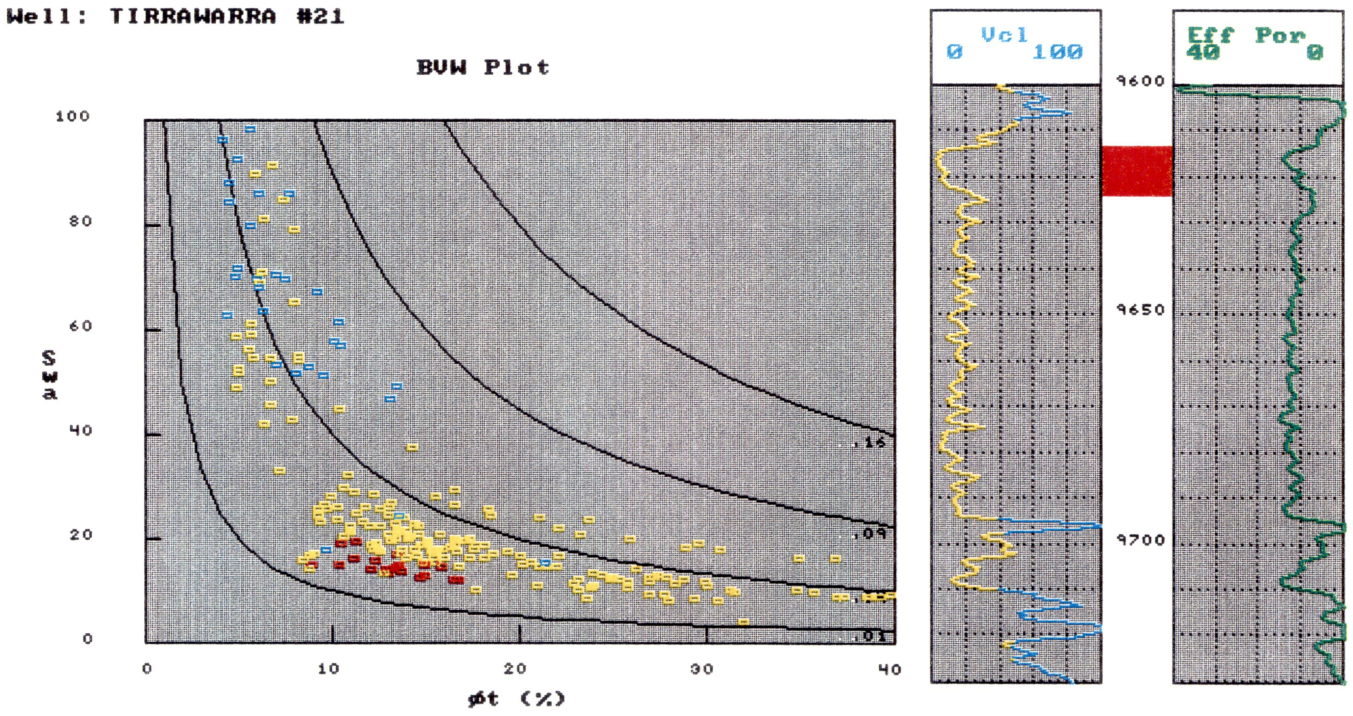

Figure VII-11. Bulk volume water plot of the Tirrawarra well 21 with reservoir flow unit 4 shown in red. Note in figures VII-11 to 15 that the different reservoir flow units plot in separate portions of the BVW plot. On each of the BVW plots the porosity on the X-axis is the density porosity. Even though the density log is optimistic it is only being used in the BVW plot for comparison.

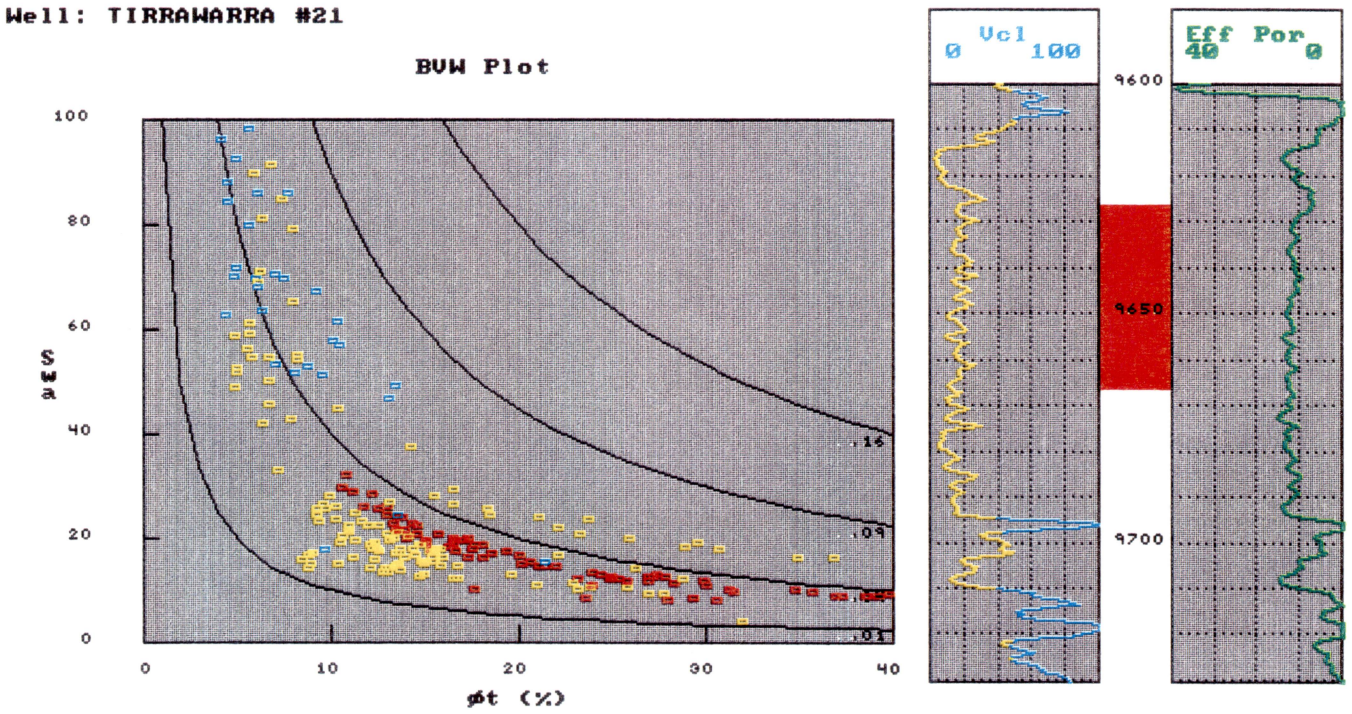

Figure VII-12. Bulk volume water plot of the Tirrawarra well 21 with reservoir flow unit 3U shown in red.

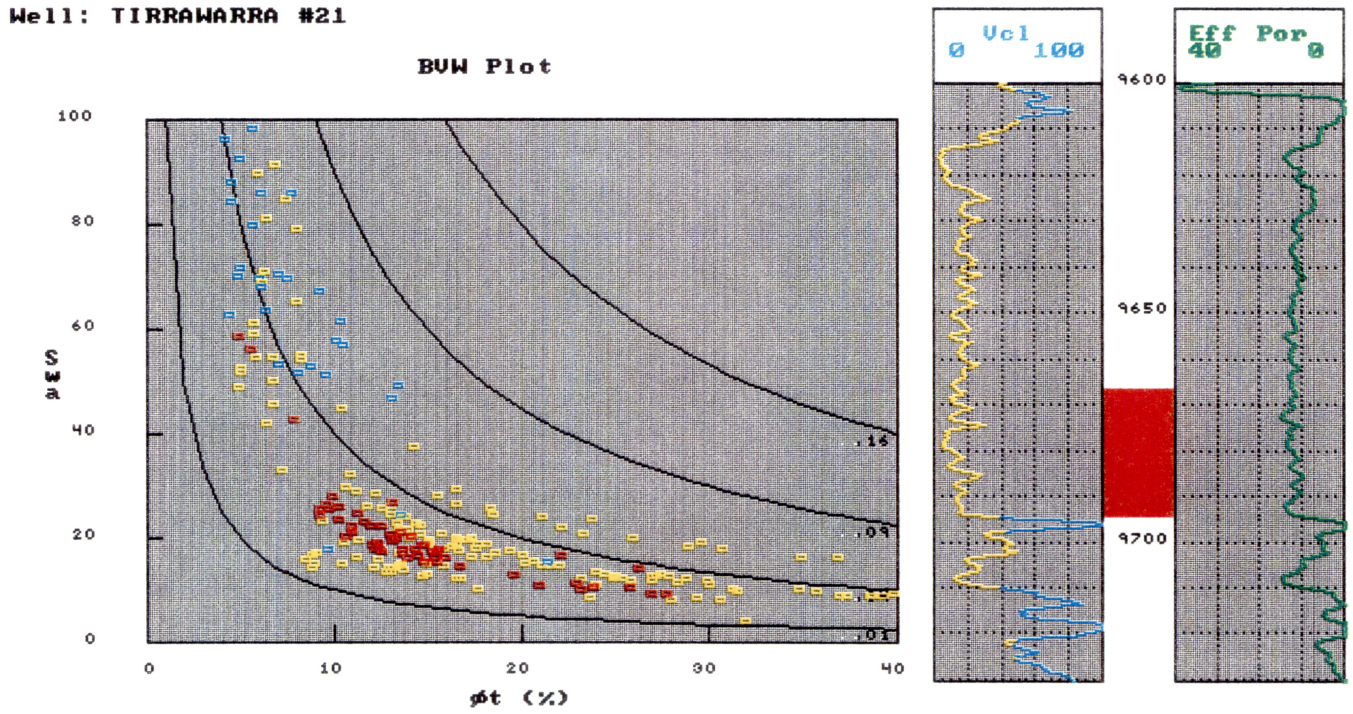

Figure VII-13. Bulk volume water plot of the Tirrawarra well 21 with reservoir flow unit 3L shown in red.

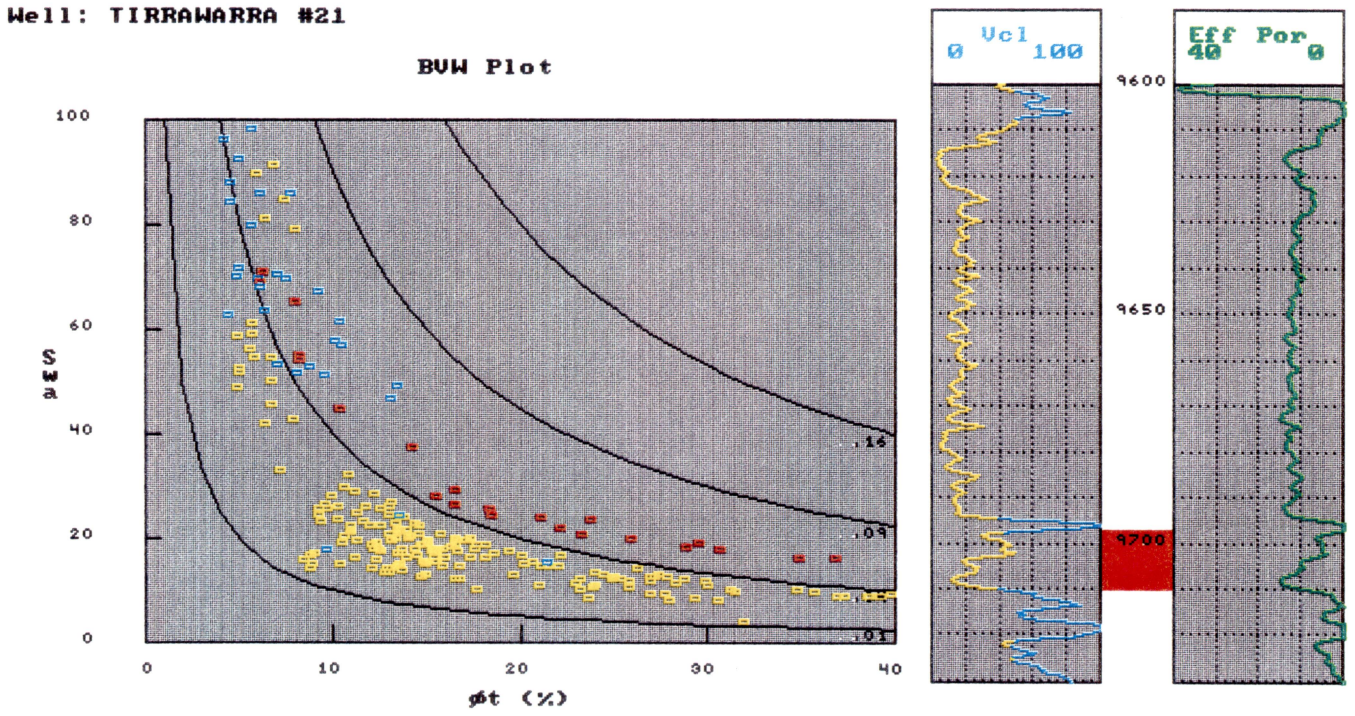

Figure VII-14. Bulk volume water plot of the Tirrawarra well 21 with reservoir flow unit 2L shown in red.

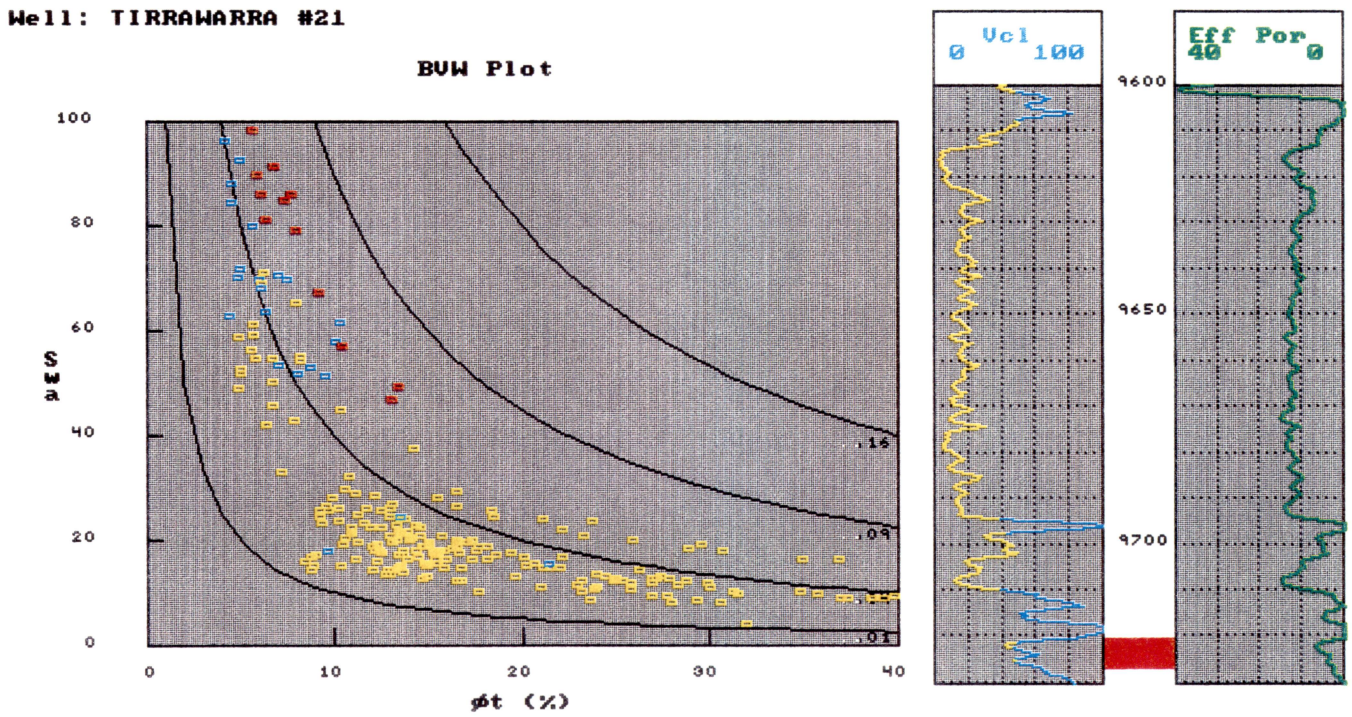

Figure VII-15. Bulk volume water plot of the Tirrawarra well 21 with reservoir flow unit 1U shown in red.

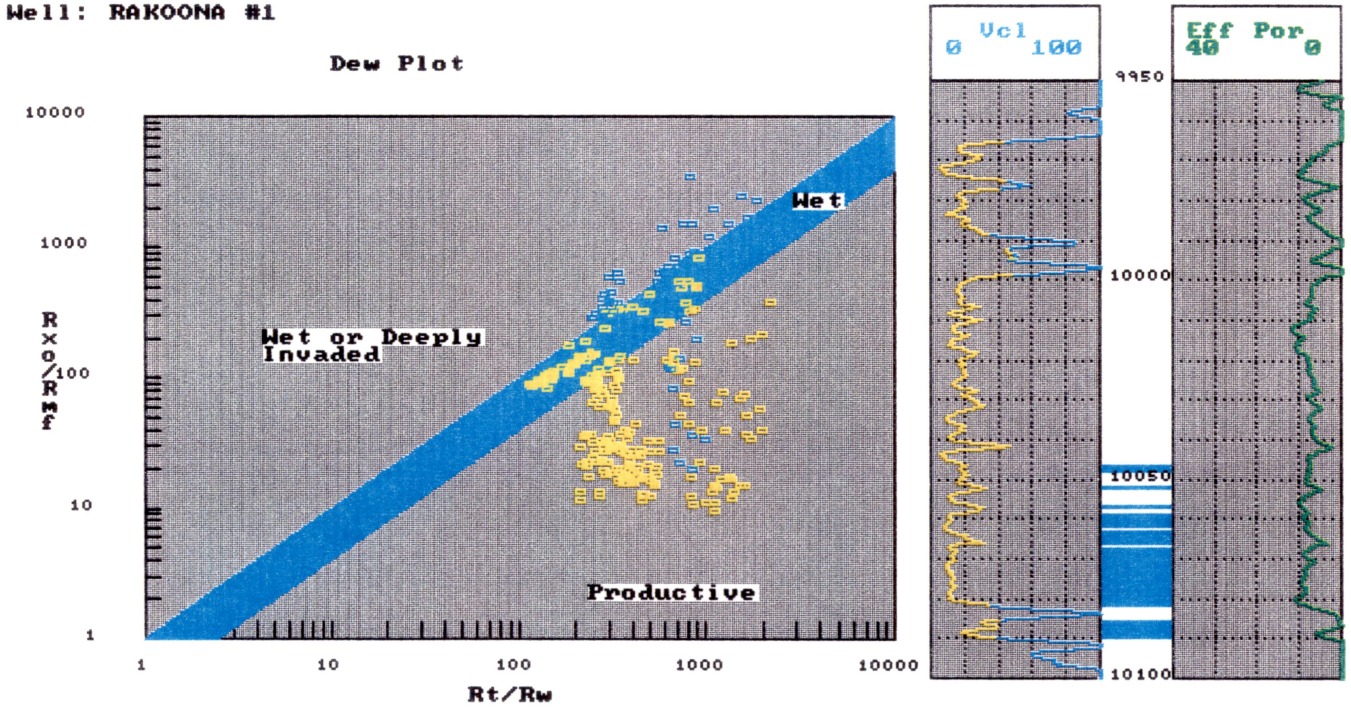

Figure VII-16. Dew plot of the downdip Rakoona well 1. Note that the lower 45 feet of this well (blue color) plot in the region of the Dew plot that indicates a lack of moved hydrocarbons (Sw/Sxo >0.7) because the zone is wet.

Vsh: 30 percent; Porosity: 9 percent; Sw: 50 percent and a core permeability cutoff of 0.5 md. Reasons for the establishment of variable petrophysical property cutoffs follow.

Volume of Shale Cutoff

Previous work on the Tirrawarra sandstones used a Vsh cutoff of 30 percent. Normally in shaly sand reservoirs with dispersed clay a 20 percent Vsh cutoff is used. However, because the dispersed clay is dickite a higher cutoff (30 percent) is appropriate because dickite and kaolinite have less effect on permeability than the other clay minerals (Neashan, 1977). Further, the presence of shale laminae and shale clasts rather than dispersed diagenetic clays in the shalier flow units supports the use of cutoffs as high as 40 percent Vsh in those flow units.

The Vsh cutoffs were determined from cross plots of log derived Vsh against core derived permeability (fig. VII-17). This plot shows that for all the core data, including all flow units, minimal pay-quality rock has a Vsh in excess of 40 percent.

Crossplots of Vsh against core permeability for each flow unit (figs. VII-18 through VII-23) show that for flow unit 4 a 40 percent Vsh cutoff is appropriate, and that a 30 percent Vsh cutoff is appropriate for flow units 3L and 3U (note that the higher Vsh values for 3U are insignificant due to the large data set for 3U). There is too little data for an adequate determination of Vsh cutoff for flow units 1U, 2U, or 2L, so the 40 percent Vsh cutoff indicated by the full data set was used for these flow units. The variation in these cutoffs on a flow-unit basis can be explained by the smaller proportion of both ductile grains and shaly laminae in flow units 3U and 3L. These ductile grains are either shale clasts or rock fragments, both of which give a significant gamma-ray response compared to the dominant clay, kaolin. The shaly laminae often have no impact on the permeability of the surrounding reservoir quality rock except on its gamma-ray response (Dewan, 1984). For flow unit 2L this effect can be substantial.

Although most of the core plug samples with Vsh values in excess of 40 percent have permeabilities less than 0.5 md (nonpay) a small but significant proportion have greater permeabilities. On this basis, rock excluded as pay by the LOGCALC program, based purely on Vsh, has been carefully reviewed during editing of the foot-by-foot log analysis results. This rock has been included as pay where ambient core permeability measurements indicate pay quality rock (greater than 0.5 md) and where thin potential pay (excluded due to high Vsh) is adjacent to other pay as well as where adjacent wells with core indicate pay with a high Vsh at this correlated level. This is especially pertinent to Flow Unit 2L which has pay-quality rock (based on core permeabilities) with Vsh values as high as 0.75.

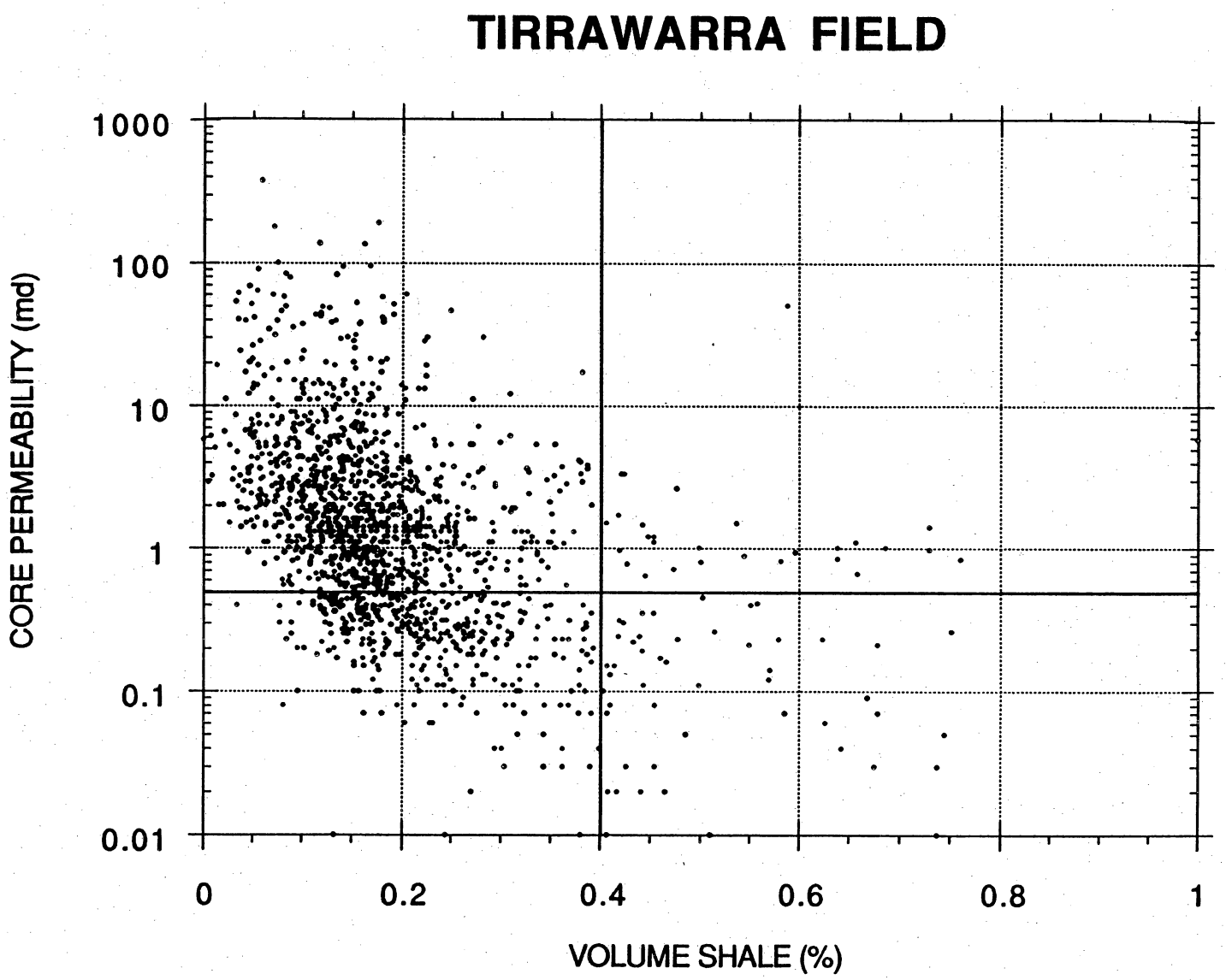

Figure VII-17. Cross plot of core permeability against log analysis calculated Volume of Shale (vsh) for all edited core data. The overall 40% Vsh cut-off is shown.

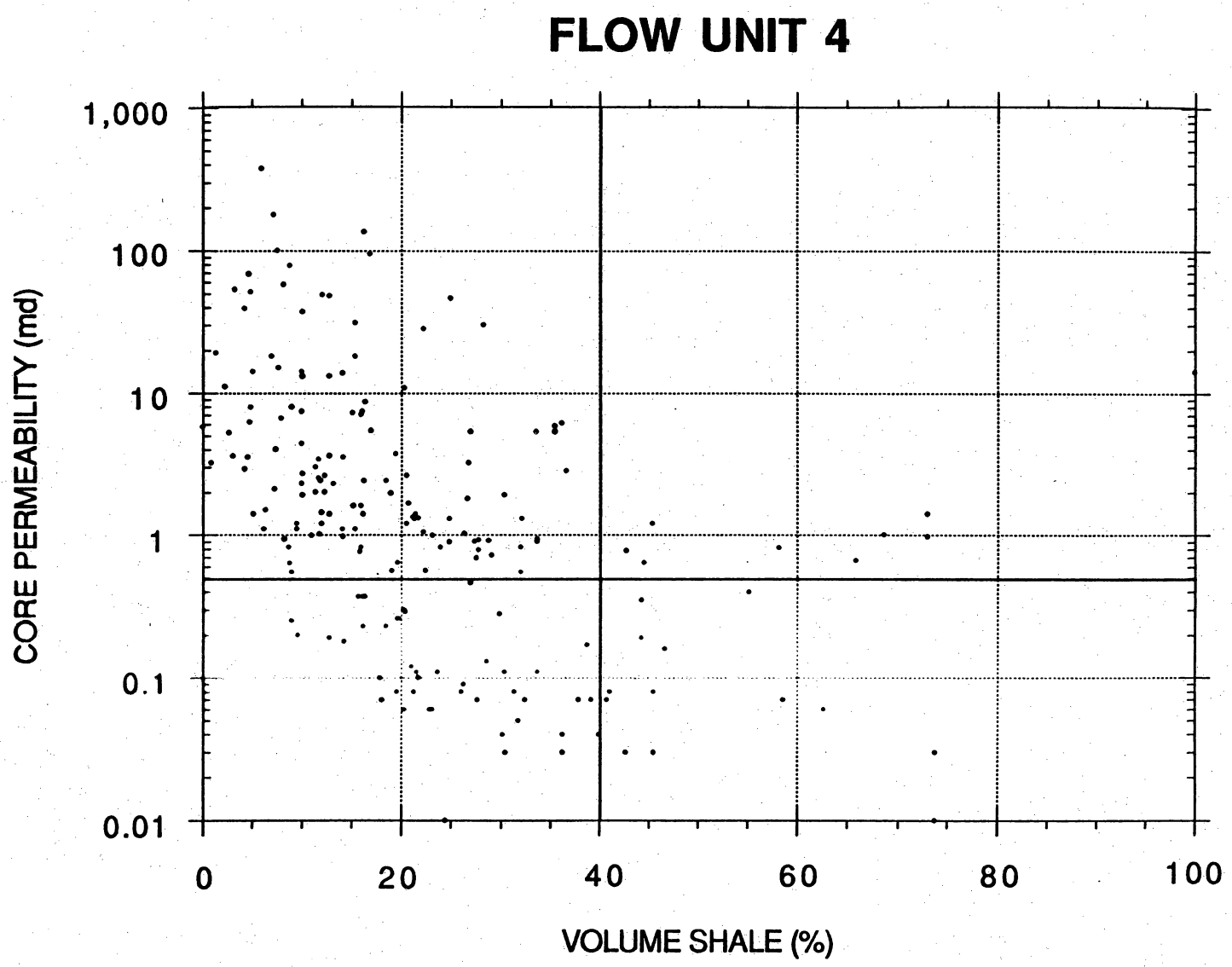

Figure VII-18. Cross plot of core permeability against log analysis calculated Volume of Shale (vsh) for all edited core data from flow unit 4. The overall 40% Vsh cut-off is shown.

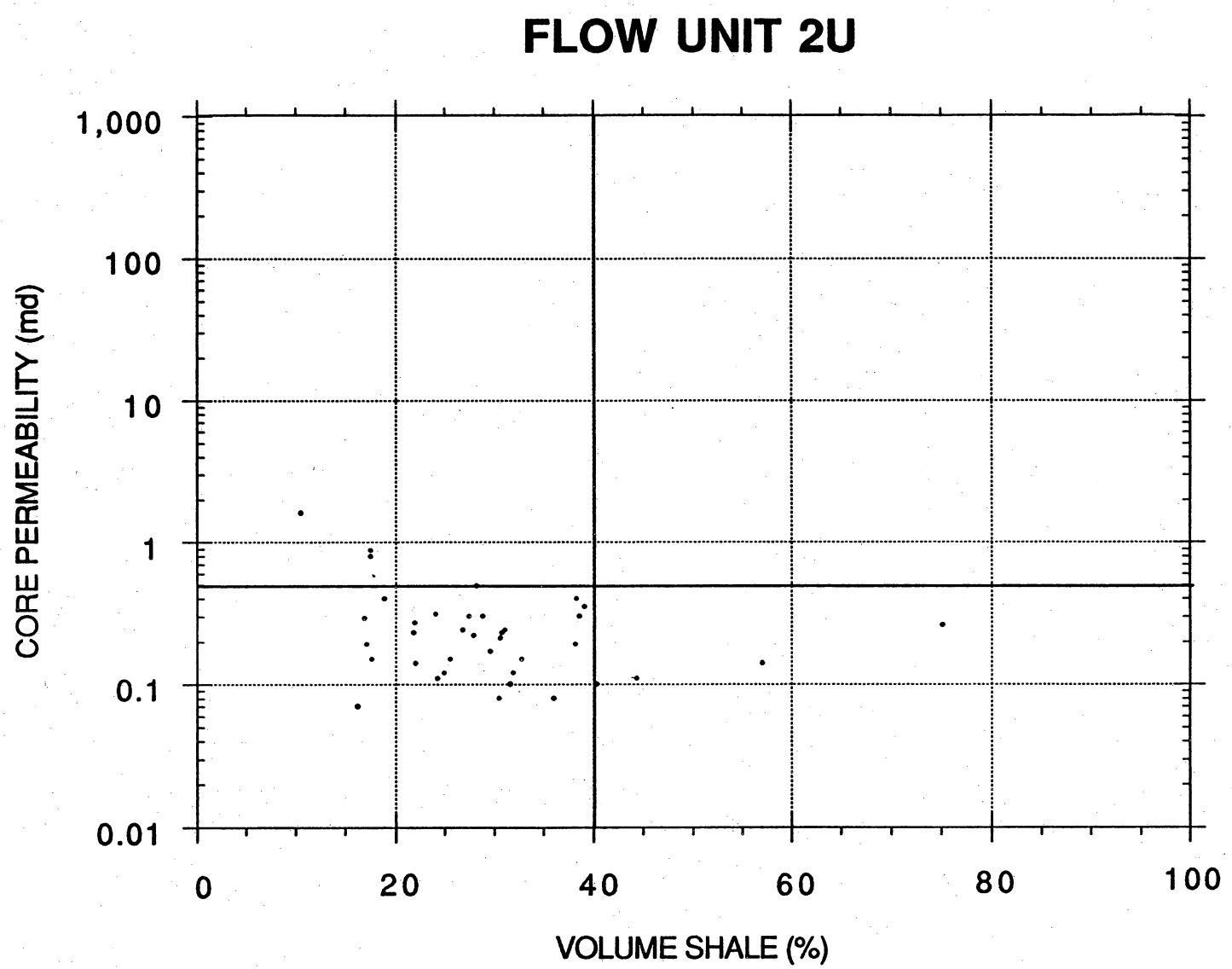

Figure VII-19. Cross plot of core permeability against log analysis calculated Volume of Shale (vsh) for all edited core data from flow unit 2U. The overall 40% Vsh cut-off is shown.

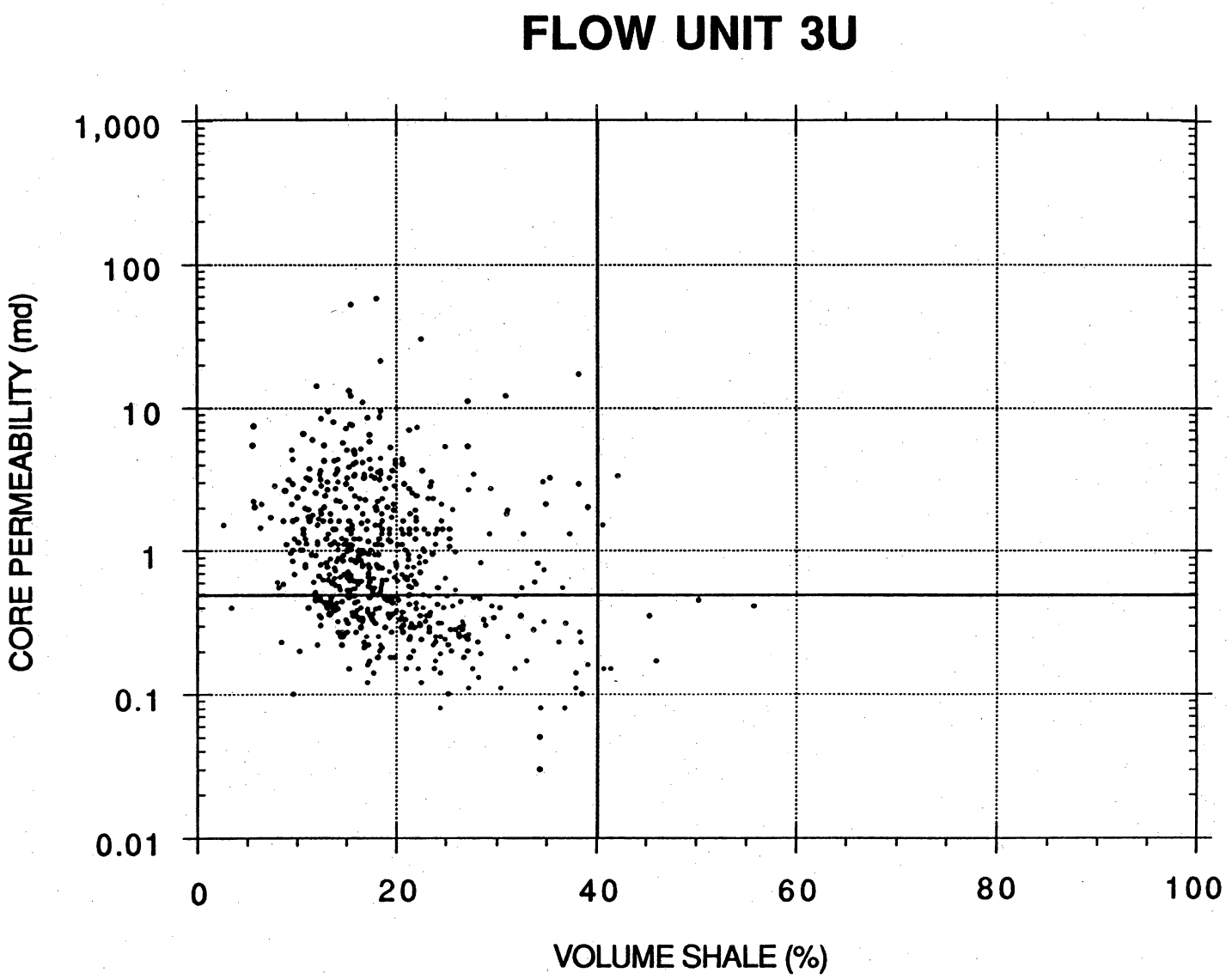

Figure VII-20. Cross plot of core permeability against log analysis calculated Volume of Shale (vsh) for all edited core data from flow unit 3U. The overall 40% Vsh cut-off is shown.

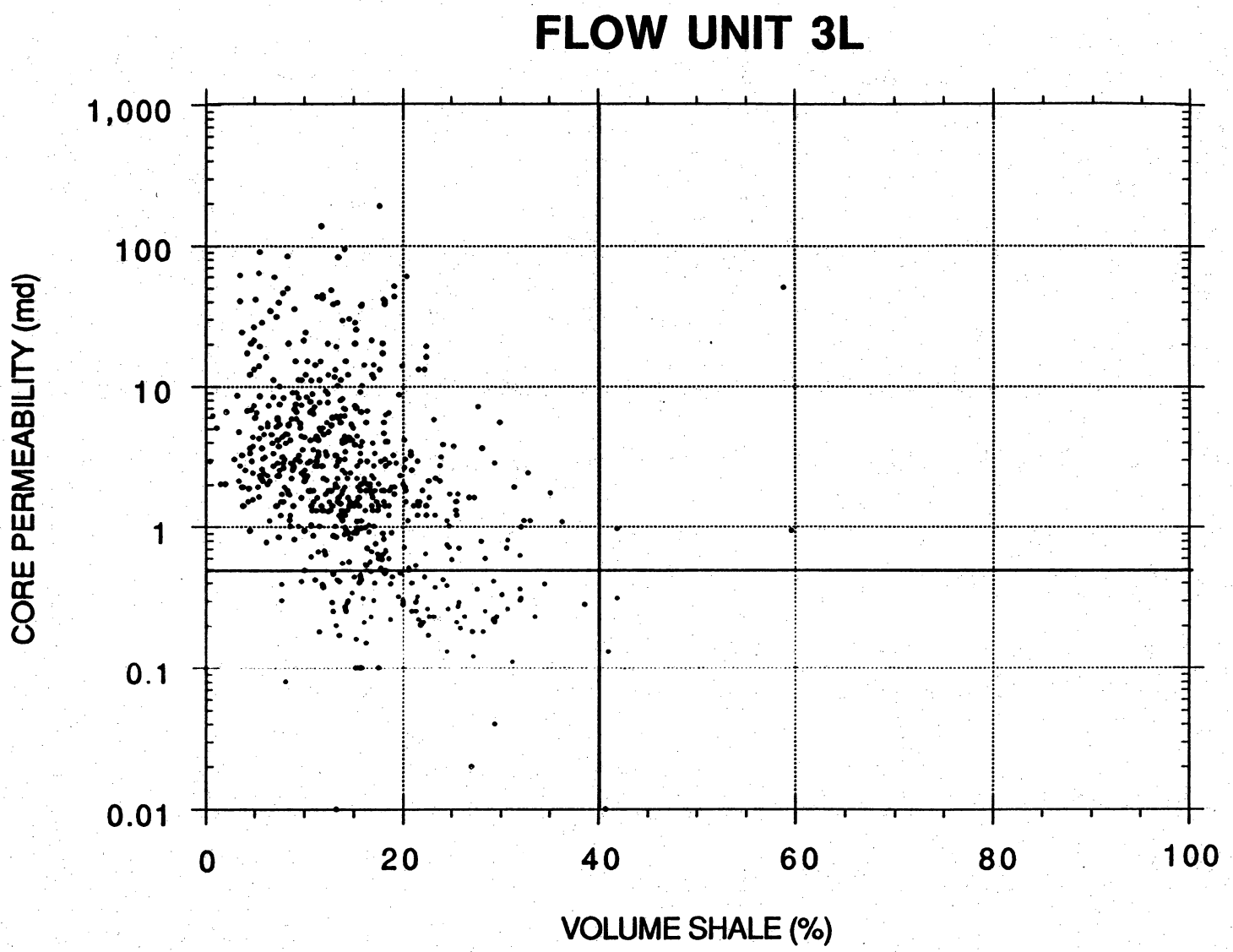

Figure VII-21. Cross plot of core permeability against log analysis calculated Volume of Shale (vsh) for all edited core data from flow unit 3L. The overall 40% Vsh cut-off is shown.

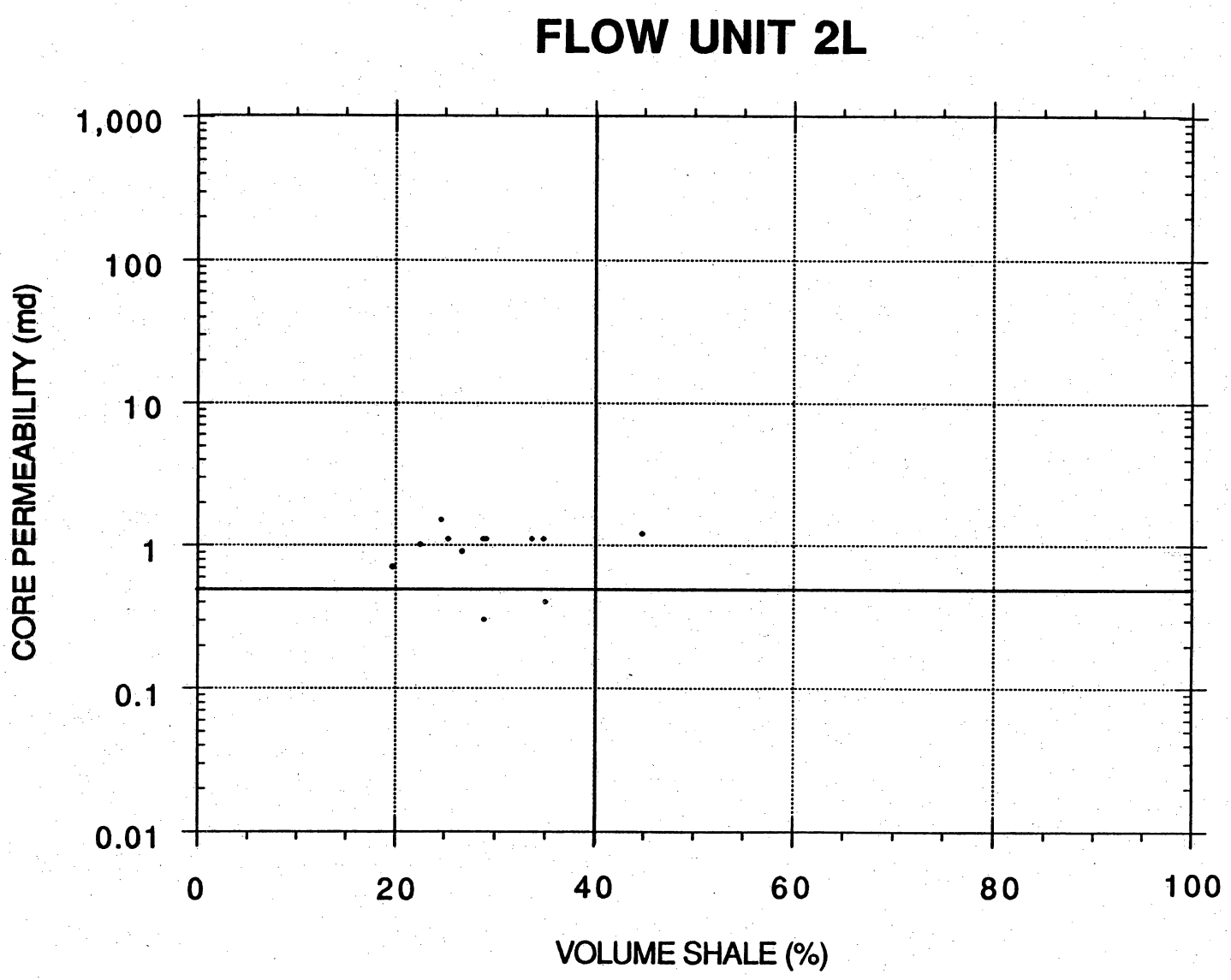

Figure VII-22. Cross plot of core permeability against log analysis calculated Volume of Shale (vsh) for all edited core data from flow unit 2L. The overall 40% Vsh cut-off is shown.

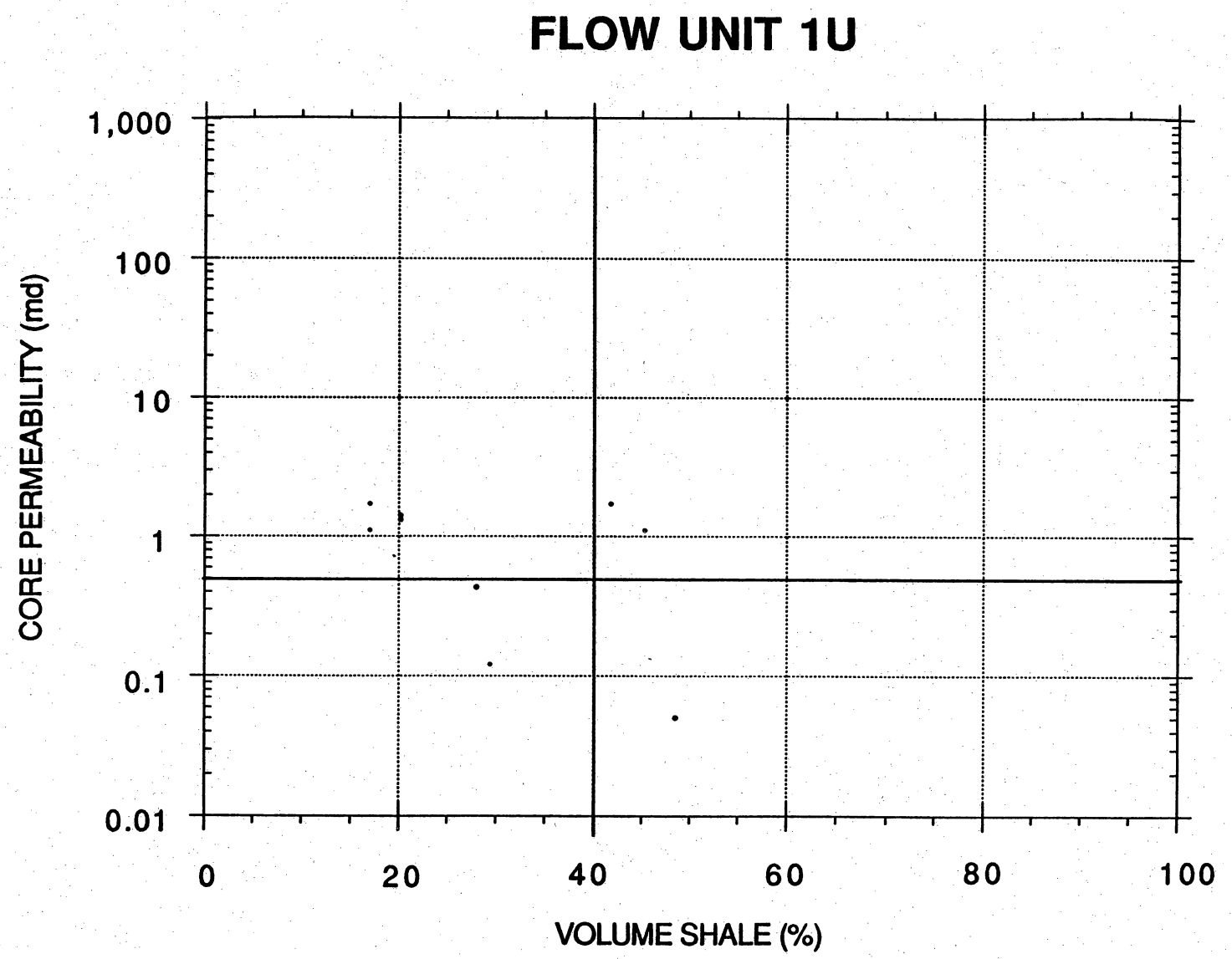

Figure VII-23. Cross plot of core permeability against log analysis calculated Volume of Shale (vsh) for all edited core data from flow unit 1U. The overall 40% Vsh cut-off is shown.

Porosity Cutoff

The porosity cutoff is related to the permeability cutoff of 0.5 md (Overton and Hamilton, 1986; Pecanek and Gulayets, 1986). The 8 percent cutoff value was derived from cross plots of core derived porosity against corresponding core-derived permeabilities, using all valid core data (figs. VII-24 through VII-30) and using a least squares line of best fit for each of these cross plots. As the different flow units have different petrophysical characteristics, a separate cross plot has been made for each flow unit. These plots show good correlation between these parameters for flow units 3L and 4 (a correlation coefficient of 0.5 or greater). A moderate correlation is calculated for flow unit 2L (a correlation coefficient of 0.4–0.5). Flow units 3U, 2U, and 1U have poor correlation for these plots (a correlation coefficient of 0.3 or less). Further, flow units 2U and 1U have statistically insignificant data populations. A porosity cutoff of 8 percent is therefore used, based on the line of best fit for the whole data set and the porosity value corresponding to 0.5 md (fig. VII-24).

Based on the line of best fit for each of these facies, 0.5 md corresponds roughly to 8 percent porosity for 3L and 4. For flow unit 3U, 0.5 md corresponds to 9 percent porosity; however, when the foot-by-foot editing is undertaken it is noted that the 8–9 percent porosity values relate to thin units of less than 5 ft, which are adjacent to the better quality reservoir. Such zones should be accessed by cross flow (Bennett & Barley, 1988). Thus, the majority of the 8–9-percent porosity sands have been included as pay for this flow unit and an 8 percent porosity cutoff has been used.

For flow unit 2L, the 0.5 md cutoff corresponds to 9 percent also. However, the arithmetic mean of the core porosity is 8.3 percent and the geometric mean of the core permeability data is 0.6 md. This variability in inferred porosity cutoff is caused by the high lithological variability in this flow unit. This variability is highlighted by a change in facies boundary interpretation which resulted in three high porosity/low permeability samples being moved from flow unit 3L to 2L and one high permeability/high porosity sample being moved to flow unit 3L from 2L. This changed the slope and intercept of the line of best fit for the data distribution so that the porosity cut off corresponding to 0.5 md changed from 8 percent to 9 percent.

As flow unit 2L is often separated from the overlying 3L flow unit by shale layers it is likely that most of this flow unit is not sweepable since most of it is less than 10 ft thick. However, reservoir simulation is the best vehicle for investigating this recovery mechanism.

This method of deriving the porosity cutoff from the line of best fit for the core porosity against core permeability cross plot has several potential errors:

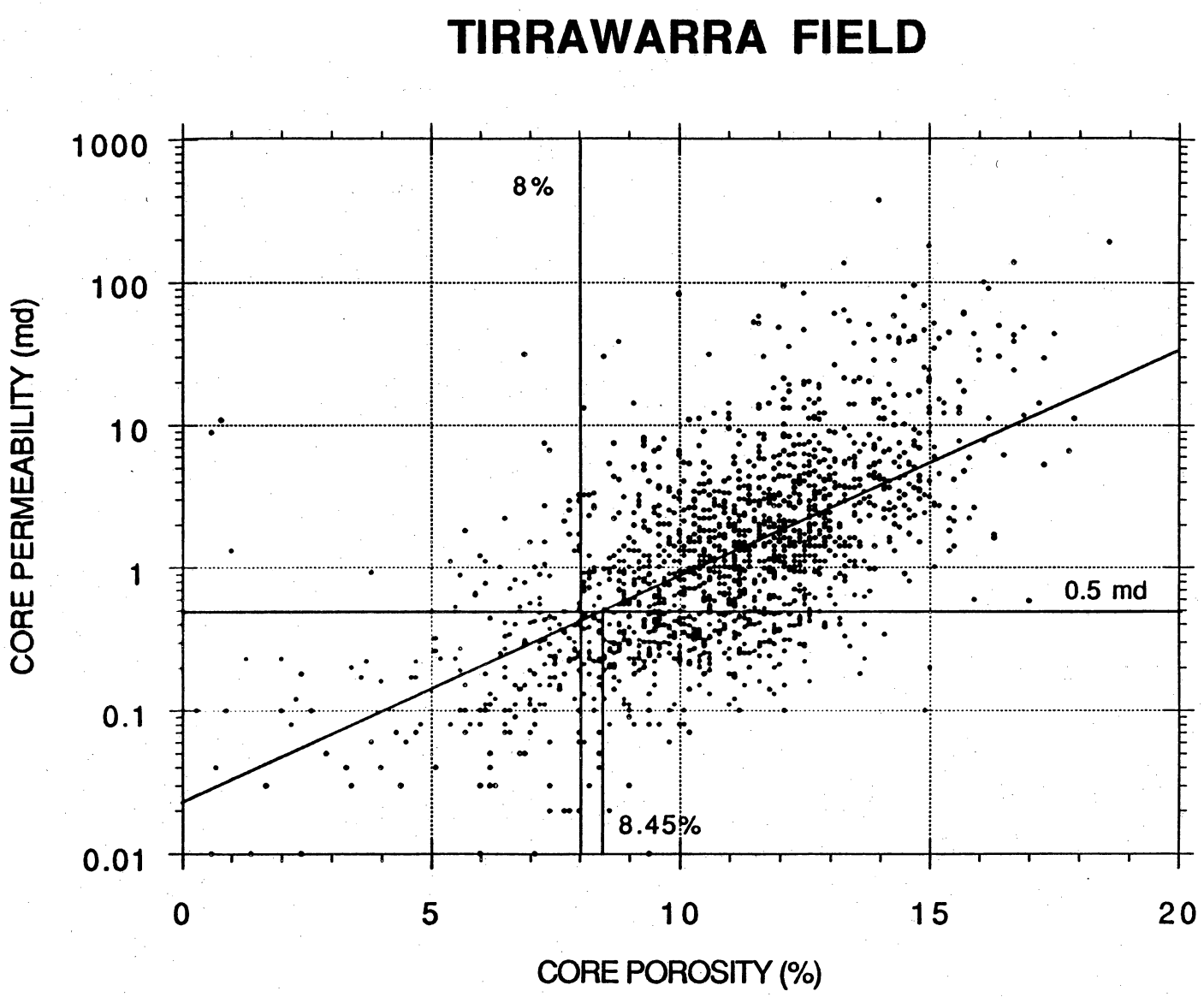

Figure VII-24. Cross plot of core permeability against core porosity for all edited core data. The equation for the line of best fit (plotted) is:

log of perm = −1.63941 + 0.158354 × core porosity
This has a correlation coefficient (R^2) of 0.39.
0.5 md corresponds to 8.45% porosity (shown) with the rounded down cut-off of 8.0% porosity also shown.

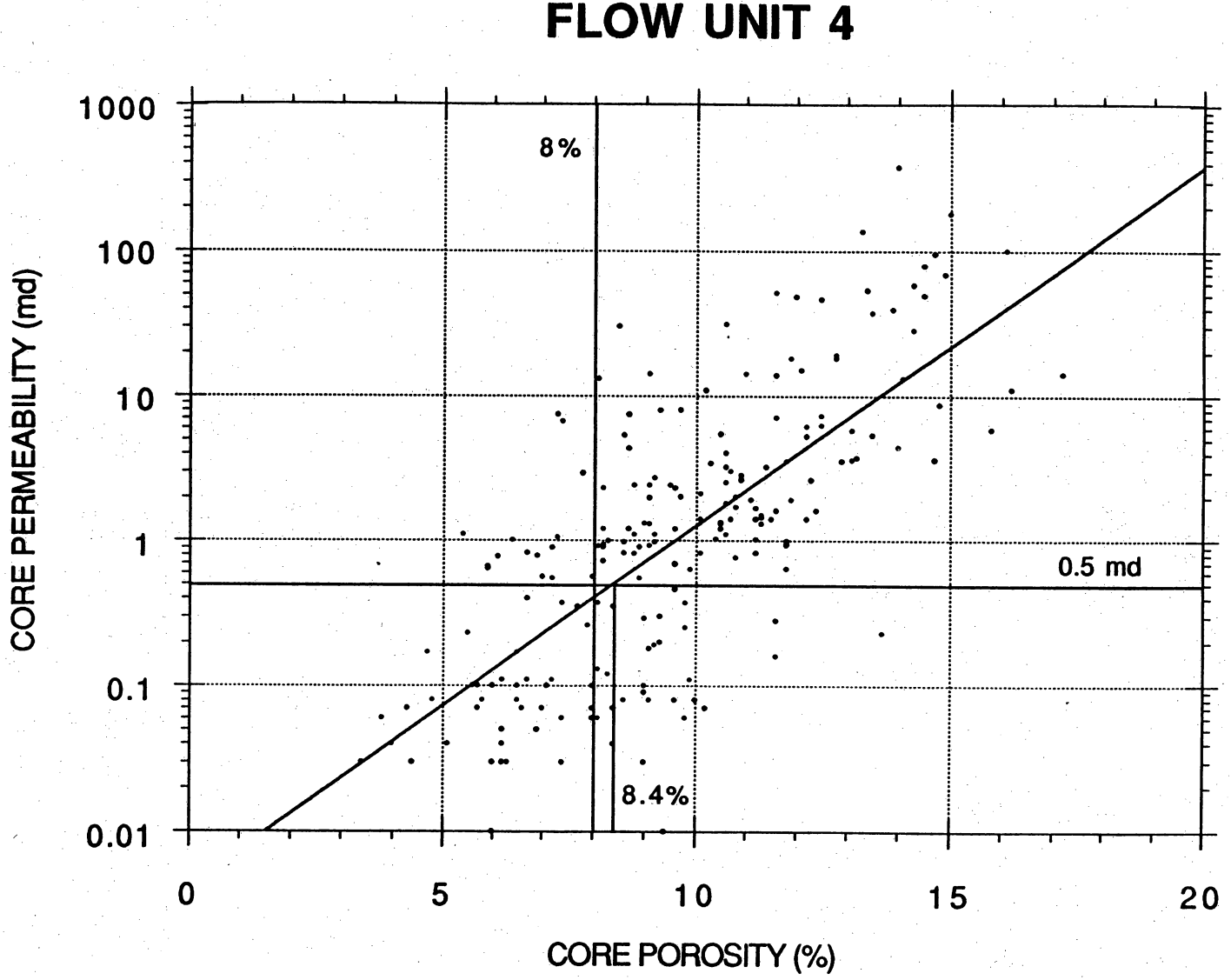

Figure VII-25. Cross plot of core permeability against core porosity for edited core data for flow unit 4. The equation for the line of best fit (plotted) is:

log of perm = −2.37241 + 0.246501 × core porosity
This has a correlation coefficient (R^2) of 0.52.
0.5 md corresponds to 8.40% porosity (shown) with the rounded down cut-off of 8.0% porosity also shown.

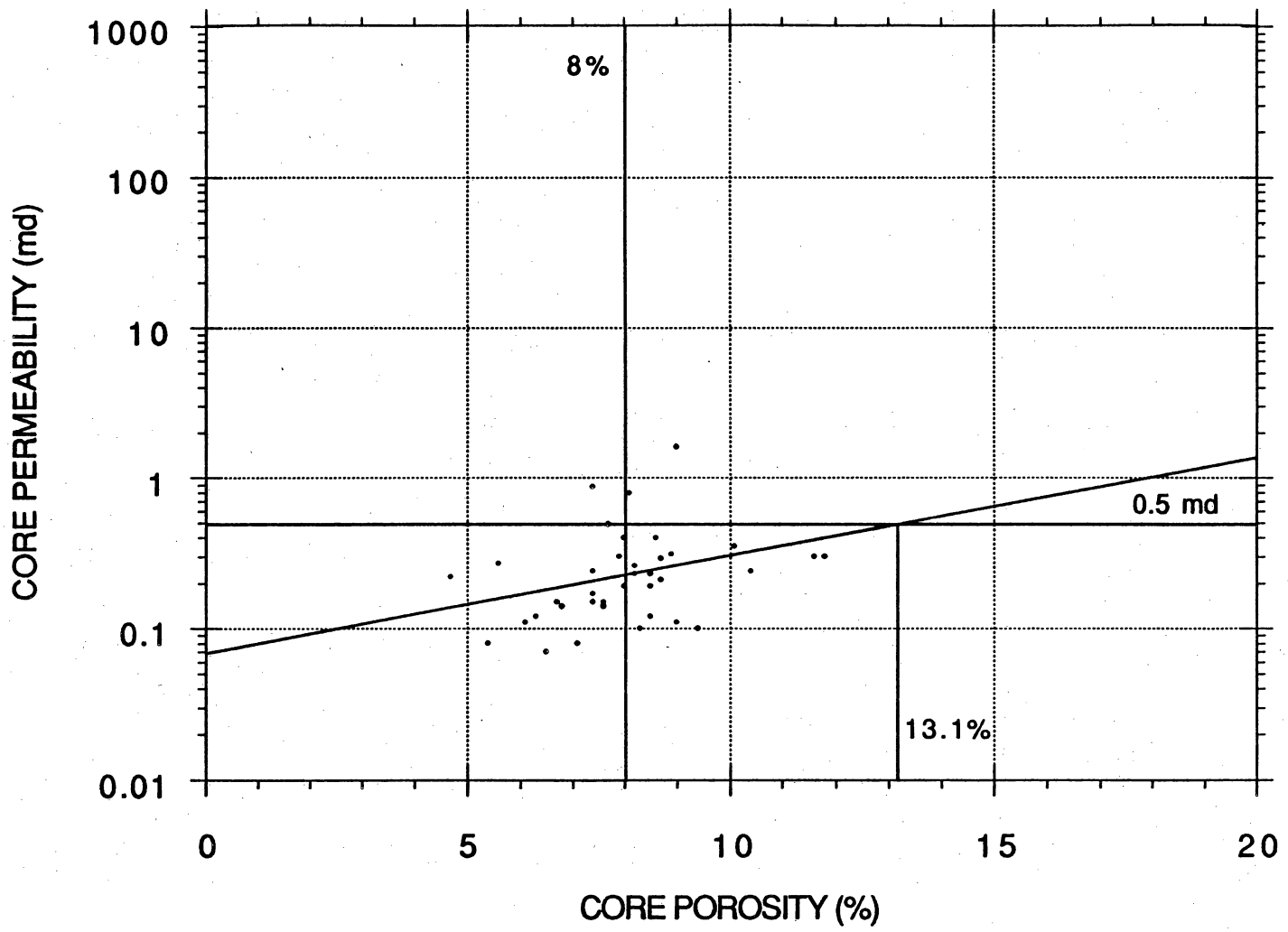

Figure VII-26. Cross plot of core permeability against core porosity for edited core data for flow unit 2U. The equation for the line of best fit (plotted) is:

log of perm = −1.19791 + 0.068463 × core porosity
This has a correlation coefficient (R^2) of 0.11.
0.5 md corresponds to 13.10% porosity (shown) with the rounded down cut-off of 8.0% porosity also shown.

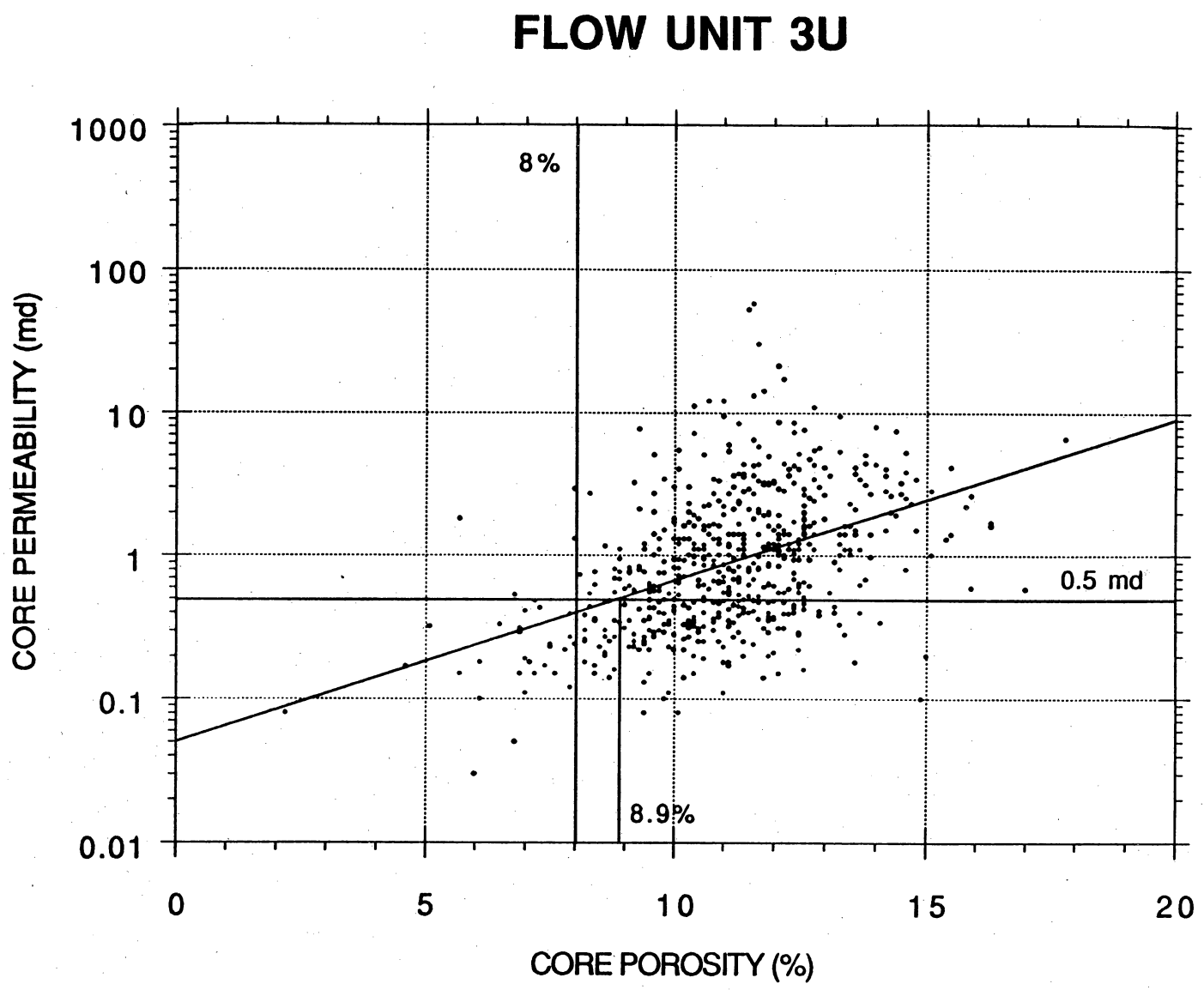

Figure VII-27. Cross plot of core permeability against core porosity for edited core data for flow unit 3U. The equation for the line of best fit (plotted) is:

log of perm = −1.30029 + 0.112277 × core porosity
This has a correlation coefficient (R^2) of 0.21.
0.5 md corresponds to 8.90% porosity (shown) with the rounded down cut-off of 8.0% porosity also shown.

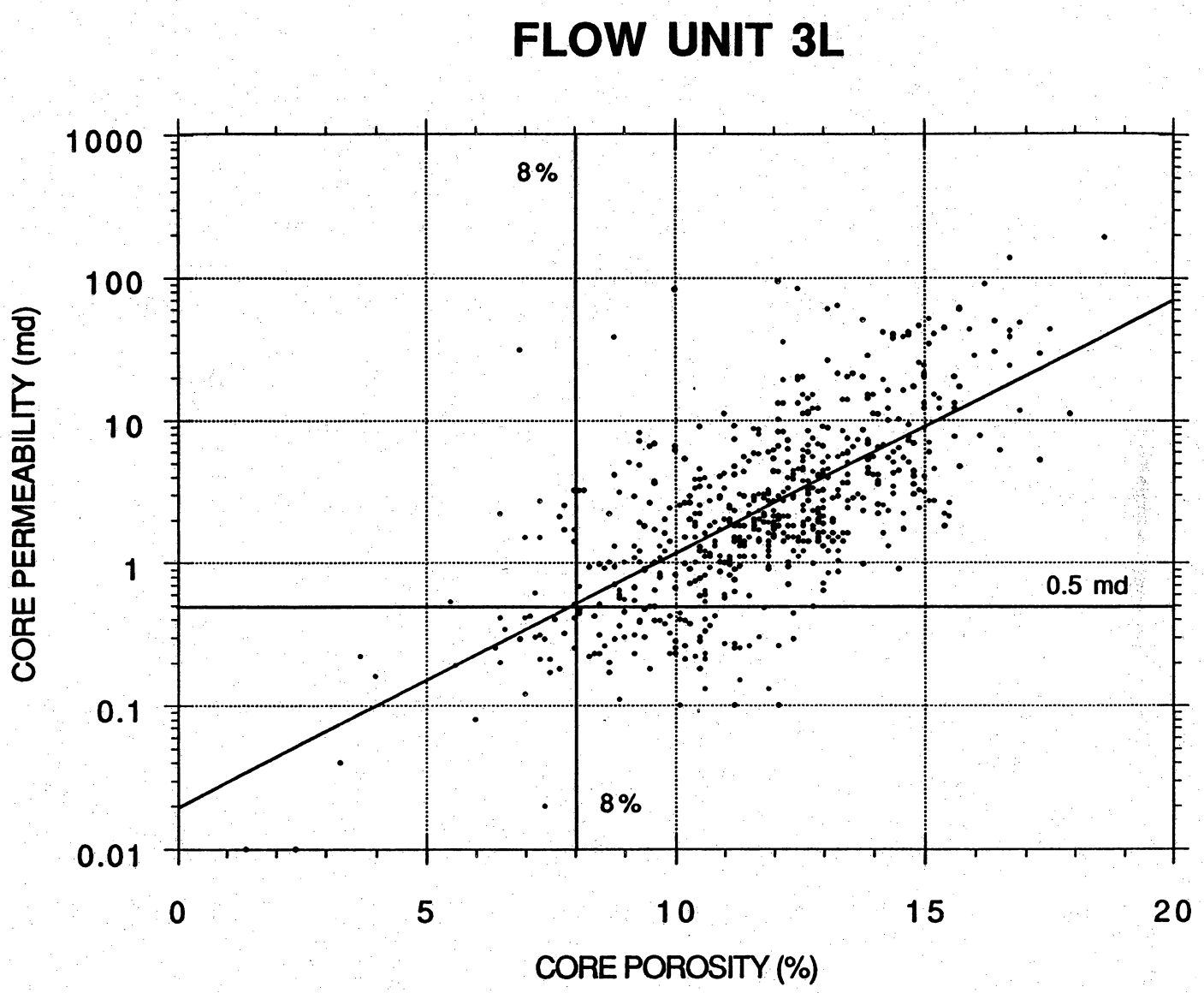

Figure VII-28. Cross plot of core permeability against core porosity for edited core data for flow unit 3L. The equation for the line of best fit (plotted) is:

log of perm = −1.68206 + 0.173446 × core porosity
This has a correlation coefficient (R^2) of 0.46.
0.5 md corresponds to 7.96% porosity (shown) with the rounded down cut-off of 8.0% porosity also shown.

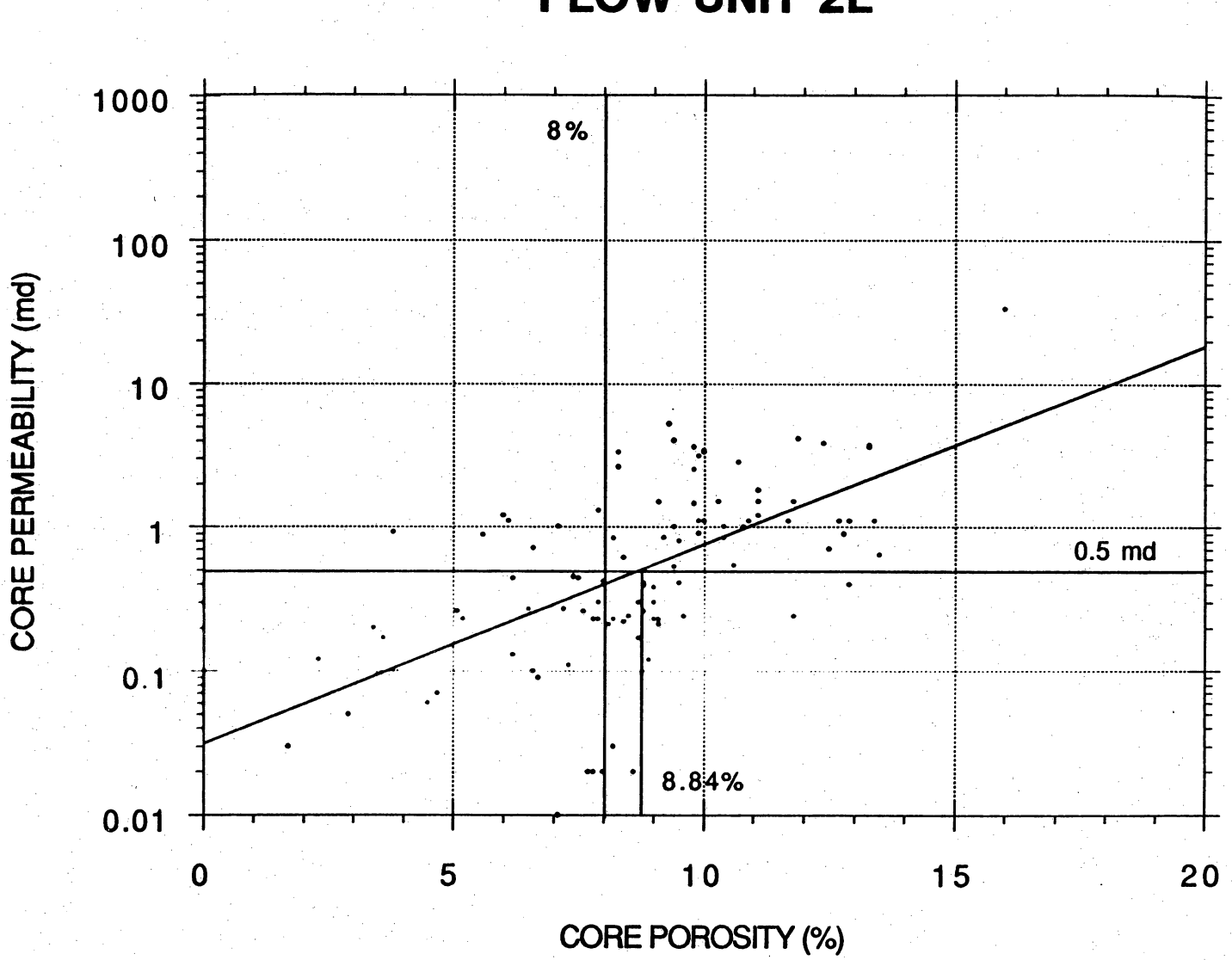

Figure VII-29. Cross plot of core permeability against core porosity for edited core data for flow unit 2L. The equation for the line of best fit (plotted) is:

log of perm = −1.51369 + 0.137160 × core porosity
This has a correlation coefficient (R^2) of 0.34.
0.5 md corresponds to 8.84% porosity (shown) with the rounded down cut-off of 8.0% porosity also shown.

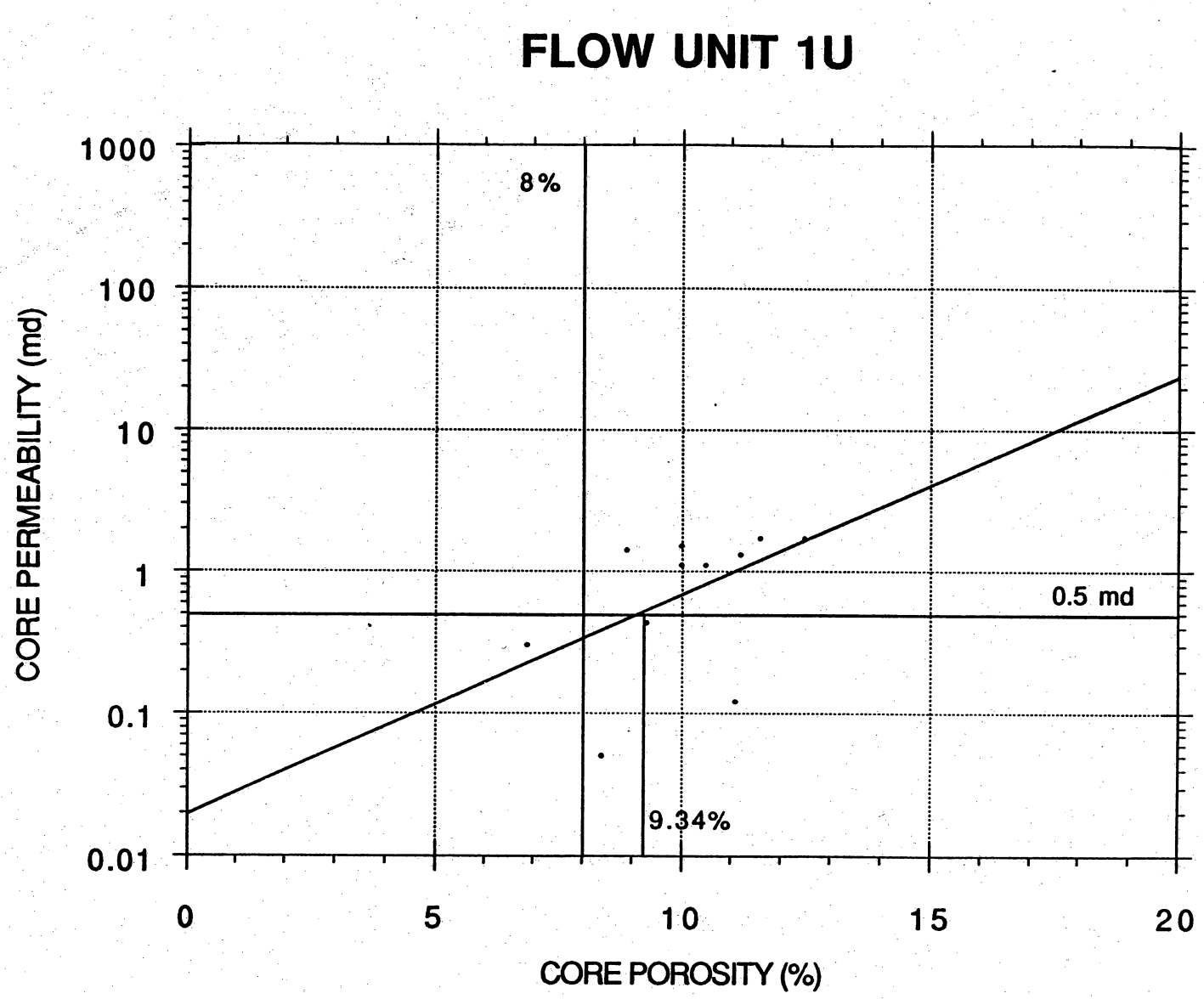

Figure VII-30. Cross plot of core permeability against core porosity for edited core data for flow unit 1U. The equation for the line of best fit (plotted) is:

log of perm = −1.75043 + 0.155103 × core porosity
This has a correlation coefficient (R^2) of 0.23.
0.5 md corresponds to 9.34% porosity (shown) with the rounded down cut-off of 8.0% porosity also shown.

- The core may not be representative of a particular flow unit. This is true for 3U, where a porosity cutoff of 9 percent is indicated due to skewing caused by the large volume of core porosity and permeability data derived from poor reservoir. Seven of the nine wells with poor 3U (78 percent) are represented by core, whereas 19 of the 64 wells with moderate to good 3U (30 percent) are represented by core.
- The large scatter of data gives a large degree of freedom to the placement of a line of best fit. A minor adjustment to facies interpretation in only one well may alter the slope and intercept of a line resulting in a different cutoff value. This occurred with flow unit 2L. Careful incorporation of all data is required for consistency during the foot-by-foot editing to give a final representative net pay distribution.

Despite these concerns, this method is valid as the number of "pay" data points excluded by this method is balanced by the number of "nonpay" data points included. Further, foot-by-foot editing allows enough leeway to correct for any obvious biases in the core data set such as the flow unit 3U sampling bias. So, the overall total net pay calculated for any well and for the field is believed to reflect the true net pay.

Water Saturation Cutoff

Any Sw cut-off determination can only be a approximation due to many factors:

- The significant transition zone (several hundreds of feet based on capillary pressure curves)
- Relative permeability effects (based on relative permeability curves and the observation that crestal wells out perform flank wells despite having equal quality reservoir)
- High irreducible water in fine grained sandstone or clayey or shaly sandstone

Gradational changes in Sw over large depth ranges are therefore expected (and observed) within most wells. It is therefore possible to have large variations in the structural position of the effective OWC in short distances over the field. Despite these concerns, Sw cut-offs are required to enable pay distribution to be mapped and original oil-in-place to be estimated.

In determining the Sw cut-off it was noted that very little water production occurs for any well within the field despite some wells having been fracture stimulated into a water zone. Relative permeability data (see Section IX) indicate that significant volumes of water should not flow and that wells with Sw's higher than 40% should have substantial oil flow impairment due to reduced relative permeability. To allow for the ability of miscible gas to mobilise oil in net sand with intermediate Sw's, a liberal approach was taken in determining the Sw cut-off. The Sw

cut-off's derived in this study would therefore be optimistic for areas where only primary recovery would occur.

A cutoff for effective water saturation of 50 percent Sw has been chosen based on the effective Sw profile for wells that have produced water prior to any hydraulic fracture stimulation. In shaly sands the cutoff for effective water saturation is normally high because shaly sands have high irreducible water saturations. Therefore, for this study an effective water saturation cutoff of 50 percent was used. This is the same as in the previous study. A higher cutoff would be inappropriate because Tirrawarra wells that tested water (Tirrawarra 3; figs. VII-31 and VII-32) commonly have water saturations as low as 60 percent. These figures show that with a change in effective water saturation cut-off from 50 percent to 60 percent the net pay increases from 38 ft to 74 ft, and 74 ft of net pay in a well that recovered 2,200 ft of water on DST is improbable. Further, almost all of the net pay in well 3 is in the upper part of the Tirrawarra (fig. VII-31) where the porosities are lower (i.e., low-permeability facies). Using net pay cutoffs of Vcl = 30 percent, effective porosity = 8 percent, and effective water saturation = 50 percent, the Tirrawarra 21 well (fig. VII-33) has 87.5 ft of net pay (8.6 HC pore-feet), and the downdip Rakoona 1 well (fig. VII-34) has 24.5 ft of net pay (1.5 HC pore-feet).

This Sw cutoff of 50 percent is appropriate for all flow units except 1U. This unit displays higher water saturations for most wells, including those high on the structure. Tirrawarra 21 is crestally located and has Sw's of up to 66 percent for sands that fit or almost fit the other pay cutoff criteria. Further, the separation between the shallow and deep laterolog curves indicate moveable hydrocarbons. Unfortunately, the low porosities and the thinness of this unit exclude it from being classified as pay.

This cutoff is further substantiated by the existing relative permeability curves for water relative to oil that show a very low initial slope that begins to steepen at between 40 and 60 percent Sw and corresponding to relative permeabilities of 0.02 to 0.1 (depending on the permeability of the sample). Water flow is therefore unlikely to be significant unless the Sw is greater than 60 percent.

Other Issues

Saturation Exponent (n)

The low water saturations in wells that recovered only water (e.g., Tirrawarra 3) and the presence of oil in finer grained facies suggest that the saturation exponent (n) for the Tirrawarra sandstone may not be 2.0 and the reservoir may not be entirely water wet. However,

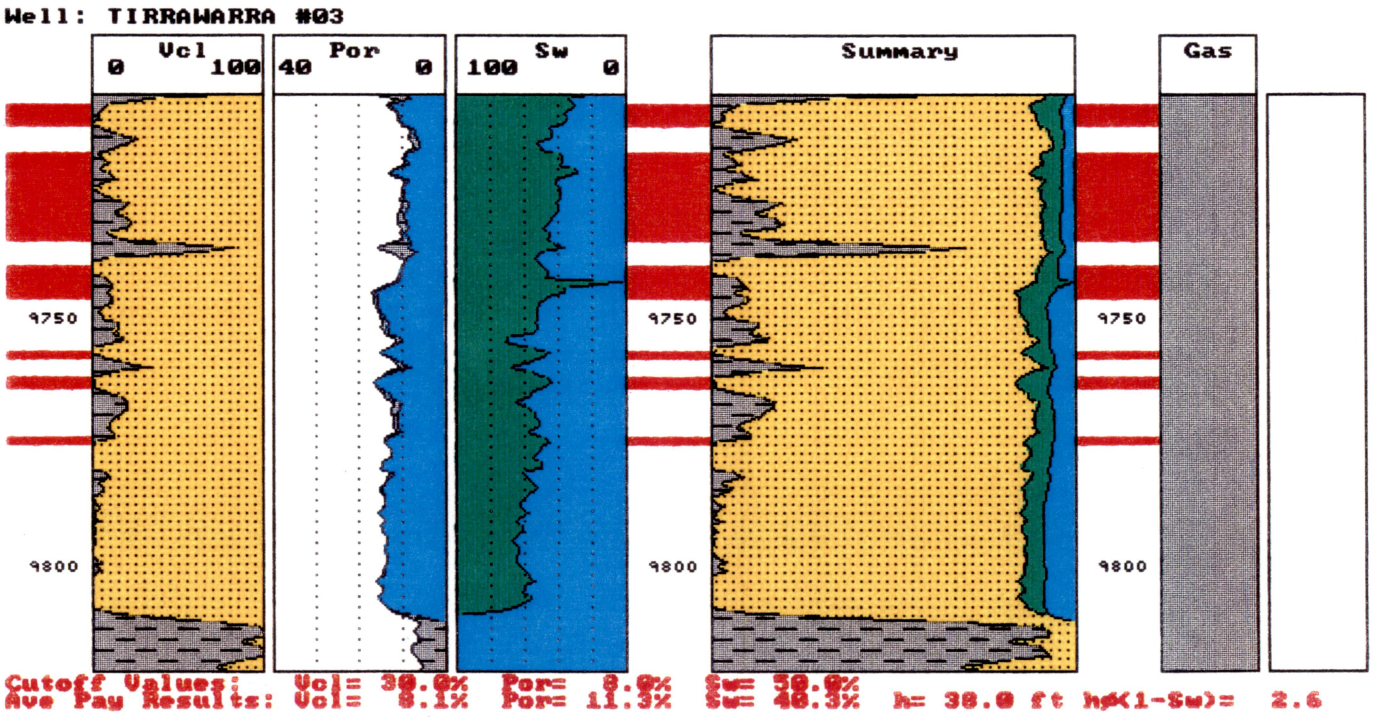

Figure VII-31. Net pay summary for the downdip Tirrawarra well 3 that tested (DST) 2,200 feet of water. Using an effective water saturation cut-off of 50% gives 38 feet of net pay in thin streaks.

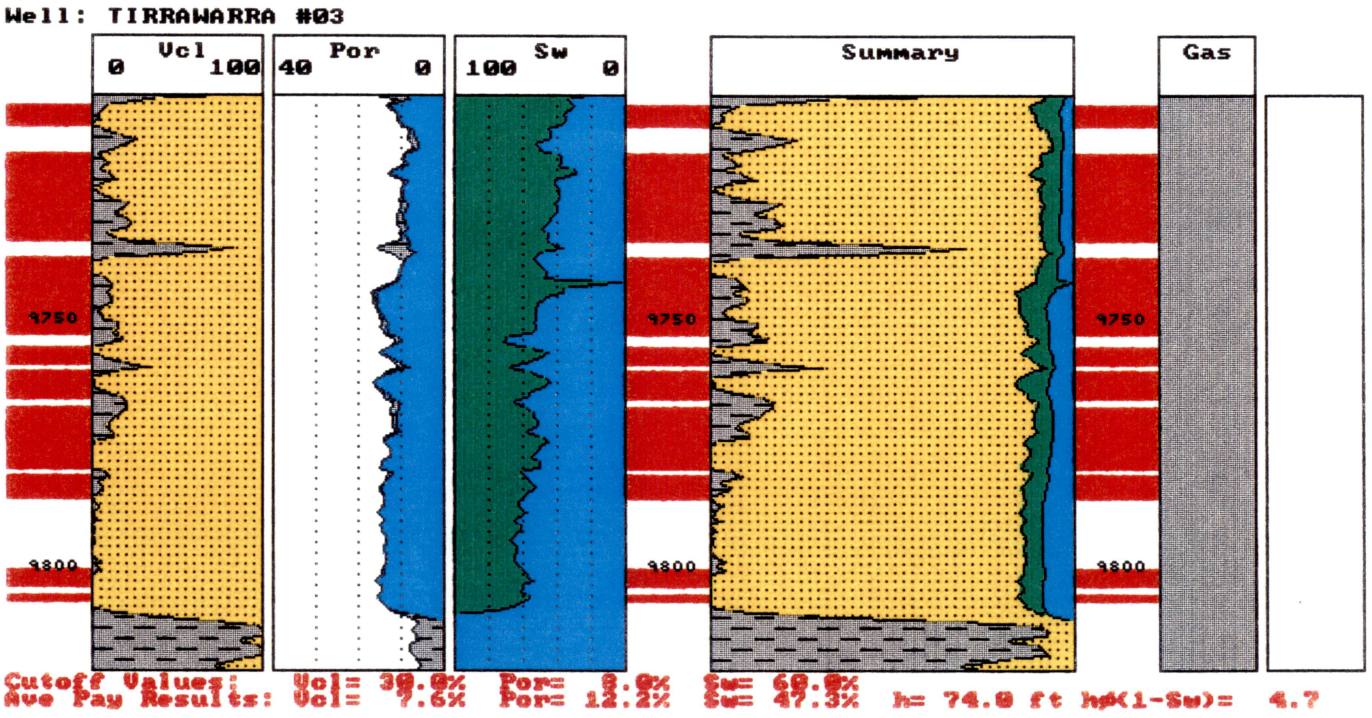

Figure VII-32. Net pay summary for the downdip Tirrawarra well 3 that tested (DST) 2,200 feet of water. Using an effective water saturation cut-off of 60% gives 74 feet of net pay much of which is in thick zones. A 60% effective water saturation cut-off is therefore too high.

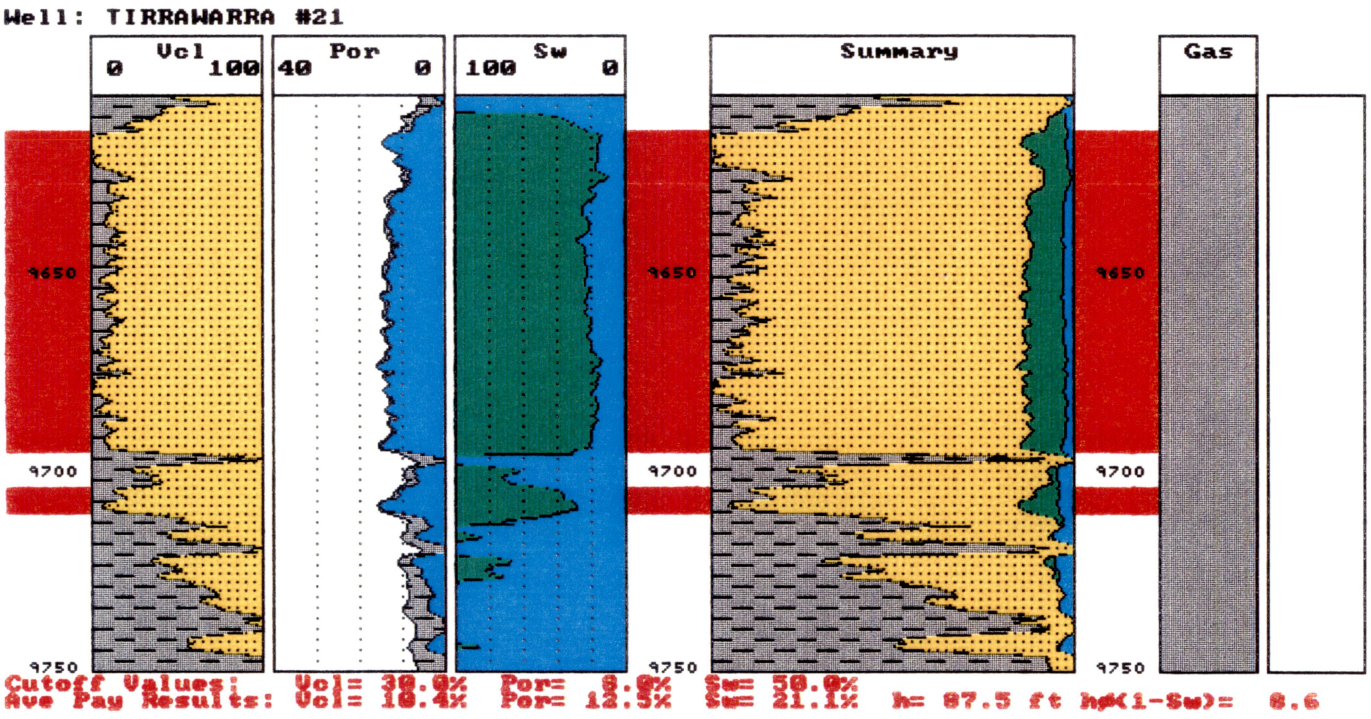

Figure VII-33. Net pay summary for the Tirrawarra well 21 near the top of the structure. The 87.5 feet of net pay in this well is present in all the reservoir facies (2–4) except facies 1 at the base.

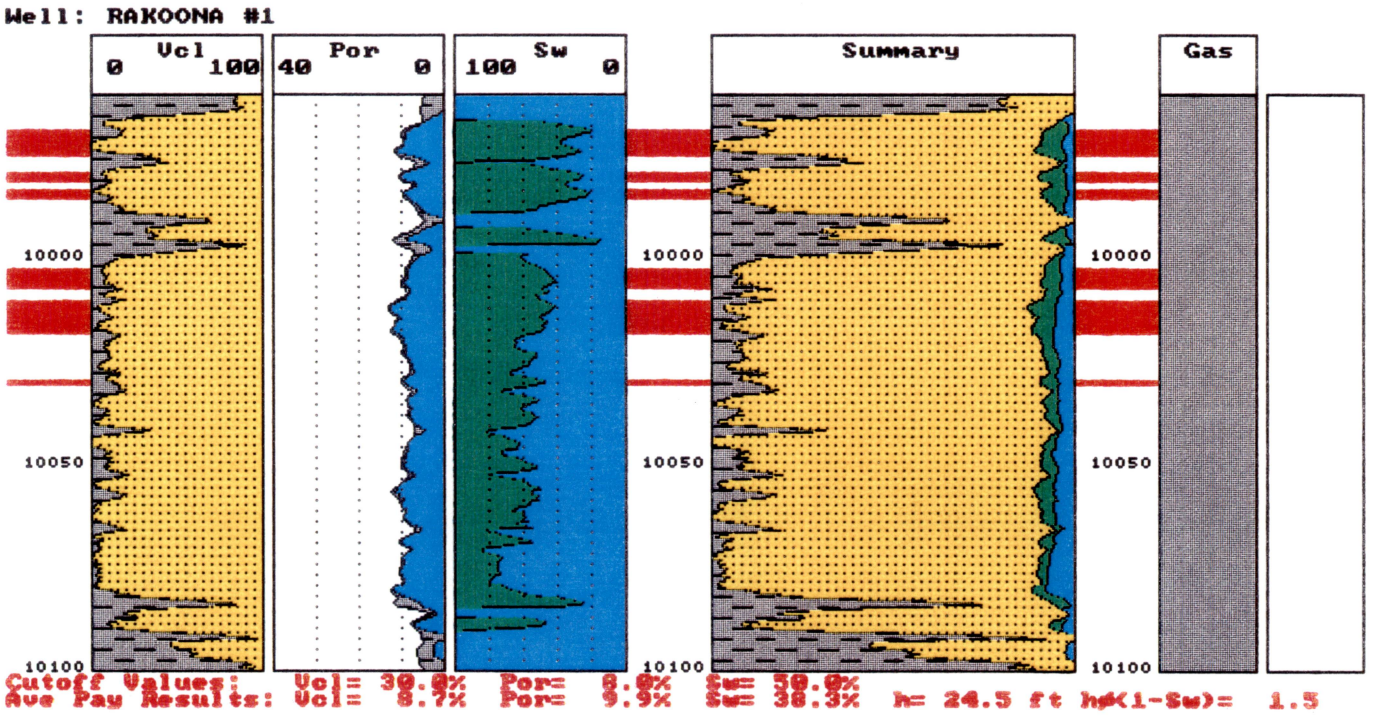

Figure VII-34. Net pay summary for the downdip Rakoona well 1. Note that there is only 24.5 feet of net pay present in three thin streaks.

the reservoir cannot be entirely or strongly oil wet because some wells do not produce water. Note, that in an entirely or strongly oil wet reservoir that does not produce water, the water cannot be a continuous phase and the resistivity should be infinity.

A comparison of Tirrawarra wells 64 and 67 (figs. VII-35 and VII-36) also suggest that the Tirrawarra reservoir is not strongly oil wet. The Tirrawarra Sandstone in Tirrawarra 67 is only 10 ft high to the Tirrawarra Sandstone in Tirrawarra 64, and the wells are only 2 km apart. However, the water saturations are much less in Tirrawarra 67 (compare: figs. VII-35 and VII-36) and the Tirrawarra Sandstone in Tirrawarra 64 has less porosity (poorer reservoir) compared to the Tirrawarra Sandstone in Tirrawarra 67. If the Tirrawarra reservoir were strongly oil wet, Tirrawarra 64 should have the lower water saturations because the oil would preferentially wet the poorer reservoir. This does not preclude intermediate wettability for this reservoir.

It is also important to note that the value of saturation exponent has 68 percent less effect on the calculated value of water saturation compared to cementation exponent. Therefore, any changes in saturation exponent will have a small effect on water saturation.

Two methods to verify the value of the saturation exponent are recommended: (1) Core analysis of a native state or restored state core, and (2) a dielectric log (EPT). The data from both of these methods could then be used a determine saturation exponent by the Archie equation using least squares summation (Asquith and Saha, 1991).

Rw Determination

Background

The current field Rw of 0.58 ohm-m at 75°F is based on a single production sample from Tirrawarra no. 16 acquired in October 1986 (FWR: 91/004). Due to anomalously high Rw values recorded from Tirrawarra no. 69 samples, a program of water sampling was undertaken for the whole field. As this program has been completed and the analyses performed, a full review of the field Rw has been included as part of this project.

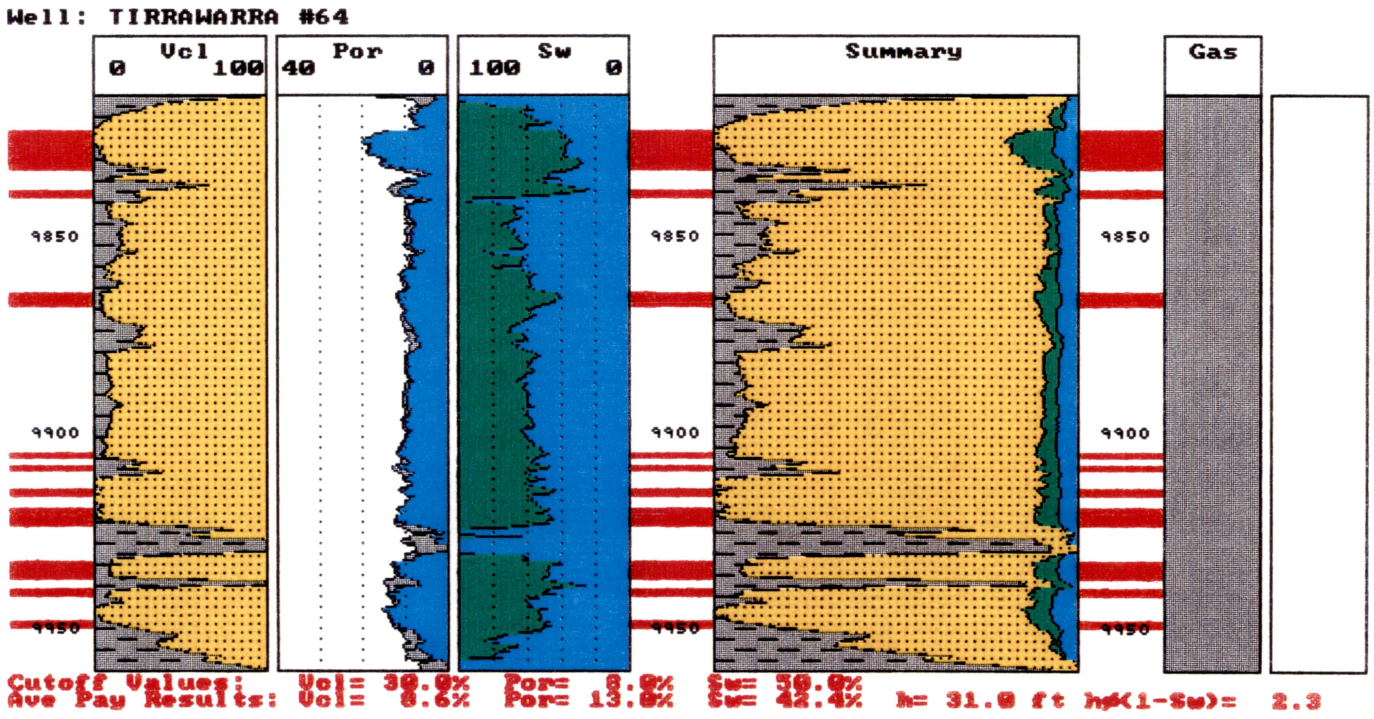

Figure VII-35. Net pay summary for the Tirrawarra well 64. Note the higher water saturations and lower porosities in this well compared to the Tirrawarra well 67 (Fig. VII-36). The Tirrawarra well 67 is located only 2 km from the Tirrawarra 64 and is structurally only 10 feet higher.

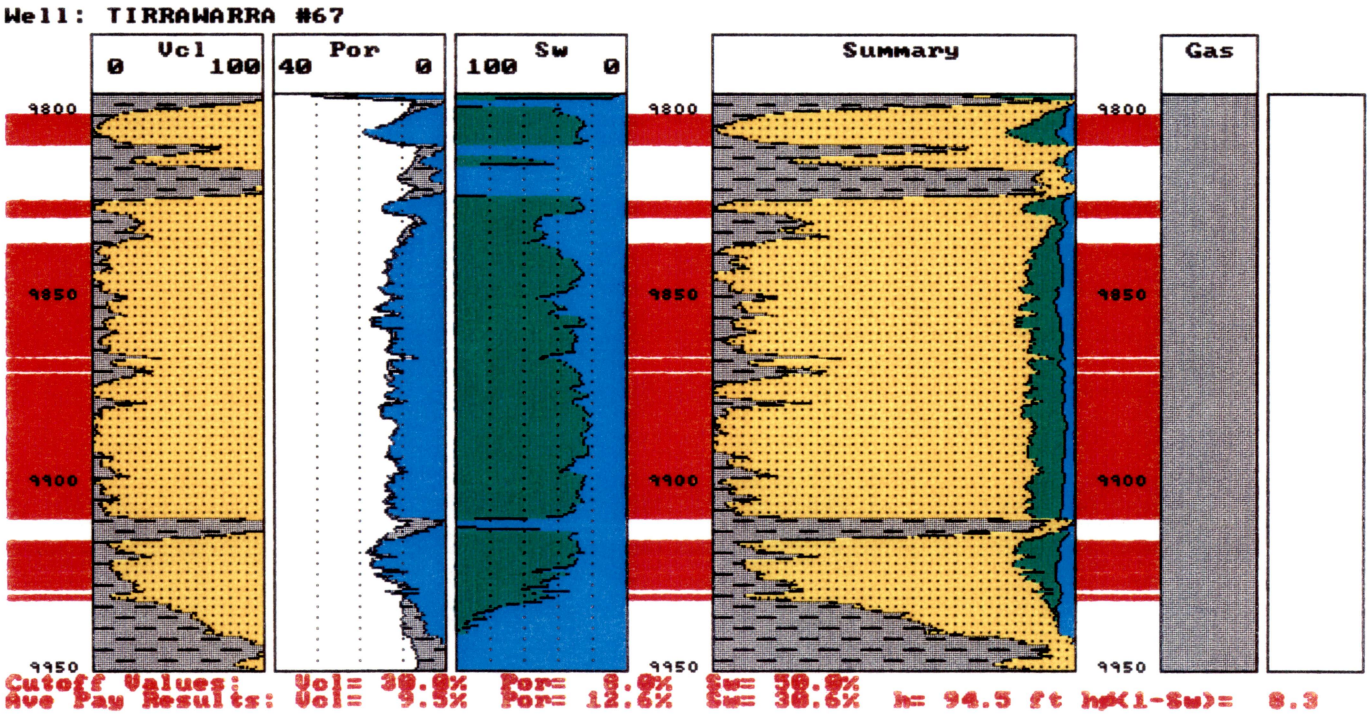

Figure VII-36. Net pay summary for the Tirrawarra well 67. The differences in water saturations between this well and the Tirrawarra 64 are the result of the capillary differences between the two wells.

Rw Determination from Water Analysis

Approximately 120 water analyses have been made for this field. As a very large range of chemical compositions and Rws exist the data were culled as follows based on Bowyer (1991):

a. Samples were excluded if they showed obvious contamination based on stiff plots, abnormal ion concentrations, and the presence of "foreign" ions (Bowyer, 1991). Samples that showed contamination which impacts little on the reliability of the sample (e.g., potassium concentrations greater than 180 mg/L but proportionally heavily outweighed by Sodium concentrations) were noted for lower weighting in the averaging calculations. For one such problem, a 50 percent weighting was used, and for two problems a 25 percent weighting was used.

b. As substantial variation in water resistivity still existed (0.47–0.87 ohm-m with an average Rw of 0.71 ohm-m) in the remaining dataset of more than 30 samples, the data were further culled. This was done by only including samples taken from wells that were flowing roughly ten barrels of water per day, or more, for the month during which the sample was taken. As samples are often taken from a very short flow period, erratic water production or very small water production maximizes the potential for contamination.

c. The remaining eleven samples (fig. VII-37) display a substantially reduced range of analyzed Rws (0.58–0.75 ohm-m with an average of 0.64 ohm-m). Two extreme values were rejected and not included in this averaging (0.81 & 0.47 ohm-m) as they stood out as clearly anomalous.

The average weighted value for these remaining data is 0.64 ohm-m at 75°F which has been rounded to 0.65 ohm-m.

Rw Estimation from Log Analysis

The formation water resistivity (Rw) determined from the SP log in several wells averages 0.41 ohm-m at 75°F. The formation water resistivity (Rw) determined by the Rwa method (Asquith, 1982) in the Rakoona 1 and Tirrawarra N-1 wells average 0.74 ohm-m at 75°F.

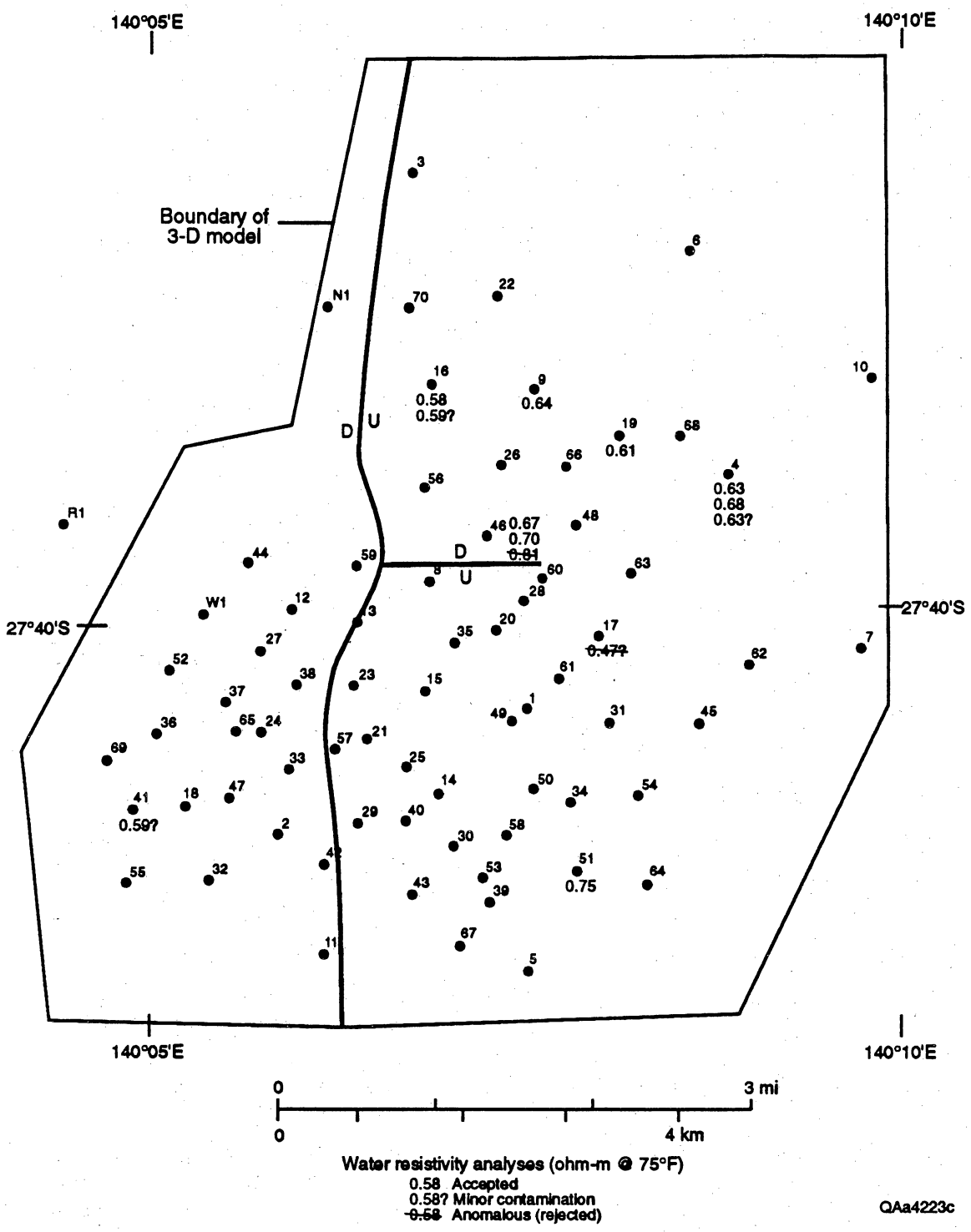

Figure VII-37. Location map of accepted water resistivities. Questioned samples have minor contamination. Two anomalous analyses are rejected.

Foot-by-Foot Log Analysis

Determination of Input Parameters for Log Analysis

The previous petrophysical calculations (SANTOS HIP: 90/130) used Shale Resistivities (Rsh), Shale Sonic Transit Times (Dts) and Gamma Ray Clean Shale (Gsh) which had been based on the shales overlying the Tirrawarra reservoir. However, these shales are carbonaceous, unlike the shale within the Tirrawarra Sandstone, resulting in incorrect values for each of these parameters. Carbonaceous matter increases the resistivity of shale and increases the sonic transit times due to the influence of coal. Carbonaceous shales also tend to accumulate radioactive ions compared to inorganic shales resulting in increased gamma ray clean shale readings. Therefore, the relatively non-carbonaceous shale coinciding with the field wide red marker horizon underlying the reservoir was used. Also, maximum or minimum values had been chosen (as appropriate) rather than an average of the cleanest shales as was performed in this analysis.

As a result, the Rsh has been reduced from the previous field wide 70 ohm-m to a well by well value ranging between 25 and 50 ohm-m but averaging 35 ohm-m; the Dts has been reduced from a field wide 70 microsec/ft to a well by well value ranging from 64 to 67 microsec/ft; and the Gsh has been reduced from a well by well range of 130 - 190 API (but averaging 170) to a well by well range of 120 - 150 (but averaging 140).

The gamma ray clean sand (Gsd) for each well was modified to ensure that the cleanest sand was 0% Vsh. This has resulted in an increase in Gsd for all wells from 20 (field wide except for Tirrawarra 68) to a well by well range of 25 - 45 but averaging roughly 30. Gsh minus Gsd is relatively constant at roughly 110 but ranges between 90 and 120 on a well by well basis. Previously the Gsh minus Gsd range between 110 and 170 and average 150.

The lower range between Gsh and Gsd and the higher Gsd value compared with the previous parameters chosen mean that Vsh calculates lower for the cleaner sands and higher for dirty sands. The cross-over in this effect (when Vsh from the previous parameters equals the Vsh calculated for the new parameters) occurs at 30 percent Vsh which is close to the overall cut-off of 40 percent. So, overall the sands will calculate slightly lower Vsh values and the impact on pay inclusions/exclusions based on Vsh will be minimal.

As the porosity is calculated by the Overton Equation which is independent of Vsh and Dts, the porosity is unaffected by these changes. Only the water saturation is affected. This has resulted in a slight reduction in water saturations for most wells. The new higher field Rw results in a slight increase in water saturations so the resultant oil saturations calculated throughout the field are minimally affected.

Log Analysis Results and Adjustments

The foot-by-foot log analysis was performed by SANTOS in-house using LOGCALC. For this, the recommended well by well input parameters, discussed above, were used, together with the recommended flow unit by flow unit cut-off parameters.

Following the receipt of the transmitted LOGCALC results, foot-by-foot analysis and editing were undertaken to determine pay from non-pay. For this the following criteria were used:

a. Pay or non-pay determinations were dependent upon core derived permeability measurements for the one-foot interval concerned. In some cases small (less than 1ft) local adjustments in core to log correlation were made so that poor reservoir in core would match poor reservoir from log analysis.
b. Poor test results and poor production data were not used as criteria for excluding pay. It is interpreted that relative permeabilities have reduced the flow potential of pay-quality sand and oil in this rock is assumed to be moveable under EOR conditions.
c. Lower porosity sands, (less than the porosity cut-off), were included as pay when adjacent to pay or surrounded by pay. This means that a one foot sand with a porosity as low as 7.5 percent has been included when adjacent to, or surrounded by thick interconnected pay. Ethane causes oil to swell and become more mobile, so sands such as these may yield hydrocarbons. The inclusion of such sand, with a porosity less than 8.0 percent represents a very small percentage of the total net pay in the field.

Implications

The main impact of the new log analysis has been to significantly increase net pay. This is mostly due to the reduction in the porosity cutoff, from 9 percent to 8 percent, and the use of well-by-well petrophysical parameters based on the low organic content shales underlying the reservoir, rather than the coaly shales overlying the reservoir. The main impact of this pay increase has been on flow units 4 and 3U. Pay has also been included for flow unit 1U and increased for the other flow units.

VIII. VOLUMETRICS

Original Oil in Place (OOIP) Mapping Procedure

The existing Top Tirrawarra Structure Depth Map (enclosure IV-36) has been used for the OOIP determination. This structure map has been converted to a Base Facies 4 Structure Contour Map by adding the isopach thicknesses of the interval between the current SANTOS top Tirrawarra and the base of Facies 4. The various total facies isopachs for each facies (see Section V) were then added to or subtracted from this structural surface to provide structure contour surfaces for the top and base of each facies. This gave the structural distribution of each facies and hence of each flow unit over the field area. These were then loaded into Stratamodel together with the interpreted oil water contact map, digitised net pay maps and the foot-by-foot LOGCALC output for each well in the field (porosity, water saturation, permeability, net pay and all well log data), as supplied by SANTOS and edited to incorporate test and core data.

As Tirrawarra wells 13 and 23 have had section faulted out, including interpreted pay, "dummy wells" have been constructed at these well locations to represent the full unfaulted section in the vicinity of the wells. In the past, thin pay (based on the shortened well section encountered) had been incorrectly interpreted for the whole area between each of these wells and the surrounding area. The "dummy wells" were constructed by estimating gross thicknesses from the flow unit isopach maps (see Section V) and then estimating net pay thickness from the net pay isopach maps (figs. VIII-1 to VIII-6) and the net pay distribution from surrounding wells. Petrophysical parameters were duplicated from the relevant facies in the well or from an adjacent well (Tirrawarra well 15).

The structure surface for the base of facies 4 was chosen as the reference horizon for structure mapping because it is subparallel to the two datum surfaces bounding the reservoir, the overlying orange time marker horizon and the underlying red time marker horizon (plate III-2).

Stratamodel has been used as the vehicle for the determination of OOIP and its distribution for the field (as well as the display of OOIP and other parameters). This software interpolates data between wells on a one foot by one foot layer basis to set parameter values in one foot thick grid cells. To account for thickening and thinning of a geological unit (in this case the respective flow units) the one foot layers must onlap or be truncated against the bounding surface of the unit. The individual flow unit net sand trends are used to set bias in the averaging and extrapolation of water saturation and porosity as they cannot be used to

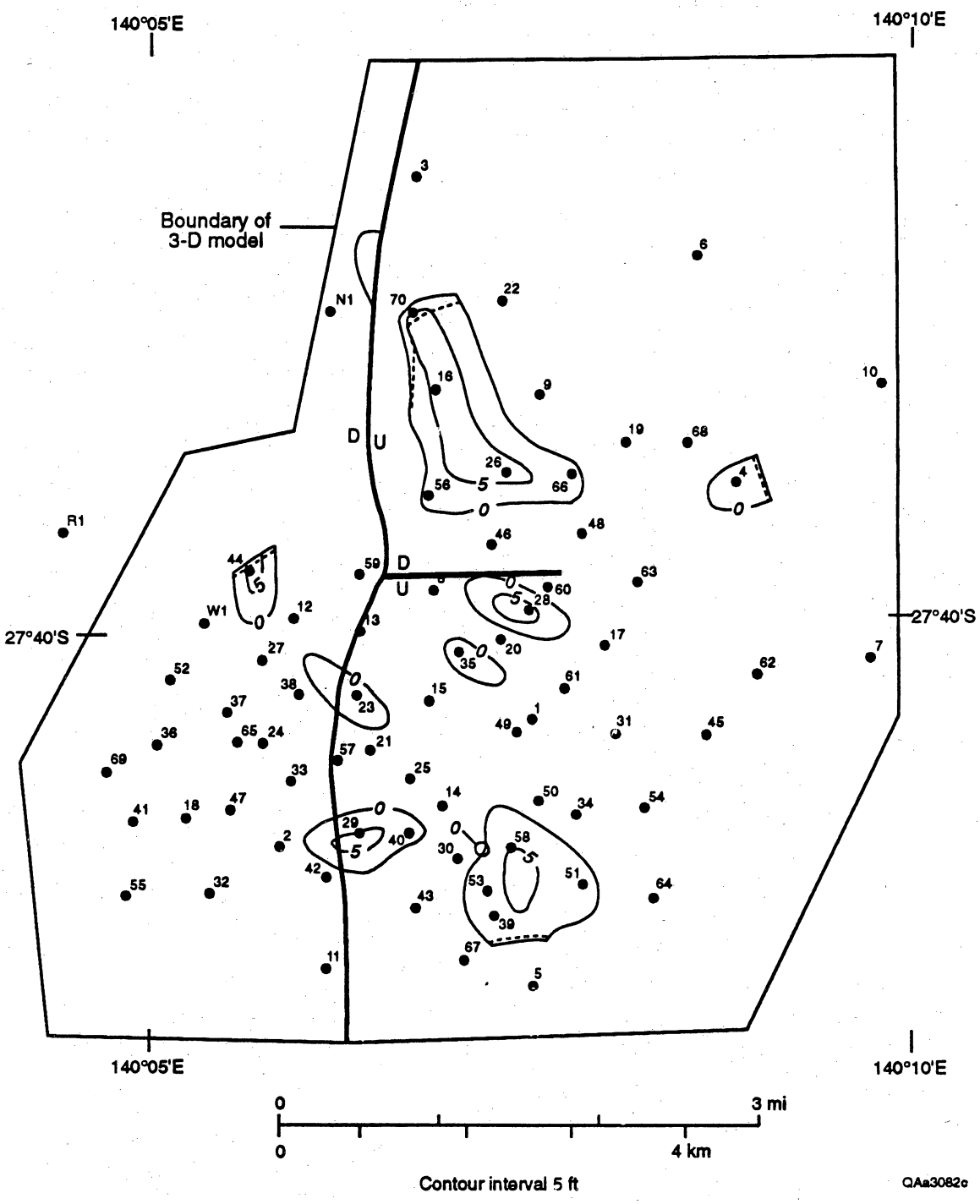

Figure VIII-1. Net pay map of flow unit 1U.

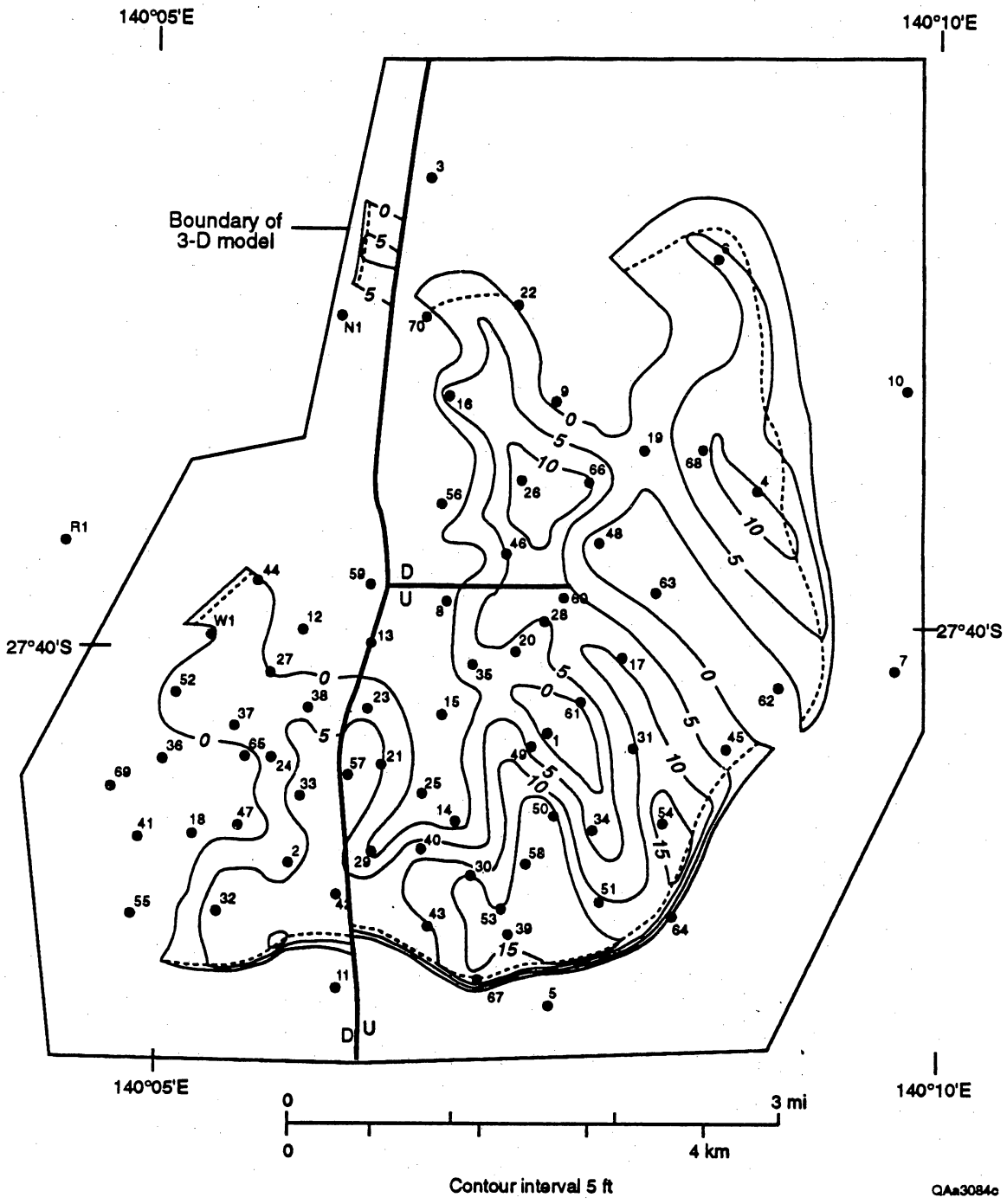

Figure VIII-2. Net pay map of flow unit 2L.

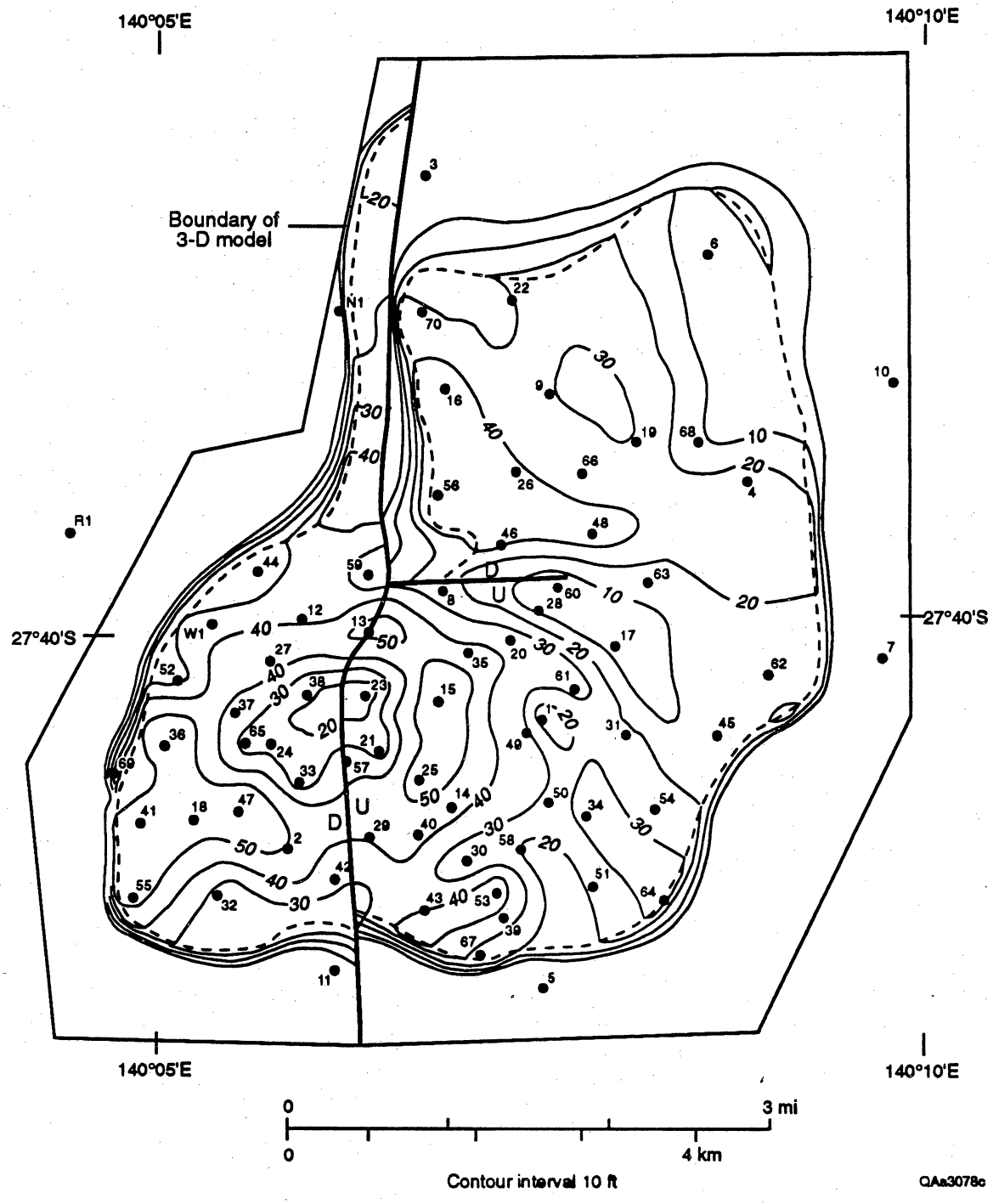

Figure VIII-3. Net pay map of flow unit 3L.

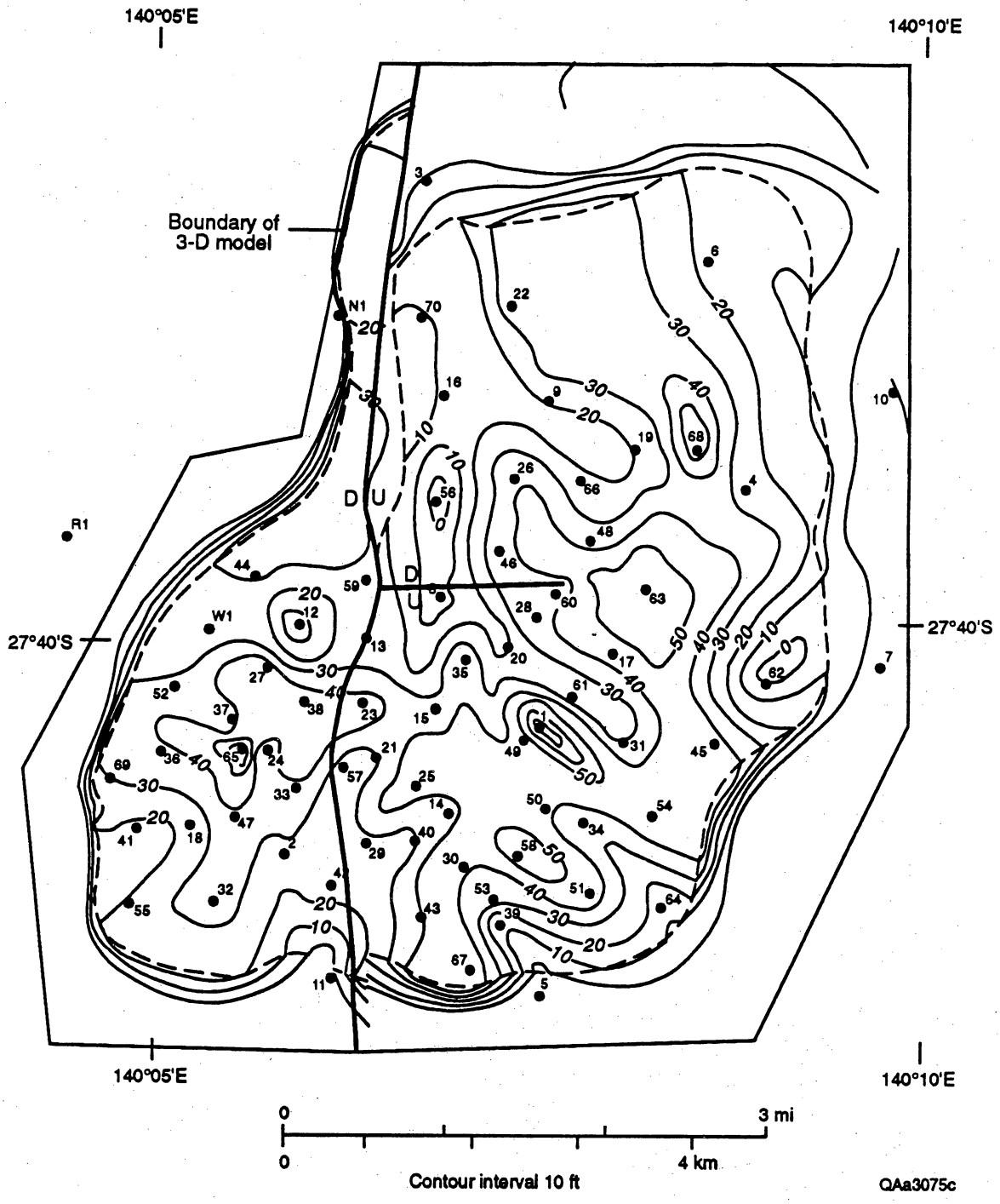

Figure VIII-4. Net pay map of flow unit 3U.

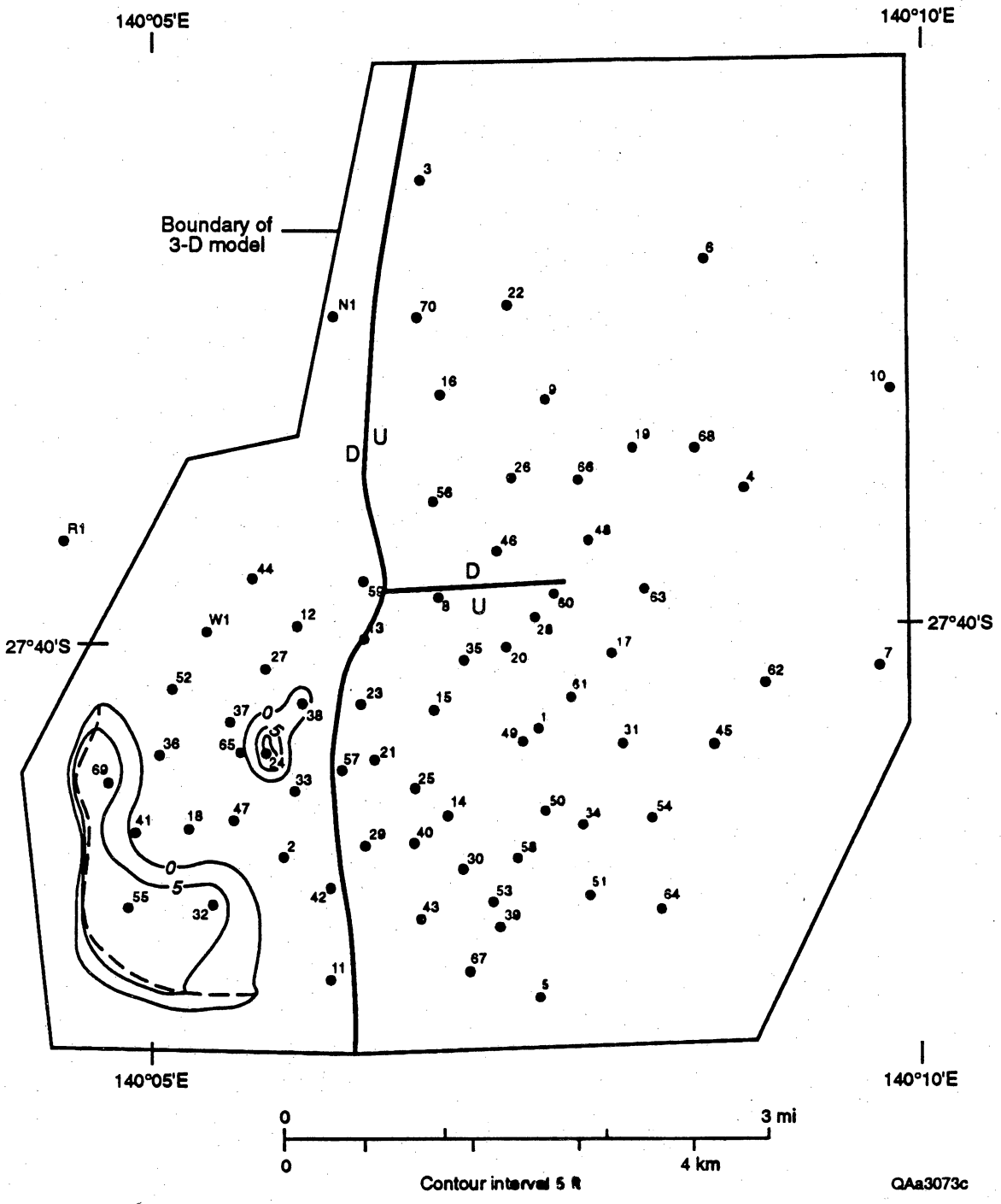

Figure VIII-5. Net pay map of flow unit 2U.

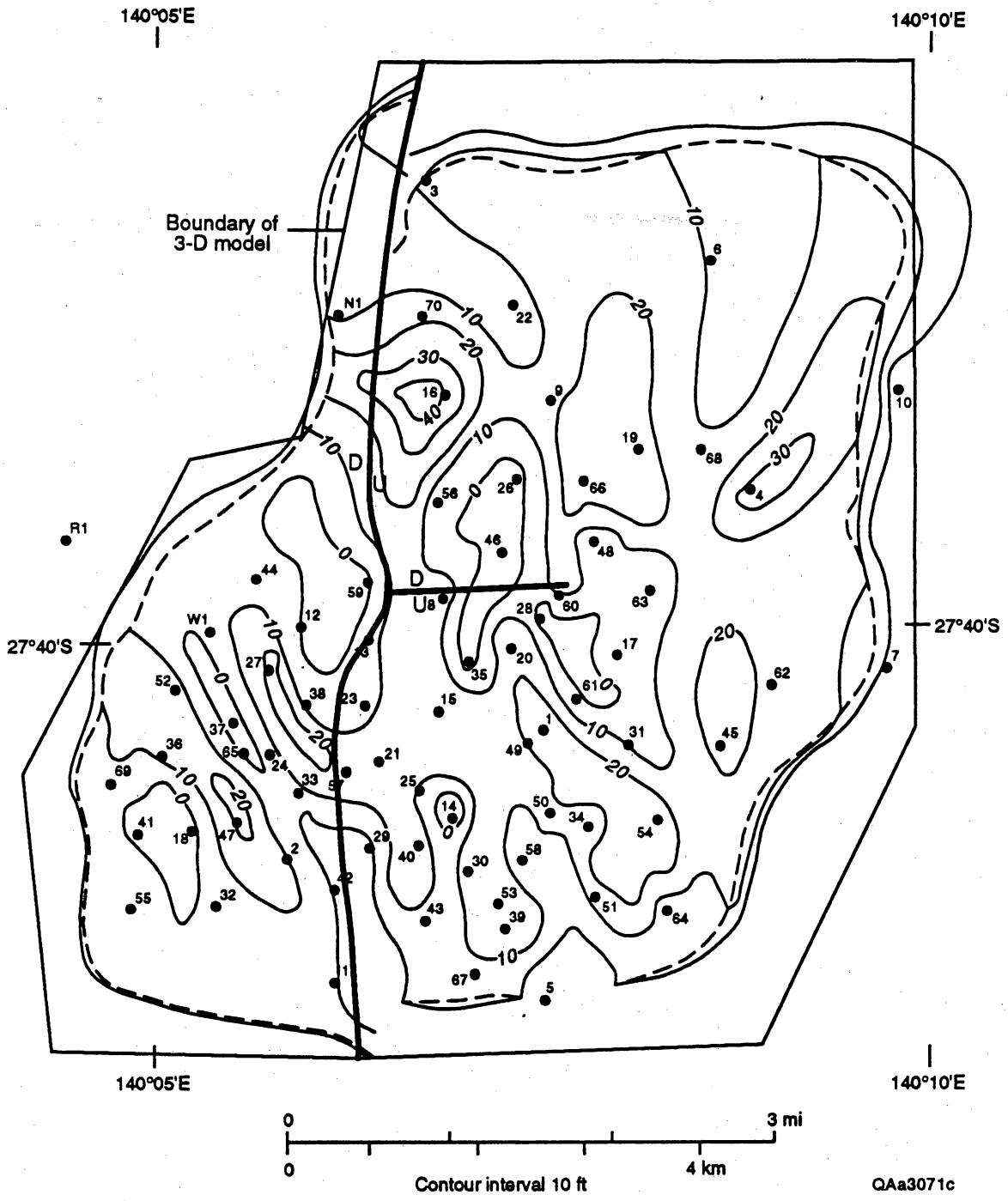

Figure VIII-6. Net pay map of flow unit 4.

influence net pay thicknesses. The hydrocarbon pore volume (HPV) is calculated on a grid cell by grid cell basis by multiplying oil saturation by porosity. The OOIP is then simply calculated by summation of the HPV of the grid cells.

Oil/Water Contact Interpretation

Any Oil Water Contact (OWC) interpretation can only be an approximation of a complex capillary relationship. This is particularly true in Tirrawarra due to the significant transition zone (based on capillary pressure curves); relative permeability effects (based on relative permeability curves and the observation that crestal wells out perform flank wells despite having equal quality reservoir) and higher irreducible water in fine grained sandstone or clayey or shaly sandstone.

Gradational changes in Sw over large depth ranges are therefore expected (and observed) within most wells. It is therefore possible to have large variations in the structural position of the effective OWC in short distances over the field. Despite these concerns, an OWC surface map is required to enable pay distribution to be mapped away from well control so that original oil in place can be estimated.

The OWC interpretation (fig. VIII-7) is tied to the Sw cut-off interpretation and to production and test data so that it honours fluid limit information.

The oil-water-contact analysis gave an interpreted flat oil/water contact (OWC) of -9910 ft (Tirrawarra well 69 lowest known oil [LKO]) in the west of the field (west of the main north-south fault). Apart from the Tirrawarra well 69 LKO, this OWC is controlled by a highest inferred water (HIW) of -9919 ft (Tirrawarra well 11) and -9917 ft (Tirrawarra N well 1), both based on log analysis, an LKO of -9896 ft (Tirrawarra well 44 production data) and a lowest inferred oil (LIO) of -9890 ft (Tirrawarra N well 1 log analysis). The analysis has also resulted in a southerly dipping OWC being interpreted over the eastern area of the field. An east-west permeability barrier in the east central part of the field associated with an east-trending fault marks a distinct break in the level of the OWC. This southerly dip is controlled by an OWC of -9615 ft in the north (Tirrawarra well 3 yielded water and minor oil on the drill stem test) and an LKO of -9792 ft in the south (Tirrawarra well 67 production statistics). The oil free water tests in Tirrawarra well 10 and well 7, in the east (highest known water (HKW) of -9682 ft and -9774 ft, respectively), provide control in that area and confirm the southerly dip in the southern segment. The presence of an LKO (-9647 ft) in Tirrawarra well 56 in the middle of the field, confirms the southerly dip of the OWC in the north. This map implies the main north-south fault to be sealing and a complex hydrodynamic and/or capillary effect to exist in the area east of the fault.

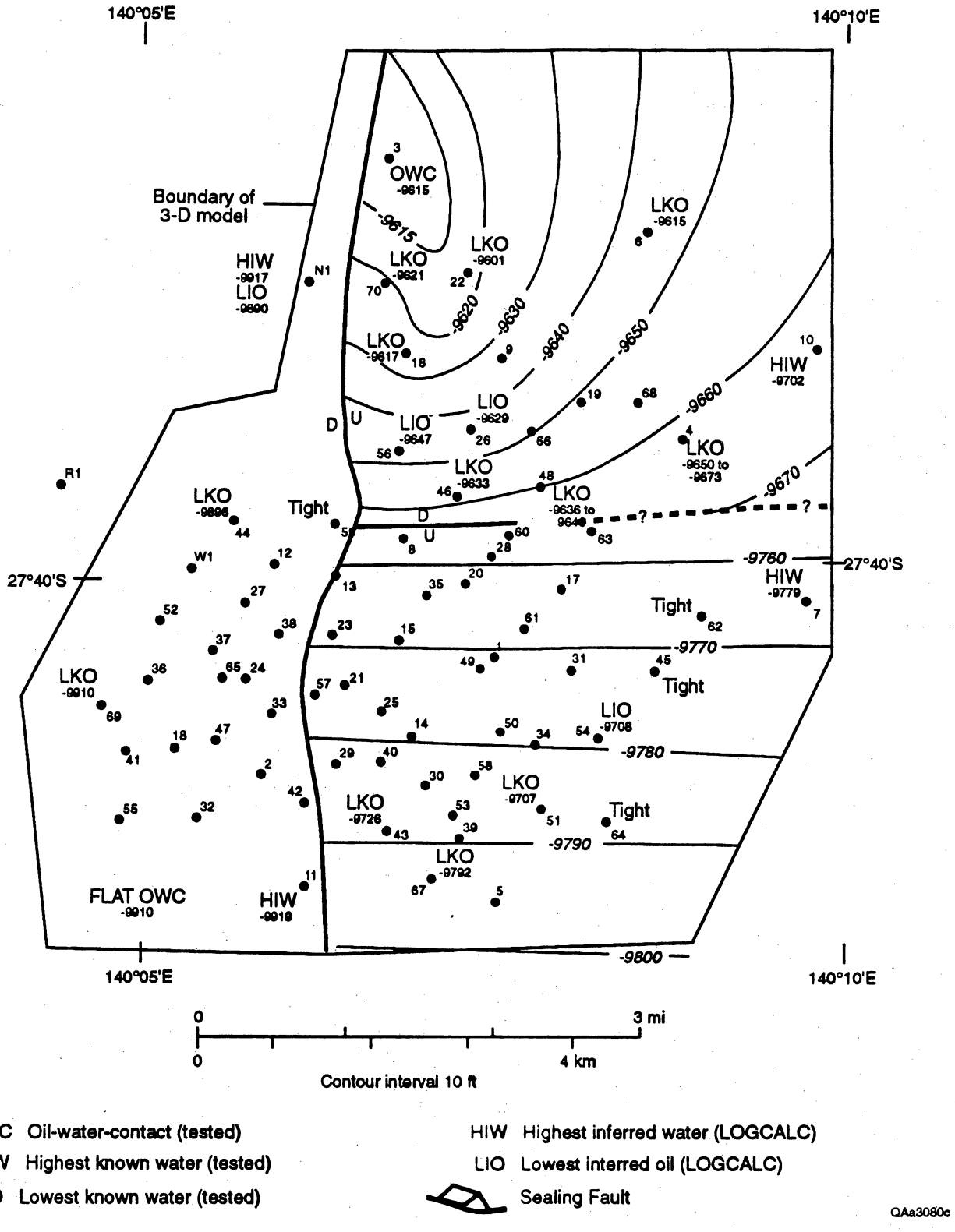

Figure VIII-7. Map of effective oil/water contact surface.

Plates VIII-1 and VIII-2 are cross-section displays from Stratamodel, showing LOGCALC calculated water saturation distribution over the field. Note that the water saturation decreases in a crestal direction with high water saturations being evident in most areas for the two basal flow units. Also note the low water saturations in the structurally low western wells and the high water saturations throughout the north of the field. The variation in water saturation in any one area attests to the complexity of the water saturation distribution. Any oil-water-contact map can therefore only be a simple model of a very complex interrelationship of rock properties, fluid properties, and structural position.

Rather than a continuous, steep gradational gradient in the east, a gentle gradient has been mapped in both the north and the south, separated by the main east–west fault, to the north of Tirrawarra well 8. This barrier is connected to a zone of complex smaller faults and tighter sand in the east between Tirrawarra wells 7 and 10. Despite the large transition zone (in excess of 400 ft) evidenced by capillary pressure curves, a steep gradient implies a very large hydrodynamic gradient across the field. As the reservoir is tight and does not have high rates of ground water movement, this is very unlikely.

The main constraint for the shallow oil/ water contact in the north, is the OWC in Tirrawarra well 3. This is further supported by significant water production from structurally shallow wells in the north. The presence of high water saturations in the best reservoir in flow unit 3L in Tirrawarra wells 22 and 16 and water production from these wells indicate that these zones have been swept. However, these wells were drilled prior to any oil production from the north of the field. These examples indicate anomalous water behavior in this northwest area.

As this area of anomalous water behavior is adjacent to the main north–south fault, it is concluded that the fault has breached seal for the high side of the fault prior to the drilling of the northern wells in the field. This had to have occurred during recent geological time because the slope on the OWC indicates that equilibrium has yet to occur. As a result of this breach of seal, water swept up high-permeability streaks from the north and the west as oil spilled across the fault, or up the fault, into shallower horizons. This explanation also accounts for the substantial oil staining and odor in lower, water productive, reservoir quality sand in Tirrawarra well 3.

The large variation in observed formation water resistivities (0.47–0.87 ohm-m) (fig. VII-37) may also support this model if they are a true representation of the field and a dual water model may be appropriate. This could account for the presence of more saline water in the northwest (0.58 ohm-m at Tirrawarra well 16), indicating movement of water from the more saline Patchawarra Formation across the main fault into the northwest area of Tirrawarra field.

Tirrawarra Field Cross–section T–12

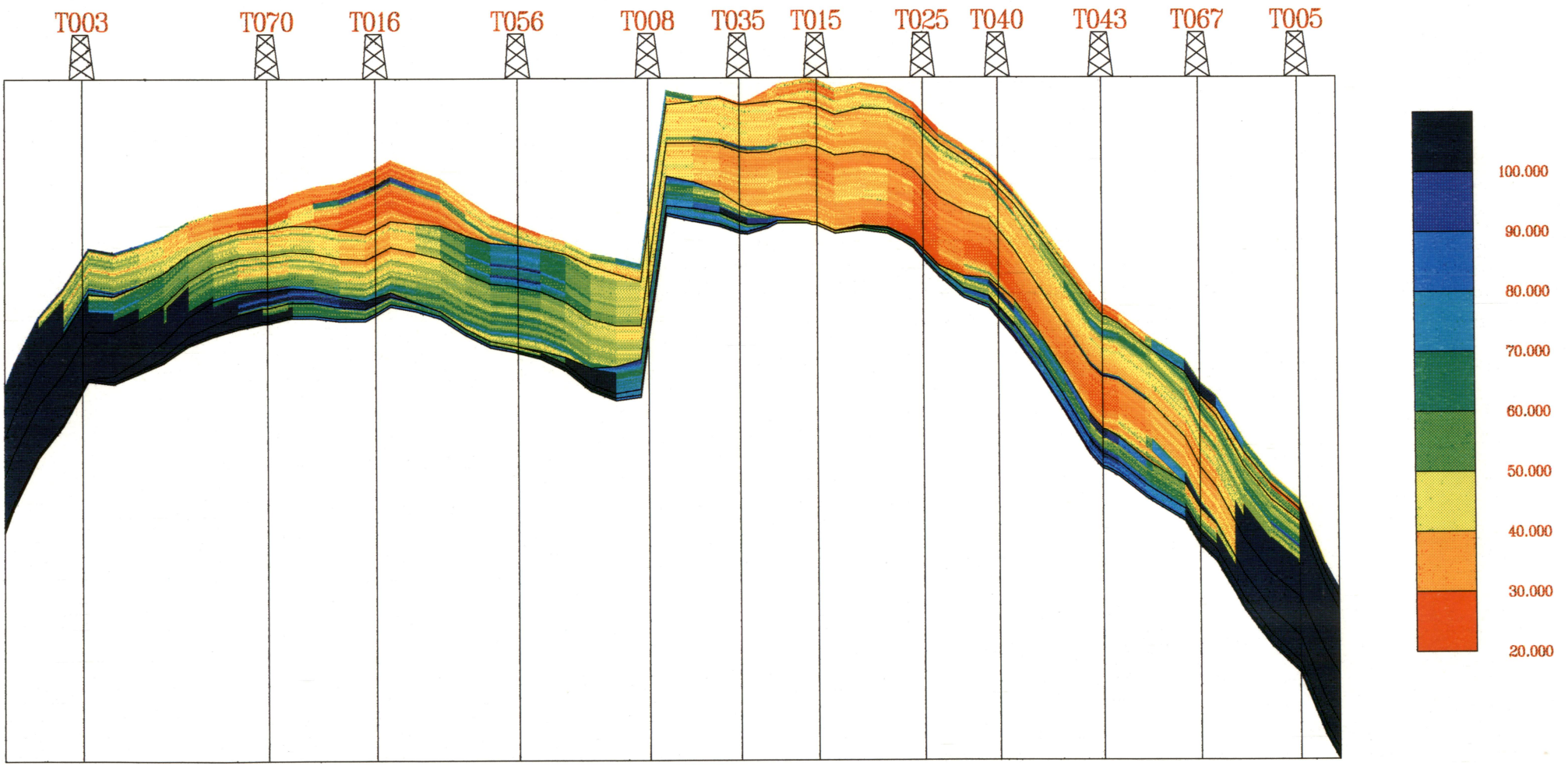

Plate VIII-1. Stratamodel cross section T12 showing LOGCALC calculated water saturations. See figure II-1 for location of section line.

Plate VIII-2. Stratamodel cross section T17 showing LOGCALC calculated water saturations. See figure II-1 for location of section line.

Tirrawarra Field Cross–section T–17

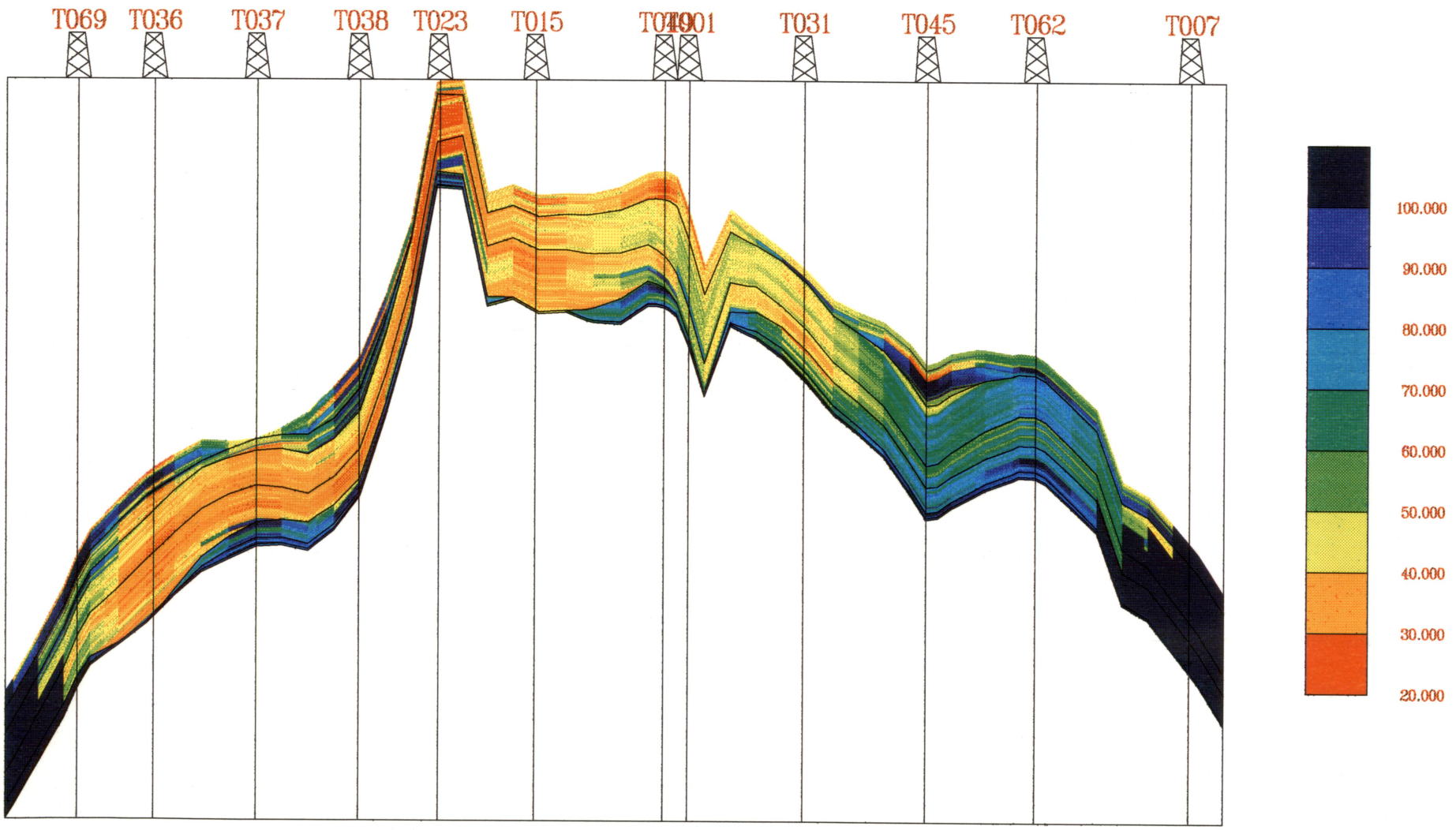

As the west side of the field has a constant OWC, controlled in part by Tirrawarra N well 1, the seal on this side of the field was not breached by the main north–south fault in the north, despite the high side being breached.

The presence of water in only the best reservoir in Tirrawarra wells 16 and 22 was initially thought to be adequate evidence for concern about the wettability of the reservoir in this field. However, tight wells have much higher calculated water saturations than adjacent productive wells at the same depth, indicating a water wet reservoir.

Tirrawarra well 64 is at the same depth as Tirrawarra well 67 yet Tirrawarra well 67 produces oil with insignificant water and has Sh of 50–70 percent and Tirrawarra well 64 (2 km away) has Sh of 30–50 percent and is tight. This wet/tight relationship is seen fieldwide throughout each well, with the exception of the wet zones in Tirrawarra wells 16 and 22. Apart from these exceptions the reservoir is behaving as if water wet, the good reservoir having lower Sw values and the tight rock having higher Sw values.

OOIP Calculation and Distribution

OOIP Distribution—Net Pay and Hydrocarbon Pore Volume

Net pay has been mapped by combining the net sandstone maps for each flow unit (figs. V-29, 32, 36, 37, 41, and 44) with the oil-water-contact structure contour map (fig. VIII-7) and the top porosity and base porosity structure contour maps for each flow unit. The structure maps provide the control for mapping the wedge-edge of the net pay. The result is a net pay map for each flow unit (figs. VIII-1 to VIII-6). The net pay maps show distribution of OOIP in terms of thickness only. However, as this provides the major parameter for OOIP calculation, and a major factor for permeability feet calculation, it has been mapped separately.

Net pay has been determined firstly by log analysis using the petrophysical cut-offs (Section VII) and by the subsequent editing of this data, based on core data and partly on production and DST data. Net sand has been defined as all sand which was interpreted to be wet or pay on this same basis. As a result, the net pay isopach equates with the Net sand map down to the wedge edge where structural surfaces also control the pay distribution.

The hydrocarbon pore volume (oil saturation * porosity * thickness) has also been calculated for each flow unit for each well and mapped (figs. VIII-8 to VIII-13). This has been calculated by summation of the So*phi (from log analysis) for each foot of net pay. The same wedge edge from the net pay mapping has been used for these maps. The hydrocarbon pore volume (HPV) maps show actual OOIP distribution in units of cumulative hydrocarbon pore feet.

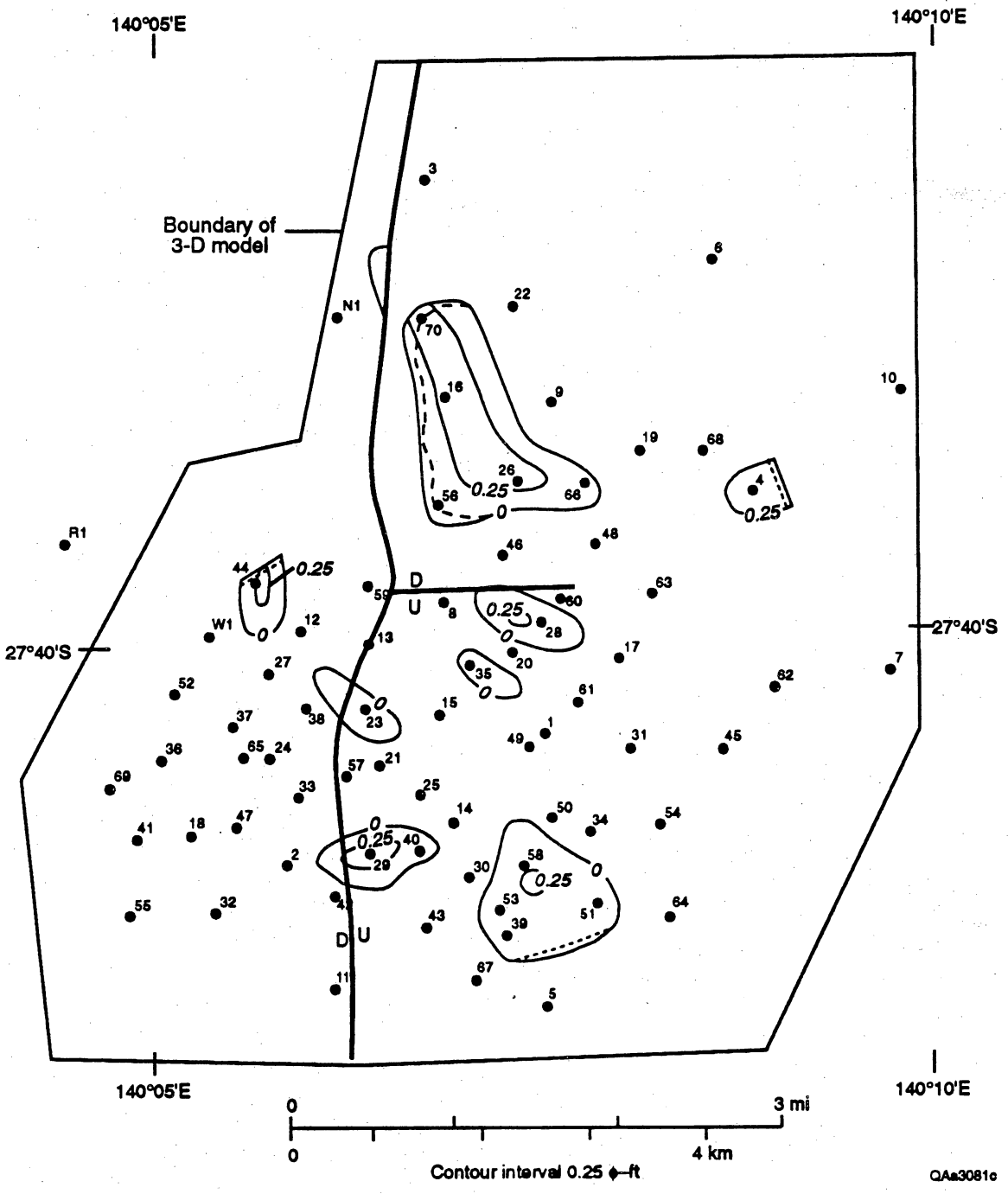

Figure VIII-8. Map of hydrocarbon pore volume, flow unit 1U.

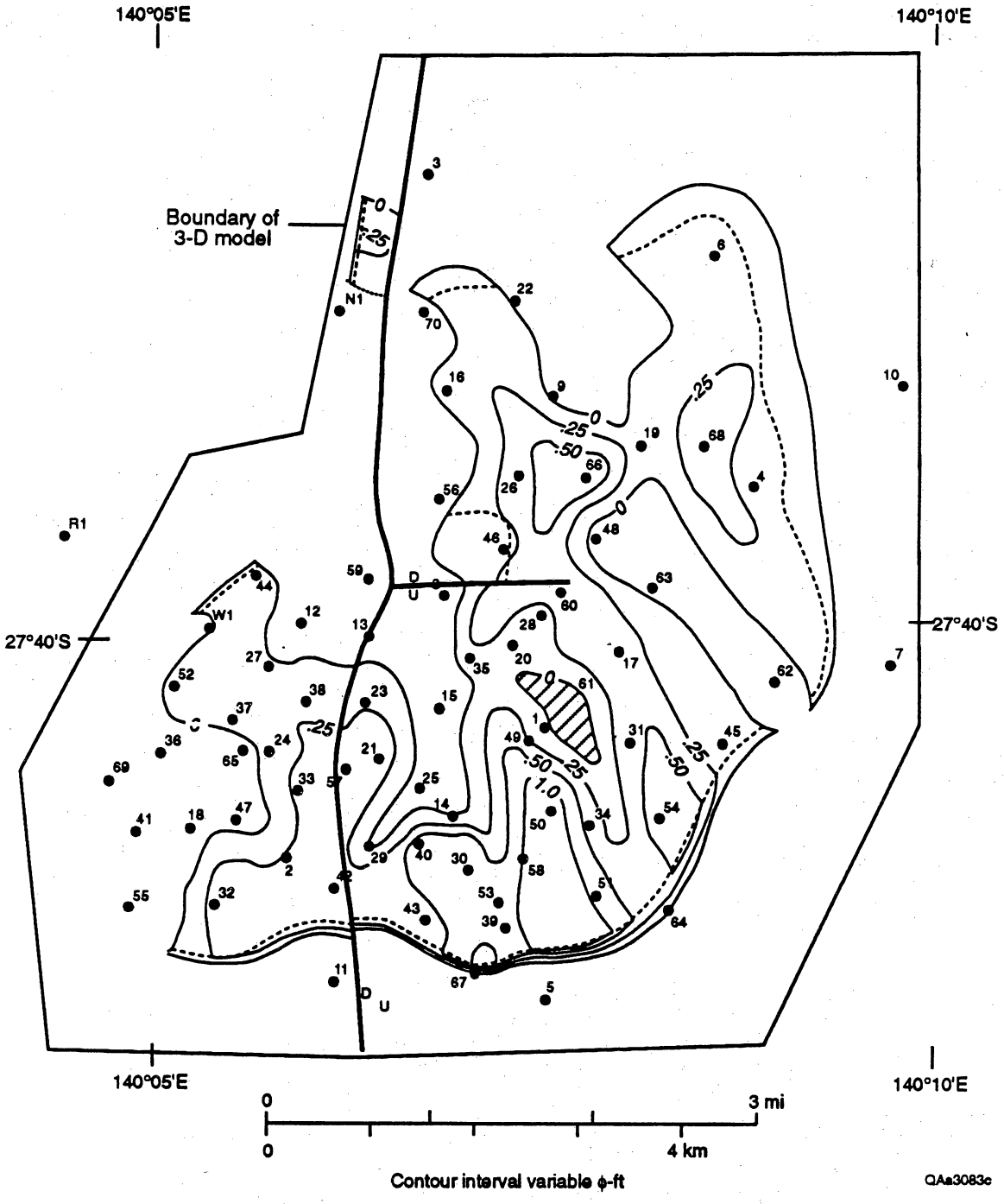

Figure VIII-9. Map of hydrocarbon pore volume, flow unit 2L.

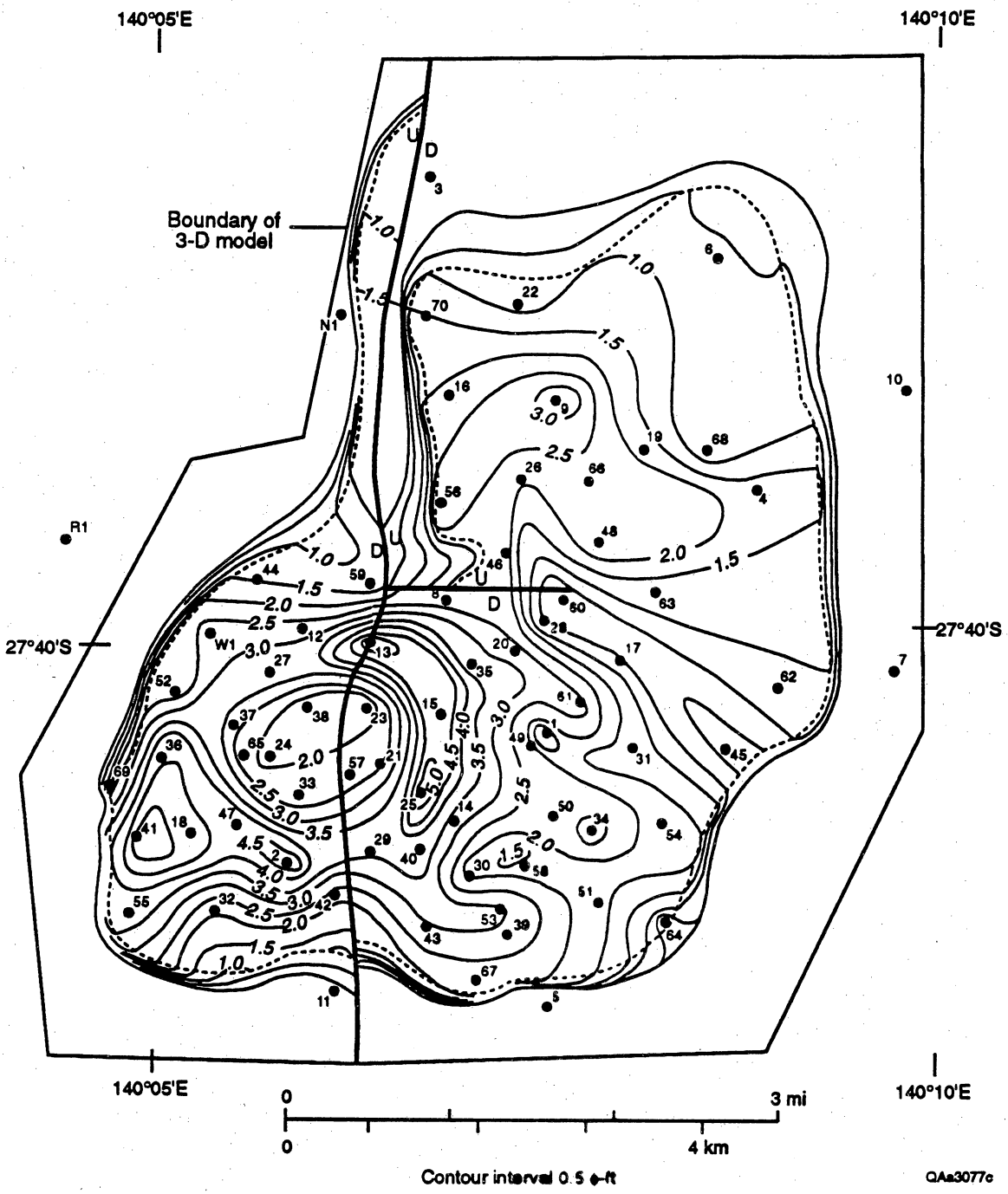

Figure VIII-10. Map of hydrocarbon pore volume, flow unit 3L.

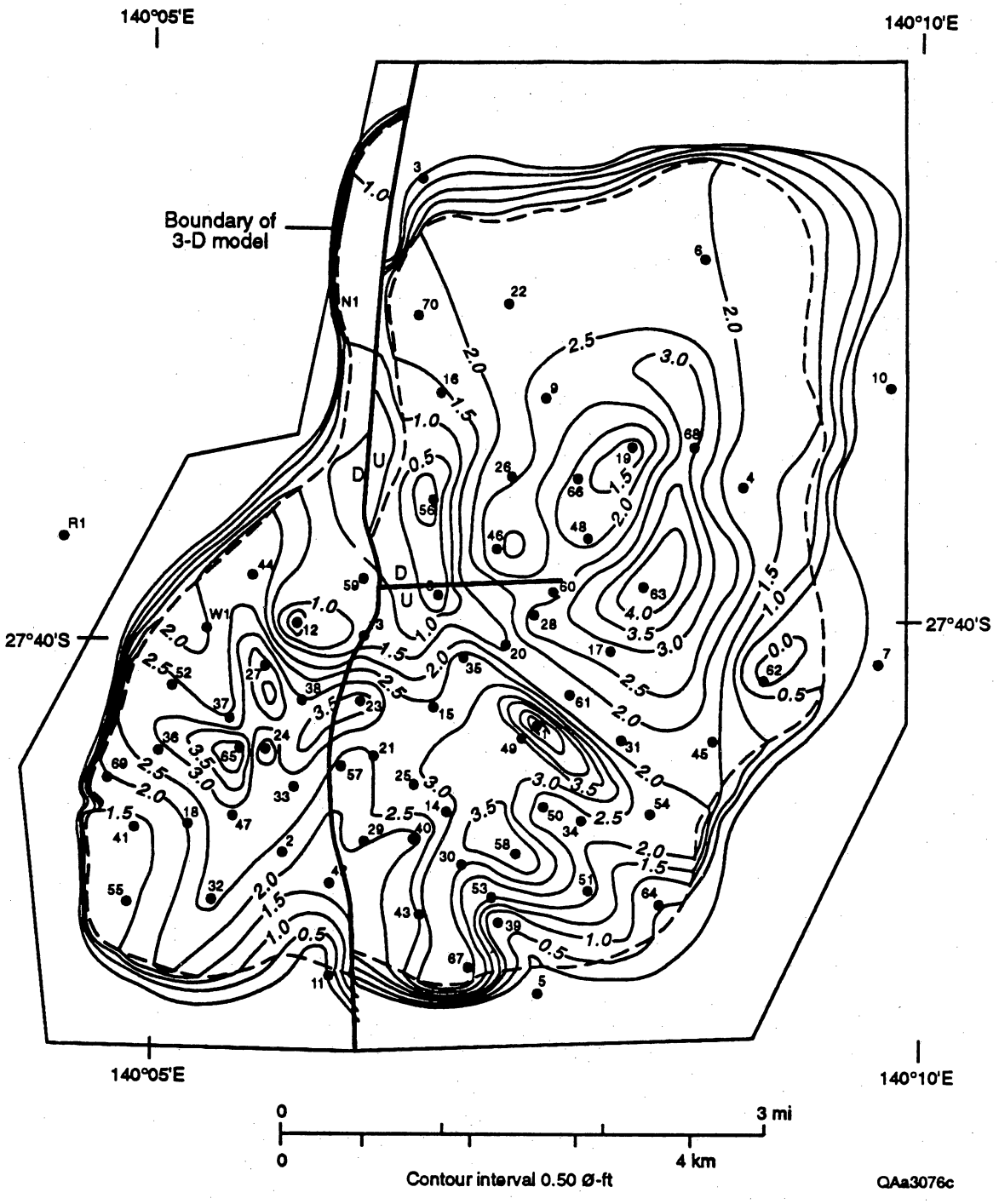

Figure VIII-11. Map of hydrocarbon pore volume, flow unit 3U.

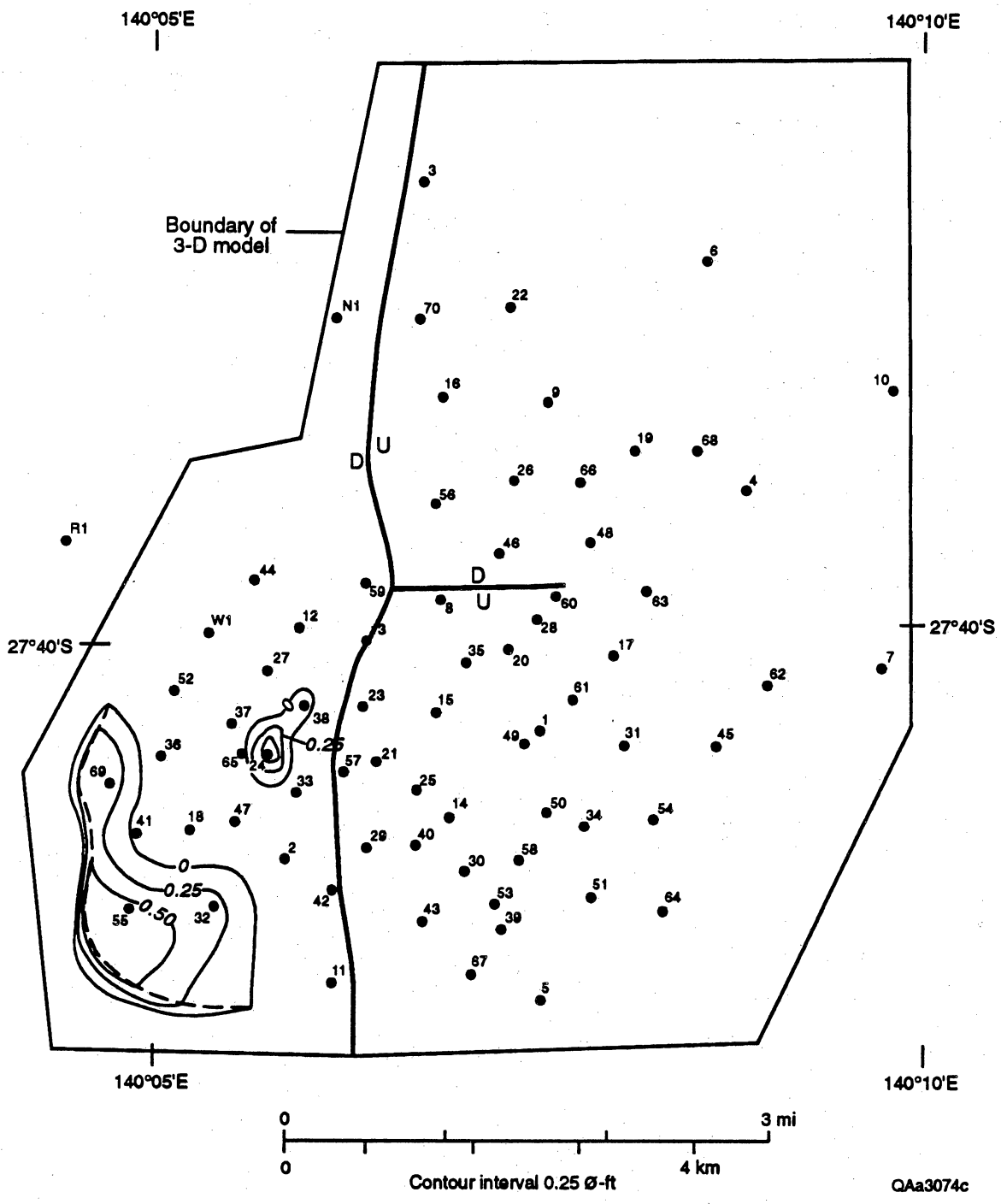

Figure VIII-12. Map of hydrocarbon pore volume, flow unit 2U.

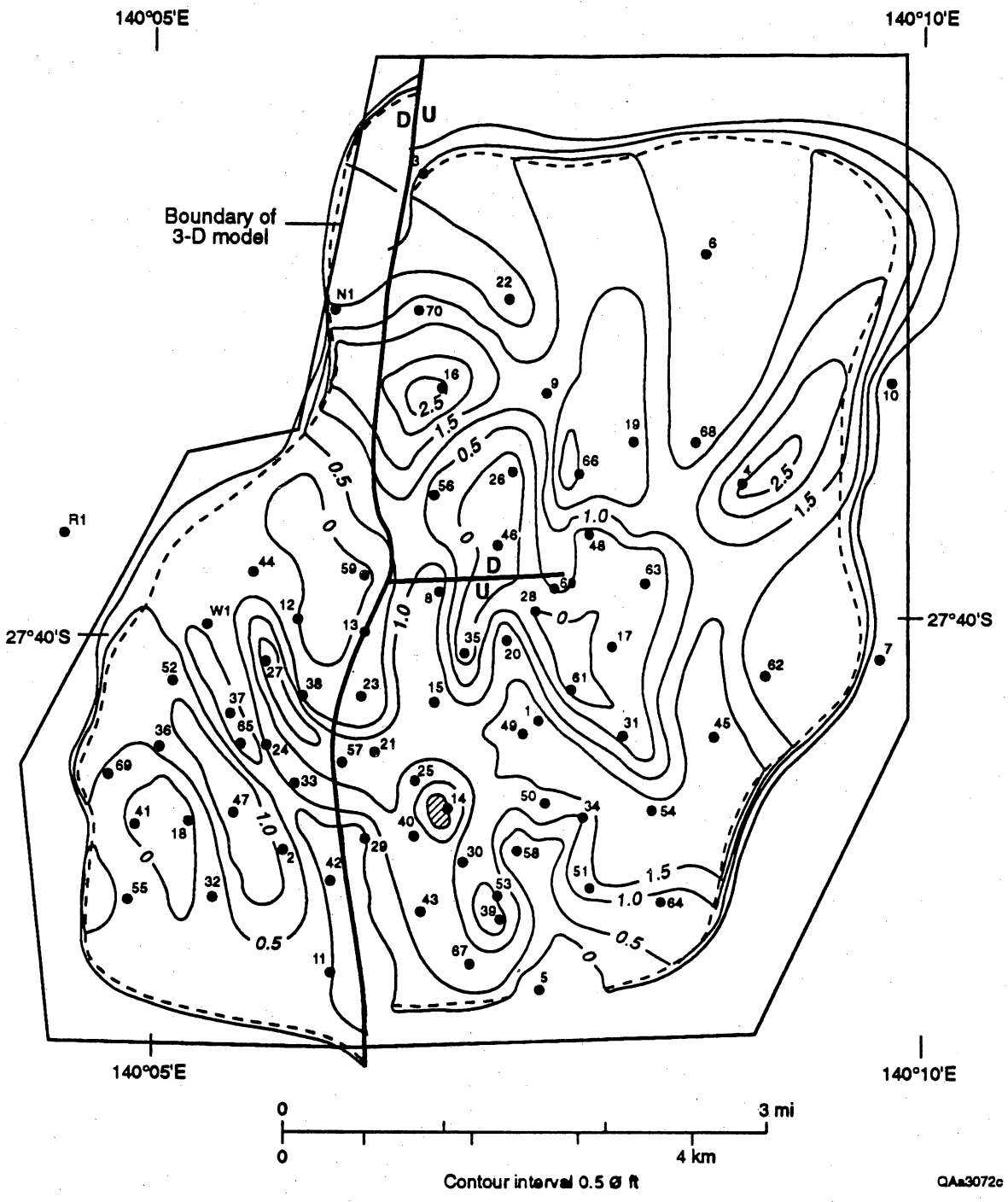

Figure VIII-13. Map of hydrocarbon pore volume, flow unit 4.

Note that the pre-existing Rw of 0.58 ohm-m at 75°F has been used for the HPV maps. This was done as the HPV maps were produced prior to the final Rw determination, however, the recommended field Rw of 0.65 ohm-m at 75°F was used for the final OOIP calculations. The HPV calculated using 0.65 ohm-m for log analysis is slightly less than that calculated using 0.58 ohm-m. For low water saturation units and areas this equates to a reduction in HPV of 1 percent, whereas in areas of high water saturation the reduction in HPV is 3 percent. Although the HPV values may be reduced from what is mapped, the reductions are minimal and regional, so the maps still reflect the OOIP distribution (figs. VIII-8 to VIII-13).

The area of contact between pay in adjacent flow units has been mapped (figs. VIII-14 to VIII-17), based on the log analysis interpretation of interconnected pay at the flow unit boundary in each well. Interconnected pay is interpreted where net pay thicker than 3 ft in one flow unit contacts net pay thicker than 3 ft in the adjacent flow unit.

Mapping of the division of OOIP, for a flow unit, into vertically isolated zones separated by nonpay rock (figs. VIII-18 through VIII-22) is also based on the log analysis interpretation. Any nonpay within a flow unit may be a barrier to vertical flow. The contour maps of the number of pay divisions do not imply any lateral extent to nonpay zones but do show the degree of pay/nonpay interlayering. This may result in flow unit compartmentalization or may simply make flow paths more tortuous.

The distribution of OOIP in terms of net pay, HPV and net pay subdivision by flow unit, and interconnectivity between flow units are described below and summarized in table VIII-1 together with Stratamodel-calculated OOIP values from table VIII-2.

Flow Unit 1U

Flow unit 1U (fig. VIII-1) has only minor net pay characterized by small, thin (<5 ft), discontinuous sand bodies. This reflects the low energy, lacustrine deltaic depositional environment of this unit. Flow unit 1U sand bodies have low porosities and high water saturations (average So*phi <5 percent) with the exception of a small isolated sand at Tirrawarra well 29 (average So*phi of 6.1 percent). The HPV isopach (fig. VIII-8) closely mirrors the net pay distribution but only attains a maximum of 0.4 hydrocarbon pore feet (Tirrawarra well 70) with the remainder being much less. Flow unit 1U is vertically connected with flow unit 2L in isolated wells (fig. VIII-14). When encountered, pay is never broken up by nonpay into thinner units. This flow unit reservoirs 1.2 MMSTB of OOIP.

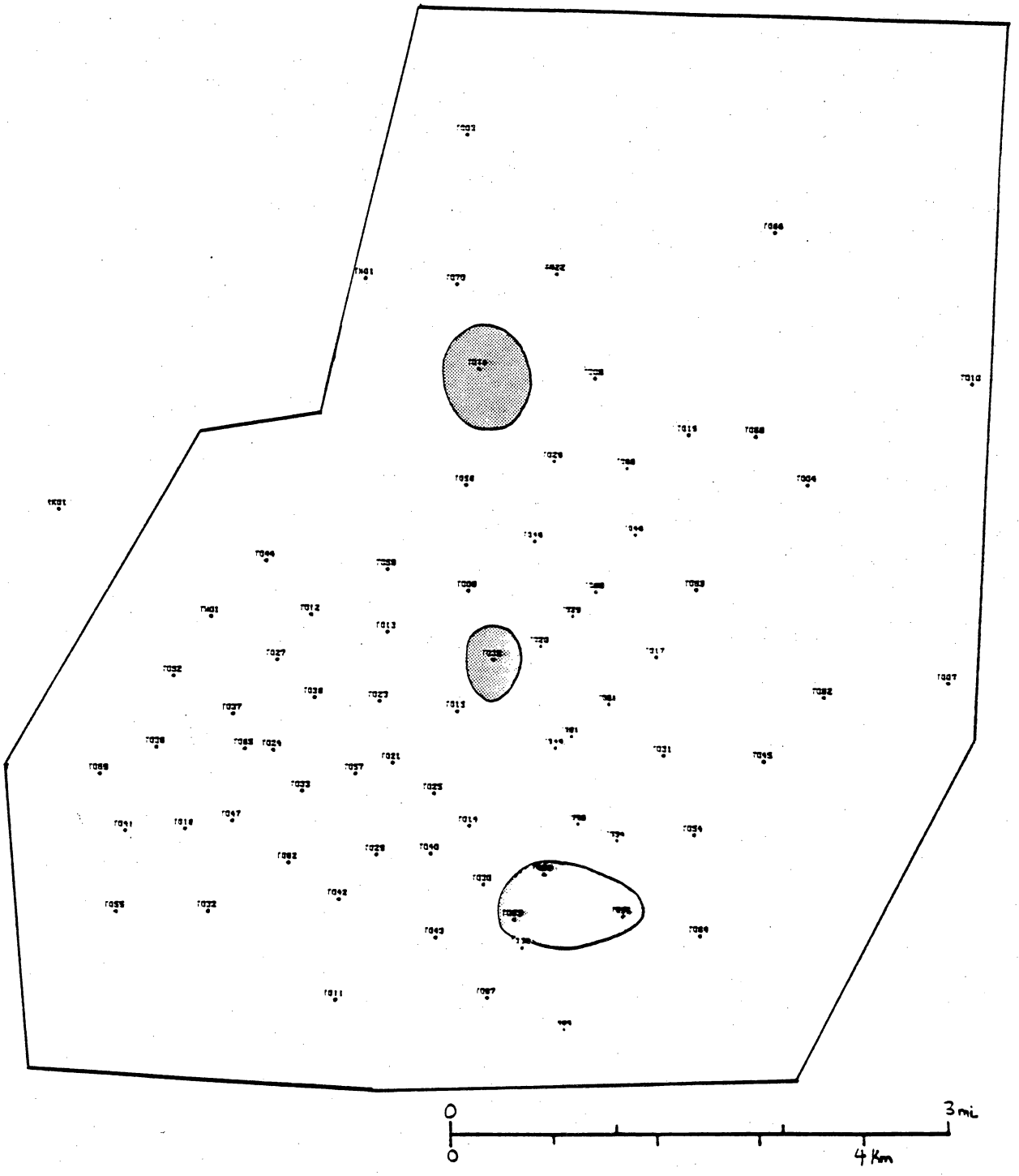

Figure VIII-14. Map of pay connectivity between flow units 2L and 1U. Outlined areas show where pay zones at least 3 ft thick are in contact along the boundary between these flow units.

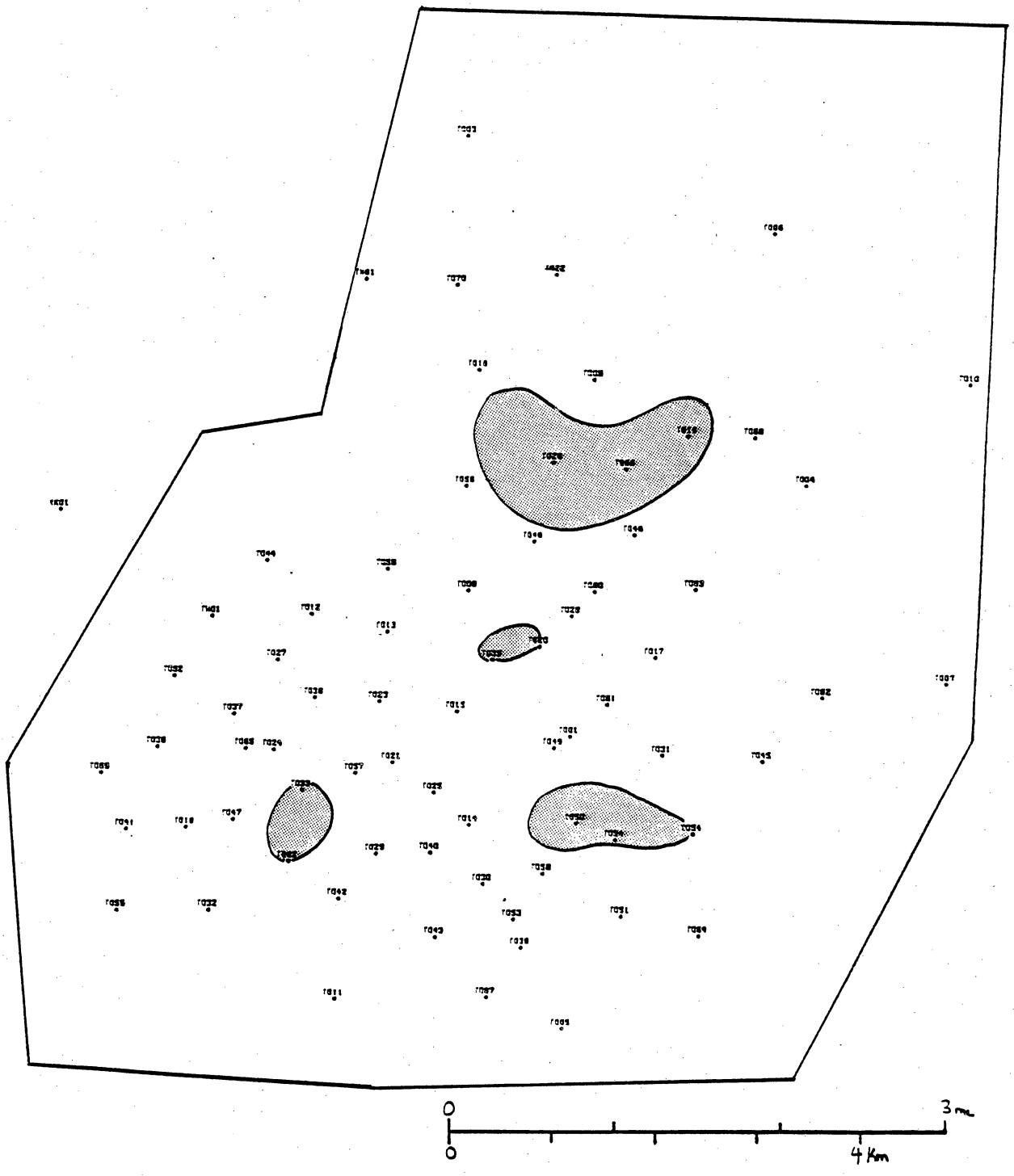

Figure VIII-15. Map of pay connectivity between flow units 3L and 2L. Outlined areas show where pay zones at least 3 ft thick are in contact along the boundary between these flow units.

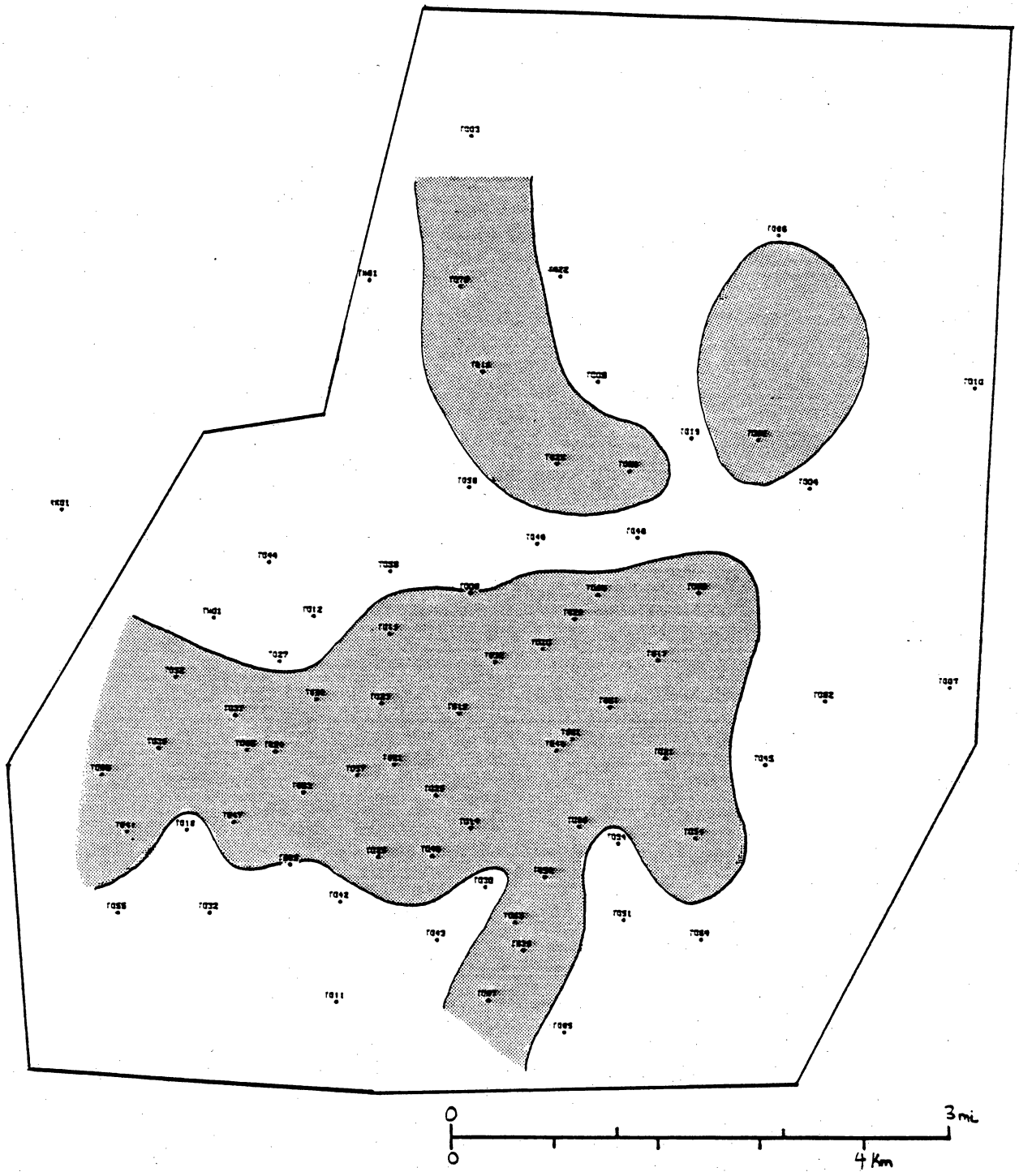

Figure VIII-16. Map of pay connectivity between flow units 3U and 3L. Outlined areas show where pay zones at least 3 ft thick are in contact along the boundary between these flow units.

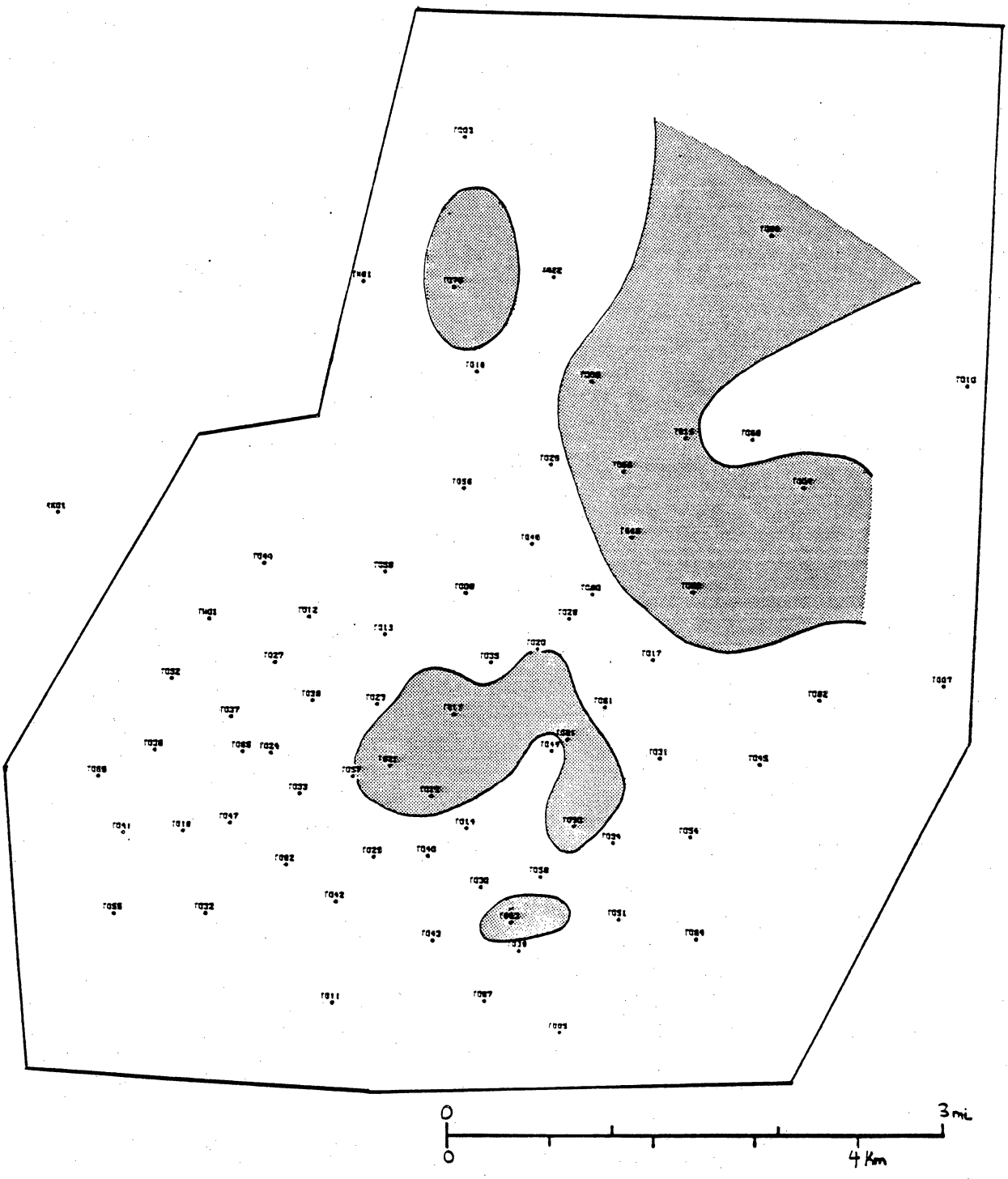

Figure VIII-17. Map of pay connectivity between flow units 4 and 3U. Outlined areas show where pay zones at least 3 ft thick are in contact along the boundary between these flow units.

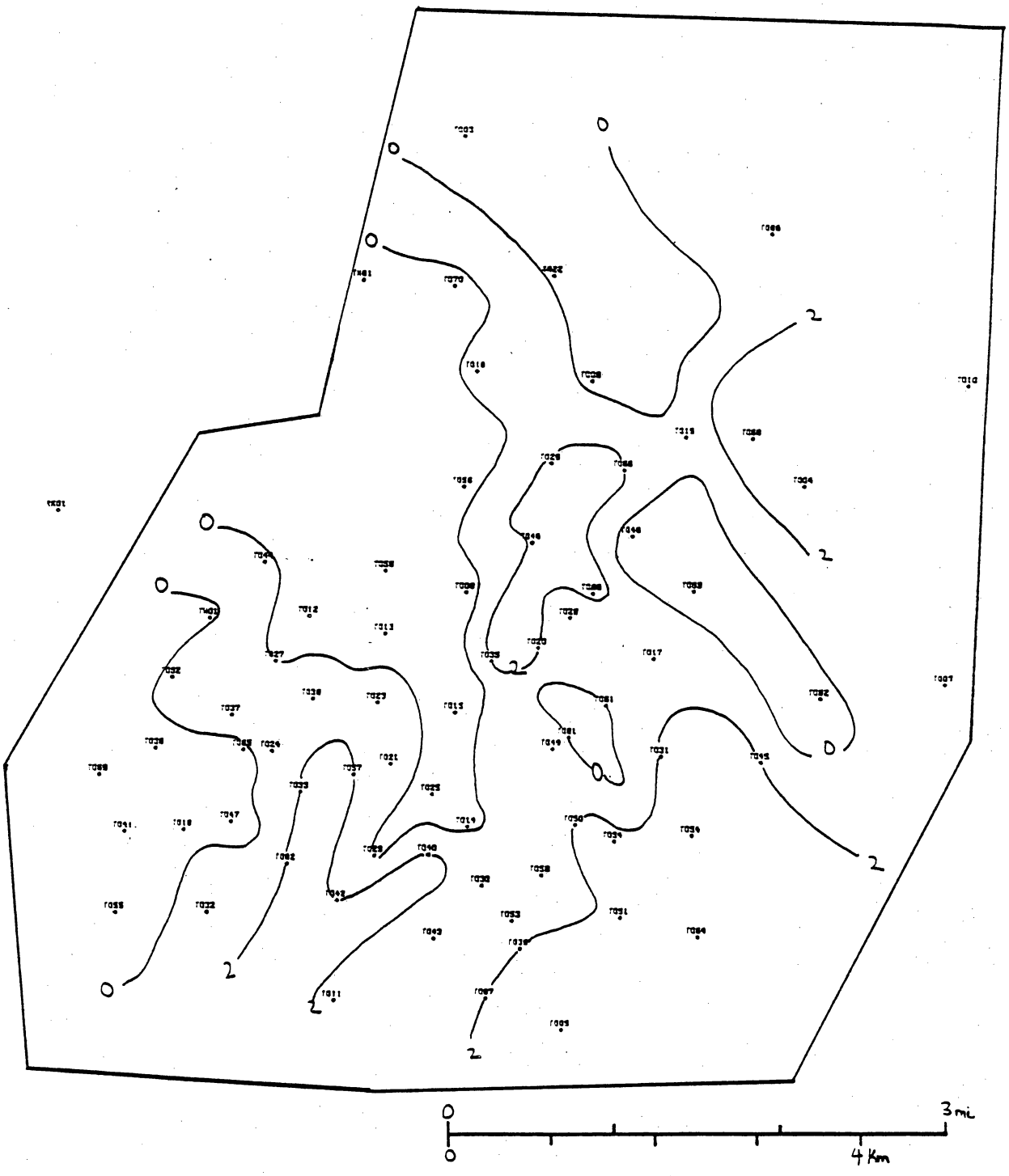

Figure VIII-18. Contour map of the number of separate pay zones in flow unit 2L. Pay zones are separated vertically by interlayered nonpay zones.

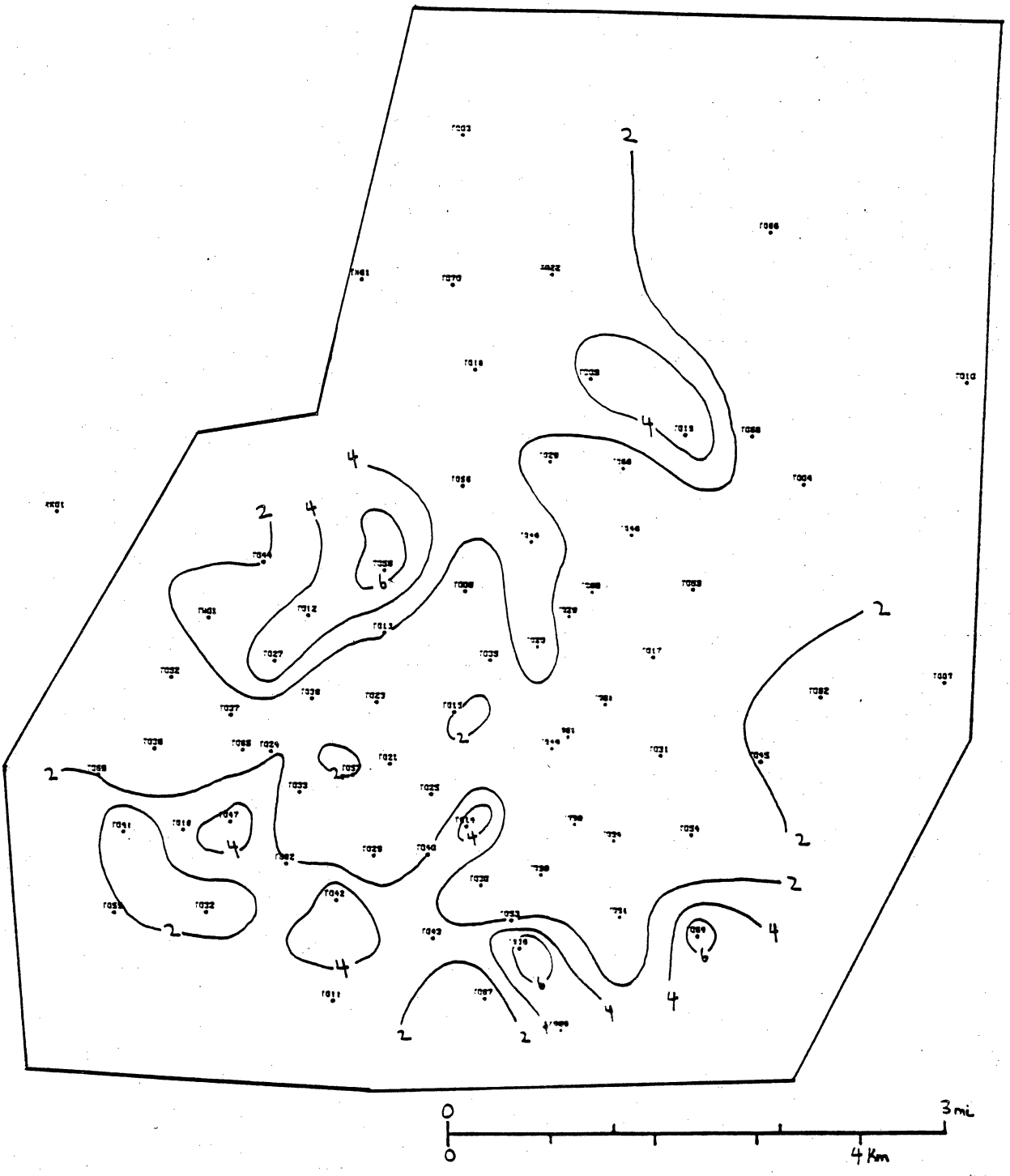

Figure VIII-19. Contour map of the number of separate pay zones in flow unit 3L. Pay zones are separated vertically by interlayered nonpay zones.

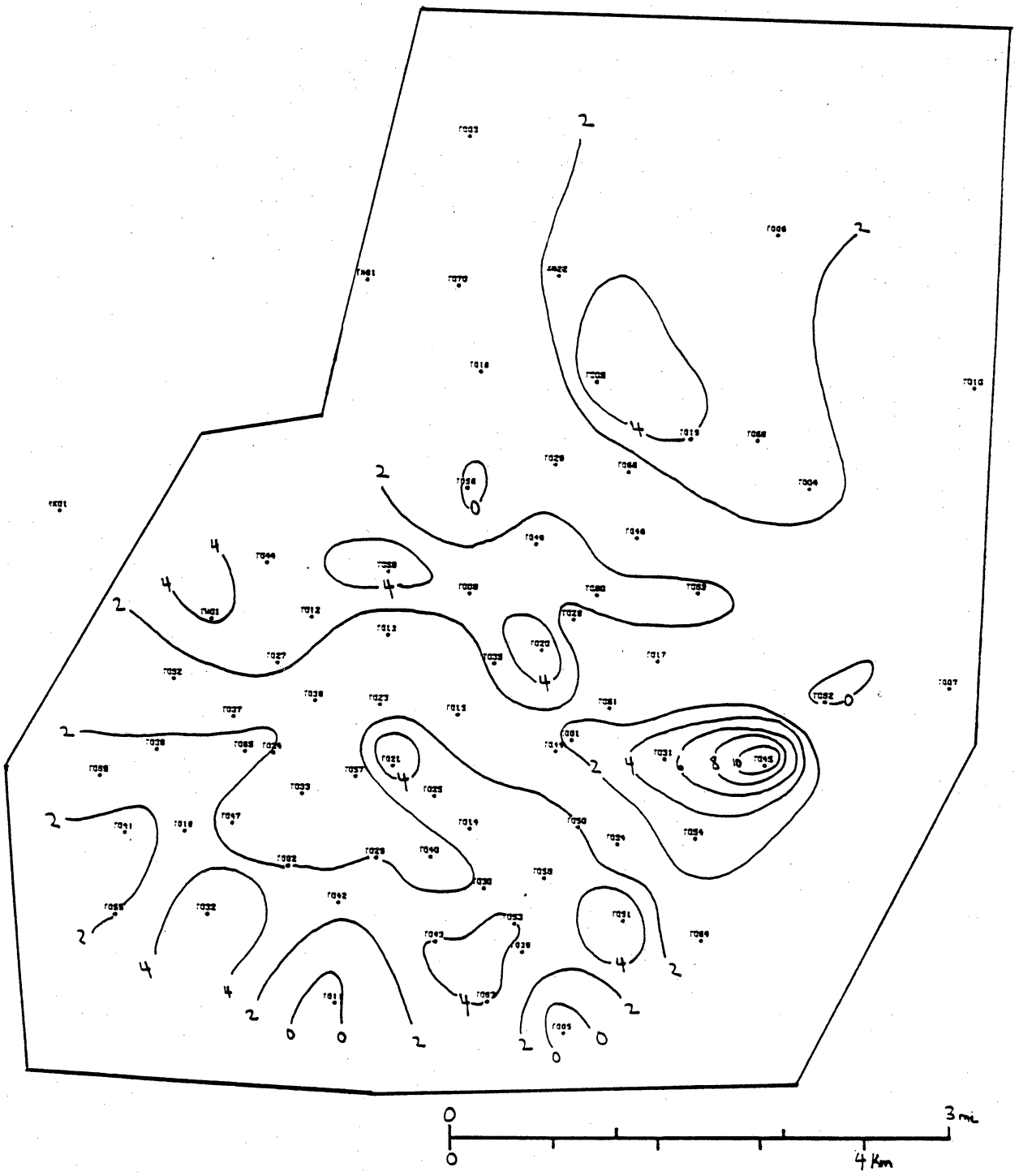

Figure VIII-20. Contour map of the number of separate pay zones in flow unit 3U. Pay zones are separated vertically by interlayered nonpay zones.

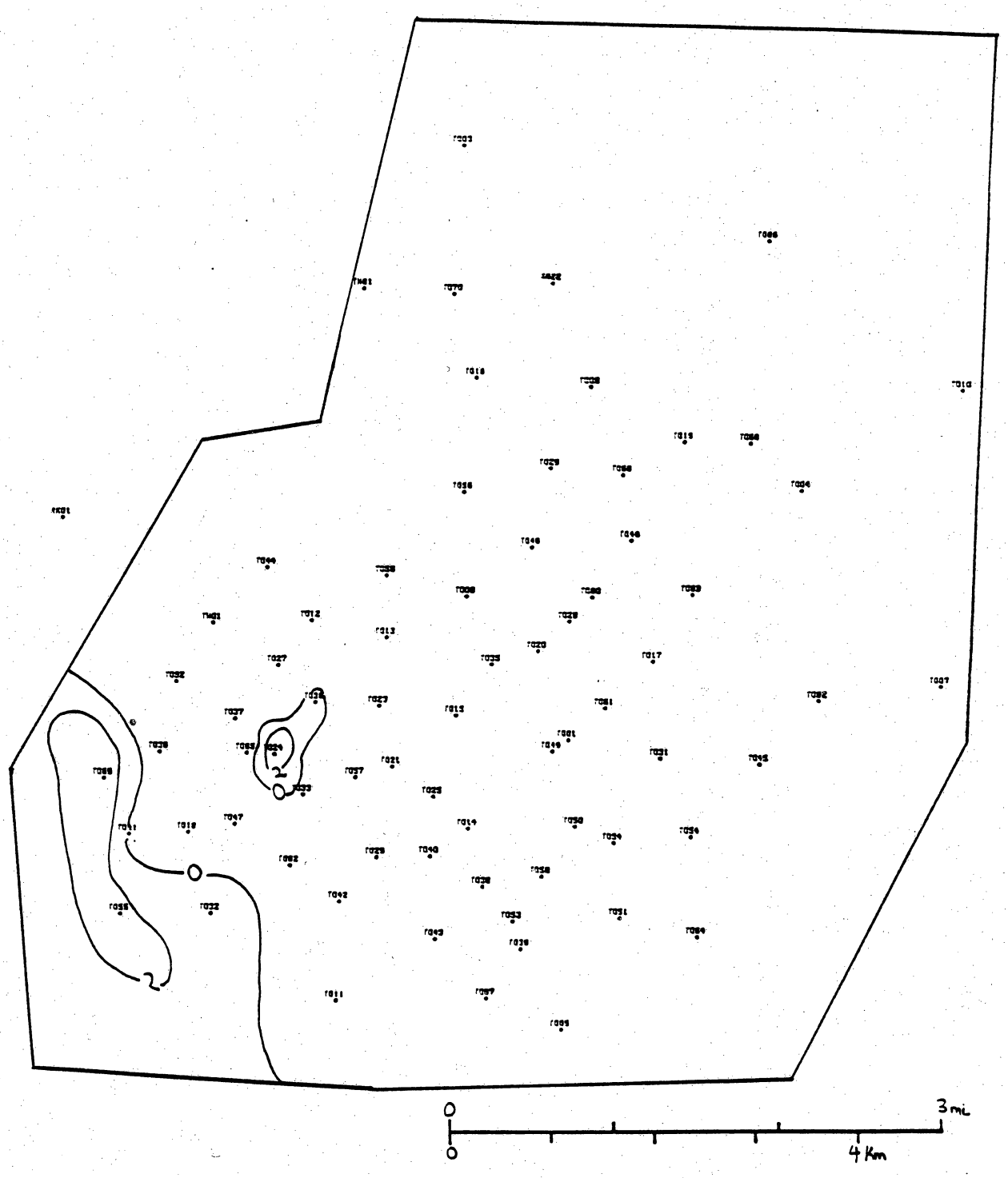

Figure VIII-21. Contour map of the number of separate pay zones in flow unit 2U. Pay zones are separated vertically by interlayered nonpay zones.

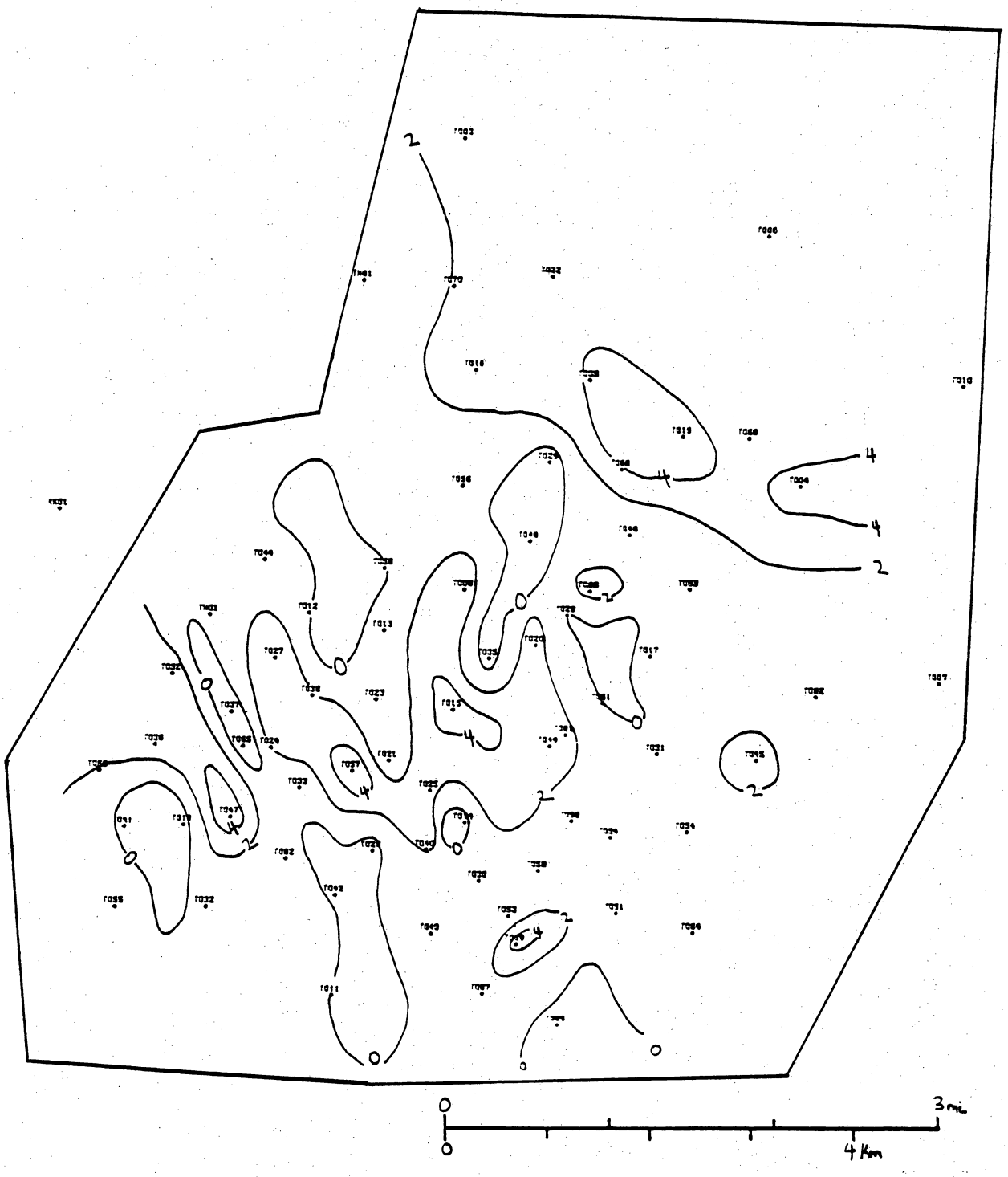

Figure VIII-22. Contour map of the number of separate pay zones in flow unit 4. Pay zones are separated vertically by interlayered nonpay zones.

Table VIII-I OOIP Distribution.

Facies	Net pay (ft)	HPV hydrocarbon pore feet	Permeability distribution md.	Average So x Ø	Connectivity	Total OOIP (MMSTBO)
FU 4	• Highly variable thickness <40' (T #16). • 10ft avg. • Best in the north.	• Highly variable. • 0-2.6 roughly 1.0 avg. • Matches net pay.	• Highly variable but up to 340md in T #16. • Kh up to 64 in t #8.	• 6%-8% up to 9.8%. • Low Ø, high So.	• Best in center and north (with 3U). • Least divided adjacent to main fault. • Best lateral connectivity in the north.	24.2
FU 2U	• <10ft restricted to the SW. • Probably small isolated pay sands.	• 0-0.6 range. • Matches net pay.	• Very low permeabilities. • Kh <.4md ft.	• 5% avg. • Low Ø, mod So.	• Not connected with other flow units. • Divided into 2-3 pay units. • Connectivity between wells unlikely.	2.8
FU 3U	• Relatively even 30ft, up to 72ft. • Best in center and south.	• 0-5.4. • 2.0 avg. • Matches net pay.	• North-south orientation near main fault. • Kh up to 30md ft in T #21. • Much of field >5md ft.	• 3.4-12.1%. • Mainly 77%. • Mod So, mod Ø.	• Well connected with 3L except for flanks. • Minimal division except NW and southern edge. • Laterally well connected.	64.7
FU 3L	• Relatively even 20ft, up to 59ft. • Best in south and SW.	• Roughly 2.0 ave. • Matches net pay	• Strong north-south orientation near main fault. • Up to 252md ft in T #25. • Most of field >10md ft.	• 4.1%-11.0%. • Mainly >7%. • High Ø, mod So.	• Well connected with 3U. • Minimal division except for NW and southern edge. • Laterally well connected.	64.3
FU 2L	• Highly variable thickness. • Channel sands. • 5ft-10ft avg. • Up to 19ft. • Best in SE.	• 0.25 avg. • <1.2. • Matches net pay.	• Up to 7.8%. • Mostly <5%. • Low Ø, low So.	• Best in T #21 area (11md ft). • 1-2md ft avg. best. • Highly erratic.	• Pay is poorly connected with 3L & 1U vertically. • Lateral connectivity with 3L is common. • Often divided into 2 separate units.	5.9
FU 1U	• Thin (<6ft) isolated small. • Best in north (T #16 area).	• <0.4. • Matches net pay.	• Mostly <5%. • V. low Ø, V. low So.	• <3.0md ft best in north (T #16 area).	• Isolated except for a few wells. • Pay is never divided.	1.2

Flow Unit 2L

Flow unit 2L (fig. VIII-2) is characterized by thin (<10 ft) elongate bodies of net pay that thicken and widen in the south east due to coalescing of these sand bodies in that area. This reflects the distributary channel and channel mouth bar depositional setting. Much of this flow unit has low porosities and high water saturations (average So*phi <5 percent), however, structurally higher wells have lower water saturations to give average So*phi values up to 7.8 percent (Tirrawarra well 21). The HPV isopach (fig. VIII-9) closely mirrors the net pay distribution with hydrocarbon pore feet values only exceeding 0.5 in the south-east and in Tirrawarra well 66. This unit has minimal pay in contact with pay in flow unit 3L (fig. VIII-15) reducing its chance of being swept to these areas unless intersected by the hydraulic fracture. However, it is often divided into 2 or more isolated sand bodies separated by non-pay (fig. VIII-18). This flow unit reservoirs 5.9 MMSTB of OOIP.

Flow Unit 3L

Flow unit 3L (fig. VIII-3) is a continuous sandstone unit having net pay thickness ranging from 3 ft (Tirrawarra well 60) to 59 ft (Tirrawarra wells 15 and 36). The geometry and interconnectedness of the pay in this unit reflects the braid delta setting of this deposit. It has high porosities and low water saturations with average So*phi values as high as 11.0 percent (Tirrawarra wells 8 and 9) with most wells having values in excess of 7 percent. Structurally lower wells have higher water saturations and some wells in the east have low porosities as well to give average So*phi values as low as 4.1 percent (Tirrawarra well 62). The HPV isopach (fig. VIII-10) is similar to the net pay distribution differing near the wedge edge and in the north where higher water saturations impact on the HPV. Hydrocarbon pore feet values are rarely less than 1.0 (near water and Tirrawarra wells 60 and 17 area) and range up to 5.5 (Tirrawarra well 25). Pay in this unit is in direct communication with pay in flow unit 3U over most of the field (fig. VIII-16) but has minimal contact with pay in flow unit 2L (fig. VIII-15). This unit is often divided into two or more isolated sand bodies separated by nonpay (fig. VIII-19). This flow unit reservoirs 64.3 MMSTB of OOIP.

Flow Unit 3U

Flow unit 3U (fig. VIII-4) is a continuous sandstone unit having net pay thickness ranging from 0 ft (Tirrawarra wells 56 and 62) to 63 ft (Tirrawarra well 65) and displaying greater

thickness variation than does flow unit 3L. The geometry and interconnectedness of this flow unit reflect its braid delta depositional setting. Net pay has high porosities and low water saturations with average So*phi values as high as 12.1 percent (Tirrawarra well 9) with most wells having average values in excess of 7 percent. Structurally lower wells have higher water saturations and some wells in the east and north have low porosities as well to give average So*phi values as low as 3.4 percent (Tirrawarrra well 45). The HPV map (fig. VIII-11) is similar to the net pay distribution differing near the wedge edge and in the north where higher water saturations impact on the HPV. Hydrocarbon pore feet values are rarely less than 1.0 (near water and Tirrawarra wells 60 and 17 area) and range up to 5.5 (Tirrawarra well 1). Pay in this unit is in direct contact with pay in Flow Unit 4 over crestal and northern parts of the field (fig. VIII-17) and is in direct contact with pay in flow unit 3L over most of the field area (fig. VIII-16). It is frequently divided into 2 or more isolated sand bodies separated by nonpay (fig. VIII-20). This flow unit reservoirs 64.7 MMSTB of OOIP.

Flow Unit 2U

Flow unit 2U (fig. VIII-5) has only minor net pay restricted to the south west of the field where it ranges in thickness from 5 to 10 ft. This pay distribution is most likely contained in poorly connecting fluvial channels. This sand body has low porosities and moderate water saturations (average So*phi approx. 5 percent). The HPV isopach (fig. VIII-12) closely mirrors the net pay distribution but only attains a maximum of 0.64 hydrocarbon pore feet (Tirrawarra well 34), the remainder being less than 0.3. Pay in this unit is not vertically connected with interconnected pay in other flow units and is usually divided into two or more isolated sand bodies separated by nonpay (fig. VIII-21). This flow unit reservoirs 2.8 MMSTB of OOIP.

Flow Unit 4

Flow unit 4 (fig. VIII-6) extends across the field area, roughly averaging 10 ft net pay thickness but ranging from 0 ft (center, south and west of the field) to 40 ft (Tirrawarra well 16). This unit is a braid plain deposit with belts of thinner and thicker net pay being a function of the channel-interchannel facies that characterize this flow unit. The net pay has low porosities and low water saturations with average So*phi values as high as 9.8 percent (Tirrawarra well 53) with most wells having values between 6.0 percent and 8.0 percent. Structurally lower wells have higher water saturations to give average So*phi values ranging between 5.0 percent and 6.0 percent. The HPV isopach (fig. VIII-13) is similar to the net pay

distribution but differing near the wedge edge, where higher water saturations impact on the HPV, and in the south east where several thin conglomerate beds improve reservoir characteristics. HPV values are irregular with most areas being between 0.5 and 2.6 (Tirrawarra well 16). Pay in this unit is in direct contact with pay in Flow unit 3U over central and northern parts of the field (fig. VIII-17). However, it is frequently divided into 2 or more isolated sand bodies separated by non-pay (fig. VIII-22). This flow unit reservoirs 24.2 MMSTB of OOIP.

Calculated OOIP and Distribution Summary

Using Stratamodel, OOIP was calculated for each flow unit over the field and each area (see fig. VIII-23). These are presented in table VIII-2.

Table VIII-2. Original Oil in Place By Flow Unit And Region.

Flow unit	North	South	West	Total OOIP (MMSTB)
4	11.950	8.949	3.322	24.230
2 UPPER	0.148	0.360	2.288	2.798
3 UPPER	23.166	24.378	17.160	64.700
3 LOWER	16.647	25.128	22.553	64.326
2 LOWER	1.327	3.696	0.901	5.924
1 UPPER	0.359	0.710	0.173	1.243
TOTAL OOIP	53.597	63.222	46.398	163.221

This represents an increase in OOIP of 36.051 MMSTB from the previous approved estimate of 127.17 MMSTB (HIP: 90/130—post Tirrawarra well 67) which is very similar to the current field OOIP estimate (123.3 MMSTB—post Tirrawarra well 70) stored in VULCAN (SANTOS volumetric software). This increase in OOIP is due to:

1. The inclusion of pay previously omitted from flow unit 4 due to the use of too high a porosity cutoff in the past (core data supports the reduction in porosity from 9 to 8 percent) (increase of approximately 15 MMSTB);
2. The recognition of the shalier flow unit 2L and finer grained flow unit 1U, requiring higher Vsh cut-offs for flow unit 2L and a higher Sw cutoff for unit 1U (increase of approximately 5 MMSTB).
3. The indication from core data that flow units 3L and 3U would contribute from rock with lower porosities requiring a reduction in porosity cutoff from 9 to 8 percent (increase of approximately 15 MMSTBO).
4. The inclusion of the wedge of OOIP located to the west of the main north–south fault and north of Tirrawarra well 59 (increase of approximately 10 MMSTBO).
5. The increase in Rw (decrease of approximately 10 MMSTBB).

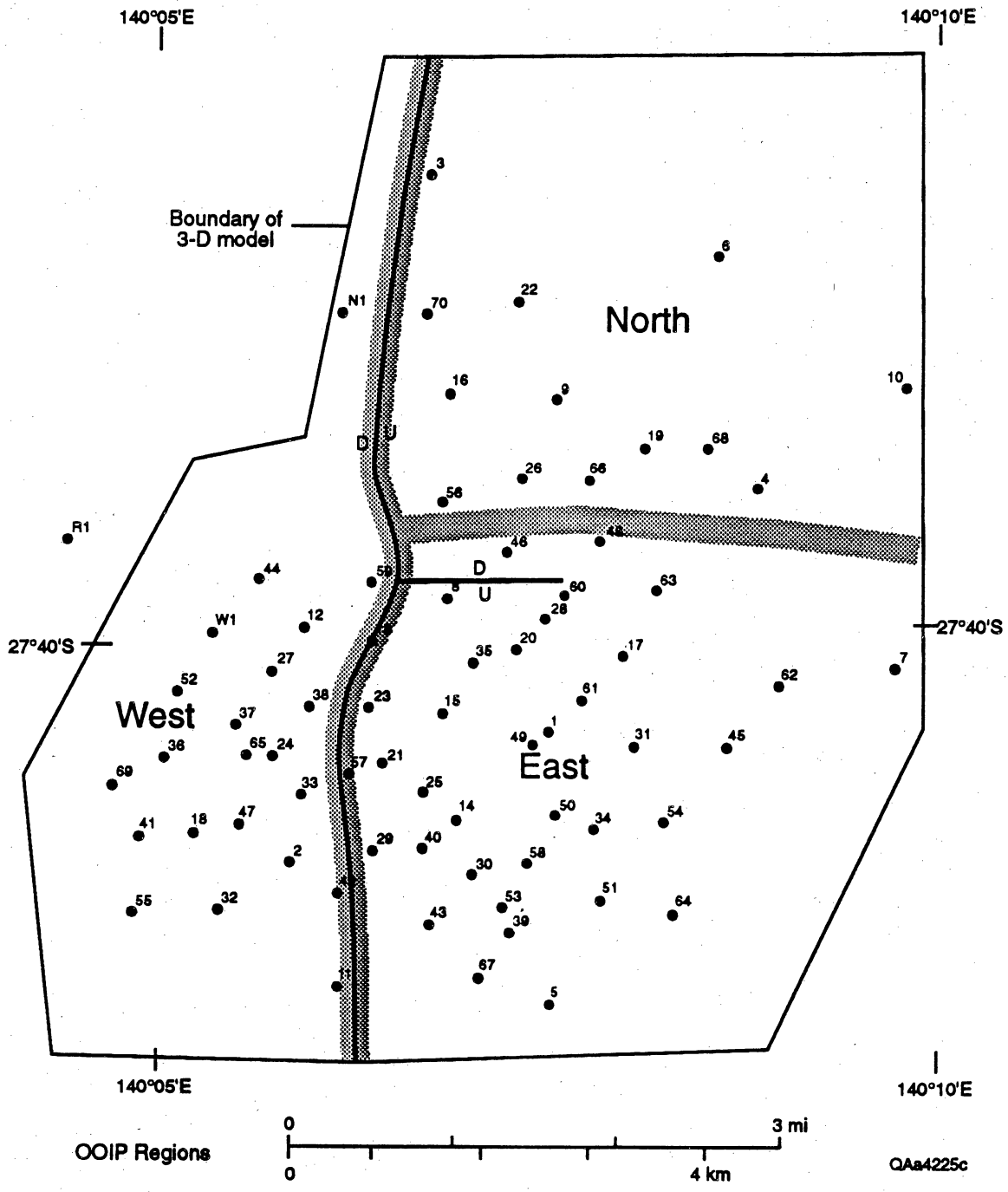

Figure VIII-23. Map showing regions used in OOIP calculations. See table VIII-2.

Note that the OOIP is reasonably evenly distributed between the three regions yet the northern area is virtually undeveloped. Further, flow unit 4 has been only partly developed but contains substantial OOIP.

IX. PRODUCTION ANALYSIS

Engineering Review

This review of the relevant available engineering data has been undertaken to confirm and refine the geologically derived reservoir description and to provide a basis for further engineering studies and projects. Engineering data provide valuable information on the reservoir quality, layering, preferred flow paths, stratigraphic heterogeneity, and structural partitioning by sealing faults within reservoir units, which can then be used to refine the geological model. Due to the low permeabilty of the Tirrawarra reservoir, two notable limitations were encountered in the engineering data:

a. the majority of Tirrawarra wells have been fracture stimulated in order to achieve commercial flow rates. This negates any tests on these wells to determine flow contribution (i.e. PLT) from each flow unit and significantly limits the layering input for this geological.
b. due to the low permeability, the radius of investigation of transient well tests is small and therefore such tests provide little information on boundaries, channel dimensions, layering, etc.

The engineering data used for this study have been divided into four sections for discussion:

1. Special core analysis (SCAL) Data
2. RFT/PLT results
3. Production data
4. Pattern performance

SCAL Data

The special core analysis data for Tirrawarra were obtained from 14 wells which provided good areal coverage of the field (fig. IX-1). The distribution of SCAL by flow unit showed a satisfactory coverage of flow units 3U and 3L and 4 but only limited data were available for flow units 2L, 2U, and 1U. Unfortunately, the core used for these SCAL tests had not been restored to its original in-situ conditions. Recent studies have shown that it is important to "soak" the core in actual reservoir oil and formation water to attempt to properly restore the true wettability of the core. It is unclear what effect this factor has on Tirrawarra core, but further SCAL work using these procedures has been planned. Major differences would only occur if the

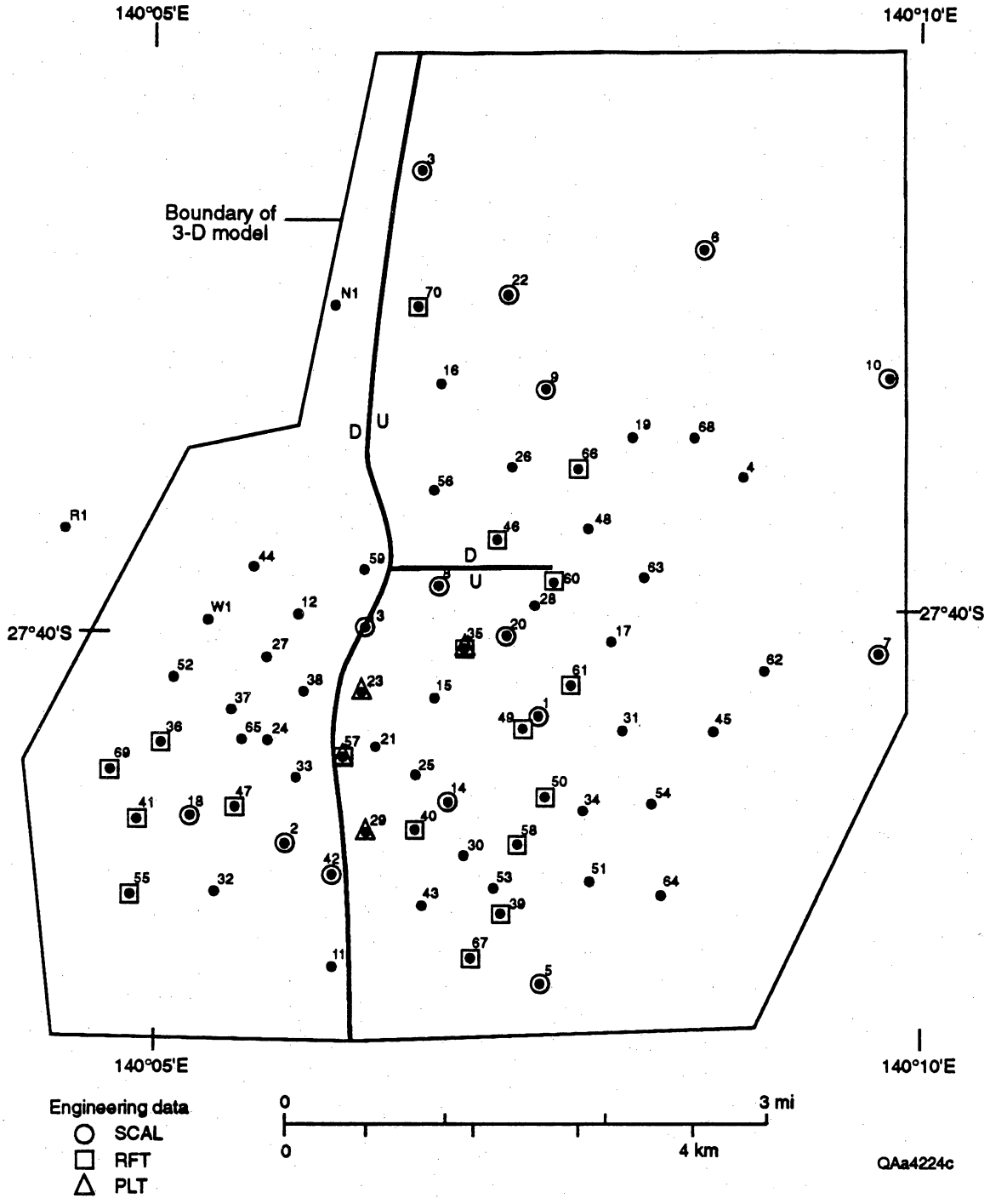

Figure IX-1. Map showing distribution of available engineering data.

Tirrawarra core was not strongly water wet which appears unlikely from the log analysis work (see Section VII).

Capillary Pressure

The capillary pressure data reviewed for this study are plotted in figure IX-2 as reservoir capillary pressure vs. water saturation and also plotted in Figure IX-3 as height above the free water level vs. water saturation.

The curves in figure IX-2 indicate a good relationship between capillary pressure and permeability and show consistency with capillary theory. Flow units are readily differentiated by the capillary pressure data. The curves which indicate the smaller transition zones are from flow unit 3L and 4 which represent the best reservoir quality rock. The poorer quality flow units such as flow unit 2 and 3U consistently show high transition zones. Flow unit 4 also shows considerable scatter between tests which is consistent with a variable quality channel sand.

Figure IX-3 shows that large transition zones occur in all flow units with zones of up to 300 ft in flow units 3L and 4 and flow units 3U and 2 may have transition zones of greater than 700 ft. These results indicate that water saturations in Tirrawarra are dependent on both the depth and the facies type. An example of this is shown in figure IX-3, where, at identical depths, flow unit 3L has an Sw of 22 percent while the poorer quality facies 2 has an Sw of 55 percent. This conforms with the water saturation results of the petrophysical analysis (Section VII) and the oil water contact analysis (Section VIII).

Figure IX-3 also highlights the difficulty in determing an OWC for the Tirrawarra field. If an OWC is defined by an Sw of 50%, figure IX-3 indicates that the OWC can vary by almost 600 ft.

Relative Permeability

Unlike the capillary pressure data, the relative permeability results are very scattered and show no grouping into flow units. Despite this scatter, two features are consistent throughout and are important to the behavior of the Tirrawarra reservoir (fig. IX-4):

- The relative permeability to oil shows a dramatic decline with increasing water saturation. For example, an increase in Sw from 30 to 40 percent relates to a drop in Kro of approximately 50 percent.
- The relative permeability to water does not increase above 0.1, indicating that water cannot easily flow through any of the Tirrawarra reservoir flow units.

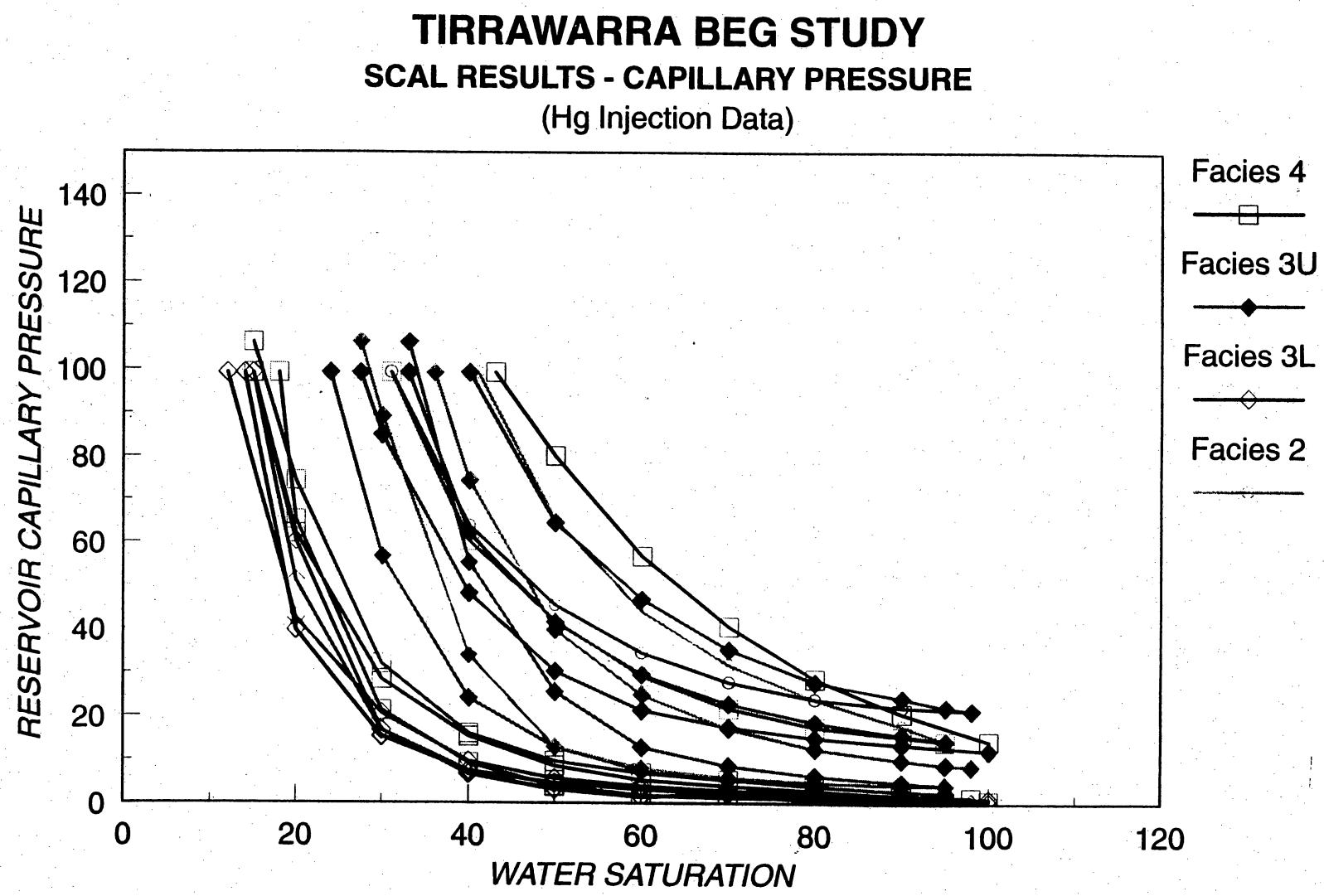

Figure IX-2. Graph showing capillary pressure versus water saturation at reservoir conditions for averaged Tirrawarra flow unit data.

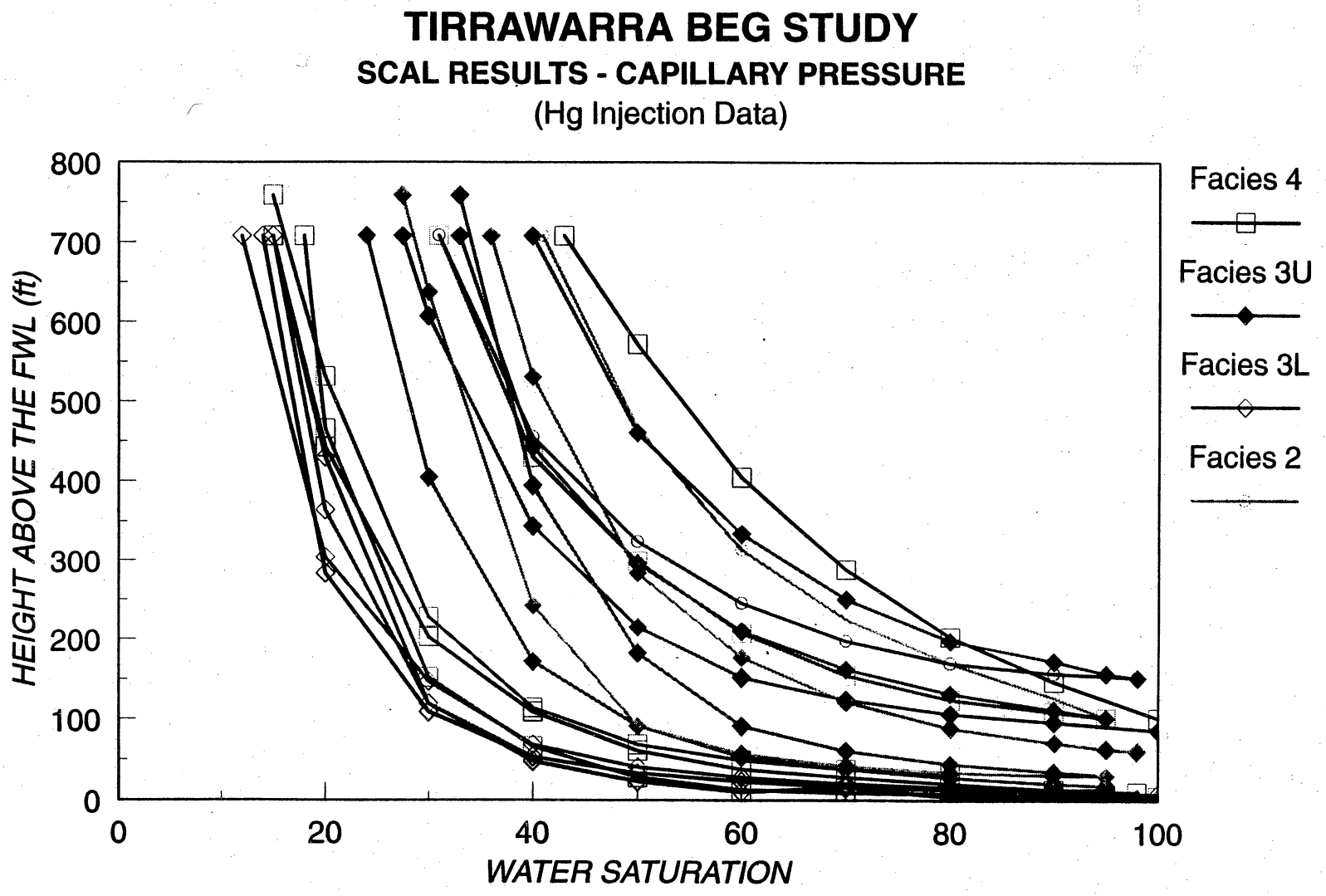

Figure IX-3. Graph showing height above the free-water level versus water saturation for averaged Tirrawarra flow unit data.

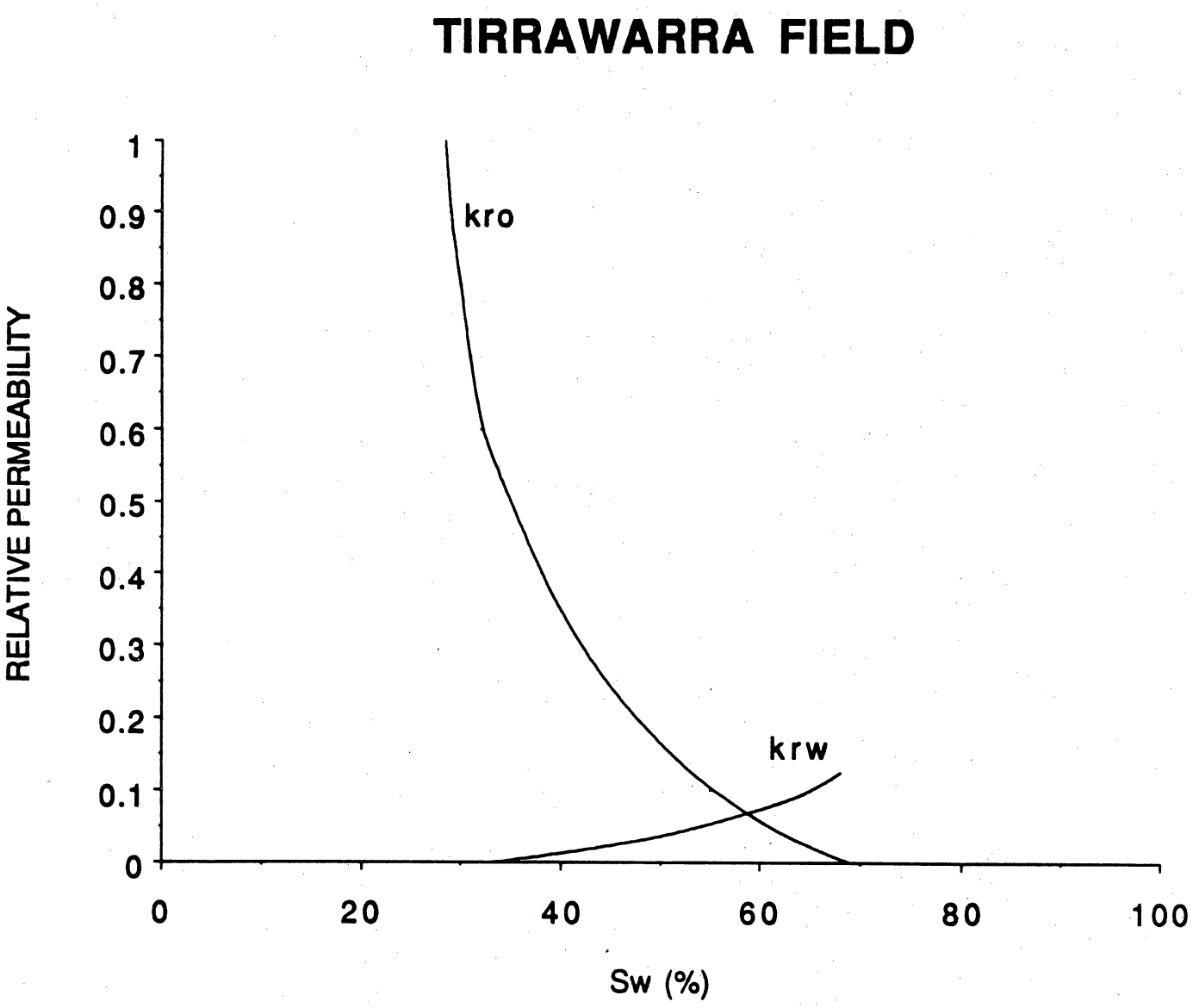

Figure IX-4. Graph showing average oil/water relative permeabilities for the Tirrawarra reservoir.

Both of these features are consistent with a strongly water wet system which, in the case of the Tirrawarra core, is a function of how the core was restored (as discussed above). If these curves are representative of the Tirrawarra reservoir, then small increases in water saturation will have a large effect on reservoir oil productivity. Wells that penetrate zones with water saturations greater than connate will have significantly poorer primary oil productivity compared with crestal wells. Water production in all off-structure wells should be minimal as the relative permeability to water always remains low.

RFT/PLT Results

Production logging tests (PLT's) have been performed on all unstimulated Tirrawarra wells, namely Tirrawarra wells 23, 29, 35, and 57 (fig. IX-1). These tests involve running a wireline spinner past the perforated intervals in order to determine the relative contribution of each flow unit. The test results on each of these wells were very similar and show that flow unit 3L dominates the production/injection behavior of the Tirrawarra EOR wells.

The PLT's in producers Tirrawarra wells 23, 35, 57 showed that, under normal operating conditions, flow unit 3L was the only unit contributing to flow. Under increased drawdown Tirrawarra wells 23 and 57 PLT's showed a minor contribution from flow unit 4. These results indicate that flow unit 3L is the only flow unit receiving any significant pressure support from the miscible flood. The fact that crossflow between flow units 3L and 4 had ceased after a shut-in period of only 3 hours indicated that flow unit 4 in Tirrawarra wells 23 and 57 is of limited extent. Facies interpretation of this unit (Section V) shows that it is composed of coalescing channels separated by fine grained interchannel deposits which result a degree of reservoir compartmentalization and thus is resistive to crossflow in this area. The PLT in Tirrawarra well 29 injector indicated that all injection gas was entering flow unit 3L.

The RFT data listed in table IX-1 gives an excellent spread of pressure data across the field. A total of 85 valid RFT points have been obtained from the Tirrawarra wells with the majority testing flow unit 3L. The data in the eastern and western sections of the field indicate that flow unit 3L is receiving good pressure support from the miscible flood. Data for the other flow units are sparse, but it should be noted that flow unit 4 has the highest depletion levels of any flow unit, indicating a lack of pressure support from the miscible flood but also that this facies has lateral connectivity between wells.

The RFT data also show local and partial vertical communication between the various flow units. Some wells indicate good vertical communication between flow units (3L and 2L in Tirrawarra well 50) (3U and 3L in Tirrawarra well 49), whereas others show areally extensive vertical barriers between the flow units (4 and 3U in Tirrawarra well 49), (3U and 3L in

Tirrawarra well 35), (4 and 3L in Tirrawarra well 41), (4 and 3L in Tirrawarra well 66). Most of these observations support the analysis of the net pay subdivision and the connectivity between pay in adjacent flow units (Section VIII). The Tirrawarra well 35 results are the only exception; however, a shale close to the 3U/3L boundary could explain the pressure difference.

Table IX-1. Tirrawarra RFT pressure results.

	Flow unit 4	Flow unit 3U	Flow unit 3L	Flow unit 2L
Eastern Area				
well 35	-	3566	3770	-
well 39	-	-	4303	-
well 40	-	-	3620	-
well 46	-	-	3975	-
well 49	3896	4040	4000	-
well 50	-	-	3930	3929
well 57	3507	-	3630	-
well 58	-	4170	3950	-
well 60	3910	-	-	-
well 61	-	3770	4250	-
well 67	-	-	4080	-
Western Area				
well 36	-	-	4270	-
well 41	3504	-	4220	-
well 47	-	-	3880	-
well 55	-	-	4000	-
well 69	-	-	4270	-
Northern Area				
well 66	3470	-	4210	-
well 70	-	-	4130	-
Average	3657	3886	4029	3929

Production Data

Production data for Tirrawarra field indicate that well productivity has a strong relationship to structural position. Crestal wells, such as those in the Tirrawarra well 15 pattern, represent the best producers in the field whereas wells drilled on the flanks of the field are significantly poorer. This feature is illustrated in figure IX-5, which is a contour map of initial oil production rates with the shaded area representing initial oil rates greater than 400 bbl/day (restricted to the crestal areas). There is a fairly smooth decline in well productivity with depth and contouring this initial rate data appears to mimic the top structure contours.

Poor well productivity in flank wells was previously explained by diminishing reservoir quality in the downdip regions of Tirrawarra field, particularly to the north due to some form of diagenesis. However, studies of reservoir stratigraphy, petrography, and petrophysics

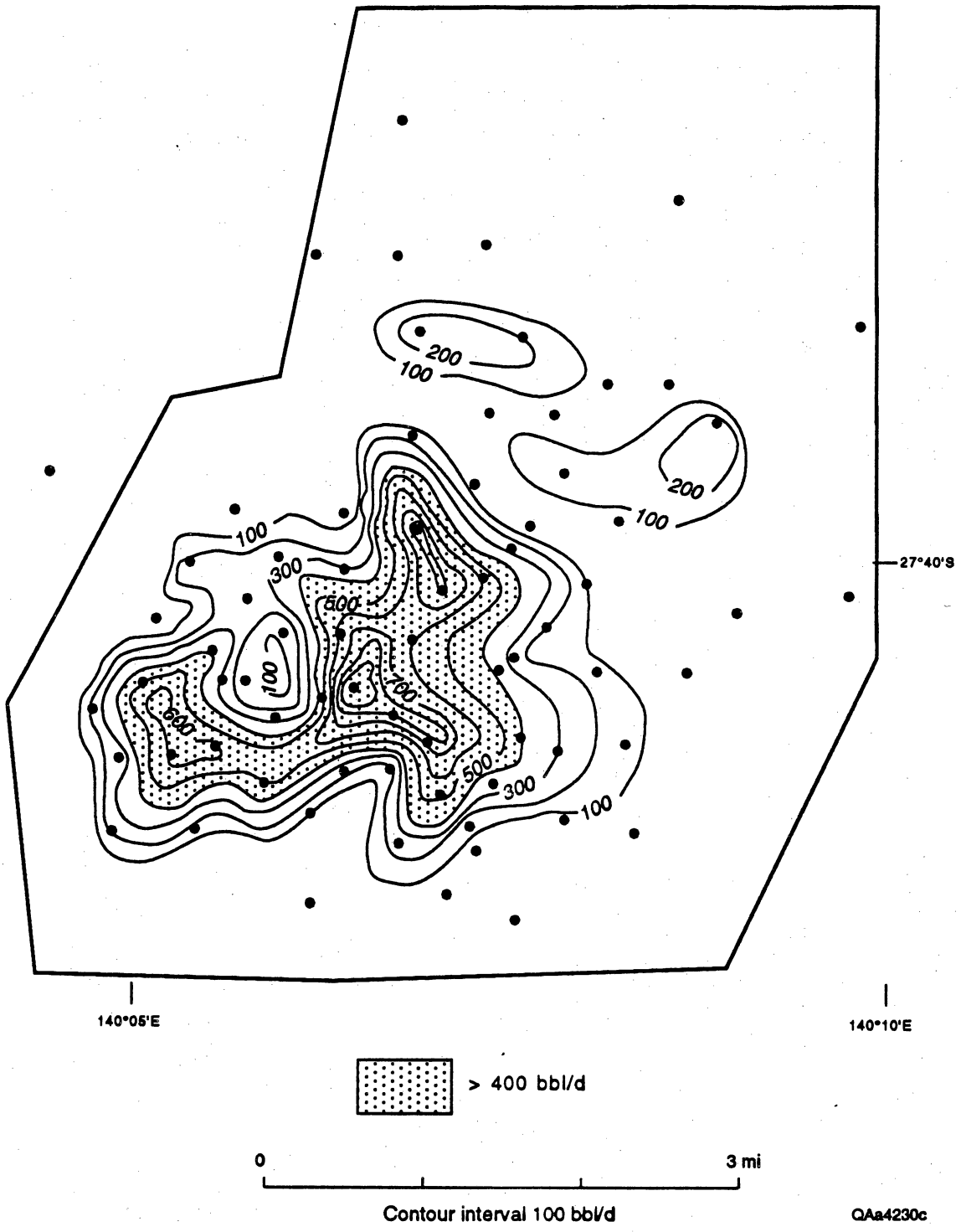

Figure IX-5. Contour map of initial oil production rates from Tirrawarra oil wells.

(Sections V, VI, and VII) did not reveal any systematic decrease in reservoir quality from the crest to the flanks of the field in any of the flow units. This is illustrated in the core data for Tirrawarra wells 4 and 8. Based on the summation of the raw foot by foot core permeability data, these wells should have similar flow capacities. However, the crestal Tirrawarra well 8 well had over three times the initial flow rate of the down dip Tirrawarra well 4 well. The explanation for this decrease in oil productivity off structure appears to be relative permeability. The capillary pressure data indicated that there is a large transition zone in all of the Tirrawarra flow units with substantial water saturation increases with depth. The relative permeability curves show a dramatic drop in oil permeability when water saturation increases above connate. Therefore, wells in the north of the field and off to the flanks of the EOR patterns appear to be affected by high water saturations and the resultant drop in oil productivity.

If this theory is correct, then there is significant scope for expanding the EOR Scheme into these areas. In northern Tirrawarra field, the development of new EOR patterns would have the following benefits:

- the reservoir oil contacted by the injection fluid (i.e., miscible bank) would have much improved mobility (by viscosity reduction) compared with original reservoir oil;
- ethane is capable of swelling oil by up to eight times its original volume at reservoir conditions. This swelling could change the saturation profile of the oil and water in the reservoir and may improve the relative permeability of the oil.

Expansion has been delayed in the past due to the perceived theory that this area contained reservoir of significantly poorer quality: an assumption that results of this project indicate may be erroneous.

Water production in Tirrawarra field is minor and only occurs in structurally low wells. Wells which have produced formation water have done so since initial production indicating that these wells either penetrated a mobile water zone (Tirrawarra wells 16 and 19) or the subsequent fracture stimulation accessed such a zone (Tirrawarra wells 4, 44, and 70). The fact that no other Tirrawarra wells have seen the onset of water production indicates that water influx in this reservoir is insignificant and water does not appear to be moving up high permeability channel sands (e.g. flow unit 4).

Wells which are affected by water production are the northern primary wells which do not have the pressure support to lift small quantities of produced formation water. Extending the EOR scheme to these wells should provide the necessary pressure support to lift this water.

Pattern Performance

One of the major engineering reviews was an analysis of the EOR patterns and how their performance relates to the geological description. Currently, there are eight EOR patterns covering large areas of the east and west sections of Tirrawarra field. Discussion is centered on the mature Tirrawarra wells 15, 18, 29, and 38 patterns due to the quantity of pattern performance, recycled gas cut information, and breakthrough times. Table IX-2 highlights the estimated recoveries of each pattern to December 1992.

Table IX-2. Pattern performance summary. (Production data to December 1992)

	Injection startup	OOIP (MMbbl)	Cumulative injection (BCF)	Cumulative production (MMbbl)	Recovery factor (percent)
EAST					
well 15	Feb. 1984	12.3	21.5	5.24	42.6
well 29	Jan. 1986	6.4	7.9	2.28	35.6
well 50	Jan. 1988	9.2	8.7	2.38	25.9
well 60	Dec. 1990	4.8	0.9	0.75	15.6
well 61	Mar. 1991	4.1	2.1	0.40	9.8
WEST					
well 18	Oct. 1985	9.5	11.6	3.47	36.5
well 38	Jan. 1986	5.0	8.1	1.49	29.8
well 52	Jan. 1992	2.5	0.2	0.27	10.8
TOTAL		53.8	61.0	16.28	30.3

In general, the performance of the mature Tirrawarra EOR patterns indicates fairly uniform reservoir properties with little evidence of the effects of heterogeneity, substantial tortuosity or sealing faults. While layering is discussed in more detail below, the uniform breakthrough in the mature patterns suggests that the miscible flood is dominated by a single interval and that high permeability channels such as in flow unit 4 are not contributing to the pattern performance. This is confirmed by the PLT data (discussed earlier) which show that flow unit 3L is the dominant layer in both the EOR injectors and producers. This uniform performance of the EOR patterns is consistent with the geological description of flow unit 3L which describes the associated facies as a broad continuous unit of consistently good quality reservoir. This flow unit has consistently high core permeability across the entire field.

To analyze pattern performance the production and injection volumes of each Tirrawarra EOR well was apportioned by pattern. While the injection allocation was straight forward, the allocation of production was determined using pattern geometry, well performance (especially GOR and oil rate), radioactive tracer trends, response to gas injection and consideration of the

general field development history. It is important to bear in mind that the EOR pattern performance comparisons discussed below are dependent on these allocation factors.

Figure IX-6 is a plot of cumulative oil production since injection start-up versus cumulative solvent injected both on a displaceable pore volume (DPV) basis. This plot gives an indication of the EOR pattern response to the injection gas. The results show very similar trends for the Tirrawarra wells 15, 18, and 29 patterns. The responses of the Tirrawarra wells 38 and 50 patterns are poorer and appear to reflect the production and injection imbalances in these patterns and is not a geological response. The recent patterns (Tirrawarra wells 52, 60, and 61) all appear to be tracking the high performing patterns although data are limited. Another plot which helps compare the pattern performance is figure IX-7 which is a plot of cumulative solvent produced versus cumulative solvent injected. This plot shows almost identical behavior for each of the EOR patterns with the exception of Tirrawarra 38, which again appears to be adversely affected by over-injection. The similarity in pattern performance in both these figures shows that the sweep efficiency for each pattern is almost identical and that the geology in these areas of the field is very uniform. Following is a brief performance summary of each of the major EOR patterns:

Tirrawarra No. 15 Pattern

This pattern is the most mature of the EOR patterns and to date is the best performer with a recovery factor to December, 1992 of 42.6 percent. This pattern covers the main crestal area of the eastern part of the field. The pattern incorporates the four best oil producers in the field (Tirrawarra wells 8, 14, 20, and 21) and a total of 5.24 MMbbl production has been allocated to this pattern.

All producers in this pattern have had injection gas breakthrough and the pattern's oil rate is in decline as a result of increasing GOR. The time to breakthrough is strongly related to well productivity with Tirrawarra well 21 being the first to produce recycled gas followed by Tirrawarra wells 8 and 20. An interesting feature of this pattern is that the cumulative oil production of each well at the time of breakthrough was very similar (110, 000 +/- 15,000 cubic meters) indicating uniform sweep and is further evidence of the homogenous nature of flow unit 3L geology in these EOR patterns (fig. IX-8).

The recovery factor for this pattern to date indicates that the volumetric sweep efficiency is high. The consistent breakthrough times and smooth nature of the recycled gas production indicates uniform sweep of a single layer. In terms of vertical sweep, the PLT data indicates that flow unit 3L is the main contributor to injection and production in the EOR areas. However, the OOIP for this unit in the Tirrawarra well 15 pattern is 6.7 MMbbl resulting in a recovery

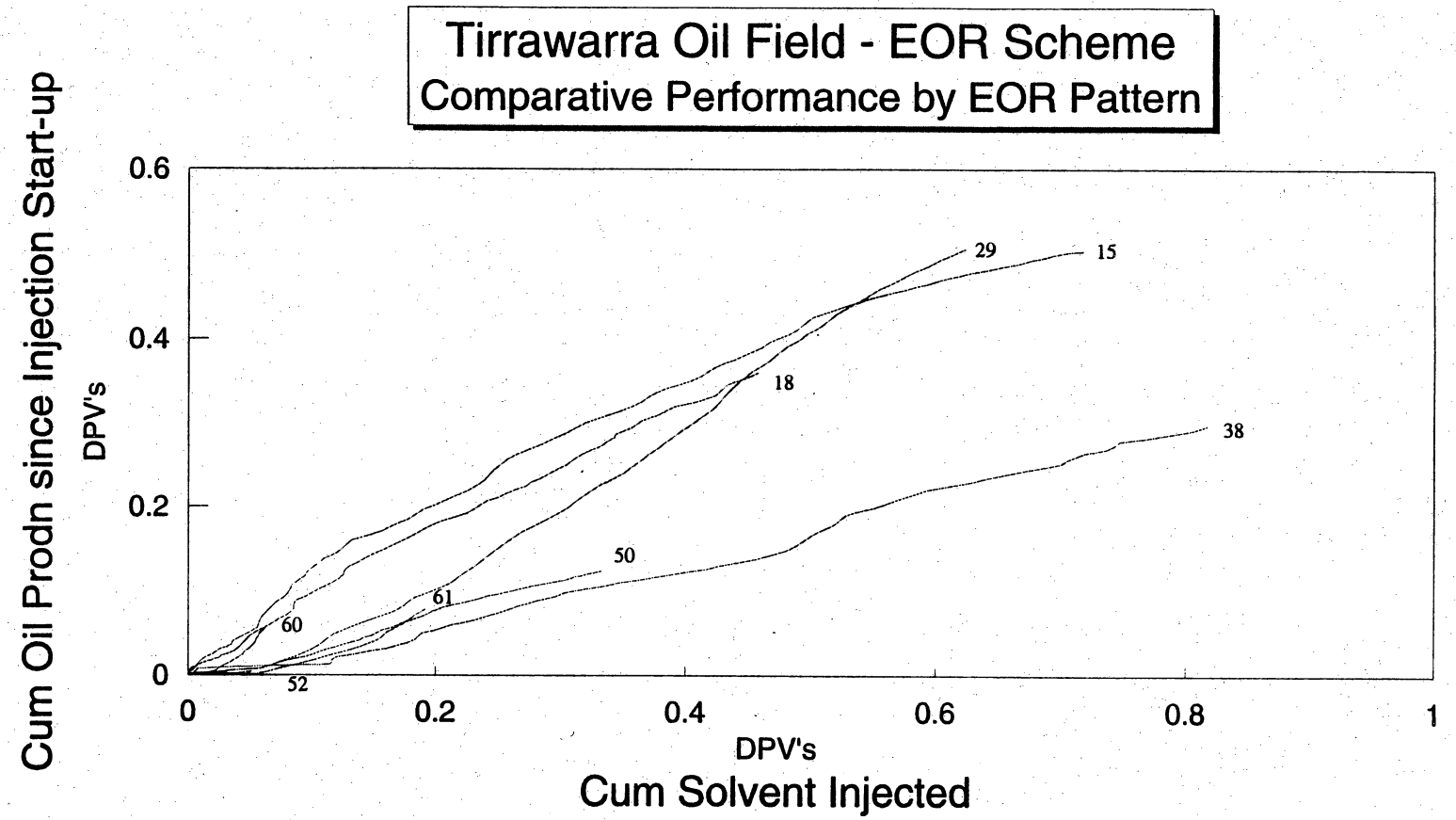

Figure IX-6. Graph of cumulative oil production since injection start-up versus cumulative solvent injected, both on a displaceable pore volume (DPV) basis, for the Tirrawarra EOR patterns.

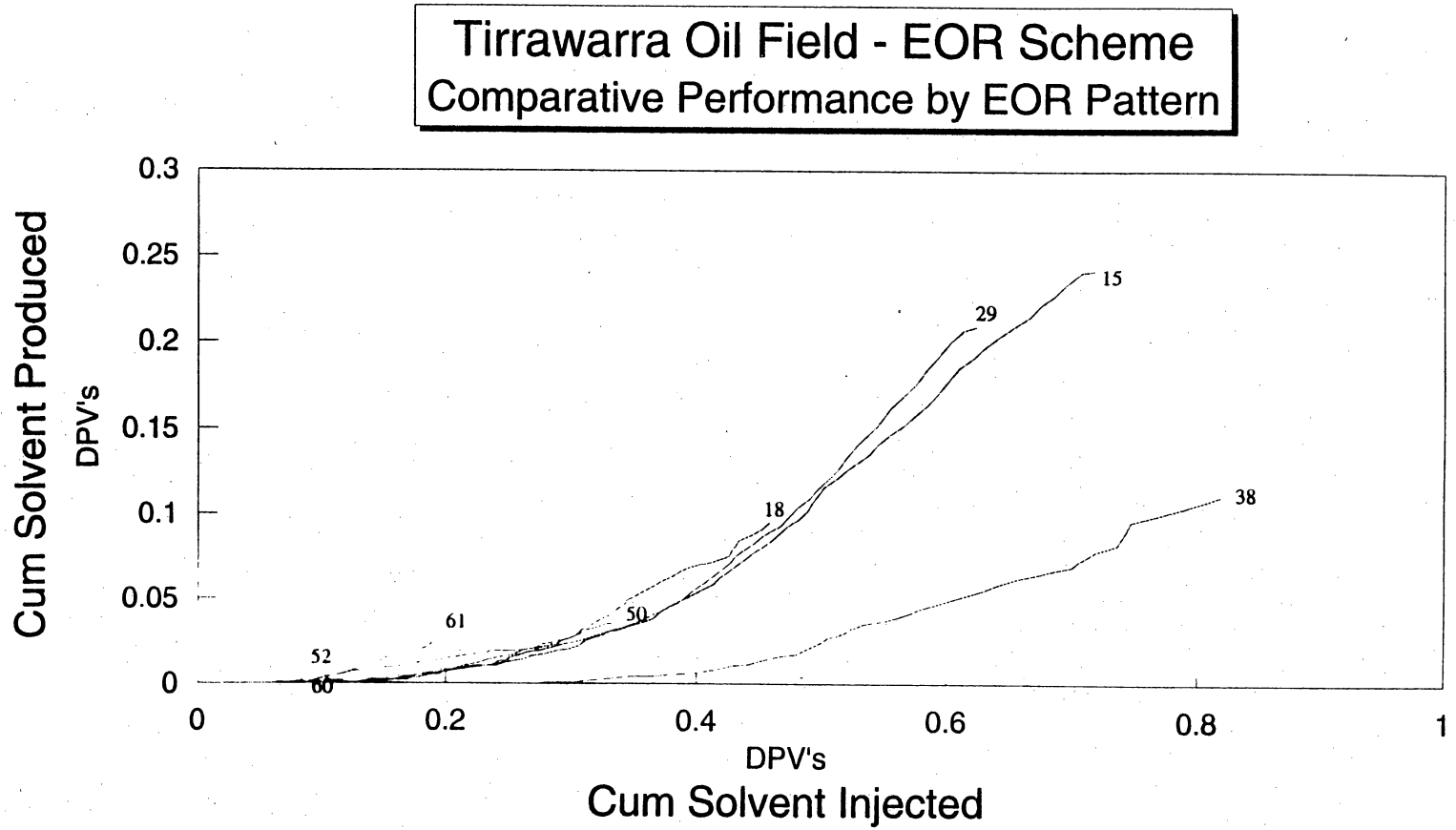

Figure IX-7. Graph of cumulative solvent produced versus cumulative solvent injected for the Tirrawarra EOR patterns.

factor (to December 1992) of almost 80 percent if this flow unit was the sole contributor. This high recovery factor suggests other facies may be contributing. One theory which explains the PLT results is vertical crossflow between layers. Due to the density of the injection gas, this fluid tends to gravity override the oil and travel along the top of flow unit 3L. This allows the injection gas to contact and increase the mobility of the oil in flow unit 3U. This altered reservoir fluid can either flow along flow unit 3U, or flow down into the productive 3L unit. Therefore, any flow unit 3U oil in vertical communication with flow unit 3L could be accessed by the miscible flood. It is unlikely that flow units 1U, 2L, 2U, and 4 are significant contributors to the EOR scheme due to their poor vertical connectivity with flow unit 3L. If this recovery mechanism is correct then potential exists to shut-in these EOR patterns prior to blowdown to allow this transfer of miscible gas into the low productivity units. This crossflow of oil between flow units is expected to occur in all the EOR patterns.

While the recovery factor of this pattern is high, there is potential to improve areal sweep by recompletion of Tirrawarra well 25. Tirrawarra 23 has recently been recompleted from a Patchawarra gas well to test the economical viability of such wells and is currently producing oil at 250 bbl/d. Gas breakthrough has just occurred here but there has been significant production to date and more is expected. Tirrawarra 25 offers similar potential.

Tirrawarra No. 18 Pattern

This pattern is also a good performer with a recovery factor to December 1992 of 36.5 percent. This pattern covers both crestal (Tirrawarra wells 36, 65, 33, and 2) and flank areas (Tirrawarra wells 55 and 32) of the western section of the field. All producing wells in this pattern have broken through and the gradually increasing pattern GOR has seen a steady decline in oil rate in recent years. Cumulative oil production to breakthrough for the Tirrawarra well 18 pattern (fig. IX-8) shows some relation to structure with the flank producers (Tirrawarra wells 55 and 32) breaking through at lower volumes than the up-structure wells (40,000 cubic meters compared with 70,000–90,000 cubic meters). This is most likely some form of relative permeability effect on flank sweep efficiency. This feature is important in understanding the performance of EOR patterns in the north which are expected to have similar relative permeability problems due to the high water saturations in this area. Tirrawarra well 41's early breakthrough is probably a result of being drilled too close to the injection well along sedimentological trend. Due to the considerable oil in place in the flanks expansion of this pattern may prove viable.

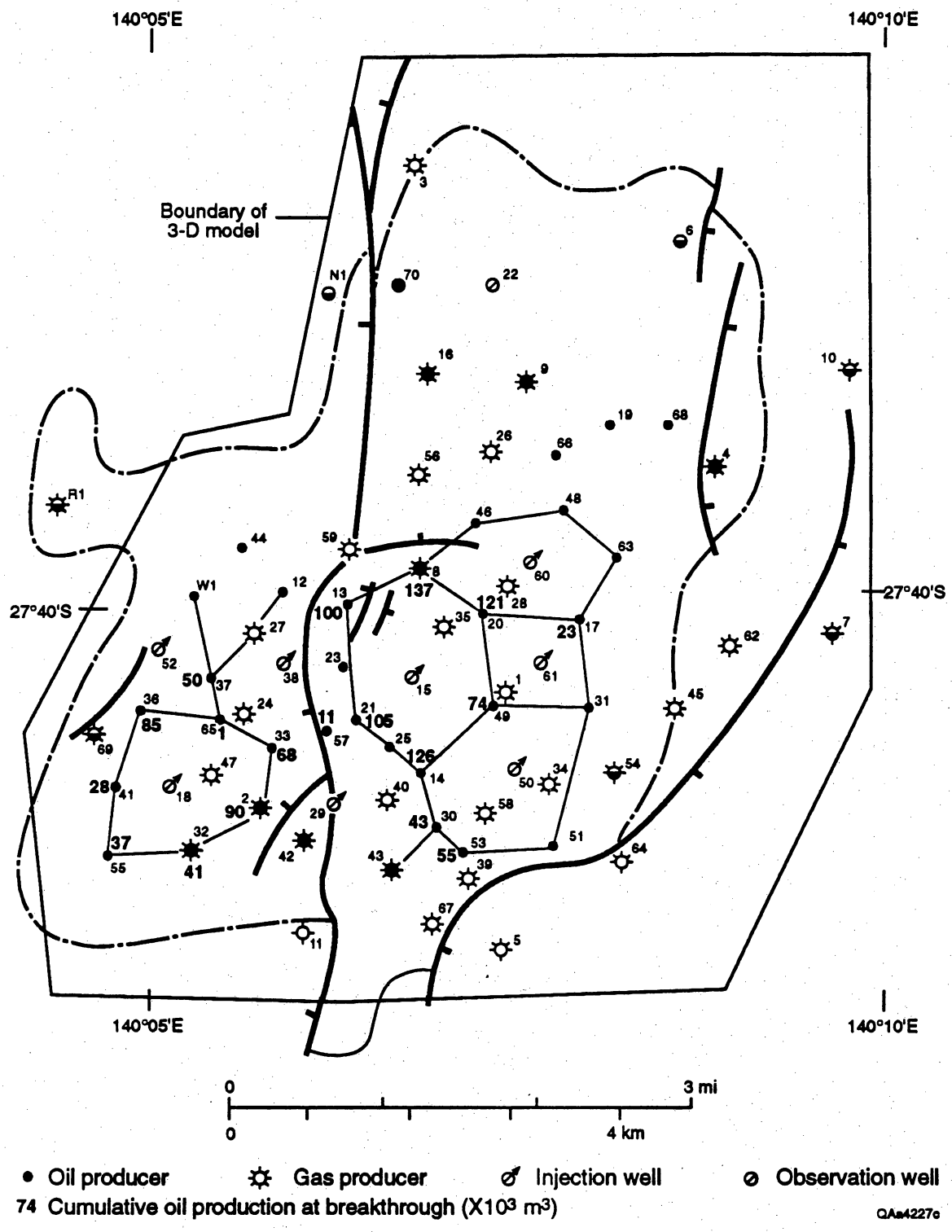

Figure IX-8. Map of Tirrawarra field showing cumulative oil production to breakthrough.

Tirrawarra No. 29 Pattern

This "half" pattern has a recovery factor of 35.6 percent to December 1992. The surrounding wells experience good pressure support from the injector with Tirrawarra well 43 the only well which has not broken through. The cumulative production to breakthrough of Tirrawarra well 30, the only well whose breakthrough can be solely attributed to Tirrawarra 29, is consistent with the flank wells in the Tirrawarra well 18 pattern.

Tirrawarra No. 38 Pattern

This "half" pattern is the worst performer of the mature patterns with a recovery factor of 29.8 percent to December 1992. Reasons for this poor performance may be as follows:

(i) inefficient pattern layout with only one well north of the injector
(ii) over injection into this pattern resulting in poor volumetric sweep efficiency
(iii) pattern shape may have allowed injection gas to be drawn outside the pattern boundaries (i.e., toward Tirrawarra West 1).

The volumetric sweep of this pattern may be improved by reducing injection rates and by drilling an infill well in a location northwest of Tirrawarra well 27. The new fault interpretation has resulted in potential infill well locations in the east of this pattern. Productivity in this area should be high and should improve the recovery of this pattern.

Tirrawarra Nos. 50, 60, and 61 Patterns

These recent patterns do not have sufficient data to discuss in detail. Following is a brief discussion of some specific features of these patterns;

- the recovery factor in the Tirrawarra well 50 pattern is not expected to be high due to the production imbalance. Because of the lower productivity of flank wells, disproportionately low offtakes have occurred from the eastern part of this pattern.
- the sweep efficiency in the Tirrawarra well 50 pattern could be improved by the completion and fracture stimulation of Tirrawarra well 54. This well appears to be similar in reservoir quality to Tirrawarra well 51 but an adverse DST result (which incorporated a separate deeper water wet sand) resulted in this well remaining cased and suspended.
- the early breakthrough of Tirrawarra well 17 is probably a result of this well being too close to the Tirrawarra well 61 injector.

- areal sweep efficiency in the Tirrawarra well 61 would be improved by locating an infill well east of Tirrawarra wells 17 and 31.
- the Tirrawarra well 60 pattern will require modification as flow unit 3L in the injector is almost completed shaled out making the well a very poor injector. As a result, pressure support at adjacent wells is limited. One option in this area is to inject into Tirrawarra well 48 which would create an 'extended' pattern at low cost which could also provide pressure support to the northern primary wells some of which have water loading problems.

Permeability Analysis

Permeability Calculation

The generation of foot-by-foot permeability values for each well in Tirrawarra field was based on the permeability versus porosity crossplots discussed in Sections V and VII. These flow unit-specific equations were used to generate the ambient permeability data from the log analysis derived porosity values and then a correction from ambient to in situ permeability was made using the following equation:

$$K_{\text{in situ}} = \frac{K_{air}^{1.33}}{6.6}$$

This equation was based on Cooper Basin-wide core measurements as there was not sufficient data to develop a field or flow unit specific equation. The foot-by-foot in situ permeabilities were then summed, for pay only, to give the overall well flow capacity (kh) for each Tirrawarra well. The final flow capacity of each well and its comparison with pre-frac test kh data is shown in table IX-3. The predicted well flow capacity for each well was then scaled up or down to match the pre-frac test results. The scaling factors applied to each well indicate that the cross plots are fairly accurate at predicting well flow capacity with an average scale up of 1.73.

Table IX-3. Comparison between well log and production test-derived flow capacity.

Well no.	Actual test kh	Log well kh	Scaling factor
2	59	65	0.9077
4	33	33	1.0000
8	206	51	4.0392
9	27	154	0.1753
12	24	14	1.7143
13	48	31	1.5484
14	74	22	3.3636
15	31	30	1.0333
16	318	24	7.7917
17	12	8	1.5000
18	29	28	1.0357
19	3.6	28	0.1286
20	37.4	22	1.7000
21	148	22	6.7273
30	16	16	1.0000
31	1.0	11	0.0909
32	24	13	1.8462
33	18	18	1.0000
34	78	22	3.5455
37	11	11	1.0000
38	42	12	3.5000
41	48	23	2.0870
42	6.7	9	0.7444
43	23	14	1.6429
44	2	11	0.1818
48	34	16	2.1250
50	15	28	0.5357
51	4	13	0.3077
53	11	20	0.5500
55	14	28	0.5000
60	26	8	3.2500
65	10	14	0.7143
	44.8	25.9	

Average scaling factor = 1.7902 R^2 = 1.8

A consistent trend was noted during the scaling process with crestal wells requiring up-scaling by as much as 7 fold (Tirrawarra well 16) and the flank wells requiring down-scaling by as much as 5 fold (Tirrawarra well 44). This trend conforms with the relative permeability data by showing suppression of the test flow capacity in flank wells. A map of the scaling factor of each well across the field (fig. IX-9) reinforces the observed relationship between relative permeability and the flow capacity of Tirrawarra wells. Scaling factors for wells without test data were developed by taking an average of the scaling factors for nearby wells. The well scaling factor was then applied to each flow unit in the well, and flow capacity maps for each flow unit were generated.

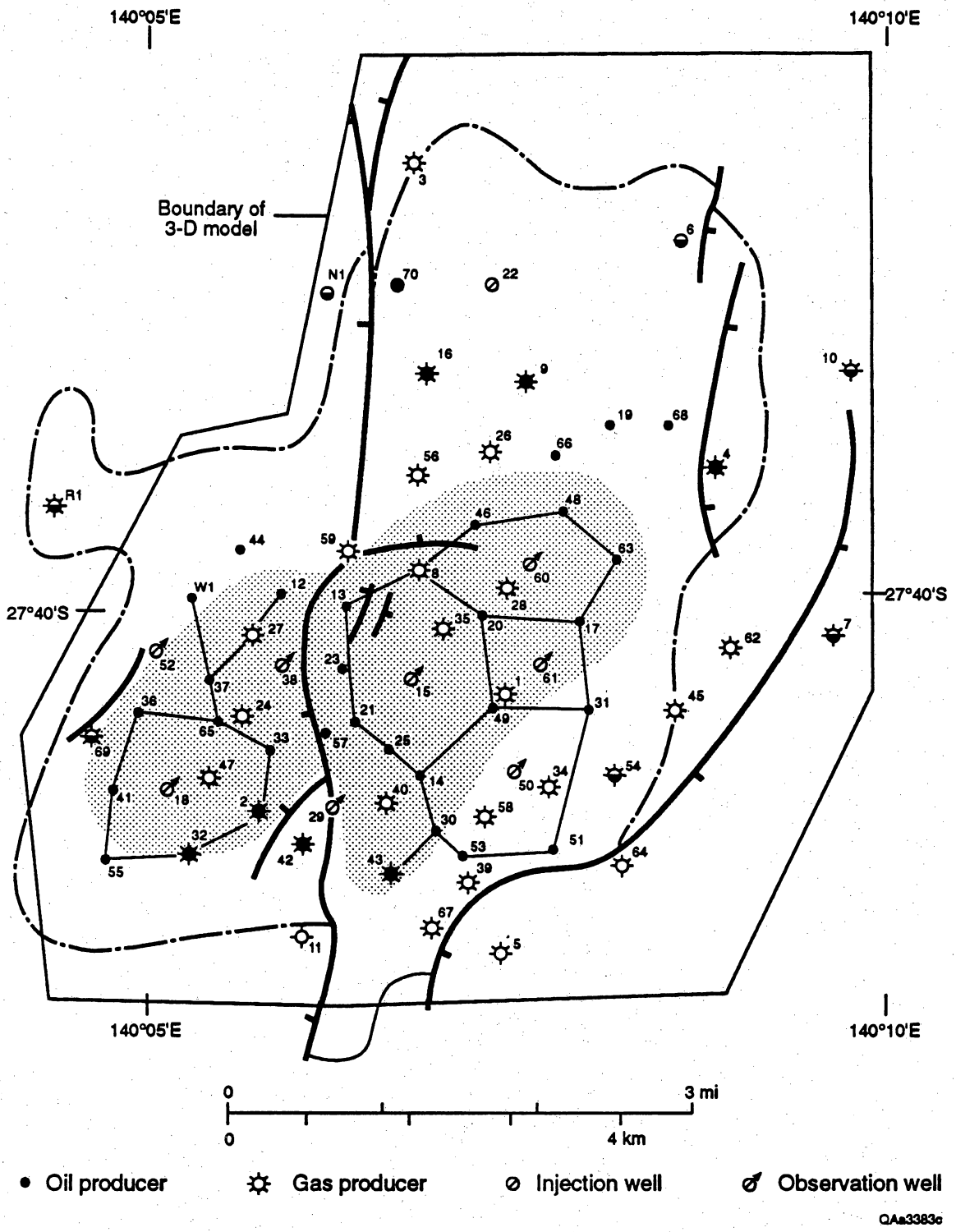

Figure IX-9. Map of Tirrawarra field showing existing EOR patterns and scaling factors. Areas where log-derived kh values were increased (scaled up) to match well test data are shaded. In unshaded areas, log-derived kh values were scaled down to match well test data.

Two areas of the field showed specific problems with the flow capacity scaling procedure. In the southeast, high calculated flow capacities corresponded to low performance based results. This was due to gravel beds at the base of flow unit 4 in this area, which, due to their high log porosities, resulted in abnormally high calculated permeabilities. DST results over these zones showed little productivity and so the flow capacities were down graded accordingly. The crestal well in the north of the field, Tirrawarra well 9, has a high calculated kh (154 md) but a low performance based kh (27 md), requiring down scaling by a factor of 5.7. The lower value was used, but concerns remain as this scaling factor has influenced the scaling factor used on an adjacent uncored well.

Due to the obvious relationship between relative permeability and the scaling factor, it was questionable as to whether flow capacity maps should be based on the unscaled or scaled data. For this study the scaled data were used because these maps give a direct indication of true oil productivity in any area of the field. For a simulation study where relative permeability is an input parameter, it would be logical to use the unscaled data and let the relative permeability curves determine reservoir productivity.

Permeability Distribution

The rough coincidence among net porous sandstone trends, hydrocarbon pore volume mapping, and permeability-thickness trends documents the influence of depositional setting on permeability distribution. Porosity and permeability have been reduced by postdepositional diagenesis, but those sandstones deposited in the highest energy environments retain the best reservoir quality (see Section VI). Permeability related to natural fractures and faults may contribute to reservoir transmissivity, but a good correlation between high core permeabilities and high permeability-thicknesses suggests that "matrix" permeability (not fracture permeability) controls fluid flow. The exception to this (apart from the influence of the scaling of the kh data which highlights the relative permeability effects) is the high permeability thickness (kh) trend, on the upside, and adjacent to, the main north-south fault which persists for each flow unit. This trend is interrupted by Tirrawarra 13 for most flow units and 23 for flow unit 4 only. The values at these wells, are reduced due to the faulting out of some flow units.

Although no structural influence was interpreted during the facies description (Section V) this north-south kh trend on the upside, and adjacent to, the main north-south fault and the isopach thinning of the reservoir section coinciding with this trend (fig. III-5) suggest that structure influenced reservoir quality. Ambient core permeability data show that although high kh wells have some very thin high permeability zones, the bulk of the permeability values are greater than 1 md in the better quality 3L and 4 flow units, whereas lower kh wells have the

bulk of the permeability in these flow units, close to, or below, 1 md. As "matrix" permeability controls fluid flow, structure must have influenced depositional energy to give this effect.

Permeability development in flow unit 1U is poor because of (1) low wave and current energies in the lacustrine nearshore environment where facies 1 delta-front siltstone and sandstone were deposited and (2) local erosional truncation of this flow unit. Porous sandstone in flow unit 1U is 0 to 5 ft thick in isolated pods (fig. V-29), and permeability-thickness (kh), which is developed only within those pods, is 0 to 2.6 md-ft (fig. V-30). Studies of core and well logs indicate that flow unit 1U displays an upward-coarsening/cleaning profile, reflecting gradual shoaling within the delta-front environment and that this profile in unit 1U is best developed in those wells having measurable kh.

In flow unit 2L, permeability-thickness trends closely coincide with the distribution limits of this flow unit (figs. V-32 and V-33). The net sandstone trends delineate the deltaic distributary channels and channel mouth bars where most of the sandstone in unit 2L was deposited. The highest kh values in unit 2L (1 to 10 md-ft) lie within the sinuous channel belts that dominate most of Tirrawarra field. Lobate channel mouth bar sandstones in the southeast part of the field have lower kh values (less than 2 md-ft) (fig. V-33), even though the net porous value there is higher (fig. V-32). Although both the distributary channel and channel mouth bar sandstones contain mud clasts and organic debris, which lower porosity and permeability generally, only the channel-fill sandstones include permeable lenses of conglomeratic sandstone and facies 3-type clean sandstone. These discontinuous lenses, which formed as channel-base lag deposits or in braided channel reaches where flow unit 2L grades laterally into flow unit 3L, represent the most favorable targets for increasing production from flow unit 2L. They are located within the sinuous channel belts delineated on the net porous sandstone map (fig. V-32).

Flow unit 2U has a composition and genesis similar to those of flow unit 2L but contains little permeable sandstone. Flow unit 2U is present only along the south and west margins of the field (fig. V-40) and includes isolated porous sandstone only in a few wells in the southwest (fig. V-41). A small amount of kh was measured in several of these wells (fig. V-42). Apparently, flow unit 2U is dominated by fine-grained interchannel and lake-margin deposits within the confines of Tirrawarra field. This unit is unlikely to contribute to productivity due to its low permeability and its isolation from pay in other flow units.

Although facies 3 forms a continuous sheet of sandstone across Tirrawarra field, permeability distribution in flow units 3L and 3U is complex. Permeability-thickness trends (figs. V-38 and V-39) coincide with the high side of the north-south fault and display only an approximate coincidence with net porous sandstone trends (figs. V-36 and V-37). In many wells having below-average thickness of porous sandstone in flow unit 3L (well 21, for example), core

permeabilities are consistently above average, and the resulting kh is high. Core data also show that layers having permeabilities greater than 50 md are generally less than 3 ft thick and are relatively rare. In well 8, for example, which includes several of these high-permeability thin beds, flow unit 3L has a high kh (fig. V-38) even though porous sandstone is relatively thin (fig. V-36).

The flow unit 3 bed-load fluvial system is laterally continuous and sandstone-dominated, and so good permeabilities are widespread. Production data suggest that flow unit 3L is the main conduit for the miscible flood and the main contributor to oil production. In flow unit 3L, kh ranges between 10 and 100 md-ft across most of Tirrawarra field (fig. V-38), and in flow unit 3U, the kh range is 5 to 20 md-ft across most of the field (fig. V-39). Greater preservation of fine-grained interchannel deposits in unit 3U accounts for generally lower kh and less production there. The internal permeability variability noted above, however, results from the lateral discontinuity of the many depositional elements that compose this fluvial system. These depositional elements are channel-fill sandstones and remnant interchannel mudstones that are coalesced laterally and vertically (fig. V-7). Each of these elements forms a reservoir compartment having a particular permeability, although flow barriers between compartments are discontinuous, and therefore intercommunication is probably good.

Permeability distribution is even more heterogeneous in flow unit 4 than it is in flow units 3L and 3U. Flow unit 4 is composed of a variety of fluvial channel types: laterally continuous bed-load channels in the lower part and more isolated mixed-load channels in the upper part. Permeability interconnectivity, therefore, decreases upward in unit 4. Interchannel mudstones and coals are more widespread and form more effective flow barriers in flow unit 4 relative to flow unit 3. Because of this greater isolation of individual channel sandstones, net porous sandstone and permeability-thickness are greatest where channels stack vertically. Superimposed channel sandstones form well-defined belts on isopach, porous sandstone, and kh maps (compare figs. V-43, V-44, and V-45). Within these belts, flow unit 4 is 30 to 60 ft thick, net porous sandstone is 10 to 40 ft, and kh is best developed, reaching 20 to 50 md-ft locally. Thin high-permeability compartments similar to those in flow units 3L and 3U also influence kh trends in flow unit 4. In the southeast part of the field, for example, several wells intersect permeable lenses of sandstone and conglomerate, 3 to 15 ft thick. Although these lenses are interpreted to be laterally discontinuous, they are best developed within the channel belts. If an injector/producer pair access such a lens, channeling of the injected gas is a likely result. The current pattern of EOR injection wells relative to permeability distribution in flow unit 4 suggests that productive zones in this unit may have been largely bypassed by the miscible flood.

The broadest permeability distribution is displayed by flow unit 3L which also has the highest widespread kh values with only flank areas in the east and north-west displaying kh's below 5 md ft. This Flow Unit is therefore interpreted to be the major contributor to oil production for the field.

Due to their poor kh development and distribution, flow units 2U, 2L, and 1U are not interpreted to be significant contributors to production.

Productivity from flow unit 4 may prove to be substantial in areas where it is well developed, but has yet to be demonstrated.

Production Allocation by kh

The assessment of the distribution of remaining oil in place by area and by flow unit required the allocation of cumulative well production into the various flow units. Because only total well production data are available for the Tirrawarra field, the production volumes were allocated to each flow unit on the basis of relative flow capacity. For example, if the flow capacity of flow unit 4 in Tirrawarra 8 was 40% of the total well flow capacity, then flow unit 4 was assigned 40% of the well's production.

The fact that cumulative production is assigned to the various flow units solely on the basis of individual flow capacity means that the results of this work can be misleading, particularly in the EOR patterns. The assumption may be applied with some accuracy to a field undergoing primary depletion where all layers are isolated and drain similar areas. For an EOR scheme such as Tirrawarra where the field is multilayered the method is deficient because it is undergoing pressure maintenance from injectors which came on line at varying times and only support certain flow units. Apart from the geological and operational aspects, the Tirrawarra EOR scheme is a miscible flood were factors such as oil swelling, gravity override, and viscous fingering play an important part in the recovery mechanism. For the northern primary wells, the method is also deficient due to the vertical communication between the various flow units. Therefore, while these methods have been utilised for this geological study, a better approach would be to utilise reservoir simulation.

The implications of applying this method to the Tirrawarra EOR pattern areas are as follows:

(a) Flow unit 3L will not be allocated sufficient cumulative production. This flow unit is the dominant facies in the Tirrawarra Field and is the main conduit for the miscible flood.

(b) Flow unit 4 has good permeability, but the interconnecting channels composing this unit are often partly isolated by interchannel mud rock. Applying the allocation purely on the basis of kh means that there will be too much production allocated to this flow unit.

(c) Facies 3U shows moderate kh values yet the engineering data available showed no evidence of contribution from this sand. It is likely that this unit will have an inflated production allocation unless there is significant vertical crossflow.

Remaining Oil in Place

The production allocation results using the kh-apportion method are detailed in Table IX-4 by flow unit across the entire field and in Table IX-5 by area and by flow unit. The cumulative production data is to December 1992.

Table IX-4. Aggregate Tirrawarra volumetrics.

Flow unit	OOIP (MMbbl)	Cumulative Production (MMbbl)	Percent	Remaining Oil (MMbbl)	Percent
4	24.1	2.3	13.4	21.8	14.9
2U	2.8	0.0	-	2.8	1.9
3U	64.8	3.2	18.6	61.6	42.2
3L	64.3	11.4	66.3	52.9	36.2
2L	5.9	0.3	1.7	5.6	3.8
1U	1.3	0.0	-	1.3	1.0
Total	163.2	17.2		146.0	

Of the 163 MMbbl of oil in the Tirrawarra Field, the vast bulk (129 MMbbl) is contained in flow units 3U and 3L. Recovery as of December 1992 totalled 17.4 MMbbl or 10.7 percent. Flow unit 3L accounts for two-thirds of this production (using the kh-allocation method). Flow units 3U and 4 account for 3.2 and 2.3 MMbbl, respectively. Unrecovered oil amounts to 146 MMbbl, and three flow units account for 93 percent of the remaining volumes. Flow units 3L, 3U, and 4 contain more than 136 MMbbl; however, the primary location of the remaining resource is in flow units 3U and 3L.

The remaining oil in place has been divided into three areas in order to group the field into wells with similar production histories and help minimise the errors resulting from the kh-apportioned method (fig. VIII-23). The east and west pattern areas were simply split along the main north-south fault (considered to be sealing). The northern breakdown was based on the fact that all wells north of Tirrawarra 48 are under primary depletion.

Table IX-5. Remaining oil in place calculated by the production allocation method for west, east, and north areas.

Flow unit	OOIP (MMbbl)			Cumulative production (MMbbl)			Remaining OIP (MMbbl)		
	West	East	North	West	East	North	West	East	North
4	3.3	8.9	11.9	0.3	1.8	0.2	3.0	7.1	11.7
2U	2.3	0.4	0.1	0.0	0.0	0.0	2.3	0.4	0.1
3U	17.2	24.4	23.2	1.0	2.1	0.1	16.2	22.3	23.1
3L	22.6	25.1	16.6	4.0	6.9	0.5	18.6	18.2	16.1
2L	0.9	3.7	1.3	0.0	0.3	0.0	0.9	3.4	1.3
1U	0.2	0.7	0.4	0.0	0.0	0.0	0.2	0.7	0.4
Total	46.4	63.2	53.6	5.4	11.1	0.8	41.2	52.1	52.7
Grand Total			163.2			17.4			146.0

Table IX-5 shows Tirrawarra oil-in-place by flow unit and by area. Flow units 3U and 3L dominate all aspects of the OOIP resource base across the field. The remaining oil in place is remarkably similar in these flow units in all three areas. The principal difference between the areas is the substantial resource remaining in flow unit 4 in the northern area. An analysis of each area follows.

West Area

The overall recovery factor for this area is 11.6% with the majority of the production from Facies 3L. The OOIP of the patterns in this western area is approximately 17.0 MMbbl indicating a significant proportion (63%) of the OOIP in the western zone is in flank locations. The recovery factors for the EOR patterns in this area are very good with Tirrawarra 18 and 38 having recovery factors of 40.0 and 44.2% respectively to December 1992.

To successfully access the flank oil in place in the western section of the reservoir as well as improve recovery from the existing EOR areas, a combination of methods including EOR pattern expansion, EOR soak, huff-and-puff, and infill drilling will be required. These will be discussed in the next chapter.

East Area

The overall recovery factor for this area is 17.6% and is the highest in the field. This recovery is representative of the excellent performance of the EOR patterns in this area and the fact that a greater proportion of this area is encompassed by the EOR scheme. Due to the larger pattern sizes in the eastern area scope exists to improve recovery from existing patterns

by infill well locations such as Tirrawarra F, Q, E, 23, 25, and 54. These wells would help improve the areal sweep efficiencies of these patterns.

The volume of oil located in the flanks of this region is similar to the west pattern (26.4 MMbbl cp. with 29.4 MMbbl in the west). The mechanisms to recover this flank oil are identical to those discussed above for the western area.

North Area

The overall recovery factor for the northern area is 1.5% and reflects a lack of development, poor productivity of the northern wells due to relative permeability effects and also the poor recovery factor expected without some form of enhanced oil recovery. This area has the greatest potential for further development as the expansion of the EOR scheme in this area would have significant benefits (See Section X).

Validation and Sensitivity of kh-Apportioned Method

Due to the concerns raised over the kh-apportioned method for determining the remaining oil in place distribution, a sensitivity was conducted assuming that 90% of each well's cumulative production was from flow unit 3L. The rationale for performing this sensitivity was that the engineering data available indicated that the majority of the flow from Tirrawarra EOR wells was from flow unit 3L. The East Area of the Tirrawarra Field was chosen for the sensitivity. The results of this work are shown in Table IX-6.

Table IX-6. Comparison of kh-apportioned method with volumes remaining assuming flow unit 3L produces 90 percent (CP_{90}) of Tirrawarra production.

		Production		Remaining Oil	
Flow unit	OOIP (MMbbl)	kh (MMbbl)	CP_{90} (MMbbl)	kh (MMbbl)	CP_{90} (MMbbl)
4	8.9	1.8	0.55	7.1	8.35
2U	0.4	-	-	0.4	0.4
3U	24.4	2.1	0.55	22.3	23.85
3L	25.1	6.9	10.0	18.2	15.1
2L	3.7	0.3	-	3.4	3.7
1U	0.7	0.0	-	0.7	0.7
Total		11.1	11.1		

Table IX-6 indicates that if it is assumed that 90 percent of the production is from flow unit 3L, the difference in unrecovered oil volumes in flow units 3L, 3U, and 4 changes by only 8 percent. The remaining resource in Tirrawarra is so large and the relative volume differences

by the two methods so small, that it is concluded that the kh-apportioned method provides a good preliminary assessment of the residency of remaining oil on a regional basis until an accurate full field simulation model is concluded.

X. OPPORTUNITIES FOR INCREMENTAL DEVELOPMENT

A substantial oil resource remains in Tirrawarra field. Current recovery efficiency is only 11 percent of the OOIP; thus, the volume of unrecovered oil amounts to 146 MMbbl. The resource is fairly evenly distributed throughout the field area, even though development has focused on the east and west sections of the field. In this chapter, a variety of strategies for optimizing recovery are addressed. These technologies include infill drilling, EOR pattern optimization, deployment of new EOR patterns, and recompletion of existing wells.

New Pattern Development

Development of EOR patterns in the north of the field has stalled in the past because of the belief that reservoir quality in the north is significantly poorer in this area. However, the detailed reservoir description and characterization have shown that the reservoir quality in the north is comparable to that in the east and west pattern areas and that the poorer productivity of the northern wells is due to relative permeability effects as a result of the higher water saturations in this region and due to water loading in the well bore. This new interpretation improves the outlook for EOR pattern development in the north as:

(a) the reservoir oil contacted by the injection fluid (i.e., miscible bank) has much improved mobility compared with original reservoir oil;

(b) pressure support gained by injection will allow producers to lift the minor volumes of water which, under primary depletion, have been killing these wells; and

(c) ethane is capable of significantly swelling the oil at reservoir conditions and may improve the relative permeability of the oil by altering the saturation profile in the reservoir.

An example of possible future pattern configurations in the north is shown in figure X-1. There is potential in this area of the field for an additional 5 EOR patterns roughly described as Tirrawarra S, Z, G, I, and AC. The first four patterns all have oil in place volumes of greater than 6.0 MMbbl, which makes them comparable with the smaller southern patterns. The small size may prove beneficial in hastening the pressure support to the producers. The down side of these patterns is that they are located in areas of higher water saturation and therefore the productivity/injectivity will be significantly less than for the southern patterns. The extent to which water saturation affects these patterns is unknown, and further work requiring detailed SCAL studies, small-scale reservoir simulation studies, and field trials/pilots will be necessary to

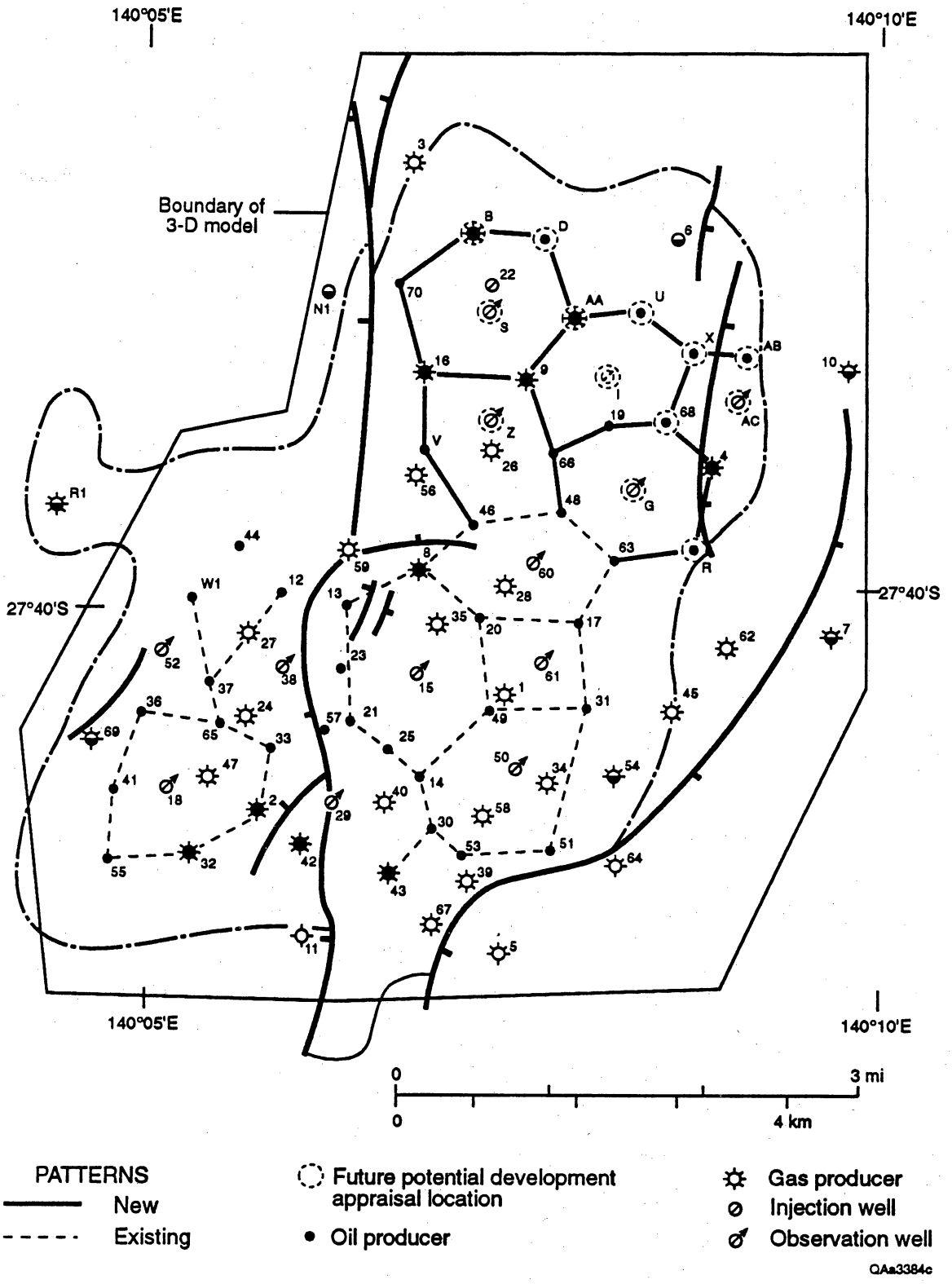

Figure X-1. Map of Tirrawarra field showing potential future EOR patterns in the north part of the field.

gain a better understanding of the mechanisms involved. Initial investigations into the establishment these patterns will center on proving injection capabilities in this area by converting an existing producer such as Tirrawarra well 16 or well 48 to injection and monitoring pressure support at surrounding wells. If this is successful, an economic analysis of the development of the full northern area is highly recommended. The proposed pattern development in the northern half of the field would access incremental OOIP of approximately 35 MMSTBO.

Optimization of Existing EOR Activities

General

The optimization of the existing patterns will require validation in the form of simulation modeling. It is obvious that the recovery of each pattern is dependent on the facies architecture and the detailed three-dimensional distribution of petrophysical characteristics, but the extent of other factors such as viscous fingering, gravity override, and crossflow between flow units is largely unknown.

The study has shown that fairly uniform sweep is being achieved within the mature patterns and that flow unit 3L is the dominant conduit for the miscible flood. Based on the fairly uniform reservoir characteristics of flow units 3U and 3L throughout the field, there is no obvious need to change the structure of existing patterns (i.e., switch to line drive). One obvious method of improving the sweep efficiency of the existing patterns is by providing recompletion and infill locations such as Tirrawarra well 25, F, and Q (fig. X-2). As noted earlier, recompletion of Tirrawarra well 23 has resulted in a 250 bbl/d well; similar yields may be possible in Tirrawarra well 25 and in infill wells F and Q.

Other methods for improving the recovery from the existing patterns concentrate on recovery mechanisms:

Low Pressure Flood

The current operation of the miscible flood aims to maintain the average pressure within each pattern at 3,200 to 3,500 psia and therefore ensures that the injection fluid is at or near first-contact-miscibility with the oil. If injection rates were reduced and average pattern pressures kept near bubblepoint (P_b = 2,960 psia), the following advantages could be gained:

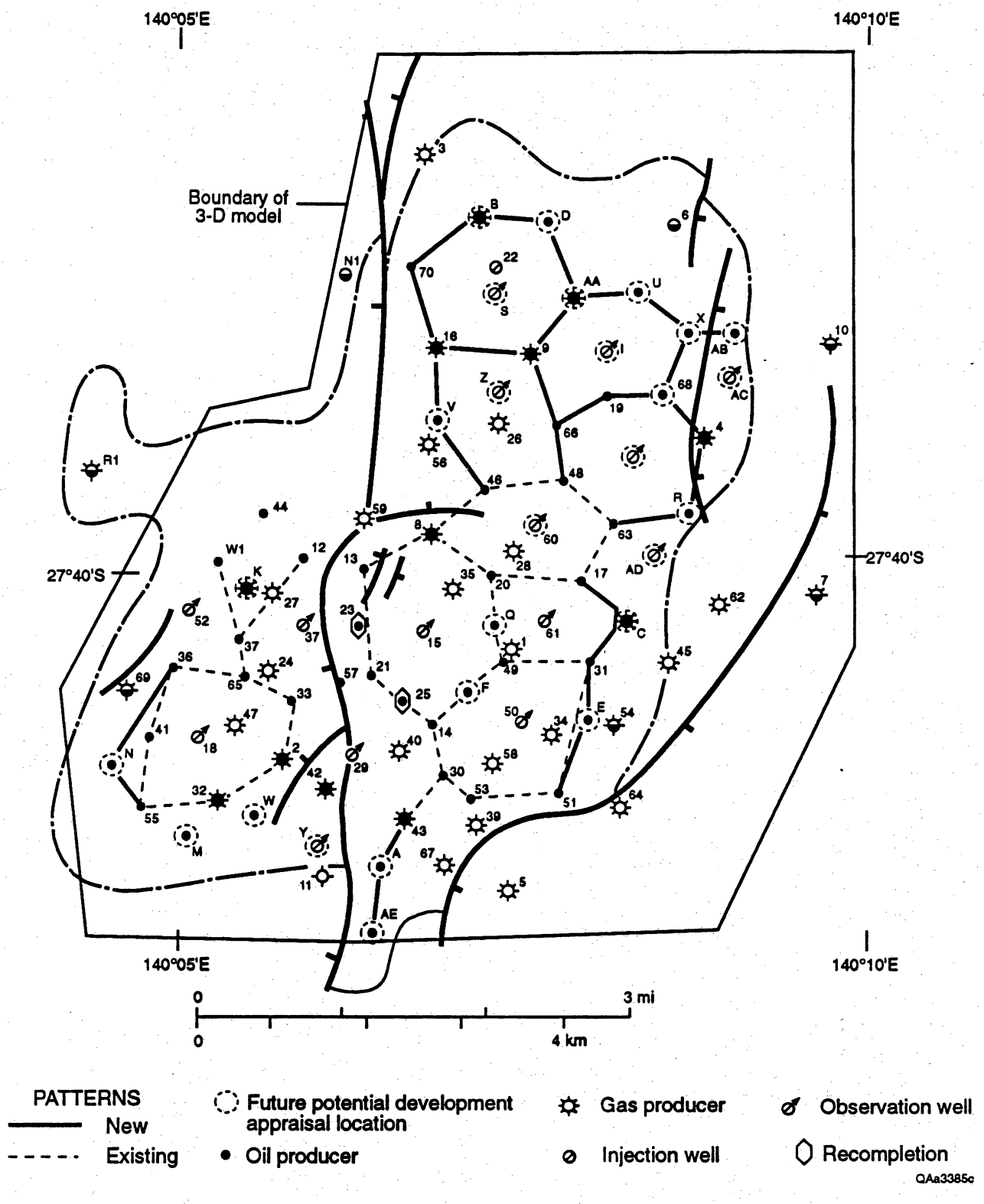

Figure X-2. Map of Tirrawarra field showing potential infill drilling and recompletion locations.

i. The flood may become immiscible, which would result in a lowering of the mobility ratio and a potential increase in sweep efficiency, without significant mass transfer losses.
ii. The pressure of the main conduit of the flood (facies 3L) would be lowered, allowing greater transfer of oil from the poorly swept facies 3U.
iii. Due to reduced injection rates, the flood would require less injection fluid, resulting in reduced operating costs and surplus ethane for expansion of EOR to the north and to other fields.

CO_2 Injection

By altering the injection fluid it is possible to improve the sweep efficiency of a miscible flood. The main advantages of CO_2 over ethane are its greater density and solubility in water. The density difference means that gravity override effects would be less severe with CO_2 and compression requirements would be reduced. The solubility of CO_2 in water allows it to access oil which has been blocked by water. This process may be significant in future northern patterns or current patterns where water saturations are high.

Pattern Soak

If flow unit 3L is the main conduit for the miscible flood, then oil in the other flow units (3U and 4) may not be being contacted by the injection fluid. One method that may assist in the contact of these flow units is to shut-in a pattern and allow the injection fluid to be soaked up into the other flow units (mainly 3U), improving oil mobility. When the pattern is brought back on line, this oil may be capable of flow, either through these flow units, or down into the productive flow unit 3L.

Flank Location Huff-and-Puff

Flank wells isolated from deployed EOR patterns could benefit from huff-and-puff injection to swell the oil and improve mobility in the wedge areas.

Infill Well Locations

Based on the new interpretation of the main north–south fault location, the possibility exists for infill wells along the western side of this fault to extend the Tirrawarra well 38 pattern. The productivity of these wells should be similar to the high-productivity wells on the other side of the fault. The wells would also help improve the efficiency of this pattern. Careful selection of drill locations based on seismic (preferably 3-D) would be required to prevent fault isolation.

Considerable oil reserves are located in the flanks of Tirrawarra field, and locations exist where the water saturation should not adversely affect well productivity. In the west, locations such as M, N, and W all appear viable and would help improve Tirrawarra well 18's sweep efficiency as well as access flank OOIP (fig. X-2). In particular, the N location would greatly improve recovery to the west of this pattern as access is currently denied due to the early breakthrough of Tirrawarra well 41.

In the east of the field, locations on the flanks such as A, C, E, AD, and R are all possibilities if pressure support can be achieved in these flank regions. The productivity of these wells would not be high (cf. Tirrawarra well 51), but they would greatly improve the sweep efficiency of the flank patterns and access oil outside the main pattern areas.

As well as these flank well locations, well locations such as F and Q may prove economic and may help improve the sweep efficiency of these mature patterns (Tirrawarra well 15 pattern and Tirrawarra well 50 pattern). These wells should not be drilled until sufficient information has been obtained from the currently programmed Tirrawarra wells 23 and 25 recompletions.

In summary, there is the possibility of up to 12 infill/flank development wells in the existing pattern areas in the east and west of the field. The drilling of these will largely depend on proof that pressure support can be achieved out in the flanks of the field and on the results of infill recompletions. Other methods such as improved artificial lift techniques, improved hydraulic fracture stimulations, and huff-and-puff techniques may also improve the commercial viability of the flank development wells.

Strategic Infill and Recompletion Opportunities

Horizontal Well

A substantial volume of the western area reserves are located along the western side of the main north–south fault between Tirrawarra well 12 and Tirrawarra West well 1 (fig. X-2). While the productivity in such areas is expected to be poor, a horizontal well drilled along this zone may prove economic. Other technology that may help the commercial viability of such areas is the use of slimholes and drainholes. These allow additional production sites with possible capital saving compared to the cost of a standard Tirrawarra well.

Recompletion Strategies

The most cost effective method of accessing incremental reserves and increasing production is to complete or recomplete existing cased wells.

One of the important findings of the study was the addition of considerable OOIP in flow unit 4, which is interpreted over the entire Tirrawarra field. There exists the potential to perforate a number of existing producers in this flow unit. This will increase recoverable reserves and should also add to the current deliverability of the field. Existing wells perforated in flow unit 4 may not be accessing this flow unit due to proppant settling during fracture stimulation. Although it should not be a problem to perforate the producers, further work is required to determine whether current injectors or wells that may become injectors in the future should be perforated in flow unit 4. Perforating the injectors in this flow unit may result in early gas breakthrough where thin, high-permeability channel sands connect injectors to producers. This early breakthrough would be detrimental to production and recovery and would not be easily remedied by cement squeezes. The southeast area is the biggest risk for such breakthrough as an interconnected gravel bed is developed there.

A number of Tirrawarra wells that are currently completed in upper Patchawarra gas sands are ideal candidates for recompletion to oil producers/injectors. These include wells such as Tirrawarra well 25 in the east and Tirrawarra wells 26 and 56 in the north. These wells provide a more economic alternative to drilling new wells if their location is not critical to the gas sand development. The preliminary success of such options is shown by Tirrawarra well 23, in the east, which was recently recompleted to an oil producer and is currently producing 250 Bbl/day of clean oil.

XI. CONCLUSIONS

A substantial oil resource remains in Tirrawarra. Detailed geological, petrophysical, and engineering characterization of the field has resulted in identification of an additional 36 MMSTB of original oil in place. Current recovery efficiency of this oil resource (as of 1992) is less than 11 percent. Thus, of the 163 MMSTB of in-place oil, 146 MMSTB remains. Much of this remaining resource is accessible through optimization of existing EOR patterns; deployment of new patterns in the northern area of the field; targeted infill drilling for improved sweep efficiency particularly in the more heterogeneous flow units 2 and 4; and, strategic recompletion of existing wells, again targeting flow unit 4, which has largely been vertically bypassed by EOR sweep. Specific conclusions regarding each project task are described below.

Task 1: Data Compilation

Successful identification of the volume and residency of this large remaining resource is the product of synergistic integration of a multidisciplinary characterization team and access to a well-organized and well-compiled data base. All available geological and petrophysical information had been compiled into comprehensive strip logs supported by comprehensive plots of engineering data as part of Santos' initial study of the field. This enabled rapid incorporation and full analysis of data during the project. As a result, all aspects of this multidisciplinary study are fully integrated in support of the conclusions reached herein. The data format established by Santos for this study fostered rapid progress of the project. For any future studies, all engineering and geological data should be fully compiled, in a similar manner, to aid data analysis by geologists and engineers to ensure fully synergistic characterization.

Tasks 2 and 3: Geological Setting and Depositional Systems Analysis

Regional stratigraphic and structural studies led to identification of regional datums throughout the Patchawarra/Tirrawarra section and the effective analysis of the structural history and broad sequence stratigraphy of the area. A constant, active stress regime was active throughout this whole period of deposition with thickening to the west of the main north–south fault, crestal thinning, and overall northward thinning (by up to 30 percent). The preexisting basement structural framework was reactivated through time to cause the complex

structure observed in the field. Palynological analysis resulted in the G confluence zone being identified in the reservoir section. This is the only indication of this zone in the basin, and its absence at nearby Fly Lake field (despite thorough sampling) implies the presence of a sequence boundary between the lower Patchawarra Formation and facies 3. The unconformity at the base of facies 4 is interpreted to be this sequence boundary.

Detailed sedimentologic analysis of the rich Tirrawarra core dataset facilitated the identification and mapping of the facies composition of the field. In conjunction with petrographic and petrophysical analysis, facies were then further divided into six flow units on the basis of porosity and permeability attributes. High-resolution mapping of flow unit distribution and their component volumetric attributes, including flow capacity and hydrocarbon pore volume, resulted in the reservoir being fully characterized with no ambiguity. As a result, the reservoir model fully accounts for all production behavior, including anomalous RFT's and previously inexplicable production trends.

Task 4: Geophysical Interpretation

Despite poor data quality at the reservoir level, existing seismic data were successfully used to map the structural grain of the field. Poor data quality is the result of the subtle but complex field structure and, importantly, signal deterioration caused by the overlying coal measure sequence. This poor data quality is manifested as interference by multiples and out-of-plane data in a very poor signal-to-noise environment. Poor data quality prevented high-resolution seismic stratigraphic analysis. Nonetheless, field structure and small-scale faults that account for several production anomalies were identified.

Task 5: Petrography

The main controls on permeability in the Tirrawarra Sandstone reservoir are grain size and volume of ductile grains, which are both functions of the original depositional environment. Tirrawarra depositional facies have distinct petrographic characteristics, and the effect of diagenesis has been to lower porosity and permeability but with depositional texture and composition determining the magnitude of loss. The highest porosity and permeability occur in those sandstones from flow units 3L and 4 that have coarser grain size, relatively quartz-rich detrital mineral composition, and high values of primary porosity. Mechnical compaction of ductile grains and chemical compaction by intergranular pressure solution and stylolitization are

major causes of porosity loss. Volume of cement is not a significant control on porosity or permeability.

Task 6: Petrophysics

Petrophysical analysis verified flow unit definition. Well log resolution and SCAL analysis of flow units showed that the flow units have different compositions and hence different pore geometries. For this reason, flow unit-specific cutoffs were established for each flow unit for foot-by-foot log analysis and pay determination. The main impact was the reduction of the porosity cutoff from 9 percent to 8 percent based on core porosity versus core permeability crossplots. The Vsh cutoff was also increased for some of the flow units due to the high shale-clast content and the presence of shale laminae. The impact was a substantial increase in net pay for most wells. Foot-by-foot editing of the log analysis verified the petrophysical cutoffs as the final results matched core data, production data, and test data for all wells.

Santos' methods of log analysis were verified (calculation of Vsh, phi, and Sw) as they are based on correlation with core data. There are reservations about the Overton equation not using corrected or normalized GR for determination, due to the impact that environmental effects (logging speed, KCl, mud, and caving) can have on the GR tool.

Task 7: Original Oil in Place Calculation and Residency

Based on detailed review of flow unit architecture and petrophysical analysis, Tirrawarra volumetrics have been substantially revised. OOIP has been increased by 28 percent to 163 MMSTB as a result of modifications to the cutoffs and recognition of a large resource in flow unit 4. Most of the OOIP resides in flow units 3U and 3L.

Task 8: Engineering Review

Engineering analysis showed that all production trends and other engineering data pertaining to the field, including previously inexplicable anomalies, can be accounted for using the reservoir characterization model. SCAL data showed a large transition zone in each of the flow units and combined with the strongly water wet relative permeabilities suggested a dramatic fall off in oil productivity to the flanks of the field. This result is consistent with production trends that showed a significant drop in well productivity off structure. The SCAL data also showed that water production should be minor, a result that is consistent with

production data. No Tirrawarra wells have seen the onset of water production, which indicates no significant water influx to the field. PLT and RFT results showed definite layering, with flow unit 3L dominating the production and injection behavior of Tirrawarra EOR wells. Of the other facies, only flow unit 4 showed any flow contribution, and the results of cross flow indicated limited channels. The RFT data also indicated sporadic communication between the various flow units, which is consistent with the geological description that showed shale barriers between certain flow units.

Performance the eight EOR patterns is consistent with a uniform geologic character of flow unit 3L. Pressure support, cumulative production to breakthrough, and the overall recovery factors of the patterns indicate no substantial tortuosity or sealing barriers. These factors, combined with the RFT/PLT results, indicate that flow unit 3L is the main contributor to the EOR patterns. However, the substantial recovery factors of the patterns to date indicate definite contributions from other facies, probably by vertical crossflow.

Permeability data were determined and related to flow units through the use of facies-dependent permeability/porosity crossplots and then summed to give predicted well flow capacities. The match with pre-fracture stimulation test data was very good, with an average scaling factor of 1.7. The scaling process to correct the predicted flow capacities with the test data showed relative permeability effects with a flank wells requiring consistent downscaling while the predicted flow capacities of crestal wells was generally conservative. The flow capacity maps for each flow unit corresponded well to the facies interpretation. Flow units 2L, 2U, and 4 showed highly irregular flow capacity distribution, which is consistent with channelized braid plain deposits. Flow units 3L and 3U indicated highly uniform flow capacity with flow unit 3L having the best and most laterally continuous reservoir quality.

Task 9: Remaining Oil in Place

Determination of the areal distribution and flow-unit residency of the unrecovered oil resource was based on allocation of production by the relative flow capacity of each flow unit. The result of this effort highlighted significant remaining oil in place with a recovery factor to December 1992 of 10.7 percent. The remaining 146 MMSTB oil in place is spread fairly evenly across the field but is dominated by flank locations in flow units 3L and 3U. Flow unit 4 also contains considerable remaining oil in place in the north.

There is considerable potential for reserve appreciation through production optimization from the field. Deployment of new EOR patterns in the north and expansion of existing patterns in the east and west together with recompletion of existing wells in these patterns to improve sweep, supported by targeted infill drilling and recompletion of 14 existing wells to

contact bypassed oil in flow unit 4, will access an incremental 50 MMSTB of oil. Based on current patterns of behavior, incremental recovery of 35 percent, or 18 MMSTB, of this resource is possible. The magnitude of incremental reserves potentially recoverable from Tirrawarra and identified by this project is equivalent to the volume of oil historically produced from the field.

XII. RECOMMENDATIONS

Tasks 2 and 3: Geological Setting and Depositional Systems Analysis

The lack of a comprehensive structural and stratigraphic framework for the region has meant that this field characterization study could not benefit from an understanding of larger scale depositional or structural patterns. Due to the lack of any knowledge of the depositional system at the time of Tirrawarra deposition, only local depositional trends could be deduced. Further, there is no geological framework for the extrapolation of the results of this study to the prediction of additional exploration targets. A detailed regional analysis of the structure, sedimentology, and stratigraphy of this important reservoir interval is recommended.

A more detailed breakdown of flow unit 4 is recommended to separate the interconnected from the unconnected pay unit. This is expected to be required prior to the targeting of this flow unit for specific development projects, especially in the south and west, where this unit is thinnest and least continuous. Flow unit 4 is composed of a basal interconnected braid plain channel system, with interconnecting pay sands, grading upward into a meanderbelt section with disconnected channel sands.

Because natural fractures are common in Tirrawarra Sandstone core and may play a role in oil production, a study focusing on Tirrawarra natural fractures may be warranted. The goal of this study would be to gain insight into the distribution, orientation, connectivity, and conductivity of natural fractures in Tirrawarra field. This study should begin with characterization of all fractures in existing Tirrawarra core. Since fracture orientation is necessary for mapping the subsurface fracture network, paleomagnetic methods might be used to orient selected intervals of existing core. Borehole imaging logs should be run in new wells, and, if cores are taken, downhole orientation techniques should be used. Regional in situ stress conditions and tectonic history must also be considered when evaluating local fracture characteristics.

Task 4: Geophysical Interpretation

It is recommended that 3-D seismic supported by VSPs be considered to overcome the imaging problems beneath the coal measure sequence. VSPs may image beneath the coals, and a 3-D seismic survey will provide the necessary resolution to image facies architecture and to

resolve the complex reservoir structure. Both of these practices will greatly reduce the risk involved in drilling infill development wells (even on the crestal areas where structural complexity may result in fault block isolation). Due to the high drilling costs involved, the avoidance of a single poor well will justify these recommendations.

Task 6: Petrophysics

Following a full review of all water analyses, including the recent sampling program, the use of a new water resistivity for the field (0.65 ohm-m at 75°F) is recommended. Further, continued water sampling is recommended as the complex OWC and the presence of lower water resistivities in the northwest indicates potential for lower resistivity Patchawarra water influx across the main fault in that area.

ACKNOWLEDGEMENTS

Funding for this study was provided by Santos Ltd., and work was conducted in close cooperation with Santos personnel. Sigrid J. Clift, Rick Edson, Senira S. Kattah, Eugene M. Kim, John M. Mendenhall, Glynis G. Morse, Virginia M. Pendleton, and Robert S. Single assisted in various phases of the project. We benefited from discussions about the Tirrawarra field with many BEG scientists, including Mark J. Burn, William E. Galloway, Douglas S. Hamilton, Mark Holtz, Martin P. A. Jackson, Stephen E. Laubach, Jerry F. Lucia, and Daniel D. Schultz-Ela. Figures in this report were prepared under the direction of Richard L. Dillon, Chief Cartographer. Word processing was done by Susan Lloyd under the direction of Amanda R. Masterson, Editor-in-Chief, who also edited the report. Assembly of the report was by Jeannette Miether and Eugene M. Kim. The contract report was pasted up by Jamie H. Coggin and Margaret L. Evans. Santos staff who provided assistance with the study were Glen A. Johnson, Tony Harrison, Marie-Louise Lees, Franz Posaner, Geoff Wood, and David Hudson. Brian Logan of the South Australian Department of Mines and Energy's Core Library was very helpful in organizing core viewing.

REFERENCES

Ashley, G. M., 1975, Rhythmic sedimentation in glacial Lake Hitchcock, Massachusetts–Connecticut, *in* Jopling, A. V., and McDonald, B. C. (eds.), Glaciofluvial and glaciolacustrine sedimentation: Society of Economic Paleontologists and Mineralogists Special Publication well 23, p. 304–320.

Asquith, G. B., 1982, Basic well log analysis for geologists: American Association of Petroleum Geologists, Methods in Exploration Series well 3, 216 p.

Asquith, G. B., 1990, Shaly sand analysis, a practical guide: American Association of Petroleum Geologists, Course Notes Series well 31, 59 p.

Asquith, G. B., and Saha, Souvick, 1991, Determining Archie parameters m and n using least squares summation and dielectric water saturations in the PASCAL computer program MN: Geobyte, v. 24, well 6, p. 24–28.

Atkins, J. E., and McBride, E. F., 1992, Porosity and packing of Holocene river, dune, and beach sands: American Association of Petroleum Geologists Bulletin, v. 76, p. 339–355.

Battersby, D. G., 1976, Cooper Basin gas and oil fields, *in* Leslie, R. B., Evans, H. J., and Knight, C. L. (eds.), Economic geology of Australia and Papua New Guinea: Australasian Institute of Mining and Metallurgy Monograph 7, Part 3, Petroleum, 3, p. 321–568.

Bennett, D. G., Barley, M. R., 1988, The significance of vertical crossflow to gas recovery from Cooper Basin Sands, RE: 020/88, unpublished SANTOS report.

Bever, J. M., Carroll, P. G., Williams, B. P. J., and Wild, E. K., 1987, Petrography and core study, Tirrawarra Sandstone, Moorari and Tirrawarra field, vols. 1 and 2: unpublished Santos report.

Boothroyd, J. C., and Ashley, G. M., 1975, Processes, bar morphology, and sedimentary structures on braided outwash fans, Northeastern Gulf of Alaska, *in* Jopling, A. V., and McDonald, B. C. (eds.), Glaciofluvial and glaciolacustrine sedimentation: Society of Economic Paleontologists and Mineralogists Special Publication well 23, p. 193–222.

Boothroyd, J. C., and Nummedal, D., 1978, Proglacial braided outwash: a model for humid alluvial fan deposits, *in* Miall, A. D. (ed.), Fluvial sedimentology: Canadian Society for Petroleum Geology, Memoir, 5, p. 641–668.

Bowyer, D. G., 1991, Recognition of formation waters from the Cooper and Ecomanga Basins: SDRN 035191, unpublished Santos report.

Campbell, C. V., 1976, Reservoir geometry of a fluvial sheet sandstone: American Association of Petroleum Geologists Bulletin, v. 60, well 7, p. 1009–1020.

Church, M., and Gilbert, R., 1975, Proglacial fluvial and lacustrine environments, *in* Jopling, A. V., and McDonald, B. C. (eds.), Glaciofluvial and glaciolacustrine sedimentation: Society of Economic Paleontologists and Mineralogists Special Publication 23, p. 22–100.

Davies, D. K., Williams, B. P. J., and Vessell, R. K., 1991, Reservoir models for meandering and straight fluvial channels; examples from the Travis Peak Formation, East Texas: Gulf Coast Association of Geological Societies Transactions, v. 61, p. 152–174.

Dewan, J. T., 1984, Essentials of modern open-hole log interpretation: Tulsa, Oklahoma, PennWell Publishing Co., 361 p.

Donaldson, A. C., Martin, R. H., and Kanes, W. H., 1970, Holocene Guadalupe delta of Texas Gulf Coast, *in* Morgan, J. P. (ed.), Deltaic sedimentation modern and ancient: Society of Economic Paleontology and Mineralogists Special Publication, 15, p. 107–137.

Dutton, S. P., 1987, Diagenesis and burial history of the Lower Cretaceous Travis Peak Formation, East Texas: The University of Texas at Austin, Bureau of Economic Geology Report of Investigations No. 164, 58 p.

Dutton, S. P., Finley, R. J., and Herrington, K. L., 1987, Organic geochemistry of the Lower Cretaceous Travis Peak Formation in East Texas: Gulf Coast Association of Geological Societies Transactions, v. 37, p. 65–74.

Fielding, C. R., and Crane, R. C., 1987, An application of statistical modelling to the prediction of hydrocarbon recovery factors in fluvial reservoir sequences: Society of Economic Paleontologists and Mineralogists, p. 321–327.

Fisher, W. L., and McGowen, J. H., 1967, Depositional systems in the Wilcox Group of Texas and their relationship to occurrence of oil and gas: Gulf Coast Association of Geological Societies Transactions, v. 17, p. 105–125.

Folk, R. L., 1974, Petrology of sedimentary rocks: Austin, Texas, Hemphill, 182 p.

Galloway, W. E., and Hobday, D. K., 1983, Terrigenous clastic depositional systems: applications to petroleum, coal, and uranium exploration, New York, Springer-Verlag, 423 p.

Gatehouse, C. G., 1972, Formations of the Gidgealpa Group in the Cooper Basin: Australasian Oil Gas Review, v. 18, well 2, p. 10–15.

Gustavson, T. C., Ashley, G. M., and Boothroyd, J. C., 1975, Depositional sequences in glaciolacustrine deltas, *in* Jopling, A. V., and McDonald, B. C. (eds.), Glaciofluvial and glaciolacustrine sedimentation: Society of Economic Paleontologists and Mineralogists Special Publication, well 23, p. 264–280.

Hamlin, H. S., 1988, Depositional and ground-water flow systems of the Carrizo–Upper Wilcox, South Texas: The University of Texas at Austin, Bureau of Economic Geology Report of Investigations No. 175, 61 p.

Hearn, C. L., Ebanks, W. J., Jr., Tye, R. S., and Ranganathan, V., 1984, Geological factors influencing reservoir performance of the Hartzog Draw field, Wyoming: Journal of Petroleum Technology, SPE Paper 12016, p. 1335–1344.

Heath, R., 1989, Exploration in the Cooper Basin: Australian Petroleum Exploration Association Journal, v. 29, well 1, p. 366–378.

Hine, A. C., and Boothroyd, J. C., 1978, Morphology, processes, and recent sedimentary history of a glacial-outwash plain shoreline, Southern Iceland: Journal of Sedimentary Petrology, v. 48, well 3, p. 901–920.

Houseknecht, D. W., 1987, Assessing the relative importance of compactional processes and cementation to the reduction of porosity in sandstones: American Association of Petroleum Geologists Bulletin, v. 71, p. 633–642.

Houseknecht, D. W., 1988, Intergranular pressure solution in four quartzose sandstones: American Association of Petroleum Geologists Bulletin, v. 58, p. 228–246.

Kantsler, A. J., Prudence, T. J. C., Cook, A. C., and Zwigulis, M., 1983, Hydrocarbon habitat of the Cooper/Eromanga Basin: Australian Petroleum Exploration Association Journal, v. 23, well 1, p. 75–92.

Kapel, A. J., 1966, The Coopers Creek Basin: Australian Petroleum Exploration Association Journal, v. 6, p. 71–75.

_____ 1972, The geology of the Patchawarra area, Cooper Basin: Australian Petroleum Exploration Association Journal, v. 12, well 1, p. 53–57.

Lomando, A. J., 1992, The influence of solid reservoir bitumen on reservoir quality: American Association of Petroleum Geologists Bulletin, v. 76, no. 8, p. 1137–1152.

Martin, C. A., 1967, The Gidgealpa and Merrimelia Formations in the Coopers Creek Basin: Australasian Oil and Gas Journal, p. 29–35.

Martin, K. R., 1981, Petrology and diagenesis of the Tirrawarra Sandstone in the Tirrawarra field, Cooper Basin: unpublished Santos report.

_____ 1984, Petrology, diagenesis, and reservoir quality of the Tirrawarra Sandstone in the Tirrawarra, Fly Lake and Moorari fields: unpublished Santos report.

McGowen, J. H., 1970, Gum Hollow fan delta, Nueces Bay, Texas: The University of Texas at Austin, Bureau of Economic Geology Report of Investigations No. 69, 91 p.

McPherson, J. G., Shanmugam, G., and Moiola, R. J., 1987, Fan-deltas and braid deltas: varieties of coarse-grained deltas: Geological Society of America Bulletin, v. 99, p. 331–340.

Miall, A. D., 1981, Analysis of fluvial depositional systems: American Association of Petroleum Geologists Education Course Note Series, well 20, 75 p.

Neashan, T. W., 1977, The morphology of dispersed clay in sandstone reservoirs and its effects on sandstone shaliness, pore space, and fluid flow properties: Society of Petroleum Engineers of the AIME meeting, Denver, SPE Paper 6858.

Overton, M., and Hamilton, N., 1986, A petrophysical review of unit fields, Cooper Basin, South Australia: SDRN 86/29, unpublished Santos report.

Pecanek, H., and Gulayets, G., 1986, Correlation of core data with flow data for Cooper Basin, Australia: Santos Reservoir Engineering Report (unpublished) RE: 067/86.

Pittman, E. D., 1979, Porosity, diagenesis, and productive capability of sandstone reservoirs, in Scholle, P. A., and Schluger, P. R. (eds.), Aspects of diagenesis: Society of Economic Paleontologists and Mineralogists Special Publication No. 26, p. 159–173.

Pryor, W. A., 1973, Permeability-porosity patterns and variations in some Holocene sand bodies: American Association of Petroleum Geologists Bulletin, v. 57, p. 162–189.

Rogers, M. A., McAlary, J. D., and Bailey, N. J. L., 1974, Significance of reservoir bitumens to thermal-maturation studies, western Canada Basin: American Association of Petroleum Geologists Bulletin, v. 58, p. 1806–1824.

Schumm, S. A., 1977, The fluvial system: New York, John Wiley, 338 p.

Smith, G. L. B., and Eriksson, K. A., 1979, A fluvioglacial and glaciolacustrine deltaic depositional model for Permo-Carboniferous coals of the Northeastern Karoo Basin, South Africa: Palaeogeography, Palaeoclimatology, Palaeoecology, 27, p. 67–84.

Thornton, R. C. N., 1979, Regional stratigraphic analysis: Geological Survey of South Australia Bulletin 49, 140 p.

Tyler, N., and Ethridge, F. G., 1983, Fluvial architecture of Jurassic uranium-bearing sandstones, Colorado Plateau, western United States: International Association of Sedimentologists Special Publication, 6, p. 533–547.

Tyler, N., and Gholston, J. C., 1988, Heterogeneous deep-sea fan reservoirs, Shackelford and Preston waterflood units, Spraberry Trend, West Texas: The University of Texas at Austin, Bureau of Economic Geology Report of Investigations No. 171, 38 p.

Van Dijk, D. E., Hobday, D. K., and Tankard, A. J., 1978, Permo-Triassic lacustrine deposits in the Eastern Karoo Basin, Natal, South Africa: International Association of Sedimentologists Special Publication, 2, p. 225–239.

Van Wagoner, J. C., Posamentier, H. W., Mitchum, R. M., Vail, P. R., Sarg, J. F., Loutit, T. S., and Hardenbol, 1988, An overview of the fundamentals of sequence stratigraphy and key definitions: Society of Economic Paleontologists and Mineralogists Special Publication, well 42, p. 39–45.

Van Wagoner, H. W., Mitchum, R. M., Campion, K. M., and Rahmanian, V. D., 1990, Siliciclastic sequence stratigraphy in well logs, cores, and outcrops: American Association of Petroleum Geologists Methods in Exploration Series, well 7, 55 p.

Vavra, C. L., Kaldi, J. G., and Sneider, R. M., 1992, Geological applications of capillary pressure: a review: American Association of Petroleum Geologists Bulletin, v. 76, well 6, p. 840–850.

Vos, R. G., 1982, Sedimentology of an Ordovician fan delta complex, Western Libya: Sedimentary Geology, v. 29, p. 153–170.

Weber, K. J., 1982, Influence of common sedimentary structures on fluid flow in reservoir models: Journal of Petroleum Technology, SPE Paper 9247, p. 665–672.

Williams, B. P. J., and Wild, E. K., 1984, The Tirrawarra sandstone and Merrimelia Formation of the Southern Cooper Basin, South Australia—the sedimentation and evolution of a glaciofluvial system: Australian Petroleum Exploration Association Journal, p. 377–392.

Wilson, M. D., and Pittman, E. D., 1977, Authigenic clays in sandstones: recognition and influence on reservoir properties and paleoenvironmental analysis: Journal of Sedimentary Petrology, v. 47, p. 3–31.